Friedrich-Schiller-Universität Jena

Chemisch-Geowissenschaftliche Fakultät

Design of Polymeric Building Blocks: Synthesis and Preparation of Different Polymer Architectures or Hybrid Materials

Dissertation

(kumulativ)

zur Erlangung des akademischen Grades

doctor rerum naturalium (Dr. rer. nat.)

vorgelegt dem Rat der Chemisch-Geowissenschaftlichen Fakultät der Friedrich Schiller Universität Jena

von M. Sc. Tobias Rudolph

geboren am 16.02.1986 in Coburg

This work was funded by a PhD scholarship of the Carl-Zeiss Foundation from 06/12-02/15.

Gutachter:

1. Jun.-Prof. Dr. Felix H. Schacher (Friedrich Schiller Universität Jena)

2. Prof. Dr. Ulrich S. Schubert (Friedrich Schiller Universität Jena)

3. Prof. Dr. Sebastian Seiffert (Freie Universität Berlin)

Tag der Verteidigung: 08. September 2015

Für alle die mich auf meinen Wegen begleitet haben

Table of Content

Documentation of authorship

This section contains a list of the individual authors' contributions to the publications reprinted in this thesis.

P1) "Synthesis and Solution Properties of Double Hydrophilic Poly(ethylene oxide)-*block*-poly(2-ethyl-2-oxazoline) (PEO-*b*-PEtOx Star Block Copolymers"

Tobias Rudolph,[1] Sarah Crotty,[2] Moritz von der Lühe,[3] David Pretzel,[4] Ulrich S. Schubert,[5] Felix H. Schacher[6]

Polymers, **2013**, 5, 1081-1101

Authors	**1**	**2**	**3**	**4**	**5**	**6**
Conceptual development/contribution	x					x
Synthesis and characterization of polymers	x		x			
MALDI-TOF MS and 2D SEC measurements		x				
Preparation of manuscript	x			x		x
Correction of manuscript	x	x	x	x	x	x
Supervision of TR						x
Supervision of MvdL	x					x
Proposed publication equivalent	**1.0**					

P2) "Controlling Aqueous Self-Assembly Mechanisms *via* Hydrophobic Interactions"

Tobias Rudolph,[#,1] Naveen K. Allampally,[#,2] Gustavo Fernandez,[3] Felix H. Schacher[4]

Chem. Eur. J., **2014**, 43, 13871-13875

[#]Both authors contributed equally.

Authors	**1**	**2**	**3**	**4**
Conceptual development/contribution	x		x	x
Synthesis and characterization of polymers	x			
Synthesis of bolaamphiphiles and characterization (NMR, SEC, FT-IR)	x			
Characterization of bolaamphiphiles and determination of mechanism		x	x	
Preparation of manuscript	x	x	x	x
Correction of manuscript	x	x	x	x
Supervision of TR				x
Proposed publication equivalent	**1.0**	1.0		

P3) "Supramolecular Three-Armed Star Polymers *via* Cyclodextrin Host/Guest Self-Assembly"

Bernhard V. K. J. Schmidt,[1] Tobias Rudolph,[2] Martin Hetzer,[3] Helmut Ritter,[4] Felix H. Schacher,[5] Christopher Barner-Kowollik[6]

Polym. Chem., **2012**, 3, 3139-3145

Authors	**1**	**2**	**3**	**4**	**5**	**6**
Conceptual development/contribution	x	x				
Synthesis and characterization of polymers	x					
Study the self-assembly process *via* DLS		x				
Study the self-assembly process *via* NMR			x			
Preparation of manuscript	x	x	x			
Correction of manuscript	x	x	x	x	x	x
Supervision of BVKJ						x
Supervision of TR					x	
Proposed publication equivalent		**0.5**				

P4) "Synthesis and Self-Assembly of Poly(ferrocenyldimethylsilane)-*block*-poly(2-alkyl-2-oxazoline) Block Copolymers"

Tobias Rudolph,[1] Adam Nunns,[2] Almut M. Schwenke,[3] Felix H. Schacher[4]

Polym. Chem., **2015**, 6, 1604-1612

Authors	**1**	**2**	**3**	**4**
Conceptual development/contribution	x			x
Synthesis and characterization of polymers	x	x		
Synthesis and characterization of block copolymers	x			
Self-assembly studies	x			
AFM measurements			x	
Preparation of manuscript	x			x
Correction of manuscript	x	x	x	x
Supervision of TR				x
Proposed publication equivalent	**1.0**			

P5) "Hierarchical Self-Assembly of Double-Crystalline Poly(ferrocenyldimethylsilane)-*block*-poly(2-*iso*-propyl-2-oxazoline) (PFDMS-*b*-PiPrOx) Block Copolymers"

Tobias Rudolph,[1] Adam Nunns,[2] Steffi Stumpf,[3] Christian Pietsch,[4] Felix H. Schacher[5]

Macromol. Rapid Commun., submitted

Submission date: 25.04.2015

Authors	**1**	**2**	**3**	**4**	**5**
Conceptual development/contribution	x				x
Synthesis and characterization of polymers	x	x			
Synthesis and characterization of block copolymers	x				
Self-assembly studies	x				
SEM measurements			x	x	
Preparation of manuscript	x				x
Correction of manuscript	x	x	x	x	x
Supervision of TR					x
Proposed publication equivalent	**1.0**				

P6) "Towards Anisotropic Hybrid Materials: Solution Self-Assembly of Linear Polyethylene-*block*-poly(2-(4-((*tert*-butoxycarbonyl)amino)butyl-2-oxazoline)–*block*-poly(2-*iso*-propyl-2-oxazoline) Triblock Terpolymers"

Tobias Rudolph,[1] Matthias Hartlieb,[2] Moritz von der Lühe,[3] Ulrich S. Schubert,[4] Franck DAgosto,[5] Felix H. Schacher[6]

In preparation

Authors	**1**	**2**	**3**	**4**	**5**	**6**
Conceptual development/contribution	x				x	x
Synthesis and characterization of polymers	x					
Synthesis of BocAmOx and deprotection of polymers		x				
DLS measurements	x					
TEM measurements			x			
Preparation of manuscript	x					x
Correction of manuscript	x	x	x	x	x	x
Supervision of TR and MvdL						x
Proposed publication equivalent	**1.0**					

P7) "Homo- and Block Copolymers of Poly(furfuryl glycidyl ether) by Living Anionic Polymerization: Towards Reversibly Core-Crosslinked Micelles"

Markus J. Barthel,[#,1] Tobias Rudolph,[#,2] Sarah Crotty,[3] Felix H. Schacher,[4] Ulrich S. Schubert[5]

J. Polym. Sci. Part A: Polym. Chem., **2012**, *50*, 4958-4965

[#]Both authors contributed equally.

Authors	**1**	**2**	**3**	**4**	**5**
Conceptual development	x	x		x	x
Synthesis and characterization of polymers	x	x			
Crosslinking study	x				
DLS measurements		x			
MALDI-ToF MS measurements			x		
Preparation of manuscript	x	x			
Correction of manuscript	x	x	x	x	x
Supervision of MJB					x
Supervision of TR				x	
Proposed publication equivalent	1.0	**1.0**			

P8) "Self-Healing Materials *via* Reversible Crosslinking of Poly(ethylene oxide)-*block*-poly(furfuryl glycidyl ether) (PEO-*b*-PFGE) Block Copolymer Films"

Markus J. Barthel,[1] Tobias Rudolph,[2] Anke Teichler,[3] Renzo M. Paulus,[4] Jürgen Vitz,[5] Stephanie Hoeppener,[6] Martin D. Hager,[7] Felix H. Schacher,[8] Ulrich S. Schubert[9]

Adv. Funct. Mater., **2013**, *23*, 4921-4932

Authors	**1**	**2**	**3**	**4**	**5**	**6**	**7**	**8**	**9**
Conceptual development/contribution	x	x						x	x
Synthesis and characterization of polymers	x	x							
Self-healing studies	x	x							
Nano-indentation measurements					x				
Profilometry and contact angle measurements			x						
DSC measurements				x					

Preparation of manuscript	x								
Correction of manuscript	x	x	x	x	x	x	x	x	x
Supervision of MJB									x
Supervision of TR								x	
Proposed publication equivalent		**0.5**							

P9) "Poly(2-vinyl pyridine)-*block*-Poly(ethylene oxide) featuring a Furan Group at the Block Junction – Synthesis and Functionalization"

Tobias Rudolph,[1,#] Markus J. Barthel,[2,#] Florian Kretschmer,[3] Ulrich Mansfeld,[4] Stephanie Hoeppener,[5] Martin D. Hager,[6] Ulrich S. Schubert,[7] Felix H. Schacher[8]

Macromol. Rapid Commun., **2014**, 35, 916-921

[#]Both authors contributed equally.

Authors	**1**	**2**	**3**	**4**	**5**	**6**	**7**	**8**
Conceptual development/contribution	x	x						x
Synthesis and characterization of polymers	x	x						
Gold-Nanoparticle preparation			x					
Mid-chain functionalization with dyes and NP	x	x						
TEM measurements				x	x			
Preparation of manuscript	x	x						x
Correction of manuscript	x	x	x	x	x	x	x	x
Supervision of MJB							x	
Supervision of TR								x
Proposed publication equivalent	**1.0**	1.0						

P10) "A Strong Cationic Brønsted Acid, $[H(OEt_2)_2][Al\{OC(CF_3)_3\}_4]$, as an Efficient Initiator for the Cationic Ring-Opening Polymerization of 2-Alkyl-2-Oxazolines"

Tobias Rudolph,[1] Kristian Kempe,[2] Sarah Crotty,[3] Renzo M. Paulus,[4] Ulrich S. Schubert,[5] Ingo Krossing,[6] Felix H. Schacher[7]

Polym. Chem., **2013***, 4,* 495-505

Authors	**1**	**2**	**3**	**4**	**5**	**6**	**7**
Conceptual development/contribution	x	x					x
Synthesis and characterization of polymers	x		x				
Monomer synthesis (2-*tert*-butyl-2-oxazoline)		x					

TGA and DSC measurements				x			
Preparation of manuscript	x						x
Correction of manuscript	x	x	x	x	x	x	x
Supervision of TR							x
Proposed publication equivalent	**1.0**						

P11) "Poly(thiolactone) Homo- and Copolymers from Maleimide Thiolactone: Synthesis and Functionalization"

Tobias Rudolph,[1] Pieter Espeel,[2] Filip E. Du Prez,[3] Felix H. Schacher[4]

Polym. Chem., **2015**, in press (DOI: 10.1039/C5PY00329F)

Authors	**1**	**2**	**3**	**4**
Conceptual development/contribution	x			x
Synthesis and characterization of monomer and polymers	x			
Double modification of polymers	x			
Preparation of manuscript	x	x		x
Correction of manuscript	x	x	x	x
Supervision of TR				x
Proposed publication equivalent	**1.0**			

P12) "Hybrid Fe_3O_4@Amino Cellulose Nanoparticles in Organic Media: Heterogeneous Ligands for Atom Transfer Radical Polymerizations"

Ludmila C. Fidale,[1] Melanie Nikolasjski,[2] Tobias Rudolph,[3] Felix H. Schacher,[4] Thomas Heinze[5]

J. Colloid Interface Sci., **2013**, 390, 25-33

Authors	**1**	**2**	**3**	**4**	**5**
Conceptual development/contribution	x	x	x	x	x
Synthesis and characterization of polymers	x		x		
Preparation of cellulose and NP formation and characterization	x	x			
DLS and TEM measurements			x		
Preparation of manuscript	x	x		x	
Correction of manuscript	x	x	x	x	x
Supervision of LCF					x

Supervision of TR				x	
Proposed publication equivalent			**0.5**		

P13) "Porous NiOx Nanostructures Templated by Polystyrene-*block*-poly(2-vinylpyridine) Diblock Copolymer Micelles"

Maximilian Bräutigam,[1] Peter Weyell,[2] Tobias Rudolph,[3] Jan Dellith,[4] Sven Krieck,[5] Holger Schmalz,[6] Felix H. Schacher,[7] Benjamin Dietzek[8]

Journal of Materials Chemistry A, **2014**, 2, 6158-6166

Authors	**1**	**2**	**3**	**4**	**5**	**6**	**7**	**8**
Conceptual development/contribution	x		x				x	x
Synthesis and characterization of polymers						x		
Micelle formation and embedding of metal ions	x	x	x					
DLS and TEM measurements	x	x	x					
SEM and CV measurements	x			x	x			
Preparation of manuscript	x		x				x	x
Correction of manuscript	x	x	x	x	x	x	x	x
Supervision of MB and PW								x
Supervision of TR							x	
Proposed publication equivalent			**0.5**					

P14) "Star-Shaped Poly-(2-ethyl-2-oxazoline) Featuring a Porphyrin Core: Synthesis, and Metal Complexation"

Tobias Rudolph,[1] Sarah Crotty,[2] Ulrich S. Schubert,[3] Felix H. Schacher[4]

e-Polymers, **2015**, in press (DOI: 10.1515/epoly-2015-0041)

Authors	**1**	**2**	**3**	**4**
Conceptual development/contribution	x			x
Synthesis and characterization polymers	x			
MALDI-TOF MS measurements		x		
Preparation of manuscript	x			x
Correction of manuscript	x	x	x	x
Supervision of TR				x
Proposed publication equivalent	**1.0**			

Erklärung zu den Eigenanteilen des Promovenden sowie der weiteren Doktoranden/Doktroandinnen als Koauthoren an den Publikationen und Zweitpublikationsrechten bei einer kumulativen Dissertation

Für alle in dieser kumulativen Dissertation verwendeten Manuskripte liegen die notwendigen Genehmigungen der Verlage ("Reprint permissions") für die Zweitpublikation vor.
Die Co-Autoren der in dieser kumulativen Dissertation verwendeten Manuskripte sind sowohl über die Nutzung als auch über die oben angegebenen Eigenanteile informiert und stimmen dem zu. Die Anteile der Co-Authoren an den Publikationen sind in den vorausgehenden Tabellen aufgeführt.

Ich bin mit der Abfassung der Dissertation als publikationsbasiert, d.h. kumulativ, einverstanden und bestätige die vorstehenden Angaben. Eine entsprechend begründete Befürwortung mit Angabe des wissenschaftlichen Anteils des Doktoranden an den verwendeten Publikationen werde ich parallel an den Rat der Fakultät der Chemisch-Geowissenschaftlichen Fakultät richten.

Prof. Dr. Felix H. Schacher _____

Datum, Ort

Tobias Rudolph _____

Datum, Ort

1 Introduction

1.1 Polymer Synthesis

Staudinger developed a general view on the covalent linkage of molecules leading to the formation of macromolecules, and therefore is regarded as one of the pioneers establishing the concept of macromolecular chemistry in 1920.[1-4] Since the development of macromolecules, the focus over the following decades was set on control over the polymerization process of different monomers. Beside classical free radical polymerization, ionic polymerization was established by Szwarc in 1956 introducing new polymerization techniques, the anionic polymerization for homo- and block copolymers *via* living polymerization.[5-8] *Via* this approach improved control over the obtained macromolecules is obtained, due to the absence of transfer or termination reactions. As high purity reagents are necessary for ionic polymerizations in comparison to radical approaches, in the recent decades controlled radical polymerization techniques (CRP) as alternative were developed, including atom transfer radical polymerization (ATRP),[9, 10] reversible addition-fragmentation chain transfer (RAFT),[11, 12] or nitroxide-mediated polymerization (NMP).[13]

All approaches have in common, that under optimized conditions various monomers can be polymerized and certain end groups can be introduced to the polymer chain. Therefore, functional initiators or functional termination agents can be used in the polymerization leading to polymer chains, which can be used for further reactions, as for example subsequent polymerizations (macromonomers), or conjugation reactions. Hence, physical properties of the resulting materials like solubility,[14, 15] thermo-responsive behavior,[16-18] or crystallization[19-22] can be controlled.

As in this study mainly anionic and cationic ring-opening polymerization (AROP and CROP) are used, a brief polymerization mechanism will be discussed for the case of 2-alkyl-

2-oxazolines (CROP) and glycidyl ethers (AROP). 2-alkyl-2-oxazolines were first polymerized by four research groups in parallel in 1966, while the interest in these monomers increased in the last decade due to their unique properties, e.g. they exhibit a similar "stealth effect" as poly(ethylene oxide) (PEO).[23-25] The initiation of the polymerization is induced by an electrophile (E), e.g. tosylate, triflate or halide, and the formation of a cationic oxazolinium species (Scheme 1). During propagation the cationic species leads to a weakening in the C-O bond facilitating the nucleophilic attack of another monomer. Under optimized conditions controlled chain growth of the active polymer chain is obtained until no further monomer is available, as one of the advantages of living polymerization includes the absence of termination and chain transfer. The termination of the reaction is obtained by the addition of a suitable nucleophile, e.g. sodium azide or water.

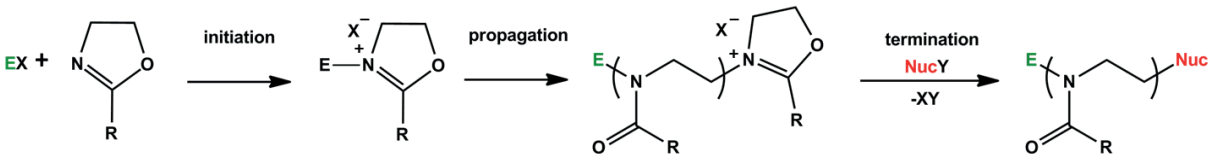

Scheme 1: Cationic ring-opening polymerization (CROP) of 2-alkyl-2-oxazolines, initiated by an electrophile and termination by the addition of nucleophiles.

In case of the anionic ring-opening polymerization (AROP) of glycidyl ethers, e.g. the most prominent example allyl glycidyl ether (AGE), the polymerization can be divided into three individual steps (Scheme 2). During the initiation step the carbanion (e.g. diphenylmethyl potassium) attacks the epoxy ring, inducing ring-opening and formation of an oxy-anion. During chain growth further repeating units are added to the reactive species, while the chain ends always remains active, until subsequent addition of a termination agent, like e.g. alcohols introducing an hydroxyl endgroup.

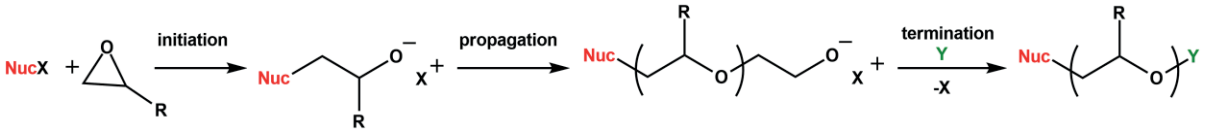

Scheme 2: Anionic ring-opening polymerization (AROP) of glycidyl ethers, initiated by a nucleophile and termination using e.g. alcohols.

Both methods, AROP and CROP, represent living polymerization techniques, therefore the initiation step is much faster than the propagation rate, and transfer or termination reactions are negligible using appropriate conditions. Due to the living character molar mass and size distribution are well controlled and block elongation is possible.

The physical properties of macromolecules can be controlled by the length of the side-chain or by varying the composition introducing a second comonomer. For the

copolymerization of two monomers alternating, random, gradient and block type monomer distributions are possible.[26] The formation of block copolymers is of special interest as in this case two individual segments are covalently connected. Due to the immiscibility of most polymers, block copolymers tend to phase separate in the bulk and in solution, leading to different morphologies.[15, 27-29] As the morphology in the bulk as well as in solution is influenced by the weight fraction of the segments the synthesis of different block copolymers and the control over the composition is necessary for in-depth studies. As an easy access for the synthesis of a library of different compositions of block copolymers, click chemistry for the conjugation of macromolecular building blocks is a powerful tool and has been intensely developed during the last decade. Therefore, the introduction of complementary groups at the polymer chain ends is a prerequisite and enabled by well-controlled polymerization techniques as described above.

1.2 Covalent Polymer Conjugation Reactions

Numerous works on click chemistry have been published within the last decades applying this technique for the synthesis of new polymers and various materials.[30-45] Sharpless et al. developed a short description for the criteria of click reactions: modular, wide in scope, giving high yields and, most important, low amounts of side products under simple reaction conditions.[30, 40] Therefore, different approaches are summarized under the title "click chemistry", including thiol-X,[39, 46] Diels-Alder,[47] and cycloaddition reactions[48, 49] between complementary motifs (Scheme 3).

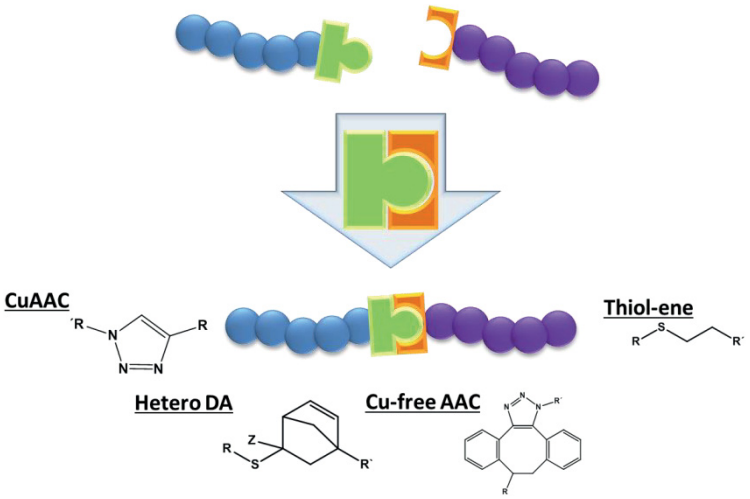

Scheme 3: Polymer-polymer conjugation reactions *via* copper-catalyzed azide-alkyne cycloaddition (CuAAC), hetero Diels-Alder (HDA), strain-promoted azide-alkyne cycloaddition, and thiol-ene reactions.

Due to its high efficiency and tolerance towards the presence of various functionalities the copper-catalyzed azide-alkyne cycloaddition (CuAAC) is one of the most prominent conjugation reactions used in polymer and material science.[30, 43, 50, 51] A bimetallic mechanism is proposed by Fokin and Finn concerning the catalytic cycle including an alkynyl ligand bond to one metal and the azide to another, leading to the formation of selectively 1,4-disubstituted triazoles.[48, 52] This approach was used for the synthesis of different polymer architectures, polymer synthesis through functional monomers, and for the preparation of block copolymers.[23, 35, 37, 42, 45]

Due to the cytotoxicity of copper, both CuAAC, as well as the classical catalyst-free azide-alkyne cycloaddition (AAC) at high temperatures (≈100 °C) are not suitable for biological applications. A more moderate approach was developed, which is the strain-promoted azide-alkyne cycloaddition (SPAAC) reaction between cylcooctyne derivatives and azides, opening up AAC methodologies for biological applications.[53-55]

Diels-Alder reactions are [4+2] cycloaddition reactions between a diene and a dienophile, which are frequently used in organic synthesis[56, 57] and polymer conjugation reactions. [58-61] Most prominent motifs for polymer conjugation or side-chain modification *via* Diels-Alder are furan or anthracene (as dienes) and maleimide (as dienophile) moieties introduced by substitution reactions or respectively functionalized molecules. Beside the efficient linkage between the complementary functionalities, the retro-Diels-Alder reaction at elevated temperatures is used for potential self-healing materials as cross-linked networks can be reversibly formed and opened under sequential temperature treatment.[62-65]

Beside this, also the Hetero Diels-Alder (HDA) reactions have been intensively investigated by Barner-Kowollik et al. Here, combinations of diene functionalized (e.g. cyclopentadiene) polymers and macromolecules containing a special RAFT group are used.[66-68] Herefore, RAFT agents with an electron-deficient dithioester were synthesized and used for the polymerization of a second building block. In a subsequent reaction both motifs react in a Hetero-Diels-Alder reaction and an efficient linkage between the individual segments is formed. This approach is even suitable for polymers with a molar mass above 100 000 g mol^{-1} within short reaction times.[66]

Another example are thiol-ene reactions for polymer-polymer conjugation *via* the radical reaction between thiol-radicals and alkene-functionalized polymer chains.[39, 41, 69] Due to limitations in reactivity, this example of click chemistry is less often used when it comes to macromolecular building blocks.[70, 71] Thiol-ene reactions are mostly used for side-chain or end-group modifications, or in Michael-type addition reactions.[70, 72-75]

Recent work on new efficient polymer linkage by the group of Du Prez et al. described triazolindiones for ultrafast and reversible linkage employing a similar mechanism as for DA reactions. This reaction leads to a quantitative polymer-polymer conjugation at ambient temperature without any additives within minutes (< 30 min) and a complete reversibility upon heating within 30 minutes as indicated by color changes.[76]

All these modular reactions are widely used in material science, biochemistry, organic synthesis and polymer science, leading to a variety of new materials and developments.[33, 49, 51, 77, 78] The list of above mentioned types for conjugation reaction is just a short excerpt of reactions used in the literature, mentioning widely used existing systems and their advantages or disadvantages. Based on these, the focus for the following work is put on copper-catalyzed azide-alkyne cycloaddition (CuAAC) reactions, mainly due to facile access to and commercial availability of functional monomers, initiators and substitution agents.

1.3 Post-Polymerization Modification Reactions

Beside the linkage between polymer chains the modification of as-synthesized polymers or copolymers is widely investigated, due to the ability to change or improve the physical properties of the respective macromolecule. Similar approaches as mentioned above are used for this task, e.g. DA, CuAAC, or thiol-X reactions (Scheme 4).[44, 49, 79] Therefore, polymers with side-chain functionalities are synthesized, characterized concerning the composition and integrity of the functional groups introduced, and subsequently used in modification steps.

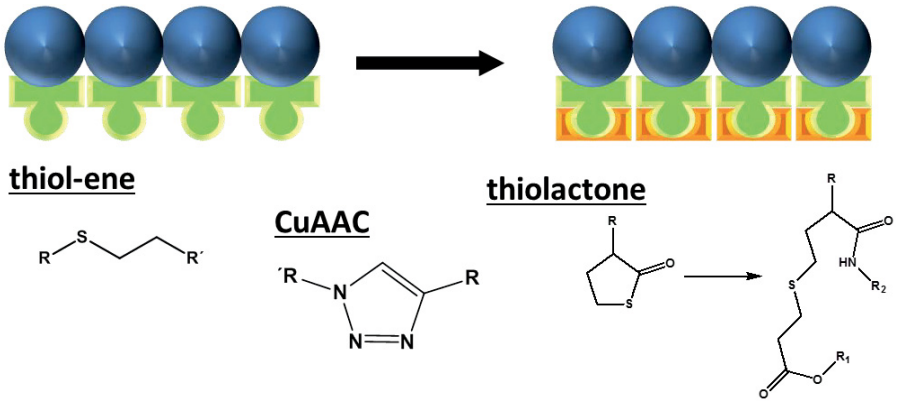

Scheme 4: Modification of side-chain functionalized polymers in a subsequent reaction by thiol-ene, CuAAC, or thiolactone chemistry.

Most of the time the side-chain functionality contains only one reactive unit, while thiolactone moieties can undergo sequential reactions with amines and acrylates, allowing a

one-pot double modification.[80] Under the attack of an amine the thiolactone ring is opened, releasing a thiol moiety, which can react with acrylates instantaneously.[81, 82]

Beside the attachment of polymers or molecules by orthogonal chemistry, also the deprotection of polymer side-chains can be seen as post-polymerization modification. Protection of functional groups in monomers, like e.g. amines or carboxyl groups, is necessary in certain cases during the polymerization. Sequential deprotection and release of the corresponding group leads to side-chain functionalized polymers.[83, 84]

1.4 Self-Assembly in Solution

The self-assembly of block copolymers and smaller building blocks in selective solvents has been intensely investigated.[14, 15, 85-92] The solvophobic block will collapse in a selective solvent, decreasing unfavorable solvent-polymer interactions and forming a collapsed core, while the soluble segments stabilize the core in solution, leading to the formation of core-corona micelles (for, e.g., AB diblock copolymers). Depending on the weight fractions of the two blocks, different morphologies can be obtained, e.g. spheres, rods, discs, or vesicles (Scheme 5).

Scheme 5: Different morphologies formed via the self-assembly of block copolymers in solution: spheres, discs, vesicles and rods.

Beside solubility, also crystallization is found in the literature as a driving force for the formation of hierarchical superstructures. Hierarchical in this case includes several periodicity within the superstructure other several length scales, the most prominent example in nature is the construction of wood.[93] Manners et al. established the term “crystallization induced supramolecular polymerization” of ferrocenyl-based block copolymers in solution.[94, 95] They were able to control the self-assembly of semi-crystalline poly(ferrocenylsilane)s (PFS) as core-forming blocks in selective solvents stabilized by a second block which formed the corona (Figure 1). Rod-like and platelet-like structures are often observed in solution. Further, the size of these crystalline rods could be tuned by sonication, and the use of pre-formed seed micelles for the controlled growth of a second, semi-crystalline poly(ferrocenylgermane)-

containing block copolymer *via* epitaxial crystallization was demonstrated. This "living polymerization" was investigated by transmission electron microscopy (TEM), wide angle x-ray scattering (WAXS) and static light scattering (SLS).[95]

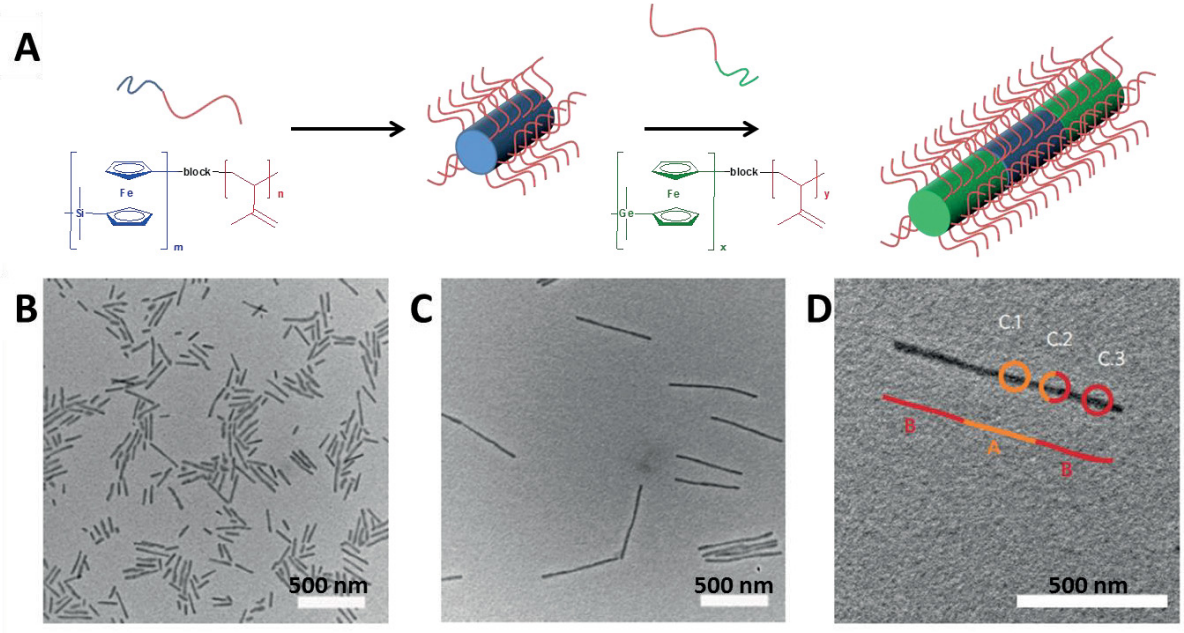

Figure 1: A) "Living crystallization-driven supramolecular polymerization" of PI-*b*-PFG from a PI-*b*-PFS-seed micelle; B) TEM micrograph of rod-like structure in hexane with a PFS core; C) TEM micrograph of linear BAB-triblock co-micelles; D) enlarged TEM micrograph of a BAB triblock co-micelle together with the triblock composition located *via* EDX.[95]

For smaller building blocks the influence of different driving forces for self-assembly in a certain solvent, like e.g. stacking, hydrogen bonds or hydrophobic interactions get more and more important in comparison to larger macromolecules.[96] Here, three different self-assembly mechanisms can be distinguished (Scheme 6). In case of the isodesmic mechanism, each addition of a building block releases the same energy as is necessary for its detachment. For cooperative self-assembly, a nucleation step is necessary, forming first dimers and a subsequent elongation of the assembly by attachments of further building blocks. In comparison, for the anti-cooperative mechanism just a dimerization of two building blocks is observed and further elongation is usually not preferred.[97]

Depending on the mechanism and the composition spherical, vesicular, rod-like or even helical structures can be observed.[96, 98]

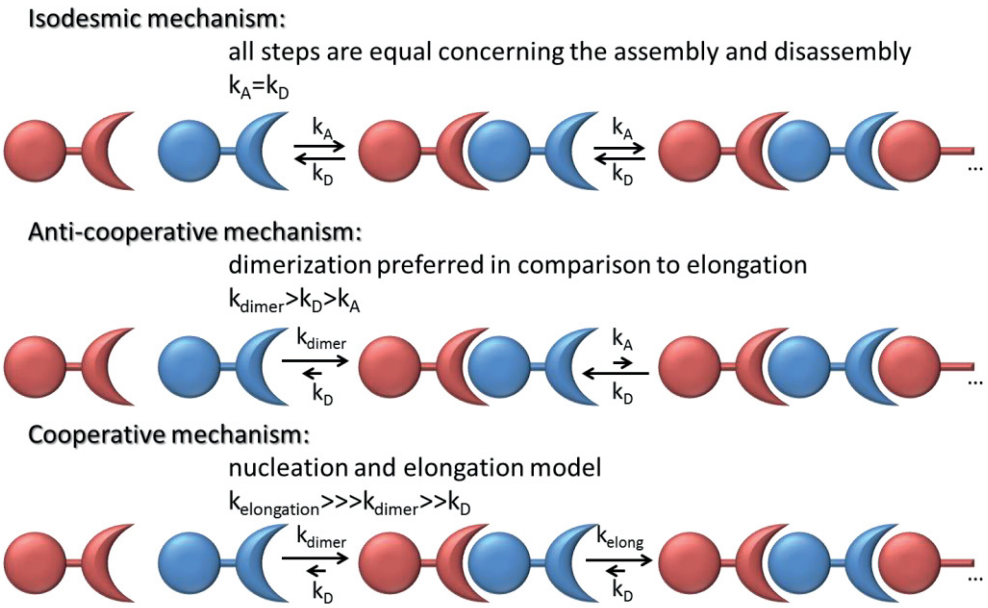

Scheme 6: Illustration of different aggregation mechanisms for smaller building blocks: isodesmic, anti-cooperative and cooperative mechanism.

1.5 Hybrid Materials using Block Copolymers

Hybrid materials of organic and inorganic components are able to combine the (physical) properties of all constituents. This combination of both materials can be divided into two different classes according to the interaction – the first class is formed by embedding and rather weak bonds between both parts, while in the second class covalent crosslinks are present.[99] By using block copolymers for the formation of hybrid materials both classes are available as functionalized macromolecules can strongly interact with inorganic surfaces or as-synthesized nanoparticles. Also, metal ions can be embedded selectively into suitable compartments within block copolymer nanostructures.[100-107] For the introduction of metal ions into the main chain of block copolymers Manners et al. investigated iron-based monomers, e.g. ferrocenyldimethylsilane, which can be copolymerized together with different monomers showing hierarchical self-assembly in solution.[21, 94, 108-112] The wide research field of hybrid materials has been extensively reviewed within the last years.[99-101, 113, 114]

Here, the focus for the selective complexation of metal ions in certain domains influenced by block copolymers in solution is briefly discussed.[115-117] Inorganic nanoparticles can be coated with suitable polymer shells, either induced by metal-polymer interactions or by electrostatic interactions (Scheme 7).[118-121] For this approach the corresponding polymer is added to a nanoparticle solution, followed by several washing cycles. Consequently, the ratio of

inorganic to organic components varies, depending on the size of the nanoparticle and the applied coating process.

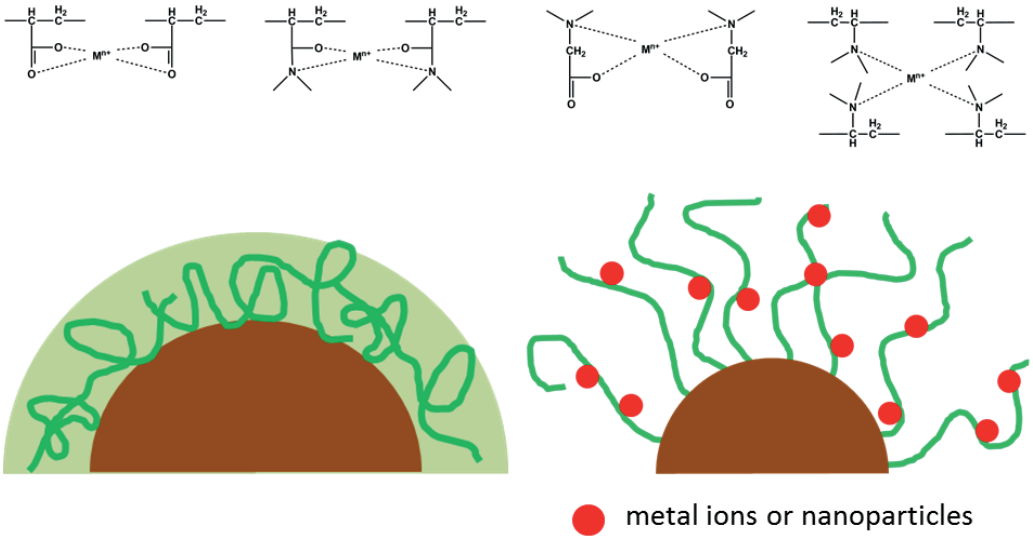

Scheme 7: Illustration of some metal-polymer interactions - differences in the formation of hybrid materials by coating of nanoparticles with polymers or the embedding of metal-ions / NP into a polymer matrix.

Alternatively, metal ions can be introduced into certain domains by selective complexation. The complexed ions can be reduced in a subsequent step, thereby in-situ forming NP within block copolymer nanostructures.[103, 104, 122] *Via* this approach typically rather small NPs are formed, which can be used for increasing contrast in certain domains for transmission electron microscopy (TEM) investigations, or the introduction and stabilization of catalytic amounts of metal ions. Müller et al. showed the formation of cylindrical core-crosslinked micelles of a triblock terpolymer, polybutadiene-*block*-poly(2-vinylpyridine)^{quaternized}-*block*-poly(methyl acrylic acid) (BVqMAA). The oppositely charged polymer segments, quaternized P2VP and MAA form a discontinuous shell of interpolyelectrolyte complex (IPEC) around the crosslinked polybutadiene segment, while the excess of PMAA stabilizes the aggregate in solution and can be addressed by different metal salt precursors ($HAuCl_4$; K_2PtBr_6) (Figure 2A-C).

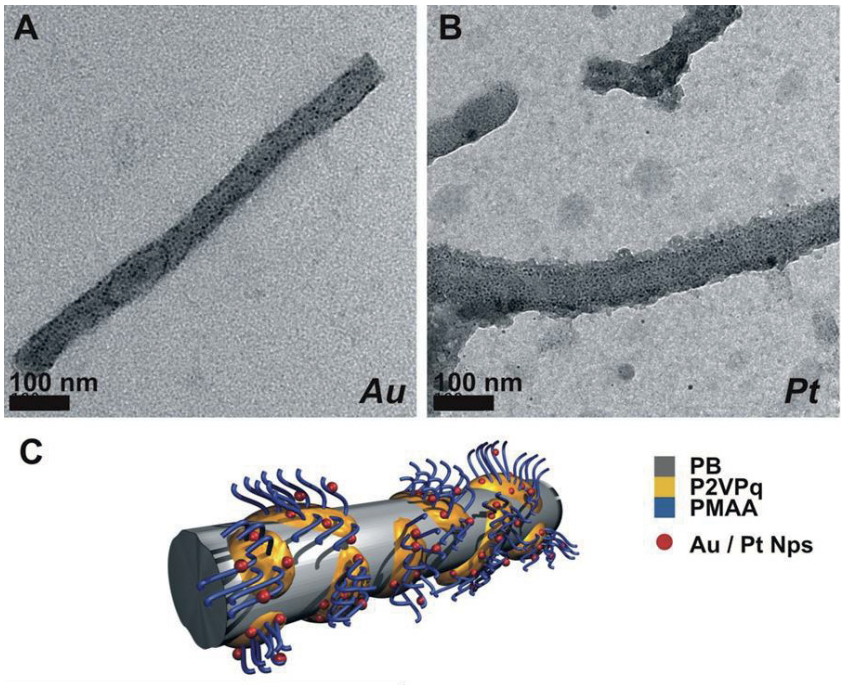

Figure 2: TEM micrographs of cylindrical core-crosslinked polybutadiene-*block*-poly(2-vinylpyridine)^{quaternized}-*block*-poly(methyl acrylic acid) ($B_{420}Vq_{280}MAA_{790}$) triblock terpolymer micelles/metal nanoparticle hybrids deposited from aqueous solution; Au (A), Pt (B), and the proposed solution structure (C).[104]

The preferential deposition of metals in certain compartments of stabilizing block copolymers might lead to the formation of new hybrid materials, which foster conceptual development for nanotechnology in both biochemical and electronic context.[123, 124]

1.6 Outline

This thesis is divided into three main chapters: polymer and (block) copolymer synthesis and functionalization, solution self-assembly, and the formation and application of organic/inorganic hybrid materials:

In the first part of this thesis, we were interested in the synthesis of end-group functionalized (co)polymers for efficient subsequent linkage between complementary motifs. Herefore, linear and star-shaped macromolecular building blocks were synthesized and functionalized. After copper-catalyzed azide alkyne cycloaddition (CuAAC) reactions, the resulting block copolymers were purified and characterized by various techniques (Chapter 2.1). On the other hand, side-group functionalized macromolecules, including new classes of monomers and the selective addressing of the functionalities in post-polymerization modification steps, like e.g. selective cross-linking, were synthesized (Chapter 2.2).

The second part focuses on the self-assembly of block copolymers in selective solvents. A new class of bolaamphiphiles is studied concerning self-assembly in aqueous solution and the influence of the polymer chain length on the underlying mechanism (Chapter 3.1). Furthermore, a morphological study of organometallic block copolymers with different composition in selective solvents is presented. Potential double crystalline block copolymers of this study were further investigated concerning the subsequent crystallization of the second segment, leading to the formation of double-crystalline materials (Chapter 3.2). In addition, the formation of star-shaped polymers by host-guest interactions of adamantyl-functionalized polymers with different molar mass and a cyclodextrine-based core is discussed in detail and investigated using a combination of dynamic light scattering and NMR experiments (Chapter 3.3).

In the third chapter the use of block copolymers for the formation of hybrid materials is described for four individual approaches: the synthesis of porphyrin-centered star-shaped polymers and the complexation of copper and iron ion within the porphyrin cavity (Chapter 4.1). Further, a template-assisted immobilization of Ni-ions in block copolymer

micelles and subsequent calcination leads to porous nickel oxide layers (Chapter 4.2). We also present investigations of triblock terpolymers for the selective complexation of metal ions or nanoparticles and the subsequent directional crystallization into hybrid fiber-like structures (Chapter 4.3). Finally, the use of macromolecule/nanoparticle suspensions for copper complexation and their subsequent use for the ATRP of styrene is presented. Due to the superparamagnetic properties of the Fe_3O_4 NP the catalyst can be removed and re-used for another polymerization batch, while the copper content in the final polymer is negligible (Chapter 4.4).

2 Synthesis of Functional Polymers *via* Controlled Polymerization Techniques

Different approaches were used for the synthesis of a broad tool box of functional materials for subsequent post-polymerization modification reactions. The introduction of these functionalities and the subsequent use of these macromolecular building blocks will be described in the following chapter, which is divided into:

1) The synthesis of end-group functionalized polymers, (**Chapter 2.1**)

2) The synthesis of side-chain functionalized polymers, (**Chapter 2.2**)

3) The formation of linear and star-shaped block copolymers (**Chapter 2.3**).

2.1 Endgroup-Functionalized Polymers

Parts of this chapter will be/have been published: **P1)** Rudolph, T.; Crotty, S.; v. d. Lühe, M.; Pretzel, D.: Schubert, U. S.; Schacher, F. H., *Polymers*, 2013, 5, 1081-1101; **P2)** Rudolph, T.; Allampally, N. K.; Fernandez, G.; Schacher, F. H., *Chem. Eur. J.,* 2014, 43, 13871-13875; **P3)** Schmidt, B.V.K.J.; Rudolph, T.; Hetzer, M.; Ritter, H.; Schacher, F.H.; Barner-Kowollik, C.; *Polym. Chem.*, 2012, 3, 3139-3145; **P4)** Rudolph, T.; Nunns, A.; Schwenk, A. M.; Schacher, F. H., *Polym. Chem.*, 2015, 6, 1604-1612; **P5)** Rudolph, T.; Nunns, A.; Stumpf, S.; Pietsch, C.; Schacher, F. H.; *submitted*; **P6)** Rudolph, T.; Hartlieb, M.; v. d. Lühe, M.; Schubert, U. S.; Hoeppener, S.; D´Agosto, F.; Schacher, F. H.; *in preparation*.

For the preparation of a tool box of endgroup-functionalized polymers containing complementary functionalities, a library of azide or alkyne functionalized macromolecules were synthesized. Exemplarily, an alkyne functionalized initiator has been used for the cationic ring-opening polymerization (CROP) of 2-alkyl-2-oxazolines or, alternatively, an azide functionality can be introduced by subsequent exchange of the endgroup. In the following (Scheme 8), some examples for linear or star-shaped homo- or block copolymers used in this thesis are depicted, which can be later covalently linked by copper catalyzed azide-alkyne cycloaddition (CuAAC) reactions.

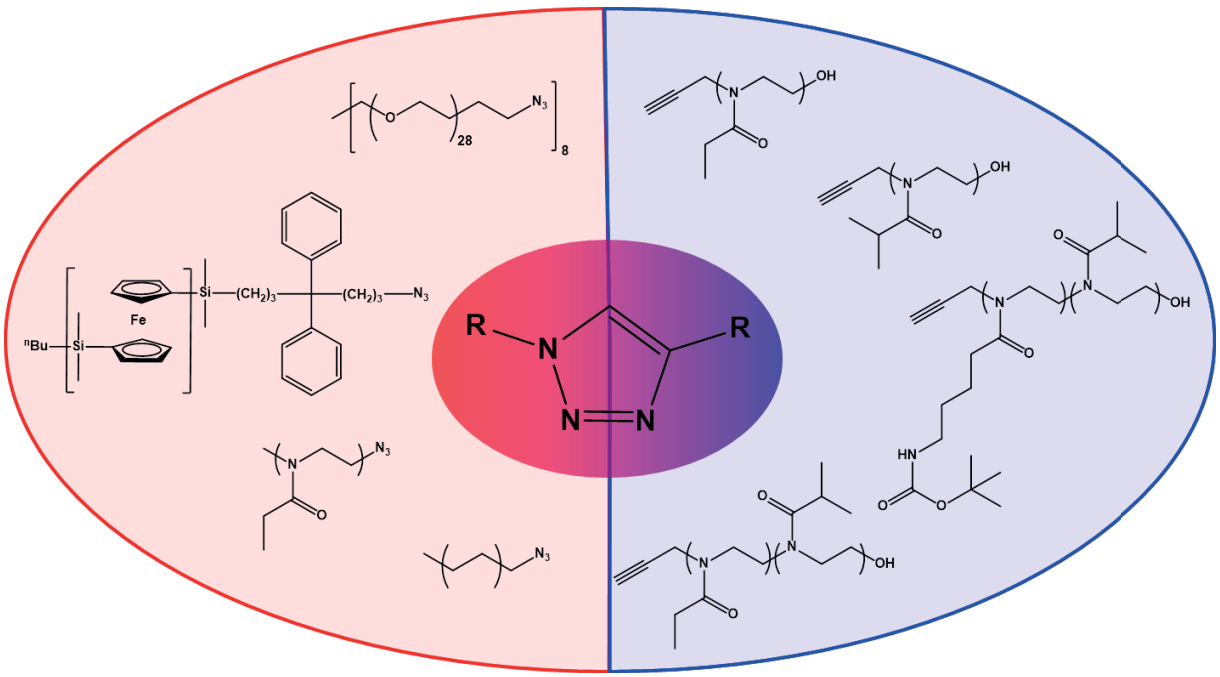

Scheme 8: Azide- and alkyne-functionalized polymers, synthesized for covalent linkage between two individual building blocks by CuAAC.

2.1.1 Synthesis of α- or ω-Functionalized Polymers

2.1.1.1 Alkyne-Functionalized Poly(2-alkyl-2-oxazoline)s (TB-POx)

For the synthesis of α-functionalized polymer chains for subsequent copper catalyzed azide-alkyne cycloaddition (CuAAC) reactions functional initiators are often used.[50] In case of the cationic ring-opening polymerization (CROP) of 2-alkyl-2-oxazolines, propargyl *p*-toluenesulfonate (TB-Ts) is used for the introduction of an alkyne-functionality (Scheme 9).

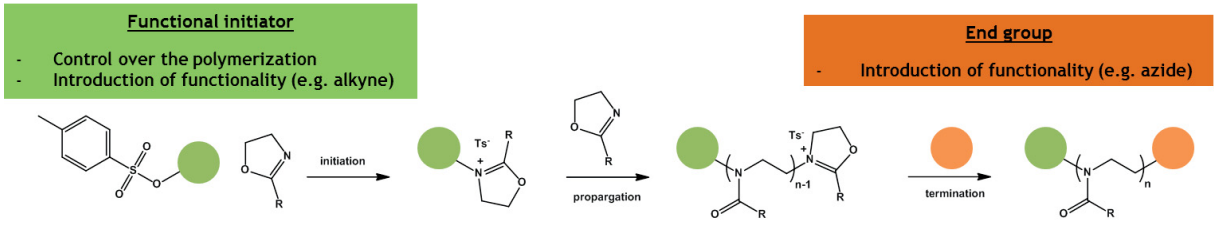

Scheme 9: Cationic ring-opening polymerization (CROP) of 2-alkyl-2-oxazolines as α- / ω- or double functional polymer chains *via* functional initiators or termination with nucleophiles.

Via this initiator homopolymers of 2-ethyl-2-oxazoline (EtOx), 2-*iso*-propyl-2-oxazolines (*i*PrOx), 2-(4-((*tert*-butoxycarbonyl)amino)butyl-2-oxazoline (BocAmOx),[84] and block copolymers of these monomers were synthesized with different molar masses (Figure 3). For the polymerization, optimized microwave-assisted reaction conditions as described in the literature were chosen.[23, 125, 126] Briefly, the monomer concentration was adjusted to 4M in acetonitrile (ACN), and the polymerization was performed at 140 °C in a microwave synthesizer. In case of block copolymerization of two different monomers, the polymerization of the first monomer is performed to full conversion, thereafter sequential addition of a second monomer leads to chain extension, indicated by a shift to lower elution volume in SEC (Figure 3C). The polymerization is terminated by the addition of water, leading to a hydroxyl endgroup. Depending on the monomer to initiator ratio ([M]/[I]), polymers with different degrees of polymerization (DP) can be obtained (Figure 3B).

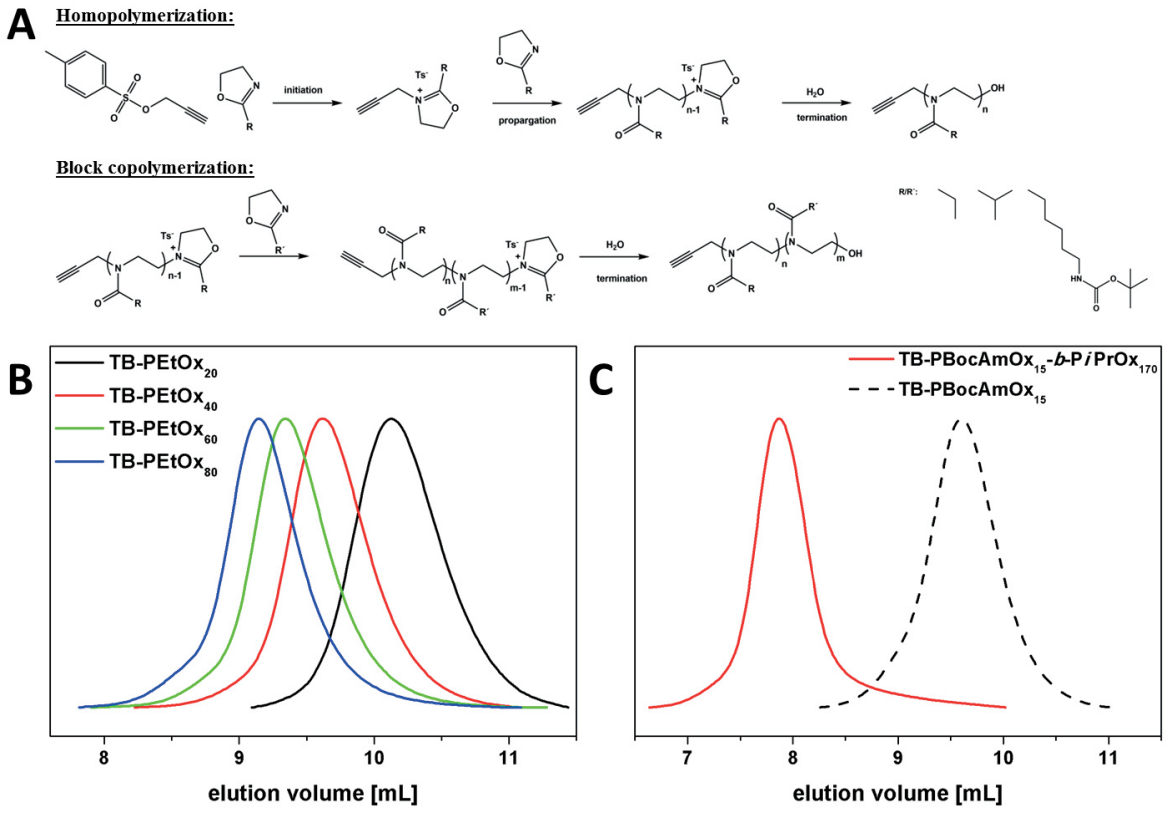

Figure 3: A) Microwave-assisted homo- and block copolymerization of 2-alkyl-2-oxazolines initiated *via* propargyl *p*-toluenesulfonate; B) comparison of SEC traces for PEtOx homopolymers with different degrees of polymerizations initiated by TB-Ts: DP20 (black curve), 40 (red curve), 60 (green curve), and 80 (blue curve); C) Comparison of SEC traces for PBocAmOx$_{15}$ (dashed line) and PBocAmOx$_{15}$-*b*-P*i*PrOx$_{145}$ (red line).

Via this approach a wide range of polymers of different molar mass and composition was synthesized. Due to the controlled mechanism of this polymerization the dispersity indices (Đ) for the obtained polymers are low up to a certain DP. Upon a [M]/[I]-ratio of 200, side reactions decrease control over the polymerization, limiting the molar mass range to 20 000 g mol^{-1} in the case of PEtOx.[127, 128] The resulting polymers are denoted as TB for the triple bond as starting group, while the subscripts represent the degree of polymerization (DP) of the corresponding polymer segment.

2.1.1.2 Azide-Functionalized Poly(2-alkyl-2-oxazoline)s (POx-N$_3$)

For α-functionalized poly(2-alkyl-2-oxazoline)s the polymerization was terminated by the addition of water, while for ω-functionalized poly(2-alkyl-2-oxazoline)s termination *via* the addition of sodium azide leads to the formation of an azide functionality at the chain end. In the literature also other endgroups were introduced to incoporate polymerizable groups[129] or for influencing the solubility of the resulting polymers in water.[130, 131]

Here, the focus is put on azide functionalized polymers and oligomers (Scheme 9), therefore azide functionalized homopolymers of EtOx were synthesized with DPs between 5 to 15 (Figure 4).

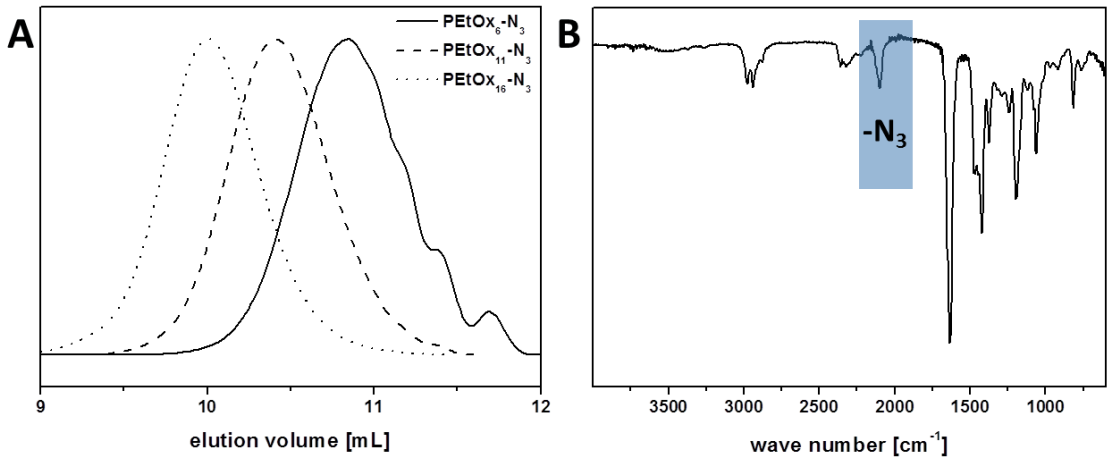

Figure 4: A) Comparison of SEC traces for $PEtOx_6$-N_3 (straight line), $PEtOx_{11}$-N_3 (dashed line), and $PEtOx_{16}$-N_3 (dotted line); B) FT-IR spectrum for $PEtOx_{11}$-N_3.

Table 1 shows a short summary of PEtOx homopolymers containing azide endgroups. The calculated DPs are close to the ones estimated corresponding to the [M]/[I] ratio, and the dispersity indices for the different polymers were narrow (< 1.12).

Table 1: Characterization data for $PEtOx_x$ homopolymers terminated via sodium azide.

Polymer	$DP^{theo,a}$	$DP^{calc,b}$	M_n[g mol^{-1}]^c	$Đ^c$
$PEtOx_6$-N_3	5	6	900	1.12
$PEtOx_{11}$-N_3	10	11	1 300	1.12
$PEtOx_{16}$-N_3	15	16	2 100	1.10

[a] Feed ratio, [b] according to NMR (300 MHz, $CDCl_3$), [c] SEC ($CHCl_3$/*i*-PrOH/TEA): PS calibration

All synthesized poly(2-alkyl-2-oxazolines), α- and ω-functionalized, respectively, were characterized concerning their molar mass, composition, and functionality *via* different methods, like e.g. size-exclusion chromatography (SEC), nuclear magnetic resonance spectroscopy (NMR), matrix-assisted laser desorption/ionization mass spectrometry (MALDI-TOF MS), and fourier-transform infrared spectroscopy (FT-IR). In case of $PEtOx_x$-N_3, for the azide functionality a characteristic signal at ≈2100 cm^{-1} (Figure 4B) is observed. *Via* these characterization methods a complete functionalization of the obtained homo- and block copolymers was confirmed.

2.1.1.3 Azide-Functionalized Poly(ferrocenyl dimethylsilane) (PFDMS-N_3)

Beside the direct termination of polymerizations by the addition of sodium azide, for some polymerization approaches it is necessary to first introduce a different substituent, which can be converted subsequently in a second step into an azide functionality. In case of the anionic ring-opening polymerization (AROP) of dimethylsilaferrocenophane, the nucleophilicity of the living polymer chain end was attenuated by the addition of 1,1-diphenylethylene (DPE) and 1,1-dimethylsilacyclobutane.[132] The reaction solution was quenched by purging the polymer solution into cold 1,3-dibromopropane, thereby introducing a bromine endgroup. After purification and drying, the bromine moiety was exchanged against an azide functionality by a substitution reaction (Figure 5).[132]

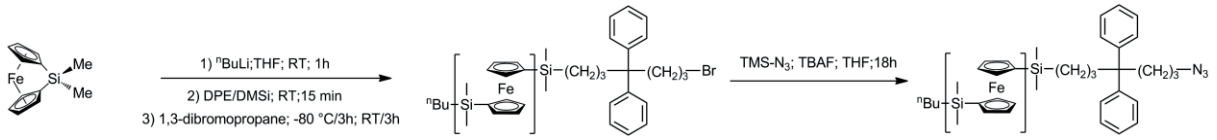

Figure 5: Synthesis of azide-functionalized PFDMS-N_3.

To conclude the library of azide and alkyne end-group functionalized polymers, cooperation partners kindly provided azide functionalized polyethylene (PE_{35}-N_3)[133] and adamantyl-functionalized poly(*N,N*-dimethylacrylamide) (Ada-PDMAAm), and poly(*N,N*-diethylacrylamide) (Ada-PDEAAm).[134]

2.1.2 Functional Star-shaped Building Blocks for CuAAC

Beside linear polymers with azide- and alkyne-functionalities, also star-shaped polymers and block copolymers were investigated. For this purpose star-shaped poly(ethylene oxide) ($[PEO_{28}\text{-}OH]_8$), commercially available with a molar mass of 10 000 g mol^{-1} and eight arms, was used for modification with an azide group. Therefore, the hydroxyl end group of the crude $[PEO_{28}\text{-}OH]_8$ (subscripts below denote the number of arms of the star-polymer) was tosylated and later substituted with sodium azide, introducing an azide functionality (Scheme 10). Full conversion of the tosylate and azide modification was confirmed by ^{1}H-, ^{13}C-NMR, FT-IR, and 2D-SEC.[135]

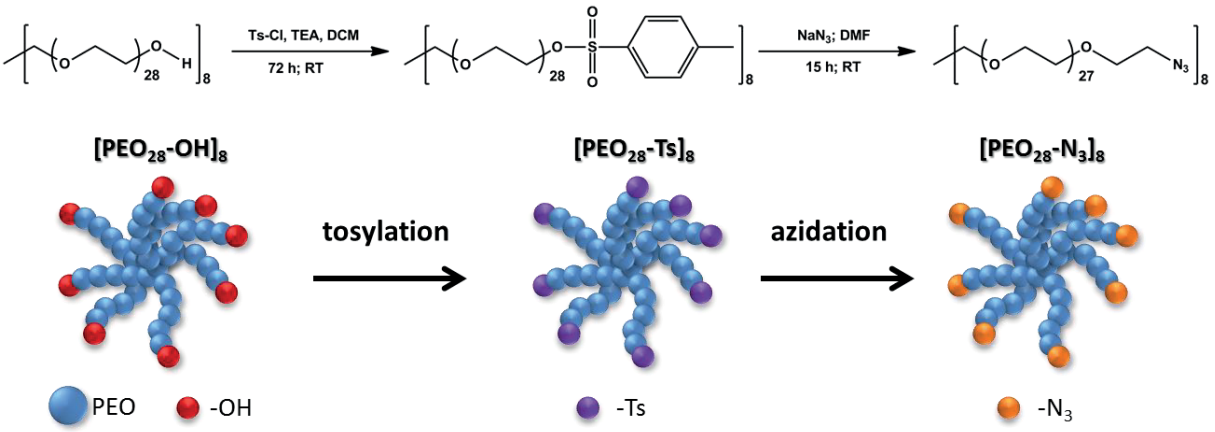

Scheme 10: Modification reactions leading from a hydroxyl functionalized star-shaped PEO ([PEO-OH]$_8$) *via* tosylation ([PEO-Ts]$_8$) to azide functionalized PEO ([PEO-N$_3$]$_8$).

As second star-shaped core, porphyrin (5,10,15,20-Tetrakis(4-hydroxyphenyl)-21H,23H-porphine (TPP)), was functionalized using propargyl bromide, thereby introducing alkyne functionalities (Figure 6). This alkyne-functionalized core can be used for the synthesis of symmetrical star-shaped polymers beside the azide-functionalized PEO ([PEO-N$_3$]$_8$), after CuAAC with suitable modified linear polymers.

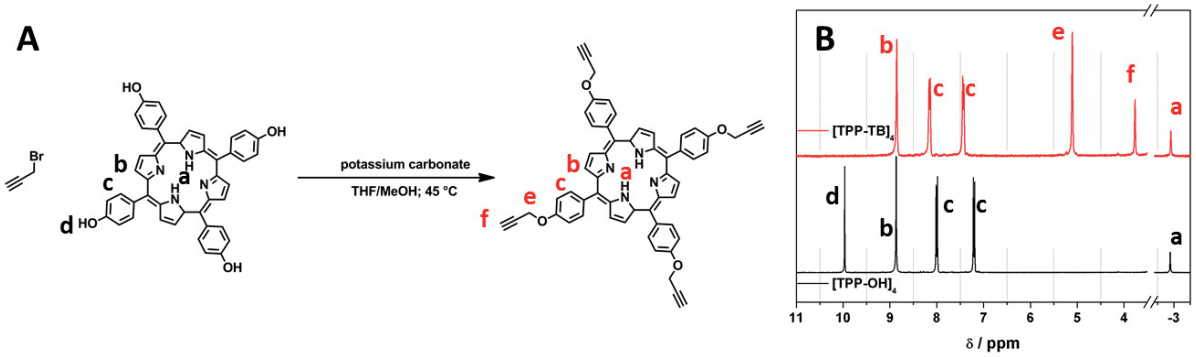

Figure 6: A) Alkyne functionalization of (5,10,15,20-Tetrakis(4-hydroxyphenyl)-21H,23H-porphine ([TPP-OH]$_4$) *via* propargyl bromide; B) comparison of NMR spectra for [TPP-OH]$_4$ (black trace) and [TB-TPP]$_4$ (red trace).

2.1.3 Summary of Clickable Building Blocks for CuAAC

In summary, a library of α- and ω-functionalized homo- and block copolymers with different composition were synthesized, which can used in later copper-catalyzed azide-alkyne cycloaddition (CuAAC) reactions, (Table 2; Table 3). Beside these, adamantyl functionalized polymers with different molar mass, were obtained, which can be used for host-guest interactions with β-cyclodextrine (CD).

Table 2: Summary of α- or ω-functionalized homopolymers synthesized for further studies.

Polymers	Degree of polymerization (x)
TB-PEtOx$_x$	20, 40, 60, 80, 100, 200
TB-P*i*PrOX$_x$	10, 20, 24, 40, 60, 75, 170
TB-BocAmOx	15
PEtOx$_x$-N$_3$	6, 11, 16, 180
PFDMS$_x$-N$_3$[b]	30, 80
PE$_x$-N$_3$[c]	35
Ada-PDMAAm$_x$[d]	31, 143, 202
Ada-PDEAAm$_x$[d]	87

a) determined *via* NMR; b) azide-functionalized poly(ferrocenyldimethylsilane); c) kindly provided by Prof. Dr. DÁgosto (University Lyon, France); d) adamantyl functionalized poly(*N,N*-dimethylacrylamide) (Ada-PDMAAm) and poly(*N,N*-diethylacrylamide) (Ada-PDEAAm) were kindly provided by the group of Prof. Dr. Barner-Kowollik (Karlsruher Institute of Technology, Germany).

Table 3: Summary of α-functionalized block copolymers synthesized for further studies.

Polymers	DP of block A[a]	DP of block B[b]
TB-PEtOx$_x$-*b*-P*i*PrOx	15	50, 80, 120, 170
TB-PBocAmOx$_x$-*b*-P*i*PrOx$_x$	15	170

a) determined *via* NMR; b) determined *via* NMR corresponding to the first block.

Beside linear motifs also star-shaped building blocks were synthesized for the formation of star-shaped diblock copolymers *via* linkage between a star-shaped [PEO-N$_3$]$_8$ or alkyne-functionalized [TB-TPP]$_4$.

2.1.4 CuAAC Click Reactions Between End-functionalized Building Blocks

By Sharpless definition click reactions are modular, wide in scope and give high yields (without byproducts), rendering copper catalyzed azide-alkyne cycloaddition (CuAAC) reactions one of the most prominent in polymer and material science.[30, 33, 40, 43, 69] This modular principle can be used for the as-synthesized building block described in Chapter 2.1.1.

2.1.4.1 ABA Bolaamphilies

Self-assembly of small building blocks in organic solvents is mostly induced by the introduction of interacting units, e.g. metal-metal[136] or ionic interactions.[137] For non-covalent interactions in water hydrogen bonding and hydrophobic interactions between different moieties are used to form defined assemblies.[138-140] The herein used OPE-based aromatic fragment, 1,4-bis[(4-ethynylphenyl)ethynyl]benzene, contains both two external and two internal alkyne functionalities. Due to the high number of alkyne functionalities being present, selective addressing of the external alkyne moieties was desired. According to literature, attack of the internal alkynes during the CuAAC with azide functionalized reagents was not expected.[141] First reactions between OPE and $PEtOx_x$-N_3 in tetrahydrofuran or dimethylformamide led to bimodal size-distributions by SEC, and the disappearance of signals for the internal alkyne signals in ^{13}C-NMR. These observations might be due to attack of internal triple bonds[52, 142] or oxidative coupling reactions.[143] Therefore, we developed an approach containing a pre-organization step for the OPE segments in a solvent mixture of THF and water (1/4; v/v) into sheet-like aggregates, most probably due to the π–π interactions of the OPE units (Figure 7). The formation of aggregates is indicated by an increase in turbidity, while $PEtOx_x$-N_3 is added together with Cu(I)Br and PMDETA. To decrease the reaction time for the CuAAC the reaction was heated to 80 °C for less than 10 minutes, and purified by precipitation after removal of the copper.

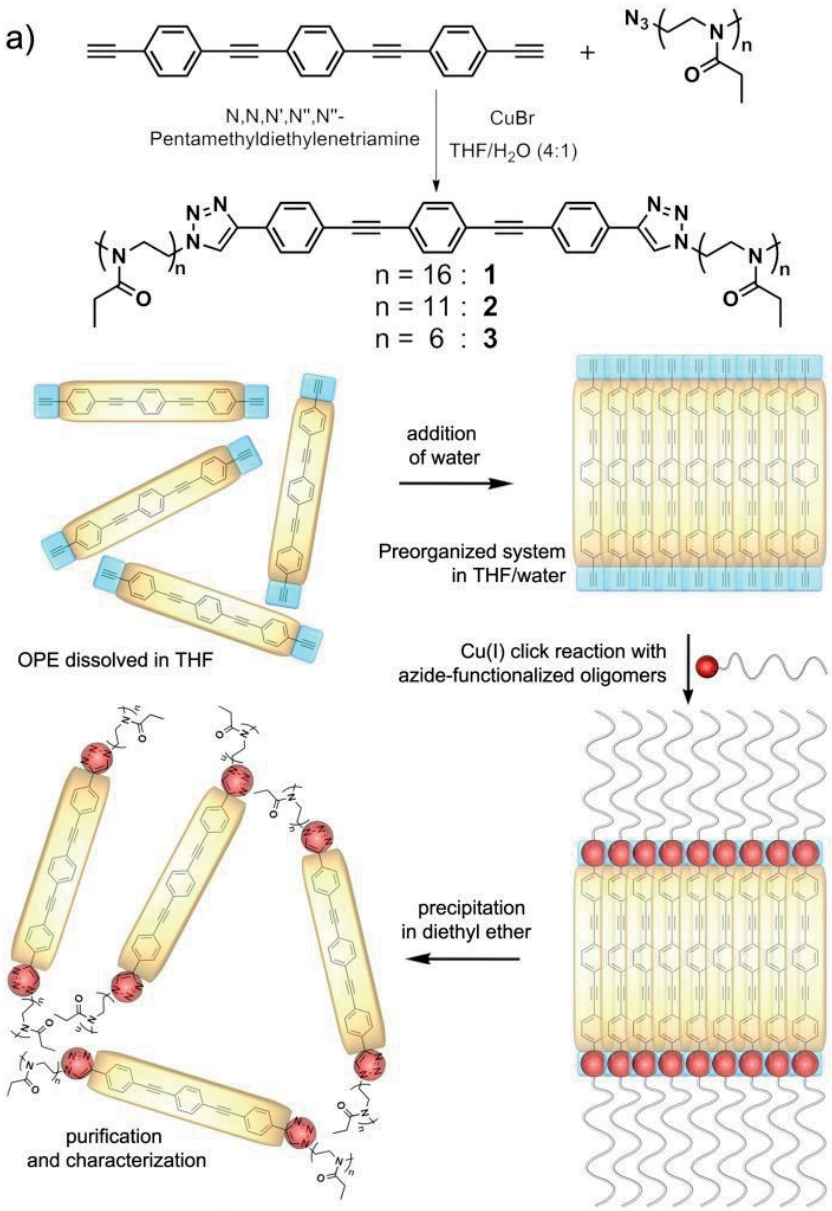

Figure 7: Synthetic scheme and strategy followed to obtain the targeted $PEtOx_x$-OPE-$PEtOx_x$ bolaamphiphiles 1–3 by selectively pre-organizing the terminal alkyne groups and formation of the bolaamphiphiles in subsequent CuAAC click reaction.

Via this approach different lengths of $PEtOx_x$-N_3 were linked to both external alkyne functionalities in aqueous media in the presence of oxygen. After the successful preparation, the bolaamphiphiles ($PEtOx_x$-OPE-$PEtOx_x$) with different DP (x = 6, 11, 16) were investigated *via* SEC (Table 4), FT-IR, and NMR, proving the presence of the internal alkynes.

Table 4: Characterization data for $PEtOx_x$-N_3 and the corresponding bolaamphiphiles $PEtOx_x$-OPE-$PEtOx_x$.

Polymer	$DP^{PEtOx\ [a]}$	$M_{n,theo}^{[a,b]}$ [g mol^{-1}]	$M_{n,SEC}^{[c]}$ [g mol^{-1}]	$Đ^{[c]}$
$PEtOx_6$-N_3[a]	6	650	900	1.12
$PEtOx_{11}$-N_3[a]	11	1 150	1 300	1.12
$PEtOx_{16}$-N_3[a]	16	1 650	2 100	1.10
$PEtOx_6$-OPE- $PEtOx_6$ (**3**)	6	1 600	2 600	1.09
$PEtOx_{11}$-OPE- $PEtOx_{11}$ (**2**)	11	2 600	3 600	1.05
$PEtOx_{16}$-OPE- $PEtOx_{16}$ (**1**)	16	3 600	4 800	1.07

[a] Feed ratio, [b] according to NMR (300 MHz, $CDCl_3$), [c] SEC ($CHCl_3$/*i*-PrOH/TEA) PS calibration

2.1.4.2 Star-shaped Block Copolymers

The CuAAC between as-synthesized azide- and alkyne functionalized polymer building blocks, as described above in chapter 2.1.1, was also investigated for the synthesis of star-shaped diblock copolymers. Therefore, azide modified star-shaped $[PEO\text{-}N_3]_8$ was combined with alkyne functionalized PEtOx (TB-PEtOx) of different molar mass. By this convergent approach, an excess of the TB-$PEtOx_x$ in comparison to the number of azide-functionalities is used to ensure full conversion of $[PEO\text{-}N_3]_8$. For the reaction, Cu(I)Br and PMDETA were applied to the reaction mixture of star-shaped and linear building block, and heated for several minutes in the microwave synthesizer at 80 °C (Figure 8). Purification of the star-shaped block copolymers ($[PEO\text{-}b\text{-}PEtOx_x]_8$) was attempted by dialysis or preparative column chromatography. The best results were obtained if the polymer mixture was dissolved in THF and placed in a freezer at -30 °C. Due to crystallization of the PEO core at low temperatures $[PEO\text{-}b\text{-}PEtOx]_8$ precipitates, while linear $PEtOx_x$-N_3 remains in the supernatant solution (Figure 9A).

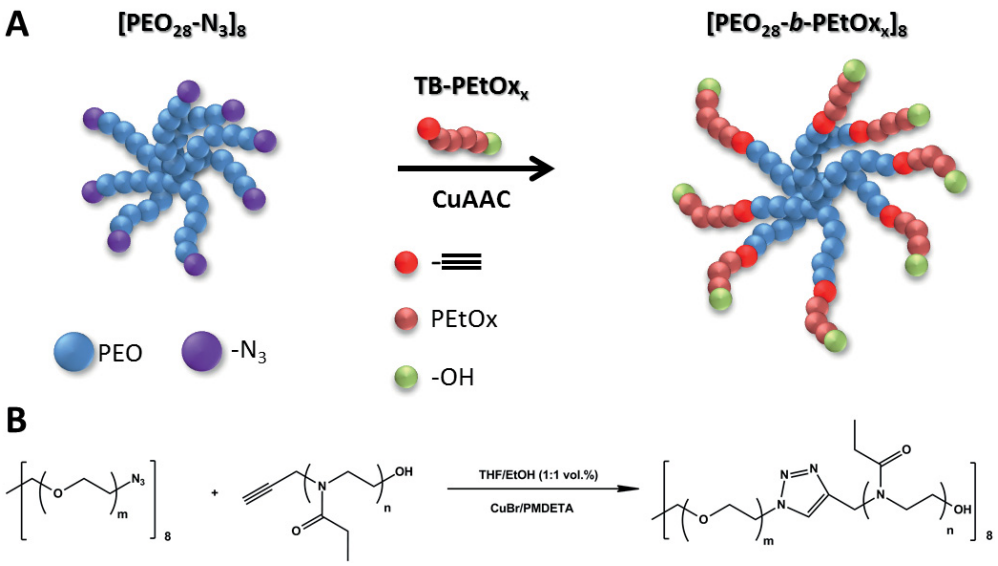

Figure 8: CuAAC click reaction between star-shape azide-functionalized $[PEO\text{-}N_3]_8$ and linear alkyne functionalized PEtOx (TB-PEtOx).

Via this method three different star-shaped diblock copolymers with different composition were obtained and characterized *via* NMR and FT-IR (Figure 9B). Beside the convergent approach for the synthesis of star-shaped block copolymers also the divergent approach is known.[144-147] Herefore, $[PEO\text{-}Ts]_8$ was used as macroinitiator for the CROP of EtOx. Even after intensive drying of the star-shaped macroinitiator *via* co-evaporation with toluene and applying high vacuum for several hours, the formation of homopolymer was observed by SEC. Three different star-shaped block copolymers with similar composition like described for the convergent approach were synthesized and investigated. As in the case of the divergent approach the accessibility and the reactivity of the functional group is limited, the length of the individual arm was not determined, while for the convergent star-shaped block copolymer the composition of the single building block is known and can be confirmed afterwards by NMR.

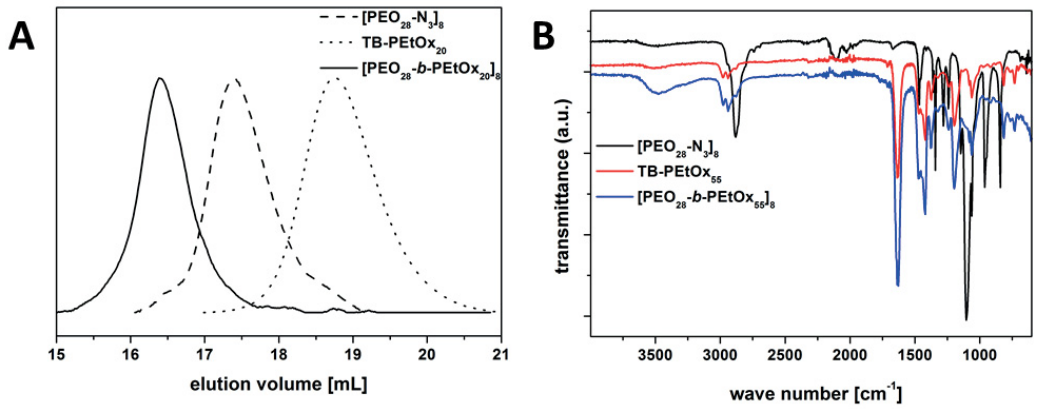

Figure 9: Comparison of SEC traces for linear (TB-PEtOx; dotted line), star-shaped ([PEO-N_3]; dashed line) building block, and the resulting purified [PEO-*b*-PEtOx]$_8$ (straight line); B) comparison of FT-IR spectra for linear (TB-PEtOx; red line), star-shaped ([PEO-N_3]; black line) building block and the resulting purified [PEO-*b*-PEtOx]$_8$ (blue line).

While the composition and the molar masses of the divergent and convergent star-shaped block copolymers of [PEO-*b*-PEtOx]$_8$ were comparable, the solution behavior in water was entirely different. For all convergent star-shaped block copolymers turbid solutions were obtained, while aqueous solutions of the divergent block copolymers remained clear. Up to now no explanation for this observation has been found.

2.1.4.3 Linear Block Copolymers Containing Two Crystalline Blocks

Under similar reaction conditions also diblock copolymers or triblock terpolymers were synthesized (Scheme 11). For the formation of diblock copolymers the azide-functionalized poly(ferrocenyldimethylsilane) (PFDMS-N_3) was used together with alkyne functionalized POx. As for all block copolymers always one segment is used in a slight excess, subsequent purification was one of the main issues as homopolymer contaminations might influence further investigations. Hence, for the formation of triblock terpolymers alkyne-functionalized diblock copolymers were used in polymer-polymer conjugation reactions as well. For triblock terpolymers polyethylene (PE) is used as azide-functionalized building block.

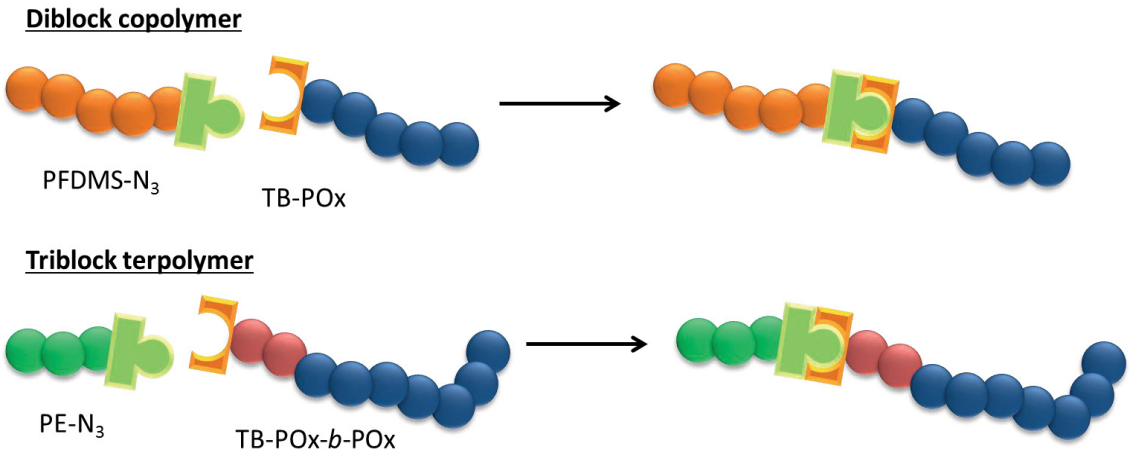

Scheme 11: Synthesis of diblock copolymers and triblock terpolymers by CuAAC reactions between complementary functionalized building blocks.

The properties and solution behavior of the obtained diblock copolymers and triblock terpolymers will be investigated in more detail in the following chapters.

2.2 Side Chain Functionalized Polymers

Parts of this chapter have been published: **P7)** Barthel, M. J.; Rudolph, T.; Crotty S.; Schacher, F. H. and Schubert, U. S.; *J. Polym. Sci. Part A: Polym. Chem.*, 2012, Vol. 50, 4958-4965; **P8)** Barthel, M. J.; Rudolph, T.; Teichler, A.; Paulus, R.; Vitz, J.; Hoeppener, S.; Hager, M. D.; Schacher, F. H.; Schubert, U. S.; *Adv. Funct. Mater.*, 2013, 23, 4921-4932; **P9)** Rudolph, T.; Barthel, M. J.; Kretschmer, F.; Mannsfeld, U.; Hoeppener, S.; Schubert, U. S.; Schacher, F. H.; *Macromol. Rapid Commun.*, 2014, 35, 916-921; **P10)** Rudolph, T.; Kempe, K.; Crotty, S.; Paulus, R. M.; Schubert, U. S.; Krossing, I.; Schacher, F. H.; *Polym. Chem.*, 2013, 4, 495–505; **P11)** Rudolph, T.; Espeel, P.; Du Prez, F. E.; Schacher, F. H.; *Polym. Chem.*, DOI: 10.1039/C5PY00329F.

Beside endgroup functionalized homo- and block copolymers, also side-chain functionalized homopolymers, copolymers and block copolymers can be used for the synthesis of functional materials. In this chapter the use of new functional monomers, like 2-*tert*-butyl-2-oxazoline (*t*ButOx; **Chapter 2.2.1**), furfuryl glycidyl ether (FGE; **Chapter 2.2.2**), or maleimide thiolactone (MITla; **Chapter 2.2.3**) for the synthesis of polymers *via* controlled polymerization techniques is described.

2.2.1 Cationic Ring-Opening Polymerization of 2-*tert*-Butyl-2-Oxazoline *via* $[H(OEt_2)_2][Al\{OC(CF_3)_3\}_4]$

Beside classical initiators for the CROP of 2-alkyl-2-oxazolines like, *e.g.* tosylates, also halides or triflates are known from literature.[125, 148-151] In our case the use of a strong Brønsted acid, $[H(OEt_2)_2][Al\{OC(CF_3)_3\}_4]$,[152] for the proton-initiated cationic ring-opening polymerization (CROP) of 2-alkyl-2-oxazolines was investigated. We speculated that the large counterion might lead to an accelerated polymerization rate and the possibility to access demanding monomers in a controlled manner. As a demanding monomer, 2-*tert*-butyl-2-oxazoline (*t*ButOx) was chosen, as for this monomer no controlled homo- or (co)polymerization was described up to now.[153-156] First, the acid was used for the CROP of 2-ethyl-2-oxazoline (EtOx) as control experiment. Therefore, typical polymerization conditions were applied at two different temperatures, 80 and 140 °C.[23] The monomer conversion for this was determined by NMR and the obtained polymers investigated *via* SEC. Upon increase of the reaction time an increase in molar mass was observed by SEC, while the dispersity index remained low (Đ ≈ 1.1; Figure 10C and D). The polymerization rate of EtOx at 140 °C increases in comparison to methyl tosylate ($k = 100$ mmol L^{-1} s^{-1})[125, 157] to 128 mmol L^{-1} s^{-1} (Figure 10B).

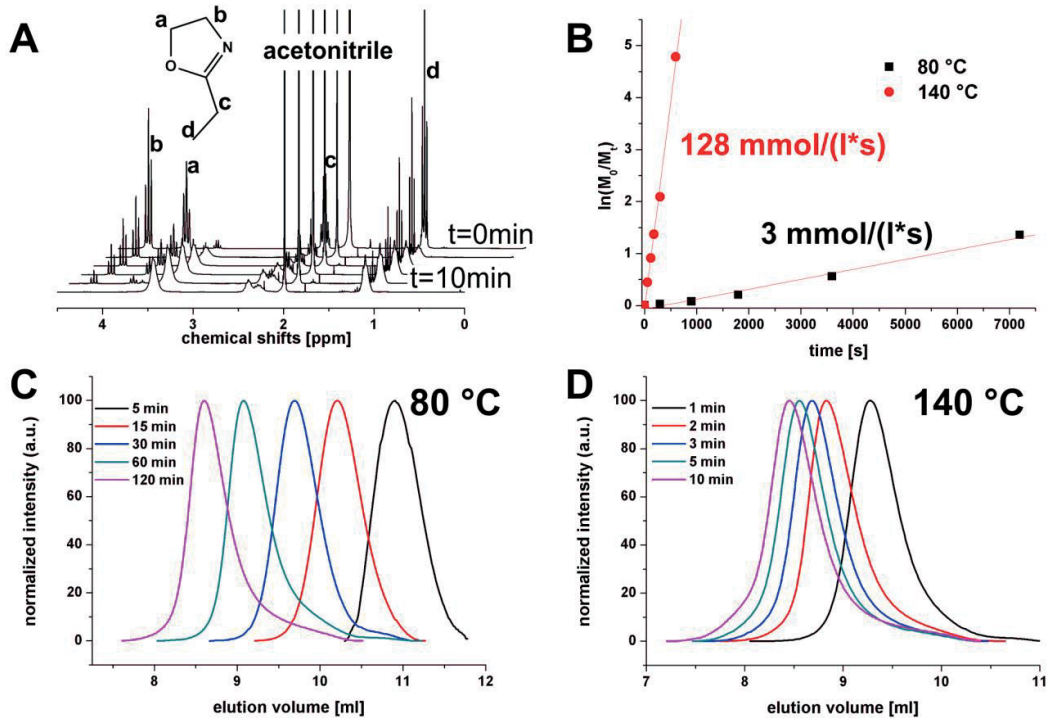

Figure 10: ^{1}H-NMR spectra for the CROP of EtOx at 140 °C at different reaction times. (A) First order time–conversion plots for the kinetic investigation of the microwave assisted polymerization of EtOx with $[H(OEt_2)_2][Al\{OC(CF_3)_3\}_4]$ as initiator at different temperatures, 80 °C (black squares) and 140 °C (red dots); the polymerization rate has been determined (B); comparison of the time dependent SEC traces for the polymerization of EtOx at 80 °C (C) and 140 °C (D).

Similar reaction conditions were also applied for the CROP of *t*ButOx, but the reaction time was increased to 16 hours to achieve full conversion. Due to the low solubility of the obtained homopolymer (P*t*ButOx) in common solvents, the characterization was limited to solid state methods like FT-IR, TGA, and X-ray scattering. Beside PEtOx and P*t*ButOx homopolymers, also copolymers with different compositions were synthesized to increase the solubility, although this was still limited even to a high content of EtOx. The obtained copolymers were investigated *via* FT-IR (Figure 11), showing changes in the peak shape and new bands corresponding to the presence of the *tert*-butyl group. The glass transition temperature (T_g) of the copolymers remained constant, at ≈ 56 °C, while *via* TGA the theoretical and the measured weight loss, due to the decomposition of the side chain confirmed the expected compositions of the copolymers (Table 5).

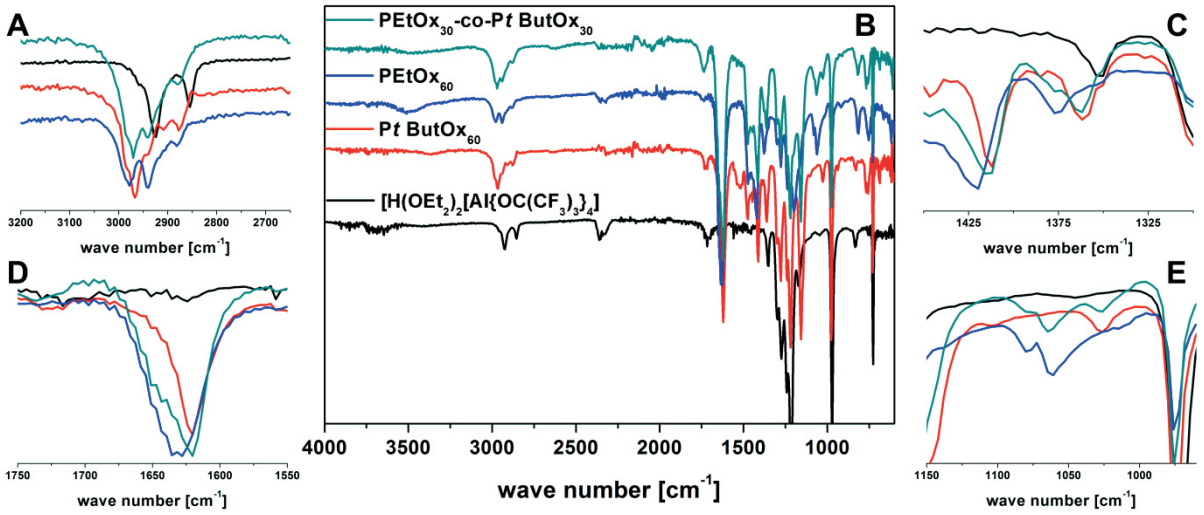

Figure 11: Fourier-transform infrared (FT-IR) spectra for $PEtOx_{60}$ (blue line), P*t*ButOx_{60} (red line), $PEtOx_{30}$-*co*-P*t*ButOx_{30} (cyan line), $[H(OEt_2)_2][Al\{OC(CF_3)_3\}_4]$ (black line), (B) and the enlargements for the important regions: (A) polymer backbone, (C) region of α-carbon next to the carbonyl group, (D) carbonyl vibration, and (E) methyl vibration.

Table 5: Comparison of the temperature dependency of the different homo- and copolymers analyzed *via* DSC and TGA.

Polymer	wt.% P*t*Bu$tOx^{a)}$	$M_{n,theo}$ [g mol^{-1}]$^{a)}$	T_g [°C]$^{b)}$	theo. weight loss [wt.%]$^{a)}$	weight loss [wt.%]$^{c)}$
$PEtOx_{60}$	0	5960	56.0		
P*t*ButOx_{60}	100	7620	37.7$^{e)}$	69	71
$PEtOx_{50}$-*co*-P*t*Bu$tOx_6$$^{d)}$	13.3	5710	53.9	9.2	15
$PEtOx_{40}$-*co*-P*t*ButOx_{20}	39.1	6500	57.0	26.9	30
$PEtOx_{30}$-*co*-P*t*ButOx_{30}	56.2	6780	56.5	38.8	38
$PEtOx_{50}$-*b*-P*t*Bu$tOx_6$$^{d)}$	13.3	5710	57.2	9.2	14

a) feed ratio; b) determined *via* the mid-value obtained by DSC from the third run; c) determined *via* TGA; d) consumption determined *via* ^{1}H-NMR; e) determined from the second DSC run

Beside the successful copolymerization of EtOx and *t*ButOx, first hints for the partial hydrolysis of, PEtOx and P*t*ButOx could be achieved. This might enable the formation of linear poly(ethylenimine) (PEI) in the presence of water.

2.2.2 Furfuryl Glycidyl Ether – A new Monomer for Living AROP

While an almost "inert" side group was described in the last chapter (**Chapter 2.2.1**), a more reactive side-group can be introduced by the use of furfuryl glycidyl ether (FGE) in anionic ring opening polymerization (AROP). We first described the AROP of FGE using different initiators. Beside homopolymerization of FGE, the chain extension of earlier synthesized poly(ethylene oxide) (PEO) was also performed. Briefly, the hydroxyl group of as-synthesized PEO was re-activated by diphenylmethyl potassium (DPMK), while FGE was added to the reaction solution (Figure 12A), leading to a change in the elution volume in SEC (Figure 12C). The corresponding block copolymer was furthermore investigated *via* NMR and MALDI-TOF MS (Figure 12B). This procedure was applied to different PEO macroinitiators, leading to block copolymers with different compositions.

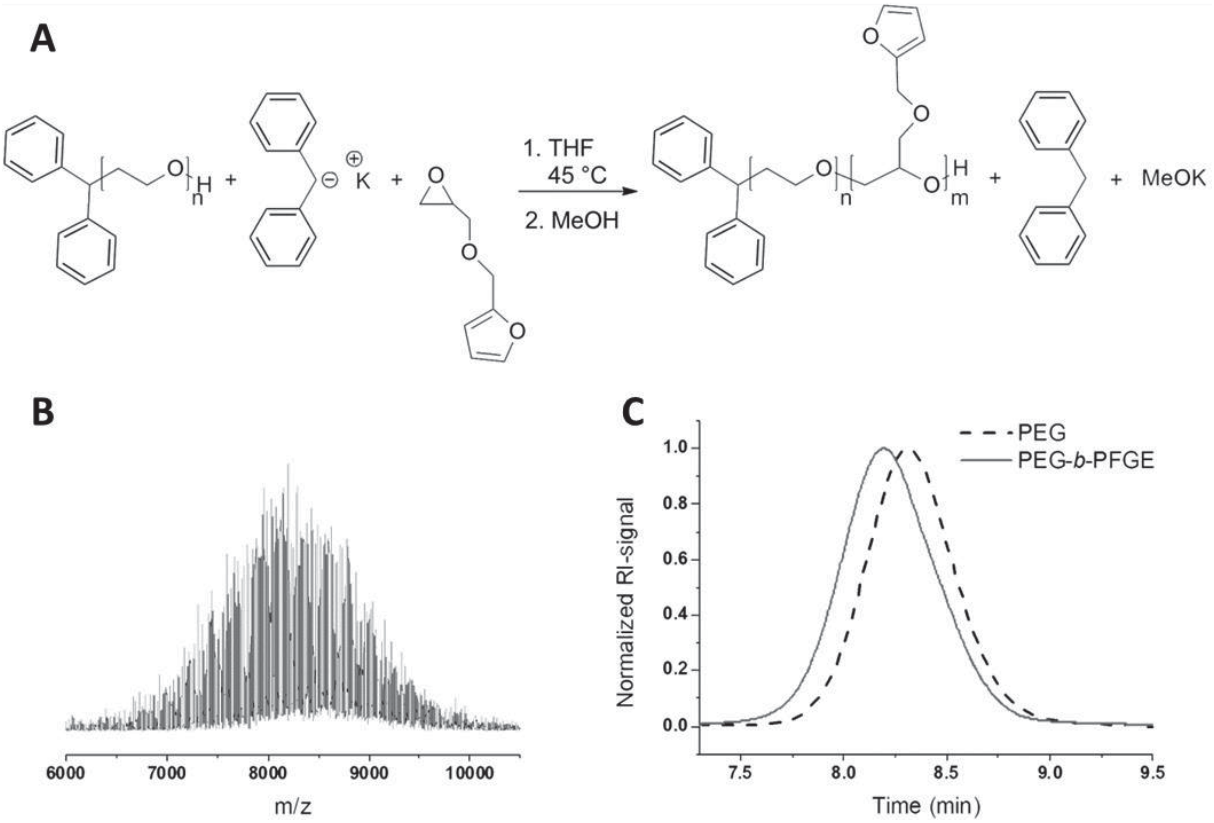

Figure 12: Synthesis of PEO-*b*-PFGE using sequential living anionic ROP (A), MALDI-TOF MS spectrum for the block copolymer (B), and SEC traces for the PEO precursor (dashed black line) and PEO-*b*-PFGE (C, solid grey line).

Due to the presence of furan moieties in the side chain, the polymers are suitable for post-polymerization modification reactions *via* Diels-Alder reactions with maleimides.[49] Therefore, the crosslinking of such block copolymers was investigated by the introduction of bismaleimides into the FGE domain in solution and in the bulk.

The amphiphilic block copolymer PEO_{139}-*b*-$PFGE_{12}$ forms micelles with a hydrodynamic radius of 6 nm in aqueous solution. For the selective crosslinking of the hydrophobic PFGE core, a bismaleimide was entrapped by dialysis from DMF (a non-selective solvent) to water. The micellar solution was subsequently heated for 30 minutes to 60 °C, obtaining core-corona micelles with a constant radius of 6 nm, as observed for the non-crosslinked micelles in aqueous media (Figure 13A and B). The crosslinked micelles were transferred into non-selective solvents like THF and DMF (*via* dialysis). The size increased slightly in comparison to water to 15 and 10 nm, respectively, as both core and corona swell in these solvents, while in water the core is fully collapsed (Figure 13C and D). In DMF and THF no unimers for the crosslinked micelles were observed *via* dynamic light scattering. Upon heating of the micellar solution in DMF for several hours to 130 °C, the retro-Diels-Alder (RDA) reaction is observed as a decrease of the hydrodynamic radius in solution to 2 nm, indicating the presence of block copolymer unimers (Figure 13E), and a partial decrease of the corresponding signals in ^{1}H-NMR.

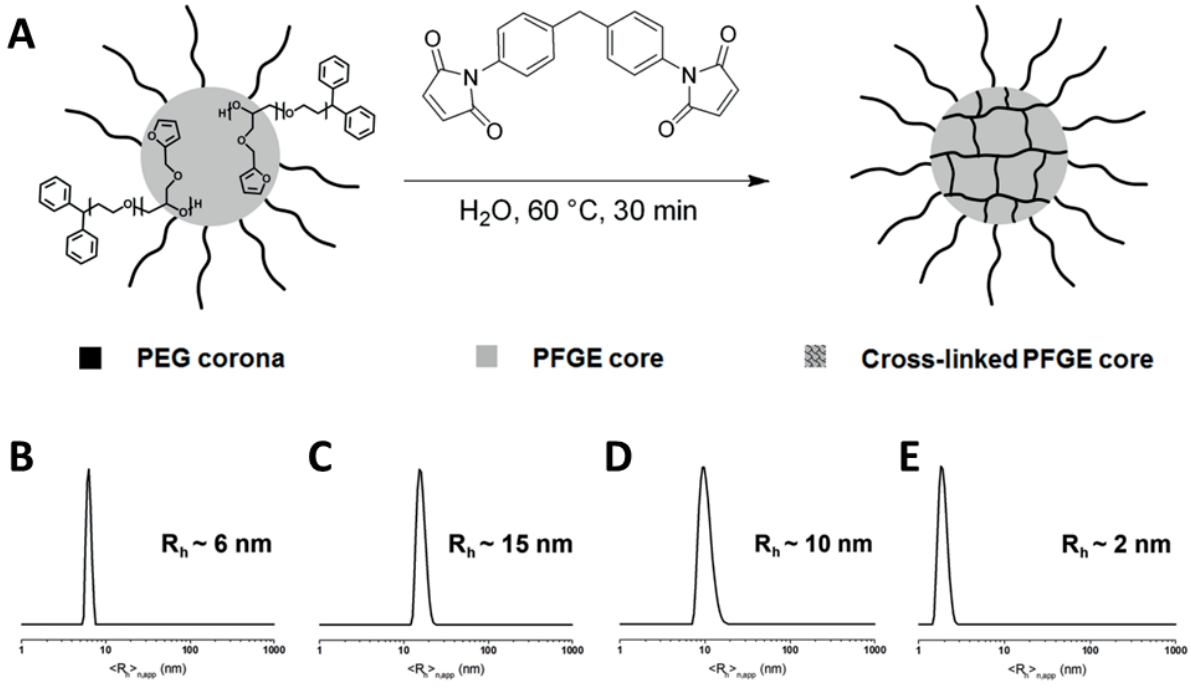

Figure 13: Crosslinking of the micellar core (A), number-weighted DLS CONTIN plots for PEO_{139}-*b*-$PFGE_{12}$ micelles in water after crosslinking (B), in THF (C), and DMF (D), and after the retro-Diels-Alder reaction in DMF (E).

After the selective crosslinking of PFGE segments in solution has been shown, we also focused on block copolymer films. Therefore, films of PEO_{330}-*b*-$PFGE_{20}$ were investigated in detail concerning the physical properties and the possibility to undergo reversible DA with maleimides. By DSC and X-ray scattering a strong indication for phase-

separation of the two polymer segments, indicated by two separate T_g´s and a lamellar morphology, was found. For the crosslinking of the block copolymer film, the material was dissolved together with the crosslinker and applied to a glass substrate. The solvent was allowed to evaporate, and the glass slide was heated for 14 hours to 65 °C. The surface of the film was investigated *via* profilometry measurements, showing a flat film with a height of ≈ 50 to 60 µm (Figure 14A). In a second step two scratches were applied to the film surface, one with a depth of 7 µm and a width of 0.45 mm, and the other with a depth of 0.9 µm and a width of 0.1 mm (Figure 14B). As the RDA reaction takes place at high temperatures, the scratched film was placed in the oven at 155 °C for 3 hours. At these temperatures the crosslinks re-open and an increase of chain mobility occurs. Afterwards, the surface was again investigated concerning the earlier made scratches, showing disappearance of the small scratch and a reduced depth for the deep scratch to 1.2 µm (Figure 14C).

This procedure could be performed up to 5 times at the same position with similar results, afterwards the efficiency decreases.

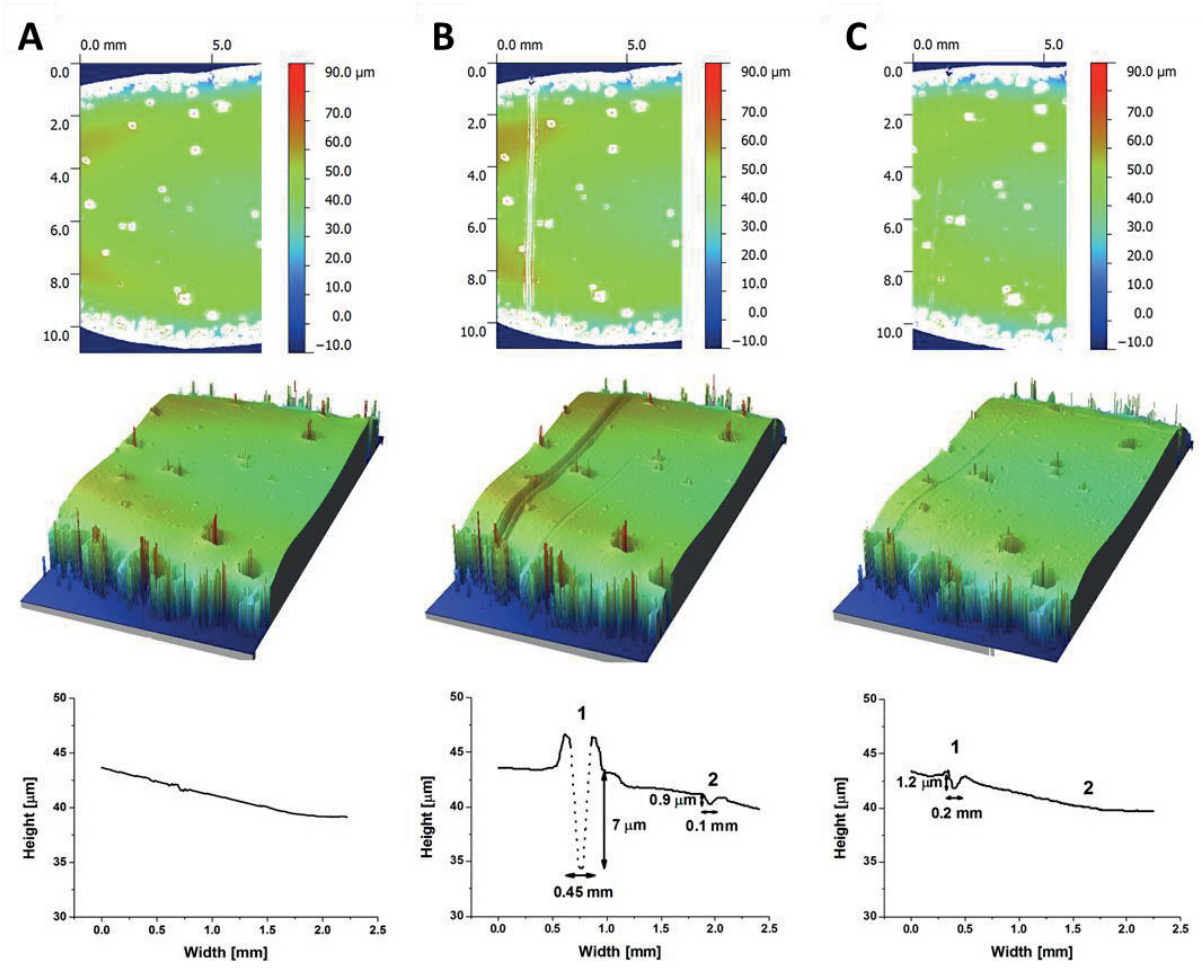

Figure 14: Profilometry measurements of PEO_{330}-*b*-$PFGE_{20}$ block copolymer films after crosslinking (A), scratching with a spatula (B), and the healing process at 155 °C (C).

Beside the formation of block copolymers, the controlled introduction of a single furan moiety at the junction point between two blocks can be achieved. In this case the anionic polymerization of 2-vinylpyridine (2VP) was initiated by *sec*-butyl lithium (*sec*-BuLi), and the polymer was endcapped *via* the addition of FGE. Due to the strong coordination of the litihium counterion, only a single furfuryl glycidyl ether repeating unit was added, and deactivated by subsequent addition of methanol. The formed hydroxyl group is reactivated *via* DPMK, followed by the polymerization of ethylene oxide (EO), yielding $P2VP_{68}$-FGE-*b*-PEO_{390}.

The furan moiety was addressed *via* attaching maleimide-functionalized pyrene, leading to UV active polymers. In case of the pyrene functionalized block copolymer, the pristine dye shows no fluorescence in water, while the block copolymer shoes an intense increase in fluorescence (Figure 15).

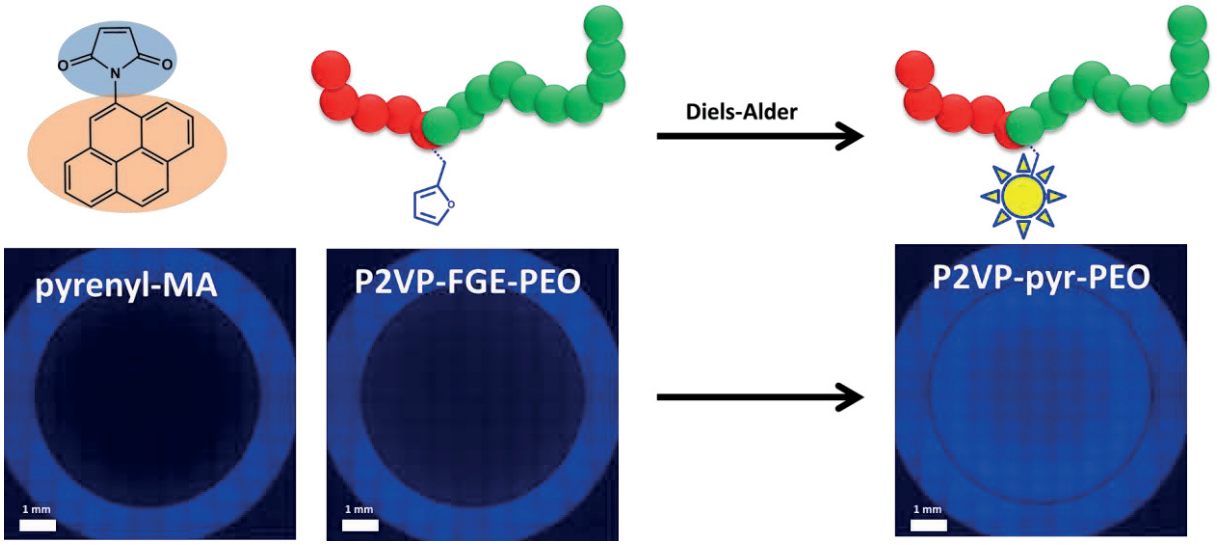

Figure 15: Diels-Alder reaction of pyrenyl maleimide and the pendant furan unit at the chain junction of a P2VP-FGE-*b*-PEO block copolymer (upper section) and fluorescence measurements of each compound (lower section).

In addition to the modification with a fluorescent dye, the mid-chain functionalized block copolymer was used for the decoration of maleimide-functionalized gold nanoparticles (Au-NP) *via* DA reactions. The stability of the Au-NP in aqueous solution at different pH values was increased afterwards, indicated by the formation of colloidally stable dispersions and changes in zeta-potential. Further studies also showed the use of thiol-functionalized PEO-*b*-PFGE block copolymers as ligands for the synthesis of AuNPs. The selective crosslinking of the PFGE segment suppressed ligand exchange upon addition of a competing ligands such as dodecanethiol.[158]

2.2.3 Maleimide Thiolactone – A new Class of Homo- and Copolymers

The composition and microstructure in copolymers can be controlled by the polymerization technique or the reactivity of the corresponding monomers. *Via* this approach a copolymer of two monomers can form random, gradient, alternating or block copolymers, depending on the reaction conditions.[26] Perfectly alternating copolymers are mostly known for donor acceptor pairing between, e.g., maleic anhydride (or maleimide) and styrene. The tendency to copolymerize in an alternating fashion is mostly due to the opposite polarity of the double bonds, leading to strong interactions during the radical chain growth reaction.[159]

In this chapter the synthesis of a new bio-based monomer combining maleimides and thiolactone[80] is demonstrated. Thiolactones undergo double modification reactions in a one-pot reaction at ambient reaction temperatures by the subsequent addition of an amine for the nucleophilic ring-opening of the thiolactone and an immediate thiol-X reaction with a thiol scavenger (e.g. acrylates).[80, 81, 160, 161]

The maleimide thiolactone (MITla) can be obtained straightforward *via* reacting maleic anhydride (MAN) and D,L-homocysteine thiolactone hydrochloride (Tla*HCl) in DMSO within 3 hours. This monomer was intensively investigated *via* NMR (Figure 16A), FT-IR, elemental analysis (EA), and ESI-MS TOF.

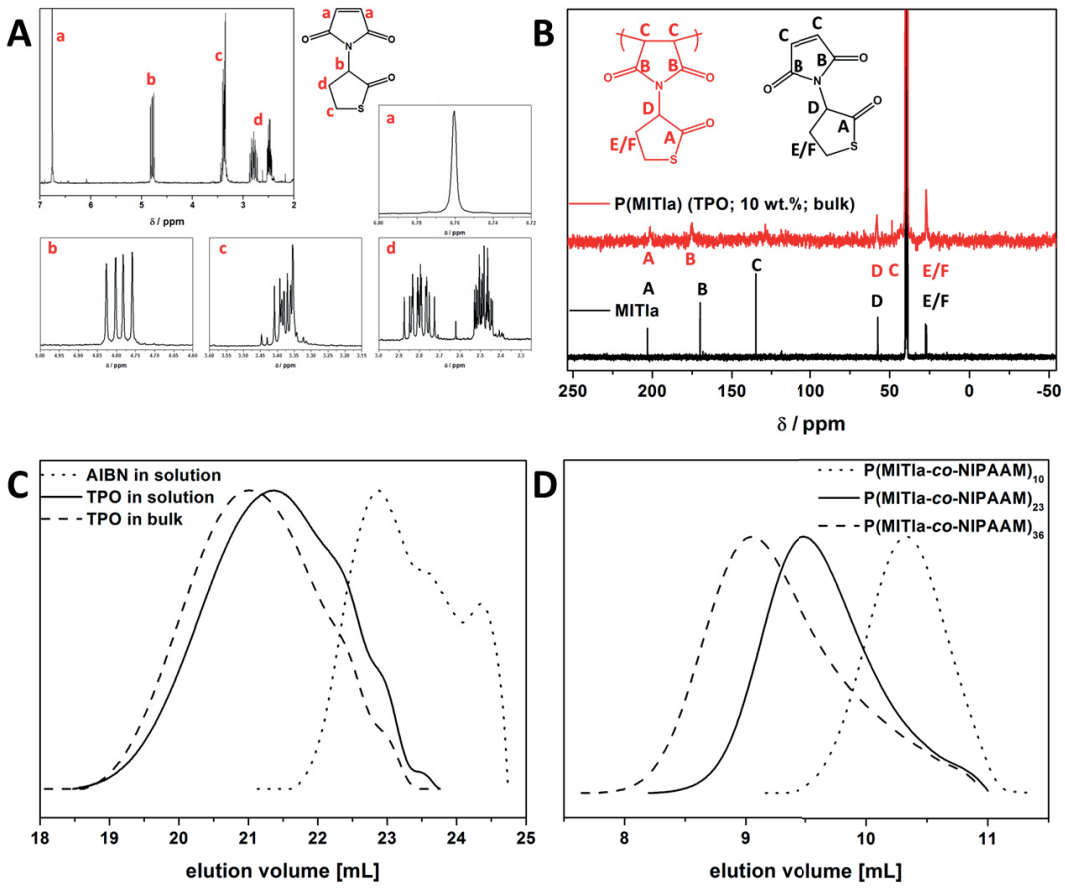

Figure 16: A) Characterization of maleimide thiolactone (MITla) *via* ^{1}H-NMR and peak assignment; B) comparison of ^{13}C-NMR of MITla (black trace) and PMITla homopolymer (red trace); C) comparison of SEC traces for PMITla homopolymers initiated *via* different initiators and reaction conditions: AIBN in solution (dotted line), TPO in solution (straight line) and in the bulk (dashed line); D) comparison of SEC traces for P(MITla-*co*-NIPAAm)$_x$ copolymers with different degrees of polymerizations (DP): DP10 (dotted line), DP23 (straight line), and DP36 (dashed line).

Along the synthesis of the maleimide thiolactone molecule the homo- and copolymerization was tested. Free radical homopolymerization, initiated with 2,2′-azobis(2-methylpropionitrile) (AIBN) or 2,4,6-trimethylbenzoyldiphenylphosphine oxide (Lucirin TPO©), was studied and investigated concerning the molar mass and integrity of the thiolactone ring after polymerization (Figure 16B). *Via* AIBN only oligomers with low molar mass were obtained while in case of TPO the molar mass could be varied depending on the reaction conditions and the monomer to initiator ratio (Figure 16C). Further, the copolymerization with styrene and *N-iso*-propylacrylamide (NIPAAm) was performed under reversible addition-fragmentation chain transfer (RAFT) conditions. Three different molar masses for, P(MITla-*alt*-S)$_x$ and P(MITla-*co*-NIPAAm)$_x$ copolymers were synthesized (Figure 16D for P(MITla-*co*-NIPAAm)$_x$). The copolymers were investigated concerning composition, molar mass, and integrity of the thiolactone ring. Copolymers with up to

50 mol.% content of thiolactone could be obtained, which in other approaches has been limited up to now to 30 mol.%.[81, 160]

The site specific double modification was performed with a combination of methyl acrylate and *n*-butylamine for homopolymers and copolymers (Figure 17A). In case of the homopolymer the post-polymerization modification of thiolactone can be easily investigated *via* SEC (Figure 17B) or NMR. In Figure 17C and D the characteristic signals for the thiolactone ring in ^{1}H- and ^{13}C-NMR disappear or broaden after the modification and the appearance of new signals corresponding to the acrylate and the amine is demonstrated.

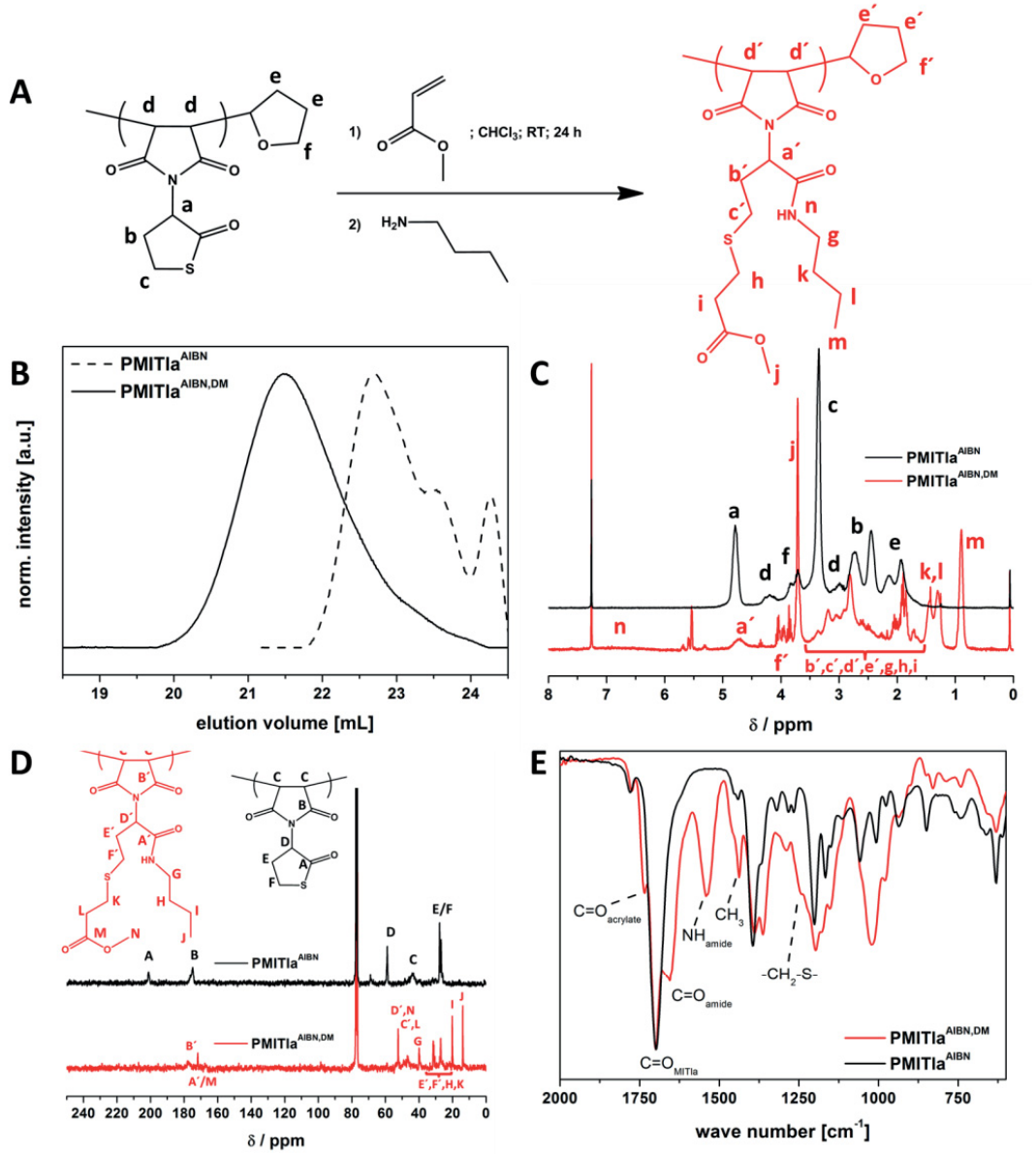

Figure 17: A) Double modification of PMITla^{AIBN} by methyl acrylate and *n*-butylamine; B) comparison of SEC traces for PMITla^{AIBN} before (dashed line) and after (straight line) double modification of the thiolactone; C) comparison of ^{1}H-NMR spectra for PMITla^{AIBN} before (black line) and after (red line) double modification; D) comparison of ^{13}C-NMR spectra for PMITla^{AIBN} before (black line) and after (red line) double modification; E) comparison of FT-IR spectra for PMITla^{AIBN} before (black line) and after (red line) double modification.

Although the successful double modification was observed for PMITla and for P(MITla-*co*-NIPAAm), the modification of P(MITla-*alt*-S)$_x$ was only possible up to 60%, although different solvents and reaction times were tested. Reasons for this might be steric demands for the modification or solubility issues, as in some cases precipitation after the addition of the amine was observed.

In our opinion, MITla offers high potential for the synthesis of block copolymers, the selective crosslinking of individual segments, the introduction of functional endgroups into polymer chains, the use of functional thiols, or the facile preparation of sequence controlled polymers.

3. Self-assembly of Block Copolymers in Selective Solvents

For the study of self-assembly for the before synthesized polymers in selective solvents, a combination of various techniques combining transmission electron microscopy (TEM), dynamic light scattering (DLS), and UV-Vis spectroscopy were applied. The chapter is divided into:

1) The investigation of the solution behavior of bolaamphiphiles and the underlying self-assembly mechanism in aqueous solution (**Chapter 3.1**)

2) A morphological study for the self-assembly of ferrocenyl-based block copolymers in selective solvents (**Chapter 3.2**)

3) The formation of star-shaped block copolymers by host-guest interaction (**Chapter 3.3**).

3.1 Solution Behavior of ABA Bolaamphiphiles in Aqueous Media

Parts of this chapter have been published: **P2)** Rudolph, T.; Allampally, N. K.; Fernandez, G.; Schacher, F. H., *Chem. Eur. J.*, 2014, 43, 13871-13875.

Assemblies of supramolecular amphiphiles are mostly formed due to noncovalent interactions, based on, e.g., π-π- interactions or hydrogen bonding.[97] Accepted mechanisms for the formation of these structures include isodesmic self-assembly (in which the equilibrium constant for all binding events is equal) or cooperative self-assembly (two-step mechanism forming first a nucleus before elongation of the aggregate).[97, 98, 162-164]

In this chapter, ABA bolaamphiphiles (**Chapter 2.1.2.1**) with different lengths of PEtOx side chains and an OPE core will be investigated concerning their aggregation mechanism in aqueous media. First, the bolaamphiphiles were investigated in pure tetrahydrofuran and THF/water mixtures *via* UV-Vis and fluorescence spectroscopy, indicating unimers in pure THF while aggregation is observed by increasing the water content due to the hydrophobicity of the central OPE part. *Via* these investigations first hints concerning different aggregation behavior can be obtained for $PEtOx_6$-OPE-$PEtOx_6$ and two $PEtOx_x$-OPE-$PEtOx_x$ with longer side chains of PEtOx (x = 11, 16).

For an in-depth study of the underlying aggregation mechanism, these bolaamphiphiles were further investigated *via* UV-Vis in dilute aqueous solution at different temperatures. Spectral changes in temperature-dependent measurements can be associated with the self-assembly mechanism. The changes at a certain wavelength in the cooling curve of the bolaamphiphile solutions can be plotted and fitted to a sigmoidal curve for $PEtOx_{11}$-OPE-$PEtOx_{11}$ and $PEtOx_{16}$-OPE-$PEtOx_{16}$, indicating an isodesmic mechanism for the aggregation process.[165] On the other hand, for $PEtOx_6$-OPE-$PEtOx_6$ a clearly non-sigmoidal shape is observed, which can be fitted to a nucleation-elongation model as developed by Meijer and coworkers.[166, 167]

The different bolaamphiphiles were further investigated *via* TEM and DLS, confirming the assembly mechanism. For the isodesmic mechanism the equilibrium constant for all binding events is equal, therefore spherical assemblies are expected and confirmed *via* TEM (Figure 18). For $PEtOx_6$-OPE-$PEtOx_6$ a cooperative mechanism is suspected, while anisotropic platelets, with a length of several μm length and several hundreds of nm in width, are observed by TEM. After the nucleation step in the mechanism an elongation of the

assembly by further addition of $PEtOx_6$-OPE-$PEtOx_6$ to the nucleus occurs over a certain period of time (Figure 18).

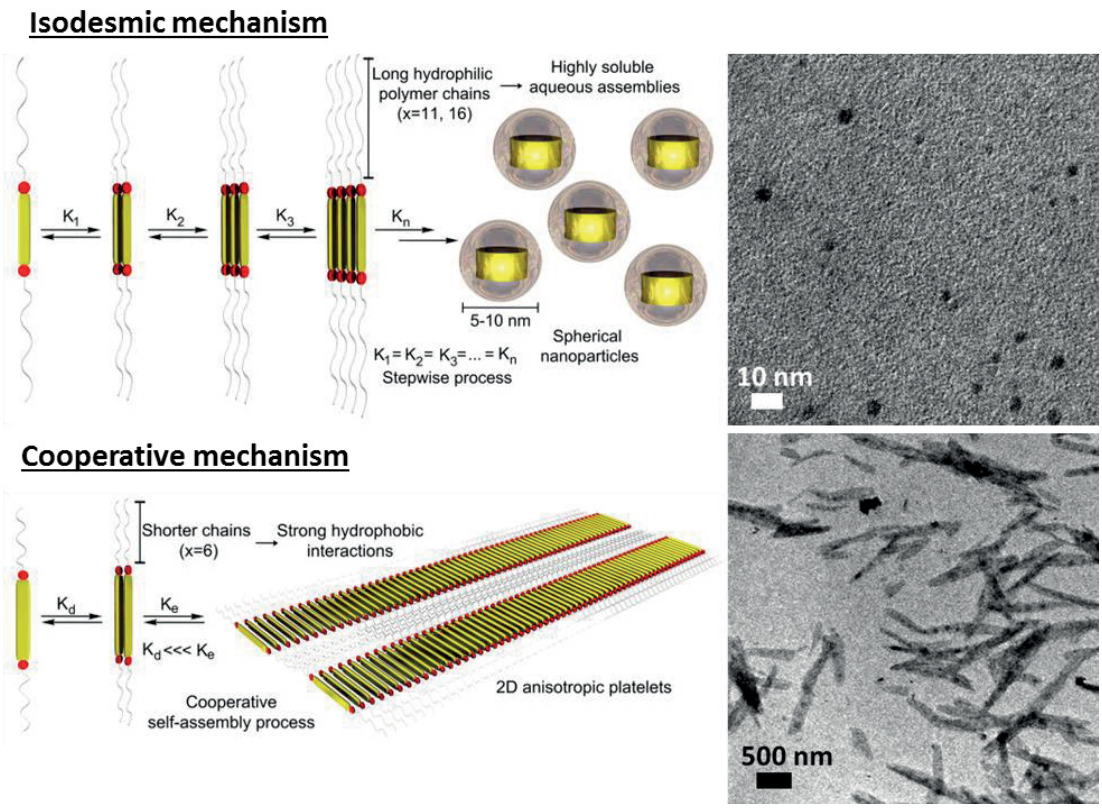

Figure 18: Isodesmic and cooperative mechanism for the aqueous self-assembly of $PEtOx_x$-OPE-$PEtOx_x$ and TEM micrographs for spherical assemblies in case of $PEtOx_{11/16}$-OPE-$PEtOx_{11/16}$ and platelets for $PEtOx_6$-OPE-$PEtOx_6$ in aqueous media.

As conclusion we were able to obtain $PEtOx_x$-OPE-$PEtOx_x$ with three different lengths of PEtOx (DP = 6, 11, 16) attached to the OPE unit. We were able to switch between an isodesmic assembly mechanism for $PEtOx_{11/16}$-OPE-$PEtOx_{11/16}$, while shortening of the PEtOx chain in case of $PEtOx_6$-OPE-$PEtOx_6$ clearly leads to a cooperative self-assembly mechanism in water, which is controlled by hydrophobic interactions.

Recent investigations show that pH-responsive units in the side chain of the attached solubilizing polymers might also increase the complexity of such materials, but may pave the way towards self-sorting systems.[168, 169]

In our case of PEtOx side chains a partial hydrolysis to poly(ethylenimine) (PEI) can be achieved, a pH-responsive polymer.[170] *Via* this, we might be able control the assembly not only by the length of the polymer chain, but also *via* the choice of the pH, leading to protonation or deprotonation of the side chains.

3.2 Linear Diblock Copolymers in Selective Solvents

Parts of this chapter will be/have been published: **P4)** Rudolph, T.; Nunns, A.; Schwenk, A. M.; Schacher, F. H., *Polym. Chem.,* 2015, 6, 1604-1612; **P5)** Rudolph, T.; Nunns, A.; Stumpf, S.; Pietsch, C.; Schacher, F. H.; *submitted*.

Manners and coworkers introduced "living crystallization-driven supramolecular polymerization" of organometallic block copolymers based on poly(ferrocenylsilane)s (PFS).[95, 110, 112, 171-173] Here, semi-crystalline PFS is the core-forming block in selective solvents, often resulting in anisotropic platelet- or rod-like morphologies, while various corona-forming blocks were used.[108, 174-176]

In this study the influence of the composition of the block copolymer on the resulting morphology in selective solvents was investigated. We aimed for ratios of 90/10, 70/30 and 50/50 wt.% for block copolymers of PFDMS$_x$-*b*-POx$_y$. As a second point, beside the variation of the ratio between PFDMS and POx, EtOx (amorph) and *i*PrOx (semi-crystalline, reported crystallization upon heating in water), were chosen as second block, forming amphiphilic block copolymers.

After the synthesis and purification of the block copolymers, different compositions were dissolved in a non-selective solvent, dichloromethane (DCM), and added dropwise into acetone (selective solvent for PFS). The solutions were allowed to stir over night, while increasing turbidity indicated aggregation, forming a semi-crystalline PFDMS core and a solubilizing POx corona. After drop casting of the solutions onto TEM grids the aggregates were investigated *via* transmission electron microscopy (Figure 19). Depending on the ratio of PFDMS/POx, the TEM micrographs show sheets (90/10 wt.%), vesicles (70/30 wt.%), or rod-like structures (50/50 wt.%), while no difference was observed between PEtOx and P*i*PrOx based PFDMS$_x$-*b*-POx$_y$ block copolymers.

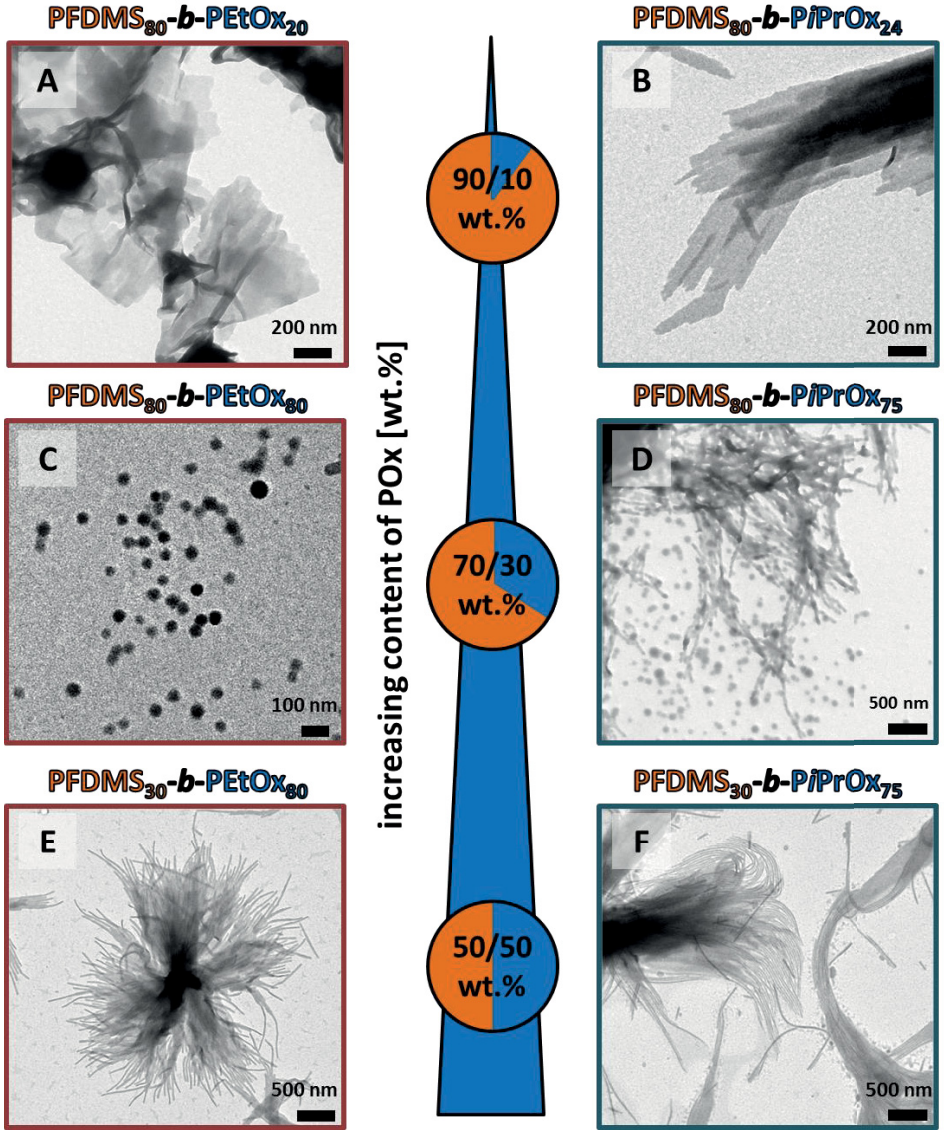

Figure 19: TEM micrographs for block copolymers with different ratios of PFDMS and POx in acetone (0.5 mg mL^{-1}),: sheet-like structures for PFDMS$_{80}$-*b*-PEtOx$_{20}$ (92/8 wt.%; A), PFDMS$_{80}$-*b*-P*i*PrOx$_{24}$ (88/12 wt.%; B); vesicular morphologies for PFDMS$_{80}$-*b*-PEtOx$_{80}$ (71/29 wt.%; C), PFDMS$_{80}$-*b*-P*i*PrOx$_{75}$ (70/30 wt.%; D); rod-like structures for PFDMS$_{30}$-*b*-PEtOx$_{80}$ (47/53 wt.%; E), PFDMS$_{30}$-*b*-P*i*PrOx$_{75}$ (46/54 wt.%; F).

PFDMS$_x$-*b*-P*i*PrOx$_y$ block copolymers are potential materials for the formation of double crystalline block copolymers. The crystallization of P*i*PrOx can be achieved in the bulk by heating the sample to elevated temperatures or heating P*i*PrOx in aqueous solution above the lower critical solution temperature (LCST).[19, 177] Schlaad and coworkers claim a combination of oriented dipolar interaction and non-hydrophobic interactions as driving force for the crystallization at elevated temperatures for P*i*PrOx homopolymers.[178] PFDMS$_x$-*b*-P*i*PrOx$_y$ (50/50 wt.%) was investigated *via* X-ray scattering at different temperatures concerning the crystallinity of the block copolymer. As can be observed in wide-angle x-ray scattering (WAXS), the presence of the characteristic reflections of PFDMS occurs already at

20 °C, while the corresponding reflections for the P*i*PrOX segment increase during the annealing process at 100 °C, as the signal for the PFDMS remains constant (Figure 20C). After the investigation in the bulk, the block copolymer $PFDMS_x$-*b*-P*i*PrOx_y (50/50 wt.%), which formed rod-like structures in acetone, was transferred from acetone into water, while the integrity of the rods was investigated *via* electron microscopy (TEM and SEM). Sequential heating of the sample in water for several hours leads to temperature-induced crystallization of P*i*PrOx, thereby embedding the PFDMS rods in a semi-crystalline matrix of P*i*PrOx (Figure 20A).

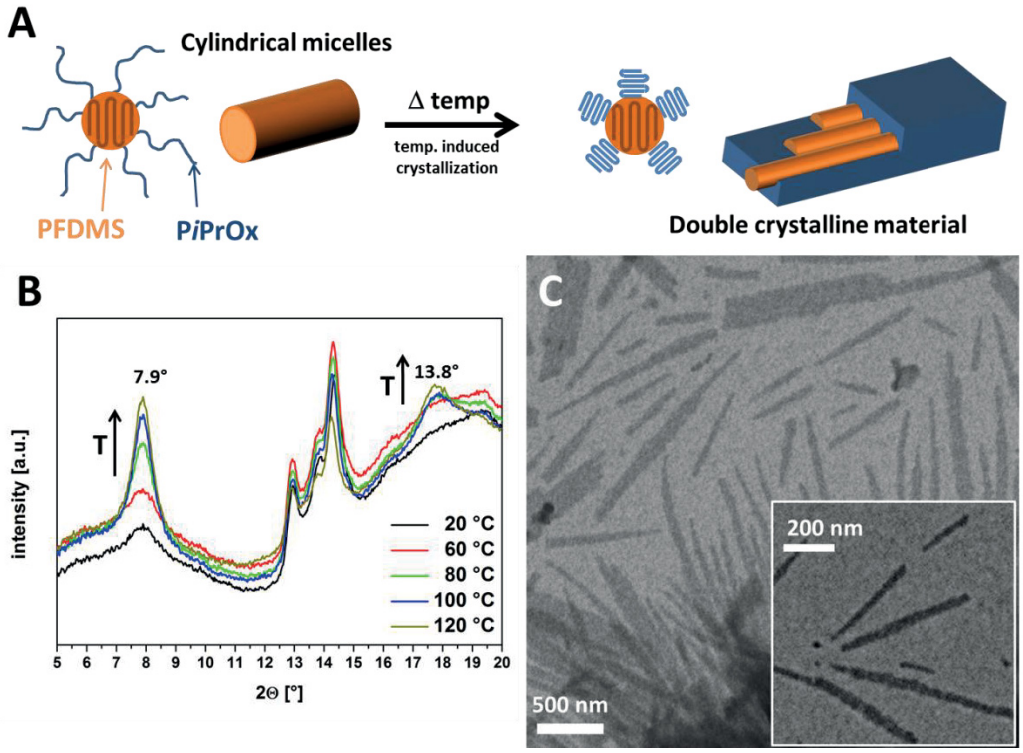

Figure 20: A) Sequential crystallization of PFDMS by solvent-induced crystallization in acetone, and transfer of the rod-like structures into water, and the sequential crystallization of P*i*PrOx forming double crystalline material; B) comparison of WAXS measurements for the block copolymer before (black trace) and after annealing at different temperature in the bulk; C) TEM micrograph of cylindrical micelles of block copolymer after transfer from acetone into aqueous solution.

In aqueous solution the crystallization was also indicated by the formation of larger structures, presumably due to uncontrolled agglomeration and precipitation. Investigations of these aggregates *via* SEM confirmed the assumption of the formation of PFDMS rods in a P*i*PrOx matrix as is shown in Figure 20A.

Up to now, we were not able to demonstrate the crystallinity of both blocks after hierarchical self-assembly in solution, which might be due to a very thin layer on the crystalline surface of

PFDMS or incomplete crystallization of P*i*PrOx. Therefore, a second rod-forming block copolymer $PFDMS_x$-*b*-P*i*$PrOx_y$ (30/70 wt.%) is currently under investigation.

3.3 Star-Shaped Polymers by Supramolecular Host-Guests Interactions

Parts of this chapter have been published: **P3)** Schmidt, B.V.K.J.; Rudolph, T.; Hetzer, M.; Ritter, H.; Schacher, F. H.; Barner-Kowollik, C.; *Polym. Chem.*, 2012, 3, 3139-3145.

Complex architectures by host/guest interactions can be achieved by, e.g., a combination of cyclodextrine and adamantyl functionalities.[179] We were interested in the synthesis of star-shaped polymers by host/guest-interactions between adamantyl-functionalized polymers with different molar mass and a cyclodextrine-functionalized (CD) star-shaped trilinker. Adamantyl-functionalized polymers of *N,N*-dimethylacrylamide (DMAAm) and *N,N*-diethylacrylamide (DEAAm) were synthesized *via* RAFT polymerization using an adamantyl-functionalized chain transfer agent. The polymers were investigated concerning the functionality and molar mass by NMR and SEC. As second motif a trilinker was obtained by the CuAAC click reaction between azide-modified cyclodextrine units (CD) and tripropargylamine.

In a subsequent investigation the formation of star-shaped polymers by self-assembly of the complementary motifs in solution was investigated (Figure 21A). The successful inclusion was mostly investigated by ROESY-NMR in D_2O by correlations between the signals of cyclodextrine and adamantyl. For first measurements *via* DLS the individual compounds were investigated in H_2O and D_2O. All polyacrylamides seemed to have lower solubility in H_2O in comparison to D_2O. Improved solubility might also lead to an increased accessibility of the adamantyl moiety for the inclusion process with CD.

The two building motifs for the supramolecular star-shaped polymers, PDMAAm (or PDEAAm) and the CD-trilinker, were dissolved in stoichiometric amounts in D_2O, stirred for 24 hours and investigated *via* DLS. The corresponding size distributions indicate a clear shift for the hydrodynamic radius (R_h) from the linear to the star-shaped polymer. In case of $PDAAm_{143}$-Ad ($M_{n,GPC}$ = 14 600 g mol^{-1}) an apparent hydrodynamic radius of 2.5 nm was obtained, while the CD-based trilinker showed a R_h of 1.3 nm (Figure 21B). After mixing of the individual macromolecular building blocks, a supramolecular star-shaped polymer with a hydrodynamic radius of 3.7 nm was observed, which was stable in solution over several days.[134]

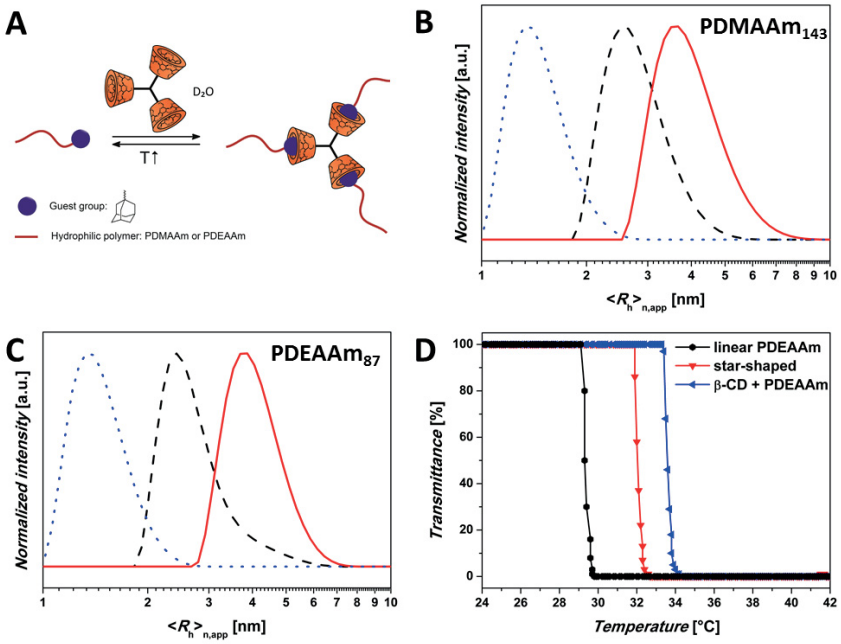

Figure 21: A) Supramolecular star-shaped polymers by host-guest inclusion complex formation between a CD functionalized trilinker and adamantyl functionalized polymers; B) comparison of number-weighted size distributions for PDMAAm$_{143}$-Ad (dashed line), the CD-trilinker (dotted line) and the resulting supramolecular star polymer (red line); C) comparison of number-weighted size distributions for PDEAAm$_{87}$-Ad (dashed line), the CD-trilinker (dotted line) and the resulting supramolecular star polymer (red line); D) turbidity measurements for PDEAAm$_{87}$-Ad (black line), the supramolecular star polymer (red line) and mixtures of PDEAAm$_{87}$-Ad and CD (blue line).

Further, the thermo-responsive polymer PDEAAm$_{87}$-Ad was used for the formation of star-shaped assemblies. PDEAAm materials show, depending on the molar mass and the respective endgroup, LCST in a temperature range of 25 to 40 °C.[180-182] First, the formation of the star-assembly was shown *via* dynamic light scattering by an increase of the hydrodynamic radius from 2.4 nm to 3.8 nm (Figure 21C). Furthermore, the temperature responsiveness was investigated by turbidimetry measurements for linear and star-shaped PDEAAm polymers. For linear PDEAAm a cloud point temperature (T_{cp}) of 29 °C was determined while the star-polymer shows a transition at 32 °C (Figure 21D). For linear PDEAAm with CD (no trilinker) a T_{cp} at 33.6 °C is observed, which can be explained by shielding of the hydrophobic adamantyl moiety by the CD and an increase in the hydrophilicity of the macromolecule. The T_{cp} for the star is in between both measurements, indicating an increase in solubility and decreasing conformational freedom at the same time. The sharp decrease of transmittance and the reproducibility of the transition are indications for the inclusion process and the inclusion of the CD-trilinker into the collapsed polymer coil.

Nevertheless, the formation of star-polymers in H_2O was not observed, which might be due to decreased solubility and accessibility of the adamantyl endgroup, as has been described for poly(*N*-*iso*-propylacrylamide).[183-185]

4) Synthesis and Applications of Hybrid Materials

For the formation of hybrid materials different approaches can be used: metal ions can be either embedded within a (block co-) polymer template by metal-polymer interactions or homogeneous coatings can be applied to nanoparticles by electrostatic adsorption of the introduction of suitable endgroups. The chapter is divided into:

1) The synthesis of porphyrin-centered star-shaped polymers incorporating copper or iron ions (**Chapter 4.1**)

2) The template-assisted loading of block copolymer micelles with nickel, followed by doctorblading, calcination, and the application of the resulting porous nickel oxide materials in photo-sensitizing experiments (**Chapter 4.2**)

3) The formation of double crystalline triblock terpolymers for the selective complexation of NP and the directional crystallization of 1D hybrid materials (**Chapter 4.3**)

4) The use of aminocellulose coated superparamagnetic NP for copper complexation and the subsequent ATRP of styrene (**Chapter 4.4**).

4.1 Metal ions Embedded into Porphyrin-Based Star Polymers

Parts of this chapter have been published: **P14)** Rudolph, T.; Crotty, S.; Schubert, U. S.; Schacher, F. H.; *e-Polymers*, 2015, in press (DOI 10.1515/epoly-2015-0041).

Macromolecular conjugation reactions between different building blocks have been extensively discussed in the chapters before. In addition, here the selective introduction of metal ions into a porphyrin cavity was investigated. Due to the planar nature of the porphyrin moiety upon inclusion of metal ions, such building blocks might be used in further assembly studies, similar to the OPE bolaamphiphiles described earlier (**Chapter 3.1**). Comparable reaction conditions for the CuAAC click reaction were applied to $[TPP\text{-}TB]_4$ and $PEtOx_5\text{-}N_3$ as established before (Figure 22A). *Via* this approach a direct inclusion of copper(II) ions during the CuAAC is observed, as by UV-Vis a collapse of two individual signals at 519 nm and 554 nm ($[TPP\text{-}TB]_4$) into one broad absorption band at 542 nm is observed. This has been described for the complexation of metal ions in the center of the porphyrin cavity (Figure 22B).[186] For the expulsion of this ion from the cavity, the star-shaped porphyrin-centered PEtOx ($[Cu\text{-}TPP\text{-}PEtOx_5]_4$) is dissolved in pure sulphuric acid. The SEC traces for $[Cu\text{-}TPP\text{-}PEtOx_5]_4$ and $[TPP\text{-}PEtOx_5]_4$ remain comparable (Figure 22C), while the absorption maxima of the porphyrin ($[TPP\text{-}PEtOx_5]_4$) return to its original position at 519 nm and 554 nm as observed for $[TPP\text{-}TB]_4$ (Figure 22D).

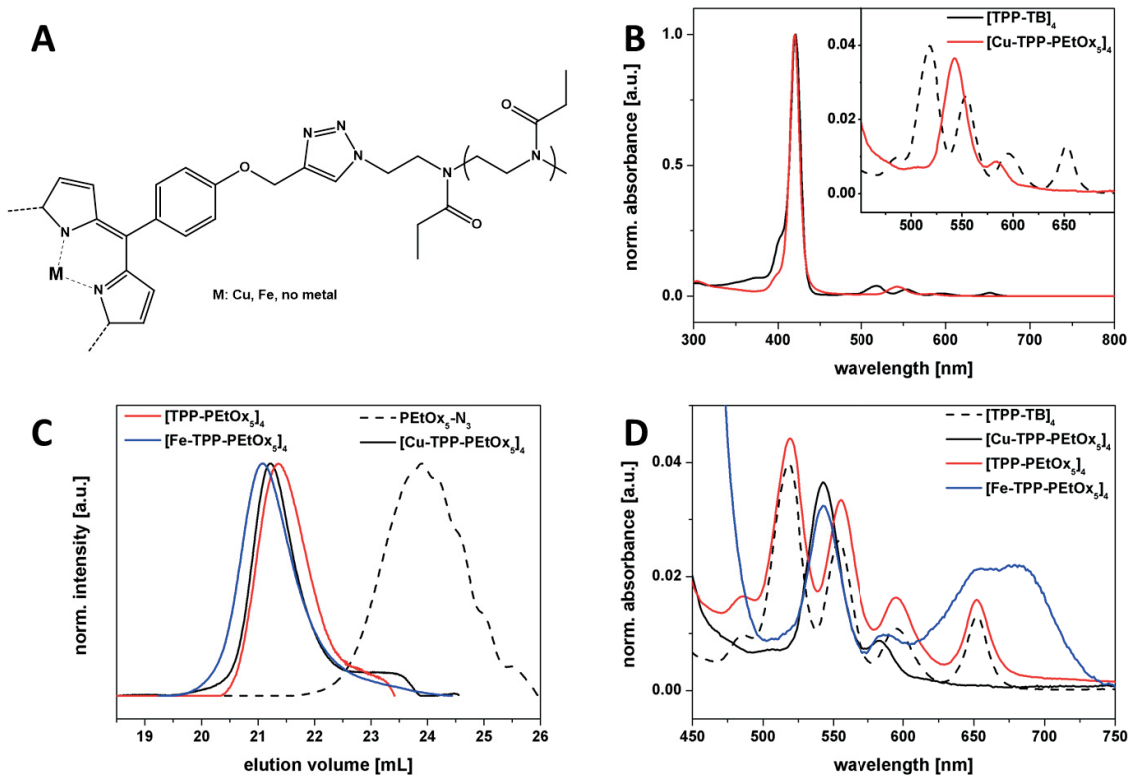

Figure 22: A) Structure of [Me-TPP-PEtOx$_5$]$_4$; B) comparison of UV-Vis spectra for [TPP-TB]$_4$ (black dashed line) and [Cu-TPP-PEtOx$_5$]$_4$; C) comparison of SEC traces for PEtOx$_5$-N$_3$ (dashed line), [Cu-TPP-PEtOx$_5$]$_4$ (black line), [Fe-TPP-PEtOx$_5$]$_4$ (blue line), and [TPP-PEtOx$_5$]$_4$ (red line); D) comparison of UV-Vis spectra for [TPP-TB]$_4$ (black dashed line), [Cu-TPP-PEtOx$_5$]$_4$ (straight black line), [TPP-PEtOx$_5$]$_4$ (red line), and [Fe-TPP-PEtOx$_5$]$_4$ (blue line).

As an alternative metal ion, iron (III) was included within the porphyrin cavity. It was not possible to obtain [Fe-TPP-PEtOx$_5$]$_4$ from [Cu-TPP-PEtOx$_5$]$_4$ or [TPP-PEtOx$_5$]$_4$, therefore an iron-centered porphyrin ([Fe-TPP-TB]$_4$) was synthesized and used instead of [TPP-TB]$_4$. Afterwards, the CuAAC reaction was conducted and the star-polymer characterized after purification. By SEC a similar trend as for [Cu-TPP-PEtOx$_5$]$_4$ and [TPP-PEtOx$_5$]$_4$ was observed, while by UV-Vis the identical signal collapse could be found, indicating the presence of iron within the cavity.

In a further step the obtained star-polymers were also investigated concerning their composition *via* MALDI-TOF MS, confirming the presence of four PEtOx arms connected to a porphyrin center and the presence of different metal ions in the corresponding cavity.
Via a combination of SEC, NMR, FT-IR, UV-Vis and MALDI-TOF MS we were able to confirm the synthesis of symmetrical porphyrin-centered star-polymers with PEtOx arms.

4.2 Porous Nickel Oxide Films via Block Copolymer Templating

Parts of this chapter have been published: **P13)** Bräutigam, M.; Weyell, P.; Rudolph, T.; Dellith, J.; Krieck, S.; Schmalz, H.; Schacher, F. H.; Dietzek, B.; *J. Mater. Chem. A*, 2014, 2, 6158-6166.

We investigated the loading capability of polystyrene-*block*-poly(2-vinylpyridine) diblock copolymer (PS-*b*-P2VP) micelles with nickel ions in solution. In a second step the nickel-loaded micelles were applied to a surface, calcinated (Figure 23) and investigated in dye sensitization experiments with coumarine 343, for a potential application in dye-sensitized solar cells (DSSCs).

Three polystyrene-*block*-poly(2-vinylpyridine) (PS-*b*-P2VP) diblock copolymers with different composition, PS_{65}-*b*-$P2VP_{35}^{230}$, PS_{68}-*b*-$P2VP_{32}^{66}$, and PS_{75}-*b*-$P2VP_{25}^{146}$, were used. The composition of the block copolymers is denoted in the subscripts in wt. % of the corresponding segment, while the superscripts denote the total molar mass of the diblock copolymer. The block copolymers were first investigated concerning their solution behavior in toluene *via* DLS.

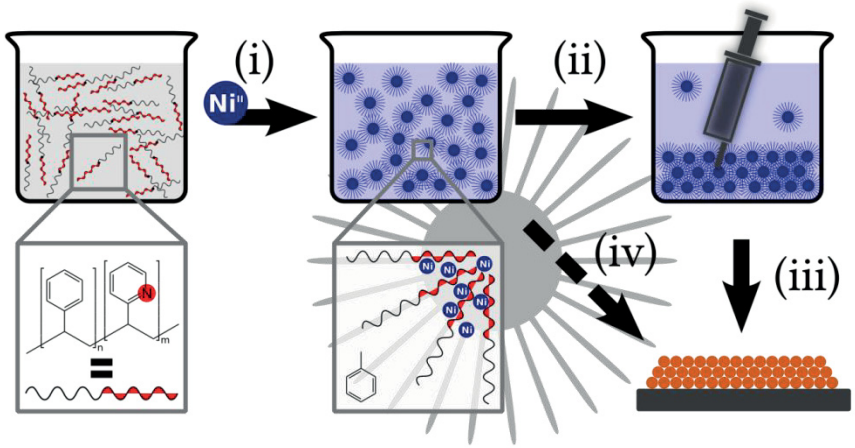

Figure 23: Synthetic route towards nanostructured NiO_x; the addition of Ni^{2+} to a PS-*b*-P2VP block copolymer solution leads to the formation of micelles (i); increasing the Ni^{2+} concentration above a critical threshold leads to precipitation (ii); this precipitate is then spin coated onto a glass substrate and calcinated at 450 °C (iii); alternatively, the initial micellar solution after step (i) can be directly applied to a suitable substrate *via* spincoating (iv).

Concentration dependent measurements of the diblock copolymers indicate the presence of unimers in toluene for PS_{68}-*b*-$P2VP_{32}^{66}$ and PS_{75}-*b*-$P2VP_{25}^{146}$, while PS_{65}-*b*-$P2VP_{35}^{230}$ starts to agglomerate upon a concentration of 5 g L^{-1} (Figure 24A). The introduction of nickel ions

(Ni^{2+}) through a stock solution of $NiCl_2$ in ethanol leads to complexation of Ni^{2+} by the vinylpyridine units and the formation of micelles. Different equivalents of Ni-ions were added with respect to the vinylpyridine units in the corresponding block copolymer. With an increasing content of nickel, the obtained micelles start to grow in size (Figure 24C). The subsequent addition of nickel of more than 1 equivalent, leads to a blue precipitate (Figure 24D), also indicated by larger size distributions in DLS experiments.

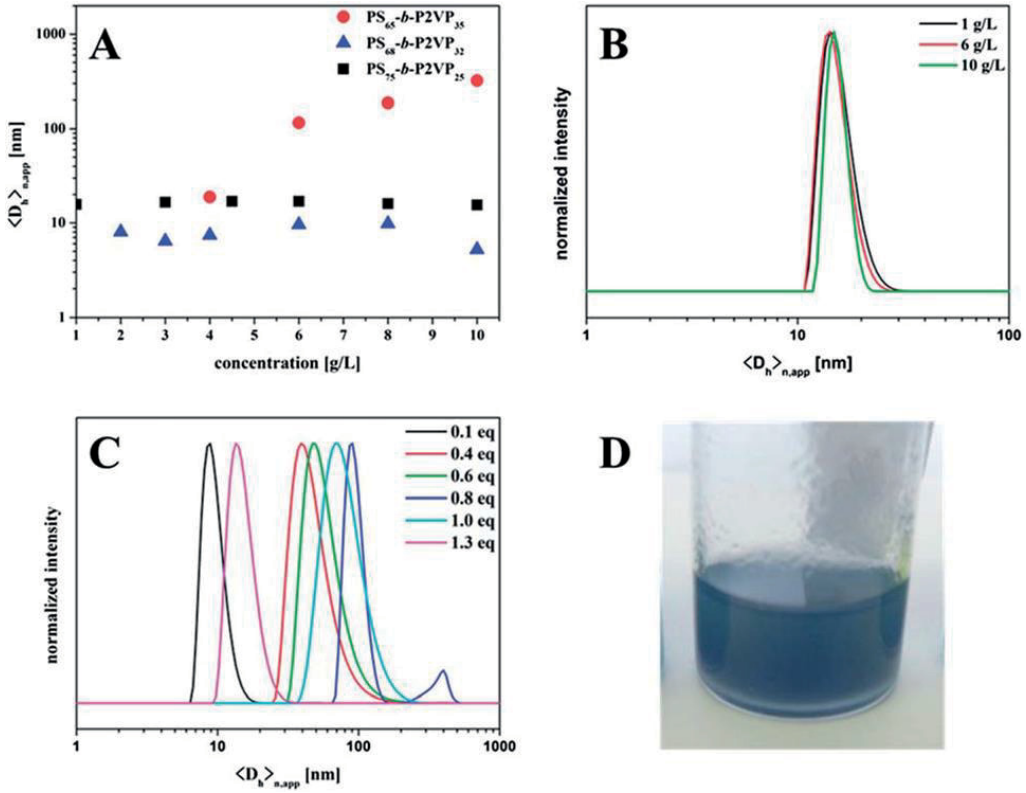

Figure 24: A) Hydrodynamic diameter of PS_{65}-*b*-$P2VP_{35}$ (red spheres), PS_{68}-*b*-$P2VP_{32}$ (blue triangles), and PS_{75}-*b*-$P2VP_{25}$ (black squares) in toluene at different concentrations. B) DLS CONTIN plots of PS_{75}-*b*- $P2VP_{25}$ at different concentrations in toluene; C) DLS CONTIN plots for PS_{75}-*b*-$P2VP_{25}$ after the addition of different amounts of Ni^{2+}: 0.1 eq. (8 nm), 0.4 eq. (40 nm), 0.6 eq. (48 nm), 0.8 eq. (90 nm), 1.0 eq. (68 nm), and 1.3 eq. (14 nm, also a macroscopic precipitate was formed) at a constant block copolymer concentration of 10 g L^{-1}; D) photograph of a vial containing a Ni^{2+}–block copolymer mixture with 1.3 eq. Ni^{2+}/VP.

According to the scope of this project, the synthesis of sub-100 nm NiOx nanoparticle synthesis, the micellar size should also stay below this value. Therefore, the best conditions were found for PS_{75}-*b*-$P2VP_{25}$[146], as these micelles remained stable up to a Ni^{2+}/2VP-ratio of 0.8 equivalents.

For the next step the micelles were deposited onto certain substrates and the substrate was heated up to 450 °C for the calcination process, forming NiO_x-films (Figure 25A). The resulting materials were investigated by SEM concerning film thickness and surface roughness. As the resulting films from colloidally stable hybrid micelles were rather thin,

which limits their use in e.g. dye-sensitized solar cells, the precipitate with a much higher Ni^{2+}-content was used for doctorblading onto the same substrates. The suspension was deposited and calcinated, leading to more homogeneous nickel oxide films (Figure 25B). The film thickness was adjusted by repeating the procedure three times, generating three layers and ending up at a film thickness of 1.4 µm according to SEM (Figure 25 C).

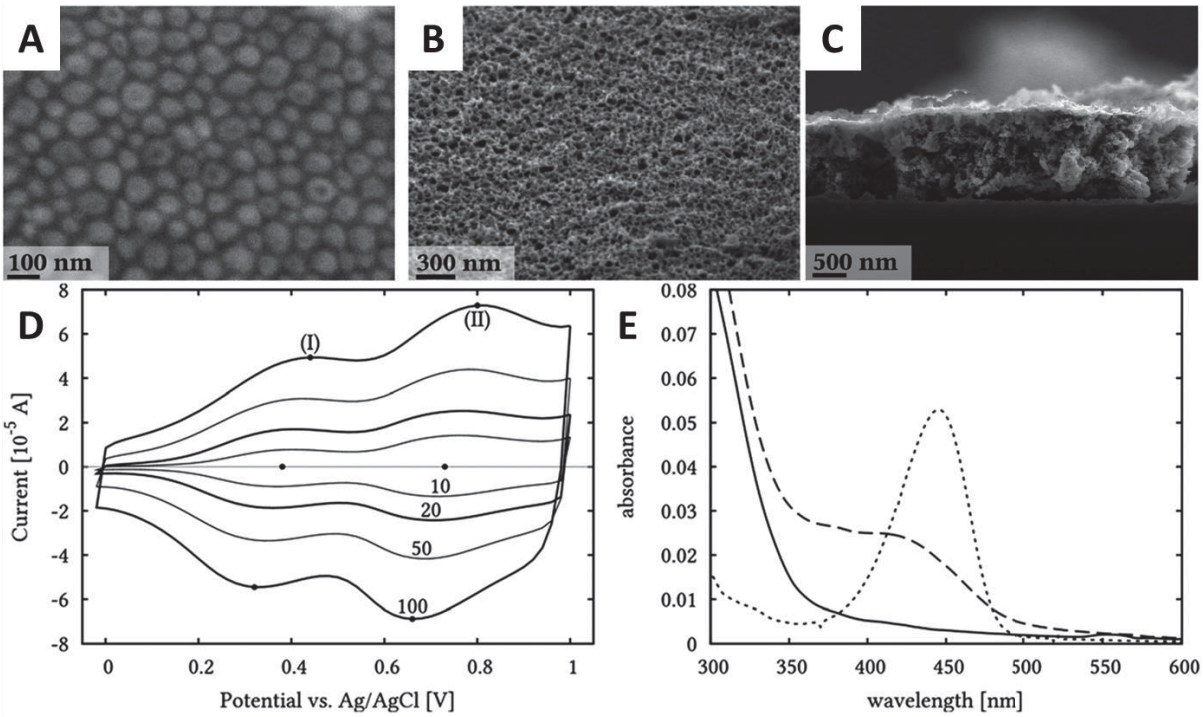

Figure 25: A) SEM micrograph of PS_{75}-*b*-$P2VP_{25}^{146}$ diblock copolymer micelles with 0.8 equivalents of Ni^{2+} (top view); B) SEM micrograph of calcinated NiO_x film; C) SEM micrograph of NiO_x cross-section after three cycles of material deposition; D) comparison of cyclic voltammograms of a NiO_x double film at four scan rates: 10, 20, 50 and 100 mVs^{-1}; E) UV-Vis spectra of coumarine 343 (dotted), of a blank NiO_x surface (solid), and the dye-senyitized NiO_x surface (dashed).

After establishing the route for obtaining homogenous and thick NiO_x films, the electrochemical properties were tested by cyclic voltammetry (CV). The distinct double peak structure in both cycles originates from the oxidation of Ni(II) to Ni(III) and Ni(IV) (Figure 25D). The observed half peak potentials are in a comparable range as the ones reported in literature.[187] The porous films appear to be stable as no differences are observed upon the fourfold cycling of each scan rate (10, 20, 50, and 100 mVs^{-1}).

In the last step the capability of the synthesized NiO_x films as dye-sensitized electrodes was tested by loading the surface with coumarine 343. After washing the surface with acetonitrile, the surface was investigated by UV-Vis spectroscopy. A new signal at 430 nm is observed, indicating the successful binding of the dye to the surface (Figure 25E).

This indicates the possibility of these nanostructured films as potential materials for photoelectrodes of dye-sensitized solar cells or (photo-) catalytic cells.

4.3 Double Crystalline Triblock Terpolymers for Metal Ion Complexation

Parts of this chapter will be published: **P6)** Rudolph, T.; Hartlieb, M.; v. d. Lühe, M.; Schubert, U. S.; Hoeppener, S.; DAgosto,F.; Schacher, F.H.; *in preparation*.

The triblock terpolymer polyethylene-*block*-poly(2-(4-((*tert*-butoxycarbonyl)amino)butyl-2-oxazoline)-*block*-poly(2-*iso*-propyl-2-oxazoline) (PE_{35}-*b*-$PBocAmOx_{15}$-*b*-*i*$PrOx_{145}$) was designed for the formation of anisotropic hybrid materials. In the first step, spherical core-shell-corona micelles with a PE core, a PBocAmOx or poly(2-(4-amino)butyl-2-oxazoline) (PAmOx) shell, and a P*i*PrOx corona are formed in aqueous media. PAmOx can be used for metal ion complexation, while directional crystallization of the P*i*PrOx corona by subsequent heating above the LCST enables the formation of anisotropic superstructures (Scheme 12).

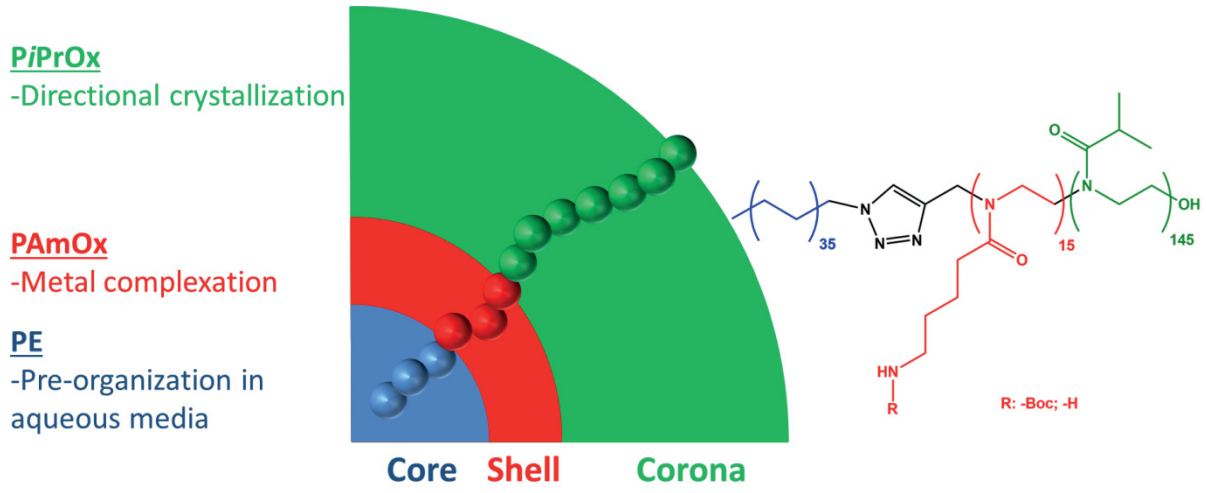

Scheme 12: Illustration of the triblock terpolymer synthesized in this study and the task of each segment involved.

The material was synthesized by covalent linkage between azide functionalized poly(ethylene) (PE_{35}-N_3) and the linear diblock copolymer TB-$PBocAmOx_{15}$-P*i*$PrOx_{145}$ using CuAAC chemistry. After purification, the middle block was deprotected, obtaining PE_{35}-*click*-$PAmOx_{15}$-P*i*$PrOx_{145}$, containing a primary amine in the side-chain. The successful synthesis of the di- and triblock terpolymers was demonstrated by SEC, NMR, and FT-IR. After characterization of the copolymers, the solution behavior was investigated in detail. Due to the low solubility of the triblock terpolymers at room temperature, turbid solutions in DMF were obtained, while it turns clear upon heating to 120 °C (above the melting temperature of

PE). The heated solutions were cooled to room temperature and dialyzed for 3 days against water (3 500 MWCO), forming core-shell-corona micelles (Figure 26A). The formation of spherical micelles was proven by dynamic light scattering (DLS) and transmission electron microscopy (TEM; Figure 26C). *Via* DLS hydrodynamic radii of 17 nm for PE_{35}-*click*-$PBocAmOx_{15}$-P*i*$PrOx_{145}$ or 13 nm for PE_{35}-*click*-$PAmOx_{15}$-P*i*$PrOx_{145}$ in aqueous solution (Figure 26B). The corresponding diblock copolymers: $PBocAmOx_{15}$-*b*-P*i*$PrOx_{145}$ and $PAmOx_{15}$-*b*-P*i*$PrOx_{145}$ led to R_h of 14 and 2 nm, respectively.

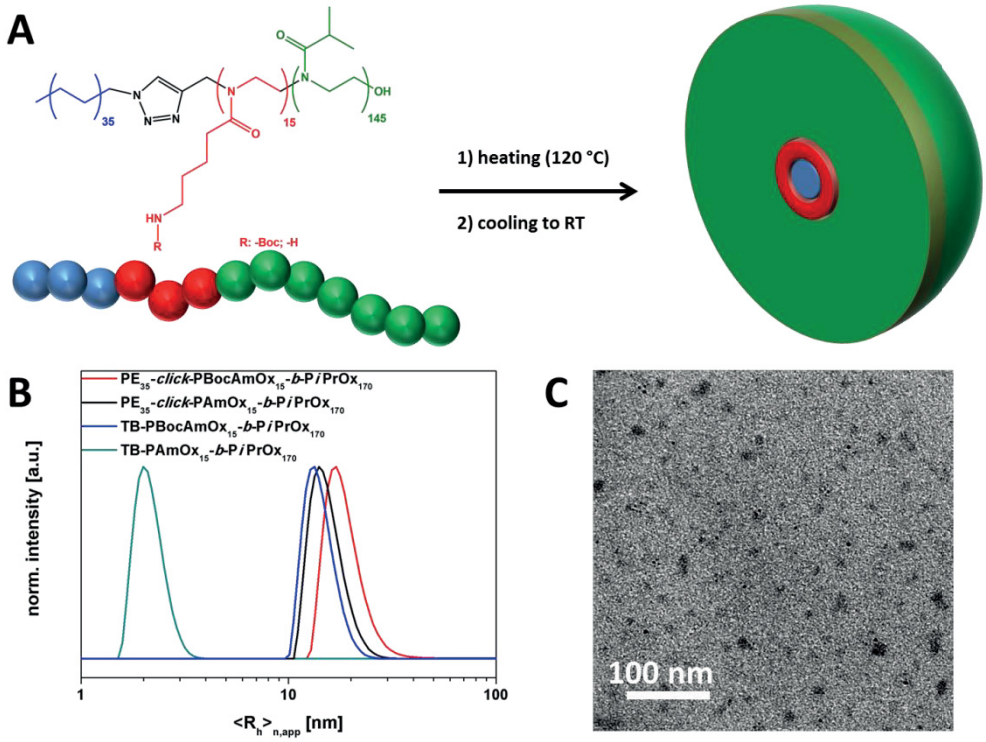

Figure 26: A) Micelle formation of PE_{35}-*click*-$PAmOx_{15}$-*b*-P*i*$PrOx_{145}$ or PE_{35}-*click*-$PBocAmOx_{15}$-*b*-P*i*$PrOx_{145}$ after heating and cooling in DMF; B) comparison of DLS size distributions for TB-$PBocAmOx_{15}$-*b*-P*i*$PrOx_{145}$ (blue curve; $<R_h>$ = 2 nm), TB-$PAmOx_{15}$-b-P*i*$PrOx_{145}$ (cyan curve; $<R_h>$ = 13 nm), PE_{35}-*click*-$PBocAmOx_{15}$-*b*-P*i*$PrOx_{145}$ (red curve; $<R_h>$ = 17 nm), and PE_{35}-*click*-$PAmOx_{15}$-*b*-P*i*$PrOx_{145}$ (black curve; $<R_h>$ = 14 nm); C) TEM micrograph for PE_{35}-*click*-$PAmOx_{15}$-*b*-P*i*$PrOx_{145}$ micelles in water (0.33 mg mL^{-1}).

In the next step, the temperature-induced crystallization of P*i*PrOx and the formation of fiber-like structures in solution as it has been described for linear P*i*PrOx was investigated.[19, 178, 188] This grants access to anisotropic superstructures with a PE core, a potentially metal containing segment/domain as shell and a crystalline P*i*PrOx outer layer. These studies could be used as a foundation for the introduction/embedding of several other metal ions and the formation of "hybrid nanowires" on the basis of linear triblock terpolymers. Herefore, the micellar solutions were heated to 65 °C for 24 hours whilst monitoring both the scattering intensity and the hydrodynamic radii by DLS. In case of TB-

PBocAmOx$_{15}$-*b*-P*i*PrOx$_{145}$ and PE$_{35}$-*click*-PAmOx$_{15}$-P*i*PrOx$_{145}$, precipitation of the material is observed over time indicated by a decrease in the scattering intensity, while for the other two block copolymers the scattering intensity remains constant. TEM micrographs of the resulting solutions show for all samples fiber-like objects of several µm length, induced by the crystallization of P*i*PrOx (Figure 27). The width of the obtained fibers was investigated by grey scale analysis, leading to an average width of ≈ 50-70 nm for all samples (Table 6). Only in the case of PE$_{35}$-*click*-PBocAmOx$_{15}$-P*i*PrOx$_{145}$, a much lower width of just 27 nm was observed.

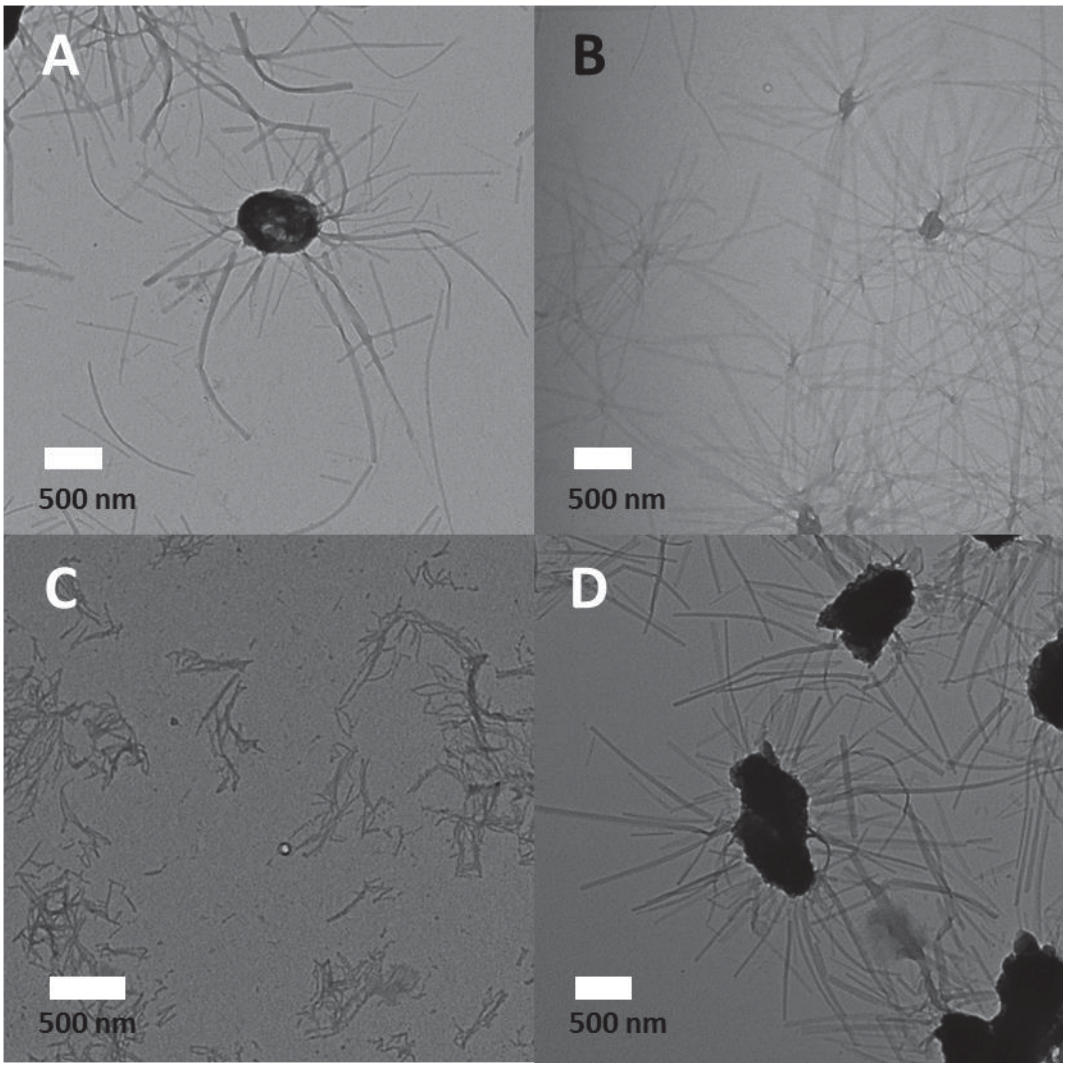

Figure 27: TEM micrographs for aggregates obtained from solution after 24 hours at 65 °C in water for: TB-PBocAmOx$_{15}$-b-P*i*PrOx$_{145}$ (A), TB-PAmOx$_{15}$-b-P*i*PrOx$_{145}$ (B), PE$_{35}$-*click*-PBocAmOx$_{15}$-b-P*i*PrOx$_{145}$ (C), and PE$_{35}$-*click*-PAmOx$_{15}$-b-P*i*PrOx$_{145}$ (D) (0.33 mg mL^{-1}).

The difference in the width might be due to differences in the crystallization process. For the diblock copolymers, the crystallization of P*i*PrOx is not influenced by the presence of PAmOx/PBocAmOx-content. For the triblock terpolymer PE$_{35}$-*click*-PBocAmOx$_{15}$-P*i*PrOx$_{145}$ with the highest hydrophobic content, the fusion of several initially spherical micelles can be

assumed. Here the core of the cylindrical micelles consists of a PE core and a PBocAmOx shell, while the crystallization of the P*i*PrOx corona leads to fixation of the superstructures in water (Figure 28A). On the other hand, PE_{35}-*click*-$PAmOx_{15}$-P*i*$PrOx_{145}$ has an increased solubility in water due to the amine functionality, which carries positive charges in the corresponding segment. Therefore, we hypothesize an inversion of the core-shell-corona micelles upon heating, observing a mixed P*i*PrOx/PE core and a PAmOx corona, presumably as short, cationally charged loops (Figure 28B).

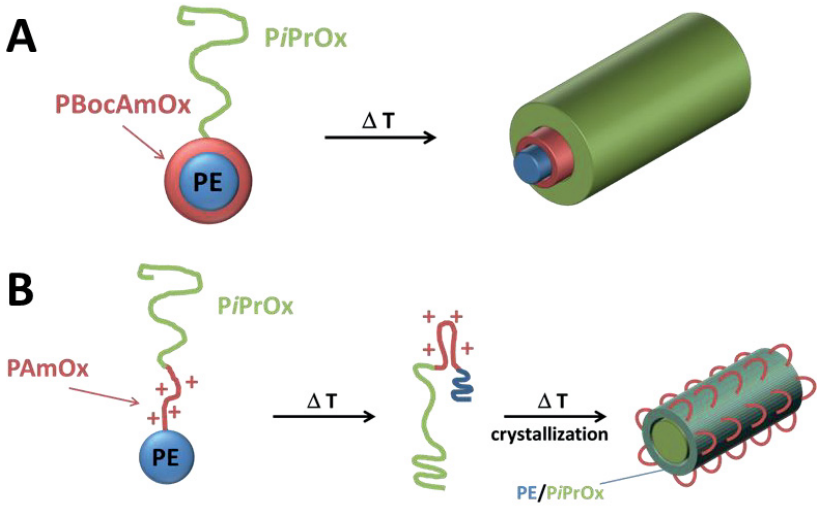

Figure 28: Formation of anisotropic superstructure from spherical micelles for: A) PE_{35}-*click*-$PBocAmOx_{15}$-P*i*$PrOx_{145}$; B) PE_{35}-*click*-$PAmOx_{15}$-P*i*$PrOx_{145}$.

Table 6: Characterization of the block copolymers concerning the hydrophilic weight fraction, hydrodynamic radius ($<R_h>$) and crystal width.

Polymer	Hydrophilic fraction[a] [wt.%]	$<R_h>_{n,app}$[b] [nm]	Crystal width[c] [nm]
TB-$PAmOx_{15}$-*b*-P*i*$PrOx_{145}$	100	2	52 +/- 12
PE_{35}-*click*-$PAmOx_{15}$-*b*-P*i*$PrOx_{145}$	95	14	71 +/- 15
TB-$PBocAmOx_{15}$-*b*-P*i*$PrOx_{145}$	82	13	64 +/- 13
PE_{35}-*click*-$PBocAmOx_{15}$-*b*-P*i*$PrOx_{145}$	78	17	27 +/- 4

a) Calculated from the block copolymer composition; b) DLS, CONTIN plot; c) average width size determined from TEM micrographs by grey-scale analysis.

For PE_{35}-*click*-$PBocAmOx_{15}$-P*i*$PrOx_{145}$ and PE_{35}-*click*-$PAmOx_{15}$-P*i*$PrOx_{145}$ the selective embedding of Au NPs and Fe_3O_4 nanocrystals within the anisotropic superstructures was investigated.[115, 189, 190] $HAuCl_4$ was applied to the micellar solution of PE_{35}-*click*-$PBocAmOx_{15}$-P*i*$PrOx_{145}$ and PE_{35}-*click*-$PAmOx_{15}$-P*i*$PrOx_{145}$ and stirred for 12 hours (in the dark). Afterwards the solutions were dialyzed against water for 2 day to remove any free

metal ions (under exclusion of light). The dialyzed solutions were clear, while the solution with PE_{35}-*click*-$PAmOx_{15}$-P*i*$PrOx_{145}$ turned bluish as the solutions were exposed to sunlight or sodium borohydride ($NaBH_4$) (Figure 29 B). This color change indicates the formation of gold nanoparticles in the case of PE_{35}-*click*-$PAmOx_{15}$-P*i*$PrOx_{145}$, presumably due to the complexation of $AuCl_4^-$-ions with the positively charged PAmOx. For the embedding of Fe_3O_4 nanocrystals ($R_{h,TEM}$ = 6 nm) the micellar solutions were allowed to stir for 12 hours, before the solutions were heated up to 65 °C for the crystallization of P*i*PrOx. Investigating the resulting precipitate *via* TEM, fiber-like aggregates are observed for both triblock terpolymers (Figure 27). Higher magnification of the fibers indicate the presence of Au NPs (Figure 29C), and Fe_3O_4 (Figure 29D) on the surface of the fibers, confirming the assumption of inverse core-shell-corona micelles in case of PE_{35}-*click*-$PAmOx_{15}$-P*i*$PrOx_{145}$ (Figure 29A; Figure 28B).

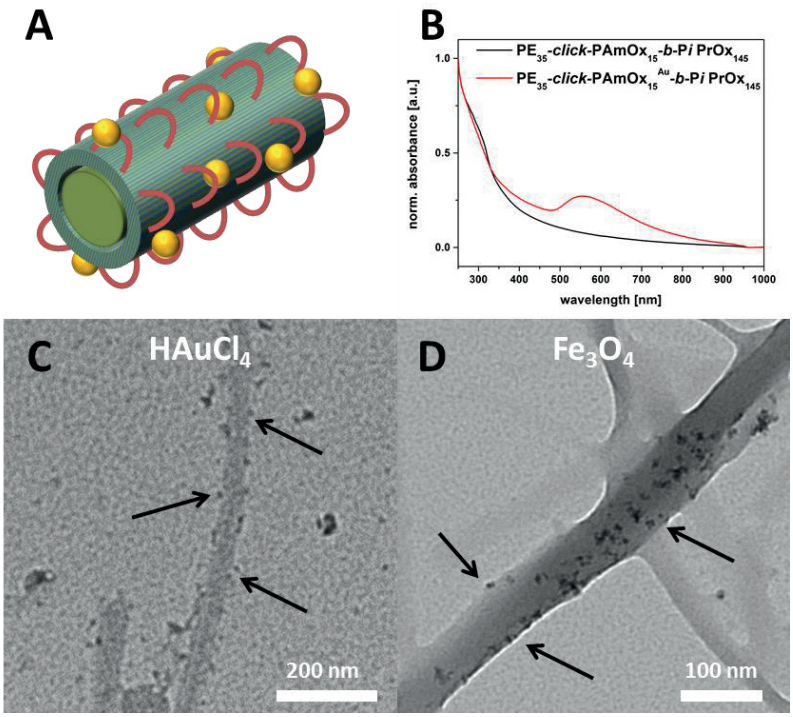

Figure 29: A) Illustration of fibers for PE_{35}-*click*-$PAmOx_{15}$-b-P*i*$PrOx_{145}$ and the complexation of metal nanoparticles; B) comparison of UV-Vis spetra for PE_{35}-*click*-$PAmOx_{15}$-b-P*i*$PrOx_{145}$ (black trace) and PE_{35}-*click*-$PAmOx_{15}^{Au}$-b-P*i*$PrOx_{145}$ (red trace); C-D) TEM micrographs of PE_{35}-*click*-$PAmOx_{15}$-b-P*i*$PrOx_{145}$ fibers with: C) Au ions (reduced in-situ by $NaBH_4$), E) Fe-NP (arrows indicate position of complexed material).

The next step would be an in-depth investigation of the crystallization of P*i*PrOx by a combination of DLS, TEM, SEM and X-ray scattering at different time intervals and concentrations. These materials are of potential interest for the formation of nano-fibers containing metal ions or nanoparticles in a certain domain of the fiber.

4.4 Hybrid Fe_3O_4@Amino Cellulose Nanoparticles in Organic Media: Heterogeneous Ligands for Atom Transfer Radical Polymerizations

Parts of this chapter have been published: **P12)** Fidale, L.C.; Nikolajski, M.; Rudolph, T.; Dutz, S.; Schacher, F. H.; Heinze, T.; *J. Colloid Interface Sci.*, 2012, 390, 25-33.

The formation of hybrid materials between magnetic nanoparticles (MNP) and different polymer shells has been described in the literature for several examples such as carboxymethylated polysaccharide, dextran, polyvinylalcohol (PVA), or polydiacetylene.[118-121, 191] In this chapter the use of superparamagnetic iron oxide nanoparticles (Fe_3O_4) coated with amino cellulose of two different molar masses (Fe_3O_4@AC_x, Figure 30A) is described. The corresponding nanoparticles were investigated concerning their composition *via* zeta-potential measurements, thermogravimetry (TGA), and vibrating sample magnetometry (VSM), indicating the presence of a cellulose shell around the Fe_3O_4 core. In case of VSM measurements (Figure 30B) the magnetic properties of the nanoparticles, pristine and Fe_3O_4@AC_x, show characteristics for superparamagnetic behavior, while the saturation magnetization decreases for the coated nanoparticles in comparison to the pristine samples. A decrease corresponds to the presence of nonmagnetic material on the surface of the NP, while the molar mass of the amino cellulose used for the coating did not influence the shell thickness, with respect to the accuracy of the measurement.[192] Beside the coating of the nanoparticles, the use of such hybrid materials for metal complexation, due to the structural similarity of the amino cellulose to *N*,*N*,*N*′,*N*″,*N*″-pentamethyldiethylenetriamine (PMDETA), was investigated as a possible ligand in controlled polymerizations. In this case the Fe_3O_4@AC_x were dispersed in *N,N*-dimethylacetamide (DMAC) together with styrene, copper bromide (CuBr), and α-bromo-*iso*-butyrate under standard ATRP reaction conditions. *Via* this approach polystyrene with different molar mass and low dispersity indices (Đ) were synthesized and investigated *via* SEC and NMR (Figure 30C).

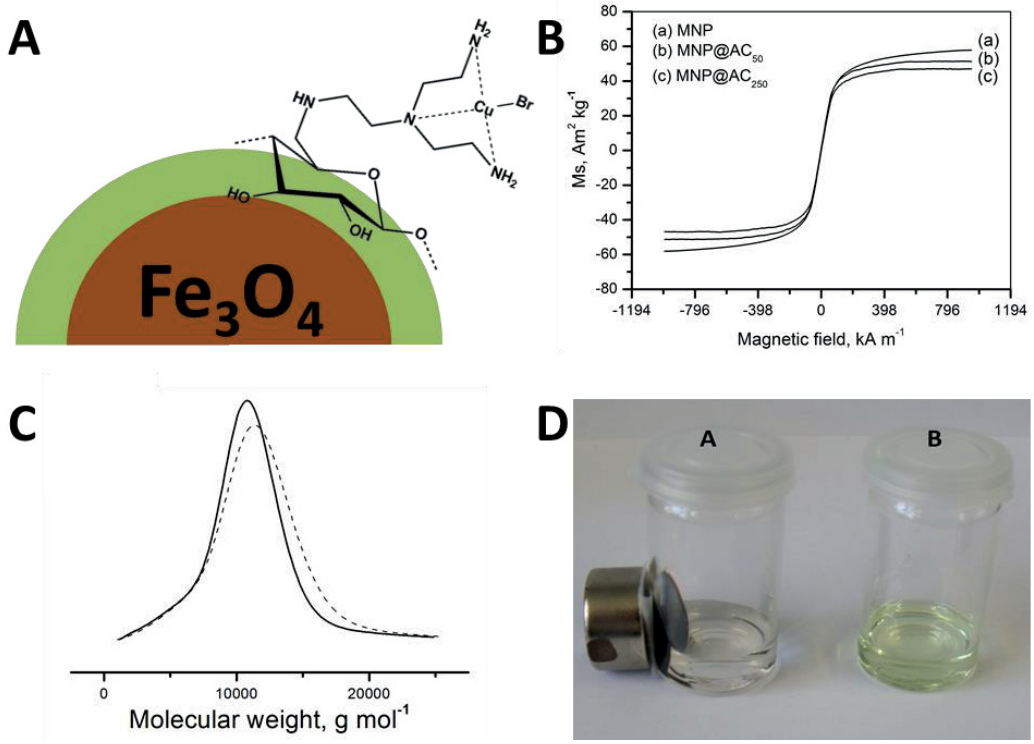

Figure 30: A) Amino cellulose and coated MNPs; B) comparison of magnetic hysteresis curves for MNP, MNP@AC$_{50}$ and MNP@AC$_{250}$; C) comparison of molar mass distributions for the ATRP of styrene in a first batch, and a second polymerization batch (straight line) with the same MNP@AC; D) images of reaction solutions after ATRP using MNP@AC (A) and PMDETA (B) as ligands.

In a second approach, the copper was removed by separating the MNP@AC hybrid particles using a magnet (Figure 30D), and the supernatant solution was removed under inert atmosphere. Afterwards, a new stock solution of monomer and initiator was added to the reaction vial. In the next step the polymerization was performed again at similar reaction conditions. The second polymerization of styrene showed similar results for the obtained PS from the first batch, confirming the ability to reuse the cellulose-coated NP for a scavenger for copper ions and their use in the ATRP of styrene (Figure 30 C). After removal of the Fe_3O_4@AC$_x$, the content of remaining copper in the obtained polymer is negligible (4.9 ppm), due to the stable complexation of the copper to the nanoparticles.

5) Summary

Controlled polymerization techniques, either radical or ionic, are powerful tools for polymer synthesis and materials with defined functionalities in either side-chain or as endgroup. In addition, efficient and reliable techniques for post-polymerization linkage of polymer chains by endgroup functionalization have been developed, like e.g. cycloaddition reactions. In this thesis the copper-catalyzed azide-alkyne cycloaddition (CuAAC) reaction was chosen, whenever direct sequential polymerization of involved monomers was challenging or not possible at all. For this purpose the synthesis of alkyne- and azide-modified macromolecular building blocks was realized by functional initiators or termination agents as described in Chapter 2.1. The subsequent linkage of the building blocks into different macromolecular architectures was shown for low molecular weight bolaamphiphiles, linear diblock copolymers, triblock terpolymers, and star-shaped polymers (Scheme 13; Chapter 2.1.4).

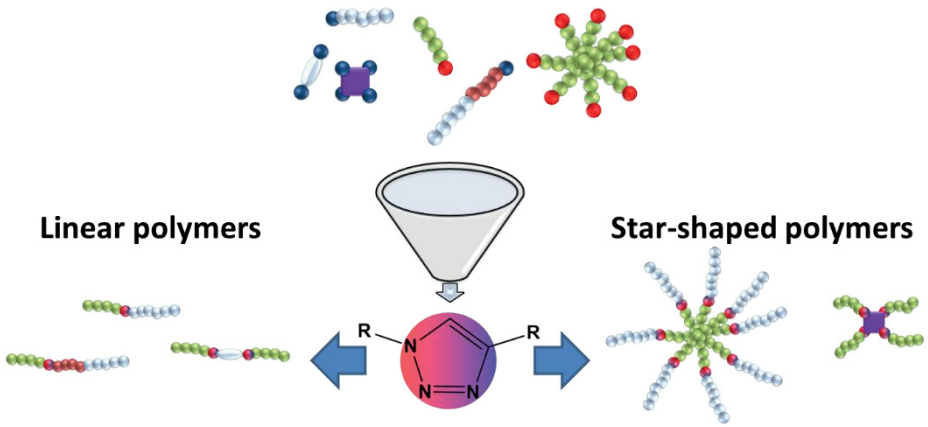

Scheme 13: Formation of linear and star-shaped (block co-) polymers by CuAAC chemistry.

On the other hand, we were interested in the synthesis of side-chain functionalized polymeric materials using the following monomer units: 2-*tert*-butyl-2-oxazoline (*t*-ButOx; Chapter 2.2.1), furfuryl glycidyl ether (FGE; Chapter 2.2.2), and maleimide thiolactone (MITla; Chapter 2.2.3).

For all monomers the homopolymerization, as well as the copolymerization was shown, and the resulting materials could be characterized by various techniques. In case of FGE containing block copolymers, controlled crosslinking of the FGE segment in solution by Diels-Alder (DA) reactions between the furan moieties and a bismaleimide was shown. This concept was further extended to block copolymer films as potentially self-healing surfaces. For this purpose, thin and homogenous films of the block copolymer were crosslinked, a scratch applied to the surfaces, and "healed" by retro-Diels-Alder (rDA) and subsequent DA reactions (Scheme 14).

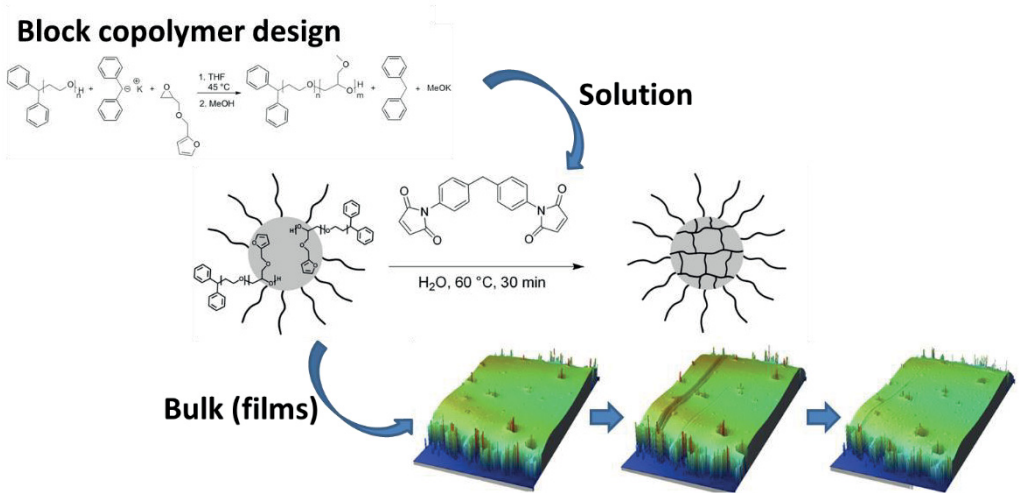

Scheme 14: Illustration of block copolymer design, and selective crosslinking in solution or block copolymer films.

In the second part, we focused on the self-assembly of different systems like bolaamphiphiles (Chapter 3.1), diblock copolymers (Chapter 3.2), and supramolecular star-shaped polymers formed by host-guest chemistry (Chapter 3.3).

For ABA bolaamphiphilies, containing an 1,4-bis[(4-ethynylphenyl)ethynyl]benzene (OPE; segment B) and two oligo(2-ethyl-2-oxazoline) based side chains with different chain length, the assembly mechanism in water was studied in detail. Two different aggregation mechanisms, isodesmic and cooperative, were found depending on the side-chain length. For the bolaamphiphiles with long side chains an isodesmic aggregation mechanism to small spherical aggregates was found, while in case of short side chains a cooperative aggregation towards plate-like aggregates occurred (Scheme 15).

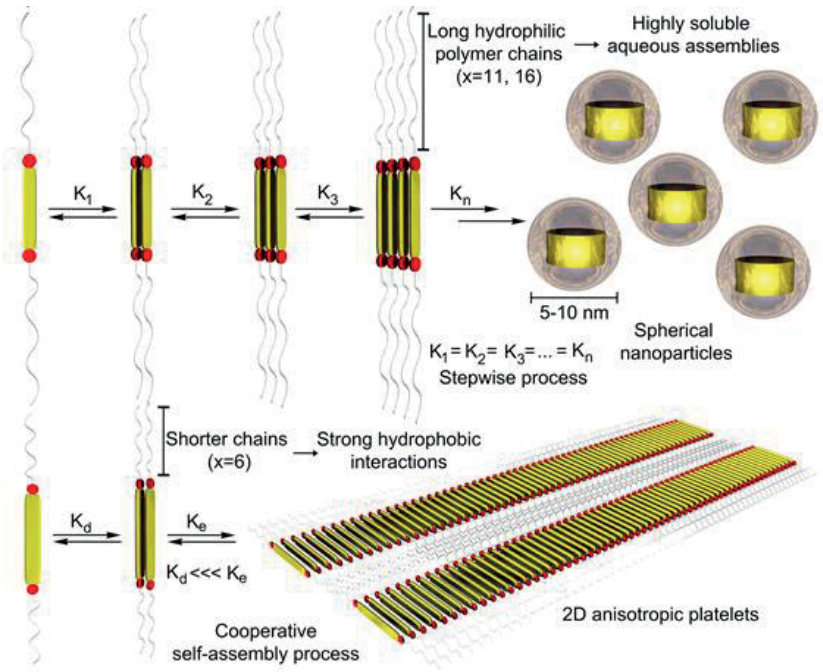

Scheme 15: Illustration of isodesmic and cooperative assembly mechanism for ABA bolaamphiphiles.

In the last part, the synthesis and formation of hybrid materials is shown by either the selective introduction of metals into certain domains of nanostructured materials or *via* metal complexation, e.g. within a porphyrin cavity (Chapter 4.1) or within triblock terpolymer micelles (Chapter 4.3). On the other hand, the template-assisted formation of nanoporous NiO_x films by block copolymer templating and subsequent calcination (Chapter 4.2) the use of core/shell hybrid nanoparticles as heterogeneous ligands for the ATRP of styrene was demonstrated (Chapter 4.4).

By using a suitably designed ABC triblock terpolymer, we were able to demonstrate a new strategy for the formation of hybrid nanowires *via* a combination of metal complexation and directional crystallization. Both Au NPs and Fe_3O_4 nanocrystals could be selectively loaded into one domain of (poly(2-(4-amino)butyl-2-oxzaoline)) and the subsequent crystallization of the poly(2-*iso*-propyl-2-oxazoline) corona led to the formation of macroscopic aggregates by directional crystallization (Figure 31).

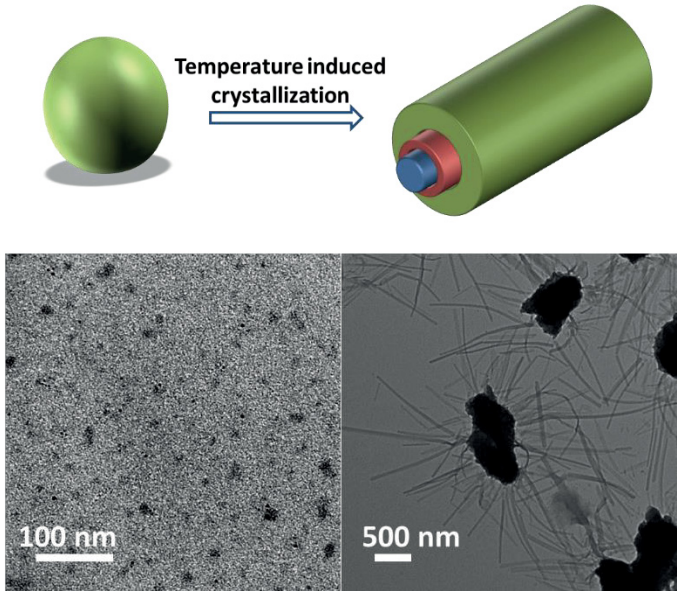

Figure 31: Illustration of sequential temperature induced crystallization of spherical micelles towards anisotropic superstructures in aqueous solution; TEM micrographs for spherical (before heating) and anisotropic superstructures obtained after heating.

In a "bottom-up" approach, this thesis showed the synthesis of functional macromolecular building blocks (endgroup and side-chain functionalized), their covalent linkage into different macromolecular architectures and, finally, self-assembly into hierarchical superstructures or hybrid materials.

The different systems demonstrated in this work combine (block co-) polymer design, functionalization, and self-assembly. Whilst in all cases bottom-up approaches are shown, materials with potential for application as coatings, sensors, or molecular electronics could be generated.

6) Zusammenfassung

Kontrollierte Polymerisationstechniken, radikalischer oder ionischer Art, sind geeignete Methoden für die Herstellung von Polymeren aus verschiedenen Monomeren und die Gewinnung von funktionalisierten Materialien, welche in den letzten Jahrzehnten weiterentwickelt wurden. Zudem können nachträgliche Verknüpfungen von Polymeren durch Einführung funktioneller Endgruppen und effizienter Reaktionen, wie zum Beispiel die Cycloaddition, erreicht werden. In dieser Arbeit wurde auf die sogenannte kupfer-katalysierte Azid-Alkin Cycloadditionsreaktion (CuAAC) zurückgegriffen, sobald eine direkte Copolymerisation von unterschiedlichen Monomeren schwierig oder nicht realisierbar war. Hierfür wurden Alkin- oder Azid-funktionalisierte makromolekulare Bausteine durch funktionelle Initiatoren oder Terminierungsreagenzien, wie in Kapitel 2.1 beschrieben, hergestellt. Deren nachgeschaltete Verknüpfung wurde an Beispielen von niedermolekularen ABA Bolaamphiphilen, linearen Diblockcopolymeren, Triblockterpolymeren und auch sternförmigen Polymeren gezeigt (Schema 16; Kapitel 2.1.4).

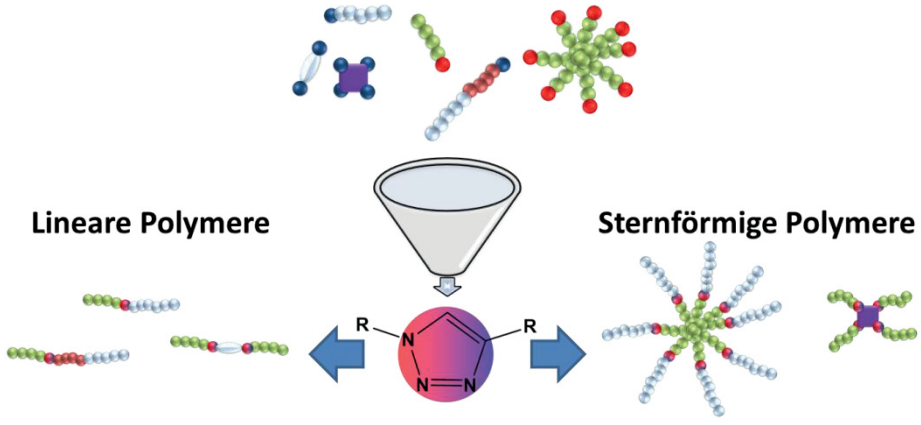

Schema 16: Darstellung der Herstellung von linearen und stern-förmigen (Co-) Polymeren mittels CuAAC.

Neben der Endgruppenfunktionalisierung wurde auch die Synthese von seitenketten-funktionalisierten Copolymeren mit folgenden Monomeren verfolgt: 2-*tert*-Butyl-2-Oxazolin (*t*ButOx; Kapitel 2.2.1), Furfurylglycidylether (FGE; Kapitel 2.2.2) und Maleimide thiolactone (MITla; Kapitel 2.2.3).

Für alle Monomere wurde sowohl die Homopolymerisation, als auch die Copolymerisation gezeigt und die erhaltenen Materialien mittels unterschiedlicher Methoden untersucht. Im Falle von FGE basierten Blockcopolymeren konnte die kontrollierte Vernetzung von FGE Segmenten in Lösung mittels Diels-Alder (DA) Reaktion zwischen Furan und Bismaleimiden gezeigt werden. Dieses Konzept wurde ferner auf Blockcopolymer-Filme erweitert, um potentiell selbstheilende Oberflächen zu generieren. Hierfür wurden dünne homogene Filme des Blockcopolymers vernetzt, ein Kratzer auf der Oberfläche zugeführt und dieser über Retro Diels-Alder (rDA) und DA Reaktionen wieder verschlossen (Schema 17).

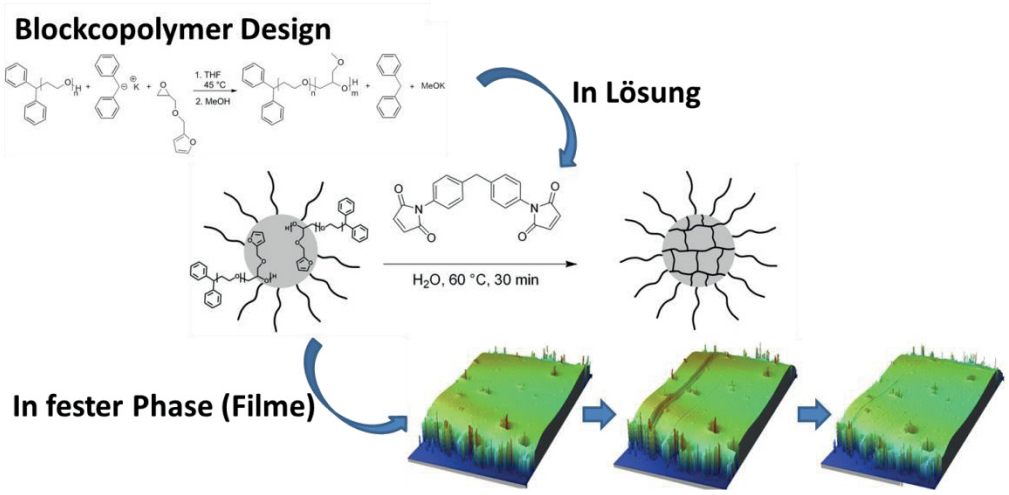

Schema 17: Darstellung eines Konzepts von Blockcopolymer-Design, über selektive Vernetzung in Lösung und in fester Phase (Filmen).

Im zweiten Teil wurde das Assemblierungsverhalten von ABA Bolaamphiphilen (Kapitel 3.1), Diblockcopolymeren (Kapitel 3.2) und sternförmige Polymeren mittels Wirts-Gast Einschlussverbindung (Kapitel 3.3) in Lösung untersucht.

Für ABA Bolaamphiphile, basierend auf 1,4-bis[4 ethynylphenyl)ethynyl]benzene (OPE, Segment B) und zwei Seitenketten aus 2-Ethyl-2-oxazolin-Oligomeren (EtOx; Segment A) mit verschiedenen Kettenlängen, konnte gezeigt werden, dass sich der Assemblierungsmechanismus in Wasser unterschiedlich darstellt. In Abhängigkeit ihrer Kettenlänge konnte zwischen einem isodesmischen und einen cooperativen Mechanismus unterschieden werden. Dies äußert sich durch die Ausbildung von sphärischen Aggregaten für lange Seitenketten (isodesmischer Prozess) und plättchenartigen Aggregaten, resultierend aus einem kooperativer Mechanismus, bei kurzen Seitenketten (Schema 18).

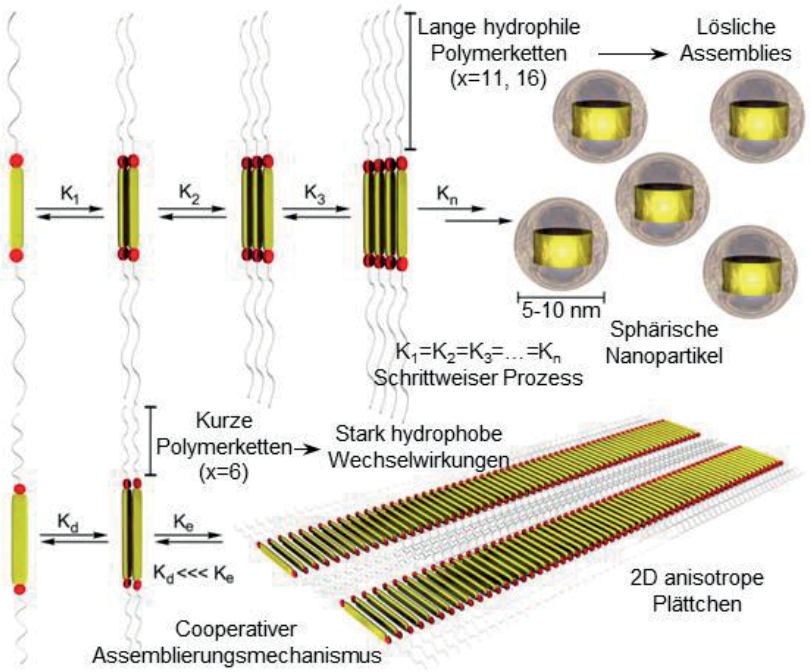

Schema 18: Darstellung des isodesmischen und kooperativen Assemblierungsmechanismus von ABA Bolaamphiphilen.

Im letzten Teil der Arbeit stand die Synthese von Hybridmaterialien, entweder durch das selektive Einbringen von Metallen in ausgewählte Bereiche der Nanostrukturen oder durch Komplexierung von Metallionen. Letzteres wurde an den Beispielen von Porphyrin (Kapitel 4.1) und Triblockterpolymer Mizellen (Kapitel 4.3) gezeigt. Während Metall/Polymer-Hybride durch Diblockcopolymer-Mizellen zur Herstellung von NiO_x Filme verwendet wurden (Kapitel 4.2) oder Polymer/Nanopartikel-Systeme als heterogener Liganden für die ATRP von Styrol verwendet wurden (Kapitel 4.4).

Des Weiteren konnte durch ein geeignetes Polymerdesign von ABC Triblockterpolymere ein neuer Weg zur Herstellung von potentiellen Hybrid Nanodrähten gezeigt werden, da sie sowohl zur Metallkomplexierung, als auch zur gezielten Kristallisation geeignet sind. Gold-Nanopartikel, als auch Fe_3O_4-Nanokristalle konnten selektiv in den Bereich von Poly(2-(4-amino)butyl-2-oxazolin) eingebracht werden, während in der nachgeschalteten Kristallisation der Poly(2-*iso*-propyl-2-oxazolin)-Korona zur Ausbildung von makroskopischen Aggregaten führte (Abbildung 32).

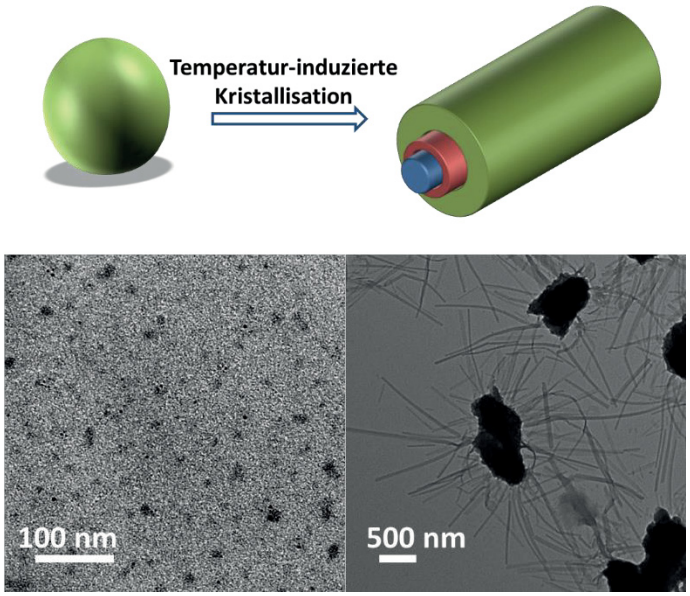

Abbildung 32: Darstellung der anschließenden Temperatur-induzierten Kristallisation von sphärischen Mizellen zu anisotropen Überstrukturen in Wasser; TEM Aufnahmen sphärischer (vorm Heizen) und Überstrukturen die nach dem Heizen beobachtet wurden.

Im Zuge des „Bottom-up"-Ansatzes konnte innerhalb dieser Arbeit die Synthese von funktionalisierten Polymeren (Endgruppen- und Seitengruppen-funktionalisiert), deren Verknüpfung zu verschieden Architekturen und zuletzt die Ausbildung zu hierarchischen Überstrukturen oder zu Hybridmaterialien zusammengefasst werden.

Die verschiedenen gezeigten Systeme dieser Arbeit vereinen (Blockco-) Polymer-Design, Funktionalisierung und Selbstassemblierung. Obwohl in allen Fällen „Bottom-up"-Ansätze verfolgt wurden, konnten Materialien zur potenziellen Anwendung in Beschichtungen, Sensorik oder Nanoelektronik realisiert werden.

7) References

1. H. Ringsdorf, *Angew. Chem. Int. Ed.*, 2004, **43**, 1064-1076.
2. R. Mülhaupt, *Angew. Chem. Int. Ed.*, 2004, **43**, 1054-1063.
3. H. Staudinger and J. Fritschi, *Helv. Chim. Acta*, 1922, **5**, 785-806.
4. H. Staudinger, *Ber. Dtsch. Chem. Ges.*, 1920, **53**, 1073-1085.
5. M. Szwarc, *Nature*, 1956, **178**, 1168-1169.
6. M. Szwarc, M. Levy and R. Milkovich, *J. Am. Chem. Soc.*, 1956, **78**, 2656-2657.
7. D. H. Richards and M. Szwarc, *Trans. Faraday Soc.*, 1959, **55**, 1644-1650.
8. K. Matyjaszewski and A. H. E. Müller, *Prog. Polym. Sci.*, 2006, **31**, 1039-1040.
9. J.-S. Wang and K. Matyjaszewski, *Macromolecules*, 1995, **28**, 7901-7910.
10. K. Matyjaszewski and J. H. Xia, *Chem. Rev.*, 2001, **101**, 2921-2990.
11. Moad G., Rizzardo E. and Thang S. H., *Aust. J. Chem.*, 2006, **10**, 669-692.
12. G. Moad, E. Rizzardo and S. H. Thang, *Aust. J. Chem.*, 2005, **58**, 379-410.
13. C. J. Hawker, A. W. Bosman and E. Harth, *Chem. Rev.*, 2001, **101**, 3661-3688.
14. A. Choucair and A. Eisenberg, *Eur. Phys. J. E.*, 2003, **10**, 37-44.
15. Y. Mai and A. Eisenberg, *Chem. Soc. Rev.*, 2012, **41**, 5969-5985.
16. C. Diehl and H. Schlaad, *Macromol. Biosci.*, 2009, **9**, 157-161.
17. V. Aseyev, H. Tenhu and F. Winnik, in *Self Organized Nanostructures of Amphiphilic Block Copolymers II*, eds. A. H. E. Müller and O. Borisov, Springer Berlin Heidelberg, 2011, vol. 242, ch. 57, pp. 29-89.
18. C. Weber, R. Hoogenboom and U. S. Schubert, *Prog. Polym. Sci.*, 2012, **37**, 686-714.
19. M. Meyer, M. Antonietti and H. Schlaad, *Soft Matter*, 2007, **3**, 430-431.
20. J. Rasburn, R. Petersen, T. Jahr, R. Rulkens, I. Manners and G. J. Vancso, *Chem. Mater.*, 1995, **7**, 871-877.
21. J. B. Gilroy, T. Gädt, G. R. Whittell, L. Chabanne, J. M. Mitchels, R. M. Richardson, M. A. Winnik and I. Manners, *Nat. Chem.*, 2010, **2**, 566-570.
22. W.-N. He and J.-T. Xu, *Prog. Polym. Sci.*, 2012, **37**, 1350-1400.
23. E. Rossegger, V. Schenk and F. Wiesbrock, *Polymers*, 2013, **5**, 956-1011.
24. K. Knop, R. Hoogenboom, D. Fischer and U. S. Schubert, *Angew. Chem. Int. Ed.*, 2010, **49**, 6288-6308.
25. H. Schlaad, C. Diehl, A. Gress, M. Meyer, A. L. Demirel, Y. Nur and A. Bertin, *Macromol. Rapid Commun.*, 2010, **31**, 511-525.
26. K. A. Davis and K. Matyjaszewski, *Adv. Polym. Sci.*, 2002, **159**, 107-152.
27. F. S. Bates and G. H. Frederickson, *Annu. Rev. Phys. Chem.*, 1990, **41**, 525-557.
28. F. S. Bates and G. H. Fredrickson, *Physics Today*, 1999, **52**, 32-38.
29. C. Auschra and R. Stadler, *Macromolecules*, 1993, **26**, 2171-2174.
30. H. C. Kolb, M. G. Finn and K. B. Sharpless, *Angew. Chem. Int. Ed.*, 2001, **40**, 2004-2021.
31. J. P. Collman, N. K. Devaraj and C. E. D. Chidsey, *Langmuir*, 2004, **20**, 1051-1053.

32. R. Luxenhofer and R. Jordan, *Macromolecules*, 2006, **39**, 3509-3516.
33. W. H. Binder and R. Sachsenhofer, *Macromol. Rapid Commun.*, 2007, **28**, 15-54.
34. H. Durmaz, A. Dag, O. Altintas, T. Erdogan, G. Hizal and U. Tunca, *Macromolecules*, 2007, **40**, 191-198.
35. D. Fournier, R. Hoogenboom and U. S. Schubert, *Chem. Soc. Rev.*, 2007, **36**, 1369-1380.
36. L. Billiet, D. Fournier and F. Du Prez, *Polymer*, 2009, **50**, 3877-3886.
37. R. K. Iha, K. L. Wooley, A. M. Nyström, D. J. Burke, M. J. Kade and C. J. Hawker, *Chem. Rev.*, 2009, **109**, 5620-5686.
38. J. Iehl and J.-F. Nierengarten, *Chem. Commun.*, 2010, **46**, 4160-4162.
39. M. J. Kade, D. J. Burke and C. J. Hawker, *J. Polym. Sci. Part A: Polym. Chem.*, 2010, **48**, 743-750.
40. C. Barner-Kowollik, F. E. Du Prez, P. Espeel, C. J. Hawker, T. Junkers, H. Schlaad and W. Van Camp, *Angew. Chem. Int. Ed.*, 2011, **50**, 60-62.
41. H. Durmaz, A. Sanyal, G. Hizal and U. Tunca, *Polym. Chem.*, 2012, **3**, 825-835.
42. K. Kempe, A. Krieg, C. R. Becer and U. S. Schubert, *Chem. Soc. Rev.*, 2012, **41**, 176-191.
43. W. Xi, T. F. Scott, C. J. Kloxin and C. N. Bowman, *Adv. Funct. Mater.*, 2014, **24**, 2572-2590.
44. P. Espeel and F. E. Du Prez, *Macromolecules*, 2015, **48**, 2-14.
45. K. Lava, B. Verbraeken and R. Hoogenboom, *Eur. Polym. J.*
46. A. B. Lowe, *Polym. Chem.*, 2010, **1**, 17.
47. A. Gandini, *Prog. Polym. Sci.*, 2013, **38**, 1-29.
48. L. Liang and D. Astruc, *Coord. Chem. Rev.*, 2011, **255**, 2933-2945.
49. A. S. Goldmann, M. Glassner, A. J. Inglis and C. Barner-Kowollik, *Macromol. Rapid Commun.*, 2013, **34**, 810-849.
50. U. Mansfeld, C. Pietsch, R. Hoogenboom, C. R. Becer and U. S. Schubert, *Polym. Chem.*, 2010, **1**, 1560-1598.
51. V. V. Rostovtsev, L. G. Green, V. V. Fokin and K. B. Sharpless, *Angew. Chem.*, 2002, **114**, 2708-2711.
52. V. O. Rodionov, V. V. Fokin and M. G. Finn, *Angew. Chem. Int. Ed.*, 2005, **44**, 2210-2215.
53. M. Shelbourne, X. Chen, T. Brown and A. H. El-Sagheer, *Chem. Commun.*, 2011, **47**, 6257-6259.
54. F. Schoenebeck, D. H. Ess, G. O. Jones and K. N. Houk, *J. Am. Chem. Soc.*, 2009, **131**, 8121-8133.
55. J. M. Baskin, J. A. Prescher, S. T. Laughlin, N. J. Agard, P. V. Chang, I. A. Miller, A. Lo, J. A. Codelli and C. R. Bertozzi, *Proc. Natl. Acad. Sci.*, 2007, **104**, 16793-16797.
56. L. Tietze and G. Kettschau, in *Stereoselective Heterocyclic Synthesis I*, ed. P. Metz, Springer Berlin Heidelberg, 1997, vol. 189, ch. 1, pp. 1-120.
57. J. D. Winkler, *Chem. Rev.*, 1996, **96**, 167-176.
58. T. Paulöhrl, A. J. Inglis and C. Barner-Kowollik, *Adv. Mater.*, 2010, **22**, 2788-2791.
59. G. Hizal, U. Tunca and A. Sanyal, *J. Polym. Sci. Part A: Polym. Chem.*, 2011, **49**, 4103-4120.
60. S. Sarkar, E. Bekyarova, S. Niyogi and R. C. Haddon, *J. Am. Chem. Soc.*, 2011, **133**, 3324-3327.
61. C. Gousse, A. Gandini and P. Hodge, *Macromolecules*, 1998, **31**, 314-321.
62. Y.-L. Liu and T.-W. Chuo, *Polym. Chem.*, 2013, **4**, 2194.
63. J. A. Syrett, C. R. Becer and D. M. Haddleton, *Polym. Chem.*, 2010, **1**, 978.

64. M. J. Barthel, T. Rudolph, A. Teichler, R. M. Paulus, J. Vitz, S. Hoeppener, M. D. Hager, F. H. Schacher and U. S. Schubert, *Adv. Funct. Mater.*, 2013, **23**, 4921-4932.
65. B. J. Blaiszik, S. L. B. Kramer, S. C. Olugebefola, J. S. Moore, N. R. Sottos and S. R. White, *Annu. Rev. Mater. Res.*, 2010, **40**, 179-211.
66. A. J. Inglis and C. Barner-Kowollik, *Macromol.Rapid Commun.*, 2010, **31**, 1247-1266.
67. A. J. Inglis, M. H. Stenzel and C. Barner-Kowollik, *Macromol. Rapid Commun.*, 2009, **30**, 1792-1798.
68. M. Langer, J. Brandt, A. Lederer, A. S. Goldmann, F. H. Schacher and C. Barner-Kowollik, *Polym. Chem.*, 2014, **5**, 5330-5338.
69. A. B. Lowe, *Polym. Chem.*, 2014, **5**, 4820-4870.
70. S. P. S. Koo, M. M. Stamenović, R. A. Prasath, A. J. Inglis, F. E. Du Prez, C. Barner-Kowollik, W. Van Camp and T. Junkers, *J. Polym. Sci. Part A: Polym. Chem.*, 2010, **48**, 1699-1713.
71. P. Derboven, D. R. D'hooge, M. M. Stamenovic, P. Espeel, G. B. Marin, F. E. Du Prez and M.-F. Reyniers, *Macromolecules*, 2013, **46**, 1732-1742.
72. P. Espeel, L. L. G. Carrette, K. Bury, S. Capenberghs, J. C. Martins, F. E. Du Prez and A. Madder, *Angew. Chem. Int. Ed.*, 2013, **52**, 13261-13264.
73. P. Espeel, F. Goethals, F. Driessen, L.-T. T. Nguyen and F. E. Du Prez, *Polym. Chem.*, 2013, **4**, 2449-2456.
74. A. Gress, A. Völkel and H. Schlaad, *Macromolecules*, 2007, **40**, 7928-7933.
75. M. J. Barthel, K. Babiuch, T. Rudolph, J. Vitz, S. Hoeppener, M. Gottschaldt, M. D. Hager, F. H. Schacher and U. S. Schubert, *J. Polym. Sci. Part A: Polym. Chem.*, 2012, **50**, 2914-2923.
76. S. Billiet, K. De Bruycker, F. Driessen, H. Goossens, V. Van Speybroeck, J. M. Winne and F. E. Du Prez, *Nat. Chem.*, 2014, **6**, 815-821.
77. D. D. Díaz, S. Punna, P. Holzer, A. K. McPherson, K. B. Sharpless, V. V. Fokin and M. G. Finn, *J. Polym. Sci. Part A: Polym. Chem.*, 2004, **42**, 4392-4403.
78. U. Tunca, *J. Polym. Sci. Part A: Polym. Chem.*, 2014, **52**, 3147-3165.
79. M. A. Gauthier, M. I. Gibson and H. A. Klok, *Angew. Chem. Int. Ed.*, 2009, **48**, 48-58.
80. P. Espeel and F. E. Du Prez, *Eur. Polym. J.*, 2015, **62**, 247-272.
81. S. Reinicke, P. Espeel, M. M. Stamenović and F. E. Du Prez, *ACS Macro Letters*, 2013, **2**, 539-543.
82. P. Espeel, F. Goethals and F. E. Du Prez, *J. Am. Chem. Soc.*, 2011, **133**, 1678-1681.
83. U. Günther, L. V. Sigolaeva, D. V. Pergushov and F. H. Schacher, *Macromol. Chem. Phys.*, 2013, **214**, 2202-2212.
84. M. Hartlieb, D. Pretzel, K. Kempe, C. Fritzsche, R. M. Paulus, M. Gottschaldt and U. S. Schubert, *Soft Matter*, 2013, **9**, 4693.
85. T. Heuser, A. K. Steppert, C. Molano Lopez, B. Zhu and A. Walther, *Nano Lett.*, 2015, **15**, 2213-2219.
86. L. Zhang and A. Eisenberg, *Polym. Adv. Technol.*, 1998, **9**, 677-699.
87. A. Walther, A. S. Goldmann, R. S. Yelamanchili, M. Drechsler, H. Schmalz, A. Eisenberg and A. H. E. Müller, *Macromolecules*, 2008, **41**, 3254-3260.
88. G. Fernández, M. Stolte, V. Stepanenko and F. Würthner, *Chem. Eur. J.*, 2013, **19**, 206-217.
89. G. Fernandez, F. Garcia, F. Aparicio, E. Matesanz and L. Sanchez, *Chem. Commun.*, 2009, 7155-7157.
90. C. Rest, M. J. Mayoral and G. Fernandez, *Int. J. Mol. Sci.*, 2013, **14**, 1541-1565.
91. J. W. Steed and J. L. Atwood, eds., *Supramolecular Chemistry*, Book; John Wiley & Son, Ltd., 2009.

92. G. V. Oshovsky, D. N. Reinhoudt and W. Verboom, *Angew. Chem. Int. Ed.*, 2007, **46**, 2366-2393.
93. R. J. Moon, A. Martini, J. Nairn, J. Simonsen and J. Youngblood, *Chem. Soc. Rev.*, 2011, **40**, 3941-3994.
94. J. A. Massey, K. Temple, L. Cao, Y. Rharbi, J. Raez, M. A. Winnik and I. Manners, *J. Am. Chem. Soc.*, 2000, **122**, 11577-11584.
95. T. Gädt, N. S. Ieong, G. Cambridge, M. A. Winnik and I. Manners, *Nat. Mater.*, 2009, **8**, 144-150.
96. J.-H. Ryu, D.-J. Hong and M. Lee, *Chem. Commun.*, 2008, 1043-1054.
97. T. F. A. De Greef, M. M. J. Smulders, M. Wolffs, A. P. H. J. Schenning, R. P. Sijbesma and E. W. Meijer, *Chem. Rev.*, 2009, **109**, 5687-5754.
98. Z. Chen, A. Lohr, C. R. Saha-Moller and F. Würthner, *Chem. Soc. Rev.*, 2009, **38**, 564-584.
99. C. Sanchez, B. Julian, P. Belleville and M. Popall, *J. Mater. Chem.*, 2005, **15**, 3559-3592.
100. S. Mann, *Nat. Mater.*, 2009, **8**, 781-792.
101. S. Förster and T. Plantenberg, *Angew. Chem. Int. Ed.*, 2002, **41**, 688-714.
102. J. Yuan, F. Schacher, M. Drechsler, A. Hanisch, Y. Lu, M. Ballauff and A. H. E. Müller, *Chem. Mater.*, 2010, **22**, 2626-2634.
103. J. Yuan, A. Walther and A. H. E. Müller, *Phys. Status Solidi*, 2010, **247**, 2436-2450.
104. F. H. Schacher, T. Rudolph, M. Drechsler and A. H. E. Müller, *Nanoscale*, 2011, **3**, 288-297.
105. H. Zhang, Y. Liu, D. Yao and B. Yang, *Chem. Soc. Rev.*, 2012, **41**, 6066-6088.
106. V. Ďorďovič, M. Uchman, A. Zhigunov, A. Nykänen, J. Ruokolainen and P. Matějíček, *ACS Macro Letters*, 2014, **3**, 1151-1155.
107. C. Hoerenz, T. Rudolph, M. J. Barthel, U. Guenther and F. H. Schacher, *Polym. Chem.*, 2015, DOI: 10.1039/C1034PY01434K.
108. D. A. Rider and I. Manners, *Polym. Rev.*, 2007, **47**, 165-195.
109. X. Wang, G. Guerin, H. Wang, Y. Wang, I. Manners and M. A. Winnik, *Science*, 2007, **317**, 644-647.
110. P. A. Rupar, L. Chabanne, M. A. Winnik and I. Manners, *Science*, 2012, **337**, 559-562.
111. A. Nunns, J. Gwyther and I. Manners, *Polymer*, 2013, **54**, 1269-1284.
112. Z. M. Hudson, C. E. Boott, M. E. Robinson, P. A. Rupar, M. A. Winnik and I. Manners, *Nat. Chem.*, 2014, **6**, 893-898.
113. D. Bogdal, S. Bednarz and K. Matras-Postolek, in *Adv. Polym. Sci.*, Springer Berlin Heidelberg, 2015, ch. 296, pp. 1-15.
114. S. Förster and M. Antonietti, *Adv. Mater.*, 1998, **10**, 195-217.
115. B. L. Rivas, E. D. Pereira and I. Moreno-Villoslada, *Prog. Polym. Sci.*, 2003, **28**, 173-208.
116. T. Kaliyappan and P. Kannan, *Prog. Polym. Sci.*, 2000, **25**, 343-370.
117. S. R. Batten, *Curr. Opin. Solid State and Mater. Sci.*, 2001, **5**, 107-114.
118. J. Wotschadlo, T. Liebert, T. Heinze, K. Wagner, M. Schnabelrauch, S. Dutz, R. Müller, F. Steiniger, M. Schwalbe, T. C. Kroll, K. Höffken, N. Buske and J. H. Clement, *J. Magn. Magn. Mater.*, 2009, **321**, 1469-1473.
119. S. Dutz, W. Andrä, R. Hergt, R. Müller, C. Oestreich, C. Schmidt, J. Töpfer, M. Zeisberger and M. E. Bellemann, *J. Magn. Magn. Mater.*, 2007, **311**, 51-54.
120. M. Chastellain, A. Petri and H. Hofmann, *J. Colloid Interface Sci.*, 2004, **278**, 353-360.

121. X. Chen, L. Li, X. Sun, Y. Liu, B. Luo, C. Wang, Y. Bao, H. Xu and H. Peng, *Angew. Chem. Int. Ed.*, 2011, **50**, 5486-5489.
122. J. Yuan and A. H. E. Müller, *Polymer*, 2010, **51**, 4015-4036.
123. M. M. Cheng, G. Cuda, Y. L. Bunimovich, M. Gaspari, J. R. Heath, H. D. Hill, C. A. Mirkin, A. J. Nijdam, R. Terracciano, T. Thundat and M. Ferrari, *Curr. Opin. Chem. Biol.*, 2006, **10**, 11-19.
124. W. Lu and C. M. Lieber, *Nat. Mater.*, 2007, **4**, 841-850.
125. R. Hoogenboom, M. W. M. Fijten and U. S. Schubert, *J. Polym. Sci. Part A: Polym. Chem.*, 2004, **42**, 1830-1840.
126. R. Hoogenboom, M. W. M. Fijten, H. M. L. Thijs, B. M. Van Lankvelt and U. S. Schubert, *Des. Monomers Polym.*, 2005, **8**, 659-671.
127. F. Wiesbrock, R. Hoogenboom, M. A. M. Leenen, M. A. R. Meier and U. S. Schubert, *Macromolecules*, 2005, **38**, 5025-5034.
128. J. M. Warakomski and B. P. Thill, *J. Polym. Sci. Part A: Polym. Chem.*, 1990, **28**, 3551-3563.
129. C. Weber, S. Rogers, A. Vollrath, S. Hoeppener, T. Rudolph, N. Fritz, R. Hoogenboom and U. S. Schubert, *J. Polym. Sci. Part A: Polym. Chem.*, 2013, **51**, 139-148.
130. M. Reif and R. Jordan, *Macromol. Chem. Phys.*, 2011, **212**, 1815-1824.
131. S. Huber, N. Hutter and R. Jordan, *Colloid Polym. Sci.*, 2008, **286**, 1653-1661.
132. A. Nunns, C. A. Ross and I. Manners, *Macromolecules*, 2013, **46**, 2628-2635.
133. R. Briquel, J. Mazzolini, T. Le Bris, O. Boyron, F. Boisson, F. Delolme, F. D'Agosto, C. Boisson and R. Spitz, *Angew. Chem. Int. Ed.*, 2008, **47**, 9311-9313.
134. B. V. K. J. Schmidt, T. Rudolph, M. Hetzer, H. Ritter, F. H. Schacher and C. Barner-Kowollik, *Polym. Chem.*, 2012, **3**, 3139-3145.
135. T. Rudolph, S. Crotty, M. v. d. Lühe, D. Pretzel, U. S. Schubert and F. H. Schacher, *Polymers*, 2013, **5**, 1081-1101.
136. M. J. Mayoral, C. Rest, V. Stepanenko, J. Schellheimer, R. Q. Albuquerque and G. Fernandez, *J. Am. Chem. Soc.*, 2013, **135**, 2148-2151.
137. M. T. Fenske, W. Meyer-Zaika, H.-G. Korth, H. Vieker, A. Turchanin and C. Schmuck, *J. Am. Chem. Soc.*, 2013, **135**, 8342-8349.
138. F. t. García, J. Buendía and L. Sánchez, *J. Org. Chem.*, 2011, **76**, 6271-6276.
139. C. M. A. Leenders, L. Albertazzi, T. Mes, M. M. E. Koenigs, A. R. A. Palmans and E. W. Meijer, *Chem. Comm.*, 2013, **49**, 1963-1965.
140. H. Frisch, J. P. Unsleber, D. Lüdeker, M. Peterlechner, G. Brunklaus, M. Waller and P. Besenius, *Angew. Chem. Int. Ed.*, 2013, **52**, 10097-10101.
141. M. Arseneault, I. Levesque and J.-F. Morin, *Macromolecules*, 2012, **45**, 3687-3694.
142. R. Huisgen, *Proc. Chem. Soc.*, 1961, 357-396.
143. B. Gerard, J. Ryan, A. B. Beeler and J. A. Porco, *Tetrahedron*, 2006, **62**, 6405-6411.
144. G. Lapienis, *Prog. Polym. Sci.*, 2009, **34**, 852-892.
145. N. Hadjichristidis, H. Iatrou, M. Pitsikalis and J. Mays, *Prog. Polym. Sci.*, 2006, **31**, 1068-1132.
146. N. Hadjichristidis, M. Pitsikalis, S. Pispas and H. Iatrou, *Chem. Rev.*, 2001, **101**, 3747-3792.
147. M. Pitsikalis, S. Pispas, J. Mays and N. Hadjichristidis, *Adv. Polym. Sci.*, 1998, **135**, 1-137.
148. Y. C. Yu, H. S. Cho, W.-R. Yu and J. H. Youk, *Polymer*, 2014.
149. M. Einzmann and W. H. Binder, *J. Polym. Sci. Part A: Polym. Chem.*, 2001, **39**, 2821-2831.

150. S. Kobayashi, H. Uyama, Y. Narita and J. Ishiyama, *Macromolecules*, 1992, **25**, 3232-3236.
151. T. K. Bera and S. Sivaram, *Macromol. Chem. Phys.*, 1995, **196**, 1515-1522.
152. T. Rudolph, K. Kempe, S. Crotty, R. M. Paulus, U. S. Schubert, I. Krossing and F. H. Schacher, *Polym. Chem.*, 2013, **4**, 495-505.
153. K. Kempe, M. Lobert, R. Hoogenboom and U. S. Schubert, *J. Comb. Chem.*, 2009, **11**, 274-280.
154. T. G. Bassiri, A. Levy and M. Litt, *J. Polymer Sci. B: Polym. Lett.*, 1967, **5**, 871-879.
155. M. Litt, F. Rahl and L. G. Roldan, *J. Polym. Sci. Part A-2: Polym. Phys.*, 1969, **7**, 463-&.
156. S. Huber and R. Jordan, *Colloid Polym. Sci.*, 2008, **286**, 395-402.
157. R. Hoogenboom, M. W. M. Fijten, H. M. L. Thijs, B. M. van Lankvelt and U. S. Schubert, *Des. Monomers Polym.*, 2005, **8**, 659-671.
158. C. Hörenz, T. Rudolph, M. J. Barthel, U. Günther and F. H. Schacher, *Polym. Chem.*, 2014.
159. M. Zamfir and J.-F. Lutz, *Nat. Comm.*, 2012, **3**, 1138.
160. P. Espeel, F. Goethals, M. M. Stamenović, L. Petton and F. E. Du Prez, *Polym. Chem.*, 2012, **3**, 1007-1015.
161. P. Espeel, F. Goethals and F. E. Du Prez, *J. Am. Chem. Soc.*, 2011, **133**, 1678-1681.
162. T. Aida, E. W. Meijer and S. I. Stupp, *Science*, 2012, **335**, 813-817.
163. C. Kulkarni, S. Balasubramanian and S. J. George, *Chem. Phys. Chem.*, 2013, **14**, 661-673.
164. D. Zhao and J. S. Moore, *Org. Biomol. Chem.*, 2003, **1**, 3471-3491.
165. C. A. Hunter, *Angew. Chem. Int. Ed.*, 2004, **43**, 5310-5324.
166. A. J. Markvoort, H. M. ten Eikelder, P. A. Hilbers, T. F. de Greef and E. W. Meijer, *Nat. Comm.*, 2011, **2**, 509.
167. H. M. M. ten Eikelder, A. J. Markvoort, T. F. A. de Greef and P. A. J. Hilbers, *J. Phys. Chem. B*, 2012, **116**, 5291-5301.
168. H. Frisch and P. Besenius, *Macromol. Rapid Commun.*, 2014, n/a-n/a.
169. H. Frisch, Y. Nie, S. Raunser and P. Besenius, *Chem. Eur. J.*, 2015.
170. F. Wendler, T. Rudolph, G. Fernandez and F. H. Schacher, *in preparation*, 2015.
171. N. McGrath, F. H. Schacher, H. Qiu, S. Mann, M. A. Winnik and I. Manners, *Polym. Chem.*, 2014, **5**, 1923.
172. S. F. Mohd Yusoff, J. B. Gilroy, G. Cambridge, M. A. Winnik and I. Manners, *J. Am. Chem. Soc.*, 2011, **133**, 11220-11230.
173. I. Korczagin, M. A. Hempenius, R. G. Fokkink, M. A. C. Stuart, M. Al-Hussein, P. H. H. Bomans, P. M. Frederik and G. J. Vancso, *Macromolecules*, 2006, **39**, 2306-2315.
174. M. Zhang, P. A. Rupar, C. Feng, K. Lin, D. J. Lunn, A. Oliver, A. Nunns, G. R. Whittell, I. Manners and M. A. Winnik, *Macromolecules*, 2013, **46**, 1296-1304.
175. J.-F. Gohy, B. G. G. Lohmeijer, A. Alexeev, X.-S. Wang, I. Manners, M. A. Winnik and U. S. Schubert, *Chem. Eur. J.*, 2004, **10**, 4315-4323.
176. A. Natalello, A. Alkan, A. Friedel, I. Lieberwirth, H. Frey and F. R. Wurm, *ACS Macro Letters*, 2013, **2**, 313-316.
177. C. Diehl, P. Cernoch, I. Zenke, H. Runge, R. Pitschke, J. Hartmann, B. Tiersch and H. Schlaad, *Soft Matter*, 2010, **6**, 3784-3788.
178. A. L. Demirel, M. Meyer and H. Schlaad, *Angew. Chem. Int. Ed.*, 2007, **46**, 8622-8624.
179. B. V. K. J. Schmidt, M. Hetzer, H. Ritter and C. Barner-Kowollik, *Prog. Polym. Sci.*, 2014, **39**, 235-249.

180. B. V. K. J. Schmidt, M. Hetzer, H. Ritter and C. Barner-Kowollik, *Macromolecules*, 2011, **44**, 7220-7232.
181. P. Kujawa, F. Segui, S. Shaban, C. Diab, Y. Okada, F. Tanaka and F. M. Winnik, *Macromolecules*, 2006, **39**.
182. L.-H. Gan, W. Cai and K. C. Tam, *Eur. Polym. J.*, 2001, **37**, 1773-1778.
183. X. Wang and C. Wu, *Macromolecules*, 1999, **32**, 4299-4301.
184. H. Mao, C. Li, Y. Zhang, S. Furyk, P. S. Cremer and D. E. Bergbreiter, *Macromolecules*, 2004, **37**, 1031-1036.
185. P. Kujawa and F. M. Winnik, *Macromolecules*, 2001, **34**, 4130-4135.
186. H. Dinçer, H. Mert, B. N. Şen, A. Dağ and S. Bayraktar, *Dyes Pigm.*, 2013, **98**, 246-254.
187. M. Bräutigam, M. Schulz, J. Inglis, J. Popp, J. G. Vos and B. Dietzek, *Phys. Chem. Chem. Phys.*, 2012, **14**, 15185-15190.
188. C. Diehl, P. Černoch, I. Zenke, H. Runge, R. Pitschke, J. Hartmann, B. Tiersch and H. Schlaad, *Soft Matter*, 2010, **6**, 3784.
189. L. M. Bronstein, S. N. Sidorov, A. Y. Gourkova, P. M. Valetsky, J. Hartmann, M. Breulmann, H. Cölfen and M. Antonietti, *Inorg. Chim. Acta*, 1998, **280**, 348-354.
190. F. Kretschmer, U. Mansfeld, S. Hoeppener, M. Hager and U. S. Schubert, *Chem. Commun.*, 2013, **50**, 88-90.
191. J. Y. Park, E. S. Choi, M. J. Baek and G. H. Lee, *Mater. Lett.*, 2009, **63**, 379-381.
192. S. Dutz and R. Hergt, *J. Nano-Electron. Phys.*, 2012, **4**, 02010.

8) List of Abbreviations

AC	Amino cellulose
Ada	Adamantyl functionalized polymer
AGE	Allyl glycidyl ether
AIBN	Azo-bis-(isobutyronitrile)
AROP	Anionic ring opening polymerization
ATRP	Atom transfer radical polymerization
BocAmOx	2-(4-((*tert*-butoxycarbonyl)amino)butyl-2-oxazoline
BuLi	Butyl lithium
CD	β-Cyclodextrine
$CHCl_3$	Chloroform
CRP	Controlled radical polymerization
CROP	Cationic ring opening polymerization
CuAAC	Copper-catalyzed azide-alkyne cycloaddition
CuBr	Copper(I) bromide
Đ	Dispersity index
D_2O	Deuterium oxide
DA	Diels-Alder
DCM	Dichloromethane
DLS	Dynamic light scattering
DMAC	Dimethylacetamide
DMF	Dimethylformamide
DMSO	Dimethylsulfoxide

DP	Degree of polymerization
DPE	Diphenylethylene
DPMK	Diphenylmethyl potassium
DSC	Differential scanning calorimetry
EA	Elemental analysis
EO	Ethylene oxide
EtOx	2-Ethyl-2-oxazoline
Fe_3O_4	Ironoxide
FGE	Furfuryl glycidyl ether
FT-IR	Fourier transformed infrared
H_2O	Water
*i*PrOx	2-*iso*-propyl-2-oxazoline
LCST	Lower critical solution temperature
MALDI-TOF	Matrix-assisted laser desorption/ionization time of flight
MAN	Maleic anhydride
MS	Mass spectrometry
MITla	Maleimide thiolactone
MNP	magnetic nanoparticle
N_3	Azide
NiO_x	Nickel oxide
NIPAAm	*N*-*iso*-propylacrylamide
NMP	Nitroxide-mediated polymerization
NMR	Nuclear magnetic resonance
NP	Nanoparticle
OPE	1,4-bis[(4-ethynylphenyl)ethynyl]benzene
P2VP	Poly(2-vinylpyridine)
PAmOx	Poly(2-(4-amino)butyl-2-oxazoline)
PBocAmOx	Poly(2-(4-((*tert*-butoxycarbonyl)amino)butyl-2-oxazoline)
PDMAAm	Poly(*N,N*-dimethylacrylamide)
PDEAAm	Poly(*N,N*-diethylacrylamide)
PE	Polyethylene
PEO	Poly(ethylene oxide)
PEG	Poly(ethylene glycol)
PEtOx	Poly(2-ethyl-2-oxazoline)

PFS	Poly(ferrocenyl silane)
PFDMS	Poly(ferrocenyldimethylsilane)
PFGE	Poly(furfuryl glycidyl ether)
P*i*PrOx	Poly(2-*iso*-propyl-2-oxazoline)
POx	Poly(2-alkyl-2-oxazoline)
PMDETA	*N*,*N*,*N*′,*N*″,*N*″-pentamethyldiethylenetriamine
PS	Polystyrene
P*t*ButOx	Poly(2-*tert*-butyl-2-oxazoline)
RAFT	Reversible addition-fragmentation chain transfer
rDA	Retro-Diels-Alder
SAXS	Small angle x-ray scattering
SEC	Size exclusion chromatography
SEM	Scanning electron microscopy
SLS	Static light scattering
T_{cp}	Cloud point temperature
T_g	Glass transition temperature
T_m	Melting temperature
TB	Trible bond
TB-Ts	Propargyl *p*-toluenesulfonate
*t*ButOx	2-*tert*-butyl-2-oxazoline
TEA	Triethylamine
TEM	Transmission electron microscopy
TGA	Thermogravimetric analysis
THF	Tetrahydrofuran
TPO	2,4,6-Trimethylbenzoyldiphenylphosphine oxide (Lucirin TPO; BASF)
TPP	5,10,15,20-Tetrakis(4-hydroxyphenyl)-21H,23H-porphine
Ts	Tosylate
WAXS	Wide angle x-ray scattering
wt.%	Weight fraction

Curriculum Vitae

Personal information:

Last name: Rudolph

First name: Tobias

Date of birth: 16th February 1986

Place of birth: Coburg, Germany

Citizenship: German

Marital status: Married

Education:

Since 10/2011	PhD-Student in macromolecular chemistry Title: "Design of Polymeric Building Blocks: Synthesis and Preparation of Different Polymer Architectures or Hybrid Materials" *Friedrich Schiller University of Jena* *Supervision:* Prof. Dr. F. H. Schacher
10/2009-10/2011	Master-Student in "Polymer Science" Title: "Core-Shell Colloids" *University of Bayreuth* *Supervision:* Prof. Dr. A. H. E. Müller *Cooperation:* Prof. Dr. F. H. Schacher (*Friedrich Schiller University of Jena*)
10/2006-10/2009	Bachelor-Student in "Polymer- and Colloid Chemistry" Title: "Cylindrical, Crosslinked Terpolymer Micelles with a Discontinuous Shell" *University of Bayreuth* *Supervision:* Prof. Dr. A. H. E. Müller
1996-2006	Abitur (corresponds A-levels) *Gymnasium Ernestinum Coburg*

Jena,

_____

Tobias Rudolph

Publication List

Peer-reviewed publications:

1) Schacher, F.; **Rudolph, T.**; Wieberger, F.; Ulbricht, M.; Müller, A. H. E.; "Double Stimuli-Responsive Ultrafiltration Membranes from Polystyrene-block-poly(N,N-dimethylaminoethyl methacrylate) Diblock Copolymers"; *ACS Appl. Mater. Int.*, **2009**, 1, 1492-1503.

2) Schacher, F. H.; **Rudolph, T.**; Drechsler, M.; Müller, A. H. E.; "Core-Crosslinked Compartmentalized Cylindrical Micelles"; *Nanoscale*, **2011**, 3, 288-297.

3) Altintas, O.; **Rudolph, T.**; Barner-Kowollik, C.; "Single Chain Self-Assembly of Well-Defined Heterotelechelic Polymers Generated by ATRP and Click Chemistry"; *J. Polym. Sci. Part A: Polym. Chem.*, **2011**, 49, 2566–2576.

4) Barthel, M. J.; Babiuch, K.; **Rudolph, T.**; Vitz, J.; Hoeppener, S.; Gottschaldt, M.; Schacher, F. H.; Schubert, U. S.; „Bis-hydrophilic and Functional Triblock Terpolymers Based on Polyethers: Synthesis and Self-Assembly in Solution"; *J. Polym. Sci. Part A: Polym. Chem.*, **2012**, 50, 2914-2923.

5) Schmidt, B.V.K.J.; **Rudolph, T.**; Hetzer, M.; Ritter, H.; Schacher, F.H.; Barner-Kowollik, C.; "Supramolecular Three-Armed Star Polymers via Cyclodextrin Host/Guest Self-Assembly"; *Polym. Chem.*, **2012**, 3, 3139-3145.

6) Barthel, M. J.; **Rudolph, T.**; Crotty S.; Schacher, F. H. and Schubert, U. S.; "Homo- and Block Copolymers of Poly(furfuryl glycidyl ether) by Living Anionic Polymerization: Towards Reversibly Core-Crosslinked Micelles"; *J. Polym. Sci. Part A: Polym. Chem.*, **2012**, 50, 4958-4965.

7) Rettler, E. F.-J.; **Rudolph, T.**; Hanisch, A.; Schacher, F. H.; Schubert, U. S.; "Crosslinking of the Polybutadiene Domains of Polystyrene-block-polybutadiene Block Copolymer Films – An In-Depth Study"; *Polymer*, **2012**, 53, 5641-5648.

8) **Rudolph, T.**; Kempe, K.; Crotty, S.; Paulus, R. M.; Schubert, U. S.; Krossing, I.; Schacher, F. H.; "A Strong Cationic Brønsted Acid, $[H(OEt_2)_2][Al\{OC(CF_3)_3\}_4]$, as an Efficient Initiator for the Cationic Ring-Opening Polymerization of 2-Alkyl-2-Oxazolines"; *Polym. Chem.*, **2013**, 4, 495-505.

9) Fidale, L. C.; Nikolajski, M.; **Rudolph, T.**; Schacher, F. H.; Heinze, T.; "Hybrid Fe3O4@Amino Cellulose Nanoparticles in Organic Media: Heterogeneous Ligands for Atom Transfer Radical Polymerizations"; *J. Coll. Inter. Sci.*, **2013**, 390, 25-33.

10) Weber, C.; Vollrath, A.; **Rudolph, T.**; Hoeppener, S.; Hoogenboom, R.; Rogers, S.; Fritz, N.; Schubert. U. S.; "Aqueous solution behavior of comb shaped poly(2-ethyl-2-oxazoline)"; *J. Polym. Sci. Part A: Polym. Chem.*, **2013**, 51, 139-148.

11) Knop, K.; Pavlov, G. M.; **Rudolph, T.**; Martin, K.; Pretzel, D.; Jahn, B. O.; Scharf, D. H.; Brakhage, A.; Schacher, F. H.; Schubert, U. S.; "Amphiphilic star-shaped block copolymers as unimolecular drug delivery systems: investigations using a novel fungicide"; *Soft Matter*, **2013**, 9, 715-726.

12) Wotschadlo, J.; Liebert, T.; Clement, J. H.; Anspach, N.; Hoeppener, S.; **Rudolph, T.**; Müller, R.; Schacher, F. H.; Schubert, U. S.; Heinze, T.; "Biocompatible Multishell Architecture for Iron Oxide Nanoparticles"; *Biomacromolecules*, **2013**, 13, 93-105.

13) Barthel, M. J.; **Rudolph, T.**; Teichler, A.; Paulus, R.; Vitz, J.; Hoeppener, S.; Hager, M. D.; Schacher, F. H.; Schubert, U. S.; "Self-Healing Materials via Reversible Crosslinking of Poly(ethylene oxide)-*block*-poly(furfuryl glycidyl ether) (PEO-b-PFGE) Block Copolymer Films"; *Adv. Funct. Mater.*, **2013**, 39, 4921-4932.

14) Knop, K.; Pretzel, D.; Urbanek, A.; **Rudolph, T.**; Scharf, D.; Schallon, A.; Schubert, S.; Kiehntopf, M.; Brakhage, A.; Wagner, M.; Schacher, F. H.; Schubert, U. S.; "Star-shaped drug carriers for doxorubicin with POEGMA and POEtOxMA brush-like shells: A structural, physical and biological comparison"; *Biomacromolecules*; **2013**, 14, 2536-2548.

15) **Rudolph, T.**; Crotty, S.; Lühe, M. v. d.; Pretzel, D.; Schubert, U. S.; Schacher, F. H.; "Synthesis and Solution Properties of Double Hydrophilic Poly(ethylene oxide)-*block*-poly(2-ethyl-2-oxazoline) (PEO-*b*-PEtOx) Star Block Copolymers" *Polymers*, **2013**, 5, 1081-1101.

16) Bräutigam, M.; Weyell, P.; **Rudolph, T.**; Dellith, J.; Krieck, S.; Schmalz, H.; Schacher, F. H.; Dietzek, B.; "Porous NiOx Nanostructures Templated by Polystyrene-*block*-poly(2-vinylpyridine) Diblock Copolymer Micelles"; *J. Mater. Chem. A*, **2014**, 2, 6158-6166 *(Emerging Investigators Special Issue).*

17) **Rudolph, T.**; Barthel, M. J.; Kretschmer, F.; Mannsfeld, U.; Hoeppener, S.; Schubert, U. S.; Schacher, F. H.; "Poly(2-vinyl pyridine)-*block*-Poly(ethylene oxide) featuring a Furan Group at the Block Junction – Synthesis and Functionalization"; *Macromol. Rapid Commun.,* **2014**, 35, 916-921.

18) **Rudolph, T.**; Allampally, N. K.; Fernandez, G.; Schacher, F. H.; "Controlling Aqueous Self-Assembly Mechanisms via Hydrophobic Interactions"; *Chem. Eur. J.,* **2014***,* 43, 13871-13875.

19) Hörenz, C.; **Rudolph, T.**; Barthel, M. J.; Günther, U.; Schacher, F. H.; "Amphiphilic Polyether-based Block Copolymers as Crosslinkable Ligands for Au Nanoparticles"; *Polym.*

Chem.; **2015**, *in press* (*DOI: 10.1039/C4PY01434K*; *invited article for the 2015 issue on young emerging investigators*).

20) Rudolph, T.; Nunns, A.; Schwenk, A.; Schacher, F. H.; "Synthesis and Self-Assembly of Poly(ferrocenyldimethylsilane)-*block*-poly(2-alkyl-2-oxazoline) Block Copolymers"; *Polym. Chem.*, **2015**, 6, 1604-1612.

21) Rudolph, T.; Crotty, S,; Schubert, U. S.; Schacher, F. H.; "Symmetrical Porphyrin Centered Star-Shaped Poly-(2-ethyl-2-oxazoline): Synthesis, Characterization and Metal Embedding", *E-polymers*, **2015**, in press (DOI: 10.1515/epoly-2015-0041).

22) Can, A.; Zhang, Q.; **Rudolph, T.**; Schacher, F. H.; Gohy, J.-F.; Schubert, U. S.; Hoogenboom, R.; "Schizophrenic thermoresponsive block copolymer micelles based on LCST and UCST behavior in ethanol-water mixtures"; **2015**, Eur. Polym. J.; in press.

23) Rudolph, T.; Espeel, P.; Du Prez, F.; Schacher, F. H.; "Poly(thiolactone) Homo- and Copolymers from Maleimide Thiolactone: Synthesis and Functionalization"; *Polym. Chem.,* **2015***,* in press (DOI: 10.1039/C5PY00329F).

24) Rudolph, T.; Nunns, A.; Stumpf, S.; Pietsch, C.; Schacher, F. H.; "Hierarchical Self-Assembly of Double-Crystalline Poly(ferrocenyldimethylsilane)-*block*-poly(2-*iso*-propyl-2-oxazoline) (PFDMS-*b*-P*i*PrOx) Block Copolymers"; *Macromol. Rapid Commun.,* submitted.

25) Rudolph, T.; Hartlieb, M.; von der Lühe, M.; Norsic, S.; Schubert, U. S.; D´Agosto, F.; Schacher, F. H.; "Towards Anisotropic Hybrid Materials: Solution Self-Assembly of Linear Polyethylene-*block*-poly(2-(4-((*tert*-butoxycarbonyl)amino)butyl-2-oxazoline)–*block*-poly(2-*iso*-propyl-2-oxazoline) Triblock Terpolymers"; *in preparation*.

Non peer-reviewed publications:

1) Schacher, F.; **Rudolph, T.**; Ulbricht, M.; Mueller, A. H. E.; "Double stimuli-responsive porous membranes from polystyrene-block-poly(N,N-dimethyl-aminoethyl methacrylate) diblock copolymers", PMSE Preprints, **2009**, 100, 243-244; 22. – 26. März 2009, ACS National Meeting, Salt Lake City.

2) Rudolph, T.; Knop, K.; Kempe, K.; Schubert, U. S.; Schacher, F. H.; "Star-shaped block copolymers with a responsive poly(2-ethyl-2-oxazoline) shell: synthesis and self-assembly in dilute solution", PMSE Preprints, **2012**, ACS Conference, 25. – 29.03.2012, San Diego.

3) Rudolph, T.; Drechsler, M.; Sugimori, H.; Jinnai, H.; Müller, A. H. E.; Schacher, F. H.; "Compartmentalized Colloidal Particles via Bulk Crosslinking of ABC Triblock Terpolymers", PMSE Preprints, **2012,** ACS Conference, 25. – 29.03.2012, San Diego.

Oral presentations:

1) Rudolph, T., Schacher, F. H., "Hierarchische Selbstorganisation von Hybridmaterialien"; Research fellowship meeting of the Carl-Zeiss foundation, 20.-21.11.2013, Oberkochen (Germany).

2) Rudolph, T.; Nunns, A.; Stumpf, S.; Manners, I.; Schacher, F.H.; "*Synthesis and hierarchical self-assembly of amphiphilic poly(ferrocenyldimethylsilane)-block-poly(2-alkyl-2-oxazoline) block copolymers in organic and aqueous media*"; 247th American Chemical Society National Meeting & Exposition, 16.-20. March 2014, Dallas (USA).

Poster presentations:

1) Rudolph, T., Müller, A. H. E., Schacher, F. H., "*Core-crosslinked Nanoparticles from Polybutadiene–block–poly(2-vinyl pyridine)–block–poly(tert-butyl methacrylate) (BVT) Triblock Terpolymers"*, GDCH-Wissenschaftsforum, 04. - 07. September 2011, Bremen (Ger)

2) Rudolph, T.; Kempe, K.; Knop, K.; Schubert, U. S.; Schacher F. H. S.; *"Poly(2-Alkyl-2-Oxazolines) of different Architecture via Macromolecular Conjugation Reactions",* Macrogroup UK International Conference on Polymer Synthesis & UKPCF International Conference on Polymer Colloids; 9.-12. July 2012; Warwick (UK)

3) Schmidt, B. V. K. J.; **Rudolph, T.**; Hetzer, M.; Ritter, H.; Schacher, F. H.; Barner-Kowollik, C.; "*Supramolecular Three-Armed Star Polymers via Cyclodextrin Host/Guest Self-Assembly*"; GDCH Fachgruppen-Tagung, 7.-9.10.2012, Mainz (Ger)

4) Hörenz, C.; **Rudolph, T.**; Barthel, M. J.; Majdanski, T.; Schubert, U. S.; Schacher, F. H.; *"Well-defined Hybrid Au-Nanoparticles with a Diblock Copolymer Shell: Preparation and Crosslinking by Thiol-ene Chemistry*"; Frontiers, 2013, Barcelona

5) Rudolph, T.; Nunns, A.; Stumpf, S.; Manners, I.; Schacher, F. H.; "*Hierarchical Self-Assembly of Linear and Star-shaped Poly(2-alkyl-2-oxazoline) Block Copolymers*"; IUPAC

10th International Conference on Advanced Polymers via Macromolecular Engineering; 18.08.-22.08.2013, Durham (UK)

6) Rudolph, T., Schacher, F. H., "*Hierarchische Selbstorganisation von Hybridmaterialien"*; Research fellowship meeting of the Carl-Zeiss foundation, 20.-21.11.2013, Oberkochen (Ger)

7) Rudolph, T.; Nunns, A.; Stumpf, S.; Manners, I.; Schacher, F. H.; *"Hierarchical Self-Assembly of Well-defined Linear and Star-Shaped Block Copolymers Containing Poly(2-alkyl-2-oxazoline) Segments"*; Makromolekulares Kolloquium, 26.-28.02.2014 Freiburg (Ger)

8) Rudolph, T.; Allampally, N. K.; Fernandez, G.; Schacher, F. H.; "*Controlling Aqueous Supramolecular Self-Assembly Mechanisms via Hydrophobic Interactions*", GDCH Fachgruppen-Tagung (Macromolecular Chemistry), 14.-16.09.2014 Jena (Ger)

9) Rudolph, T., Schacher, F. H., "*Hierarchische Selbstorganisation von Hybridmaterialien"*; Research fellowship meeting of the Carl-Zeiss foundation, 16.-17.10.2014, Mainz (Ger)

Acknowledgements / Danksagung

Anhand der Publikationsliste wird schnell klar, dass meine Arbeit nicht ohne zahlreiche Co-Autoren möglich gewesen wären, die mir stets mit Rat und Tat zur Seite standen. In diesem Zusammenhang möchte ich mich bei all denjenigen bedanken, die mir bei Experimenten, Messungen oder Interpretationen geholfen haben.

Ein besonderer Dank geht an Prof. Felix H. Schacher, der mich in den letzten Jahren auf meinem Weg begleitet und geführt hat. Ich bin sehr dankbar für die Unterstützung, viele Diskussionen und das Vertrauen in mich. In meinen Jahren in der Gruppe wurde es mir immer wieder ermöglicht mich mit anderen Arbeitsgruppen (national wie auch international) im Rahmen von Forschungsaufenthalten oder Konferenzen auszutauschen, was mich um viele Erfahrungen bereichert hat.

Ein weiterer Dank geht zudem an Prof. U. S. Schubert, für all die Mühen und die Unterstützung der AG Schacher, wobei wir stets auf die Infrastruktur in seiner Gruppe zurückgreifen durften und er bei Problemen zur Verfügung stand.

Des Weiteren möchte ich mich auch bei Prof. C. Barner-Kowollik und Prof. A.H. E. Müller für ihre große Unterstützung bereits während meines Studiums und die Aufnahme ihn ihren Gruppen (Karlsruhe und Bayreuth) in dieser Zeit bedanken, sowie die kontinuierliche Unterstützung auch im Anschluss. I would like to thank Prof. F. E. Du Prez and Prof I. Manners for hosting me in their groups during my stay, as well as a lot of fruitful discussions concerning my projects and the great experiences I made.

Finanzielle Unterstützung erhielt ich hauptsächlich durch die Carl-Zeiss Stiftung im Rahmen eines Doktoranden-Stipendiums, sowie den Deutschen Akademischer Austauschdienst (DAAD) für Reisestipendien und der „European Science Foundation“ (ESF) für einen Auslandsaufenthalt.

Special thanks for all external cooperation partners during my work, like Özcan Altintas, Bernhard Schmidt, Naveen Allampally, Gustavo Fernandez, Pieter Espeel, Prof. Ingo

Krossing, Sebastien Norsic, Prof. Franck DÁgosto, from different Institutes corresponding to different projects I worked during my thesis.

Besonderer Dank geht auch an:
Uwe Köhn (Rat in Sicherheitsfragen), Renzo Paulus (Messungen und IT), Jürgen Vitz (Anionik, Glovebox, Rat und Tat), Katrin Knop (Diskussionen, Rat und Tat), Kristian Kempe (Rat und Tat), Matthias Hartlieb (Polymere, Projekte, Gespräche, Rat und Tat), Sandra Köhn (offenes Ohr), Sarah Crotty (alle Messungen), alle Sekretärinnen (für bürokratische Hilfestellung), Christine Weber, Florian Kretschmer, Lutz Tauhardt, Steffi Stumpf, Stephanie Höppener, Almut Schwenke, …. und noch vielen mehr.
Wen ich auch nicht vergessen will, ist die technische Seite, die alles am Laufen hält und ohne die die entsprechende Analytik nicht möglich wäre: Grit Festag (SEC), Dr. Günther und Frau Sentis (NMR Abteilung OC), Stephanie (TEM), Jürgen und Renzo, Hausmeister, ….

Besonders möchte ich mich auch bei meinen ehemaligen Kollegen und Praktikanten (oftmals ein und dieselbe Person) bedanken. Ihr habt mir häufig den Tag versüßt, konnten wir doch oft lachen und haben etliche schöne Stunden miteinander verbracht. Wen ich nie vergessen werde, wird Ulrike „Freier-Günther“ sein, da sie Bezugsperson der ersten Stunde in Jena für mich war und wir einfach sehr viel miteinander erlebt haben.
Eine weitere solche Person ist Markus Barthel, mit dem ich zahlreiche positive Erinnerungen verbinde. Unsere Zeit war doch sehr kreativ und ich hoff wir werden uns noch oft auf unseren Wegen treffen.
Sarah, Christoph, Moritz, Bob, Felix W., Mark: Wir haben so manch einen netten Abend miteinander verbracht und ich hoff wir verbleiben im Guten. Bleibt wie ihr seid ;-)
Meine Freunde aus Bayreuther Zeiten kann ich natürlich auch nicht ganz vergessen, da das Studium doch ein bedeutender Teil meines Weges bis hier her war. Diese Zeit war eine der lehrreichsten und ereignisreichsten und ich kann nur jedem danken der mich damals begleitet hat.

Eine wichtige Stütze durchs Studium und auch danach war stets meine Familie, die mich seelisch und moralisch unterstützt hat und während meiner Promotion durch meine Hochzeit noch weiter gewachsen ist.

Mein letzter Dank soll an meine Freundin, Wegbegleiterin und Frau Stefanie gehen. Ohne deine Unterstützung, Hilfe und Zureden wären Alltag, Studium/Promotion und alles andere nicht miteinander vereinbar gewesen. Kein anderer war so geduldig und aufmerksam, auch wenn ich nur von meinem langweiligen Laboralltag erzählt hab, wie du. Vielleicht konntest du selbst bis zu Letzt meine Begeisterung für die Polymerchemie nicht teilen, aber dennoch wusstest du stets wie du mich auf meinem nicht immer linearen Weg unterstützen kannst.

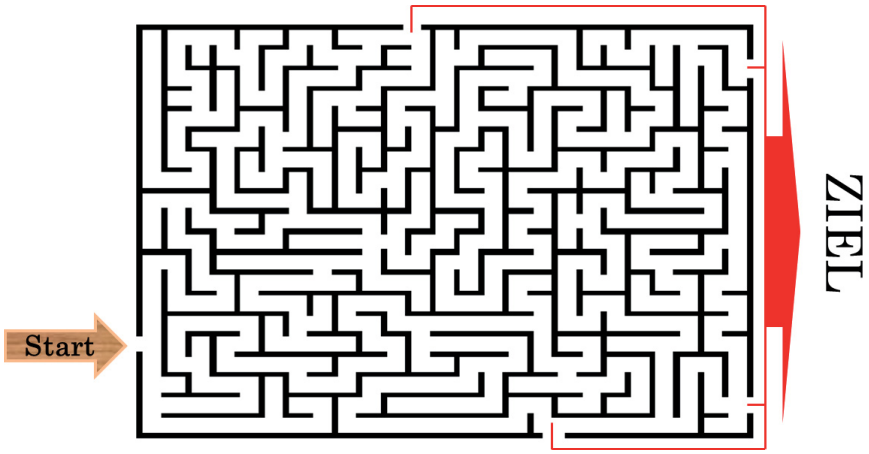

http://www.blume-programm.de/ab/boerse/jan_15/knobeln/mazes/25x20-01.gif (aufgerufen am 13.02.2015)

Declaration of Authorship / Selbstständigkeitserklärung

Ich erkläre, dass ich die vorliegende Arbeit selbständig und unter Verwendung der angegebenen Hilfsmittel, persönlichen Mitteilungen und Quellen angefertigt habe.

Jena, _____

Tobias Rudolph

Publication P1 – P14

Publication P1

“Synthesis and Solution Properties of Double Hydrophilic Poly(ethylene oxide)-*block*-poly(2-ethyl-2-oxazoline) (PEO-*b*-PEtOx Star Block Copolymers”

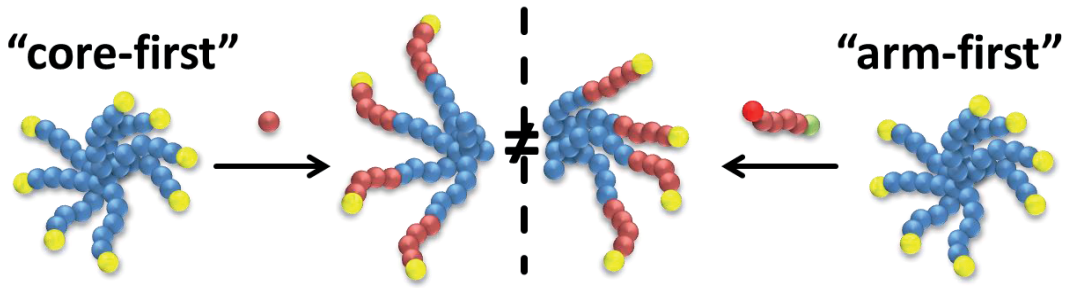

Tobias Rudolph, Sarah Crotty, Moritz von der Lühe, David Pretzel, Ulrich S. Schubert, Felix H. Schacher

Polymers, **2013**, 5, 1081-1101

Polymers **2013**, *5*, 1081-1101; doi:10.3390/polym5031081

OPEN ACCESS

polymers

ISSN 2073-4360

www.mdpi.com/journal/polymers

Article

Synthesis and Solution Properties of Double Hydrophilic Poly(ethylene oxide)-*block*-poly(2-ethyl-2-oxazoline) (PEO-*b*-PEtOx) Star Block Copolymers

Tobias Rudolph [1,2], Sarah Crotty [1,2,3], Moritz von der Lühe [1,2], David Pretzel [1,2], Ulrich S. Schubert [1,2,3] and Felix H. Schacher [1,2,*]

[1] Laboratory of Organic and Macromolecular Chemistry (IOMC), Friedrich Schiller University Jena, Humboldtstr. 10, Jena 07743, Germany; E-Mails: tobias.rudolph@uni-jena.de (T.R.); sarah.crotty@uni-jena.de (S.C.); moritz.von-der-luehe@uni-jena.de (M.L.); david.pretzel@uni-jena.de (D.P.); ulrich.schubert@uni-jena.de (U.S.S.)

[2] Jena Center for Soft Matter (JCSM), Friedrich Schiller University Jena, Philosophenweg 7, Jena 07743, Germany

[3] Dutch Polymer Institute, P.O. Box 902, Eindhoven 5600 AX, The Netherlands

* Author to whom correspondence should be addressed; E-Mail: felix.schacher@uni-jena.de; Tel.: +49 (0) 3641-9-48250; Fax: +49 (0) 3641-9-48252.

Received: 28 June 2013; in revised form: 27 July 2013 / Accepted: 19 August 2013 / Published: 2 September 2013

Abstract: We demonstrate the synthesis of star-shaped poly(ethylene oxide)-*block*-poly(2-ethyl-2-oxazoline) $[PEO_m$-*b*-$PEtOx_n]_x$ block copolymers with eight arms using two different approaches, either the "arm-first" or the "core-first" strategy. Different lengths of the outer PEtOx blocks ranging from 16 to 75 repeating units were used, and the obtained materials $[PEO_{28}$-*b*-$PEtOx_x]_8$ were characterized via size exclusion chromatography (SEC), nuclear magnetic resonance spectroscopy (NMR), and Fourier-transform infrared spectroscopy (FT-IR) measurements. First investigations regarding the solution behavior in water as a non-selective solvent revealed significant differences. Whereas materials synthesized via the "core-first" method seemed to be well soluble (unimers), aggregation occurred in the case of materials synthesized by the "arm-first" method using copper-catalyzed azide-alkyne click chemistry.

Keywords: poly(2-ethyl-2-oxazoline); star-shaped block copolymers; double hydrophilic block copolymers

1. Introduction

The synthesis of polymer-based materials using different monomers, material compositions and macromolecular architectures can be realized via a multitude of synthetic methodologies. Mainly living and controlled polymerization techniques were developed to obtain polymers with narrow molar mass distributions, adjustable chain length and precisely positioned functional groups [1]. Thereby, the architecture has a large influence on the physical properties of the final material. Moreover, the monomer distribution and composition along the polymer backbone directly influences the solubility and other physical properties [2–4]. This has been demonstrated for random, gradient, graft and block copolymers synthesized by different polymerization techniques [5–9]. In the case of linear homo- and (block) copolymers, the solution behavior has become quite predictable after a manifold of systematic studies for different monomer combinations and sequences during the last few decades [10–14]. On the other hand, the combination of polymer chains in one central point leads to star-shaped materials and can result in unprecedented morphologies, as well as solution behavior in selective and non-selective solvents [15–18].

Star-shaped amphiphilic block copolymers are of special interest in drug delivery applications, due to the absence of a critical micellar concentration (cmc, depending on the hydrophilic-to-hydrophobic balance of the system) and the possibility to take up and release suitable drugs. The "load" can be encapsulated into the inner part (core, hydrophobic) of the materials, while the outer shell (hydrophilic) stabilizes the system in, e.g., aqueous solution [19]. If poly(ethylene oxide) (PEO) is used as the shell, "stealth"-behavior can be observed, also known as "PEGylation", preventing the recognition of such materials by our immune system. This renders such approaches suitable for the preparation of long-circulating polymer-based drug nanocontainers [20–22].

For the synthesis of star-shaped block copolymers, mainly two approaches have been employed, the divergent ("core-first") and the convergent ("arm-first") method [20,23–27]. The divergent approach uses a multifunctional initiator, but typically not all initiation sites are easily accessible, which drastically influences the number of arms and the overall degree of polymerization. Nevertheless, with increasing distance between the core and the initiation site, the initiation efficiency can be improved. Nevertheless, star-star coupling often occurs during, e.g., radical polymerizations, and limits the monomer conversion (arm length) in such attempts [2,4,28,29]. As an alternative, the convergent approach employs pre-synthesized arms, which are subsequently connected to the core covalently in the final step, often providing superior control over arm length and number; moreover, an in-depth characterization of the constituting building blocks prior to joining the core and shell is possible. Such approaches have been described in the literature via supramolecular chemistry [24,30,31], metal-complexation [32] or click-chemistry [23,33,34].

Herein, we demonstrate the synthesis of star-shaped poly(ethylene oxide)-*block*-poly(2-ethyl-2-oxazoline) $[PEO_m$-*b*-$PEtOx_n]_x$ block copolymers with eight arms using two different approaches, either the "arm-first" or the "core-first" strategy. Regarding the core block, PEO-based materials of different architectures have been thoroughly investigated concerning solution behavior [35,36] or the possibility of being scaffolds in medical applications [19,20,22]. The outer block, poly(2-ethyl-2-oxazoline) (PEtOx), is water-soluble and non-toxic, and the pseudo-peptide character of this material has been shown to induce similar "stealth" behavior, as observed for PEO [19,22,37–39]. PEtOx can be

synthesized with a wide range of functional groups, being present via cationic ring-opening polymerization (CROP) [40–43]. We used different lengths of the outer PEtOx blocks, and the obtained [PEO_{28}-*b*-$PEtOx_x$]$_8$ materials were characterized via size exclusion chromatography (SEC), nuclear magnetic resonance spectroscopy (NMR) and Fourier-transform infrared spectroscopy (FT-IR). Whereas similar compositions could be prepared using either "core-first" or "arm-first" approaches, first investigations regarding the solution behavior in water as a non-selective solvent revealed significant differences.

2. Experimental Section

2.1. Instruments

NMR: Proton nuclear magnetic resonance (^{1}H-NMR) spectra were recorded in $CDCl_3$ on a Bruker AC 300 MHz spectrometer at 298 K. Chemical shifts are given in parts per million (ppm, δ scale) relative to the residual signal of the deuterated solvent. Carbon NMR (^{13}C-NMR) spectra were recorded with 75 MHz.

SEC: Size exclusion chromatography was measured on a Shimadzu system equipped with a SCL-10A system controller, an LC-10AD pump, an RID-10A refractive index detector and both a PSS Gram30 and a PSS Gram1000 column [Polymer Standards Services GmbH (Mainz, Germany)] in series, whereby *N*,*N*-dimethylacetamide (DMAC) with 5 mmol of lithium chloride (LiCl) was used as an eluent at a 1 mL min^{-1} flow rate. The column oven was set to 60 °C. The system was calibrated with polystyrene (PS; 100 to 1,000,000 g mol^{-1}) standards. Furthermore, a Shimadzu system equipped with an SCL-10A system controller, an LC-10AD pump and an RID-10A refractive index detector using a solvent mixture containing chloroform ($CHCl_3$), triethylamine (TEA) and *iso*-propanol (*i*-PrOH) (94:4:2) at a flow rate of 1 mL min^{-1} on a PSS SDV linear M 5 µm column. The system was calibrated using PS (100 to 100,000 g mol^{-1}) and PEO (440 to 44,700 g mol^{-1}) standards.

MALDI-ToF MS: Matrix-assisted laser desorption/ionization time of flight mass spectrometry was performed on an Ultraflex III TOF/TOF (Bruker Daltonics, Bremen, Germany), equipped with a Nd:YAG laser and with *trans*-2-[3-(4-*tert*-butylphenyl)-2-methyl-2-propenylidene] malononitrile (DCTB) as the matrix and NaCl as the doping agent in reflector and linear mode. The instrument was calibrated prior to each measurement with an external poly(methyl methacrylate) (PMMA) standard from PSS Polymer Standards Services GmbH (Mainz, Germany).

FT-IR Infra-red spectroscopy: Dry powders of the copolymers were directly placed on the crystal of the ATR-FTIR (Affinity-1 FTIR, Shimadzu) for measurements in the range of 4000 to 600 cm^{-1}.

Microwave-assisted polymerizations were carried out utilizing an Initiator Sixty single-mode microwave synthesizer from Biotage, equipped with a non-invasive IR sensor (accuracy: 2%). Microwave vials (conical, 0.5 to 2 mL) were heated at 110 °C overnight and allowed to cool to room temperature under nitrogen atmosphere. All polymerizations were carried out using temperature control.

DLS: Dynamic light scattering was performed at a scattering angle of 90° on an ALV CGS-3 instrument equipped with a He-Ne laser operating at a wavelength of 633 nm at 25 °C. Tetrahydrofuran (THF) [polytetrafluoroethylene (PTFE); 0.45 µm] and MilliQ-water [glass faser (GF); 1–2 µm] were filtered before usage. The CONTIN algorithm was applied to analyze the obtained

correlation functions. For temperature control, the DLS is equipped with a Lauda thermostat. Apparent hydrodynamic radii were calculated according to the Stokes-Einstein equation. All CONTIN plots shown are number-weighted.

SLS: For static light scattering (SLS), different concentrations between 1.5 and 3.5 mg mL^{-1} were prepared in THF and measured at 25 °C and different scattering angles (30° to 150°). Prior to the measurements, the samples and all solvents were filtered with PTFE-syringe filters (0.45 μm).

Liquid Chromatography under Critical Conditions (LCCC): High-performance liquid chromatography (HPLC) was measured on an Agilent system (series 1200) equipped with a binary pump, an autosampler and an evaporative light scattering detector (ELSD, Softa Corporation, Model 400). For the LCCC separation, a Nucleosil octadecylsilyl (ODS) column (Knauer, 100 mm × 3 mm, particle size 5 μm, pore size 100 Å) was used. The mobile phase consisted of a mixture of acetonitrile (ACN) and water (55/45, v/v) delivered by the binary pump at a flow rate of 0.5 mL min^{-1}. The column oven temperature was set to 45 °C. For the detection part, the ELSD was used with an evaporator temperature of 90 °C. The samples were dissolved at a concentration of 2 mg mL^{-1} in the same solvent mixture as the mobile phase and for each measurement, 20 μL were injected. The data was acquired using the WINGPC Unity software from PSS. To characterize the star-shaped PEO samples prior to 2D measurements, size exclusion chromatography (SEC) was measured separately on a Shimadzu system equipped with an SCL-10A system controller, an LC-10AD pump and an RID-10A refractive index detector using 100% THF as the solvent at a flow rate of 3 mL min^{-1} on a PSS-SDV-linear S column (PSS GmbH Mainz, 300 mm × 8 mm, particle size 5 μm) at 45 °C. The system was calibrated with PEO (M_n = 1470 to 7000 g mol^{-1}) standards purchased from PSS.

Two-dimensional liquid chromatography (2D-LC): For the first dimension LCCC of PEO, the analytical conditions were used as described above, except that the flow rate was set to 0.02 mL min^{-1} to enable the subsequent SEC separation of the LCCC fractions for the 2D analysis. The different sample fractions of the LCCC separation were automatically transferred to the second dimension (SEC) via an eight-port valve system with 100 μL sample loops. On the SEC system, the fractions were separated on an SDV HighSpeed linear S column from PSS (50 mm × 20 mm, particle size 5 μm) using THF as eluent at a flow rate of 3 mL min^{-1} at 45 °C and the ELSD. For the 2D measurements, higher concentrated polymer solutions (7 mg mL^{-1}) were prepared, and 50 μL were used as the injection volume. The data acquisition was done by the PSS WINGPC unity software, including a 2D software module.

Transmission electron microscopy (TEM): The formed aggregates were analyzed using a TEM (Zeiss-CEM 902A, Oberkochen, Germany) operated at 80 kV. Images were recorded using a 1 k TVIPS FastScan CCD camera. TEM samples were prepared by applying a drop of an aqueous sample solution onto the surface of a plasma-treated carbon coated copper grid (Holey Carbon Grid + 2 nm C; Quantifoil Micro-Tools GmbH, Jena, Germany).

2.2. Materials

Star-shaped poly(ethylene oxide) ($[PEO\text{-}OH]_8$; supplier information: M_n = 10,000 g mol^{-1}; SEC ($CHCl_3$/*i*-PrOH/Et_3N): M_n = 6100 g mol^{-1}, Đ 1.07; SEC (DMAC/LiCl): M_n = 6800 g mol^{-1}; Đ= 1.11; MALDI-ToF MS: M_p = 9900 g mol^{-1}) (JenKem Technology, China) was dissolved in THF and

precipitated in cold diethyl ether, filtered and dried under vacuum before usage. Tetrahydrofuran (THF), acetonitrile (ACN) and dichloromethane (DCM) were purified using a Solvent Purification System (SPS, Innovative Technology, PM-400-3-MD) equipped with two activated alumina columns. 2-Ethyl-2-oxazoline (EtOx) and propargyl *p*-toluenesulfonate (Aldrich) were distilled over barium oxide under reduced pressure before polymerization and stored under argon. Triethylamine was distilled over CaH_2 and stored under argon. All other chemicals were used as purchased if not otherwise mentioned in the text.

2.2.1. Tosylation of Star-Shaped $[PEO_{28}\text{-}OH]_8$

The tosylation of $[PEO_{28}\text{-}OH]_8$ (6 g; 0.6 mmol) was achieved in a slightly modified way as described in the literature [44,45]. Briefly, the educts were dissolved in DCM and stirred at room temperature for at least 72 h, obtaining $[PEO_{28}\text{-}Ts]_8$ via extraction and precipitation in cold diethyl ether.

SEC ($CHCl_3$/*i*-PrOH/Et_3N): M_n = 6300 g mol^{-1}; Đ = 1.10 (PEO-calibration); SEC (DMAC/LiCl): M_n = 5800 g mol^{-1}; Đ = 1.22 (PEO-calibration); ^{1}H NMR (300 MHz, $CDCl_3$, δ): 7.84–7.14 (aromatic C*H*), 4.15 (t, Ts–CH_2–CH_2–O–), 3.80–3.46 (b, –CH_2–CH_2–O–), 2.44 (s, methyl) ppm; ^{13}C-NMR (75 MHz, $CDCl_3$, δ): 125–130 (aromatic *C*H), 71–70 (backbone), ppm 69.1 (–*C*H_2–CH_2–Ts), 68.5 (–CH_2–*C*H_2–Ts), 21.2 (Ts-*C*H_3) ppm.

2.2.2. Preparation of Star-Shaped $[PEO_{28}\text{-}N_3]_8$

$[PEO_{28}\text{-}Ts]_8$ (4 g; 0.4 mmol) was dissolved in DMF (10 mL) and stirred together with sodium azide (NaN_3, 20 equiv) overnight at room temperature. The solvent was removed under reduced pressure and the remainder diluted with chloroform and extracted with water, filtered and dried over sodium sulfate. The resulting $[PEO_{28}\text{–}N_3]_8$ was obtained as a brownish powder via precipitation in cold diethyl ether.

SEC ($CHCl_3$/*i*-PrOH/Et_3N): M_n = 7000 g mol^{-1}; Đ = 1.10 (PEO-calibration); SEC (DMAC/LiCl): M_n = 5800 g mol^{-1}; Đ = 1.21 (PEO-calibration); ^{1}H NMR (300 MHz, $CDCl_3$, δ): 3.80–3.46 (b, –CH_2–CH_2–O–) ppm; ^{13}C-NMR (75 MHz, $CDCl_3$, δ): 71–70 (backbone), ppm 69.8 (–*C*H_2–CH_2–N_3), 50.5 (–CH_2–*C*H_2–N_3) ppm; ATR-FT-IR: 2110 cm^{-1} (azide).

2.2.3. Synthesis of Alkyne-Functionalized TB-$PEtOx_x$

Propargyl *p*-toluenesulfonate and 2-ethyl-2-oxazoline (EtOx) were dissolved in acetonitrile (ACN) at different monomer to initiator ratios ([M]/[I] = 20, 60 and 80) at a monomer concentration of 4 M. The capped vials were placed in a microwave synthesizer at 140 °C. The polymerization was terminated via the addition of water. The polymers were obtained after extraction with $NaHCO_3$ solution, brine and dried under vacuum. After precipitation in cold diethyl ether, the polymer was filtered and dried under vacuum.

TB-$PEtOx_{18}$: SEC ($CHCl_3$/*i*-PrOH/Et_3N): M_n = 2700 g mol^{-1}; Đ = 1.12 (PS-calibration); SEC (DMAC/LiCl): M_n = 3900 g mol^{-1}; Đ = 1.18 (PS-calibration); TB-$PEtOx_{55}$: SEC ($CHCl_3$/*i*-PrOH/Et_3N): M_n = 5600 g mol^{-1}; Đ = 1.09 (PS-calibration); SEC (DMAC/LiCl): M_n = 9700 g mol^{-1}; Đ = 1.16 (PS-calibration); TB-$PEtOx_{75}$: SEC ($CHCl_3$/*i*-PrOH/Et_3N): M_n = 7000 g mol^{-1}; Đ = 1.10 (PS-calibration); SEC (DMAC/LiCl): M_n = 12,000 g mol^{-1}; Đ = 1.19 (PS-calibration); ^{1}H NMR

(300 MHz, $CDCl_3$, δ): 3.6–3.2 (br, –N–C*H*$_2$–C*H*$_2$–), 2.5–2.2 (br, CO–C*H*$_2$–CH$_3$), 1.2–0.9 (br, CO–CH$_2$–C*H*$_3$).

2.2.4. Copper catalyzed Azide-Alkyne Cycloaddition (CuAAC) Click Reaction between $[PEO_{28}\text{-}N_3]_8$ and TB-$PEtOx_x$

For the microwave-assisted copper-catalyzed azide-alkyne cycloaddition click chemistry (CuAAC) click reaction $[PEO_{28}\text{-}N_3]_8$ (1 equiv) and TB-$PEtOx_x$ (16 equiv) were dissolved in a solvent mixture of ethanol (EtOH) and THF (1:1 vol %). Copper bromide (CuBr; 10 equiv) and *N*,*N*′,*N*′′,*N*′′-Pentamethyldiethylenetriamine (PMDETA; 10 equiv) were added under argon flux, purged for 15 min with argon and placed in the microwave-synthesizer for 30 min at 80 °C. The solvent was removed under reduced pressure, and the copper was removed via a short aluminum oxide (AlOxN) column. The homopolymer was removed via precipitation in THF at −30 °C.

$[PEO_{28}\text{-}b\text{-}PEtOx_{18}]_8$: SEC (DMAC/LiCl): M_n = 22,000 g mol^{-1}; Đ = 1.13 (PS-calibration); $[PEO_{28}\text{-}b\text{-}PEtOx_{55}]_8$: SEC (DMAC/LiCl): M_n = 46,000 g mol^{-1}; Đ = 1.18 (PS-calibration); $[PEO_{28}\text{-}b\text{-}PEtOx_{75}]_8$: SEC (DMAC/LiCl): M_n = 42,000 g mol^{-1}; Đ = 1.14 (PS-calibration); ^{1}H NMR (300 MHz, $CDCl_3$, δ): 4.0–3.0 (br, backbone), 2.6–2.2 (br, CO–C*H*2–CH3), 1.2–0.8 (br, CO–CH$_2$–C*H*$_3$).

2.2.5. Polymerization of 2-Ethyl-2-oxazoline using a Star-Shaped PEO Macroinitiator

For the polymerization of EtOx via a star-shaped macroinitiator $[PEO_{28}\text{-}Ts]_8$, different initiator to monomer ratios were chosen, and the polymerization was conducted in acetonitrile (1 M) in a microwave-synthesizer at 140 °C. The reaction was stopped via cooling the reaction mixture after 15 min and the addition of 0.2 mL of water. The final polymer was obtained via precipitation in THF at −30 °C.

$[PEO_{28}\text{-}b\text{-}PEtOx_{16}]_8$: SEC (DMAC/LiCl): M_n = 24,000 g mol^{-1}; Đ = 1.24 (PS-calibration); $[PEO_{28}\text{-}b\text{-}PEtOx_{50}]_8$: SEC (DMAC/LiCl): M_n = 35,000 g mol^{-1}; Đ = 1.15 (PS-calibration); ^{1}H NMR (300 MHz, $CDCl_3$, δ): 4.0–3.0 (br, backbone), 2.6–2.2 (br, CO–C*H*$_2$–CH$_3$), 1.2–0.8 (br, CO–CH$_2$–C*H*$_3$).

2.2.6. Kinetic Investigation of the Polymerization of 2-Ethyl-2-oxazoline using a Star-Shaped PEO-Macroinitiator

A stock solution of the macroinitiator $[PEO_{28}\text{-}Ts]_8$ and 2-ethyl-2-oxazoline (EtOx) were mixed with acetonitrile at a monomer to initiator ratio of 40 and a monomer concentration of 1 M. The capped vials were placed in a microwave synthesizer at 140 °C. The polymerization was terminated via the addition of water. The pure star-shaped block copolymers were received after precipitation in THF at −30 °C.

3. Results and Discussion

We were interested in the solution properties of well-defined star-shaped block copolymers containing two hydrophilic blocks. In particular, the influence of the length used for the outer block on the behavior in non-selective solvents (*i.e.*, water) for a system with a given arm number (here: eight

arms) was our focus for this study. We chose poly(ethylene oxide) as the core, due to its wide solubility in common solvents, its commercial availability and chemical inertness, enabling various chemical modifications. As the outer block (shell), we used poly(2-ethyl-2-oxazoline), a well-studied material with proven biocompatibility [22] and temperature-responsive properties (lower critical solution properties, LCST) above a threshold-molar mass in aqueous media [46,47].

Regarding the synthesis of star-shaped poly(ethylene oxide)-*block*-poly(2-ethyl-2-oxazoline) block copolymers with eight arms, we chose to compare two different strategies: for the "arm-first" approach, the macromolecular conjugation (azide-alkyne click reaction [27,48]) between azide-functionalized $[PEO_{28}\text{-}N_3]_8$ and alkyne-functionalized TB-$PEtOx_x$ of different molar mass was used. In the case of the "core-first" strategy, tosylated $[PEO_{28}\text{-}Ts]_8$ (the subscripts denote the degree of polymerization of the corresponding block, and the subscripts after the brackets represent the arm number of the herein described star-shaped block copolymers) was used as a macroinitiator for the cationic ring-opening polymerization (CROP) of 2-ethyl-2-oxazoline (EtOx). In both cases, the length of the PEtOx block can be easily varied within a certain range. In the following, first, both synthetic routes will be described separately, and afterwards, the solution properties in water as a non-selective solvent for both blocks will be compared.

3.1. Star Synthesis via Macromolecular Conjugation ("Arm-First"-Approach)

Core: First, a commercially available star-shaped poly(ethylene oxide) (PEO) with eight arms and a total molar mass (M_n) of 10,000 g mol^{-1} (1250 g mol^{-1} per arm) was modified. For this purpose, the hydroxyl end group was tosylated first by a nucleophilic substitution reaction using *p*-toluenesulfonyl chloride (Ts-Cl; Scheme 1), obtaining $[PEO\text{-}Ts]_8$. Whereas this modification for linear PEO is often described as being performed within a few hours [44,45], in our case, the reaction time needed to be increased to at least 72 h at room temperature to achieve full functionalization (determined via ^{1}H-NMR; Figure S1C).

Scheme 1. Preparation of $[PEO_{28}\text{-}Ts]_8$ and $[PEO_{28}\text{-}N_3]_8$.

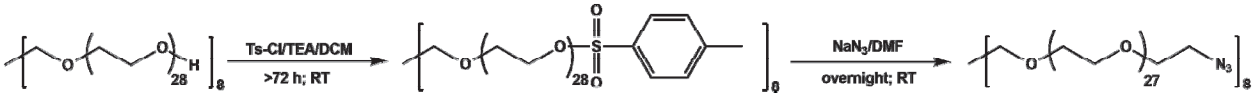

Afterwards, $[PEO_{28}\text{-}Ts]_8$ was converted to $[PEO_{28}\text{-}N_3]_8$ using sodium azide (Scheme 1). After purification, for $[PEO_{28}\text{-}N_3]_8$, slight amounts (<5%) of residual aromatic signals, corresponding to the tosyl-moiety, were observed via ^{1}H NMR (Figure S1C). Nevertheless, the azide group could be clearly detected by ATR FT-IR measurements (2110 cm^{-1}; Figure S1B).

To ensure full end-group conversion of the modified star-shaped macromolecules, the polymers were investigated via ^{13}C-NMR and 2D-LC (LCCC × SEC). In the latter case, liquid chromatography under critical conditions for PEO (LCCC) should enable the separation according to the end-group polarity and further coupled to SEC for the molar range [49–53]. After careful adjustment of the critical conditions for PEO (Figure S2), the stars with different end-groups ($[PEO_{28}\text{-}OH]_8$, $[PEO_{28}\text{-}Ts]_8$ and $[PEO_{28}\text{-}N_3]_8$) were investigated (Figure 1). As can be seen, $[PEO_{28}\text{-}OH]_8$ exhibits only one distribution, with a peak maximum at 0.62 mL (Figure 1A), whereas for $[PEO_{28}\text{-}Ts]_8$, two distributions

at 0.80 mL (97%) and 0.62 mL (3%, unfunctionalized material) were observed (Figure 1B). This is in good agreement with the error of the NMR spectroscopy, where no $[PEO_{28}\text{-}OH]_8$ could be detected. For $[PEO_{28}\text{-}N_3]_8$, also, two distributions at 0.80 mL (90%) and at 0.62 (10%) were observed (Figure 1C). We tentatively attribute this observation to a slow exchange of the azide functionality by hydroxyl groups under these conditions. This assumption can be confirmed by time-dependent investigations, leading to a ratio of 90:10 for both distributions directly after sample preparation, while 75:25 is found after 30 min (Figure S3). If the sample was stored overnight in solution, a ratio of 50:50 is observed. As many reactions using azides are described in the literature in water [49,54], this exchange process might be facilitated here, as the sample is heated to 45 °C and remains for 100 min within the system to elute/separate.

Figure 1. 2D-LC results (acetonitrile (ACN)/H_2O 55/45 v/v) for $[PEO_{28}\text{-}OH]_8$ (**A**), $[PEO_{28}\text{-}Ts]_8$ (**B**) and $[PEO_{28}\text{-}N_3]_8$ (**C**); in comparison with the SEC traces obtained for $[PEO_{28}\text{-}OH]_8$ (solid black line), $[PEO_{28}\text{-}Ts]_8$ (solid red line) and $[PEO_{28}\text{-}N_3]_8$ (solid blue line; THF was used as eluent).

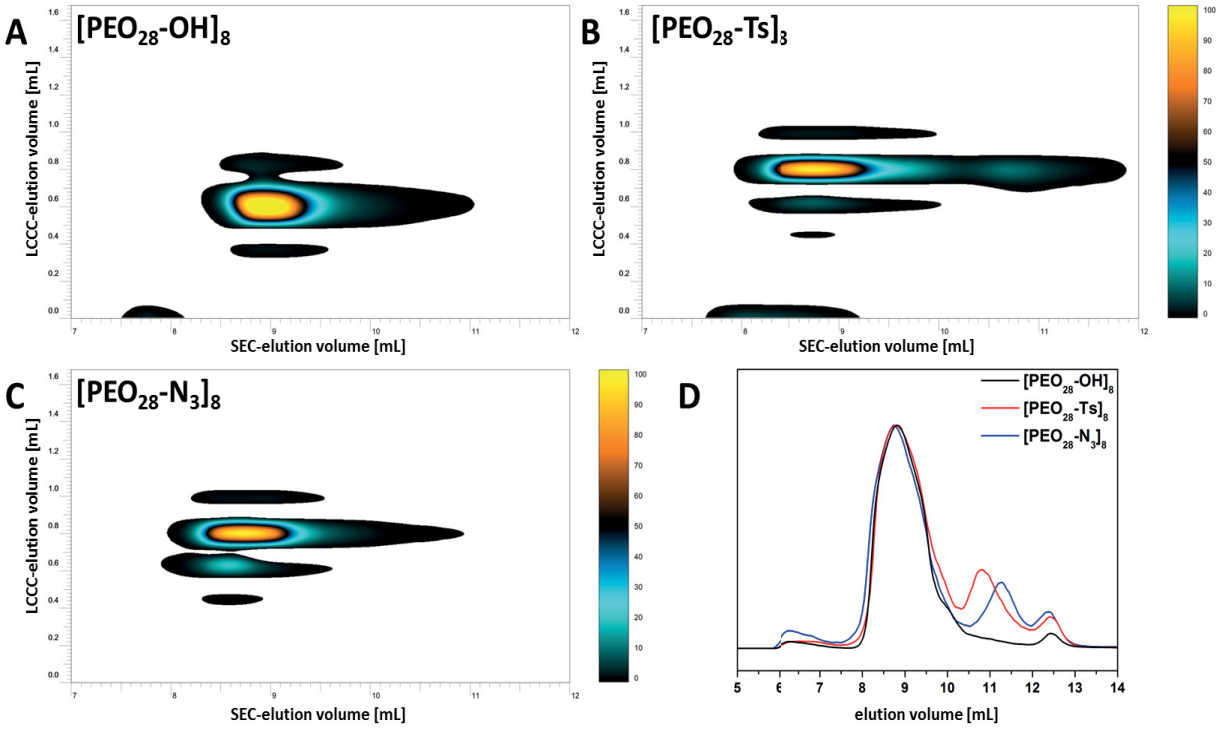

The elution behavior in LCCC was similar for $[PEO_{28}\text{-}Ts]_8$ and $[PEO_{28}\text{-}N_3]_8$, again, somewhat surprising. During SEC, further small distributions appear at higher elution volumes, which might be due to a higher flow rate of 3 mL min^{-1} (Figure 1D), as under flow rates of 1 mL min^{-1}, only monomodal distributions were observed.

Due to the results obtained for $[PEO_{28}\text{-}N_3]_8$ using 2D-LC experiments, additional ^{13}C-NMR measurements in $CDCl_3$ were carried out. Here, the signals for the tosyl-group, as well as the CH_2-group located next to the hydroxyl-end-group at 61.5 ppm are not observed, and also, two new signals for the two CH_2 groups next to the azide functionality at 50.5 and 79.8 ppm (Figure S4) confirm the successful conversion, at least within the experimental error of the NMR [45,55].

Arm: Alkyne-functionalized 2-ethyl-2-oxazoline homopolymers (TB-PEtOx$_x$) with different molar masses and low polydispersity indices (Đ; <1.1) were obtained via microwave-assisted cationic ring-opening polymerization (CROP) of 2-ethyl-2-oxazoline (EtOx) [25]. Therefore, solutions containing a functional initiator, propargyl *p*-toluenesulfonate, with different monomer-to-initiator ratios ([M]/[I]) at a constant monomer concentration of 4 M were prepared and polymerized in a microwave-synthesizer at 140 °C. The degrees of polymerization (DP) obtained via ^{1}H NMR and MALDI-ToF MS slightly differ from the theoretically calculated values, according to the feed ratios used for the polymerizations. For a theoretical DP of 20, a DP of 18 (TB-PEtOx$_{18}$), for a DP of 60, a DP of 55 (TB-PEtOx$_{55}$), and for a DP of 80, a DP of 75 (TB-PEtOx$_{75}$) were found (Table 1, SEC in Figure S6A).

Table 1. Selected characterization data for alkyne-functionalized poly(2-ethyl-2-oxazoline)s (TB-PEtOx$_x$) and star-shaped [PEO$_{28}$-Y]$_8$.

Sample	DP [a]	M_n [b] [g mol^{-1}]	M_n [c] [g mol^{-1}]	Đ [c]	M_p [d] [g mol^{-1}]	Building Block
TB-PEtOx$_{18}$ [b,e]	20	1800	2700	1.12	1500	**arm in chloroform**
TB-PEtOx$_{55}$ [b,e]	60	5500	5600	1.09	5400	
TB-PEtOx$_{75}$ [b,e]	80	7500	6700	1.10	7200	
TB-PEtOx$_{18}$ [e,f]	20	1800	3900	1.18	–	**arm in DMAC**
TB-PEtOx$_{55}$ [e,e]	60	5500	9700	1.16	–	
TB-PEtOx$_{75}$ [e,e]	80	7500	12,000	1.19	–	
[PEO$_{28}$-OH]$_8$ [b,e]	–	10,000	6100 [h]	1.07	9,900	**star-shaped core**
[PEO$_{28}$-Ts]$_8$ [b,e]	–	11,000	7000 [h]	1.04	–	
[PEO$_{28}$-N$_3$]$_8$ [b,e]	–	10,300	7000 [h]	1.07	–	
[PEO$_{28}$-N$_3$]$_8$ [e,g]	–	10,300	12,000 [g]	1.15	–	

[a] feed ratio [M]/[I]; [b] calculated from nuclear magnetic resonance spectroscopy (NMR) and Matrix-assisted laser desorption/ionization time of flight mass spectrometry (MALDI-ToF MS); [c] size exclusion chromatography (SEC) ($CHCl_3$/*i*-PrOH/TEA) (PS-calibration); [d] MALDI-ToF MS (matrix/doping agent *trans*-2-[3-(4-*tert*-butylphenyl)-2-methyl-2-propenylidene] malononitrile (DCTB) /NaCl); [e] subscripts denote the degree of polymerization; [f] SEC (DMAC/LiCl) (PS-calib.); [g] SEC (DMAC/LiCl) (PEO-calib.); [h] SEC ($CHCl_3$/*i*-PrOH/TEA) (PEO-calib.).

The molar masses of the polymers increase linearly with the monomer-to-initiator ratio and are also in good agreement with the values obtained by MALDI-ToF MS measurements (Table 1). As the molar masses of the star-shaped block copolymers after arm attachment will exceed the exclusion volume of the utilized $CHCl_3$ SEC, the homopolymers (arms) were also subjected to another SEC instrument featuring a higher molar mass range (here, *N*,*N*-dimethylacetamide (DMAc) was used as the eluent, Figure S6B). The slight broadening of the Đ-values can be ascribed to polymer-column interactions, and, furthermore, the apparent molar masses are higher in comparison to the values obtained using chloroform as the eluent.

For the synthesis of [PEO$_{28}$-*b*-PEtOx$_x$]$_8$, star-shaped block copolymers [PEO$_{28}$-N$_3$]$_8$ and different TB-PEtOx$_x$ were used in copper-catalyzed azide-alkyne cycloaddition reactions (CuAAC; Scheme 2). First, the conditions had to be optimized by variation of the solvent, the reaction temperature and the reaction time. The best conditions were obtained in a THF-ethanol mixture (1:1 v/v) at 80 °C using a four-fold excess of TB-PEtOx$_x$ in comparison to the azide-functionality and a reaction time of only 15 min in the microwave synthesizer. Under these conditions, it was possible to obtain the desired

$[PEO_{28}$-*b*-$PEtOx_x]_8$ materials. Purification was achieved via selective precipitation of the block copolymer in THF at −30 °C, while $PEtOx_x$ homopolymers are still soluble under these conditions. The obtained polymers were characterized using SEC (Table 2), FT-IR and NMR (Figure S7).

Scheme 2. Schematic representation of the synthesis of star-shaped $[PEO_{28}$-*b*-$PEtOx_x]_8$ block copolymers using copper-catalyzed azide-alkyne cycloaddition click chemistry (CuAAC).

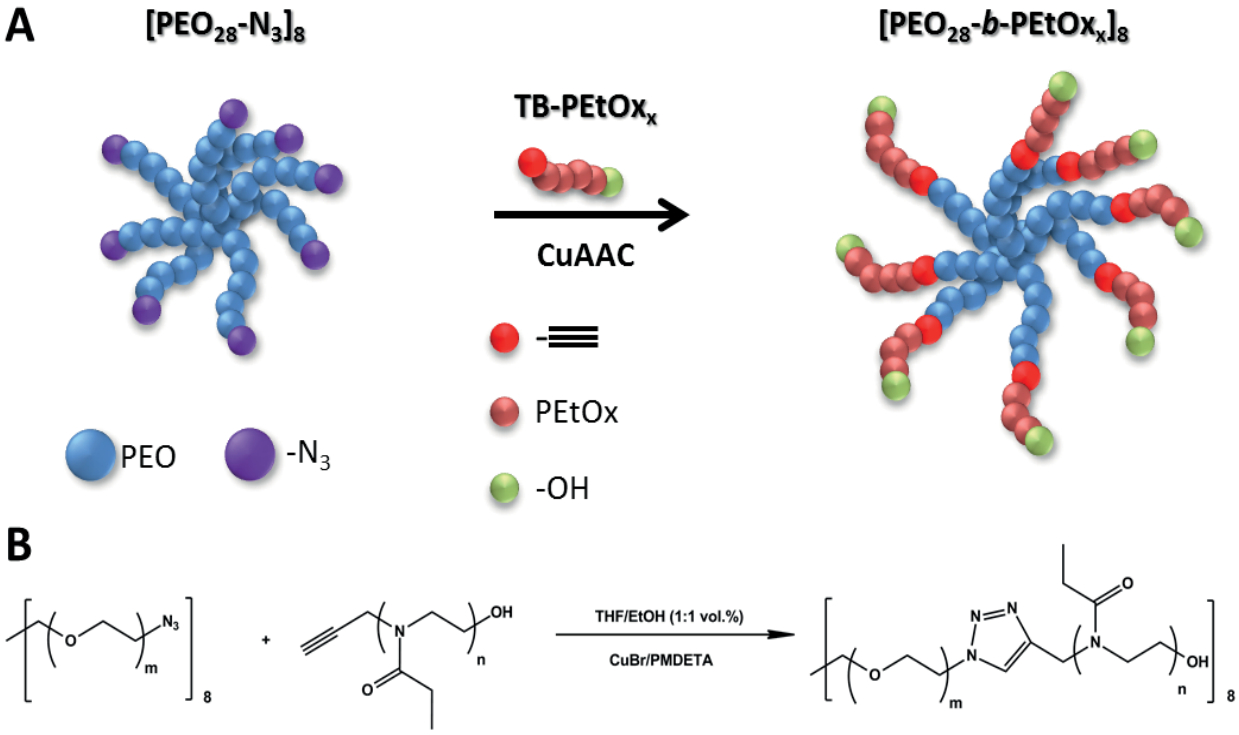

Table 2. Selected characterization data for star-shaped $[PEO_{28}$-*b*-$PEtOx_x]_8$ block copolymers obtained via the "core-first" or "arm-first" approach.

Sample	M_n [a] [g mol^{-1}]	Đ [a]	$M_{n,calc}$ [b] [g mol^{-1}]	$M_{w,SLS}$ [d] [g mol^{-1}]	Approach
$[PEO_{28}$-*b*-$PEtOx_{18}]_8$ [c]	22,000	1.13	22,000	–	
$[PEO_{28}$-*b*-$PEtOx_{55}]_8$ [c]	46,000	1.18	54,000	–	**arm-first**
$[PEO_{28}$-*b*-$PEtOx_{75}]_8$ [c]	42,000	1.14	67,000	–	
$[PEO_{28}$-*b*-$PEtOx_{16}]_8$ [c]	24,000	1.24	22,000	–	**core-first**
$[PEO_{28}$-*b*-$PEtOx_{50}]_8$ [c]	35,000	1.15	50,000	54,000	

[a] SEC (DMAC/LiCl) (PS-calib.); [b] calculated from the single compound molar masses obtained via MALDI-ToF MS ("arm-first") or ^{1}H-NMR ("core-first"); [c] subscripts denote the number of repeating units; [d] static light scattering at 25 °C in THF (dn/dc = 0.0915 mL g^{-1}; $A_2 = 1 \times 10^{-8}$ mol dm^3 g^{-2}).

SEC elution traces using DMAC/LiCl (0.21 wt % LiCl) as the eluent for the individual building blocks and the star-shaped block copolymers are shown in Figure 2. The corresponding characterization data are shown in Table 2. Via this approach, three different star-shaped block copolymers, $[PEO_{28}$-*b*-$PEtOx_{18}]_8$, $[PEO_{28}$-*b*-$PEtOx_{55}]_8$ and $[PEO_{28}$-*b*-$PEtOx_{75}]_8$, were obtained. Owing to the star architecture, the elution behavior of the star-shaped block copolymers leads to lower molar masses than expected during SEC measurements. This effect has already been described for other

star-shaped and branched systems [3]. According to the SEC traces, e.g., in the case of $[PEO_{28}$-*b*-$PEtOx_{18}]_8$, a clear shift for $[PEO_{28}$-*b*-$PEtOx_{18}]_8$, if compared to TB-$PEtOx_{18}$ and $[PEO_{28}$-$N_3]_8$, can be observed. Moreover, after purification, the sample contained neither an excess of the arm (TB-$PEtOx_{18}$) nor the core $[PEO_{28}$-$N_3]_8$. The apparent molar masses of $[PEO_{28}$-*b*-$PEtOx_{18}]_8$ obtained by SEC are 22,000 g mol^{-1} with a narrow Đ-value of 1.13 (PS-calibration). The apparent molar masses for $[PEO_{28}$-*b*-$PEtOx_{55}]_8$ and $[PEO_{28}$-*b*-$PEtOx_{75}]_8$ are in a comparable range with 46,000 and 42,000 g mol^{-1}. The composition of the star-shaped block copolymers was further confirmed using ^{1}H-NMR (Figure S7B).

Figure 2. SEC traces using DMAC/LiCl as the eluent for TB-$PEtOx_x$ (dotted line), $[PEO_{28}$-$N_3]_8$ (scattered line) and the obtained purified star-shaped $[PEO_{28}$-*b*-$PEtOx_x]_8$ (solid line): (**A**) $[PEO_{28}$-*b*-$PEtOx_{18}]_8$; (**B**) $[PEO_{28}$-*b*-$PEtOx_{55}]_8$; (**C**) $[PEO_{28}$-*b*-$PEtOx_{75}]_8$.

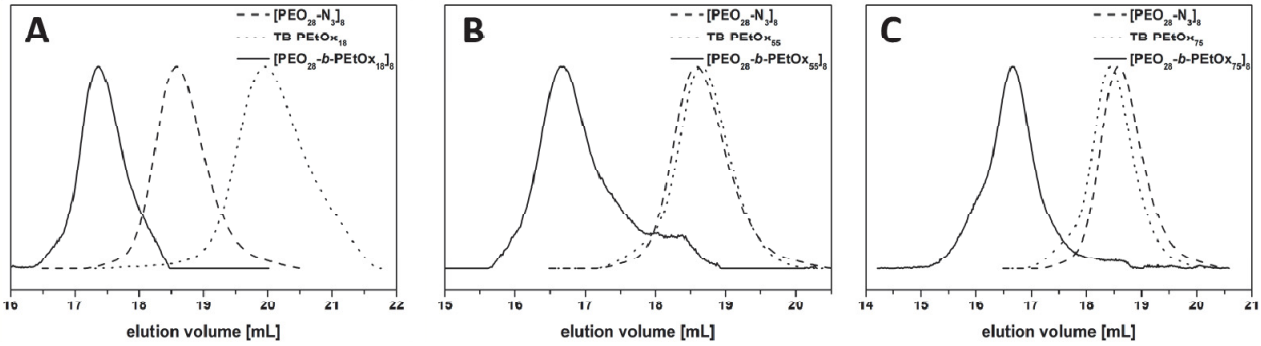

3.2. Star Synthesis via CROP of 2-Ethyl-2-oxazoline Using a Star-Shaped Macroinitiator ("Core-First"-Approach)

Furthermore, here, commercially available $[PEO_{28}$-$OH]_8$ was modified via tosylation as described above and purified until no further unreacted Ts-Cl could be observed in the ^{1}H-NMR spectra. As PEO is rather hydroscopic, the macroinitiator was co-evaporated with toluene, dried under vacuum for at least 24 h and stored in a glove box. After the preparation of the macroinitiator, we first carried out a kinetic study for the polymerization of EtOx (Figure 3). Therefore, a stock solution of $[PEO_{28}$-$Ts]_8$ and monomer ([M]/[I] = 40) was prepared in ACN (1M) and divided into several microwave vials. The vials were subsequently placed in the microwave-synthesizer and analyzed after different polymerization times at 140 °C via ^{1}H-NMR and SEC. A pseudo-linear first-order kinetic was observed for the monomer consumption over time, while in SEC elution traces, two distributions were observed (Figure 3B).

Taking into account the slope of the fit in Figure 3A, a propagation rate (k_p) of 337 L mol^{-1} s^{-1} × 10^{-3} can be calculated (corresponding to 42 L mol^{-1} s^{-1} × 10^{-3} per arm). However, as indicated by the second distribution in the SEC elution traces in Figure 3B, with increasing polymerization time, also homopolymer (PEtOx) is formed, presumably due to transfer reactions. Although $[PEO_{28}$-$Ts]_8$ has been extracted and co-evaporated with toluene several times prior to use, followed by drying for at least 24 h under vacuum, traces of impurities seem to persist.

Figure 3. First order time-conversion plot for the kinetic investigation of the microwave assisted polymerization of EtOx with $[PEO_{28}\text{-}Ts]_8$ as the initiator at 140 °C (**A**); comparison of the time-dependent SEC traces ($CHCl_3$) for the polymerization of EtOx (**B**).

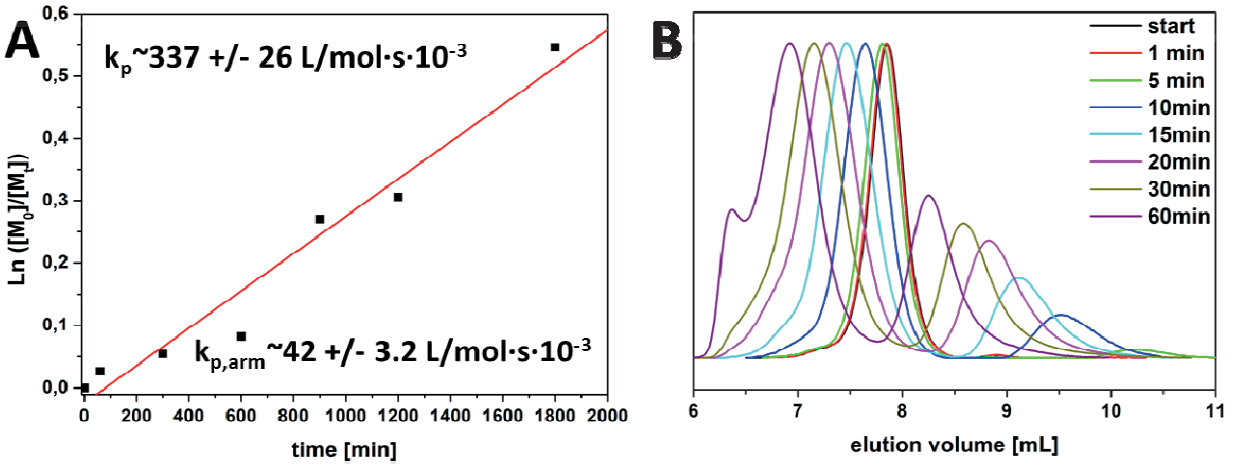

One way to determine the actual amount of incorporated PEtOx within the star-shaped $[PEO_{28}\text{-}b\text{-}PEtOx_x]_8$ block copolymers is to remove the generated homopolymer via fractionated precipitation in THF at −30 °C. The results are depicted in Figure 4. Therefore, differences of up to 50% between the expected and the real PEtOx content can be observed. The monomer conversion obtained from the reaction solution seems to be up to 50% (DP = 20), but the monomer conversion determined via NMR from the purified product leads to 25% (DP = 10).

Figure 4. Time-dependent EtOx conversion (black squares) and the corresponding degrees of polymerization per arm (red squares) determined from the reaction mixture (filled squares) and after purification of the star-shaped block copolymers (empty squares) via NMR (**A**); SEC traces before (dashed line) and after purification via fractionated precipitation (**B**) (solid lines; $CHCl_3$ was used as the eluent).

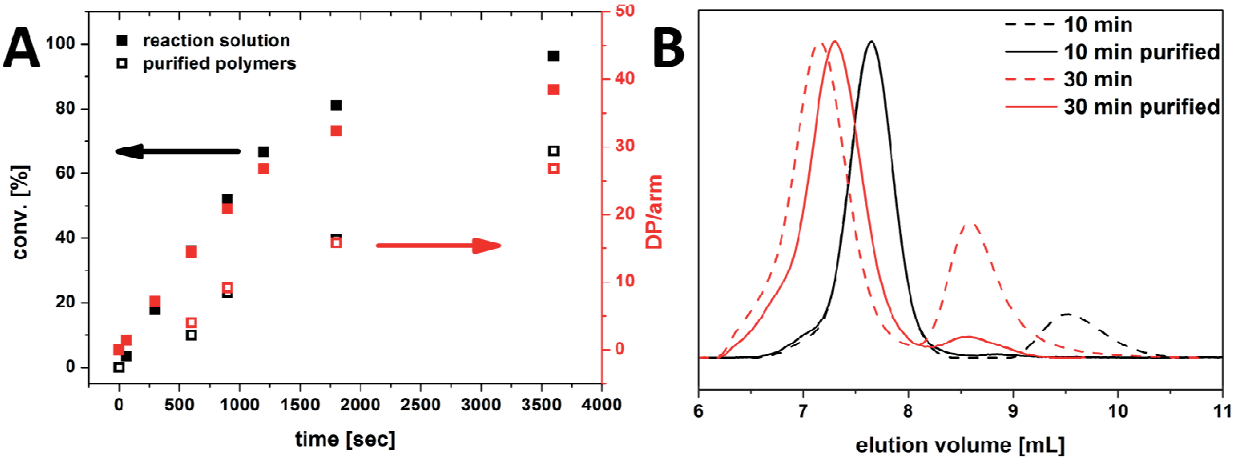

As can be seen in Figure 3B, after a polymerization time of 15 min, a considerable and clear shift of the desired product is visible in the elution traces and, at the same time, the amount of homopolymer formed is mediocre. The overall monomer conversion is around 50%, and we chose this as the conditions for the synthesis of samples with different PEtOx block lengths. Due to the fact that not

many differences were observed between $[PEO_{28}$-*b*-$PEtOx_{55}]_8$ and $[PEO_{28}$-*b*-$PEtOx_{75}]_8$ (Table 2), according to SEC measurements, $[PEO_{28}$-*b*-$PEtOx_{20}]_8$ and $[PEO_{28}$-*b*-$PEtOx_{60}]_8$ were targeted using the "core-first" approach, and the corresponding polymerizations were stopped at around 50% monomer conversion. The results are summarized in Table 2. In the case of the purified $[PEO_{28}$-*b*-$PEtOx_{50}]_8$, static light scattering (SLS) in THF was used in addition for the determination of the absolute molar mass (M_W). While in theory, a molar mass of 50,000 g mol^{-1} would be expected for $[PEO_{28}$-*b*-$PEtOx_{50}]_8$ by the [M]/[I]-ratio and NMR, SLS leads to a value of 54,000 g mol^{-1}, being in quite good agreement (Table 2).

We also compared the elution volume of star-shaped block copolymers with similar composition, but synthesized via two different approaches (Figure 5). As can be seen, for systems with a similar DP of roughly 20, the elution behavior is comparable via SEC (Figure 5A), as in NMR, the DP for the "arm-first" approach was 16, compared to 18 in the case of the "core-first" sample. For the star block copolymer with a higher amount of PEtOx (DP of 50), a shift to lower elution volume for the "core-first" product can be seen. Here, actual degrees of polymerization of 55 ("arm-first") and 50 ("core-first") for PEtOx were determined.

Figure 5. Comparison of the SEC traces obtained via the "core-first" (solid red lines) and the "arm-first" approach (solid black lines) in comparison to $[PEO_{28}$-Ts$]_8$ (dashed line) for two compositions: (**A**) $[PEO_{28}$-*b*-$PEtOx_{16}]_8$ (core-first; red curve) and $[PEO_{28}$-*b*-$PEtOx_{18}]_8$ (arm-first; black curve); and (**B**) $[PEO_{28}$-*b*-$PEtOx_{50}]_8$ (core-first; red curve) and $[PEO_{28}$-*b*-$PEtOx_{55}]_8$ (arm-first; black curve).

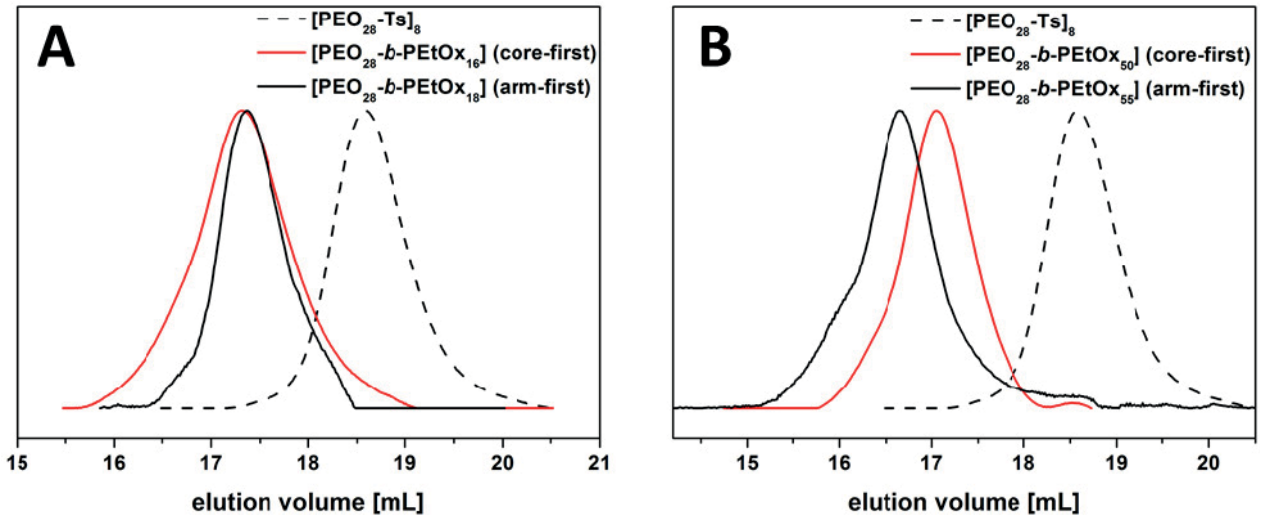

3.3. Study of Star-Shaped $[PEO_{28}$-b-$PEtOx_x]_8$ in Non-Selective Solvents

We were now interested in the solution properties of star-shaped $[PEO_{28}$-*b*-$PEtOx_x]_8$ block copolymers in non-selective solvents, for example, tetrahydrofuran (THF) or water. First, the hydrodynamic radii in solution were determined using dynamic light scattering (DLS). Therefore, the samples were dissolved in THF, filtered (0.45 µm, PTFE) and the size was compared to the crude $[PEO_{28}$-OH$]_8$ star polymer (Figure 6). According to the CONTIN plots depicted in Figure 6A, for $[PEO_{28}$-OH$]_8$, an apparent hydrodynamic radius of $\langle R_h \rangle_{n,app}$ = 1.5 nm was observed, whereas for the

star-shaped block copolymers prepared via the "arm-first" approach, apparent hydrodynamic radii of 2.5 ([PEO_{28}-*b*-$PEtOx_{18}$]$_8$), 4 nm ([PEO_{28}-*b*-$PEtOx_{55}$]$_8$) and 5 nm ([PEO_{28}-*b*-$PEtOx_{75}$]$_8$) were determined under these conditions (Table 3). These results, in our opinion, both confirm the formation of unimers in THF and the elution behavior observed in SEC with increasing length of the outer PEtOx block. The hydrodynamic radii obtained for "core-first" [PEO_{28}-*b*-$PEtOx_{16}$]$_8$ (3 nm) and [PEO_{28}-*b*-$PEtOx_{50}$]$_8$ (3 nm) are comparable.

Figure 6. DLS CONTIN plot for "arm-first" approach stars in different solvents: in THF: [PEO_{28}-OH]$_8$ (dashed black line, $<R_h>_{n,app}$ = 1.5 nm), [PEO_{28}-*b*-$PEtOx_{18}$]$_8$ (red line, $<R_h>_{n,app}$ = 2.5 nm), [PEO_{28}-*b*-$PEtOx_{55}$]$_8$ (green line, $<R_h>_{n,app}$ = 4 nm) and [PEO_{28}-*b*-$PEtOx_{75}$]$_8$ (blue line, $<R_h>_{n,app}$ = 5 nm) (2 g L^{-1}) (**A**); in water [PEO_{28}-OH]$_8$ (dotted black line, $<R_h>_{n,app}$ = 3 nm), [PEO_{28}-*b*-$PEtOx_{18}$]$_8$ (red dashed, $<R_h>_{n,app}$ = 6 nm) and [PEO_{28}-*b*-$PEtOx_{75}$]$_8$ (blue line, $<R_h>_{n,app}$ = 14 nm) (0.5 g L^{-1}, filtered) (**B**).

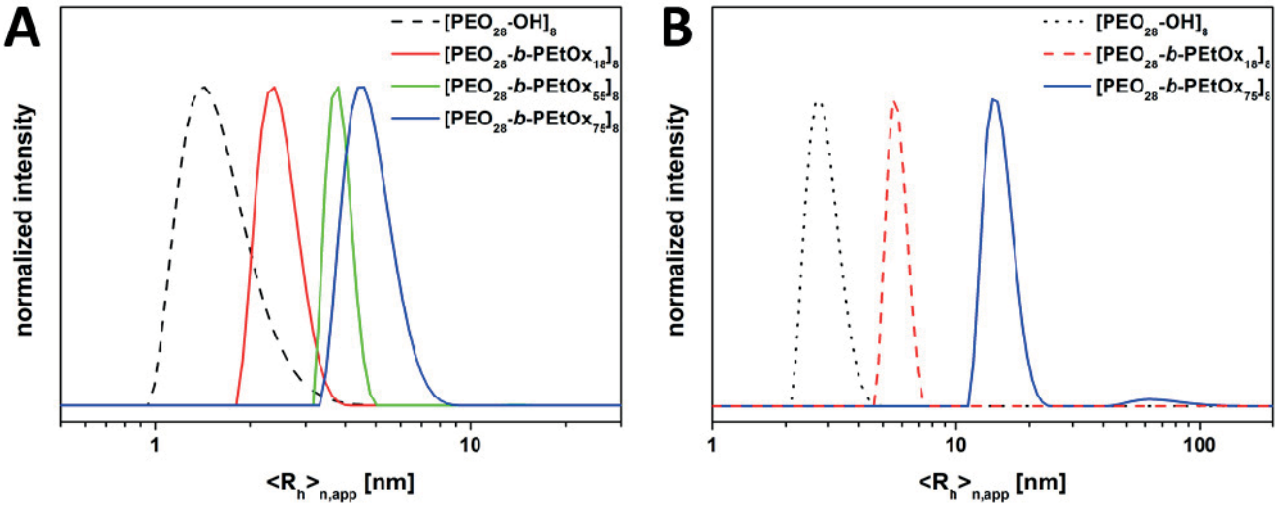

Table 3. Determination of the apparent hydrodynamic radius ($<R_h>_{n,app}$) for different star (block co-) polymer systems in non-selective solvents via DLS.

Sample	approach	$<R_h>_{n,app}$ [a] [nm] in THF	$<R_h>_{n,app}$ [a] [nm] in H_2O
[PEO_{28}-OH]$_8$	–	1.5	3
[PEO_{28}-*b*-$PEtOx_{18}$]$_8$	arm	2.5	6
[PEO_{28}-*b*-$PEtOx_{16}$]$_8$	core	3	3
[PEO_{28}-*b*-$PEtOx_{55}$]$_8$	arm	4	9
[PEO_{28}-*b*-$PEtOx_{50}$]$_8$	core	3	3
[PEO_{28}-*b*-$PEtOx_{75}$]$_8$	arm	5	14/62
[PEO_{28}-*b*-$PEtOx_{18}$]$_8$ [c]	arm	–	92/283 [b]
[PEO_{28}-*b*-$PEtOx_{75}$]$_8$ [c]	arm	–	72 [b]

[a] determined via CONTIN plot; [b] CONTIN plots in the Supporting Information part Figure S7; [c] non filtered sample.

However, if these "arm-first" materials are directly dissolved in water, again, a non-selective solvent for both PEO and PEtOx, turbid solutions are obtained. Transferring the materials from THF to water, via dialysis or evaporation of the organic co-solvent, leads to the same result. The turbidity did

not decrease after heating (up to 100 °C), cooling (~5 °C for one week), changing the pH (0 to 12), prolonged sonication or the addition of different salts (e.g., KSCN, NaCl, KCl). For these turbid solutions, hydrodynamic radii of up to several hundred nm were observed, even at very low concentrations (<0.5 g L^{-1}, Table 3, Figure S8). At this point, we assume that this turbidity originates from the aggregation of the star-shaped block copolymers, although both blocks are of hydrophilic nature. Such behavior has also been described for water-soluble homo- and block copolymers in the literature [12,19,56–58]. In some cases, the unexpected aggregation of double-hydrophilic block copolymers was explained by slight differences in the hydrophilicity of both blocks [50,58].

If, on the other hand, star-shaped $[PEO_{28}$-*b*-$PEtOx_x]_8$ block copolymers synthesized via the "core-first" approach were treated the same way, clear aqueous solutions with hydrodynamic radii of ~3 nm (both cases) are obtained. Somehow, the effect of aggregation in aqueous media is limited to samples prepared by click chemistry, for which we have no conclusive explanation up to now. No detectable amounts of copper were found in atom absorption spectroscopy (AAS), and therefore, an influence of residual copper from the CuAAC reaction can be excluded.

Applying shear forces via filtration (syringe filter, 1 µm, GF) to the turbid solutions of all described "arm-first" samples leads to clear solutions. To ensure that no material was removed by filtration, a defined concentration was filtered and dried afterwards, and the weight loss was below 5%. In Figure 6B, the DLS CONTIN plots for $[PEO_{28}$-OH$]_8$ (dashed black line, $<R_h>_{n,app}$ = 3 nm), $[PEO_{28}$-*b*-$PEtOx_{18}]_8$ (red line, $<R_h>_{n,app}$ = 6 nm) and $[PEO_{28}$-*b*-$PEtOx_{75}]_8$ (blue line, $<R_h>_{n,app}$ = 14 nm) are depicted. The obtained size distributions by DLS are slightly larger if compared to THF ($<R_h>_{n,app}$ = 1.5 nm, 2.5 nm and 5 nm), respectively. This might be an indication for the formation of aggregates by entanglements or that the star-shaped block copolymers are highly swollen.

It is well known that PEtOx materials exhibit lower critical solution temperatures (LCST), depending on the chain length [47,59]. To probe this for the herein described star-shaped systems, solutions of $[PEO_{28}$-*b*-$PEtOx_{20}]_8$ and $[PEO_{28}$-*b*-$PEtOx_{80}]_8$ (2.5 mg mL^{-1}, non-filtered aqueous solution) were heated up to 100 °C, and the turbidity was recorded. In both cases, the solutions did not show cloud points. We ascribe the absence of LCST behavior to the presence of a double-hydrophilic system and, in the case of $[PEO_{28}$-*b*-$PEtOx_{20}]_8$, to the short PEtOx arms.

As another peculiarity, it has been reported by Demirel *et al*. that PEtOx with a molar mass of 500 kg mol^{-1} (1 mg mL^{-1}) crystallizes after being heated in dilute solutions for several days at 70 °C [60]. We therefore were interested in whether similar observations can be made for star-shaped systems of different composition. Solutions of $[PEO_{28}$-*b*-$PEtOx_{18}]_8$ and $[PEO_{28}$-*b*-$PEtOx_{75}]_8$ were heated to 80 °C in water for three days. No changes could be detected for the materials synthesized using the "core-first" approach, whereas larger aggregates were found by DLS and transmission electron microscopy (TEM) for $[PEO_{28}$-*b*-$PEtOx_{18}]_8$ and $[PEO_{28}$-*b*-$PEtOx_{80}]_8$ prepared via the "arm-first" methodology (Figure 7, only if unfiltered solutions were used). The structure of such aggregates was different, depending on whether $[PEO_{28}$-*b*-$PEtOx_{18}]_8$ (55 wt % PEtOx) or $[PEO_{28}$-*b*-$PEtOx_{75}]_8$ (82 wt % PEtOx) was used. In the case of $[PEO_{28}$-*b*-$PEtOx_{18}]_8$, sharp, crystal-like structures were observed, possibly due to partial crystallization of PEtOx, which was also observed by Güner *et al*., [60] leading to an alignment in a rod-like fashion (Figure 7A). Assemblies of several hundred nm in length and ~200 nm width were obtained. For $[PEO_{28}$-*b*-$PEtOx_{75}]_8$, a slightly different aggregation mechanism might take place: here, the superstructures, rather, look like micellar clusters,

which might be the result of an initial formation of unimolecular micelles, followed by further agglomeration (Figure 7B) [61,62]. Tentatively, the hydrophilicity of PEtOx might be lower in comparison to PEO; we assume a partial collapse of the outer PEtOx shell over time, leading to aggregation. However, as this effect was only observed for star-shaped block copolymers prepared via the "arm first" approach and only if non-filtered solutions were used, we hypothesize that a certain pre-organization is required. The aggregation behavior of PEO depending on the treatment before was also discussed by Güner *et al*. for linear polymers [56], and differences in hydrophilicity were described by Ke *et al*. [50,60].

Figure 7. TEM micrographs of aggregates formed by $[PEO_{28}$-*b*-$PEtOx_{18}]_8$ (**top**) and $[PEO_{28}$-*b*-$PEtOx_{75}]_8$ (**bottom**) after heating for three days at 80 °C (unfiltered solutions, "arm-first" approach).

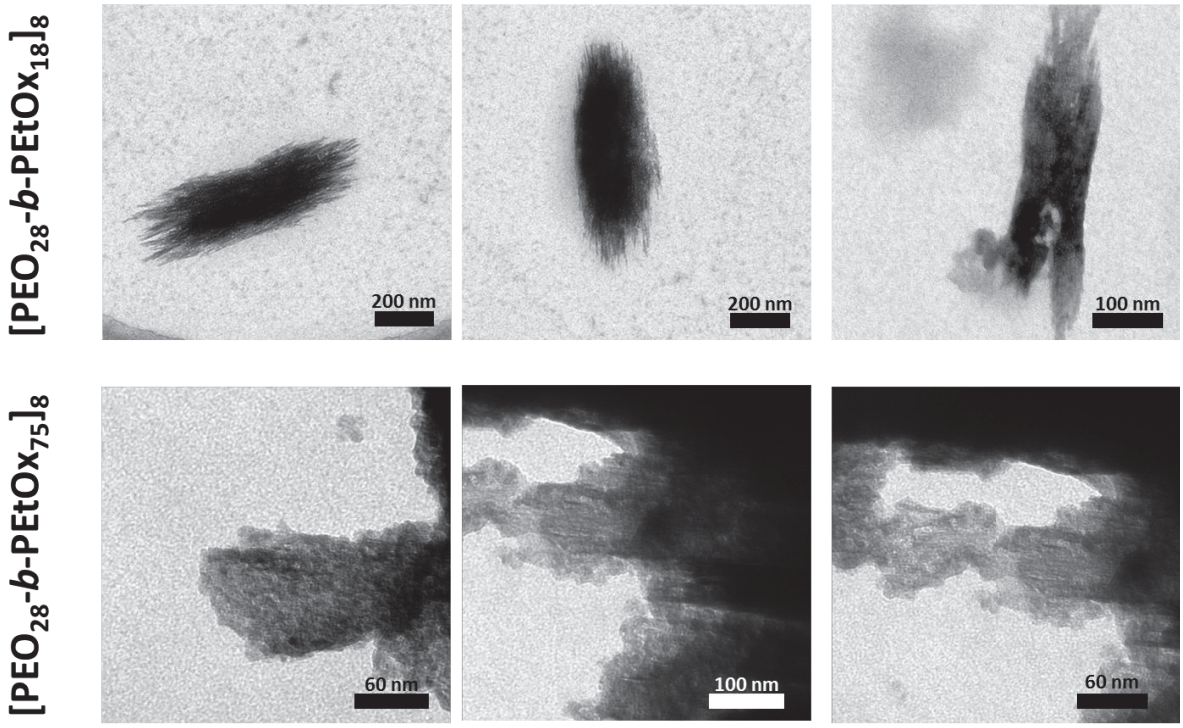

4. Conclusions

We demonstrated the synthesis of a series of well-defined star-shaped $[PEO_{28}$-*b*-$PEtOx_x]_8$ block copolymers using two different approaches, either "core-first" using $[PEO_{28}$-Ts$]_8$ as a macroinitiator for the CROP of EtOx or by copper-catalyzed azide-alkyne cycloadditions between $[PEO_{28}$-$N_3]_8$ and TB-$PEtOx_x$ ("arm-first"). In both cases, different block lengths for the outer PEtOx block were used, and comparable molar masses and hydrodynamic radii in THF as a non-selective solvent were observed. In dilute aqueous solutions, samples prepared via the "arm-first" approach showed aggregate formation, whereas this was not the case for the "core-first" materials. Although this behavior is not fully understood at this point, we could exclude several factors (salt, copper impurities, differences in the molar mass) as the origin of this peculiarity, and we could show that after filtration (1 μm pore size), also, here, smaller hydrodynamic radii are found. At this point, our hypothesis is that small differences in hydrophilicity are the main driving force for this behavior. More importantly, such loose

aggregates from star-shaped block copolymers could be used for the temperature-induced formation of larger agglomerates, where first investigations hint towards an influence of the weight ratio PEO:PEtOx on the morphology of the superstructures formed.

Acknowledgments

We thank Grit Festag for help with the SEC analysis, Sandra Köhn for AAS measurements, Nicole Fritz for help with the 2D-LC and Frank Steiniger and Christine Kämnitz (Electron Microscope Center Jena) for help with the TEM. F.H.S. and T.R. are further grateful to the Thuringian Ministry for Education, Science and Culture (TMBWK; #B515-10065, ChaPoNano) for financial support. F.H.S. thanks the VCI for a starting an independent researcher fellowship, and T.R. acknowledges the Carl-Zeiss foundation for a PhD-scholarship. We also wish to acknowledge the Dutch Polymer Institute (DPI, technology area high-throughput-experimentation, project #690) and the Thuringian Ministry for Education, Science and Culture (grants #B514-09051, NanoConSens, #B515-11028, SWAXS-JCSM and #03WKCB01C, BASIS and #B515-07008) for financial support of this study.

Conflicts of Interest

The authors declare no conflict of interest.

References

1. Barner-Kowollik, C.; Lutz, J.-F.; Perrier, S. New methods of polymer synthesis. *Polym. Chem.* **2012**, *3*, 1677–1679.
2. Pitsikalis, M.; Pispas, S.; Mays, J.W.; Hadjichristidis, N. Nonlinear Block Copolymer Architectures. In *Blockcopolymers–Polyelectrolytes–Biodegradation*; Advances in Polymer Science; Springer-Verlag: Berlin/Heidelberg, Germany, 1998; Volume 135, pp. 1–137.
3. Burchard, W. Solution Properties of Branched Macromolecules. *Adv. Polym. Sci.* **1999**, *143*, 113–194.
4. Hadjichristidis, N.; Pispas, S.; Pitsikalis, M.; Iatrou, H.; Vlahos, C. Asymmetric Star Polymers: Synthesis and Properties; In *Branched Polymers I*; Advances in Polymer Science; Roovers, J., Ed.; Springer: Berlin/Heidelberg, Germany, 1999; Volume 142, pp. 71–127.
5. Plamper, F.A.; McKee, J.R.; Laukkanen, A.; Nykanen, A.; Walther, A.; Ruokolainen, J.; Aseyev, V.; Tenhu, H. Miktoarm stars of poly(ethylene oxide) and poly(dimethylaminoethyl methacrylate): manipulation of micellization by temperature and light. *Soft Matter* **2009**, *5*, 1812–1821.
6. Hadjichristidis, N.; Pitsikalis, M.; Pispas, S.; Iatrou, H. Polymers with Complex Architecture by Living Anionic Polymerization. *Chem. Rev.* **2001**, *101*, 3747–3792.
7. Matyjaszewski, K.; Xia, J.H. Atom transfer radical polymerization. *Chem. Rev.* **2001**, *101*, 2921–2990.
8. Moad, G.; Rizzardo, E.; Thang, S.H. Living radical polymerization by the RAFT process. *Aust. J. Chem.* **2005**, *58*, 379–410.

9. Schacher, F.H.; Rupar, P.A.; Manners, I. Functional Block Copolymers: Nanostructured Materials with Emerging Applications. *Angew. Chem. Int. Ed.* **2012**, *51*, 7898–7921.
10. Zhang, J.; Lu, Z.-Y.; Sun, Z.-Y. Self-assembly structures of amphiphilic multiblock copolymer in dilute solution. *Soft Matter* **2013**, *9*, 1947–1954.
11. Gröschel, A.H.; Schacher, F.H.; Schmalz, H.; Borisov, O.V.; Zhulina, E.B.; Walther, A.; Müller, A.H.E. Precise hierarchical self-assembly of multicompartment micelles. *Nat. Commun.* **2012**, *3*, 710.
12. Riess, G. Micellization of block copolymers. *Prog. Polym. Sci.* **2003**, *28*, 1107–1170.
13. Schacher, F.; Walther, A.; Muller, A.H.E. Dynamic Multicompartment-Core Micelles in Aqueous Media. *Langmuir* **2009**, *25*, 10962–10969.
14. Förster, S.; Abetz, V.; Müller, A.H.E. *Polyelectrolyte Block Copolymer Micelles*; Springer Berlin: Heidelberg, Germany, 2004.
15. Iatridi, Z.; Tsitsilianis, C. Water-Soluble Stimuli Responsive Star-Shaped Segmented Macromolecules. *Polymers* **2011**, *3*, 1911–1933.
16. Schacher, F.H.; Elbert, J.; Patra, S.K.; Mohd Yusoff, S.F.; Winnik, M.A.; Manners, I. Responsive Vesicles from the Self-Assembly of Crystalline-Coil Polyferrocenylsilane-*block*-Poly(ethylene Oxide) Star-Block Copolymers. *Chem. Eur. J.* **2012**, *18*, 517–525.
17. Schacher, F.H.; Freier, U.; Steiniger, F. Hierarchical self-assembly of star-shaped organometallic crystalline-coil block copolymers in solution. *Soft Matter*. **2012**, *8*, 6968–6978.
18. Steinschulte, A.A.; Schulte, B.; Erberich, M.; Borisov, O.V.; Plamper, F.A. Unimolecular Janus Micelles by Microenvironment-Induced, Internal Complexation. *ACS Macro Lett.* **2012**, *1*, 504–507.
19. Knop, K.; Pavlov, G.M.; Rudolph, T.; Martin, K.; Pretzel, D.; Jahn, B.O.; Scharf, D.H.; Brakhage, A.A.; Makarov, V.; Mollmann, U.; Schacher, F.H.; Schubert, U.S. Amphiphilic star-shaped block copolymers as unimolecular drug delivery systems: investigations using a novel fungicide. *Soft Matter* **2013**, *9*, 715–726.
20. Lapienis, G. Star-shaped polymers having PEO arms. *Prog. Polym. Sci.* **2009**, *34*, 852–892.
21. Quaglia, F.; Ostacolo, L.; Nese, G.; Canciello, M.; de Rosa, G.; Ungaro, F.; Palumbo, R.; la Rotonda, M.I.; Maglio, G. Micelles based on amphiphilic PCL-PEO triblock and star-shaped diblock copolymers: Potential in drug delivery applications. *J. Biomed. Mater. Res. A* **2008**, *87A*, 563–574.
22. Knop, K.; Hoogenboom, R.; Fischer, D.; Schubert, U.S. Poly(ethylene glycol) in Drug Delivery: Pros and Cons as Well as Potential Alternatives. *Angew. Chem. Int. Ed.* **2010**, *49*, 6288–6308.
23. Hanisch, A.; Schmalz, H.; Müller, A.H.E. A Modular Route for the Synthesis of ABC Miktoarm Star Terpolymers via a New Alkyne-Substituted Diphenylethylene Derivative. *Macromolecules* **2012**, *45*, 8300–8309.
24. Altintas, O.; Vogt, A.P.; Barner-Kowollik, C.; Tunca, U. Constructing star polymers via modular ligation strategies. *Polym. Chem.* **2012**, *3*, 34–45.
25. Fijten, M.W.M.; Haensch, C.; van Lankvelt, B.M.; Hoogenboom, R.; Schubert, U.S. Clickable poly(2-oxazoline)s as versatile building blocks. *Macromol. Chem. Phys.* **2008**, *209*, 1887–1895.

26. Hadjichristidis, N.; Iatrou, H.; Pitsikalis, M.; Pispas, S.; Avgeropoulos, A. Linear and non-linear triblock terpolymers. Synthesis, self-assembly in selective solvents and in bulk. *Prog. Polym. Sci.* **2005**, *30*, 725–782.
27. Kempe, K.; Krieg, A.; Becer, C.R.; Schubert, U.S. "Clicking" on/with polymers: A rapidly expanding field for the straightforward preparation of novel macromolecular architectures. *Chem. Soc. Rev.* **2012**, *41*, 176–191.
28. Tsitsilianis, C.; Lutz, P.; Graff, S.; Lamps, J.P.; Rempp, P. Core-first synthesis of star polymers with potentially ionogenic branches. *Macromolecules* **1991**, *24*, 5897–5902.
29. Knischka, R.; Lutz, P.J.; Sunder, A.; Mülhaupt, R.; Frey, H. Functional Poly(ethylene oxide) Multiarm Star Polymers: Core-First Synthesis Using Hyperbranched Polyglycerol Initiators. *Macromolecules* **2000**, *33*, 315–320.
30. Schmidt, B.V.K.J.; Rudolph, T.; Hetzer, M.; Ritter, H.; Schacher, F.H.; Barner-Kowollik, C. Supramolecular three-armed star polymers via cyclodextrin host-guest self-assembly. *Polym. Chem.* **2012**, *3*, 3139–3145.
31. Altintas, O.; Tunca, U.; Barner-Kowollik, C. Star and miktoarm star block (co)polymers via self-assembly of ATRP generated polymer segments featuring Hamilton wedge and cyanuric acid. *Polym. Chem.* **2011**, *2*, 1146–1155.
32. Hochwimmer, G.; Nuyken, O.; Schubert, U.S. 6,6′-Bisfunctionalized 2,2′-bipyridines as metallo-supramolecular initiators for the living polymerization of oxazolines. *Macromol. Rapid Comm.* **1998**, *19*, 309–313.
33. Altintas, O.; Yankul, B.; Hizal, G.; Tunca, U. One-pot preparation of 3-miktoarm star terpolymers via click [3 + 2] reaction. *J. Polym. Sci. A Polym. Chem.* **2007**, *45*, 3588–3598.
34. Johnson, J.A.; Finn, M.G.; Koberstein, J.T.; Turro, N.J. Construction of Linear Polymers, Dendrimers, Networks, and Other Polymeric Architectures by Copper-Catalyzed Azide-Alkyne Cycloaddition "Click" Chemistry. *Macromol. Rapid Comm.* **2008**, *29*, 1052–1072.
35. Chen, C.H.; Wilson, J.; Chen, W.; Davis, R.M.; Riffle, J.S. A light-scattering study of poly(2-alkyl-2-oxazoline)s: effect of temperature and solvent type. *Polymer* **1994**, *35*, 3587–3591.
36. Carmichael, A.Y.; Caba, B.L.; Huffstetler, P.P.; Davis, R.M.; Riffle, J.S. Synthesis and solution properties of poly(ethylene oxide-*b*-2-ethyl-2-oxazoline) and poly(ethylene oxide-*b*-ethyleneimine). *Polym. Prepr.* **2004**, *45*, 476–477.
37. Schlaad, H.; Diehl, C.; Gress, A.; Meyer, M.; Demirel, A.L.; Nur, Y.; Bertin, A. Poly(2-oxazoline)s as Smart Bioinspired Polymers. *Macromol. Rapid Commun.* **2010**, *31*, 511–525.
38. Park, J.-S.; Kataoka, K. Comprehensive and Accurate Control of Thermosensitivity of Poly(2-alkyl-2-oxazoline)s via Well-Defined Gradient or Random Copolymerization. *Macromolecules* **2007**, *40*, 3599–3609.
39. Bauer, M.; Lautenschlaeger, C.; Kempe, K.; Tauhardt, L.; Schubert, U.S.; Fischer, D. Poly(2-ethyl-2-oxazoline) as Alternative for the Stealth Polymer Poly(ethylene glycol): Comparison of in vitro Cytotoxicity and Hemocompatibility. *Macromol. Biosci.* **2012**, *12*, 986–998.

40. Rudolph, T.; Kempe, K.; Crotty, S.; Paulus, R.M.; Schubert, U.S.; Krossing, I.; Schacher, F.H. A strong cationic Bronsted acid, $[H(OEt_2)_2][Al\{OC(CF_3)_3\}_4]$, as an efficient initiator for the cationic ring-opening polymerization of 2-alkyl-2-oxazolines. *Polym. Chem.* **2013**, *4*, 495–505.
41. Tauhardt, L.; Kempe, K.; Knop, K.; Altuntaş, E.; Jäger, M.; Schubert, S.; Fischer, D.; Schubert, U.S. Linear Polyethyleneimine: Optimized Synthesis and Characterization—On the Way to "Pharmagrade" Batches. *Macromol. Chem. Phys.* **2011**, *212*, 1918–1924.
42. Einzmann, M.; Binder, W.H. Novel functional initiators for oxazoline polymerization. *J. Polym. Sci. A Polym. Chem.* **2001**, *39*, 2821–2831.
43. Kobayashi, S.; Uyama, H.; Narita, Y.; Ishiyama, J. Novel multifunctional initiators for polymerization of 2-oxazolines. *Macromolecules* **1992**, *25*, 3232–3236.
44. Knop, K.; Jahn, B.O.; Hager, M.D.; Crecelius, A.; Gottschaldt, M.; Schubert, U.S. Systematic MALDI-TOF CID Investigation on Different Substituted mPEG 2000. *Macromol. Chem. Phys.* **2010**, *211*, 677–684.
45. Li, Z.; Chau, Y. A facile synthesis of branched poly(ethylene glycol) and its heterobifunctional derivatives. *Polym. Chem.* **2011**, *2*, 873–878.
46. Güner, P. T.; Demirel, A.L. Effect of Anions on the Cloud Point Temperature of Aqueous Poly(2-ethyl-2-oxazoline) Solutions. *J. Phys. Chem. B* **2012**, *116*, 14510–14514.
47. Christova, D.; Velichkova, R.; Loos, W.; Goethals, E.J.; Prez, F.D. New thermo-responsive polymer materials based on poly(2-ethyl-2-oxazoline) segments. *Polymer* **2003**, *44*, 2255–2261.
48. Kolb, H.C.; Finn, M.G.; Sharpless, K.B. Click Chemistry: Diverse Chemical Function from a Few Good Reactions. *Angew. Chem. Int. Ed.* **2001**, *40*, 2004–2021.
49. Rostovtsev, V.V.; Green, L.G.; Fokin, V.V.; Sharpless, K.B. A Stepwise Huisgen Cycloaddition Process: Copper(I)-Catalyzed Regioselective "Ligation" of Azides and Terminal Alkynes. *Angew. Chem. Int. Ed.* **2002**, *114*, 2708–2711.
50. Ke, F.; Mo, X.; Yang, R.; Wang, Y.; Liang, D. Association of Block Copolymer in Nonselective Solvent. *Macromolecules* **2009**, *42*, 5339–5344.
51. Malik, M.I.; Ahmed, H.; Trathnigg, B. Liquid chromatography under critical conditions: practical applications in the analysis of amphiphilic polymers. *Anal. Bioanal. Chem.* **2009**, *393*, 1797–1804.
52. Falkenhagen, J.; Much, H.; Stauf, W.; Müller, A.H.E. Characterization of Block Copolymers by Liquid Adsorption Chromatography at Critical Conditions. 1. Diblock Copolymers. *Macromolecules* **2000**, *33*, 3687–3693.
53. Jiang, W.; Khan, S.; Wang, Y. Retention Behaviors of Block Copolymers in Liquid Chromatography at the Critical Condition. *Macromolecules* **2005**, *38*, 7514–7520.
54. Sharghi, H.; Khalifeh, R.; Doroodmand, M.M. Immobilization of Porphyrinatocopper Nanoparticles onto Activated Multi-Walled Carbon Nanotubes and a Study of its Catalytic Activity as an Efficient Heterogeneous Catalyst for a Click Approach to the Three-Component Synthesis of 1,2,3-Triazoles in Water. *Adv. Synth. Catal.* **2009**, *351*, 207–218.
55. Ziegast, G.; Pfannemüller, B. Linear and star-shaped hybrid polymers, 1. A new method for the conversion of hydroxyl end groups of poly(oxyethylene) and other polyols into amino end groups. *Makromol. Chem.* **1984**, *5*, 363–371.

56. Özdemir, C.; Güner, A. Solubility profiles of poly(ethylene glycol)/solvent systems, I: Qualitative comparison of solubility parameter approaches. *Eur. Polym. J.* **2007**, *43*, 3068–3093.
57. Nakashima, K.; Bahadur, P. Aggregation of water-soluble block copolymers in aqueous solutions: Recent trends. *Adv. Col. Int. Sci.* **2006**, *123–126*, 75–96.
58. Casse, O.; Shkilnyy, A.; Linders, J.; Mayer, C.; Häussinger, D.; Völkel, A.; Thünemann, A.F.; Dimova, R.; Cölfen, H.; Meier, W.; Schlaad, H.; Taubert, A. Solution Behavior of Double-Hydrophilic Block Copolymers in Dilute Aqueous Solution. *Macromolecules* **2012**, *45*, 4772–4777.
59. Lambermont-Thijs, H.M.L.; Kuringen, H.P.C.V.; Put, J.P.W.V.D.; Schubert, U.S.; Hoogenboom, R. Temperature Induced Solubility Transitions of Various Poly(2-oxazoline)s in Ethanol-Water Solvent Mixtures. *Polymers* **2010**, *2*, 188–199.
60. Guner, P.T.; Miko, A.; Schweinberger, F.F.; Demirel, A.L. Self-assembled poly(2-ethyl-2-oxazoline) fibers in aqueous solutions. *Polym. Chem.* **2012**, *3*, 322–324.
61. Cheng, L.; Zhang, G.; Zhu, L.; Chen, D.; Jiang, M. Nanoscale tubular and sheetlike superstructures from hierarchical self-assembly of polymeric janus particles. *Angew. Chem. Int. Ed.* **2008**, *47*, 10171–10174.
62. Liu, C.; Zhang, K.; Chen, D.; Jiang, M.; Liu, S. Transforming spherical block polyelectrolyte micelles into free-suspending films via DNA complexation-induced structural anisotropy. *Chem. Commun.* **2010**, *46*, 6135–6137.

Supporting Information

Figure S1. Characterization data for the modification steps performed to obtain star-shaped $[PEO_{28}\text{-}N_3]_8$ via: (**A**) reaction scheme for the tosylation and azidation of $[PEO_{28}\text{-}OH]_8$ and the characterization via: (**B**) ATR-FT-IR; (**C**) ^{1}H-NMR $[PEO_{28}\text{-}OH]_8$ (black curve), $[PEO_{28}\text{-}Ts]_8$ (red curve), and $[PEO_{28}\text{-}N_3]_8$ (blue curve); (**D**) SEC (DMAC) of $[PEO_{28}\text{-}OH]_8$ (dashed line) and $[PEO_{28}\text{-}N_3]_8$ (solid line).

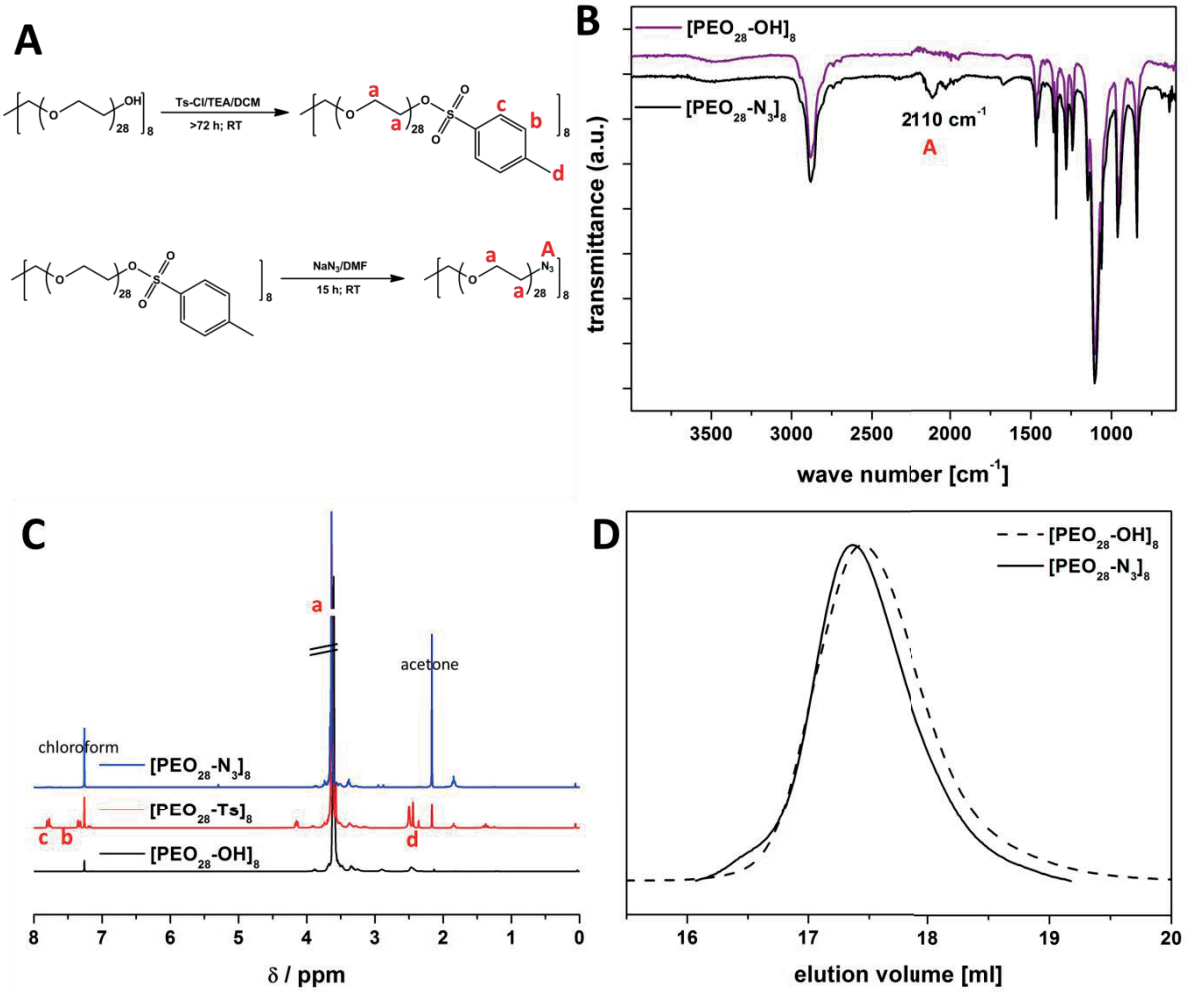

Figure S2. LCCC chromatograms at the critical conditions of PEO standards from PSS ($H(C_2H_4O)_nH$ (mobile phase composition acetonitrile and water (55/45, v/v))).

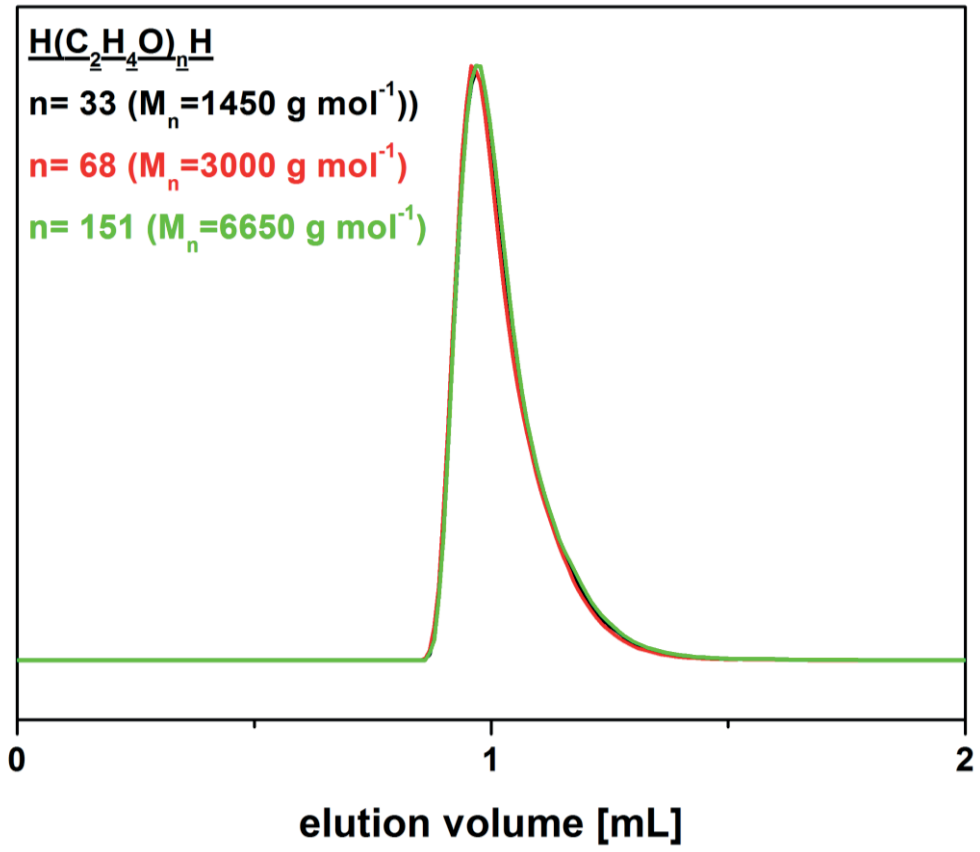

Figure S3. Comparison of 2D-LC results obtained for $[PEO_{28}\text{-}N_3]_8$ after different times in solution; (**A**) freshly prepared; (**B**) 30 min after preparation; (**C**) stored overnight in ACN/H_2O mixture of the eluent; *y*-axis elution at critical conditions (LCCC), *x*-axis SEC mode.

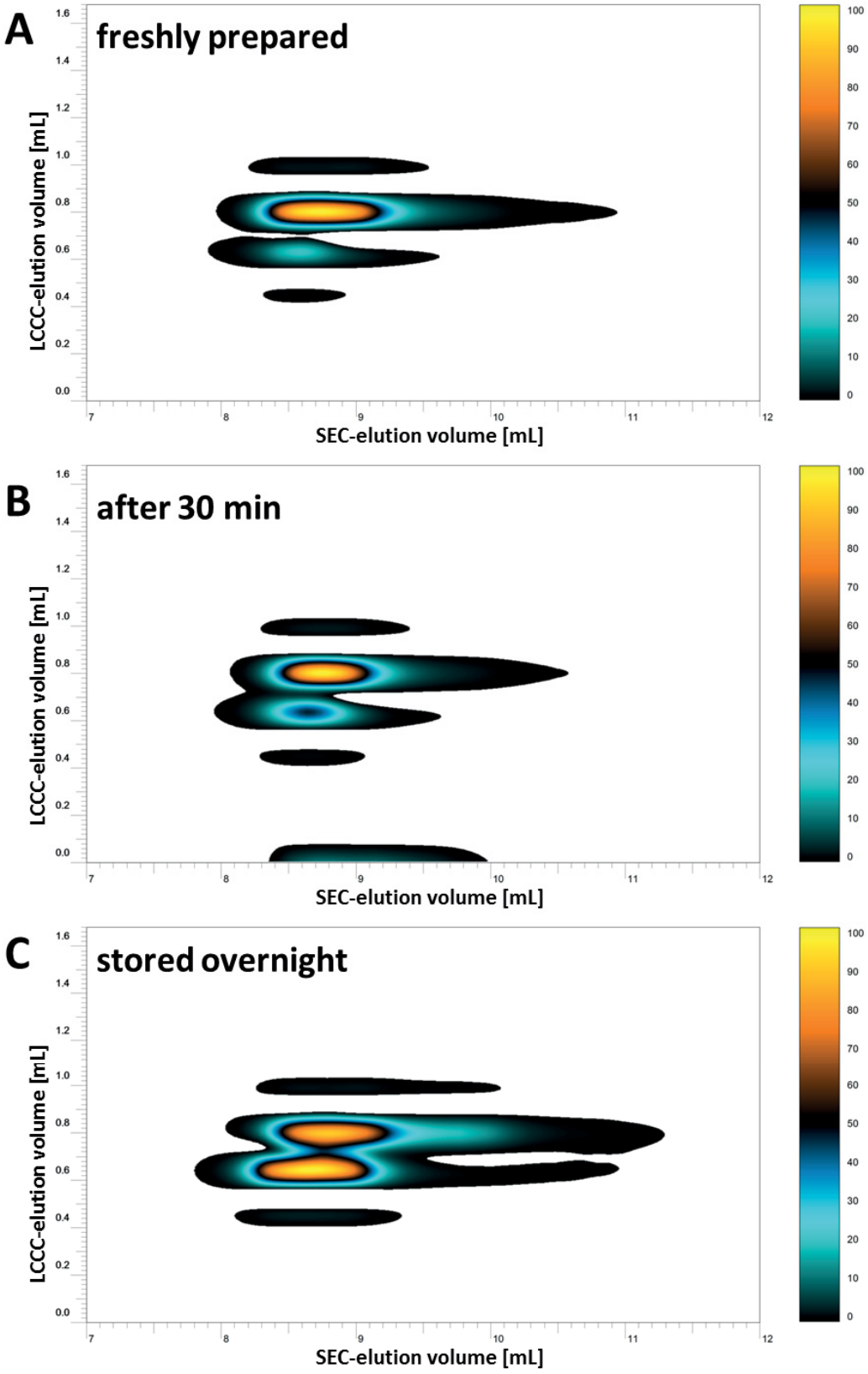

Figure S4. Comparison of characteristic signals in the ^{13}C-NMR spectra for $[PEO_{28}\text{-}OH]_8$ (black), $[PEO_{28}\text{-}Ts]_8$ (red), and $[PEO_{28}\text{-}N_3]_8$ (blue); (**A**) backbone $-CH_2-$ groups; (**B**) $-CH_2-OH$; (**C**) $-CH_2-N_3$.

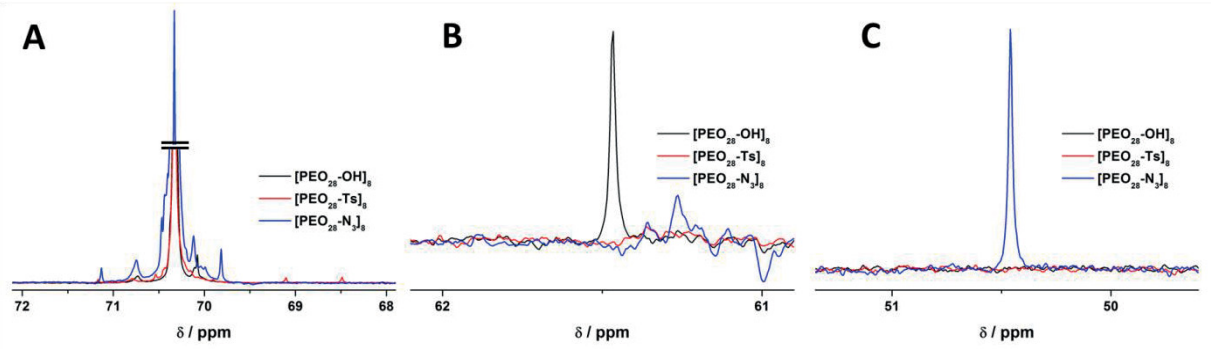

Figure S5. Schematic representation of the CROP of 2-ethyl-2-oxazoline initiated by $[PEO_{28}\text{-}Ts]_8$.

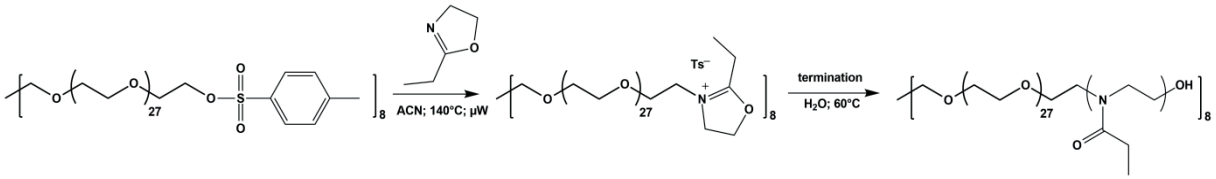

Figure S6. SEC traces for TB-$PEtOx_{20}$-OH (straight line), TB-$PEtOx_{60}$-OH (dashed line), and TB-$PEtOx_{80}$-OH (dotted line) on the chloroform (**A**) and dimethylacetamide (**B**) SEC.

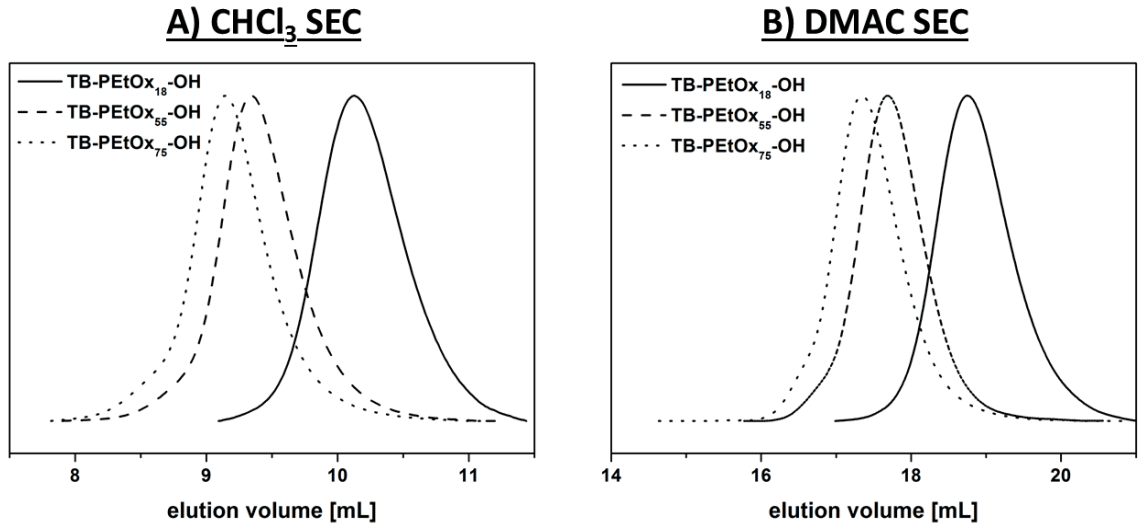

Figure S7. Characterization of the star-shaped block copolymer $[PEO_{28}$-*b*-$PEtOx_{55}]_8$ via: (**A**) NMR and (**B**) ATR-FT-IR.

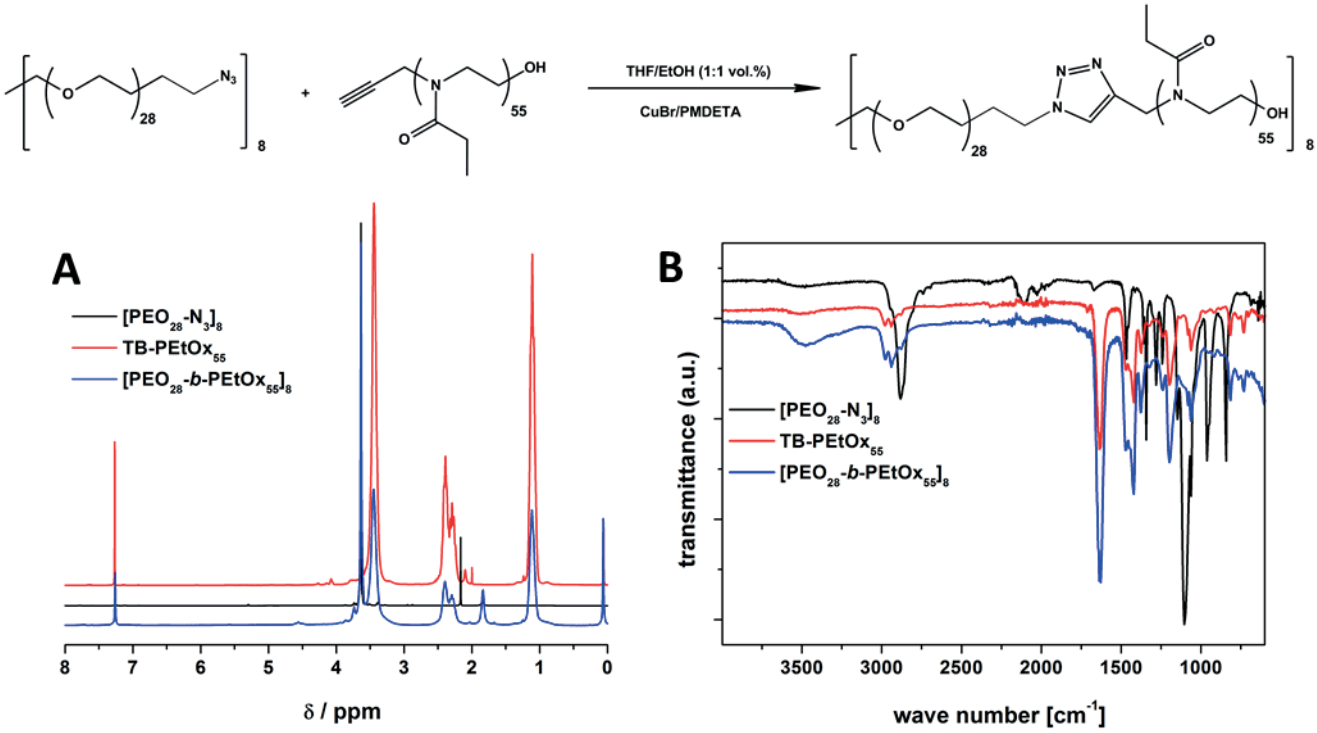

Figure S8. DLS CONTIN plots of the unfiltered samples of $[PEO_{28}$-*b*-$PEtOx_{18}]_8$ (black curve) and $[PEO_{28}$-*b*-$PEtOx_{75}]_8$ (red curve) in water.

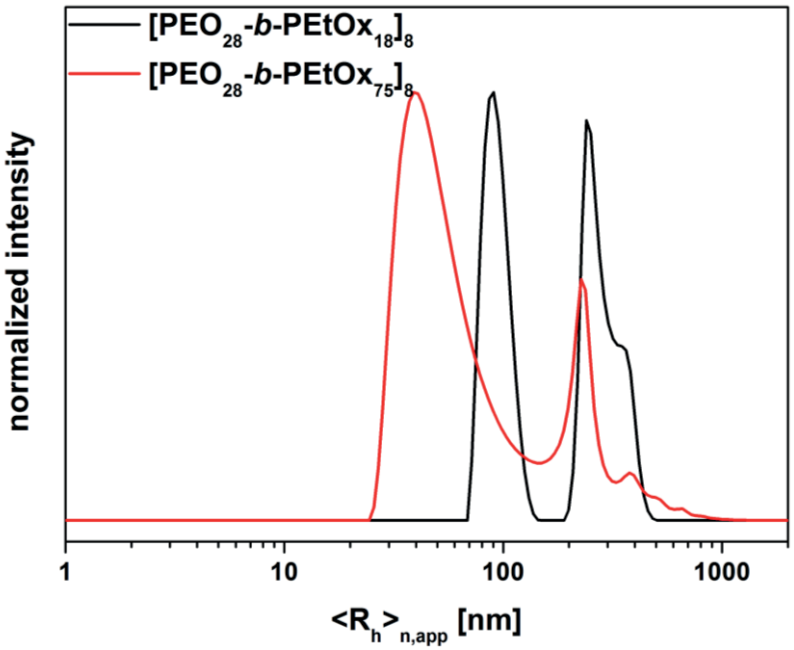

Publication P2

"Controlling Aqueous Self-Assembly Mechanisms via Hydrophobic Interactions"

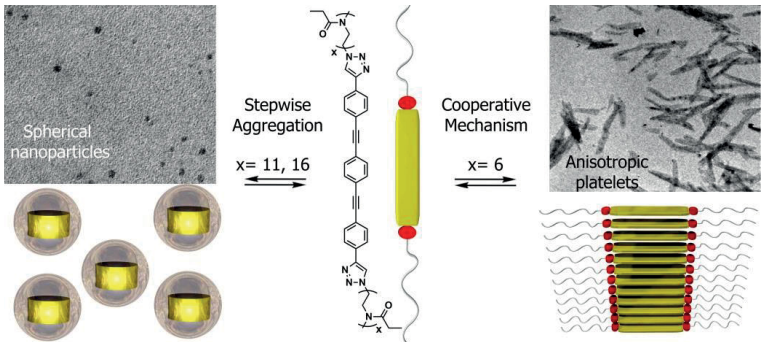

Tobias Rudolph,[#] Naveen K. Allampally,[#] Gustavo Fernandez, Felix H. Schacher

[#]Both authors contributed equally to this publication.

Chem. Eur. J., **2014**, 43, 13871-13875

ChemPubSoc Europe

DOI: 10.1002/chem.201404141

CHEMISTRY
A European Journal
Communication

Polymers

Controlling Aqueous Self-Assembly Mechanisms by Hydrophobic Interactions

Tobias Rudolph,[a] Naveen Kumar Allampally,[b] Gustavo Fernández,*[b] and Felix H. Schacher*[a]

Abstract: We report an innovative template-assisted synthetic protocol for the selective functionalization of terminal triple bonds in oligophenyleneethynylenes (OPE) by pre-organization in aqueous solution. By this approach, three new OPE-based bolaamphiphiles substituted with hydrophilic poly(2-ethyl-2-oxazoline) (PEtOx) chains of different length have been synthesized. The chain length was observed to strongly influence the aqueous supramolecular polymerization: bolaamphiphiles with longer hydrophilic chains aggregate into spherical nanoparticles in a stepwise fashion, whereas 2D anisotropic platelets are formed cooperatively if shorter PEtOx chains are used. Our results demonstrate that hydrophobic interactions can be strong enough to trigger cooperative effects in aqueous self-assembly processes.

Living systems extensively exploit various non-covalent interactions to create adaptive and multifunctional anisotropic self-assembled structures, such as the intracellular biopolymer scaffolding that is present in all cells, the cytoskeleton.[1] The degree of order of such systems is largely dependent on the mechanism followed by their constitutive repeating units to self-assemble.[2] If the equilibrium constant for all binding events is equal (isodesmic mechanism), random-coil supramolecular polymers without internal order are formed.[3] In contrast, two-state cooperative (nucleation–elongation) pathways[2,3] lead to the formation of highly organized structures when a certain activation step (nucleation) has been overcome. Hierarchical supramolecular polymers in organic media based on cooperative π–π interactions and hydrogen bonding,[4] metal–ligand,[5] dipolar,[6] ionic,[7] or metal–metal interactions[8] have been reported. Controlling noncovalent interactions in water, however, is certainly more challenging[9] and to date, cooperative aqueous self-assembly has been accomplished by introducing additional noncovalent forces, that is, hydrogen bonding, to already existing hydrophobic interactions.[10]

Herein, we demonstrate that aqueous supramolecular polymerization mechanisms can be exclusively controlled by tuning the balance between hydrophobic and hydrophilic fragments of the underlying building blocks. The systems under scrutiny (**1**–**3**) feature a hydrophobic π-conjugated oligophenyleneethynylene (OPE)-based segment functionalized with hydrophilic azide-substituted poly(2-ethyl-2-oxazoline) (PEtOx$_x$-N$_3$) side groups of variable length (Figure 1). Our motivation to design these systems is two-fold: 1) the high degree of pre-organization and excellent optical properties of OPEs[11] should ensure a predictable self-assembly through π–π and hydrophobic interactions that can be readily monitored by various spectroscopic techniques and 2) PEtOx groups combine the high solubility, biocompatibility, and similar "stealth effect" as polyethylene glycol (PEG)[12] and the possibility to balance solvophilic/solvophobic interactions as demonstrated for block copolymers[13] in selective solvents. The OPE-based aromatic fragment (1,4-bis[(4-ethynylphenyl)ethynyl]benzene) has been synthesized according to literature procedures,[14] whereas the corresponding PEtOx$_x$-N$_3$ precursors ($x=6$, 11, 16) with different molar mass and low dispersity indices ($Đ$; <1.2) have been obtained by microwave-assisted cationic ring-opening polymerization (CROP) of EtOx (for synthetic details see Scheme S1 and Table S1 in the Supporting Information). The attachment of the PEtOx side groups to the hydrophobic OPE fragment was accomplished by copper-catalyzed azide–alkyne cycloaddition (CuAAC) click chemistry,[15] which is a widely used procedure for the synthesis of monomers,[16] polymers,[17] post-polymerization modification reactions,[18] and various polymeric architectures.[19] However, typical CuAAC reaction conditions in THF or DMF at room temperature or elevated temperatures (~80 °C) generated a significant amount of undesired side products, as both internal and terminal alkyne functionalities seem to participate in the reaction (see Figure S2 in the Supporting Information).[20] To circumvent this problem, we envisaged that the pre-organization of the OPE precursor by means of self-assembly in a selective solvent mixture would hinder the reactivity of internal triple bonds and enable the selective functionalization of the terminal alkynes. To that end, we dissolved the OPE precursor in THF and added water until a slight

[a] *T. Rudolph,[+] F. H. Schacher*
Laboratory of Organic and Macromolecular Chemistry
Friedrich Schiller University Jena, Humboldtstr. 10
07743 Jena (Germany) and Jena Center for Soft Matter (JCSM)
Friedrich Schiller University Jena, Philosophenweg 7
07743 Jena (Germany)
E-mail: felix.schacher@uni-jena.de

[b] *N. Kumar Allampally,[+] G. Fernández*
Institut für Organische Chemie and Center for Nanosystems Chemistry, Universität Würzburg
Am Hubland, 97074 Würzburg (Germany)
E-mail: gustavo.fernandez@uni-wuerzburg.de

[+] *These authors contributed equally to this work.*

Supporting information for this article is available on the WWW under http://dx.doi.org/10.1002/chem.201404141.

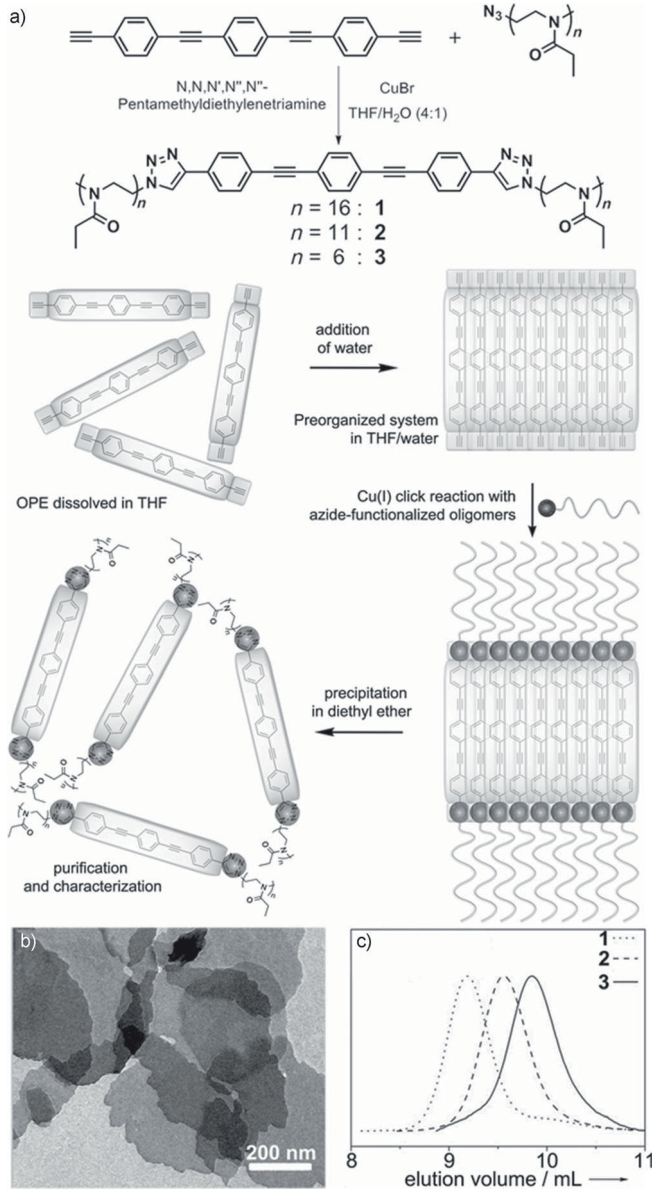

Figure 1. a) Synthetic scheme and strategy followed to obtain the targeted $PEtOx_x$-OPE-$PEtOx_x$ amphiphiles **1**–**3** by selectively pre-organizing the terminal alkyne groups. b) TEM micrograph showing the sheet-like structures formed by the OPE starting material in THF/H_2O (4:1, v/v, 2.5 mg mL^{-1}) on a carbon-coated copper grid. c) Comparison of SEC traces for **1**–**3**.

turbidity was observed (~4:1, v/v, THF/H_2O), which is indicative of aggregate formation (Figure 1a). Transmission electron microscopy (TEM) studies demonstrate the formation of sheet-like aggregates of several hundred nanometers width (Figures 1b and S6) in which the internal alkyne groups are most likely located within the interior of the structure,[21] whereas the more polar terminal triple bonds are exposed to the aqueous medium. This has been confirmed by the fact that only the desired $PEtOx_x$-OPE-$PEtOx_x$ ($x=16$ (**1**), $x=11$ (**2**), $x=6$ (**3**)) bolaamphiphiles are obtained in good yields (>75%) upon treatment with $PEtOx_x$-N_3, CuBr, and *N*,*N*,*N*′,*N*′,*N*″-pentamethyldiethylenetriamine in the microwave synthesizer at 80°C for 10 min (see Figures 1c and Figures S3–5 in the Supporting Information for characterization details). Well-defined bolaamphiphiles **1**–**3** have been characterized by ^{1}H- and ^{13}C-NMR, FTIR, and size exclusion chromatography (SEC, see Table S1 in the Supporting Information).

The influence of the length of the attached PEtOx chains on the self-assembly of $PEtOx_x$-OPE-$PEtOx_x$ **1**–**3** in solution has been investigated by using a combination of UV/Vis, fluorescence, dynamic light scattering (DLS), and TEM experiments. All materials are present in the monomeric state in both THF and $CHCl_3$, showing π–π absorption maxima around 343 nm and a shoulder at 366 nm (Figures 2a,c and Figure S7 in the Supporting Information). Aggregation can now be induced by adding different amounts of water to the corresponding solutions of **1**–**3** in THF. For the derivative with the longest side chains ($PEtOx_{16}$-OPE-$PEtOx_{16}$, **1**), aggregation only occurs if pure water is used as the solvent, as evidenced by a broadening and blue-shift of the absorption maximum from 343 to 328 nm (Figure 2a). Emission studies in various THF/water mixtures show a noticeable drop-off in the fluorescence intensity only in pure water (Figure 2b), which hints towards the association of the aromatic segments.[22] On the basis of both absorption and emission experiments, the longer and water soluble PEtOx chains of **1** appear to counterbalance the propensity of the short OPE fragment to self-assemble through π–π and hydrophobic interactions, thereby yielding highly water soluble assemblies. Comparable results are observed for $PEtOx_{11}$-OPE-$PEtOx_{11}$ (**2**) featuring slightly shorter PEtOx chains (see Figure S7 in the Supporting Information), in which a slightly increased fluorescence quenching in water compared to **1** is observed. On the other hand, for the amphiphilic system with the shortest hydrophilic PEtOx side chains ($PEtOx_6$-OPE-$PEtOx_6$, **3**), aggregates are formed even in the presence of 10% of THF as a result of increased hydrophobic interactions (Figure 2c).[23] In addition, the fluorescence quenching is significantly increased compared to **1** and **2** and the emission band spreads up to ~600 nm (Figure 2d), which suggests a distinctly different aggregation behavior than in both other cases.

To ascertain whether this assumption holds true, we have investigated the self-assembly mechanisms of all materials in water. Figure 3a shows temperature-dependent UV/Vis spectra of an aqueous solution of $PEtOx_{16}$-OPE-$PEtOx_{16}$ (**1**) at 2.4×10^{-5} M between 358 and 278 K. Upon cooling from a molecularly dissolved state at a rate of 1 K min^{-1}, spectral changes associated with the formation of self-assembled species can be observed, such as a broadening of the transitions at 333 and 368 nm (Figure 3a). The presence of isosbestic points at 363 and 305 nm confirms that the process is thermodynamically reversible under these conditions. A cooling curve is monitored from 358 to 278 K at 320 nm, which can be clearly fitted to a Boltzmann function, confirming that the self-assembly of **1** follows an isodesmic (non-cooperative) mechanism (Figures 3b and S8 in the Supporting Information).[24] All thermodynamic parameters are listed in Table 1. Each event in the self-assembly process is occurring with a binding constant of 9.6×10^4 M^{-1} (Table 1). For $PEtOx_{11}$-OPE-$PEtOx_{11}$ (**2**), a similar behavior has been observed, although the value of the binding constant is considerably higher (3.6×10^6 M^{-1}, Table 1) as a result of in-

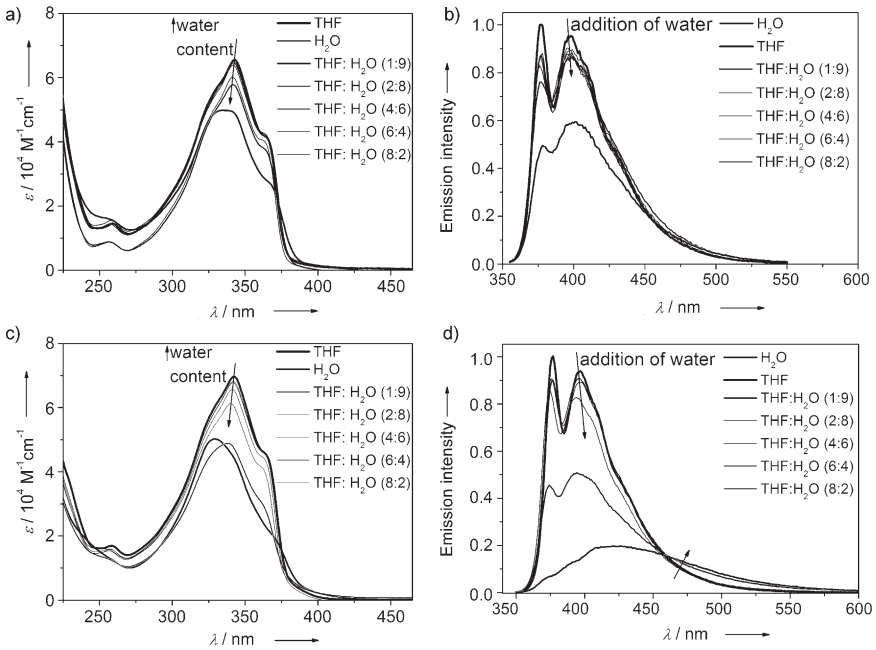

Figure 2. UV/Vis (a,c) and emission spectra (b,d) of **1** (a,b) and **3** (c,d), in various THF/water mixtures at 6×10^{-6} M for **1** and 1.47×10^{-5} M for **3**.

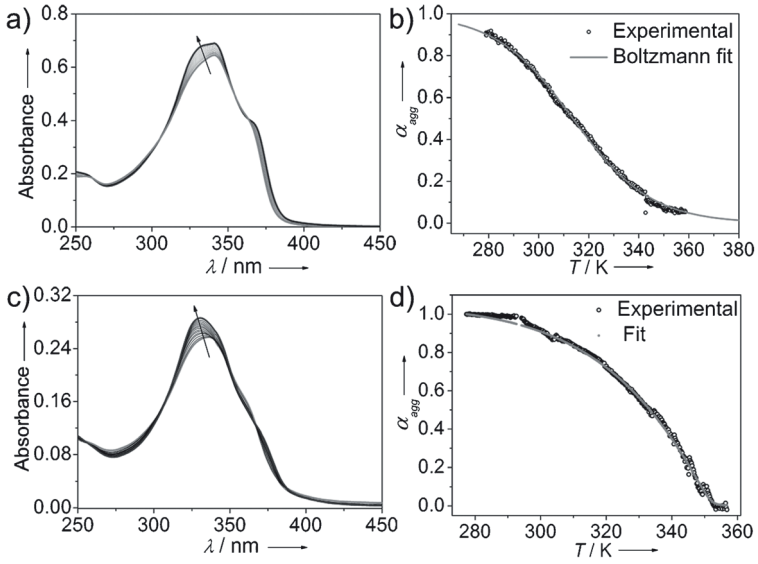

Figure 3. Temperature-dependent UV/Vis spectra of **1** at 2.4×10^{-5} M (a) and **3** at 6×10^{-6} M (c) in water from 358 to 278 K. Arrows indicate the spectral changes upon temperature decrease. Cooling curves obtained by monitoring the spectral changes observed in temperature-dependent experiments at 320 nm for **1** (b) and **3** (d) and corresponding fits to the isodesmic model for **1** (b) and nucleation–elongation model for **3** (d).

creased hydrophobic interactions (see Figure S9 in the Supporting Information).

Interestingly, the behaviour of $PEtOx_6$-OPE-$PEtOx_6$ (**3**), exhibiting the highest hydrophobic character of the series, turned out to be entirely different. Figure 3c shows the temperature dependent UV/Vis spectra of an aqueous 6×10^{-6} M solution of **3**. Upon cooling a monomer solution from 358 to 278 K at a rate of 1 K min^{-1}, different spectral changes are observed. For instance, the absorption maximum is shifted from 335 to 330 nm along with two clear isosbestic points at 308 and 367 nm, again confirming thermodynamic equilibrium between monomeric and self-assembled species (Figure 3c). However, the shoulder present in the case of **1** and **2** at 365 nm becomes now less pronounced (Figure 3c), which suggests a distinct arrangement of the OPE segments in the aggregated state.[25] In addition, the cooling curve extracted from temperature-dependent studies at 320 nm is clearly non-sigmoidal in shape, which is characteristic of a cooperative self-assembly process.[2] The curve can be unambiguously fitted to a nucleation–elongation model developed by ten Eikelder, Markvoort, Meijer, and co-workers[26] (Figure 3d) and the respective thermodynamic parameters are listed in Table 1. According to our results, **3** initially forms nuclei consisting of two molecules at high temperature with a small value of the binding constant K_d (18.4 M^{-1}) and this step can be considered as highly unfavorable. Upon further decreasing the temperature, the formed dimers then elongate into ordered self-assembled superstructures with a significantly larger value of the binding constant K_e (1.43×10^6 M^{-1}, Table 1). Our results indicate that hydrophobic interactions are the main driving force for the observed cooperativity, as $PEtOx_6$-OPE-$PEtOx_6$ (**3**) with the shortest PEtOx hydrophilic chains is the only sample of our series for which self-assembly in a cooperative fashion is found. However, other interactions, such as those between the hydrophilic polymer chains as well as hydrogen bonds involving triazole units of the PEtOx chains and surrounding water molecules (IR experiments show the appearance of a broad band between 3700–3200 cm^{-1}—see also Figure S3), are also most likely contributing to the cooperative effects in our system.

The influence of the self-assembly pathways of **1**–**3** on the aggregate morphology has been examined using TEM and DLS studies. At concentrations of 2 mg mL^{-1}, **1** and **2** form narrowly dispersed spherical aggregates of 5–12 nm in diameter according to TEM, which is in good agreement with DLS measurements ($\langle R_{h,app}\rangle = 7$ nm, Figures 4a, c and Figure S10 in the Supporting Information). The large size and water solubility of the PEtOx chains of **1** and **2** compared to the relatively short OPE fragment is most likely responsible for

Table 1. Thermodynamic parameters for the aqueous self-assembly of different $PEtOx_x$-OPE-$PEtOx_x$ bolaamphiphiles.

Sample	c [M]	K_a [M^{-1}]	T_m/K	DP_N	ΔH [kJ mol^{-1}]	ΔS [J mol^{-1}]	ΔG [kJ mol^{-1}]
1	2.4×10^{-5}	9.6×10^{4}	313.5	1.4	−60.7	−108.9	−28.5
2	5.6×10^{-6}	3.6×10^{6}	334.9	1.4	−83.2	−153.4	−37.4

Sample	c [M]	K_d [M^{-1}]	K_e [M^{-1}]	σ	T_e [K]	N	ΔH [kJ mol^{-1}]	ΔS [J mol^{-1}]	$\triangle H_{nucl}$ [kJ mol^{-1}]
3	6×10^{-6}	18.4	1.43×10^{6}	1.3×10^{-5}	351.2	2	−35.11	0	−27.90

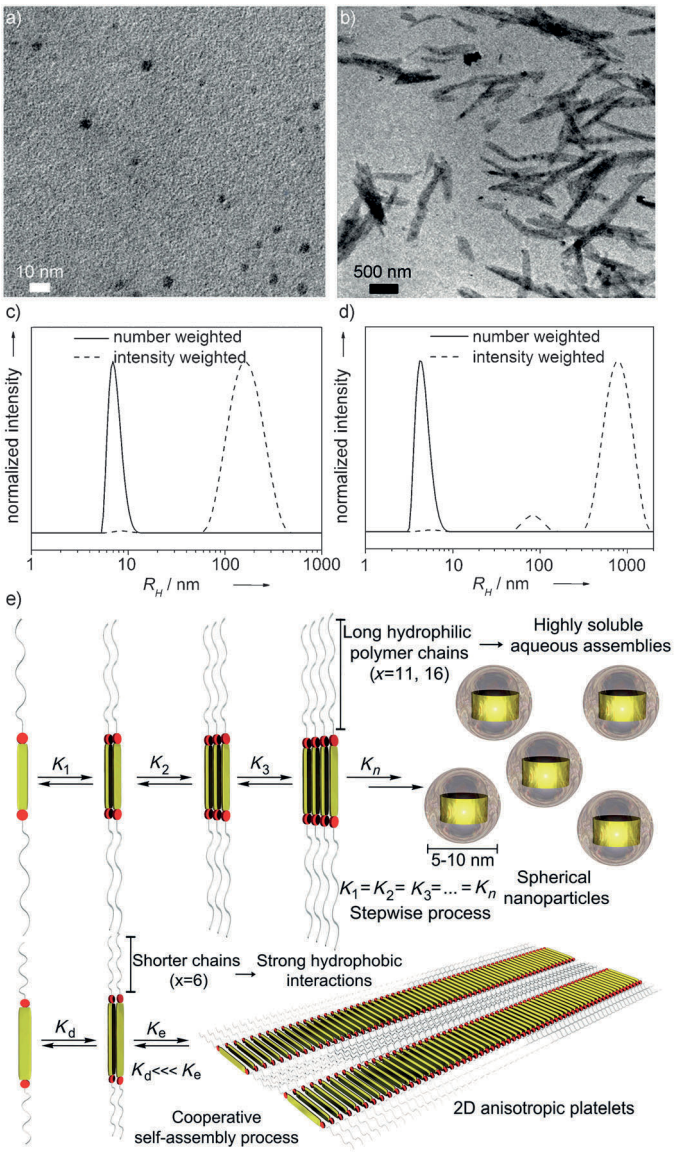

Figure 4. TEM micrographs of a) **1** and b) **3** in water at 2 mg mL^{-1} on a carbon-coated copper grid. c–d) DLS CONTIN plots of a) **1** and d) **3** in water at 2 mg mL^{-1}. e) Cartoon representation of the self-assembly pathways of **1** and **2** (top) and **3** (bottom).

the formation of low-dimensional associates in which the OPE fragments are shielded by the peripheral polymer chains (Figure 4e, top). In sharp contrast, more hydrophobic $PEtOx_6$-OPE-$PEtOx_6$ (**3**) self-assembles into anisotropic two-dimensional (2D) platelets of up to 2 μm in length and ~100–300 nm in width (Figure 4b). Although the schematic depiction shows a monolayer in the case of the anisotropic aggregates, the rather high contrast in TEM as well as the large hydrophobic surface of the OPE stacks suggests that also stacks of these sheets are observed.

DLS studies show a good correlation between the aggregate dimensions observed by TEM and the existence of several size distributions ($\langle R_{h,app}\rangle$ = ~4, 80, 800 nm) observed in solution (Figure 4d). Considering these data, the increased hydrophobicity of **3** induces a stronger packing of the OPE fragments in a preferred direction driven by π–π and hydrophobic interactions, resulting in the formation of anisotropic superstructures. Further lateral interactions involving the PEtOx chains ultimately lead to 2D plate-like structures that possess a higher degree of organization than the associates of **1** and **2** (Figure 4e, bottom).

In conclusion, we have synthesized three $PEtOx_x$-OPE-$PEtOx_x$ bolaamphiphiles (x = 16 (**1**), 11 (**2**), 6 (**3**)) by introducing a strategy for template-assisted and selective CuAAC chemistry, in which pre-organization of the OPEs resulted in the selective functionalization of the terminal alkyne moieties. The aqueous self-assembly of **1**–**3** can be effectively controlled by the length of attached side chains, as demonstrated by UV/Vis, fluorescence, DLS and TEM studies. Thus, whereas highly water soluble derivatives **1** and **2** self-assemble into spherical nanoparticles following an isodesmic (non-cooperative) mechanism, shortening of the $PEtOx_x$ chains in **3** induces the formation of anisotropic platelets of higher dimensionality in a cooperative fashion. We have demonstrated that cooperative supramolecular polymerization processes in water can be primarily controlled by hydrophobic interactions. Our results underline that a thorough analysis of self-assembly mechanisms is a prerequisite for understanding both the degree of organization and the morphology of supramolecular structures.

Experimental Section

General experimental details

^{1}H, ^{13}C NMR, FTIR, DLS, UV/Vis spectra, and further TEM micrographs are provided in the Supporting Information.

Acknowledgements

F.H.S. thanks the VCI for an independent researcher fellowship, and T.R. the Carl-Zeiss foundation for a PhD scholarship. F.H.S. and T.R. also acknowledge the Thuringian Ministry for Education, Science and Culture (grants #B514-09051, NanoConSens and #B515-10065, ChaPoNano) for financial support. G. F. thanks the Humboldt Foundation for financial support (Sofja Kovalevskaja Award) and Prof. Würthner for helpful discussions. F.H.S. further acknowledges U.S. Schubert for continuous support.

Keywords: amphiphilic systems · cooperativity · π-conjugated systems · polymers · self-assembly

[1] F. Huber, J. Schnauß, S. Rönicke, P. Rauch, K. Müller, C. Fütterer, J. Käs, *Adv. Phys.* **2013**, *62*, 1 – 112.

[2] a) C. Kulkarni, S. Balasubramanian, S. J. George, *ChemPhysChem* **2013**, *14*, 661 – 673; b) T. F. A. De Greef, M. M. J. Smulders, M. Wolffs, A. P. H. J. Schenning, R. P. Sijbesma, E. W. Meijer, *Chem. Rev.* **2009**, *109*, 5687 – 5754; c) Z. Chen, A. Lohr, C. R. Saha-Moller, F. Würthner, *Chem. Soc. Rev.* **2009**, *38*, 564 – 584; d) D. Zhao, J. S. Moore, *Org. Biomol. Chem.* **2003**, *1*, 3471 – 3491.

[3] T. Aida, E. W. Meijer, S. I. Stupp, *Science* **2012**, *335*, 813 – 817.

[4] a) C. Rest, M. J. Mayoral, K. Fucke, J. Schellheimer, V. Stepanenko, G. Fernández, *Angew. Chem. Int. Ed.* **2014**, *53*, 700 – 705; *Angew. Chem.* **2014**, *126*, 716 – 722; b) F. Fennel, S. Wolter, Z. Xie, P.-A. Plötz, O. Kühn, F. Würthner, S. Lochbrunner, *J. Am. Chem. Soc.* **2013**, *135*, 18722 – 18725; c) Y.-J. Tian, E. W. Meijer, F. Wang, *Chem. Commun.* **2013**, *49*, 9197 – 9199; d) F. Wang, M. A. J. Gillissen, P. J. M. Stals, A. R. A. Palmans, E. W. Meijer, *Chem. Eur. J.* **2012**, *18*, 11761 – 11770; e) F. García, L. Sánchez, *J. Am. Chem. Soc.* **2012**, *134*, 734 – 742;f) F. Aparicio, E. Matesanz, L. Sanchez, *Chem. Commun.* **2012**, *48*, 5757 – 5759; g) F. García, P. M. Viruela, E. Matesanz, E. Ortí, L. Sánchez, *Chem. Eur. J.* **2011**, *17*, 7755 – 7759; h) T. Seki, A. Asano, S. Seki, Y. Kikkawa, H. Murayama, T. Karatsu, A. Kitamura, S. Yagai, *Chem. Eur. J.* **2011**, *17*, 3598 – 3608; i) M. M. J. Smulders, A. P. H. J. Schenning, E. W. Meijer, *J. Am. Chem. Soc.* **2008**, *130*, 606 – 611; j) M. Bellot, L. Bouteiller, *Langmuir* **2008**, *24*, 14176 – 14182; k) L. Bouteiller, O. Colombani, F. Lortie, P. Terech, *J. Am. Chem. Soc.* **2005**, *127*, 8893 – 8898.

[5] a) J. W. Wackerly, J. S. Moore, *Macromolecules* **2006**, *39*, 7269 – 7276; b) M. T. Stone, J. S. Moore, *J. Am. Chem. Soc.* **2005**, *127*, 5928 – 5935.

[6] G. Fernández, M. Stolte, V. Stepanenko, F. Würthner, *Chem. Eur. J.* **2013**, *19*, 206 – 217.

[7] M. T. Fenske, W. Meyer-Zaika, H.-G. Korth, H. Vieker, A. Turchanin, C. Schmuck, *J. Am. Chem. Soc.* **2013**, *135*, 8342 – 8349.

[8] M. J. Mayoral, C. Rest, V. Stepanenko, J. Schellheimer, R. Q. Albuquerque, G. Fernandez, *J. Am. Chem. Soc.* **2013**, *135*, 2148 – 2151.

[9] a) J. B. Matson, S. I. Stupp, *Chem. Commun.* **2012**, *48*, 26 – 33; b) H.-J. Kim, T. Kim, M. Lee, *Acc. Chem. Res.* **2011**, *44*, 72 – 82; c) B. Rybtchinski, *ACS Nano* **2011**, *5*, 6791 – 6818; d) E. Krieg, B. Rybtchinski, *Chem. Eur. J.* **2011**, *17*, 9016 – 9026; e) T. Rehm, C. Schmuck, *Chem. Commun.* **2008**, 801 – 813; f) J.-H. Ryu, D.-J. Hong, M. Lee, *Chem. Commun.* **2008**, 1043 – 1054; g) G. V. Oshovsky, D. N. Reinhoudt, W. Verboom, *Angew. Chem. Int. Ed.* **2007**, *46*, 2366 – 2393; *Angew. Chem.* **2007**, *119*, 2418 – 2445.

[10] a) F. García, J. Buendía, L. Sánchez, *J. Org. Chem.* **2011**, *76*, 6271 – 6276; b) S. Han, S. Cao, Y. Wang, J. Wang, D. Xia, H. Xu, X. Zhao, J. R. Lu, *Chem. Eur. J.* **2011**, *17*, 13095 – 13102; c) C. M. A. Leenders, L. Albertazzi, T. Mes, M. M. E. Koenigs, A. R. A. Palmans, E. W. Meijer, *Chem. Commun.* **2013**, *49*, 1963 – 1965; d) E. Obert, M. Bellot, L. Bouteiller, F. Andrioletti, C. Lehen-Ferrenbach, F. Boué, *J. Am. Chem. Soc.* **2007**, *129*, 15601 – 15605; e) H. Frisch, J. P. Unsleber, D. Lüdeker, M. Peterlechner, G. Brunklaus, M. Waller, P. Besenius, *Angew. Chem. Int. Ed.* **2013**, *52*, 10097 – 10101; *Angew. Chem.* **2013**, *125*, 10282 – 10287.

[11] a) A. Beeby, K. Findlay, P. J. Low, T. B. Marder, *J. Am. Chem. Soc.* **2002**, *124*, 8280 – 8284; b) U. H. F. Bunz, *Chem. Rev.* **2000**, *100*, 1605 – 1644.

[12] K. Knop, R. Hoogenboom, D. Fischer, U. S. Schubert, *Angew. Chem. Int. Ed.* **2010**, *49*, 6288 – 6308; *Angew. Chem.* **2010**, *122*, 6430 – 6452.

[13] a) Y. Mai, A. Eisenberg, *Chem. Soc. Rev.* **2012**, *41*, 5969 – 5985; b) A. Choucair, A. Eisenberg, *Eur. Phys. J. E* **2003**, *10*, 37 – 44; c) D. A. Rider, I. Manners, *Polym. Rev.* **2007**, *47*, 165 – 195; d) F. H. Schacher, P. A. Rupar, I. Manners, *Angew. Chem. Int. Ed.* **2012**, *51*, 7898 – 7921; *Angew. Chem.* **2012**, *124*, 8020 – 8044.

[14] M. S. Khan, A. K. Kakkar, N. J. Long, J. Lewis, P. Raithby, P. Nguyen, T. B. Marder, F. Wittmann, R. H. Friend, *J. Mater. Chem.* **1994**, *4*, 1227 – 1232.

[15] a) V. V. Rostovtsev, L. G. Green, V. V. Fokin, K. B. Sharpless, *Angew. Chem.* **2002**, *114*, 2708 – 2711; b) H. C. Kolb, M. G. Finn, K. B. Sharpless, *Angew. Chem. Int. Ed.* **2001**, *40*, 2004 – 2021; *Angew. Chem.* **2001**, *113*, 2056 – 2075.

[16] S. Beghdadi, I. A. Miladi, D. Addis, H. B. Romdhane, J. Bernard, E. Drockenmuller, *Polym. Chem.* **2012**, *3*, 1680 – 1692.

[17] C. Lang, D. Voll, A. J. Inglis, N. Dingenouts, A. S. Goldmann, L. Barner, C. Barner-Kowollik, *Macromol. Rapid Commun.* **2011**, *212*, 831 – 839.

[18] A. S. Goldmann, M. Glassner, A. J. Inglis, C. Barner-Kowollik, *Macromol. Rapid Commun.* **2013**, *34*, 810 – 849.

[19] a) T. Rudolph, S. Crotty, M. v. d. Lühe, D. Pretzel, U. S. Schubert, F. H. Schacher, *Polymers* **2013**, *5*, 1081 – 1101; b) B. V. K. J. Schmidt, T. Rudolph, M. Hetzer, H. Ritter, F. H. Schacher, C. Barner-Kowollik, *Polym. Chem.* **2012**, *3*, 3139 – 3145; c) A. Hanisch, H. Schmalz, A. H. E. Müller, *Macromolecules* **2012**, *45*, 8300 – 8309.

[20] M. Arseneault, I. Levesque, J.-F. Morin, *Macromolecules* **2012**, *45*, 3687 – 3694.

[21] G. Fernandez, F. Garcia, F. Aparicio, E. Matesanz, L. Sanchez, *Chem. Commun.* **2009**, 7155 – 7157.

[22] J.-H. Ryu, H.-J. Kim, Z. Huang, E. Lee, M. Lee, *Angew. Chem. Int. Ed.* **2006**, *45*, 5304 – 5307; *Angew. Chem.* **2006**, *118*, 5430 – 5433.

[23] C. A. Hunter, *Angew. Chem. Int. Ed.* **2004**, *43*, 5310 – 5324; *Angew. Chem.* **2004**, *116*, 5424 – 5439.

[24] M. M. J. Smulders, M. M. L. Nieuwenhuizen, T. F. A. de Greef, P. van der Schoot, A. P. H. J. Schenning, E. W. Meijer, *Chem. Eur. J.* **2010**, *16*, 362 – 367.

[25] M. J. Mayoral, C. Rest, J. Schellheimer, V. Stepanenko, G. Fernandez, *Chem. Eur. J.* **2012**, *18*, 15607 – 15611.

[26] a) A. J. Markvoort, H. M. ten Eikelder, P. A. Hilbers, T. F. de Greef, E. W. Meijer, *Nat. Commun.* **2011**, *2*, 509; b) H. M. M. ten Eikelder, A. J. Markvoort, T. F. A. de Greef, P. A. J. Hilbers, *J. Phys. Chem. B* **2012**, *116*, 5291 – 5301.

Received: June 26, 2014
Published online on September 8, 2014

CHEMISTRY
A European Journal

Supporting Information

Controlling Aqueous Self-Assembly Mechanisms by Hydrophobic Interactions

Tobias Rudolph,[a] Naveen Kumar Allampally,[b] Gustavo Fernández,*[b] and Felix H. Schacher*[a]

chem_201404141_sm_miscellaneous_information.pdf

Supporting Information

Controlling Aqueous Self-Assembly Mechanisms *via* Hydrophobic Interactions

Tobias Rudolph,[1,+] Naveen Kumar Allampally,[2,+] Gustavo Fernandez,[2,*] Felix H. Schacher[1,*]

+ Author Tobias Rudolph and Author Naveen Kumar Allampally equally contributed to this work

[1] Laboratory of Organic and Macromolecular Chemistry, Friedrich Schiller University Jena, Humboldtstr. 10, 07743 Jena, Germany
E-mail: felix.schacher@uni-jena.de

[2] Institute for Organic Chemistry and Center for Nanosystems Chemistry, Julius-Maximaillians-University of Würzburg, Am Hubland, 97074Würzburg, Germany

E-mail: gustavo.fernandez@uni-wuerzburg.de

Experimental Section

Instruments:

NMR: Proton nuclear magnetic resonance (^{1}H-NMR) spectra were recorded in $CDCl_3$ on a Bruker AC 300 MHz spectrometer at 298 K. Chemical shifts are given in parts per million (ppm, δ scale) relative to the residual signal of the deuterated solvent. Carbon NMR (^{13}C-NMR) spectra were recorded with 75 MHz.

SEC: Size exclusion chromatography was measured on a Shimadzu system equipped with an SCL-10A system controller, an LC-10AD pump and an RID-10A refractive index detector using a solvent mixture containing chloroform ($CHCl_3$), triethylamine (TEA) and *iso*-propanol (*i*-PrOH) (94:4:2) at a flow rate of 1 mL min^{-1} on a PSS SDV linear M 5 µm column. The system was calibrated using polystyrene (100 to 100,000 g mol^{-1}) standards.

FT-IR Infra-red spectroscopy: Dry powders of the materials were directly placed on the crystal of the ATR-FTIR (Affinity-1 FTIR, Shimadzu) for measurements in the range of 4000 to 600 cm^{-1}.

Microwave-assisted polymerizations were carried out utilizing an Initiator Sixty single-mode microwave synthesizer from Biotage, equipped with a non-invasive IR sensor (accuracy: 2%). Microwave vials (conical, 0.5 to 2 mL) were heated at 110 °C overnight and allowed to cool to room temperature under nitrogen atmosphere. All polymerizations were carried out using temperature control.

DLS: Dynamic light scattering was performed at a scattering angle of 90° on an ALV CGS-3 instrument equipped with a He-Ne laser operating at a wavelength of 633 nm at 25 °C. Tetrahydrofuran

(THF) (polytetrafluoroethylene (PTFE); 0.45 µm) and MilliQ-water (glass faser (GF); 1–2 µm) were filtered before usage. The CONTIN algorithm was applied to analyze the obtained correlation functions. For temperature control, the DLS is equipped with a Lauda thermostat. Apparent hydrodynamic radii were calculated according to the Stokes-Einstein equation.

Transmission electron microscopy (TEM): The formed aggregates were analyzed using a TEM (Zeiss-CEM 902A, Oberkochen, Germany) operated at 80 kV. Images were recorded using a 1k TVIPS FastScan CCD camera. TEM samples were prepared by applying a drop of an aqueous sample solution onto the surface of a plasma-treated carbon coated copper grid (Holey Carbon Grid + 2nm C; Quantifoil Micro-Tools GmbH, Jena, Germany).

UV-Vis and Fluorescence spectroscopy: For all spectroscopic measurements, spectroscopic grade solvents (Uvasol) from Merck were used. The standard UV-Vis measurements were carried out on a Perkin-Elmer Lambda 35 at room temperature. λ is denoted in nm and ε in M^{-1} cm^{-1}. The steady-state fluorescence spectra were recorded on a PTI QM4-2003 fluorescence spectrometer and corrected against photomultiplier (type R928) and lamp intensity of the 75 W Xenon lamp (type Ushio UXL-75 XE).

Materials

Acetonitrile (ACN) for the polymerizations was purified using a Solvent Purification System (SPS, Innovative Technology, PM-400-3-MD) equipped with two activated alumina columns. 2-Ethyl-2-oxazoline (EtOx) and Methyl *p*-toluenesulfonate (MeOTs) (Aldrich) were distilled over barium oxide under reduced pressure before polymerization and stored under argon. For the synthesis OPE, 1,4-diiodobenzene, $Pd(PPh_3)_2Cl_2$, CuI, triethylamine, K_2CO_3, diisopropylamine, and trimethylsilylacetylene were purchased from Sigma-Aldrich, Merck and TCI. All other chemicals were used as purchased if not otherwise mentioned in the text.

Synthesis of Azide-Functionalized $PEtOx_x$-N_3

Methyl *p*-toluenesulfonate and 2-ethyl-2-oxazoline (EtOx) were dissolved in acetonitrile (ACN) at different monomer to initiator ratios ([M]/[I] = 5, 10 and 15) and at a monomer concentration of 4 M. The capped vials were placed in a microwave synthesizer at 140 °C. The polymerization was terminated *via* the addition of dried sodium azide under inert conditions. The polymers were obtained after extraction with $NaHCO_3$ solution, brine and dried under vacuum. After precipitation in cold diethyl ether, the polymer was filtered and dried under vacuum.

$PEtOx_6$-N_3: SEC ($CHCl_3$/*i*-PrOH/Et_3N): M_n = 900 g mol^{-1}; Đ = 1.12 (PS-calibration); **$PEtOx_{11}$-N_3: SEC ($CHCl_3$/*i*-PrOH/Et_3N):** M_n = 1300 g mol^{-1}; Đ = 1.12 (PS-calibration); **$PEtOx_{16}$-N_3: SEC ($CHCl_3$/*i*-PrOH/Et_3N):** M_n = 2100 g mol^{-1}; Đ = 1.10 (PS-calibration); **^{1}H-NMR (300 MHz, $CDCl_3$, δ):** 3.6–3.2 (br, –N–CH_2–CH_2–), 2.5–2.2 (br, CO–CH_2–CH_3), 1.2–0.9 (br, CO–CH_2–CH_3) ppm. **^{1}H-NMR (300 MHz, d_6-DMSO, δ):** 3.9–3.1 (br, –N–CH_2–CH_2–), 2.45–2.1 (br, CO–CH_2–CH_3), 1.2–0.7 (br, CO–CH_2–CH_3) ppm. **13C-NMR (75 MHz, d_6-DMSO, δ):** 173.6-172.2 (*C*=O), 50-41 (backbone), 26-23 (CO–*C*H_2–CH_3), 10-8 (CO–CH_2–*C*H_3) ppm. **ATR-FT-IR:** 2100 cm^{-1} (azide)

Synthesis of 1,4-bis((4-ethynylphenyl)ethynyl)benzene (OPE)

1,4-bis((4-ethynylphenyl)ethynyl)benzene was synthesized as described in the literature *via* coupling reactions.

^{1}H-NMR (300 MHz, $CDCl_3$, δ): 7.6-7.4 (aromatic, 12H), 3.2 (CH, 2H) ppm. **^{1}H-NMR (300 MHz, DMSO, δ):** 7.7-7.5 (aromatic, 12H), 4.4 (CH, 2H) ppm. **^{13}C-NMR (75MHz, DMSO, δ):** 133-131 (aromatic C), 123-122 (aromatic C), 91 (mid-chain triple bond), 83 (triple bond) ppm.

Copper catalyzed Azide-Alkyne Cycloaddition (CuAAC) Click Reaction between $PEtOx_x$-N_3 and OPE under non-optimized conditions

For the CuAAC click reaction 2 mg of the OPE (0.062 mmol) were dissolved in 1 mL THF (or 1 mL DMF; 2 g L^{-1}). $PEtOx_x$-N_3, 1.5 equivalents of the azide in comparison to the alkyne functionality, was dissolved into 1 mL THF (or 1 mL DMF) and added dropwise to the OPE-solution. Copper bromide (CuBr; 1.1 eq.) and *N*,*N*,*N*′,*N*′,*N*″-pentamethyldiethylenetriamine (PMDETA; 1.1 eq.) were added to the reaction mixture and placed into the microwave synthesizer at 80°C for 10 min (or overnight at room temperature). The solution was diluted with THF and passed through an AlOx N column to remove the copper. The yellowish material was obtained after precipitation into cold diethyl ether and drying under vacuum.

Afterwards, the SEC traces show multiple size distributions (Figure S2), and ^{13}C-NMR shows the partial disappearance of the internal alkyne carbon signals.

Copper catalyzed Azide-Alkyne Cycloaddition (CuAAC) Click Reaction between PEtOx$_x$-N$_3$ and OPE under optimized conditions

For the CuAAC click reaction 20 mg of the OPE (0.062 mmol) were dissolved in 8 mL THF (2.5 g L^{-1}). Afterwards 4 mL of water were added dropwise under vigorous stirring until an aggregation/precipitation of the OPE was observed. PEtOx$_x$-N$_3$, 1.1 equivalents of the azide in comparison to the alkyne functionality, was dissolved into 8 mL THF and added dropwise to the OPE-suspension, until an opaque solution was observed. Copper bromide (CuBr; 1.1 eq.) and *N*,*N*′,*N*′,*N*″-pentamethyldiethylenetriamine (PMDETA; 1.1 eq.) were added to the reaction mixture and placed into the microwave synthesizer at 80°C for 10 min. The solution was diluted with THF and passed through an AlOx N column to remove the copper. The yellowish material was obtained after precipitation into cold diethyl ether and drying under vacuum.

PEtOx$_6$-OPE-PEtOx$_6$: SEC (CHCl$_3$/*i*-PrOH/Et$_3$N): M_n = 2 600 g mol^{-1}; Đ = 1.09 (PS-calibration), yield: 75%; **PEtOx$_{11}$-OPE-PEtOx$_{11}$: SEC (CHCl$_3$/*i*-PrOH/Et$_3$N):** M_n = 3 600 g mol^{-1}; Đ = 1.05 (PS-calibration), yield: 90%; **PEtOx$_{16}$-OPE-PEtOx$_{16}$: SEC (CHCl$_3$/*i*-PrOH/Et$_3$N):** M_n = 4 800 g mol^{-1}; Đ = 1.07 (PS-calibration), yield: 90%; **^{1}H-NMR (300 MHz, CDCl$_3$, δ):** 8.0-7.3 (aromatic), 3.6–3.2 (br, –N–C*H*$_2$–C*H*$_2$–), 2.5–2.2 (br, CO–C*H*$_2$–CH$_3$), 1.2–0.9 (br, CO–CH$_2$–C*H*$_3$) ppm. ^{1}H-NMR (300 MHz, DMSO, δ): 8.7-7.5 (aromatic), 3.6-3.2 (br, –N–C*H*$_2$–C*H*$_2$–), 2.4–2.1 (br, CO–C*H*$_2$–CH$_3$), 1.1–0.7 (br, CO–CH$_2$–C*H*$_3$) ppm. **^{13}C-NMR (75 MHz, DMSO, δ):** 174-172 (*C*=O), 145 (*C*=CH triazol), 133-130 (aromatic *C*H, tiazol *C*H), 125-120 (*C* aromatic), 92-90 (mid-chain triple bond), 48-42 (backbone), 26-24 (*C*H$_2$, PEtOx), 10-8 (*C*H$_3$, PEtOx) ppm.

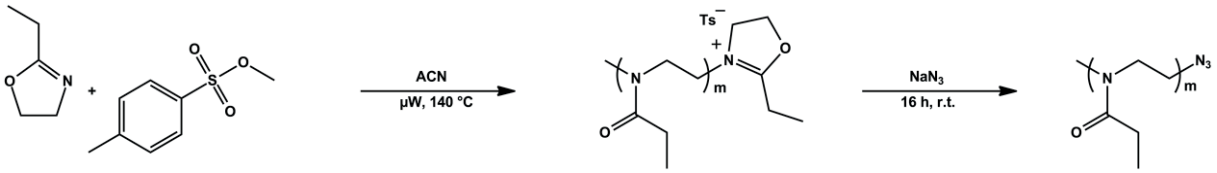

Scheme S1: Microwave-assisted cationic ring-opening polymerization (CROP) of 2-ethyl-2-oxazoline (EtOx) initiated *via* methyl *p*-toluenesulfonate and terminated using sodium azide.

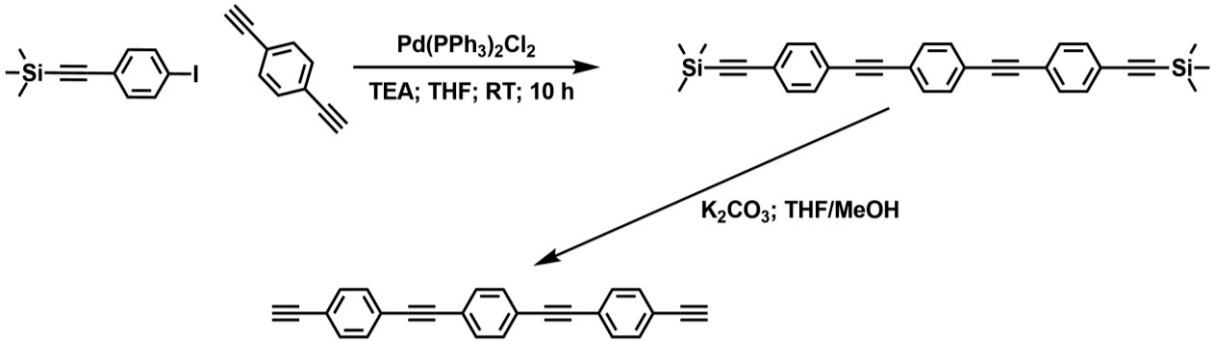

Schem S2: Synthesis of the 1,4-bis((4-ethynylphenyl)ethynyl)benzene (OPE) *via* coupling and subsequent deprotection.

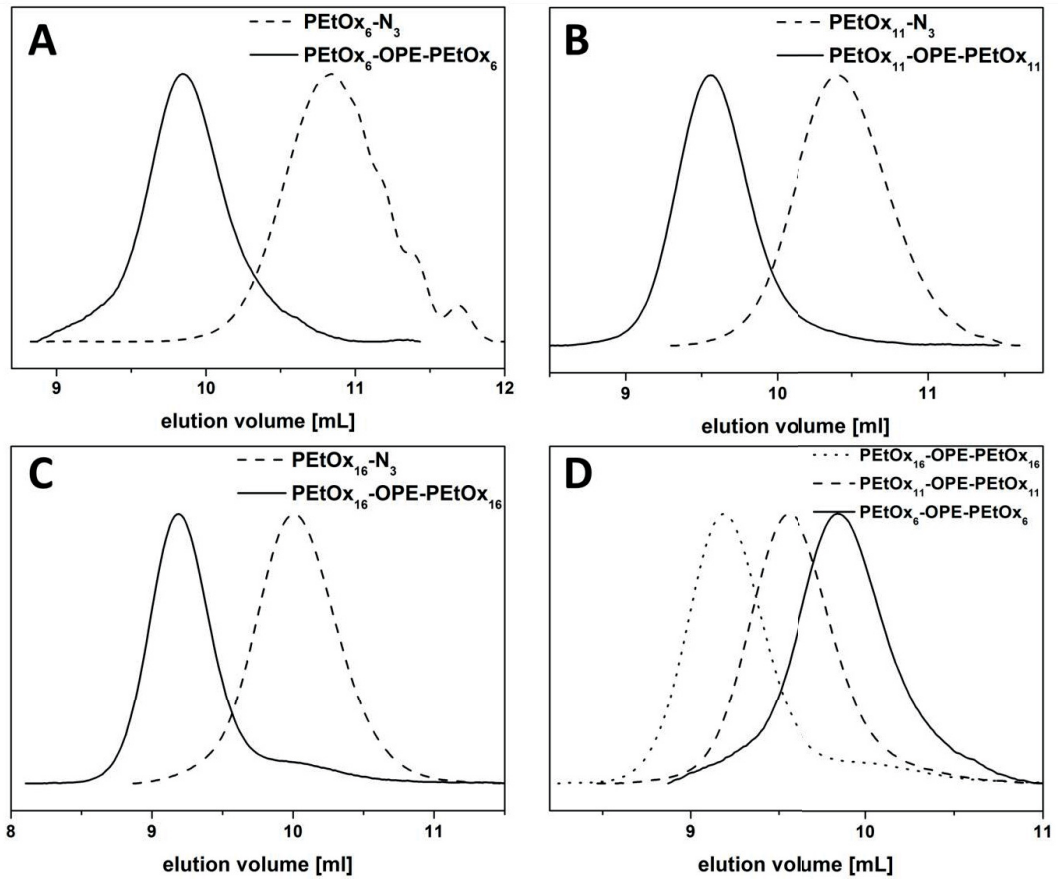

Figure S1: A) SEC traces of $PEtOx_6$-N_3 (dashed line) and $PEtOx_6$-OPE-$PEtOx_6$ (solid line); B) SEC traces of $PEtOx_{11}$-N_3 (dashed line) and $PEtOx_{11}$-OPE-$PEtOx_{11}$ (solid line); C) SEC traces of $PEtOx_{16}$-N_3 (dashed line) and $PEtOx_{16}$-OPE-$PEtOx_{16}$ (solid line); D) comparison of SEC traces for $PEtOx_6$-OPE-$PEtOx_6$ (straight line), $PEtOx_{11}$-OPE-$PEtOx_{11}$ (dashed line), $PEtOx_{16}$-OPE-$PEtOx_{16}$ (dotted line).

Table S1. Characterization data for $PEtOx_x$-N_3 and the corresponding products $PEtOx_x$-OPE-$PEtOx_x$.

Polymer	$DP^{PEtOx\ [a]}$	$M_{n,theo}$[a,b] [g mol^{-1}]	$M_{n,SEC}$[c] [g mol^{-1}]	$Đ$[c]
$PEtOx_6$-N_3[a]	6	650	900	1.12
$PEtOx_{11}$-N_3[a]	11	1 150	1 300	1.12
$PEtOx_{16}$-N_3[a]	16	1 650	2 100	1.10
$PEtOx_6$-OPE- $PEtOx_6$ (**3**)	6	1 600	2 600	1.09
$PEtOx_{11}$-OPE- $PEtOx_{11}$ (**2**)	11	2 600	3 600	1.05
$PEtOx_{16}$-OPE- $PEtOx_{16}$ (**1**)	16	3 600	4 800	1.07

[a] Feed ratio, [b] according to NMR (300 MHz, $CDCl_3$), [c] SEC ($CHCl_3$/*i*-PrOH/TEA) PS calibration

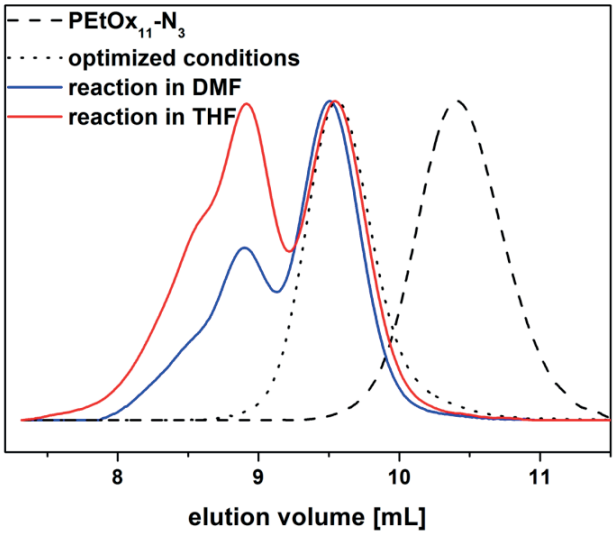

Figure S2: Comparison of SEC traces for the click products obtained in THF (red curve), in DMF (blue curve), and under optimized conditions (pre-organized system, dotted line) in comparison to the pristine $PEtOx_{11}$-N_3 (dashed line).

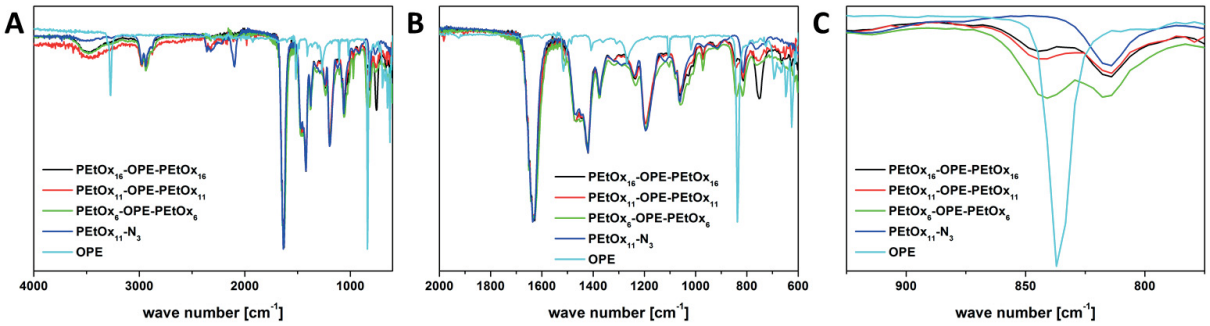

Figure S3: Comparison of FT-IR spectra for the different compositions of PEtOx and OPE for $PEtOx_{16}$-OPE-$PEtOx_{16}$ (**1**, black curve), $PEtOx_{11}$-OPE-$PEtOx_{11}$ (**2**, red curve), $PEtOx_6$-OPE-$PEtOx_6$ (**3**, green curve), $PEtOx_{11}$-N_3 (blue curve), OPE (cyan curve): A) full spectra; B) fingerprint area; C) zoom into the aromatic region.

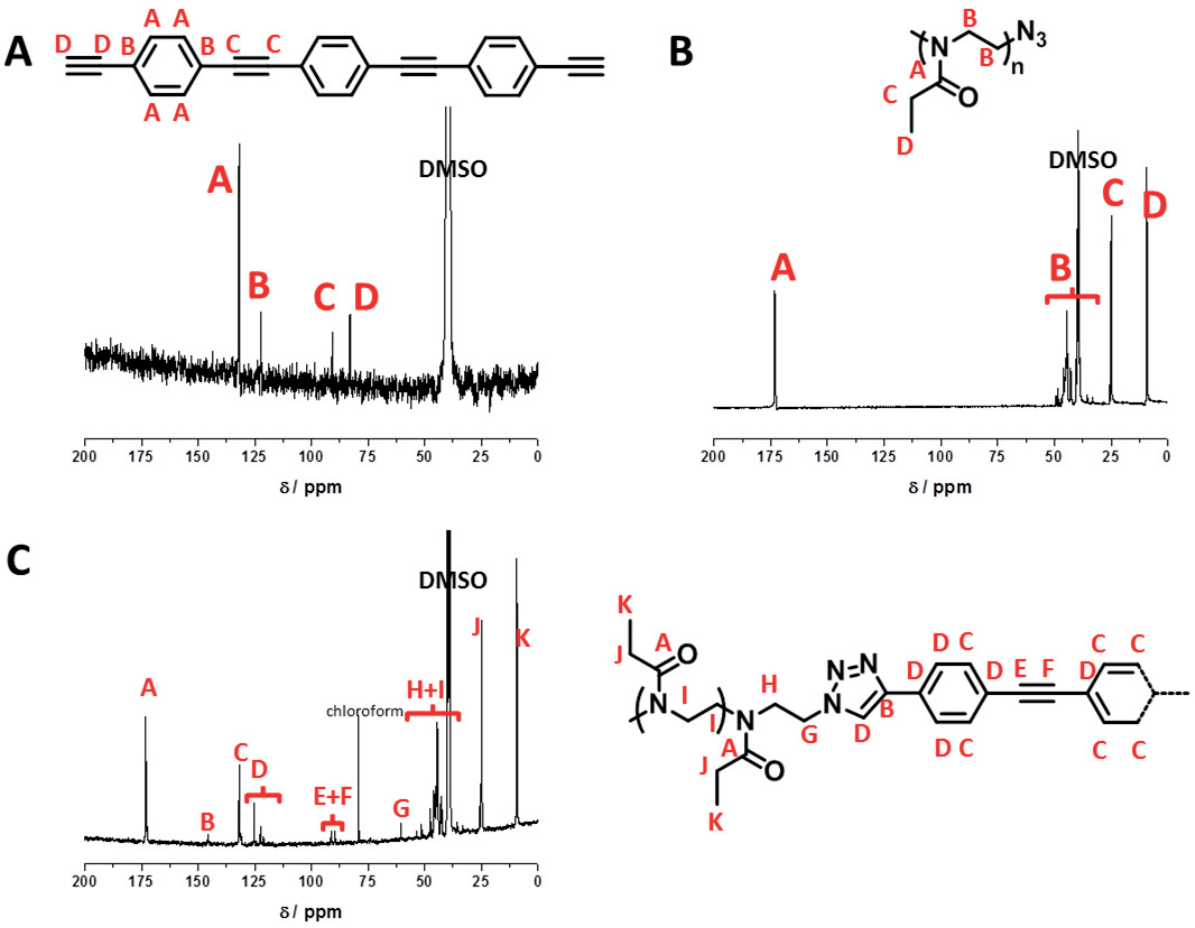

Figure S4: Characterization of OPE (A), $PEtOx_{16}$-N_3 (B), $PEtOx_{16}$-OPE-$PEtOx_{16}$ (C) *via* ^{13}C-NMR in d_6-DMSO.

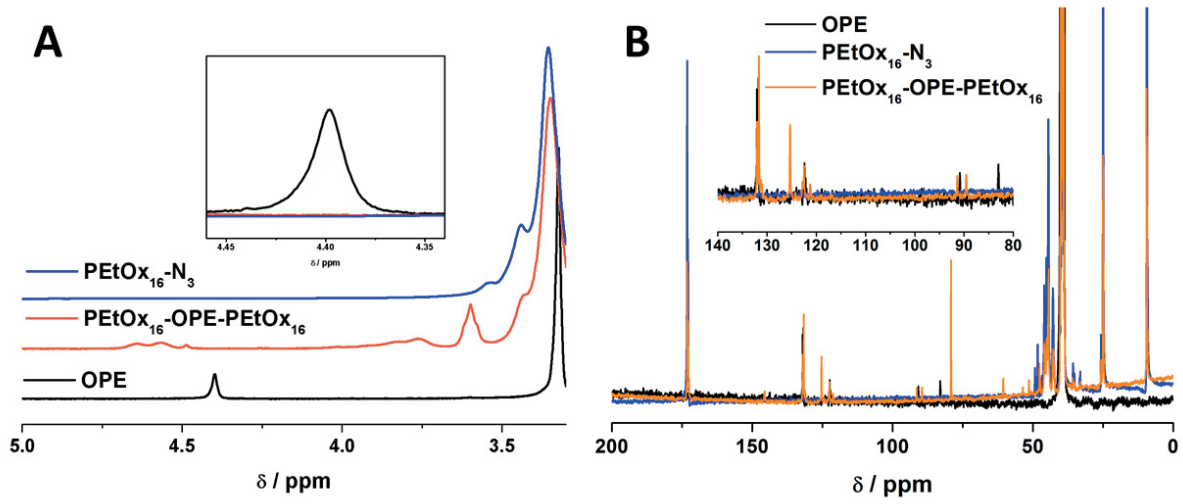

Figure S5: Comparison of the NMR traces for $PEtOx_{16}$-N_3 (blue curve), $PEtOx_{16}$-OPE-$PEtOx_{16}$ (orange curve), and OPE (black curve) in ^{1}H-NMR (A) and ^{13}C-NMR (B).

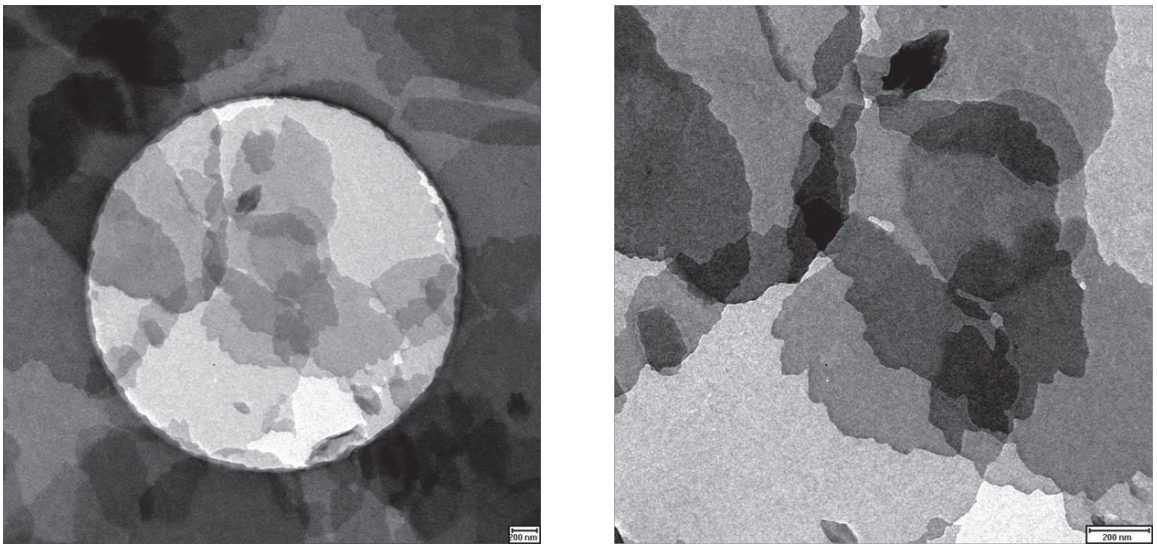

Figure S6: TEM micrographs of pre-organized structures of OPE in THF-water mixtures (4:1 v/v).

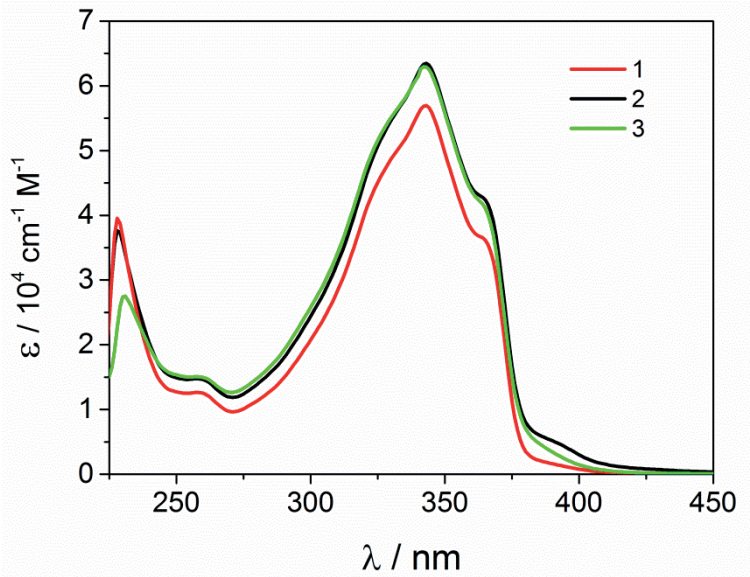

Figure S7: UV-Vis spectra of 1-3 in $CHCl_3$ at room temperature (conc. ~ 5 x 10^{-5} M).

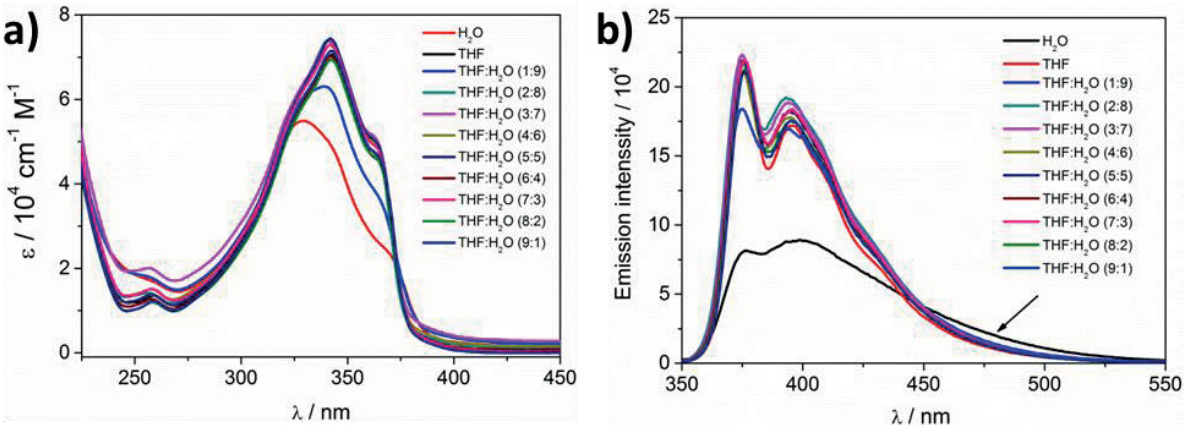

Figure S7: a) UV-Vis (conc. ~ 5 x 10^{-5} M) and b) emission spectra (conc. ~ 5 x 10^{-6} M) of $PEtOx_{11}$-OPE-$PEtOx_{11}$ in water and THF mixture at room temperature at room temperature.

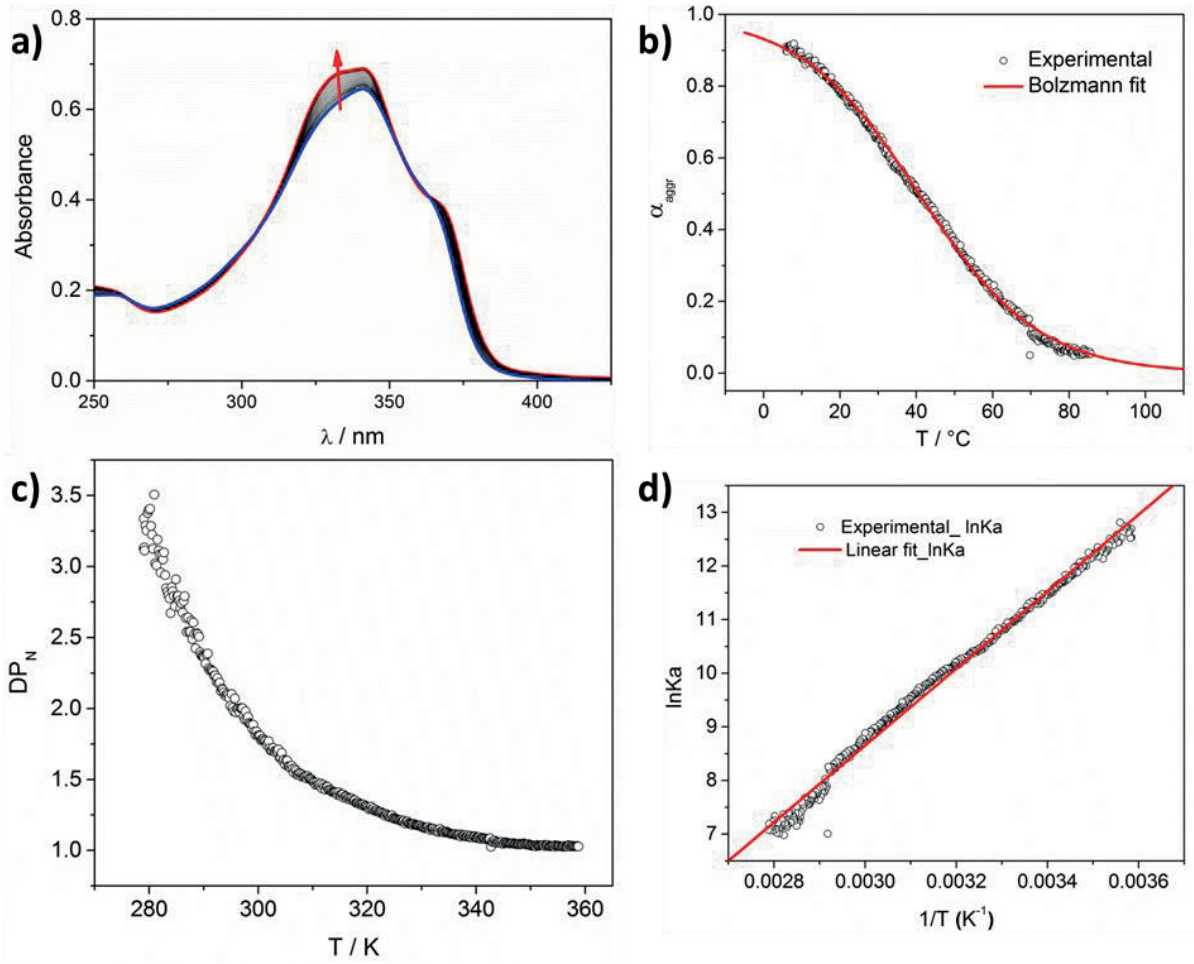

Figure S8: a) Temperature dependent (cooling) UV-Vis spectra of $PEtOx_{16}$-OPE-$PEtOx_{16}$ in water (conc. $2.4x10^{-5}$ M), b) Boltzmann fit of cooling curve monitored at 320 nm for $PEtOx_{16}$-OPE-$PEtOx_{16}$ in water (conc. 2.4 x 10-6 M), c) Number-averaged degree of polymerization (DP_N) of 1 at different temperatures and d) Van't Hoff plot for the temperature dependence of the aggregation constant K of 1 in water .

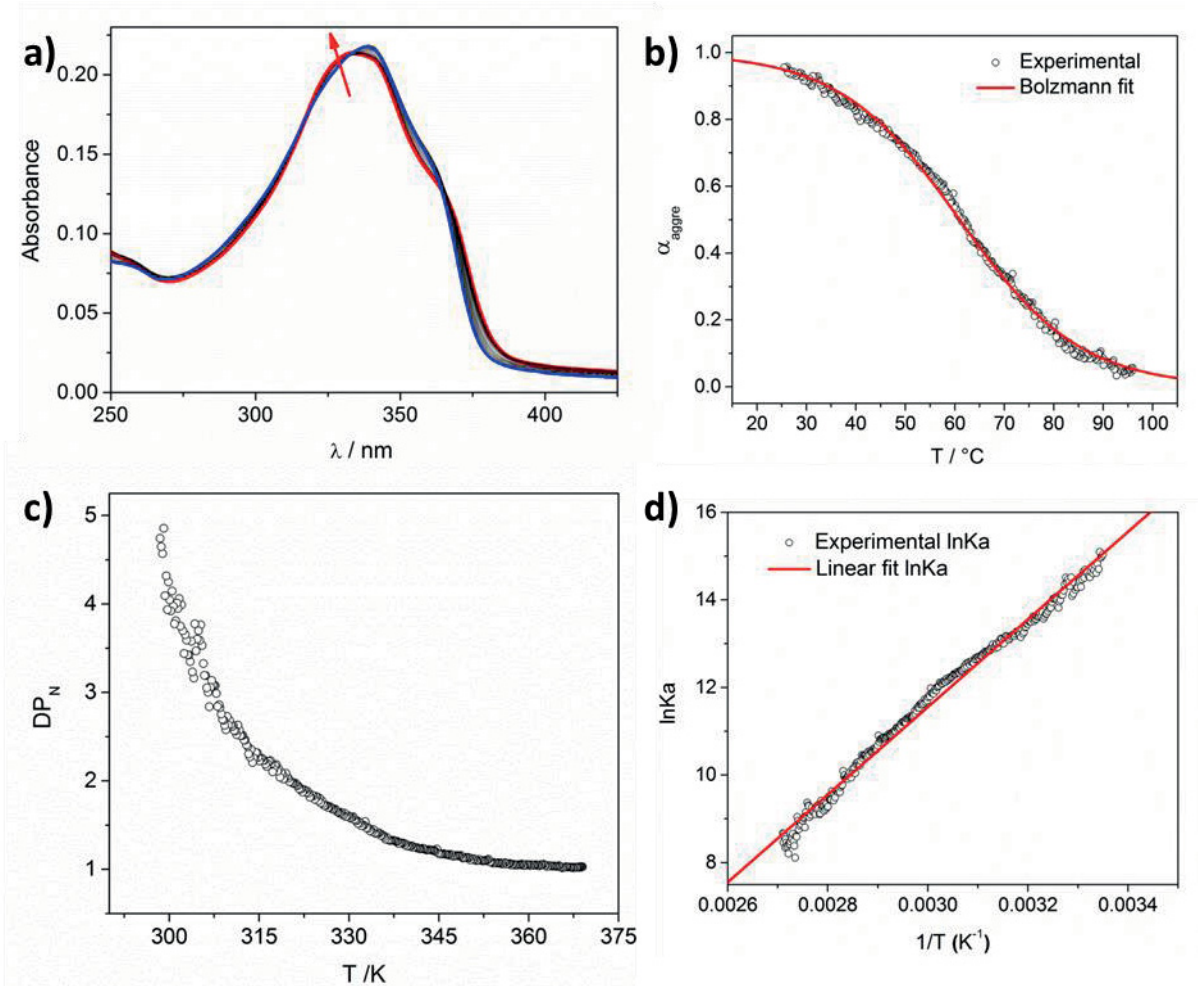

Figure S9: a) Temperature dependent (cooling) UV-Vis spectra of Poly 11 in water (conc. 5.2 x 10^{-5} M), b) Boltzmann fit of cooling curve monitored at 300 nm for Poly 11 in water (conc. 5.2 x 10^{-5} M), c) Number-averaged degree of polymerization (DP_N) of 1 at different temperatures and d) Van't Hoff plot for the temperature dependence of the aggregation constant K of 1 in water.

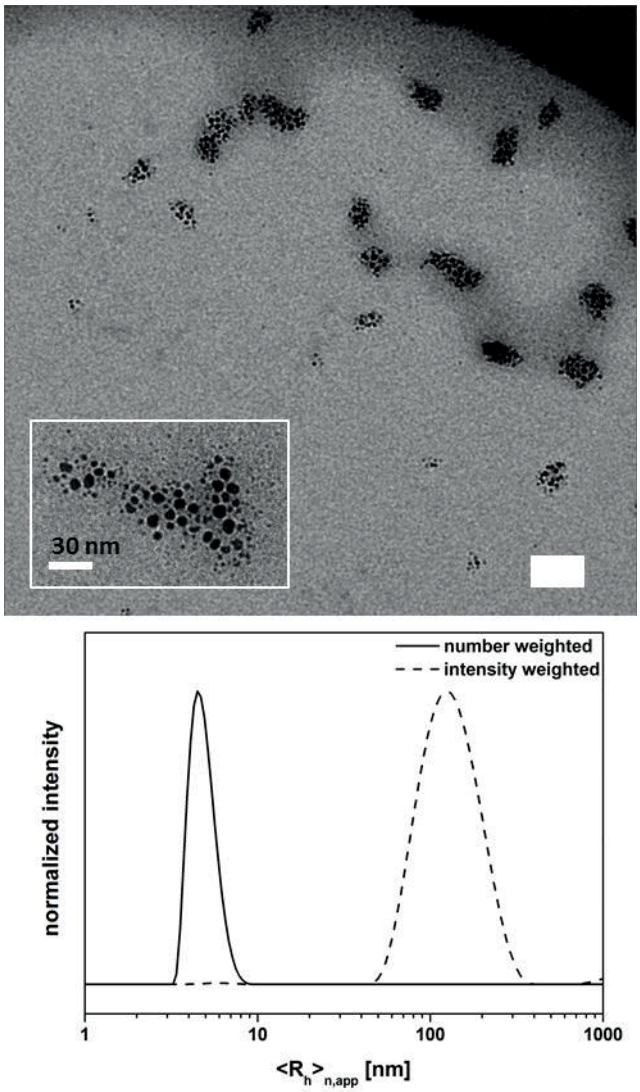

Figure S10: TEM images and DLS measurements (lower panel) of $PEtOx_{11}$-OPE-$PEtOx_{11}$ (conc. 2 mg mL^{-1}) in water.

Publication P3

“Supramolecular Three-Armed Star Polymers via Cyclodextrin Host/Guest Self-Assembly”

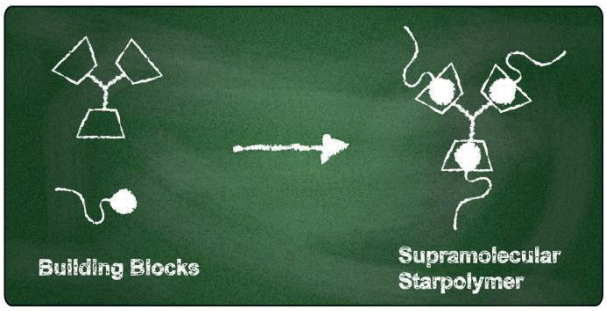

Bernhard V. K. J. Schmidt, Tobias Rudolph, Martin Hetzer, Helmut Ritter, Felix H. Schacher, Christopher Barner-Kowollik

Polym. Chem., **2012**, 3, 3139-3145

Polymer Chemistry

Cite this: *Polym. Chem.*, 2012, **3**, 3139

www.rsc.org/polymers

PAPER

Supramolecular three-armed star polymers *via* cyclodextrin host–guest self-assembly†

Bernhard V. K. J. Schmidt,[a] Tobias Rudolph,[bc] Martin Hetzer,[d] Helmut Ritter,*[d] Felix H. Schacher*[bc] and Christopher Barner-Kowollik*[a]

Received 2nd May 2012, Accepted 25th May 2012
DOI: 10.1039/c2py20293j

Three-armed star polymers with a cyclodextrin core and polyacrylamide arms were prepared *via* inclusion complex formation. A novel adamantyl-functionalized chain transfer agent was utilized in the reversible addition–fragmentation chain transfer (RAFT) polymerization of *N*,*N*-dimethylacrylamide and *N*,*N*-diethylacrylamide to afford guest-functionalized polymers. In combination with a three-pronged β-cyclodextrin core, supramolecular self-assembly was exploited for the formation of star-shaped architectures. This was demonstrated *via* a combination of dynamic light scattering (DLS) and 2D rotating frame nuclear Overhauser effect spectroscopy (ROESY) in D_2O. Furthermore, turbidity measurements in the case of PDEAAm showed a rise in the LCST of the system. The complex formation was shown to be reversible, as DLS at elevated temperatures (70 °C) indicated a complete disassembly of the star polymers.

Introduction

Star polymers are an important class of polymers that have attracted significant attention in the last few years.[1–3] This can be attributed to unique properties originating from their condensed structure, non-linear shape, and multiple chain ends per macromolecule. Many applications for such systems have been discussed in the literature, *e.g.* as unimolecular nanocontainers,[4] for drug-delivery[5] or in organic light-emitting diodes.[6]

Traditionally, the synthesis of star polymers has been carried out *via* living polymerization techniques, *i.e.* anionic[1] or cationic[7,8] methodologies. According to these synthetic strategies, one can distinguish between multifunctional initiators, *i.e.* the core-first approach,[9] or multifunctional termination agents, *i.e.* the arm-first approach.[10] Especially the introduction of controlled radical polymerization techniques, *e.g.* nitroxide mediated polymerization (NMP),[11] atom transfer radical polymerization (ATRP),[12] and reversible addition–fragmentation chain transfer (RAFT)[13,14] polymerization, has led to the generation of a broad range of star polymers in core-first approaches *via* multifunctional initiators or chain transfer agents (CTAs).[15–17] As an alternative, modular conjugation reactions can be employed for the synthesis of such architectures, *e.g. via* click chemistry,[2,18] in an arm-first approach. Several methods have been employed in that regard benefiting from high efficiency, short reaction times, and possible equimolarity of the reactions that fulfil the respective criteria.[19] Some examples include the copper-catalyzed azide–alkyne cycloaddition (CuAAc),[20,21] the thiol–ene reaction,[22] or the RAFT hetero Diels–Alder reaction.[23] As these strategies represent orthogonal approaches, they are nowadays also widely employed for the synthesis of miktoarm star polymers.[2,18,24]

New opportunities arise from the synthesis of supramolecular star polymers. Here the formation of the star polymer is driven by supramolecular interactions that offer reversible and potentially stimuli-responsive bond-formation amongst other properties. The mainly utilized types of supramolecular interactions comprise hydrogen bonding,[25–27] metal–ligand coordination[28–30] or host–guest complexation.[31] A very important class of hosts in the realm of host–guest complexations are cyclodextrins (CDs) due to their availability and the ease of chemical modification. From the point of view of star polymer synthesis the ability of CDs to form inclusion complexes with hydrophobic guest molecules leads to the possibility to form new materials. Apart from the formation of new macromolecular architectures, this ability is widely used in polymer chemistry, *e.g.* for drug- or siRNA-delivery,[32–34] to solubilize hydrophobic chain-transfer agents[35] or monomers.[36–38] In the case of star polymers CD has

[a]*Preparative Macromolecular Chemistry, Institut für Technische Chemie und Polymerchemie, Karlsruhe Institute of Technology (KIT), Engesserstr. 18, 76131 Karlsruhe, Germany. E-mail: christopher.barner-kowollik@kit.edu; Fax: +49 72160845740*
[b]*Laboratory of Organic and Macromolecular Chemistry (IOMC), Friedrich-Schiller-University Jena, Lessingstraße 8, 07743 Jena, Germany. E-mail: felix.schacher@uni-jena.de; Fax: +49 3641948202*
[c]*Jena Center for Soft Matter (JCSM), Friedrich-Schiller-University Jena, Humboldtstr. 10, 07743 Jena, Germany*
[d]*Lehrstuhl für Präparative Polymerchemie, Institut für Organische Chemie und Makromolekulare Chemie, Heinrich-Heine Universität, Universitätsstrasse 1, Geb. 26.33.00, 40225 Düsseldorf, Germany. E-mail: h.ritter@uni-duesseldorf.de; Fax: +49 2118115840*

† Electronic supplementary information (ESI) available: Additional experimental procedures and characterization data. See DOI: 10.1039/c2py20293j

been mainly used as a core molecule in the past, *e.g.* in ATRP,[39] RAFT,[40] or in a combination of ATRP and NMP.[41] Here, however, the arms were covalently attached to the CD core. In an alternative example CD-centered star polymers were reported, where two cores are bound using supramolecular interactions.[42,43]

We herein report the formation of supramolecular three-armed star polymers using CD host–guest interactions. The materials consist of adamantyl-functionalized polyacrylamides as arms and a three-fold β-CD-functionalized core molecule. An adamantyl-functionalized CTA was utilized in the RAFT polymerization of *N*,*N*-dimethylacrylamide (DMAAm) and *N*,*N*-diethylacrylamide (DEAAm) for the synthesis of the arms, which were subsequently characterized *via* ESI-MS, NMR and size exclusion chromatography (SEC). In aqueous solution, supramolecular complexes were formed and the existence of three-armed star polymers was proven *via* 2D rotating frame nuclear Overhauser effect spectroscopy (ROESY) NMR as well as dynamic light scattering (DLS) (Scheme 1).

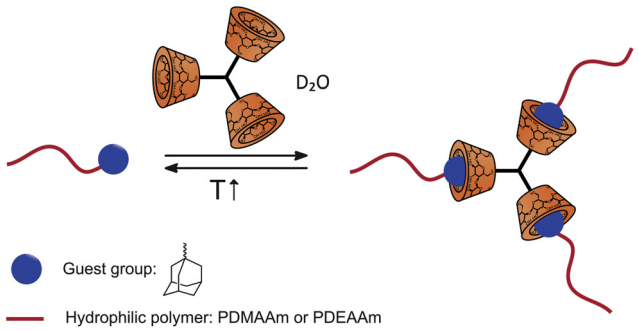

Scheme 1 Schematic representation of supramolecular star polymer formation *via* host–guest inclusion complexes between adamantyl-functionalized polyacrylamides (polymer: red; adamantyl-group: blue) and a three-pronged β-CD linker (orange).

Experimental part

Materials

1-Adamantylamine hydrochloride (ABCR, 99%), 2-bromoisobutyric acid (Sigma Aldrich, 98%), aluminium chloride (ABCR, 99%), β-cyclodextrin (β-CD; Wacker, pharmaceutical grade), carbon disulfide (Acros, 99.9%), copper bromide (Sigma Aldrich, 99%), deuterium oxide (D_2O; Euriso-top, 99.9%), *N*,*N*′-dicyclohexylcarbodiimide (DCC; ABCR, 99%), *N*,*N*-dimethylaminopyridine (DMAP; Sigma Aldrich, 99%), *N*,*N*-dimethylformamide (DMF; ABCR, 99%), ε-caprolactone (Alfa Aesar, 99%), ethanethiol (Acros, 99%), ethylenediaminetetraacetic acid disodium salt (EDTA; ABCR, 99%), *p*-toluenesulfonyl chloride (ABCR, 98%), *N*,*N*,*N*′,*N*″,*N*″′-pentamethyldiethyltriamine (PMDETA; Merck, 99.9%), potassium phosphate monohydrate (Sigma Aldrich, puriss.), silica gel (Merck, Geduran SI60. 0.063–0.200 mm), sodium azide (Acros, 99%), sodium hydroxide (Roth, 99%), triethylamine (Acros, 99%) and tripropargylamine (Sigma Aldrich, 98%) were used as received. Anhydrous dichloromethane (DCM) was purchased from Acros (extra dry over molecular sieves) and used as received. All other solvents were of analytical grade and used as received. Milli-Q water was obtained from a purification system by Thermo Fisher Scientific (TKA Micro-Pure; 0.055 μS cm^{-1}). 2,2′-Azobis(2-methylpropionitrile) (AIBN; Fluka, 99%) was recrystallized twice from methanol. *N*,*N*-Diethylacrylamide (DEAAm; TCI, 99%) and *N*,*N*-dimethylacrylamide (DMAAm; TCI, 99%) were passed over a short column of basic alumina prior to use. *N*-(Adamantan-1-yl)-6-hydroxyhexanamide[44] (also described in the SI), 2-((((ethylthio)carbonothioyl)thio)-2-methylpropanoic acid (EMP),[35,45] mono-(6-azido-6-desoxy)-β-CD (β-CD-N_3)[46] and *N*,*N*,*N*-(tris-1-(mono-(6-desoxy)-β-CD)-1*H*-1,2,3-triazol-4-yl)methanamine (β-CD_3)[47] (also described in the SI) were prepared according to the noted literature procedures.

Synthesis of 6-(adamantan-1-ylamino)-6-oxohexyl 2-(((ethylthio)carbonothioyl)thio)-2-methylpropanoate (CTA1)

In a 50 mL Schlenk-flask, 0.84 g EMP (3.75 mmol, 1.0 eq.), 1.00 g *N*-(adamantan-1-yl)-6-hydroxyhexanamide (3.77 mmol, 1.0 eq.) and 0.09 g DMAP (0.74 mmol, 0.2 eq.) were dissolved in 15 mL anhydrous DCM. At 0 °C a solution of 1.17 g DCC (5.67 mmol, 1.5 eq.) in 10 mL anhydrous DCM was added. After one hour the solution was warmed to ambient temperature, stirred overnight, filtered and concentrated under reduced pressure. The residual oil was purified *via* column chromatography on silica-gel with a 5 : 1 mixture of *n*-hexane : ethylacetate as eluent. The product was obtained as yellow oil (1.08 g, 2.29 mmol, 61%).

^{1}H-NMR (400 MHz, $CDCl_3$): [δ, ppm] = 1.27–1.43 (m, 5H, C***H***$_3$–CH_2; C***H***$_2$–*CH*$_2$–*CH*$_2$–*O*), 1.53–1.73 (m, 16H, 2× C–C***H***$_3$; C***H***$_2$–*CH*$_2$–*O*; C***H***$_2$–*CH*$_2$–*C* =O; 3× C***H***$_{2,adamantyl}$), 1.98 (d, 6H, 3× NH–C–C***H***$_{2,adamantyl}$), 2.02–2.10 (m, 5H, 3× C***H***$_{adamantyl}$; C***H***$_2$–C = O–NH), 3.28 (q, 2H, C***H***$_2$–CH_3), 4.08 (t, 2H, C***H***$_2$–O), 5.11 (br s, 1H, N***H***). ^{13}C-NMR (100 MHz, $CDCl_3$): [δ, ppm] = 13.1 (***C***H_3–CH_2), 25.5, 25.7 and 28.3 (***C***H_2–CH_2–C = O; ***C***H_2–CH_2–CH_2–C = O; ***C***H_2–CH_2–C=O–NH; 2× ***C***H_3–C = O), 29.6 (3× ***C***$H_{adamantyl}$), 31.3 (CH_3–***C***H_2), 36.5 (3× ***C***$H_{2,adamantyl}$), 37.8 (***C***H_2–C = O–NH), 41.9 (3× ***C***$H_{2,adamantyl}$–C–NH), 52.0 (***C***–NH), 56.2 (***C***$(CH_3)_2$), 66.0 (CH_2–CH_2–O), 172.1 (NH–***C***=O), 173.1 (O–***C***=O), 221.4 (***C***=S). ESI-MS: $[M + Na^+]_{exp}$ = 494.42 *m*/*z* and $[M + Na^+]_{calc}$ = 494.1833 *m*/*z*.

Exemplary procedure for the RAFT polymerization

CTA1 (60.0 mg, 0.13 mmol, 1.0 eq.), DMAAm (1.26 g, 12.72 mmol, 97.9 eq.), AIBN (4.2 mg, 0.03 mmol, 0.2 eq.), DMF (6.0 mL) and a stirring-bar were added into a Schlenk-tube. After three freeze–pump–thaw cycles the tube was backfilled with argon, sealed, placed into an oil bath at 60 °C and removed after 24 h. The tube was subsequently cooled with liquid nitrogen to stop the reaction. A NMR-sample was withdrawn for the determination of conversion, inhibited with a pinch of hydroquinone (approx. 5 mg) and $CDCl_3$ was added. A quantitative conversion was calculated based on the NMR data (see Characterization Methods for details of the calculation). The residue was dialysed with a SpectraPor3 membrane (MWCO = 1000 Da) for 3 days at ambient temperature. The solvent was removed *in vacuo* to yield the polymer as a yellow solid (1.20 g, 99%, GPC (DMAc): M_{nGPC} = 14 600 g mol^{-1}, $Đ_M$ = 1.12).

Exemplary procedure for the self-assembly of the adamantyl-functionalized PDMAAm with β-CD_3

Adamantyl-functionalized PDMAAm (M_{nGPC} = 13 200 g mol^{-1}, 55.4 mg, 0.0042 mmol, 3.0 eq.) and β-CD_3 (5.0 mg, 0.0014 mmol, 1.0 eq.) were dissolved in D_2O (0.5 mL, c = 120 mg·mL^{-1}) and stirred at ambient temperature overnight. Subsequently, the formed complex was characterized *via* 2D ROESY-NMR. For DLS measurements Milli-Q water and D_2O (c = 5 mg mL^{-1}) were utilized instead.

Characterization methods

NMR measurements were carried out on a Bruker AM250 spectrometer at 250 MHz for hydrogen nuclei for conversion determination and a Bruker AM400 spectrometer at 400 MHz for hydrogen nuclei and at 100 MHz for carbon nuclei for structure verification. 2D ROESY (rotating frame nuclear Overhauser effect spectroscopy) NMR spectra were measured on a Bruker Avance III 600 spectrometer at 600 MHz. For the determination of the conversion of DMAAm the integrals of one vinylic proton (5.78–5.89 ppm) and the backbone protons (0.75–2.00 ppm) were employed. The conversion of DEAAm was determined with the integral of one vinylic proton (5.57–5.73 ppm) and with the integral of the side chain methyl groups and backbone protons (0.81–1.97 ppm).

Size exclusion chromatography (SEC) was performed on a Polymer Laboratories PL-GPC 50 Plus Integrated System, comprising an autosampler, a PLgel 5 μm bead-size guard column (50 7.5 mm) followed by three PLgel 5 μm MixedC columns (300 7.5 mm) and a differential refractive index detector using *N*,*N*-dimethylacetamide (DMAc) containing 0.03 wt% LiBr as eluent at 50 °C with a flow rate of 1.0 mL min^{-1}. The SEC system was calibrated against linear poly(styrene) standards with molecular weights ranging from 160 to 6 × 10^6 g mol^{-1}. All SEC calculations were carried out relative to poly(styrene) calibration (Mark–Houwink parameters $K = 14.1 \times 10^{-5}$ dL g^{-1}; $\alpha = 0.7$).[48]

Electrospray ionization-mass spectrometry (ESI-MS) was performed on a LXQmass spectrometer (ThermoFisher Scientific, San Jose, CA) equipped with an atmospheric pressure ionization source operating in the nebulizer-assisted electrospray mode. The instrument was calibrated in the *m*/*z* range 195–1822 Da using a standard containing caffeine, Met–Arg–Phe–Ala acetate (MRFA), and a mixture of fluorinated phosphazenes (Ultramark 1621) (all from Aldrich). A constant spray voltage of 4.5 kV was used, and nitrogen at a dimensionless sweep gas flow rate of 2 (~3 L min^{-1}) and a dimensionless sheath gas flow rate of 12 (~1 L min^{-1}) were applied. The capillary voltage, the tube lens offset voltage, and the capillary temperature were set to 60 V, 110 V, and 275 °C respectively. Adamantyl-functionalized polymers were measured in THF/methanol 3/2 doped with 100 μM sodium trifluoroacetic acid and β-CD_3 was measured in Milli-Q water doped with 100 μM sodium iodide.

Dynamic light scattering (DLS) was performed at a scattering angle of 90° on an ALV CGS-3 instrument and a He–Ne laser operating at a wavelength of λ = 633 nm at 25 °C. The CONTIN algorithm was applied to analyze the obtained correlation functions. For temperature dependent measurements the DLS is equipped with a Lauda thermostat. Apparent hydrodynamic radii were calculated according to the Stokes–Einstein equation. All CONTIN plots are number-weighted.

Turbidity measurements were performed in a temperature range from 5 °C to 100 °C with a heating and cooling ramp of 1 °C min^{-1} under stirring (700 rpm). During these controlled heating/cooling cycles, the transmission was monitored in a Crystal 16 TM (Avantium Technologies) instrument.

Theoretical molecular weights were calculated with the following equation:

$$M_{ntheo} = \text{conversion} \times M_w(\text{Monomer}) \times \frac{[\text{Monomer}]_0}{[\text{CTA}]_0} + M_w(\text{CTA})$$

Results and discussion

Synthesis and characterization of guest- and host-functionalized building blocks

For the formation of supramolecular star polymers two types of building blocks were synthesized (Scheme 2): adamantyl end-functionalized polymers as arms (guest) and a three-pronged β-CD-functionalized core as the host.

The adamantyl-functionalized polymers were synthesized *via* RAFT-polymerization using a trithiocarbonate-containing CTA (**CTA1**). The prominent adamantyl moiety was chosen as guest group due to its high complexation constants with β-CD of up to 10^5.[49] The CTA was synthesized starting from an adamantyl-containing alcohol *via* DCC coupling with EMP as shown in Scheme 2a. The adamantyl moiety was separated from the trithiocarbonate group with a C5-spacer to improve its accessibility in the inclusion process. Subsequently, RAFT

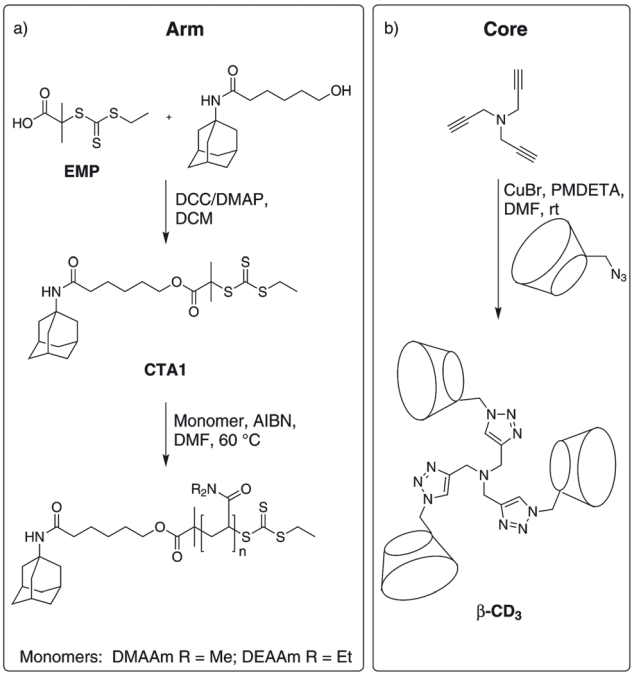

Scheme 2 Synthesis of the building blocks utilized for star polymer formation: (a) adamantyl-functionalized RAFT-agent (**CTA1**), followed by the synthesis of polyacrylamides, and (b) synthesis of the three-pronged β-CD core (β-CD_3).

polymerizations were conducted with DMAAm and DEAAm utilizing several CTA/monomer ratios. Polymerization degrees ranging from 31 to 202 with M_n ranging from 3500 to 20 500 g mol^{-1} and low $Đ_M$ < 1.25 were achieved for PDMAAm. Furthermore, the thermoresponsive adamantyl-functionalized PDEAAm was prepared *via* RAFT polymerization with **CTA1** affording a polymerization degree of 87 with a M_n of 11 500 g mol^{-1} and a low $Đ_M$ (see Table 1).

The RAFT polymerization of DMAAm and DEAAm with **CTA1** yielded unimodal molecular weight distributions (Fig. 1). For higher molecular weights a certain tailing to higher elution volumes was observed, presumably due to interactions with the column during SEC. The structure of the obtained polymers was verified *via* ^{1}H-NMR and ESI-MS (refer to the ESI, Fig. S5–S9†).

The three-pronged CD-functional building block β-CD$_3$ was synthesized *via* CuAAc starting from tripropargylamine and β-CD-N$_3$ (Scheme 2b).[47] The product was analyzed *via* ^{1}H-NMR and ESI-MS (Fig. S10 and S11†).

Star polymer formation: investigations using light scattering

Light scattering experiments are a powerful method for the *in situ* investigation of polymeric systems in solution. Before mixing the arms and the core moiety, all individual compounds were analyzed *via* DLS at ambient temperature in H_2O and D_2O. Surprisingly, all polyacrylamide compounds seemed to be better soluble in D_2O, resulting in an increase of ~20% of the hydrodynamic radius (Fig. S12 and S13†), while for β-CD$_3$ no difference was observed. Such an effect has also been observed for poly(*N*-isopropylacrylamide),[50–52] although the reason was not fully understood. The increased hydrodynamic volumes of the polymer chains should, however, lead to a better accessibility of the adamantyl moiety for the inclusion process with the β-CD$_3$ core. Therefore, all following experiments were performed in D_2O at a polymer concentration of 5 mg mL^{-1}. In addition, control experiments in H_2O were carried out (Fig. S13†).

Adamantyl-functionalized PDMAAm with three molar masses was combined in stoichiometric amounts (3 : 1) with the β-CD$_3$ core, dissolved in D_2O, stirred and analysed using DLS after 12 and 24 hours (also after several days, Fig. S13†), showing a clear shift to higher hydrodynamic radii with time. For PDMAAm$_{31}$-Ad (M_{nGPC} = 3500 g mol^{-1}) an apparent hydrodynamic radius R_h = 1.8 nm was observed, while the β-CD$_3$ exhibits a radius of R_h = 1.3 nm. After 12 hours at ambient temperature, an increase in size to R_h = 2.3 nm was found, which remained constant over several days. The proposed structure formation mechanism is depicted in Scheme 3. The same procedure was utilized for PDMAAm$_{143}$-Ad and PDMAAm$_{202}$-Ad and a R_h of 2.5 and 3.3 nm for the unimolecular polymer chains was observed, respectively. After stoichiometric mixing in a molar ratio of 3 : 1 with the CD-core moiety, a distinct increase in size can be observed in both cases. For PDMAAm$_{143}$-Ad, supramolecular star polymers with R_h = 3.7 nm were observed whereas in the case of PDMAAm$_{202}$-Ad the aggregate size was even larger, with R_h = 4.6 nm, owing to longer polyacrylamide arms. We therefore calculated an expansion ratio of 1.5 and 1.4 (Table 2). In all cases, monomodal number-weighted size distributions were observed, indicating full inclusion of the guest-polymer chains into the CD core (Fig. 2).

For all investigated combinations of arms and core, an increase of the hydrodynamic radius was observed, hinting at the formation of star-shaped aggregates. The expansion ratio (Table 2) yields comparable values for all polymers investigated.

Table 1 Results for the RAFT polymerization of DMAAm (top) and DEAAm (bottom) with **CTA1** at 60 °C in DMF

	Monomer/ CTA/AIBN	*Conv.*[a]	$M_{n,theo}$ [g mol^{-1}]	$M_{n,GPC}$ [g mol^{-1}][b]	$Đ_M$
DMAAm	31/1/0.1	Quant.	2550	3500	1.08
	143/1/0.2	Quant.	10 370	14 600	1.12
	202/1/0.2	96%	23 400	20 500	1.23
DEAAm	87/1/0.2	Quant.	13 300	11 500	1.11

[a] Based on NMR-data. [b] Relative to poly(styrene) standards.

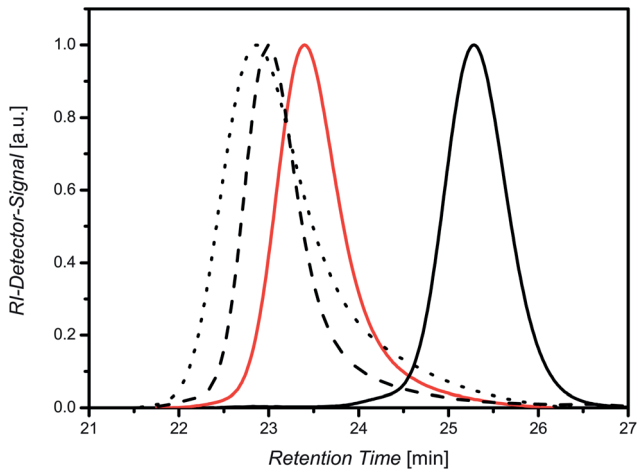

Fig. 1 SEC-traces for PDMAAm$_{31}$-Ad (solid black line), PDMAAm$_{143}$-Ad (dashed black line), PDMAAm$_{202}$-Ad (dotted black line), and PDEAAm$_{87}$-Ad (solid red line).

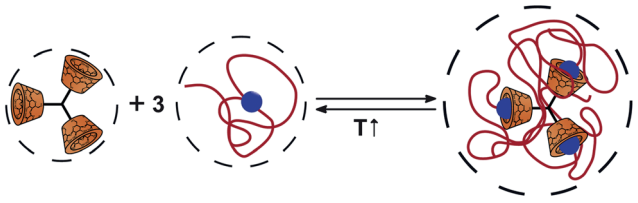

Scheme 3 Schematic representation of the formation of supramolecular star polymers, indicating the expected changes in hydrodynamic radius (R_h dashed circles).

Table 2 DLS results (number-weighted hydrodynamic radii) for the individual building blocks, the supramolecular star polymers after self-assembly, and the respective expansion ratio at 25 °C in D_2O

Polymer	Crude polymer $\langle R_{h,app}^{max} \rangle$ [nm]	Polymer@β-CD$_3$ $\langle R_{h,app}^{max} \rangle$ [nm]	Expansion ratio
β-CD$_3$	1.3	—	—
PDMAAm$_{31}$-Ad	1.8	2.3	1.3
PDMAAm$_{143}$-Ad	2.5	3.7	1.5
PDMAAm$_{202}$-Ad	3.3	4.6	1.4
PDEAAm$_{87}$-Ad	2.4	3.8	1.6

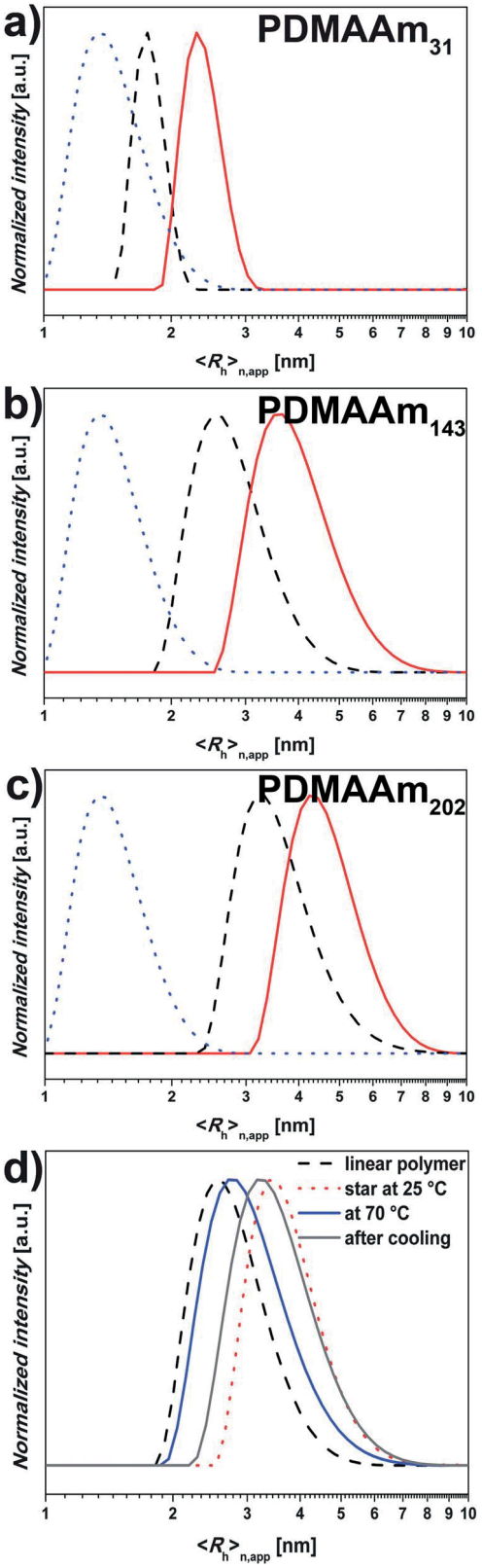

Fig. 2 Number-weighted size distributions for PDMAAm$_x$-Ad: (a) 31, (b) 143 and (c) 202 (dashed black lines), the β-CD$_3$ core molecule (dotted blue line), and the resulting supramolecular star polymers in a molar ratio of 3 : 1 after 24 hours in D_2O at 25 °C (solid red lines). (d) Investigations regarding the reversibility of the inclusion process by heating to 70 °C (blue line), followed by cooling and reformation of the aggregates.

Adamantyl-functionalized polymers with higher molecular weight lead to higher hydrodynamic radii. Furthermore, the size distributions of the adamantyl-functionalized polymers were measured after the addition of crude β-CD (refer to Fig. S13b†) to prove that the increase in R_h is due to the three-pronged nature of β-CD$_3$.

The reversibility of star polymer formation at higher temperatures was also investigated *via* DLS (Fig. 2d). Therefore, the temperature was increased from 25 to 70 °C in 2 hours and the sample was kept at this temperature for further 30 min. As a result, a decrease of the R_h from 3.7 nm to 2.8 nm was observed. This might well correspond to the expulsion of the adamantyl moiety from the β-CD$_3$ core (Fig. 2d, blue line). Afterwards, the sample solution was cooled down to 25 °C and, subsequently, the hydrodynamic radius increased again.

Comparable investigations were carried out using PDEAAm$_{87}$-Ad (Fig. 3a), a polymer which exhibits LCST behaviour.[53] Depending on the molar mass and the respective endgroup, PDEAAm materials undergo a coil-to-globule transition in the temperature range of 25 to 40 °C.[35,53,54] Again, stoichiometric amounts of PDEAAm$_{87}$-Ad and the CD-core were mixed in D_2O and the resulting assemblies were investigated using DLS. An increase in R_h from 2.4 to 3.8 nm was observed, corresponding to an expansion ratio of 1.6, similar values if compared to the earlier discussed PDMAAm systems (Fig. 3a).

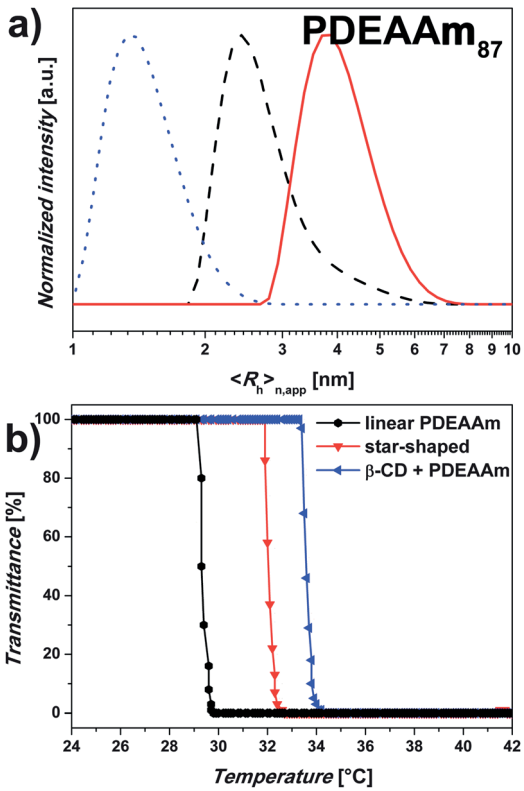

Fig. 3 (a) Number-weighted size distributions for the supramolecular star polymer (solid red line), PDEAAm$_{87}$-Ad (dashed black line), and the β-CD$_3$ core (dotted blue line) in a molar ratio of 3 : 1 after 24 hours at 25 °C. (b) Turbidity measurements for PDEAAm$_{87}$-Ad (black line), the supramolecular star polymer (red line), and a mixture of PDEAAm$_{87}$-Ad and β-CD (blue line) in D_2O.

To elucidate the temperature-dependent solubility of the PDEAAm-based supramolecular star polymers in D_2O, turbidimetry measurements were carried out. Any changes in temperature were performed with a heating/cooling rate of 1 K min^{-1}. The cloud point temperature (T_{cp}) was determined at a transmittance of 50%. Three samples, $PDEAAm_{87}$-Ad, the supramolecular star polymer, and a mixture of β-CD and $PDEAAm_{87}$, were investigated in a temperature range of 5–100 °C in D_2O. For $PDEAAm_{87}$-Ad, a T_{cp} of 29.3 °C was found, while the mixture with CD led to a higher value (T_{cp} = 33.6 °C). This observation can be explained by the complexation of the adamantyl moiety by β-CD and therefore the formation of a less hydrophobic endgroup. In the case of the star-shaped system a cloud point at 32.0 °C was observed in between the values for $PDEAAm_{87}$-Ad and the β-CD containing mixture (Fig. 3b). This might be explained by a shielding of the hydrophobic adamantyl groups due to the inclusion complex and – at the same time – decreased conformational freedom of the polymer chains by connecting three arms to the core moiety. The sharp decrease of the transmittance and the reversibility of the turbidimetry measurements (at least three times) are an additional indication for the successful formation of supramolecular star polymers *via* host–guest inclusion complexes. The collapse of the PDEAAm arms leads to an inclusion of the β-CD_3 into the collapsed polymer coil at a temperature far below the dissociation of the host–guest complex (~70 °C, as demonstrated using DLS in Fig. 2d).

Investigations of the self-assembly *via* ROESY NMR

ROESY NMR (Fig. 4) is a perfectly suitable tool to investigate the formation of inclusion complexes. The cross-correlation peaks in the ROESY spectrum can be assigned to protons that are closely situated (<4 Å).[55] While DLS experiments probe the molecular nature of the star polymers, ROESY NMR was performed to demonstrate the formation of the inclusion complex between the adamantyl moiety of polymer arms and the β-CD_3 core.

The 2D ROESY NMR spectrum (Fig. 4 and S16-S19†) shows six cross-correlation peaks that can be assigned to the adamantyl moiety and the β-CD moiety. The a, b and c protons of the adamantyl group have signals at 1.7, 2.0 and 2.1 ppm respectively whereas the inner protons H3 and H5 of β-CD have resonances at 3.7 and 3.8 ppm. In the 2D spectrum, the signals are located at the corresponding intersections that are expected for an inclusion complex of β-CD and the adamantyl moiety. Thus, a close distance between the protons of the adamantyl and β-CD moiety can be concluded, confirming the formation of an inclusion complex.[56] To exclude complex formation between the CD and the side chains of PDMAAm, a control sample of PDMAAm without the adamantyl moiety and β-CD was investigated as well, where the respective cross-correlation peaks were absent in the 2D NMR (Fig. S14, S15 and S20 in the ESI†).

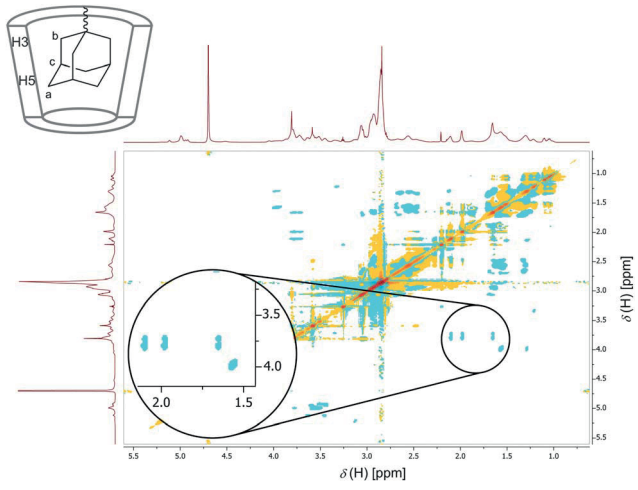

Fig. 4 2D ROESY NMR spectrum of a 3 : 1 molar mixture of $PDMAAm_{31}$-Ad (M_{nGPC} = 3500 g mol^{-1}, $Đ_M$ = 1.08) and the β-CD_3 core in D_2O at 25 °C, with the inset showing a magnification of the relevant peaks.

Conclusions

In summary, we present the formation of supramolecular star polymers *via* the formation of inclusion complexes between adamantyl-functionalized polyacrylamides and a three-pronged CD-core moiety. The synthesis of PDMAAm-Ad and PDEAAm-Ad was carried out *via* RAFT polymerization with a novel adamantyl-functionalized chain transfer agent (**CTA1**). The core, β-CD_3, was synthesized *via* CuAAc techniques. All building blocks were characterized *via* SEC, ^{1}H-NMR and ESI-MS.

The formation of supramolecular star polymers was carried out in D_2O and proven *via* a combination of light scattering (DLS) and 2D ROESY NMR. In the case of star polymers with PDEAAm arms, additional turbidity measurements revealed a change in temperature-dependent solution behaviour. The star polymer formation was shown to be reversible, as heating to 70 °C leads to an expulsion of the individual polymer arms and cooling to 25 °C to reformation of the complex.

Acknowledgements

C. B.-K. and H. R. are grateful for financial support for the current project from the German Research Council (DFG). C.B.-K. acknowledges additional financial support from the Karlsruhe Institute of Technology (KIT) in the context of the Excellence Initiative for leading German universities and the Ministry for Science and Arts of the state of Baden-Württemberg. F. H. S. and T. R. are grateful to the Thuringian Ministry for Education, Science and Culture (TMBWK; grants #B514-09051, NanoConSens and #B515-10065, ChaPoNano) for financial support.

Notes and references

1 T. Higashihara, M. Hayashi and A. Hirao, *Prog. Polym. Sci.*, 2011, **36**, 323–375.
2 K. Khanna, S. Varshney and A. Kakkar, *Polym. Chem.*, 2010, **1**, 1171–1185.
3 K. Inoue, *Prog. Polym. Sci.*, 2000, **25**, 453–571.
4 G. Kreutzer, C. Ternat, T. Q. Nguyen, C. J. G. Plummer, J.-A. E. Månson, V. Castelletto, I. W. Hamley, F. Sun, S. S. Sheiko, A. Herrmann, L. Ouali, H. Sommer, W. Fieber, M. I. Velazco and H.-A. Klok, *Macromolecules*, 2006, **39**, 4507–4516.
5 J. Liu, H. Duong, M. R. Whittaker, T. P. Davis and C. Boyer, *Macromol. Rapid Commun.*, 2012, **33**, 760–766.
6 L. Chen, P. Li, H. Tong, Z. Xie, L. Wang, X. Jing and F. Wang, *J. Polym. Sci., Part A: Polym. Chem.*, 2012, **50**, 2854–2862.
7 S. Kanaoka, M. Sawamoto and T. Higashimura, *Macromolecules*, 1991, **24**, 2309–2313.

8 H. Schlaad, C. Diehl, A. Gress, M. Meyer, A. L. Demirel, Y. Nur and A. Bertin, *Macromol. Rapid Commun.*, 2010, **31**, 511–525.
9 T. Hirano, H. S. Yoo, Y. Ozama, A. Abou El-Magd, K. Sugiyama and A. Hirao, *J. Inorg. Organomet. Polym. Mater.*, 2010, **20**, 445–456.
10 J. E. L. Roovers and S. Bywater, *Macromolecules*, 1974, **7**, 443–449.
11 C. J. Hawker, A. W. Bosman and E. Harth, *Chem. Rev.*, 2001, **101**, 3661–3688.
12 W. A. Braunecker and K. Matyjaszewski, *Prog. Polym. Sci.*, 2007, **32**, 93–146.
13 J. Chiefari, Y. K. Chong, F. Ercole, J. Krstina, J. Jeffery, T. P. T. Le, R. T. A. Mayadunne, G. F. Meijs, C. L. Moad, G. Moad, E. Rizzardo and S. H. Thang, *Macromolecules*, 1998, **31**, 5559–5562.
14 *Handbook of RAFT-Polymerization*, ed. C. Barner-Kowollik, Wiley-VCH, Weinheim, Germany, 2008.
15 K. Jankova, M. Bednarek and S. Hvilsted, *J. Polym. Sci., Part A: Polym. Chem.*, 2005, **43**, 3748–3759.
16 C. Barner-Kowollik, T. P. Davis and M. H. Stenzel, *Aust. J. Chem.*, 2006, **59**, 719–727.
17 C. J. Hawker, *Angew. Chem., Int. Ed. Engl.*, 1995, **34**, 1456–1459.
18 O. Altintas, A. P. Vogt, C. Barner-Kowollik and U. Tunca, *Polym. Chem.*, 2012, **3**, 34–45.
19 C. Barner-Kowollik, F. E. Du Prez, P. Espeel, C. J. Hawker, T. Junkers, H. Schlaad and W. Van Camp, *Angew. Chem., Int. Ed.*, 2011, **50**, 60–62.
20 H. Gao and K. Matyjaszewski, *Macromolecules*, 2006, **39**, 4960–4965.
21 M. W. M. Fijten, C. Haensch, B. M. van Lankvelt, R. Hoogenboom and U. S. Schubert, *Macromol. Chem. Phys.*, 2008, **209**, 1887–1895.
22 J. W. Chan, B. Yu, C. E. Hoyle and A. B. Lowe, *Chem. Commun.*, 2008, 4959–4961.
23 A. J. Inglis, S. Sinnwell, M. H. Stenzel and C. Barner-Kowollik, *Angew. Chem., Int. Ed.*, 2009, **48**, 2411–2414.
24 B. Iskin, G. Yilmaz and Y. Yagci, *Polym. Chem.*, 2011, **2**, 2865–2871.
25 J. Bernard, F. Lortie and B. Fenet, *Macromol. Rapid Commun.*, 2009, **30**, 83–88.
26 O. Altintas, T. Muller, E. Lejeune, O. Plietzsch, S. Bräse and C. Barner-Kowollik, *Macromol. Rapid Commun.*, 2012, **33**, 977–983.
27 A. Likhitsup, S. Yu, Y.-H. Ng, C. L. L. Chai and E. K. W. Tam, *Chem. Commun.*, 2009, 4070–4072.
28 X. Wu and C. L. Fraser, *Macromolecules*, 2000, **33**, 7776–7785.
29 U. S. Schubert and M. Heller, *Chem.–Eur. J.*, 2001, **7**, 5252–5259.
30 I. Gadwal, S. De, M. C. Stuparu, R. J. Amir, S. G. Jang and A. Khan, *J. Polym. Sci., Part A: Polym. Chem.*, 2012, **50**, 1844–1850.
31 (*a*) F. Huang, D. S. Nagvekar, C. Slebodnick and H. W. Gibson, *J. Am. Chem. Soc.*, 2004, **127**, 484–485; (*b*) B. V. K. J. Schmidt, M. Hetzer, H. Ritter and C. Barner-Kowollik, *Polym. Chem.*, 2012, DOI: 10.1039/C2PY20214J.
32 M. E. Davis, *Mol. Pharmaceutics*, 2009, **6**, 659–668.
33 F. Yhaya, J. Lim, Y. Kim, M. Liang, A. M. Gregory and M. H. Stenzel, *Macromolecules*, 2011, **44**, 8433–8445.
34 J. Zhou and H. Ritter, *Polym. Chem.*, 2010, **1**, 1552–1559.
35 B. V. K. J. Schmidt, M. Hetzer, H. Ritter and C. Barner-Kowollik, *Macromolecules*, 2011, **44**, 7220–7232.
36 H. S. Köllisch, C. Barner-Kowollik and H. Ritter, *Chem. Commun.*, 2009, 1097–1099.
37 H. Ritter, B. E. Mondrzik, M. Rehahn and M. Gallei, *Beilstein J. Org. Chem.*, 2010, **6**, No. 60.
38 L. Ding, Y. Li, J. Deng and W. Yang, *Polym. Chem.*, 2011, **2**, 694–701.
39 K. Ohno, B. Wong and D. M. Haddleton, *J. Polym. Sci., Part A: Polym. Chem.*, 2001, **39**, 2206–2214.
40 M. H. Stenzel and T. P. Davis, *J. Polym. Sci., Part A: Polym. Chem.*, 2002, **40**, 4498–4512.
41 Y. Miura, A. Narumi, S. Matsuya, T. Satoh, Q. Duan, H. Kaga and T. Kakuchi, *J. Polym. Sci., Part A: Polym. Chem.*, 2005, **43**, 4271–4279.
42 Z.-X. Zhang, X. Liu, F. J. Xu, X. J. Loh, E.-T. Kang, K.-G. Neoh and J. Li, *Macromolecules*, 2008, **41**, 5967–5970.
43 Z.-X. Zhang, K. L. Liu and J. Li, *Macromolecules*, 2011, **44**, 1182–1193.
44 Z. Yu, A. R. Sawkar, L. J. Whalen, C.-H. Wong and J. W. Kelly, *J. Med. Chem.*, 2006, **50**, 94–100.
45 J. Skey and R. K. O'Reilly, *Chem. Commun.*, 2008, 4183–4185.
46 S. Amajjahe, S. Choi, M. Munteanu and H. Ritter, *Angew. Chem., Int. Ed.*, 2008, **47**, 3435–3437.
47 R. Dong, Y. Liu, Y. Zhou, D. Yan and X. Zhu, *Polym. Chem.*, 2011, **2**, 2771–2774.
48 C. Kuo, T. Provder and M. E. Koehler, in *Int. GPC Symposium Proceeding*, 1991, pp. 147–159.
49 M. V. Rekharsky and Y. Inoue, *Chem. Rev.*, 1998, **98**, 1875–1918.
50 P. Kujawa and F. M. Winnik, *Macromolecules*, 2001, **34**, 4130–4135.
51 H. Mao, C. Li, Y. Zhang, S. Furyk, P. S. Cremer and D. E. Bergbreiter, *Macromolecules*, 2004, **37**, 1031–1036.
52 X. Wang and C. Wu, *Macromolecules*, 1999, **32**, 4299–4301.
53 L. H. Gan, W. Cai and K. C. Tam, *Eur. Polym. J.*, 2001, **37**, 1773–1778.
54 P. Kujawa, F. Segui, S. Shaban, C. Diab, Y. Okada, F. Tanaka and F. M. Winnik, *Macromolecules*, 2005, **39**, 341–348.
55 H.-J. Schneider, F. Hacket, V. Rüdiger and H. Ikeda, *Chem. Rev.*, 1998, **98**, 1755–1786.
56 H. Liu, Y. Zhang, J. Hu, C. Li and S. Liu, *Macromol. Chem. Phys.*, 2009, **210**, 2125–2137.

Electronic Supplementary Material (ESI) for Polymer Chemistry

Supplementary Information

Supramolecular Three-Armed Star Polymers via Cyclodextrin Host/Guest Self-Assembly

Bernhard V. K. J. Schmidt,[a] *Tobias Rudolph,*[b,c] *Martin Hetzer,*[d] *Helmut Ritter,*[d*] *Felix H. Schacher*[b,c*] *and Christopher Barner-Kowollik*[a*]

[a] Preparative Macromolecular Chemistry, Institut für Technische Chemie und Polymerchemie, Karlsruhe Institute of Technology (KIT), Engesserstr. 18, 76128 Karlsruhe, Germany

[b] Laboratory of Organic and Macromolecular Chemistry (IOMC), Friedrich-Schiller-University Jena, Lessingstraße 8, 07743 Jena, Germany

[c] Jena Center for Soft Matter (JCSM), Friedrich-Schiller-University Jena, Humboldtstr. 10, 07743 Jena, Germany

[d] Lehrstuhl für Präparative Polymerchemie, Institut für Organische Chemie und Makromolekulare Chemie, Heinrich-Heine Universität, Universitätsstrasse 1, Geb. 26.33.00, 40225 Düsseldorf, Germany

[*](C.B.-K.) Tel (+49) 721 608-45642; Fax (+49) 721 608-45740; e-mail: christopher.barner-kowollik@kit.edu;

[*](F.H.S.) Tel (+49) 3641 9-48250; Fax (+49) 3641 9-48202; e-mail: felix.schacher@uni-jena.de;

[*](H.R.) Tel (+49) 211 81-14760; Fax: (+49) 211 81-15840; e-mail: h.ritter@uni-duesseldorf.de.

Additional Experimental Procedures

Synthesis of N-(adamantan-1-yl)-6-hydroxyhexanamide

According to the literature procedure,[1] 11.8 g aluminium chloride (88.50 mmol, 2.2 eq.) were suspended in 100 mL of anhydrous DCM. At 0 °C 17.2 mL triethylamine (124.08 mmol, 3.1 eq.) were added dropwise via a syringe. After stirring for 15 minutes at 0 °C, the mixture was warmed to ambient temperature. Subsequently, a solution of 4.2 mL ε-caprolacton (39.74 mmol, 1.0 eq.), 6.1 mL triethylamine (46.89 mmol, 1.2 eq.) and 8.25 g adamantylamine hydrochloride (43.95 mmol, 1.1 eq.) in 100 mL anhydrous DCM was added dropwise. The mixture was stirred over night and subsequently poured into an ice cold solution of 30 g sodium carbonate in 300 mL ice water. The organic phase was separated and the aqueous phase extracted three times with 200 mL DCM. The combined organic extracts were washed with 500 mL deionized water, 500 mL brine, dried over sodium sulfate, filtered and concentrated in vacuo. The resulting solid was recrystallized from an acetonitrile/methanol mixture to give 7.09 g (26.72 mmol, 67%) of the product as off-white crystals.

^{1}H-NMR (400 MHz, $CDCl_3$): [δ, ppm] = 1.31 – 1.43 (m, 2H, C***H***$_2$-CH_2-CH_2-O), 1.51 – 1.73 (m, 10H, C***H***$_2$-CH_2-O; C***H***$_2$-CH_2-C=O; 3x C***H***$_{2,adamantyl}$), 1.92-2.00 (m, 6H, 3x NH-C-C***H***$_{2,adamantyl}$), 2.01 - 2.12 (m, 5H, 3x C***H***$_{adamantyl}$; C***H***$_2$-C=O-NH), 3.63 (t, 2H, C***H***$_2$-OH), 5.17 (br s, 1H, N***H***).

^{13}C-NMR (100 MHz, $CDCl_3$): [δ, ppm] = 25.4 (***C***H_2-CH_2-C=O; ***C***H_2-CH_2-CH_2-C=O), 29.6 (3x ***C***$H_{adamantyl}$), 32.4 (***C***H_2-CH_2-OH), 36.5 (3x ***C***$H_{2,adamantyl}$), 37.7 (***C***H_2-C=O), 41.8 (3x ***C***$H_{2,adamantyl}$-C-NH), 51.9 (***C***-NH), 62.6 (***C***H_2-OH), 172.3 (***C***=O).

ESI-MS: $[M + Na^+]_{exp}$ = 288.36 *m*/*z* and $[M + Na^+]_{calc}$ = 288.1939 *m*/*z*.

Synthesis of N,N,N-(tris-1-(mono-(6-desoxy)-β-CD)-1H-1,2,3-triazol-4-yl)methanamine (β-CD_3)

This compound was prepared from a modified literature procedure.[46] In a 50 mL Schlenk-tube tripropargylamine (34 mg, 0.26 mmol, 1.0 eq.), β-CD-N_3 (1.00 g, 0.86 mmol, 3.3 eq.) and PMDETA

(0.16 mL, 0.77 mmol, 3.0 eq.) were dissolved in DMF (11mL). After three freeze-pump-thaw cycles the tube was backfilled with Argon and CuBr (112 mg, 0.78 mmol, 3.0 eq.) was added under a flow of Argon. The tube was sealed again and subjected to two freeze-pump-thaw cycles. Subsequently the tube was backfilled with Argon and immersed in an oil bath at 70 °C for 4 days. After cooling to ambient temperature the product was precipitated in an excess of acetone. The product was filtered, dissolved in 10 mL EDTA-solution (5 wt%) and dialyzed with a SpectraPor3 membrane (MWCO = 2000 Da) for 3 days at ambient temperature. Finally the solvent was removed in vacuo to yield β-CD_3 (574 mg, 0.16 mmol, 61%) as an off-white solid.

^{1}H NMR (400 MHz, D_2O): [δ, ppm] = 3.18 (d, 3H, N-NC*H(gem)*$_2$), 3.32 (d, 3H, N-NC*H(gem)*$_2$), 3.37 - 4.14 (m, 124H, CD-*H*2,3,4,5,6), 4.24 (t, 3H, NC*H(gem)*$_2$-C), 4.66 (dd, 3H, NC*H(gem)*$_2$-C), 4.93 - 5.18 (m, 21H, CD-*H*1), 8.02 (s, 3H, $H_{triazole}$).

ESI-MS: $[M + 2Na^{2+}]_{exp}$ = 1828.33 *m*/*z* and $[M + 2Na^{2+}]_{calc}$ = 1828.0926 *m*/*z* (refer to Figure S11 for a more detailed ESI-MS characterization)

Preparation for dynamic light scattering experiments

Adamantyl-functionalized polymer, e.g. PDMAAm (M_{nGPC} = 14600 g·mol^{-1}, 12.4 mg, 3.0 eq.) and β-CD_3 (1.4 mg, 1.0 eq.) were dissolved in D_2O (1 mL, c = 5 mg·mL^{-1}) and stirred at 25 °C.

Control experiments in dynamic light scattering

For control experiments, the linear polymer was dissolved together with the linker molecule β-CD_3 in H_2O and analyzed over several days without any change in the hydrodynamic radius being observed (Figure S12a). $PDMAAm_{143}$ was additionally mixed with variable amounts of β-CD (Figure S12b) and no increase in size was observed. In Figure S12c the increase of the hydrodynamic radius with time is depicted. As a further control the β-CD_3 was mixed in an excess with the polymer (Figure S12d).

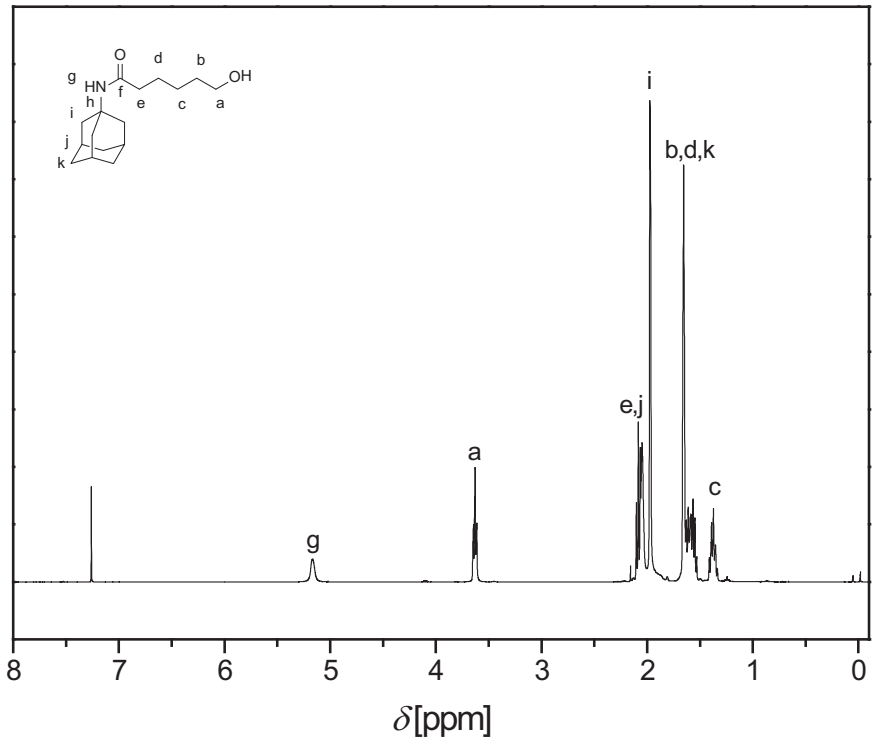

Figure S1. ^{1}H-NMR spectrum of *N*-(adamantan-1-yl)-6-hydroxyhexanamide.

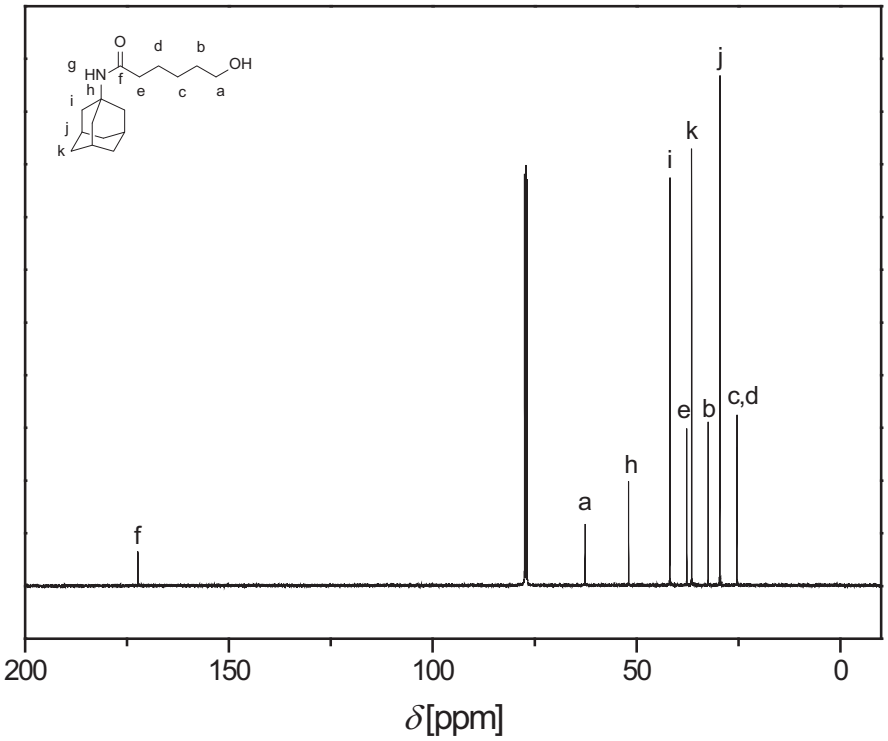

Figure S2. ^{13}C-NMR spectrum of *N*-(adamantan-1-yl)-6-hydroxyhexanamide.

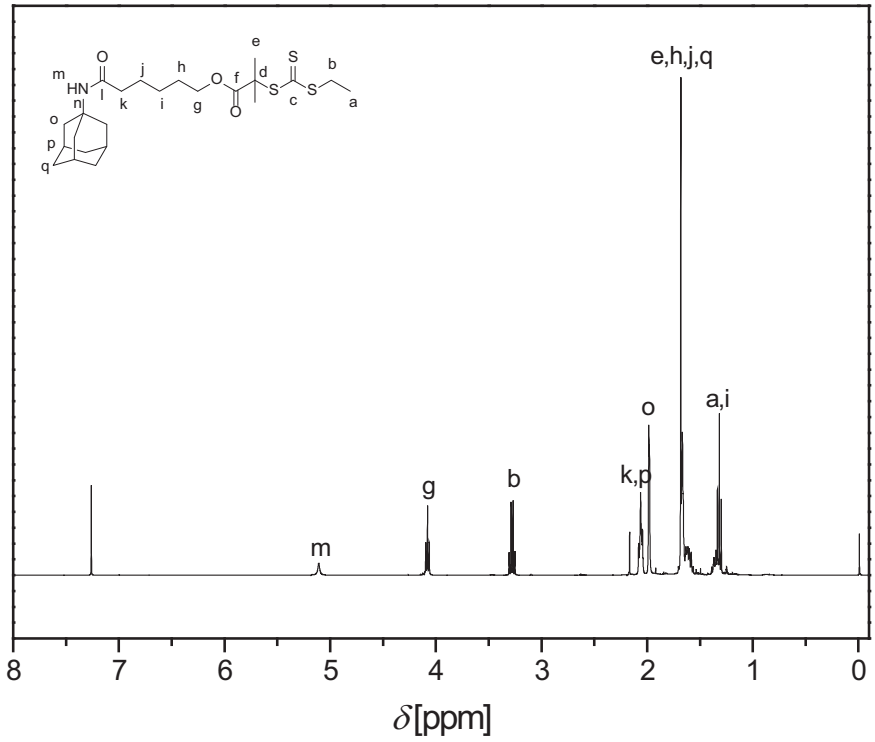

Figure S3. ^{1}H-NMR spectrum of 6-(adamantan-1-ylamino)-6-oxohexyl 2-(((ethylthio)carbonothioyl)thio)-2-methylpropanoate (**CTA1**).

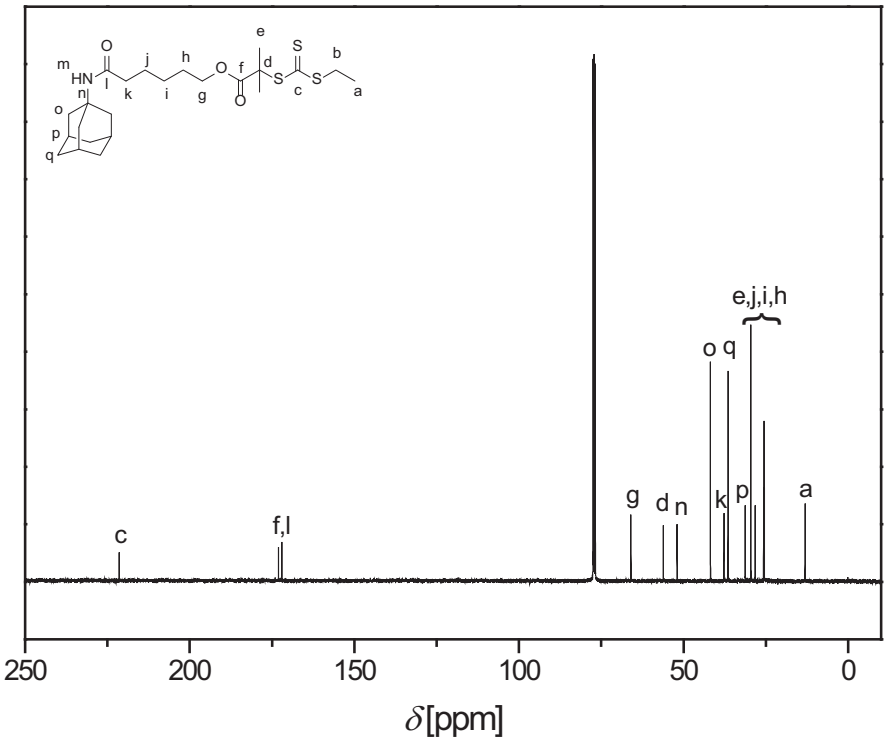

Figure S4. ^{13}C-NMR spectrum of 6-(adamantan-1-ylamino)-6-oxohexyl 2-(((ethylthio)carbonothioyl)thio)-2-methylpropanoate (**CTA1**).

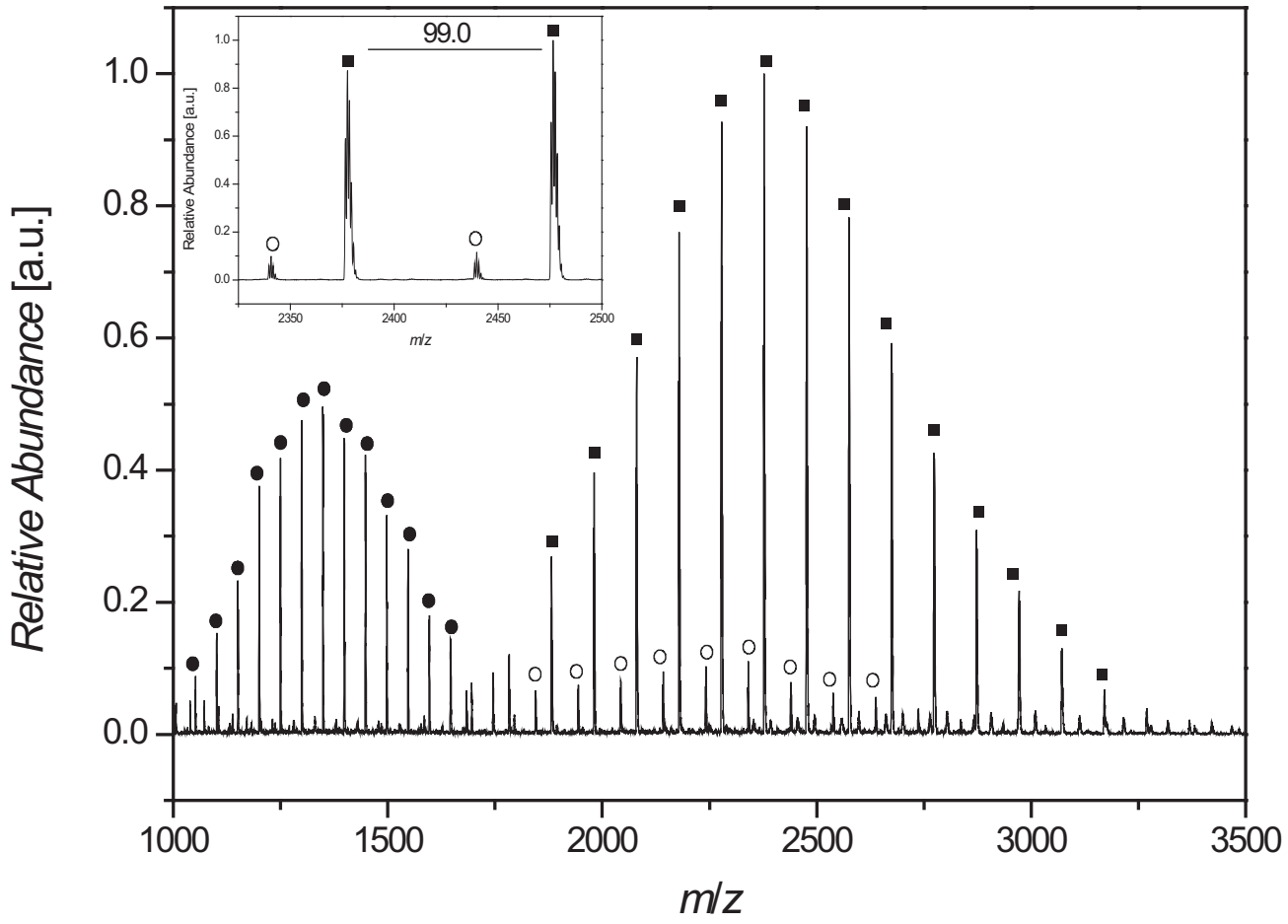

Figure S5. ESI-MS-spectrum of an adamantyl-functionalized PDMAAm (M_{nGPC} = 3900 g·mol^{-1}, $Đ_M$ = 1.07) polymerized with **CTA1**.

Table S1. Theoretical and experimental *m*/*z* of PDMAAm polymerized with **CTA1**.

Species	m/z_{theo}	$m/z_{exp.}$	Δ m/z
■ [**CTA1**(DMAAm)$_{20}$+Na]$^+$	2476.5550	2476.55	0.00
● [**CTA1**(DMAAm)$_{23}$+2Na]$^{2+}$	1348.8408	1348.82	0.02
○ [**CTA1**(DMAAm)$_{25}$-Adamantyl+Na]$^+$	2440.5060	2439.82	0.69

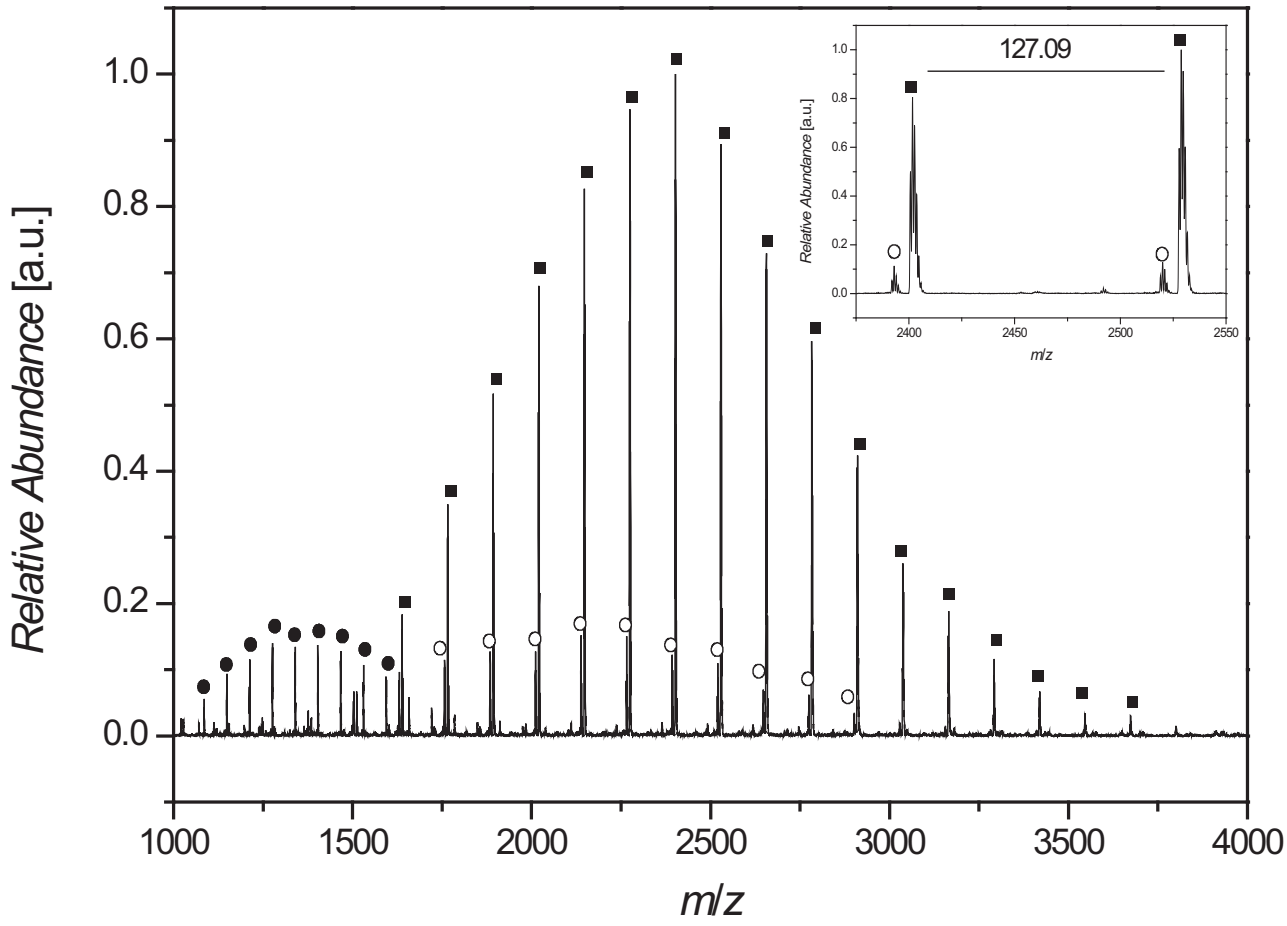

Figure S6. ESI-MS-spectrum of an adamantyl-functionalized PDEAAm (M_{nGPC} = 2700 g·mol^{-1}, $Đ_M$ = 1.08) polymerized with **CTA1**.

Table S2. Theoretical and experimental *m*/*z* of PDEAAm polymerized with **CTA1**.

Species	m/z_{theo}	$m/z_{exp.}$	Δ m/z
■ [**CTA1**(DEAAm)$_{16}$+Na]$^+$	2528.7821	2528.82	0.04
● [**CTA1**(DEAAm)$_{17}$+2Na]$^{2+}$	1339.4358	1339.45	0.01
○ [**CTA1**(DEAAm)$_{17}$-Adamantyl+Na]$^+$	2520.7644	2520.00	0.76

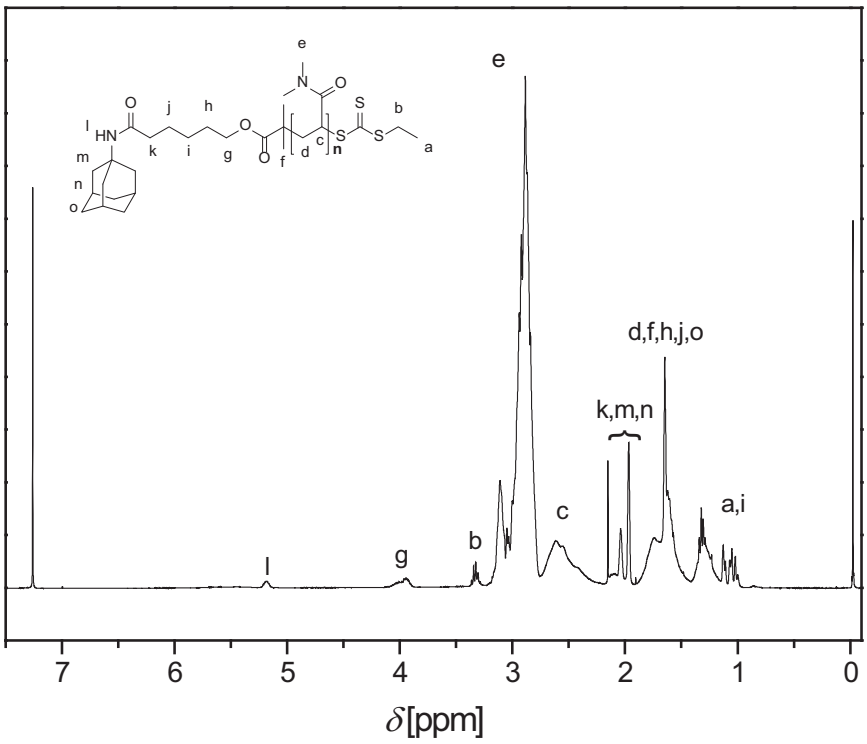

Figure S7. ^{1}H-NMR spectrum of an adamantyl-functionalized PDMAAm (M_{nGPC} = 3900 g·mol^{-1}, $Đ_M$ = 1.07) recorded in $CDCl_3$ at 25 °C.

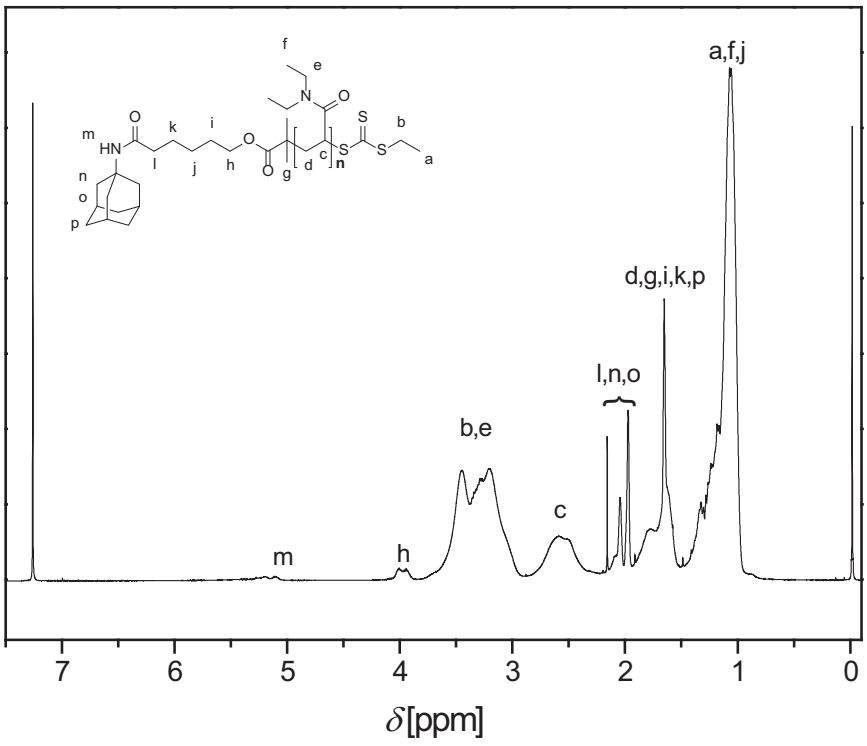

Figure S8. ^{1}H-NMR spectrum of an adamantyl-functionalized PDEAAm (M_{nGPC} = 2700 g·mol^{-1}, $Đ_M$ = 1.08) recorded in $CDCl_3$ at 25 °C.

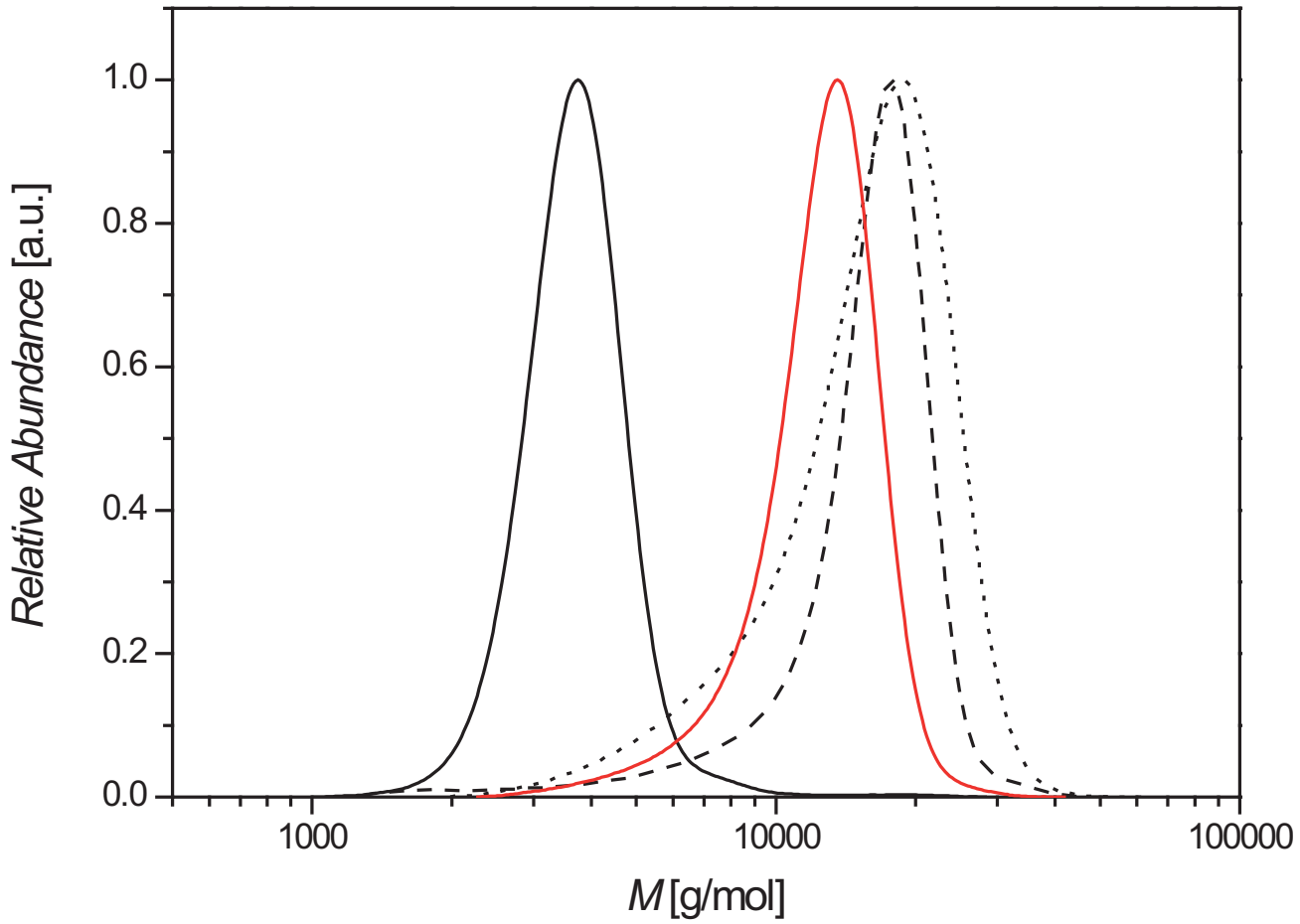

Figure S9 Molecular weight distributions for $PDMAAm_{31}$-Ad (solid black line), $PDMAAm_{143}$-Ad (dashed black line), $PDMAAm_{202}$-Ad (dotted black line), and $PDEAAm_{87}$-Ad (solid red line).

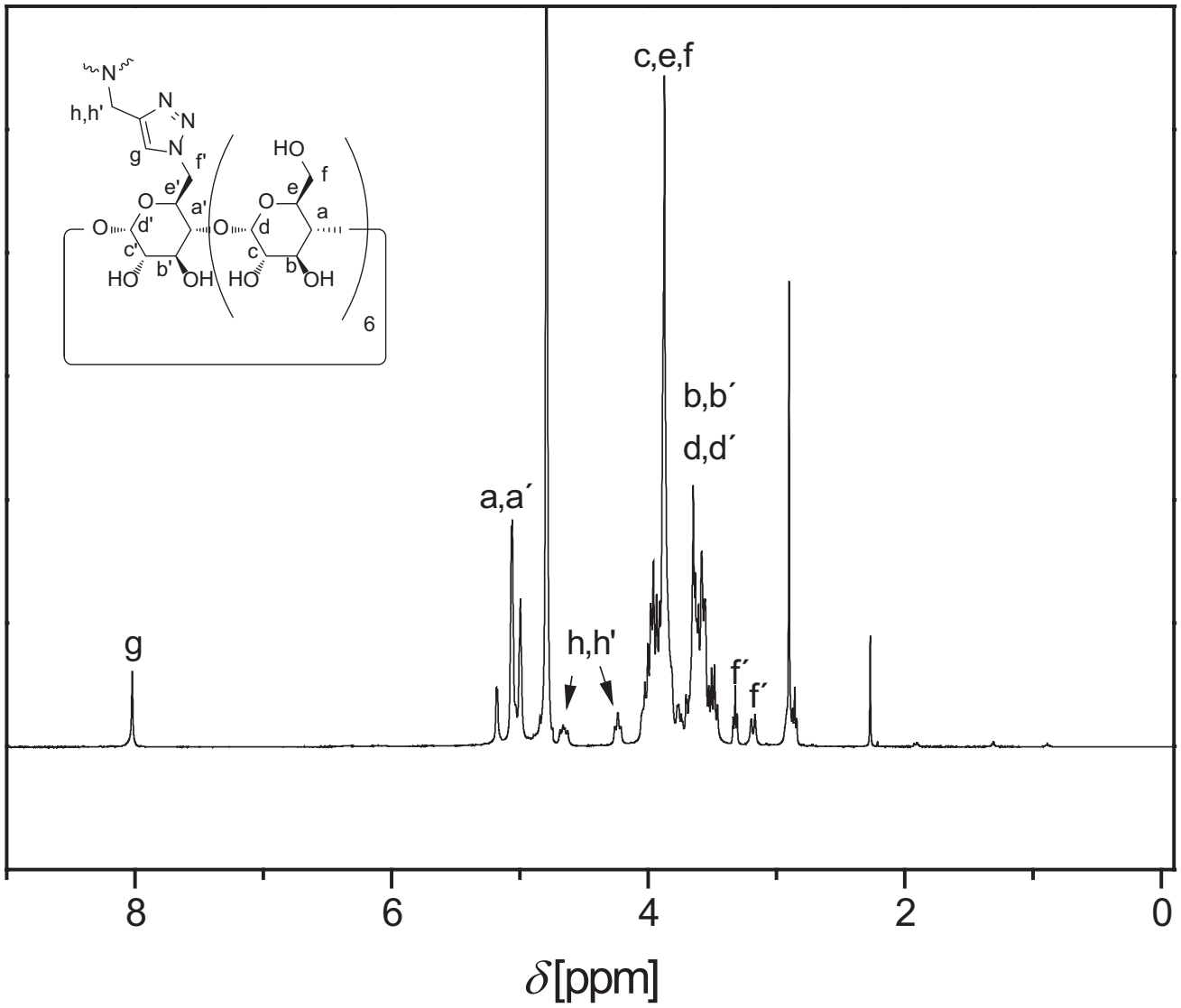

Figure S10. ^{1}H-NMR spectrum of the three-pronged β-CD core (β-CD_3) recorded in D_2O at 25 °C.

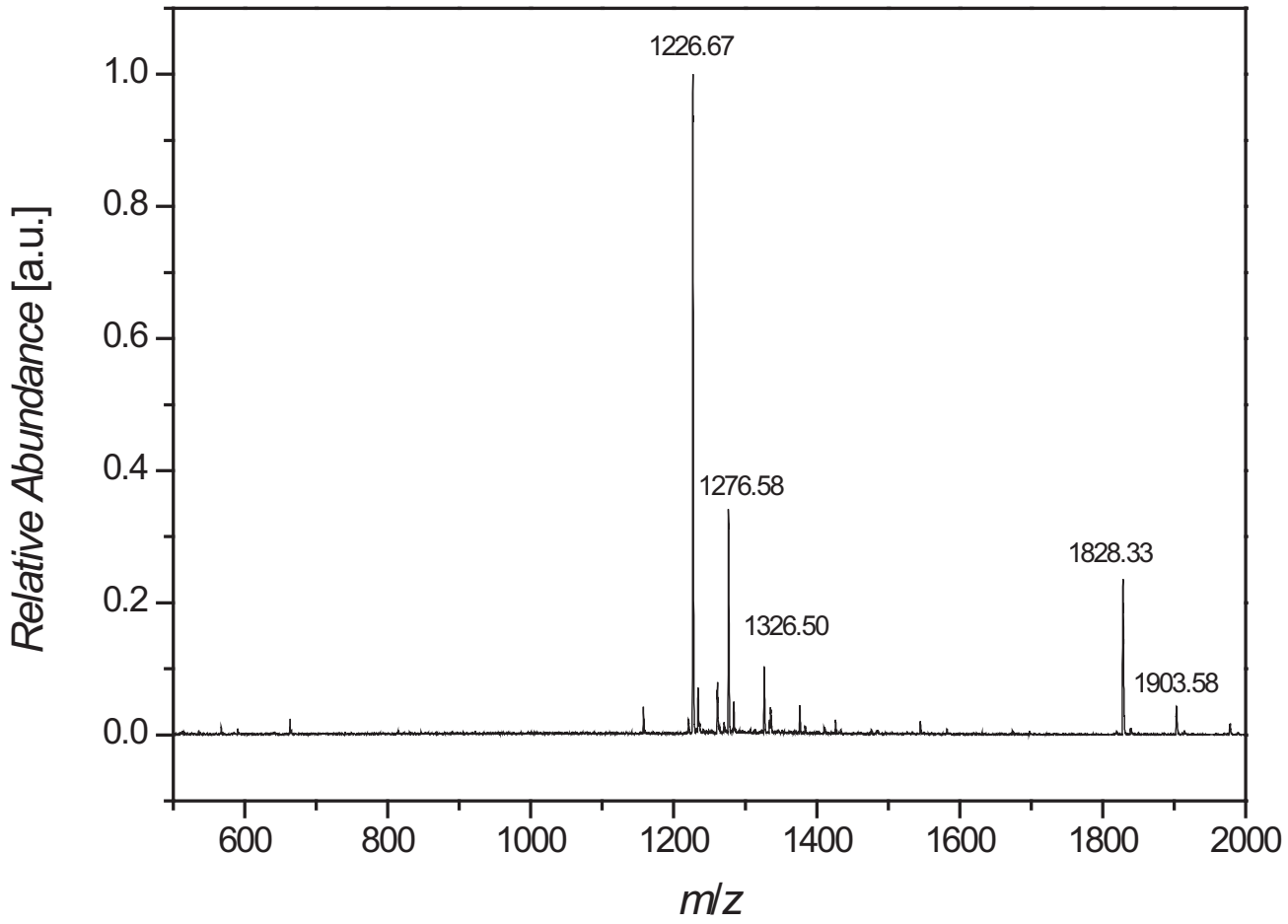

Figure S11. ESI-MS-spectrum of the three-pronged β-CD core (β-CD_3) (ionized with NaI).

Table S3. Theoretical and experimental *m*/*z* of β-CD_3 (ionized with NaI).

Species	m/z_{theo}	$m/z_{exp.}$	Δ *m*/*z*
$[\beta\text{-}CD_3+2Na]^{2+}$	1828.0926	1828.33	0.24
$[\beta\text{-}CD_3+I^-+3Na]^{2+}$	1903.0397	1903.58	0.54
$[\beta\text{-}CD_3+3Na]^{3+}$	1226.3916	1226.67	0.28
$[\beta\text{-}CD_3+I^-+4Na]^{3+}$	1276.6564	1276.58	0.22
$[\beta\text{-}CD_3+2I^-+5Na]^{3+}$	1326.3211	1326.50	0.18

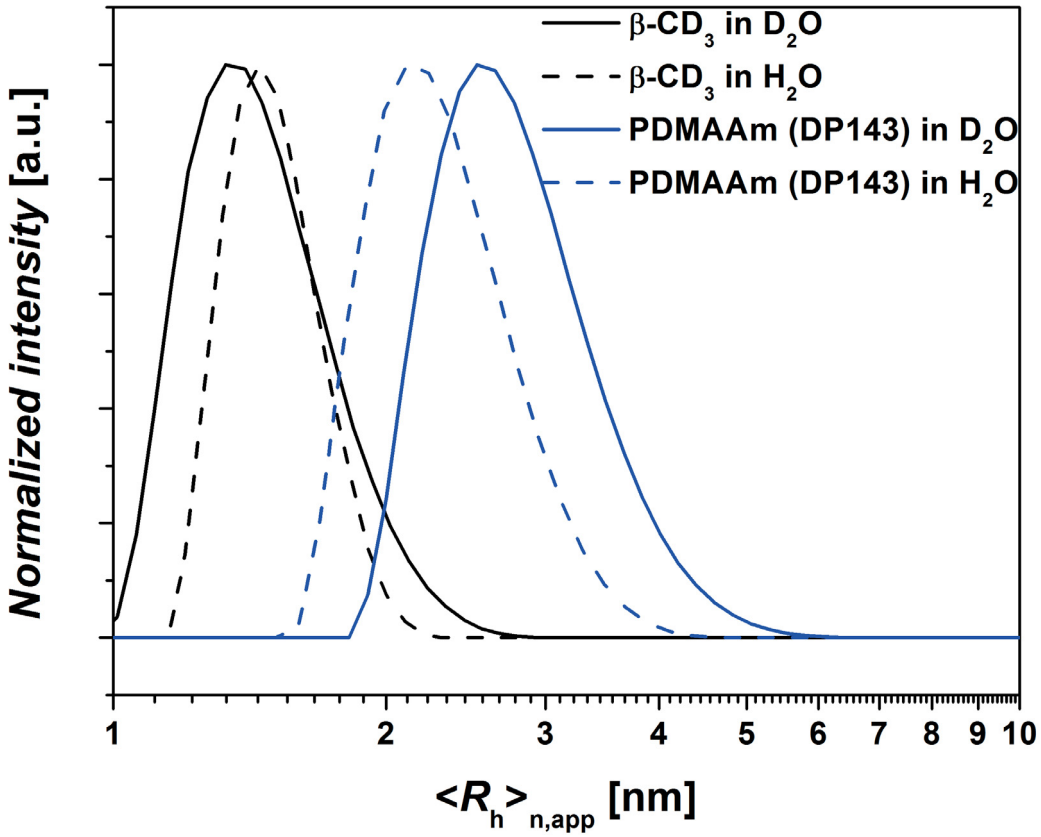

Figure S12. Comparison of the number averaged hydrodynamic radii for the core (β-CD_3) (black line) and $PDMAAm_{143}$ (blue line) in different solvents: H_2O (dashed line) and D_2O (straight line) at 25 °C.

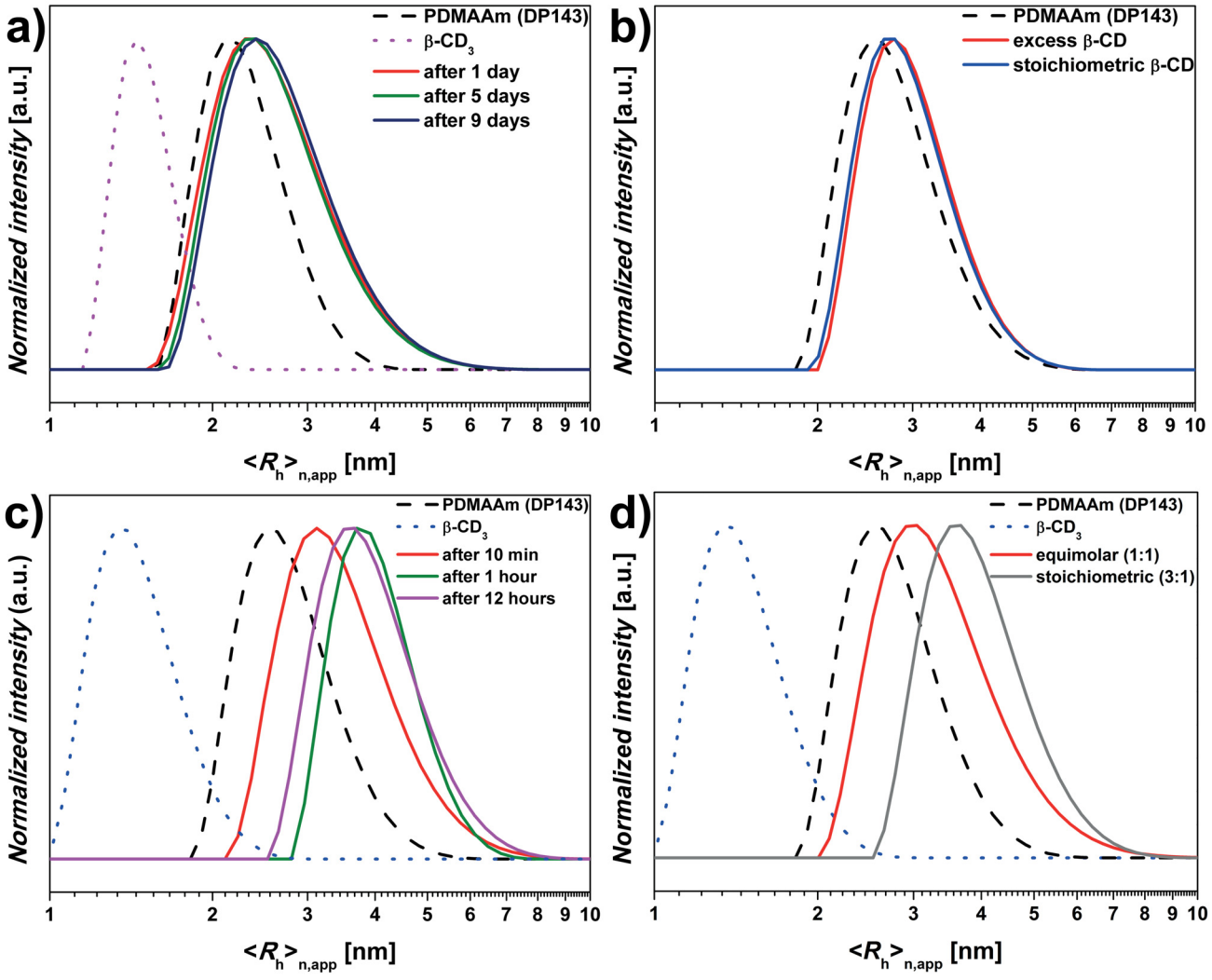

Figure S13. Number averaged hydrodynamic radii a) for $PDMAAm_{143}$ mixed with the β-CD_3 core and the resulting supramolecular star polymers over several days in H_2O at 25 °C; b) for $PDMAAm_{143}$ mixed with β-CD at 25 °C in D_2O; c) for $PDMAAm_{143}$ mixed with the β-CD_3 core in a time dependent investigation of the self-assembly process; d) for $PDMAAm_{143}$ mixed with a molar excess of 3:1 of the β-CD_3 core (red line) and for a stoichiometric mixture of $PDMAAm_{143}$ and the β-CD_3 core with a molar ratio of 3:1 (grey line) (D_2O, 25 °C).

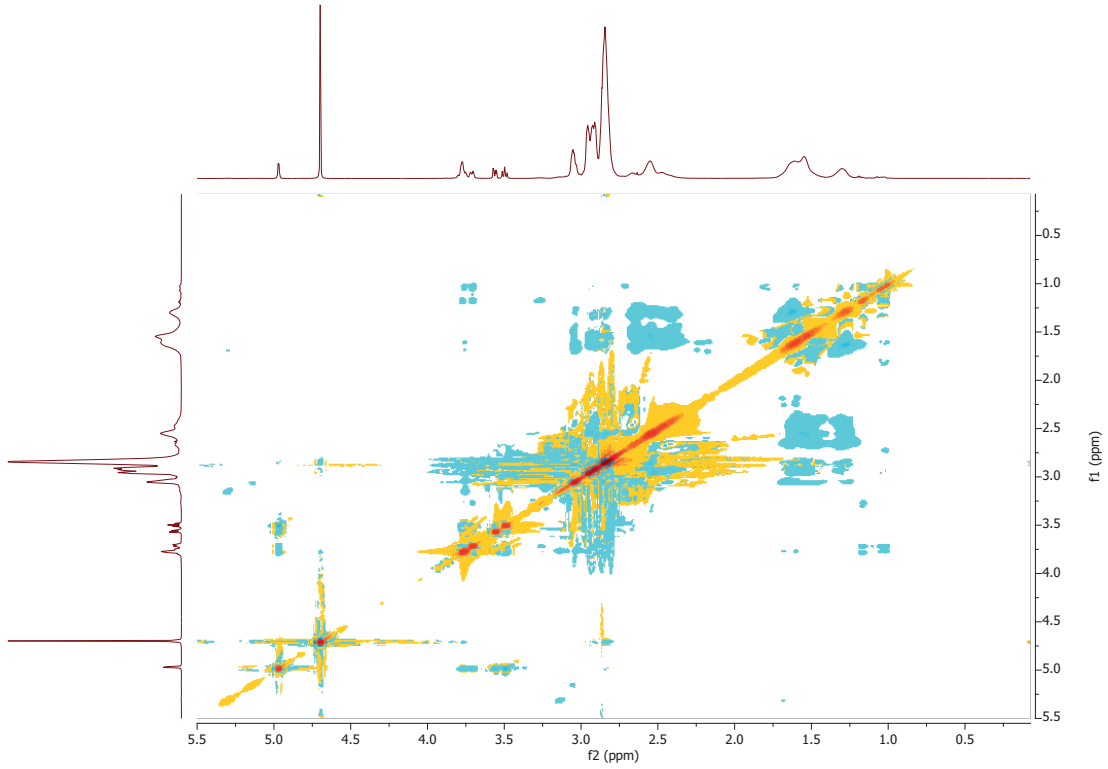

Figure S14. 2D ROESY NMR spectrum of a 1:1.1 molar mixture of PDMAAm (M_{nGPC} = 12800 g·mol^{-1}, $Đ_M$ = 1.10) polymerized with EMP and β-CD in D_2O at 25 °C.

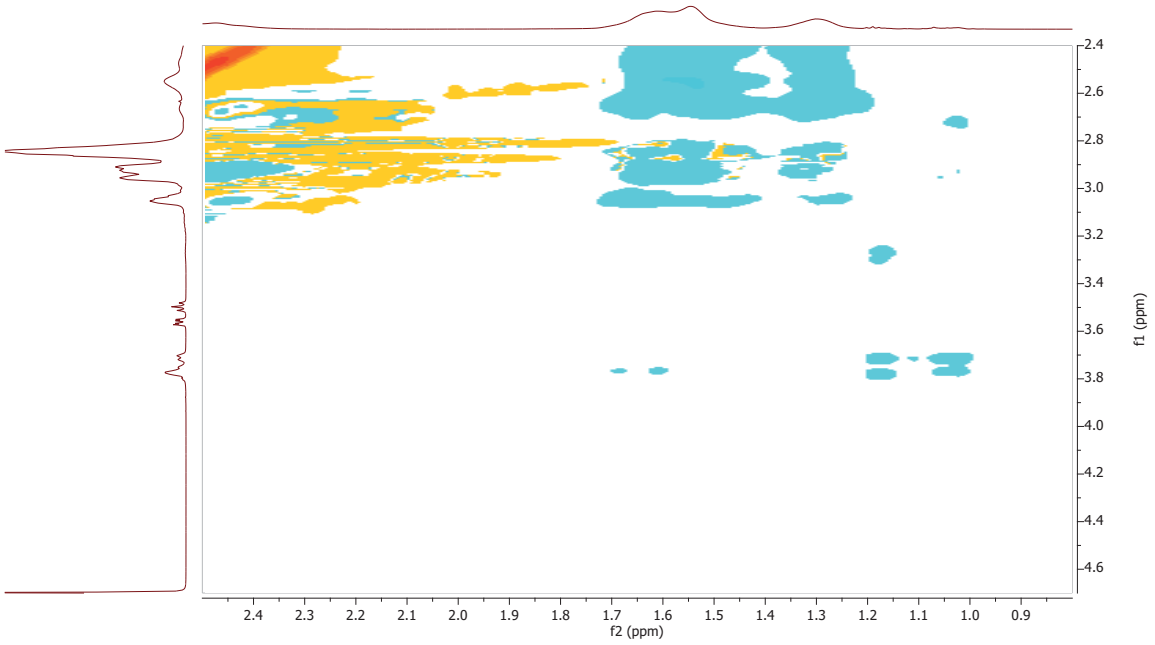

Figure S15. Magnification of the 2D ROESY NMR spectrum of a 1:1.1 molar mixture of PDMAAm (M_{nGPC} = 12800 g·mol^{-1}, $Đ_M$ = 1.10) polymerized with EMP and β-CD in D_2O at 25 °C.

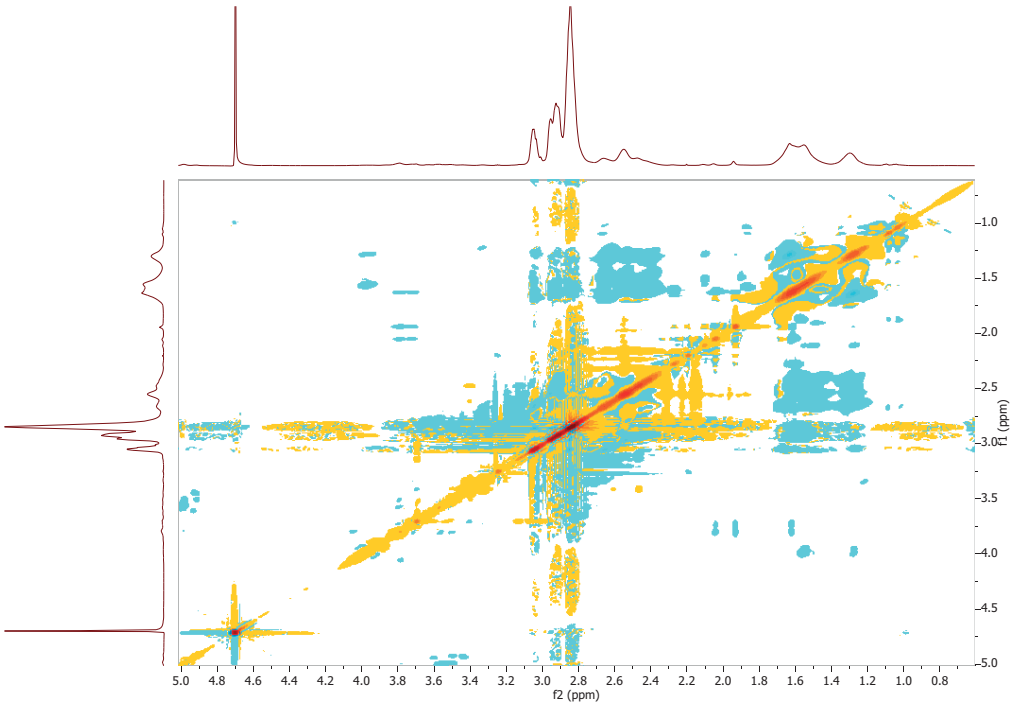

Figure S16. 2D ROESY NMR spectrum of a 3:1 molar mixture of an adamantyl-functionalized PDMAAm (M_{nGPC} = 14600 g·mol^{-1}, $Đ_M$ = 1.12) polymerized with **CTA1** and the β-CD_3 core in D_2O at 25 °C.

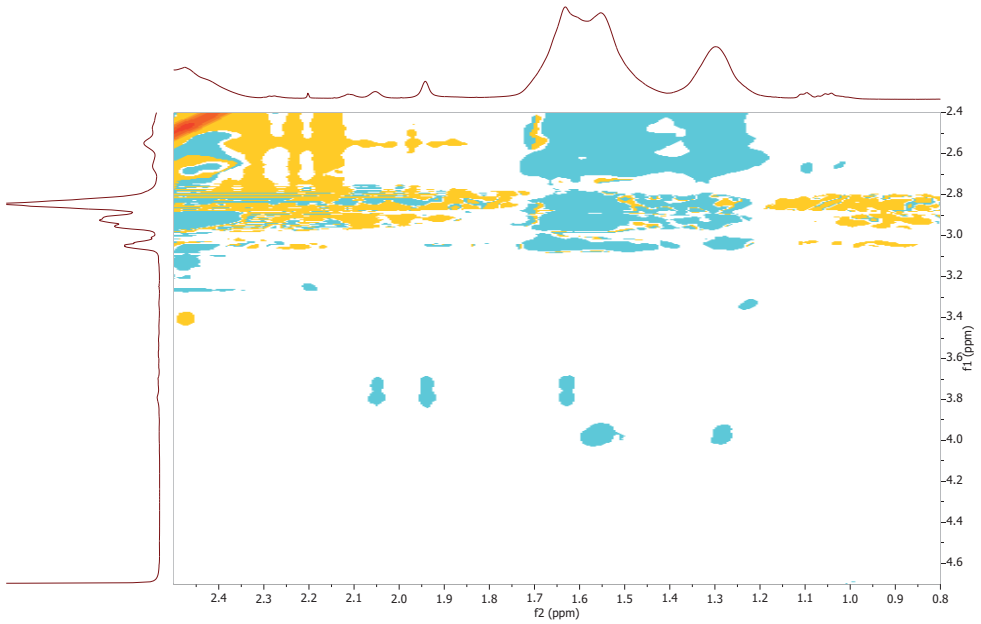

Figure S17. Magnification of the 2D ROESY NMR spectrum of a 3:1 molar mixture of an adamantyl-functionalized PDMAAm (M_{nGPC} = 14600 g·mol^{-1}, $Đ_M$ = 1.12) polymerized with **CTA1** and the β-CD_3 core in D_2O at 25 °C.

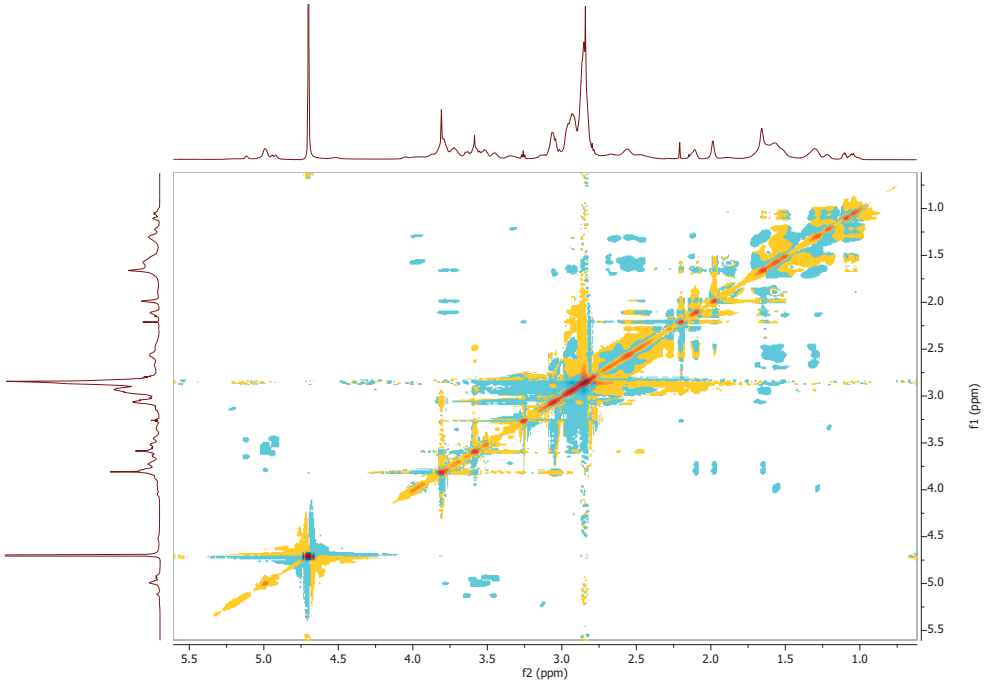

Figure S18. 2D ROESY NMR spectrum of a 3:1 molar mixture of an adamantyl-functionalized PDMAAm (M_{nGPC} = 3900 g·mol^{-1}, $Đ_M$ = 1.07) polymerized with **CTA1** and the β-CD_3 core in D_2O at 25 °C.

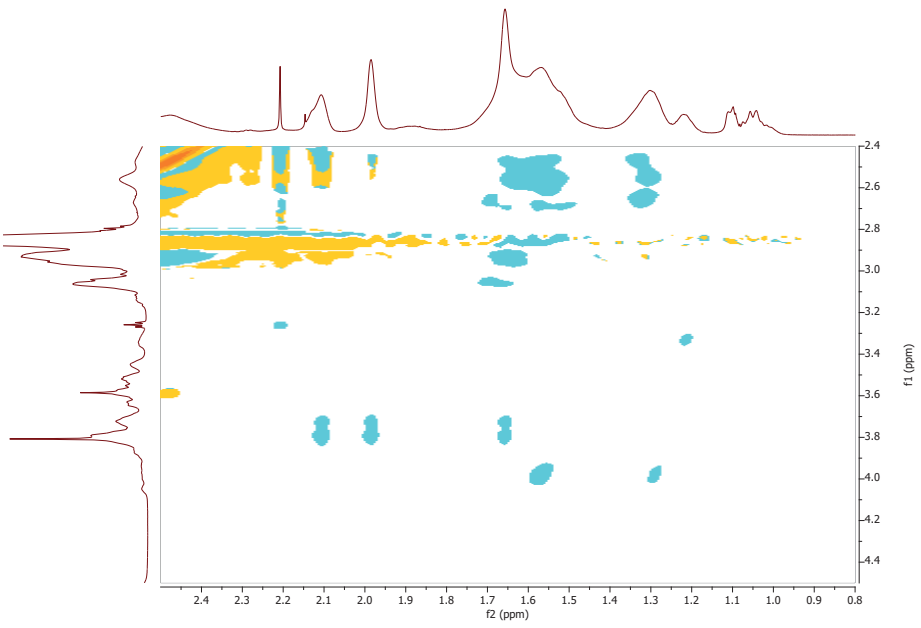

Figure S19. Magnification of the 2D ROESY NMR spectrum of a 3:1 molar mixture of an adamantyl-functionalized PDMAAm (M_{nGPC} = 3900 g·mol^{-1}, $Đ_M$ = 1.07) polymerized with **CTA1** and the β-CD_3 core in D_2O at 25 °C.

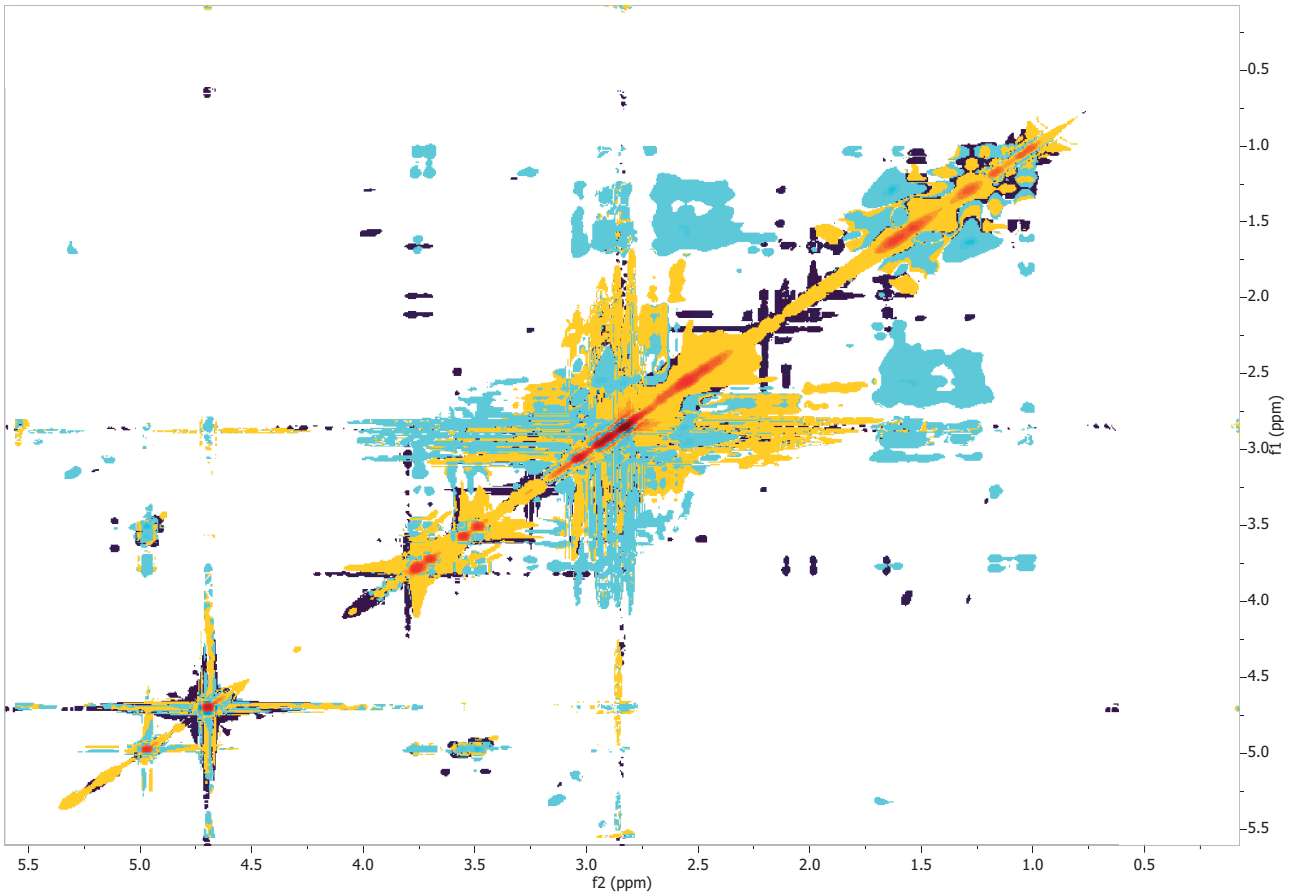

Figure S20. Overlay of the 2D ROESY NMR spectra in D_2O at 25 °C. Violet: 3:1 molar mixture of an adamantyl-functionalized PDMAAm (M_{nGPC} = 3900 g·mol^{-1}, $Đ_M$ = 1.08) polymerized with **CTA1** and the β-CD_3 core. Turquoise: 1:1.1 molar mixture of PDMAAm (M_{nGPC} = 12800 g·mol^{-1}, $Đ_M$ = 1.10) polymerized with EMP and β-CD.

References

1. Z. Yu, A. R. Sawkar, L. J. Whalen, C.-H. Wong and J. W. Kelly, *Journal of Medicinal Chemistry*, 2006, **50**, 94-100.

Publication P4

"Synthesis and Self-Assembly of Poly(ferrocenyldimethylsilane)-*block*-poly(2-alkyl-2-oxazoline) Block Copolymers"

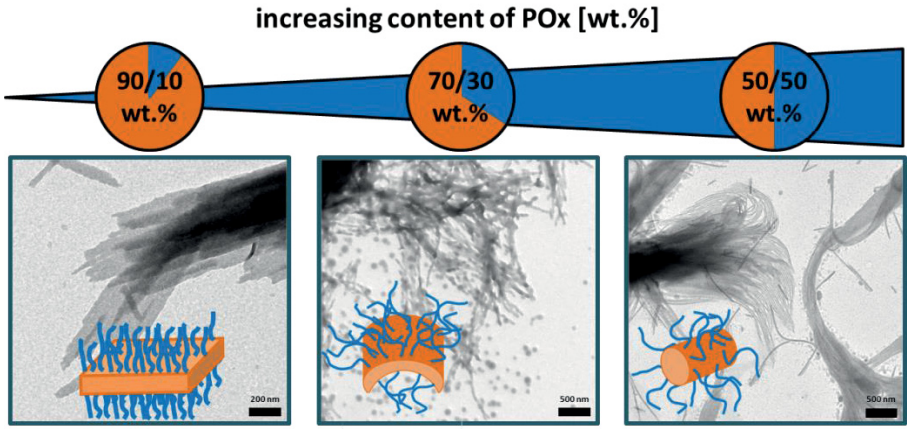

Tobias Rudolph, Adam Nunns, Almut M. Schwenke, Felix H. Schacher

Polym. Chem., **2015**, 6, 1604-1612

Polymer Chemistry

PAPER

View Article Online
View Journal | View Issue

Cite this: *Polym. Chem.*, 2015, **6**, 1604

Synthesis and self-assembly of poly(ferrocenyldimethylsilane)-*block*-poly(2-alkyl-2-oxazoline) block copolymers†

Tobias Rudolph,[a,b] Adam Nunns,[c] Almut M. Schwenke[a,b] and Felix H. Schacher*[a,b]

Received 6th November 2014,
Accepted 9th December 2014

DOI: 10.1039/c4py01512f

www.rsc.org/polymers

Herein, we demonstrate the synthesis of chain-end functionalized poly(ferrocenyldimethylsilane) (PFDMS) and poly(2-alkyl-2-oxazoline)s (POx) of different molar mass, and the subsequent macromolecular conjugation to organometallic PFDMS-*b*-POx block copolymers of different composition *via* copper-catalyzed azide–alkyne cycloaddition (CuAAC). We distinguish between amphiphilic crystalline-coil PFDMS-*b*-PEtOx (poly(2-ethyl-2-oxazoline)) and potentially double crystalline PFDMS-*b*-P*i*PrOx (poly(2-isopropyl-2-oxazoline)) materials. After characterization of the obtained block copolymers *via* SEC, NMR, FT-IR and X-ray scattering, the solution behavior in acetone as a non-solvent for PFDMS was investigated. We found various aggregate morphologies with a PFDMS core and a POx corona (sheets, vesicles, rods), depending on the weight fraction of the organometallic PFDMS segment.

Introduction

Modern synthetic approaches enable superior control over molecular weight, chain-end functionality, composition, and architecture of polymeric materials, including homo- and copolymers.[1] Especially (block) copolymers have been intensively studied because, depending on the composition and architecture (random, gradient-, graft-, or block copolymers), they can combine the properties of different monomers within one single material. The synthesis of block copolymers can be realized *via* different sequential polymerization techniques.[2–4] However, the preparation of block copolymers consisting of building blocks requiring different polymerization methodologies is often challenging. Especially for switching from anionic towards cationic polymerization only few approaches are known in the literature,[2,5–7] even less for the combination of ionic ring-opening polymerizations (anionic (AROP) and cationic (CROP)). This difficulty originates from the different reactivity of the monomers, which often is a limiting factor for ionic polymerization techniques.[8,9] Therefore, macromolecular conjugation reactions between two polymeric building blocks carrying orthogonal endgroups represent quite an attractive alternative. This strategy is mostly realized *via* the copper catalyzed azide alkyne cycloaddition (CuAAC) click reaction introduced by Sharpless.[10,11] *Via* this approach a large number of linear block copolymers[12–18] and different polymeric architectures[19–22] have been reported.[23,24] Besides this particular example, also other conjugation reactions are described in the literature,[17] *e.g.* Diels–Alder reactions,[25,26] or thiol–ene chemistry,[27,28] the latter typically showing some reactivity-related limitations.[29]

One intriguing feature of block copolymers is that by the covalent linkage of at least two unlike segments macroscopic phase separation is prevented whilst the incompatibility of most building blocks leads to microphase segregation in various environments.[30] Depending on the weight fractions of the constituting blocks, different morphologies like lamellae, cylinders, or gyroidal structures have been reported.[31,32] These defined morphologies in the bulk featuring periodicities of typically 10–100 nm are of use in different fields of nanotechnology,[33–37] or for the formation of micellar structures *via* transfer into selective solvents for one of the blocks.[38,39] In the latter case especially amphiphilic block copolymers have been in the focus over the past decades.[40] In some cases, the assembly of these structures into superstructures is also termed "supramolecular polymerization". Here, the principle of polymerization is taken to a higher level by using supramolecular units with functional groups as "monomers".[8,41,42]

Regarding "supramolecular polymerization" one of the most fascinating recent examples is the "living crystallization-driven supramolecular polymerization" of organometallic block copolymers.[36,43–47] In this case, it was possible to control the self-assembly of, *e.g.*, semi-crystalline poly(ferrocenyl-

[a]*Laboratory of Organic and Macromolecular Chemistry, Friedrich Schiller University Jena, Humboldtstr. 10, 07743 Jena, Germany. E-mail: felix.schacher@uni-jena.de*
[b]*Jena Center for Soft Matter (JCSM), Friedrich Schiller University Jena, Philosophenweg 7, 07743 Jena, Germany*
[c]*School of Chemistry, University of Bristol, Bristol BS8 1TS, UK*
†Electronic supplementary information (ESI) available. See DOI: 10.1039/c4py01512f

silane)s (PFSs) as core forming blocks in selective solvents. The resulting structures, often anisotropic platelet- or rod-like morphologies, were stabilized by different soluble corona-forming blocks. Further, the length of these core-crystalline micelles can be tuned by sonication, and the use of pre-formed seed micelles for epitaxial growth of semi-crystalline poly(ferrocenylgermane)-containing block copolymers was demonstrated.[43] This "living polymerization" can be regarded as a supramolecular analogue to classical living polymerization techniques and was investigated by transmission electron microscopy (TEM), wide angle X-ray scattering (WAXS) and static light scattering (SLS).[43]

While there are quite a few studies on crystalline-coil block copolymers, double crystalline materials comprising two semi-crystalline blocks have been less frequently reported.[48] One possibility is the combination of PFS with poly(2-alkyl-2-oxazolines) (POx), which have been shown to crystallize depending on the side-chain substitution pattern.[49] Well-defined PFS materials are typically prepared *via* AROP,[50] while POx are synthesized *via* CROP.[51] POx, especially poly(2-ethyl-2-oxazoline) (PEtOx), is water-soluble, non-toxic, and the pseudo-peptide character of this material has been shown to induce similar "stealth"-behavior as observed for poly(ethylene oxide) (PEO).[52–56] Linear poly(2-ethyl-2-oxazoline) (PEtOx) and poly(2-iso-propyl-2-oxazoline) (P*i*PrOx) exhibit different lower critical solution temperatures (LCST), depending on the molecular weight of the material investigated.[57] In case of P*i*PrOx the crystallization at elevated temperatures in water has also been reported.[58–60]

Herein, we demonstrate the synthesis of chain-end functionalized poly(ferrocenyldimethylsilane) (PFDMS) and POx of different molar mass and the subsequent macromolecular conjugation *via* CuAAC click reactions into poly(ferrocenyldimethylsilane)-*block*-poly(2-alkyl-2-oxazoline) (PFDMS-*b*-POx) block copolymers with different weight fractions. After characterization of the obtained organometallic block copolymers *via* size exclusion chromatography (SEC), nuclear magnetic resonance (NMR), Fourier-transform infra-red spectroscopy (FT-IR), and X-ray scattering, the solution behavior in acetone as a selective solvent for the POx block was investigated. In that way, micellar structures featuring a solvophobic PFDMS core and a POx corona are formed. As POx segment, both poly(2-ethyl-2-oxazoline) (PEtOx) and poly(2-*iso*-propyl-2-oxazoline) (P*i*PrOx) were used. Depending on the weight fraction of the organometallic PFDMS segment, different morphologies such as sheets, rods, and vesicular structures were found. For selected examples, we also compared these findings to the bulk morphology with regard to the observed domain size.

Materials and instruments

Instruments

NMR. Proton nuclear magnetic resonance (^{1}H-NMR) spectra were recorded in $CDCl_3$ and toluene-d_8 on a Bruker AC 300 MHz spectrometer at 298 K. Chemical shifts are given in parts per million (ppm, δ scale) relative to the residual signal of the deuterated solvent.

SEC. Size exclusion chromatography was measured on a Shimadzu system equipped with a SCL-10A system controller, a LC-10AD pump, and a RID-10A refractive index detector using a solvent mixture containing chloroform, triethylamine, and iso-propanol (94 : 4 : 2) at a flow rate of 1 mL min^{-1} on a PSS SDV linear M 5 μm column. The system was calibrated using PS (100 to 100 000 g mol^{-1}) and PEO (440 to 44 700 g mol^{-1}) standards.

MALDI-ToF MS. Matrix-assisted laser desorption/ionization time of flight mass spectrometry was performed on an Ultraflex III TOF/TOF (Bruker Daltonics, Bremen, Germany), equipped with a Nd:YAG laser and with *trans*-2-[3-(4-*tert*-butylphenyl)-2-methyl-2-propenylidene] malononitrile (DCTB) as matrix and NaCl as doping agent in reflector and linear mode. The instrument was calibrated prior to each measurement with an external PMMA standard from PSS Polymer Standards Services GmbH (Mainz, Germany).

FT-IR Infra-red spectroscopy. Dry powders of the block copolymers were directly placed on the crystal of the ATR-FTIR (Affinity-1 FTIR, Shimadzu) for measurements in the range of 4000 to 600 cm^{-1}.

Microwave-assisted reactions: The described synthetic steps were carried out using an Initiator Sixty single-mode microwave synthesizer from Biotage, equipped with a non-invasive IR sensor (accuracy: 2%). Microwave vials (conical, 0.5 to 2 mL) were heated at 110 °C overnight, and allowed to cool to room temperature under nitrogen atmosphere. All polymerizations were carried out using temperature control.

Transmission electron microscopy (TEM). The formed aggregates were analyzed using a TEM (Zeiss-CEM 902A, Oberkochen, Germany) operated at 80 kV. Images were recorded using a 1k TVIPS FastScan CCD camera. TEM samples were prepared by applying a drop of an aqueous sample solution onto the surface of a carbon coated copper grid (in case of aqueous solutions plasma treated grids were used) (Quantifoil Micro-Tools GmbH, Jena, Germany).

Wide and small angle X-ray scattering (WAXS and SAXS). Measurements on dried powders of the polymers were performed on a Bruker AXS Nanostar (Bruker, Karlsruhe, Germany), equipped with a microfocus X-ray source (Incoatec ImSCu E025, Incoatec, Geesthacht, Germany), operating at λ = 1.54 Å. A pinhole setup with 750 mm, 400 mm, and 1000 mm (in the order from source to sample) was used and the sample-to-detector distance was 107 cm (SAXS) and 12 cm (WAXS). Samples were mounted on a metal rack and fixed using tape. The scattering patterns were corrected for the beam stop and the background (Scotch tape) prior to evaluations.

Atomic force microscopy (AFM). For AFM analysis diluted solutions were dropcasted on silicon which was beforehand cleaned with Argon-Plasma. The AFM imaging was performed with a Solver LS scanning probe microscope (NT-MDT, Moscow, Russia) in semi-contact mode utilizing NSC35 cantilevers (μ-masch). Gwyddion was applied for image processing and analysis.

DLS. Dynamic light scattering was performed at a scattering angle of 90° on an ALV CGS-3 instrument and a He–Ne laser operating at a wavelength of 633 nm at 25 °C. The CONTIN algorithm was applied to analyze the obtained correlation functions. For temperature control the DLS is equipped with a Lauda thermostat. Apparent hydrodynamic radii were calculated according to the Stokes–Einstein equation. All CONTIN plots shown are intensity-weighted.

Materials

Dimethylsila[1]ferrocenophane was synthesized according to literature procedures and stored in a glovebox.[61] THF was distilled and for the polymerization of dimethylsilaferrocenophane further purified *via* titration with *sec*-BuLi prior to usage. 1,1-diphenylethylene (DPE), and 1,1-dimethylsiletane from Aldrich were distilled prior to use. Propargyl *p*-toluenesulfonate, 2-ethyl-2-oazoline (EtOx) and 2-iso-propyl-2-oxazoline (iPrOx) were distilled over barium oxide and stored under argon. Tetrahydrofuran (THF), acetonitrile (ACN) and dichloromethane (DCM) were purified using a Solvent Purification System (SPS, Innovative Technology, PM-400-3-MD) equipped with two activated alumina columns. Copper bromide (CuBr), *N*,*N*,*N*′,*N*″,*N*″-Pentamethyldiethylenetriamine (PMDETA), *n*-butyllithium (*n*-BuLi) (1.6 M in hexanes) and *sec*-butyllithium (*sec*-BuLi) (1.4 M in cyclohexane), trichloromethylsilane, trimethylsilyl azide, 1,3-dibromopropane, tetrabutylammonium fluoride (TBAF; 1.0 M in THF) were purchased from Aldrich and used as received.

Anionic ring-opening polymerization of ferrocenyldimethylsilane obtaining azide-modified poly(ferrocenyldimethylsilane) ($PFDMS_x$-N_3)[62]

500 mg dimethylsilaferrocenophane (2.1 mmol) were dissolved in 2.5 mL distilled tetrahydrofuran (THF). *n*-Butyllithium (*n*-BuLi) was added under vigorous stirring. After 1 hour at room temperature, diphenylethylene (4 equiv.) and dimethylsiletane (2 equiv.) were added to the reaction mixture. Meanwhile, 1,3-dibromopropane (20 equiv.) was dissolved in 1 mL THF and cooled to −80 °C. After 15 min a color change from orange to deep red was observed for the polymer solution and it was added to the 1,3-dibromopropane solution under vigorous stirring. The solution was allowed to stir for 3 hours at −80 °C, afterwards was allowed to get to room temperature and was stirred for another 3 hours at room temperature. All steps were performed under inert conditions in a glove box. Afterwards the reaction mixture was removed from the glove box and precipitated into methanol three times and dried under vacuum at 50 °C overnight.

The purified brominated poly(ferrocenyldimethylsilane) was dissolved in THF and stirred together with trimethylsilyl azide (TMS-N_3; 10 eq.) and tetrabutylammonium fluoride (TBAF; 10 eq.) overnight. Afterwards, the polymer was precipitated in methanol, filtered and dried under vacuum at 50 °C.

***$PFDMS_{30}$-N_3*:** SEC ($CHCl_3$/*i*-PrOH/TEA) (PS-calib.): M_n = 7000 g mol^{-1}; PDI 1.08; ***$PFDMS_{80}$-N_3*:** SEC ($CHCl_3$/*i*-PrOH/TEA): M_n = 30 000 g mol^{-1}; PDI 1.06; ***^{1}H NMR*:** (300 MHz, toluene, δ): 4.23 (bs, Cp–H), 4.06 (bs, Cp–H), 0.52 (bs, Si–(CH_3)$_2$) ppm.

Synthesis of alkyne-modified poly(2-*iso*-propyl-2-oxazoline) (TB-P*i*PrOx_y)[63]

Propargyl *p*-toluenesulfonate and 2-iso-propyl-2-oxazoline (iPrOx) were dissolved in acetonitrile at different monomer to initiator ratios ([M]/[I] = 20, 25, and 75) and a monomer concentration of 4M. The capped vials were placed in a microwave synthesizer at 140 °C. The polymer was terminated *via* the addition of water and the final polymer was obtained after extraction with $NaHCO_3$ solution, brine, dried over sodium sulfate and the solvent was removed under vacuum.

***TB-PiPrOx_{24}*:** SEC ($CHCl_3$/*i*-PrOH/TEA) (PS-calib.): M_n = 3100 g mol^{-1}; PDI 1.09; MALDI-TOF-MS: M_p = 2800 g mol^{-1}; ***TB-PiPrOx_{75}*:** SEC ($CHCl_3$/*i*-PrOH/TEA): M_n = 8800 g mol^{-1}; PDI 1.07; **^{1}H NMR** (300 MHz, $CDCl_3$, δ): 3.6–3.2 (br, –N–CH_2–CH_2–), 2.5–2.2 (br, CO–C*H*–(CH_3)$_2$), 1.2–0.9 (br, CO–CH–(CH_3)$_2$) ppm.

Synthesis of alkyne-functionalized poly(2-ethyl-2-oxazoline)s (TB-PEtOx_y)

Propargyl *p*-toluenesulfonate and 2-ethyl-2-oxazoline (EtOx) were dissolved in acetonitrile (ACN) at different monomer to initiator ratios ([M]/[I] = 20 and 80) at a monomer concentration of 4 M. The capped vials were placed in a microwave synthesizer at 140 °C. The polymerization was terminated *via* the addition of water. The polymers were obtained after extraction with $NaHCO_3$ solution, brine, and dried under vacuum. After precipitation in cold diethyl ether the polymer was filtered and dried under vacuum.

***TB-PEtOx_{20}*:** SEC ($CHCl_3$/*i*-PrOH/TEA) (PS-calib.): M_n = 3000 g mol^{-1}; PDI 1.11; MALDI-TOF-MS: M_p = 1900 g mol^{-1}; ***TB-PEtOx_{80}*:** SEC ($CHCl_3$/*i*-PrOH/TEA): M_n = 8000 g mol^{-1}; PDI 1.12; MALDI-TOF-MS: M_p = 7900 g mol^{-1}; **^{1}H NMR** (300 MHz, $CDCl_3$, δ): 3.6–3.2 (br, –N–CH_2–CH_2–), 2.5–2.2 (br, CO–CH_2–CH_3), 1.2–0.9 (br, CO–CH_2–CH_3) ppm.

Exemplarily CuAAC click-reaction between $PFDMS_x$-N_3 and TB-POx_y

For the click reaction the alkyne functionalized POx (TB-P*i*PrOx_y; 2 eq.) and the azide functionalized PFDMS ($PFDMS_x$-N_3; 1 eq.) were dissolved in a solvent mixture of THF and ethanol until a clear solution was observed (PFDMS/POx (wt%) – THF–EtOH (v/v): 90/10-3/1; 75/25-2/1; 50/50-1/1) and purged for 5 minutes with argon. Copper bromide (CuBr) and PMDETA (1.1 eq.) were added under argon flux, and the solution was purged with argon for additional 5 minutes. Afterwards the solution was placed in the microwave synthesizer and heated to 80 °C for 15 minutes.

The polymer solution was passed through a short AlOxN column to remove any copper from the reaction mixture. The block copolymer was precipitated from DCM into acetone, centrifuged on the next day (5000 rpm, 1 min), and the supernatant solution was removed. The orange precipitate was dried under vacuum. Even for the sample with lowest molar mass,

the triazole signal of the resulting block copolymers could not be observed in NMR.

SEC ($CHCl_3$/*i*-PrOH/TEA) (PS-calib.): **$PFDMS_{80}$-*b*-$PEtOx_{20}$:** M_n = 33 000 g mol^{-1}; PDI 1.09; **$PFDMS_{80}$-*b*-$PEtOx_{80}$:** M_n = 39 000 g mol^{-1}; PDI 1.09; **$PFDMS_{30}$-*b*-$PEtOx_{80}$:** M_n = 17 000 g mol^{-1}; PDI 1.12; **$PFDMS_{80}$-*b*-P*i*$PrOx_{24}$:** M_n = 32 000 g mol^{-1}; PDI 1.10; **$PFDMS_{30}$-*b*-P*i*$PrOx_{24}$:** M_n = 10 000 g mol^{-1}; PDI 1.09; **$PFDMS_{80}$-*b*-P*i*$PrOx_{75}$:** M_n = 38 000 g mol^{-1}; PDI 1.06; **$PFDMS_{30}$-*b*-P*i*$PrOx_{75}$:** M_n = 15 000 g mol^{-1}; PDI 1.22; **^{1}H-NMR:** (300 MHz, $CDCl_3$, δ): 4.3–4.1 (bs, Cp-H), 4.1–3.9 (Cp-H), 3.6–3.2 (br, –N–CH_2–CH_2–), 2.5–2.2 (br, CO–CH_2–CH_3), 1.2–0.9 (br, CO–CH_2–CH_3), 0.5–0.4 (Si–$(CH_3)_2$) ppm.

Transfer of the block copolymers into selective solvents

5 mg of the block copolymer were dissolved in 1 mL DCM and added under vigorous stirring into 5 mL acetone. The solution was stirred overnight to evaporate the DCM from the solution while acetone was added subsequently to maintain a constant concentration (1 mg mL^{-1}). For further investigations (DLS, TEM) the solution was diluted to a concentration of 0.5 mg mL^{-1}.

Results and discussion

We were interested in the solution behavior of poly(ferrocenyldimethylsilane)-*block*-poly(2-alkyl-2-oxazoline) (PFDMS-*b*-POx) diblock copolymers for two reasons: first, suitable POx materials are soluble in water and enable the later formation of amphiphilic core-crystalline micelles and, second, the use of poly(2-*iso*-propyl-2-oxazoline) as building block leads to double crystalline block copolymers. Earlier studies on double crystalline amphiphiles are described in the literature, but are limited to PEO-*b*-PFDMS,[64,65] while other amphiphiles were not double crystalline, *e.g.* PFS-*b*-PDMAEMA.[8,15] We therefore focused on two POx segments, poly(2-ethyl-2-oxazoline) (PEtOx) and poly(2-*iso*-propyl-2-oxazoline) (P*i*PrOx), and synthesized the corresponding PFDMS-*b*-POx diblock copolymers with different compositions. For the synthesis we used copper-catalyzed azide–alkyne cycloaddition (CuAAC) reactions, by which the weight fractions of the PFDMS and the POx segment can be easily varied.

Block copolymer synthesis

First, dimethylsilaferrocenophane (FDMS) was polymerized *via* anionic ring-opening polymerization (AROP) initiated with *n*-butyllithium at two different monomer to initiator concentrations ([M]/[I]) in THF at room temperature under inert conditions. The polymerization was terminated *via* 1,3-dibromopropane and the exchange of the bromide moiety with an azide functionality was carried out as described in the literature (Fig. S1†).[62] Two $PFDMS_x$-N_3 samples with molar masses of 7000 g mol^{-1} and 20 000 g mol^{-1} and low dispersity indices ($Đ$ < 1.1) were obtained and characterized *via* SEC, NMR and FT-IR (Table 1; Fig. S2†). The degree of polymerization (DP) for these polymers was determined *via* NMR, confirming the formation of $PFDMS_{30}$-N_3 and $PFDMS_{80}$-N_3, where the subscripts denote the degrees of polymerization (DP). *Via* SEC a small amount of coupling product at lower elution volume was observed, which is due to chain–chain coupling during the functionalization step with 1,5-dibromopentane. For alkyne functionalized POx (TB-PEtOx and TB-P*i*PrOx, Fig. S3†), the respective monomer was polymerized *via* microwave-assisted cationic ring-opening polymerization (CROP) and molar masses of 2000, 2400, and 8000 g mol^{-1} were synthesized in both cases. Therefore, solutions containing a functional initiator, propargyl *p*-toluenesulfonate, with different monomer-to-initiator ratios ([M]/[I]) at a constant monomer concentration of 4M were prepared and polymerized in a microwave-synthesizer at 140 °C. The DP obtained *via* NMR and MALDI-TOF MS for PEtOx were DP 20 (TB-$PEtOx_{20}$), and 80 (TB-$PEtOx_{80}$), while for P*i*PrOx DPs of 20 (TB-P*i*$PrOx_{20}$), 24 (TB-P*i*$PrOx_{24}$), and 75 (TB-P*i*$PrOx_{75}$) were found (Table 1, SEC in Fig. S4†).

Table 1 Details for different obtained homo- and block copolymers of $PFDMS_x$-N_3 and TB-POx_y

Polymer	Ratio PFDMS/POx[a] [wt%]	M_n[a] [g mol^{-1}]	M_n[b] [g mol^{-1}]	$Đ$[b]	M_p[c] [g mol^{-1}]	
$PFDMS_{30}$-N_3[d]	—	7300	7300	1.08	7500[e]	Homopolymers
$PFDMS_{80}$-N_3[d]	—	20 000	29 000	1.06	—	
TB-$PEtOx_{20}$[d]	—	2000	3000	1.11	1900	
TB-$PEtOx_{80}$[d]	—	8000	9500	1.09	7900	
TB-P*i*$PrOx_{20}$[d]	—	2300	2400	1.12	2300	
TB-P*i*$PrOx_{24}$[d]	—	2800	3000	1.10	2900	
TB-P*i*$PrOx_{75}$[d]	—	8600	8000	1.08	8800	
$PFDMS_{80}$-*b*-P*i*$PrOx_{24}$[d]	88/12	23 000	32 000	1.10	—	Block copolymers
$PFDMS_{30}$-*b*-P*i*$PrOx_{24}$[d]	75/25	10 000	10 000	1.09	—	
$PFDMS_{80}$-*b*-P*i*$PrOx_{75}$[d]	70/30	29 000	38 000	1.06	—	
$PFDMS_{30}$-*b*-P*i*$PrOx_{75}$[d]	46/54	16 000	15 000	1.22	—	
$PFDMS_{80}$-*b*-$PEtOx_{20}$[d]	92/8	22 000	33 000	1.09	—	
$PFDMS_{80}$-*b*-$PEtOx_{80}$[d]	71/29	28 000	39 000	1.09	—	
$PFDMS_{30}$-*b*-$PEtOx_{80}$[d]	47/53	16 000	17 000	1.12	—	

[a] Calculated according to the constituting building blocks. [b] SEC ($CHCl_3$/TEA/*i*-PrOH) PS-calibration. [c] MALDI-TOF MS (DCTB/NaCl). [d] Subscripts denote the degree of polymerization for the corresponding block. [e] MALDI-ToF MS (dithranol).

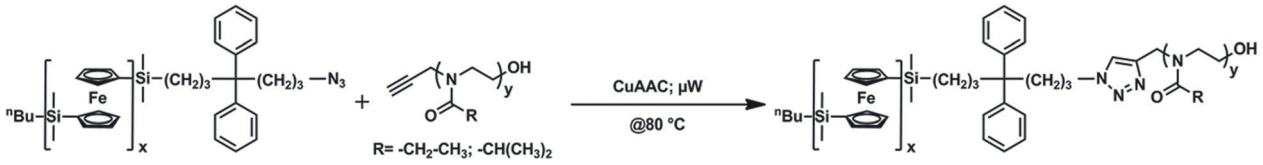

Scheme 1 Synthesis of $PFDMS_x$-*b*-POx_y block copolymers *via* CuAAC click chemistry between $PFDMS_x$-N_3 and TB-POx_y.

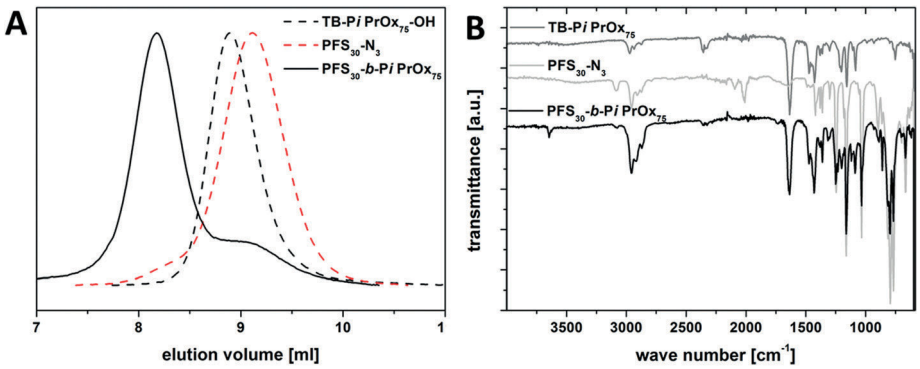

Fig. 1 Comparison of elugrams of PFDMS-N_3 (dashed red line), TB-P*i*PrOx$_{75}$ (dashed black line) and $PFDMS_{30}$-*b*-P*i*PrOx$_{75}$ (solid black line), (B) FT-IR of PFDMS-N_3 (light grey line), TB-P*i*PrOx$_{75}$ (dark grey line) and $PFDMS_{30}$-*b*-P*i*PrOx$_{75}$ (black line) (C).

As the next step, different combinations of $PFDMS_x$-N_3 and TB-POx_y were used in copper catalyzed alkyne azide cycloaddition (CuAAC) click reactions to yield amphiphilic diblock copolymers (Scheme 1). Typically, TB-POx_y was used in excess (2 eq.) in comparison to the azide-functionality of $PFDMS_x$-N_3 in the presence of copper(I) bromide (CuBr) and *N*,*N*′,*N*′,*N*″-pentamethyldiethylenetriamine (PMDETA) to ensure full conversion of the PFDMS building block. A series of different compositions was obtained *via* this approach (Table 1; Fig. 1 and S5†).

The resulting block copolymers were purified *via* transfer into a selective solvent for the POx block (acetone). Thereby, aggregation into micellar structures with a PFDMS core and a POx corona occurs, followed by centrifugation. In that way, unreacted TB-POx_y can be removed by decanting the supernatant solution afterwards. These block copolymers were characterized *via* SEC, FT-IR, and the composition was determined using NMR. Except for one composition, the excess TB-POx_y homopolymer could be completely removed. However, in case of $PFDMS_{30}$-*b*-P*i*PrOx$_{75}$ (Fig. 1A) a shoulder was observed in the corresponding SEC traces, which can be ascribed to remaining P*i*PrOx$_{75}$ polymer chains. For all other block copolymers a clear shift of the SEC trace to lower elution volume in comparison to the corresponding homopolymers is observed and a complete disappearance of the individual building blocks (Fig. S5†). Table 1 summarizes the molar masses and the corresponding weight fractions (wt%) of all obtained block copolymers.

To be able to study a wide compositional range, weight ratios from 92/8 to 47/53 for PFDMS-*b*-PEtOx and 88/12 to 46/54 for PFDMS-*b*-P*i*PrOx were prepared. By this, the PFDMS content changes from the majority phase ($PFDMS_{80}$-*b*-PEtOx$_{20}$ and $PFDMS_{80}$-*b*-P*i*PrOx$_{24}$) to values slightly below 50% ($PFDMS_{30}$-*b*-PEtOx$_{80}$ and $PFDMS_{30}$-*b*-P*i*PrOx$_{75}$). The molar masses of the different block copolymers vary from 10 000 to 30 000 g mol^{-1}. Furthermore, two PFDMS-*b*-P*i*PrOx block copolymers with almost similar weight fractions but different molar mass (10 000 g mol^{-1} ($PFDMS_{30}$-*b*-P*i*PrOx$_{24}$, 75/25) and 30 000 g mol^{-1} $PFDMS_{80}$-*b*-P*i*PrOx$_{75}$, 70/30) were synthesized to investigate the influence of the molar mass on the self-assembly in the bulk and in solution.

Self-assembly in the bulk

For initial bulk studies, we decided to focus on potentially double crystalline block copolymers, $PFDMS_x$-*b*-P*i*PrOx$_y$. The corresponding materials were investigated *via* X-ray scattering. Therefore, the block copolymers were dissolved in a non-selective solvent, in this case dichloromethane, and drop-casted for small-angle X-ray scattering (SAXS) studies at room temperature. In Fig. 2A the SAXS pattern of $PFDMS_{30}$-*b*-P*i*PrOx$_{75}$ (50/50 wt%) and $PFDMS_{30}$-*b*-P*i*PrOx$_{24}$ (75/25 wt%) is depicted. The lamellar morphology was confirmed for $PFDMS_{30}$-*b*-P*i*PrOx$_{75}$ and the characteristic peaks for such structural motifs at integer multiples of the first order peak are visible. The relative reflex positions 1 : 2 are related to the [100] : [200] reflections. From the SAXS measurements, the long period was calculated to d_{LAM} = 19 nm (with Θ = 0.46° for [100]) and is in good agreement with the results obtained from TEM micrographs of thin-film cuts prepared with an ultramicrotome after embedding in an epoxy resin (d_{LAM}, TEM = 20 nm; Fig. 2B). In case of TEM, the rather poor ordering can be partially ascribed to the sample preparation procedure. In case of the 75/25 wt%

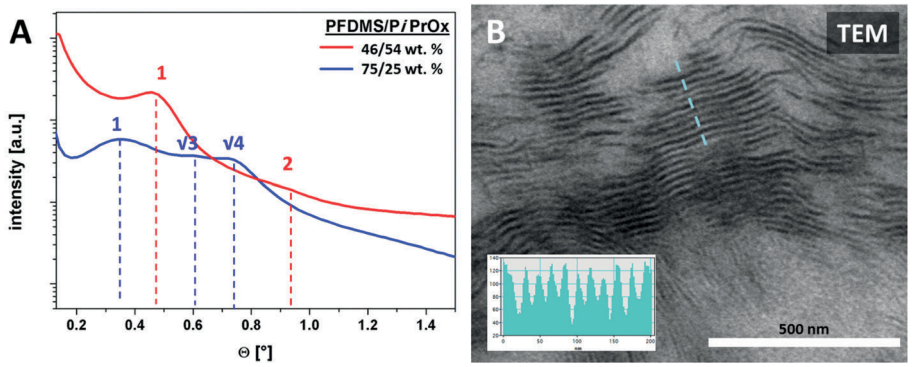

Fig. 2 (A) Comparison of SAXS data for PFDMS$_x$-*b*-P*i*PrOx$_y$ block copolymers with different compositions (wt%): 46/54 (PFDMS$_{30}$-*b*-P*i*PrOx$_{75}$; red curve), 75/25 (PFDMS$_{30}$-*b*-P*i*PrOx$_{24}$; blue curve); (B) TEM micrograph of a thin-film cut of PFDMS$_{30}$-*b*-P*i*PrOx$_{75}$.

ratio of PFDMS/P*i*PrOx, the resulting pattern leads us to the assumption of hexagonally packed cylinders of PFDMS as reflex positions of $1:\sqrt{3}:\sqrt{4}$ correspond to the $[100]:[110]:[200]$ reflections. In case of 88/12 and 70/30 wt% of PFDMS/P*i*PrOx, the corresponding X-ray patterns unfortunately showed distinctly lower signal intensity in comparison to PFDMS$_{30}$-*b*-P*i*PrOx$_{75}$ and prevented an unambiguous morphology assignment (Fig. S6†).

We were further interested in whether films from PFDMS$_{30}$-*b*-P*i*PrOx$_{75}$ (highest content of P*i*PrOx with 54 wt%) are indeed double crystalline. Wide-angle X-ray scattering (WAXS) studies show the characteristic reflections for PFDMS already at room temperature.[47] The corresponding reflections for P*i*PrOx, at ~8° and 21° get more prominent during annealing at 100 °C for 2 h (Fig. S9†), while the signals for PFDMS remain constant.[66,67]

Self-assembly in selective solvents for PEtOx and P*i*PrOx

The PFDMS$_x$-*b*-PEtOx$_y$ and PFDMS$_x$-*b*-P*i*PrOx$_y$ block copolymers of different composition (Table 1) were now investigated regarding their solution behavior in a selective solvent for the POx segment. Therefore, the materials were first dissolved in a non-selective solvent for both blocks, dichloromethane (DCM, 5 mg mL^{-1}) and added dropwise into acetone (5 mL), a selective solvent for POx, under vigorous stirring. All solutions were allowed to stir over night at RT and, during that time, considerably increased in turbidity. Eventually evaporated acetone was replaced the next day and samples for TEM were prepared by drop-casting (Fig. 3). Under these conditions, the PFDMS segment is expected to form the (crystalline) micellar core and the respective POx block serves as corona and provides solubility in acetone. We have shown earlier that micelles of PFDMS-containing block copolymer exhibit crystalline cores in acetone.[47]

For the materials showing the highest weight fractions of PFDMS, PFDMS$_{80}$-*b*-PEtOx$_{20}$ (92/8 wt%) and PFDMS$_{80}$-*b*-P*i*PrOx$_{24}$ (88/12 wt%), the formation of sheet-like aggregates with a PFDMS core and rather short POx corona chains can be expected.[68] Indeed, this morphology can be found for both PFDMS-*b*-POx systems (Fig. 3A and 3B), where sheets with a length of several μm are shown. The obtained structures show several size distributions in dynamic light scattering experiments (DLS; Fig. S7†) and the aggregates start to settle/precipitate if the solutions are not continuously agitated. Investigations *via* atomic force microscopy (AFM), confirmed the presence of sheets with 15–30 nm in height (Fig. S8†), lengths up to several μm and widths of more than 100 nm.

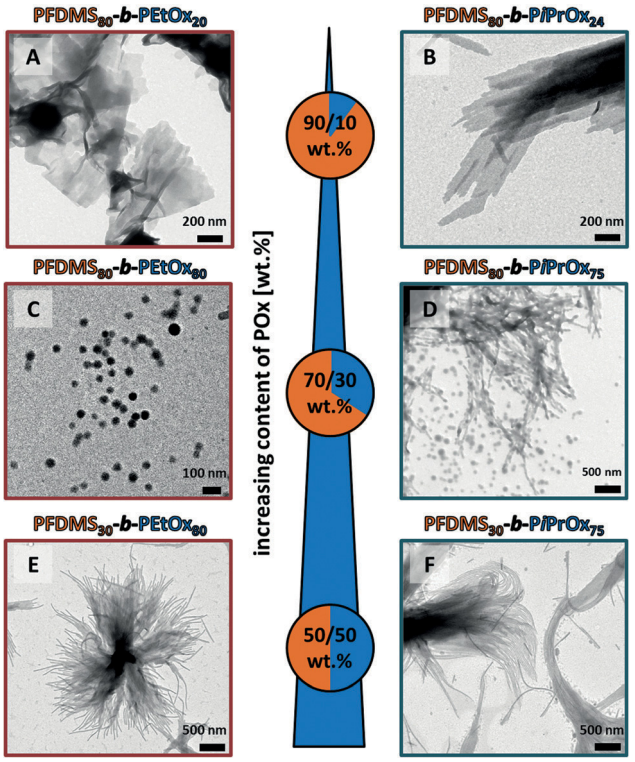

Fig. 3 TEM micrographs for block copolymers with different ratios of PFDMS and POx in acetone (0.5 mg mL^{-1}), forming: sheet-like structures for PFDMS$_{80}$-*b*-PEtOx$_{20}$ (92/8 wt%; (A), PFDMS$_{80}$-*b*-P*i*PrOx$_{24}$ (88/12 wt%; (B); vesicular morphologies for PFDMS$_{80}$-*b*-PEtOx$_{80}$ (71/29 wt%; (C), PFDMS$_{80}$-*b*-P*i*PrOx$_{75}$ (70/30 wt%; (D); rodlike structures for PFDMS$_{30}$-*b*-PEtOx$_{80}$ (47/53 wt%; (E), PFDMS$_{30}$-*b*-P*i*PrOx$_{75}$ (46/54 wt%; (F).

The theory of small amphiphilic molecules can, to certain extend, as well applied to block copolymers, explaining the

transition from sheets to vesicles (bending).[68–72] This can be seen for PFDMS$_{80}$-*b*-P*i*PrOx$_{75}$ (75/25 wt%, Fig. 3C) and PFDMS$_{80}$-*b*-PEtOx$_{80}$ (71/29 wt%, Fig. 3D). In both cases, radii of roughly 50 nm were found in DLS experiments (Fig. S7†), and spherical aggregates with diameters between 50–100 nm were found in TEM, both methods being in good agreement. According to our experience with star-shaped PEO-*b*-PFDMS block copolymers with comparable weight fractions of PFDMS, we hypothesized that these structures represent vesicles with a PFDMS membrane wall.[65,73] As can be seen for PFDMS$_{80}$-*b*-P*i*PrOx$_{75}$, these aggregates start to form anisotropic superstructures by fusion of several individual particles, which has also been found in our earlier studies when using THF–EtOH mixtures. Here, vesicles with a size of 100 to 200 nm and tubular superstructures thereof were observed.[65,73] The superstructures found here are likely to be formed by the fusion of several spherical aggregates and coexist with a small fraction of sheets and spheres (~10 nm) as found *via* TEM. This did not occur in case of PFDMS$_{80}$-*b*-PEtOx$_{80}$, which at the moment we attribute to slight differences in composition. We further tried to verify our assumption of vesicles being formed by static light scattering. Unfortunately, the structures start to agglomerate and precipitate within minutes, if the solutions are not constantly agitated. This could be observed even at concentrations below 0.07 mg mL^{-1}. AFM studies (not shown) also only indicated the presence of spherical objects. At this point, we cannot provide a definite proof for a vesicular morphology and the spherical objects identified could also represent large compound micelles. The formation of core-corona structures with a PFDMS core and a P*i*PrOx corona is doubtful as the particle diameter with 50–100 nm is rather large if the molecular weight of the involved unimers is considered. Nevertheless, earlier experience and the fact that fusion towards anisotropic superstructures can be observed hints towards the formation of vesicles.

For materials featuring a roughly symmetric composition (~50/50 wt%), rod-like morphologies with a length of several μm and a width of ~20 nm, which is also comparable to the widths of the corresponding lamellae in the bulk state (Fig. 2A), are observed for PFDMS$_{30}$-*b*-PEtOx$_{80}$ (47/53 wt%, Fig. 3E) and PFDMS$_{30}$-*b*-P*i*PrOx$_{75}$, respectively (46/54 wt%, Fig. 3F). Beside the formation of rods, also agglomerates of rods are observed, which can be explained by the drying process.

Via variation of the weight fractions within PFDMS-*b*-POx block copolymers a wide range of morphologies (sheets, vesicles, cylinders) can be accessed in acetone as selective solvent. This can be explained by the different spatial demand of the POx chains of different length in the corona of the aggregates, increasing the curvature of the PFDMS core of the structures.

Another interesting aspect is whether the molar mass of the block copolymer, in addition to the weight fraction, influences the aggregation behavior in acetone. For this, we specifically chose the material where, initially, spherical building blocks are formed, followed by further aggregation into anisotropic superstructures (*cf.* Fig. 3D). Two PFDMS$_x$-*b*-P*i*PrOx$_y$ diblock copolymers with comparable weight fractions but different molar masses were synthesized: PFDMS$_{30}$-*b*-P*i*PrOx$_{24}$ (75/25 wt%, $M_{n,\,theo}$ 10 500 g mol^{-1}) and PDFMS$_{80}$-*b*-P*i*PrOx$_{75}$ (70/30 wt%, $M_{n,\,theo}$ 29 000 g mol^{-1}), both showing monomodal size distributions in SEC experiments. Both materials were dissolved in DCM and transferred to acetone. In both cases, spherical particles reminiscent of vesicles with sizes of 50–100 nm in diameter can be found in TEM afterwards, which is in both cases in agreement with the DLS results (Fig. S7;† Fig. 4).

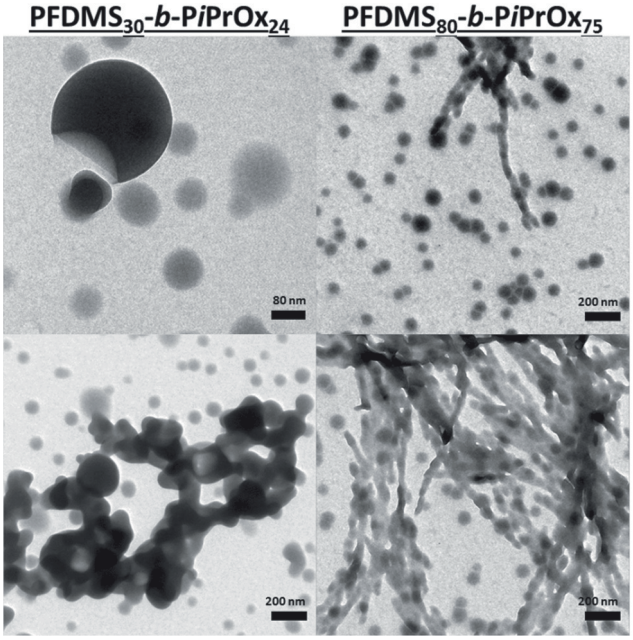

Fig. 4 TEM micrographs for vesicular aggregates of PFDMS$_{30}$-*b*-P*i*PrOx$_{24}$ (75/25 wt%; left row) and PFDMS$_{80}$-*b*-P*i*PrOx$_{75}$ (70/30 wt%; right row) with similar weight fractions in acetone (0.5 mg mL^{-1}).

Conclusion

We described the synthesis of amphiphilic poly(ferrocenyldimethylsilane)-*block*-poly(2-alkyl-2-oxazoline) block copolymers of different composition *via* conjugation reactions between two orthogonally functionalized building blocks. After the successful copper catalyzed azide–alkyne cycloaddition click reaction the purified block copolymers were investigated regarding composition and microphase segregation in the bulk and in acetone as selective solvent for the POx segments. We found that, depending on the weight fraction of the crystallizable PFDMS segments, platelet-like, potentially vesicular, and rod-like aggregates were formed. Regarding further studies, the transfer of PFDMS$_x$-*b*-POx$_y$ systems with a sufficiently high content of POx into aqueous solution and the subsequent temperature-induced crystallization of the POx segment will be investigated.

Acknowledgements

We thank Frank Steiniger and Christine Kämnitz (Electron Microscope Center Jena) for help with the TEM studies, Sarah

Crotty for MALDI-ToF MS measurements, Robert Deubler for performing part of the SAXS measurements, and Stephanie Hoeppener for discussions concerning AFM measurements. The authors would also like to thank Prof. Ian Manners for fruitful discussions and giving T. R. the possibility for joining his group for a few weeks. Jan Schröder is acknowledged for preparing microtome-cut samples for TEM. F. H. S. and T. R. are further grateful to the Thuringian Ministry for Education, Science, and Culture (TMBWK; #B515-10065, ChaPoNano and #B515-11028, SWAXS-JCSM) for financial support. F. H. S. thanks the VCI for a starting independent researcher fellowship and T. R. acknowledges the Carl-Zeiss foundation for a PhD-scholarship. F. H. S. is grateful to Ulrich S. Schubert for continuous support.

References

1 M. A. Tasdelen, M. U. Kahveci and Y. Yagci, *Prog. Polym. Sci.*, 2011, **36**, 455–567.
2 M. Hillmyer, *Curr. Opin. Solid State Mater. Sci.*, 1999, **4**, 559–564.
3 J. Jagur-Grodzinski, *React. Funct. Polym.*, 2001, **49**, 1–54.
4 C. Barner-Kowollik, J.-F. Lutz and S. Perrier, *Polym. Chem.*, 2012, **3**, 1677–1679.
5 J. Feldthusen, B. Ivan and A. H. E. Müller, *Macromolecules*, 1998, **31**, 578–585.
6 T. Higashihara, R. Faust, K. Inoue and A. Hirao, *Macromolecules*, 2008, **41**, 5616–5625.
7 Y. Yagci and M. Atilla Tasdelen, *Prog. Polym. Sci.*, 2006, **31**, 1133–1170.
8 D. A. Rider and I. Manners, *Polym. Rev.*, 2007, **47**, 165–195.
9 O. Nuyken and S. Pask, *Polymers*, 2013, **5**, 361–403.
10 H. C. Kolb, M. G. Finn and K. B. Sharpless, *Angew. Chem., Int. Ed.*, 2001, **40**, 2004–2021.
11 T. Aida, E. W. Meijer and S. I. Stupp, *Science*, 2012, **335**, 813–817.
12 K. Satoh, J. E. Poelma, L. M. Campos, B. Stahl and C. J. Hawker, *Polym. Chem.*, 2012, **3**, 1890–1898.
13 D. Fournier, R. Hoogenboom and U. S. Schubert, *Chem. Soc. Rev.*, 2007, **36**, 1369–1380.
14 K. Kempe, A. Krieg, C. R. Becer and U. S. Schubert, *Chem. Soc. Rev.*, 2012, **41**, 176–191.
15 M. Zhang, P. A. Rupar, C. Feng, K. Lin, D. J. Lunn, A. Oliver, A. Nunns, G. R. Whittell, I. Manners and M. A. Winnik, *Macromolecules*, 2013, **46**, 1296–1304.
16 K. Kempe, K. L. Killops, J. E. Poelma, H. Jung, J. Bang, R. Hoogenboom, H. Tran, C. J. Hawker, U. S. Schubert and L. M. Campos, *ACS Macro Lett.*, 2013, **2**, 677–682.
17 A. S. Goldmann, M. Glassner, A. J. Inglis and C. Barner-Kowollik, *Macromol. Rapid Commun.*, 2013, **34**, 810–849.
18 D. Quemener, T. P. Davis, C. Barner-Kowollik and M. H. Stenzel, *Chem. Commun.*, 2006, 5051–5053.
19 B. V. K. J. Schmidt, T. Rudolph, M. Hetzer, H. Ritter, F. H. Schacher and C. Barner-Kowollik, *Polym. Chem.*, 2012, **3**, 3139–3145.
20 A. Hanisch, H. Schmalz and A. H. E. Müller, *Macromolecules*, 2012, **45**, 8300–8309.
21 T. Rudolph, S. Crotty, M. v. d. Lühe, D. Pretzel, U. S. Schubert and F. H. Schacher, *Polymers*, 2013, **5**, 1081–1101.
22 S. Li, J. Han and C. Gao, *Polym. Chem.*, 2013, **4**, 1774–1787.
23 C. Barner-Kowollik, F. E. Du Prez, P. Espeel, C. J. Hawker, T. Junkers, H. Schlaad and W. Van Camp, *Angew. Chem., Int. Ed.*, 2011, **50**, 60–62.
24 J. A. Johnson, M. G. Finn, J. T. Koberstein and N. J. Turro, *Macromol. Rapid Commun.*, 2008, **29**, 1052–1072.
25 M. Langer, J. Brandt, A. Lederer, A. S. Goldmann, F. H. Schacher and C. Barner-Kowollik, *Polym. Chem.*, 2014, **5**, 5330–5338.
26 H. Durmaz, A. Sanyal, G. Hizal and U. Tunca, *Polym. Chem.*, 2012, **3**, 825–835.
27 P. Espeel, F. Goethals and F. E. Du Prez, *J. Am. Chem. Soc.*, 2011, **133**, 1678–1681.
28 A. B. Lowe, *Polym. Chem.*, 2010, **1**, 17.
29 S. P. S. Koo, M. M. Stamenović, R. A. Prasath, A. J. Inglis, F. E. Du Prez, C. Barner-Kowollik, W. Van Camp and T. Junkers, *J. Polym. Sci., Part A: Polym. Chem.*, 2010, **48**, 1699–1713.
30 T. P. Lodge, *Macromol. Chem. Phys.*, 2003, **204**, 265–273.
31 C. Auschra and R. Stadler, *Macromolecules*, 1993, **26**, 2171–2174.
32 F. Schacher, J. Yuan, H. G. Schoberth and A. H. E. Müller, *Polymer*, 2010, **51**, 2021–2032.
33 A. S. Abd-El-Aziz and E. A. Strohm, *Polymer*, 2012, **53**, 4879–4921.
34 A. Nunns, J. Gwyther and I. Manners, *Polymer*, 2013, **54**, 1269–1284.
35 C. Park, J. Yoon and E. L. Thomas, *Polymer*, 2003, **44**, 6725–6760.
36 P. A. Rupar, L. Chabanne, M. A. Winnik and I. Manners, *Science*, 2012, **337**, 559–562.
37 F. H. Schacher, P. A. Rupar and I. Manners, *Angew. Chem., Int. Ed.*, 2012, **51**, 7898–7921.
38 Y. Mai and A. Eisenberg, *Chem. Soc. Rev.*, 2012, **41**, 5969–5985.
39 A. Choucair and A. Eisenberg, *Eur. Phys. J. E*, 2003, **10**, 37–44.
40 S. B. Darling, *Prog. Polym. Sci.*, 2007, **32**, 1152–1204.
41 N. Petzetakis, A. P. Dove and R. K. O'Reilly, *Chem. Sci.*, 2011, **2**, 955–960.
42 Z. M. Hudson, C. E. Boott, M. E. Robinson, P. A. Rupar, M. A. Winnik and I. Manners, *Nat. Chem.*, 2014, **6**, 893–898.
43 T. Gädt, N. S. Ieong, G. Cambridge, M. A. Winnik and I. Manners, *Nat. Mater.*, 2009, **8**, 144–150.
44 S. F. Mohd Yusoff, J. B. Gilroy, G. Cambridge, M. A. Winnik and I. Manners, *J. Am. Chem. Soc.*, 2011, **133**, 11220–11230.
45 J. Qian, G. Guerin, Y. Lu, G. Cambridge, I. Manners and M. A. Winnik, *Angew. Chem., Int. Ed.*, 2011, **50**, 1622–1625.
46 I. Korczagin, M. A. Hempenius, R. G. Fokkink, M. A. C. Stuart, M. Al-Hussein, P. H. H. Bomans,

P. M. Frederik and G. J. Vancso, *Macromolecules*, 2006, **39**, 2306–2315.
47 N. McGrath, F. H. Schacher, H. Qiu, S. Mann, M. A. Winnik and I. Manners, *Polym. Chem.*, 2014, **5**, 1923.
48 J. Schmelz, F. H. Schacher and H. Schmalz, *Soft Matter*, 2013, **9**, 2101.
49 K. Kempe, M. Lobert, R. Hoogenboom and U. S. Schubert, *J. Polym. Sci., Part A: Polym. Chem.*, 2009, **47**, 3829–3838.
50 V. Bellas and M. Rehahn, *Angew. Chem., Int. Ed.*, 2007, **46**, 5082–5104.
51 E. Rossegger, V. Schenk and F. Wiesbrock, *Polymers*, 2013, **5**, 956–1011.
52 H. Schlaad, C. Diehl, A. Gress, M. Meyer, A. L. Demirel, Y. Nur and A. Bertin, *Macromol. Rapid Commun.*, 2010, **31**, 511–525.
53 J.-S. Park and K. Kataoka, *Macromolecules*, 2007, **40**, 3599–3609.
54 K. Knop, G. M. Pavlov, T. Rudolph, K. Martin, D. Pretzel, B. O. Jahn, D. H. Scharf, A. A. Brakhage, V. Makarov, U. Mollmann, F. H. Schacher and U. S. Schubert, *Soft Matter*, 2013, **9**, 715–726.
55 K. Knop, R. Hoogenboom, D. Fischer and U. S. Schubert, *Angew. Chem., Int. Ed.*, 2010, **49**, 6288–6308.
56 M. Bauer, C. Lautenschlaeger, K. Kempe, L. Tauhardt, U. S. Schubert and D. Fischer, *Macromol. Biosci.*, 2012, **12**, 986–998.
57 C. Weber, R. Hoogenboom and U. S. Schubert, *Prog. Polym. Sci.*, 2012, **37**, 686–714.
58 N. Atılkan, Y. Nur, J. Hacaloglu and H. Schlaad, *Macromol. Chem. Phys.*, 2012, **213**, 945–951.
59 C. Diehl, I. Dambowsky, R. Hoogenboom and H. Schlaad, *Macromol. Rapid Commun.*, 2011, **32**, 1753–1758.
60 C. Diehl, P. Cernoch, I. Zenke, H. Runge, R. Pitschke, J. Hartmann, B. Tiersch and H. Schlaad, *Soft Matter*, 2010, **6**, 3784–3788.
61 D. A. Rider, K. A. Cavicchi, K. N. Power-Billard, T. P. Russell and I. Manners, *Macromolecules*, 2005, **38**, 6931–6938.
62 A. Nunns, C. A. Ross and I. Manners, *Macromolecules*, 2013, **46**, 2628–2635.
63 M. W. M. Fijten, C. Haensch, B. M. van Lankvelt, R. Hoogenboom and U. S. Schubert, *Macromol. Chem. Phys.*, 2008, **209**, 1887–1895.
64 J. F. Gohy, B. G. Lohmeijer, A. Alexeev, X. S. Wang, I. Manners, M. A. Winnik and U. S. Schubert, *Chemistry*, 2004, **10**, 4315–4323.
65 F. H. Schacher, U. Freier and F. Steiniger, *Soft Matter*, 2012, **8**, 6968–6978.
66 M. Meyer, M. Antonietti and H. Schlaad, *Soft Matter*, 2007, **3**, 430–431.
67 A. L. Demirel, M. Meyer and H. Schlaad, *Angew. Chem., Int. Ed.*, 2007, **46**, 8622–8624.
68 A. Blanazs, S. P. Armes and A. J. Ryan, *Macromol. Rapid Commun.*, 2009, **30**, 267–277.
69 J. N. Israelachvili, in *Intermolecular and Surface Forces*, ed. J. N. Israelachvili, Academic Press, San Diego, 3rd edn, 2011, pp. 503–534.
70 N. S. Cemeron, M. K. Corbierre and A. Eisenberg, *Can. J. Chem.*, 1999, **77**, 1311–1326.
71 T. Smart, H. Lomas, M. Massignani, M. V. Flores-Merino, L. R. Perez and G. Battaglia, *Nano Today*, 2008, **3**, 38–46.
72 J.-H. Ryu, D.-J. Hong and M. Lee, *Chem. Commun.*, 2008, 1043–1054.
73 F. H. Schacher, J. Elbert, S. K. Patra, S. F. Mohd Yusoff, M. A. Winnik and I. Manners, *Chem. – Eur. J.*, 2012, **18**, 517–525.

Electronic Supplementary Material (ESI) for Polymer Chemistry.

Supporting information

Synthesis and Self-Assembly of Poly(ferrocenyldimethylsilane)-*block*-poly(2-alkyl-2-oxazoline) Block Copolymers

Tobias Rudolph,[1,2] Adam Nunns,[3] Almut Schwenke,[1,2] Felix H. Schacher[1,2,*]

[1] Laboratory of Organic and Macromolecular Chemistry, Friedrich Schiller University Jena, Humboldtstr. 10, 07743 Jena, Germany

E-mail: felix.schacher@uni-jena.de

[2] Jena Center for Soft Matter (JCSM), Friedrich Schiller University Jena, Philosophenweg 7, 07743 Jena, Germany

[3] School of Chemistry, University of Bristol, Bristol BS8 1TS, U.K

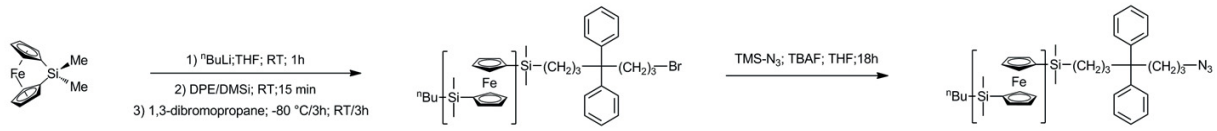

Figure S1: Synthesis of azide-functionalized PFDMS-N_3 of different molar mass.

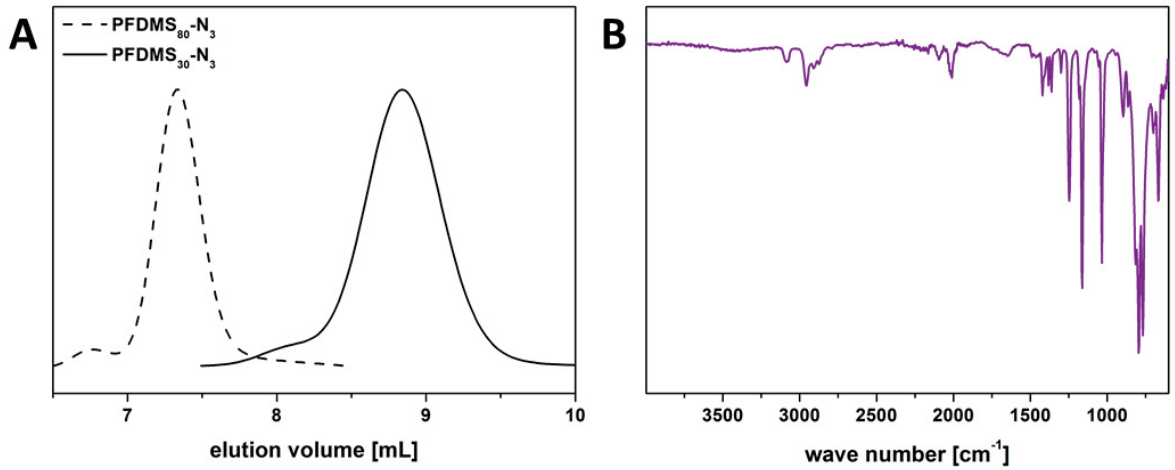

Figure S2: A) Comparison of the SEC traces for azide-modified PFDMS-N_3 with two different molar mass of 7 000 g mol^{-1} ($PFDMS_{30}$-N_3; straight black line) and 20 000 g mol^{-1} ($PFDMS_{80}$-N_3; dashed line); B) FT-IR spectrum for $PFDMS_{30}$-N_3.

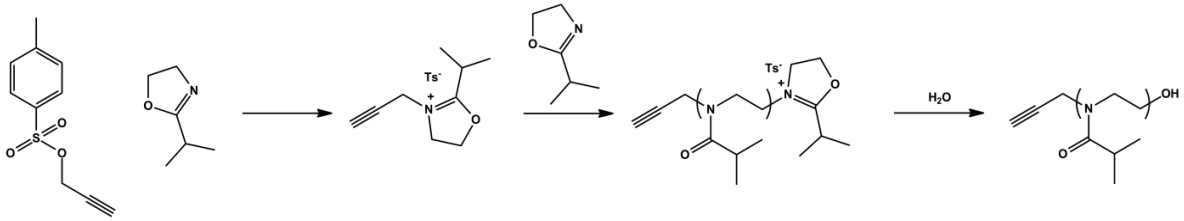

Figure S3: Synthesis of alkyne-functionalized P*i*PrOx *via* CROP initiated by propargyl *p*-toluenesulfonate.

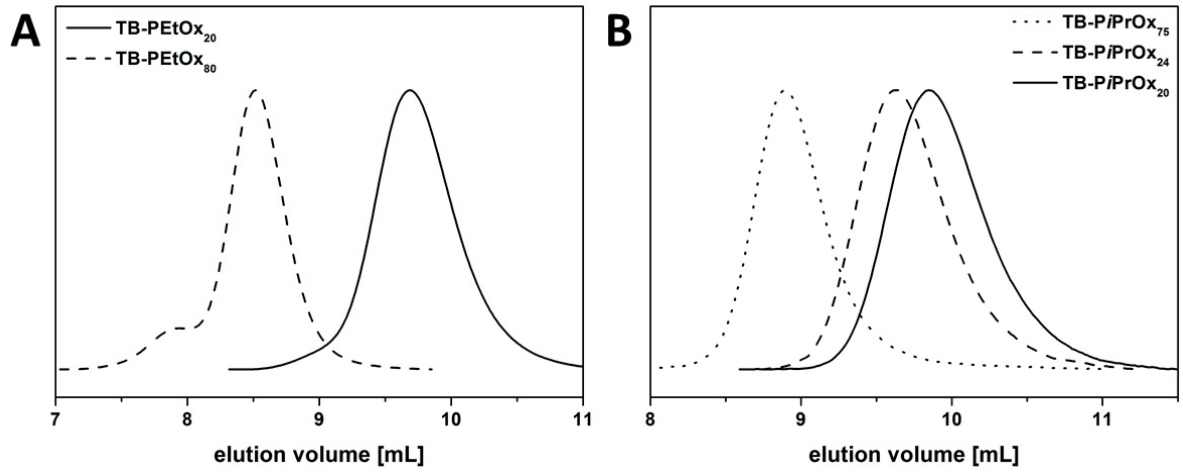

Figure S4: Comparison of SEC traces obtained for: A) TB-PEtOx$_{20}$ (straight line), TB-PEtOx$_{80}$ (dashed line); B) TB-P*i*PrOx$_{20}$ (straight line), TB-P*i*PrOx$_{24}$ (dotted line), and TB-P*i*PrOx$_{75}$ (dashed line).

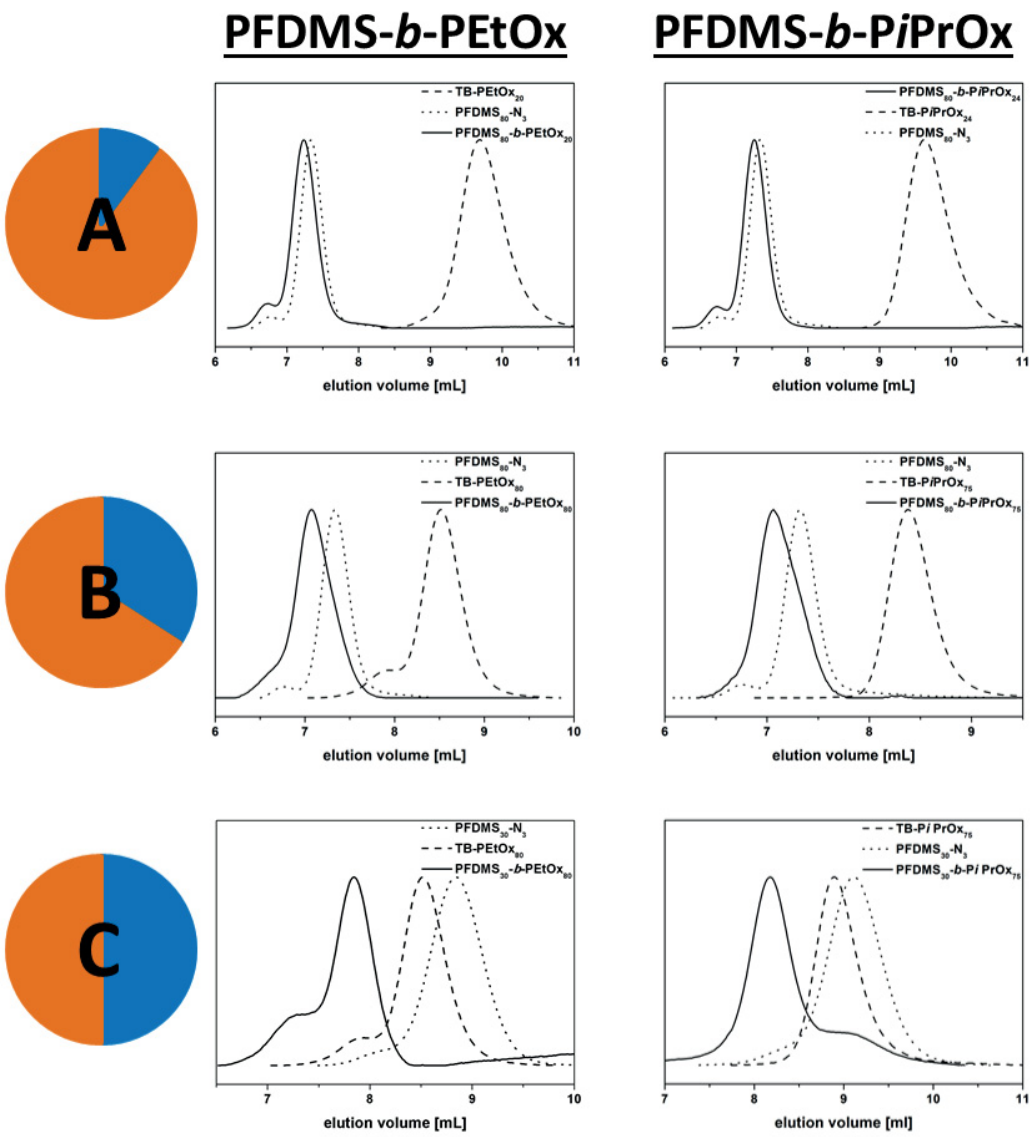

Figure S5: Comparison of SEC traces for the CuAAC click reaction between $PFDMS_x$-N_3 (dotted line) and various TB-POx_y (dashed line) synthesized block copolymers (straight line) with different ratios: A) $PFDMS_{80}$-*b*-$PEtOx_{20}$ (92/8 wt. %), $PFDMS_{80}$-*b*-P*i*$PrOx_{24}$ (88/12 wt. %); B) $PFDMS_{80}$-*b*-$PEtOx_{80}$ (71/29 wt. %), $PFDMS_{80}$-*b*-P*i*$PrOx_{75}$ (70/30 wt. %); C) $PFDMS_{30}$-*b*-$PEtOx_{80}$ (47/53 wt. %), $PFDMS_{30}$-*b*-P*i*$PrOx_{75}$ (46/54 wt. %).

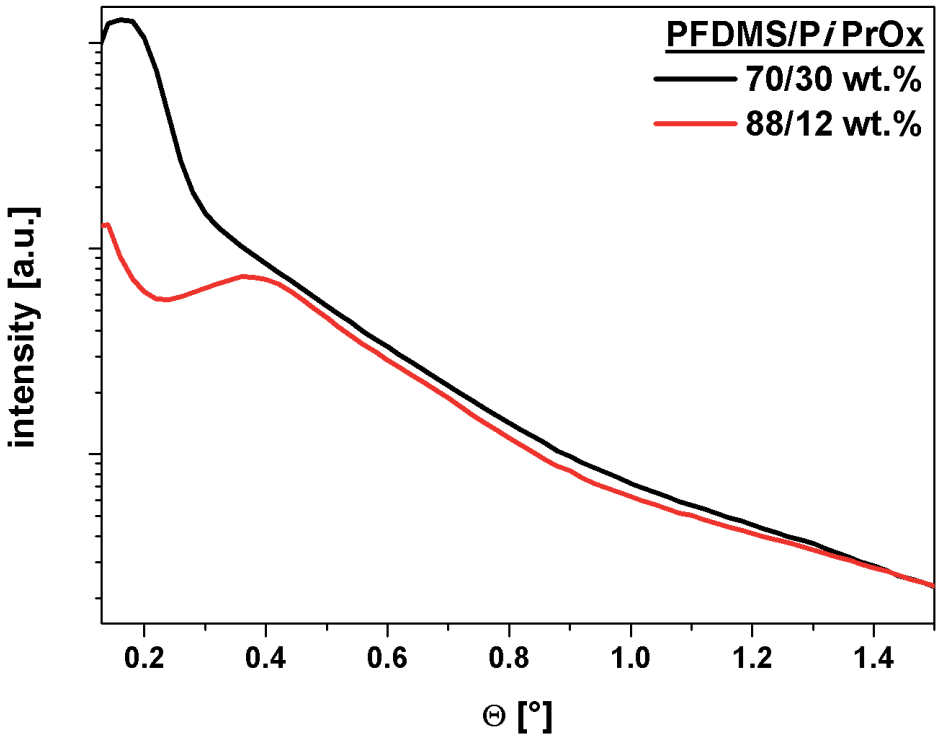

Figure S6: Comparison of SAXS patterns for different PFDMS$_x$-*b*-P*i*PrOx$_y$ diblock copolymers: 70/30 wt. % (PFDMS$_{80}$-*b*-P*i*PrOx$_{75}$; black curve), 88/12 wt. % (PFDMS$_{80}$-*b*-P*i*PrOx$_{24}$; red curve).

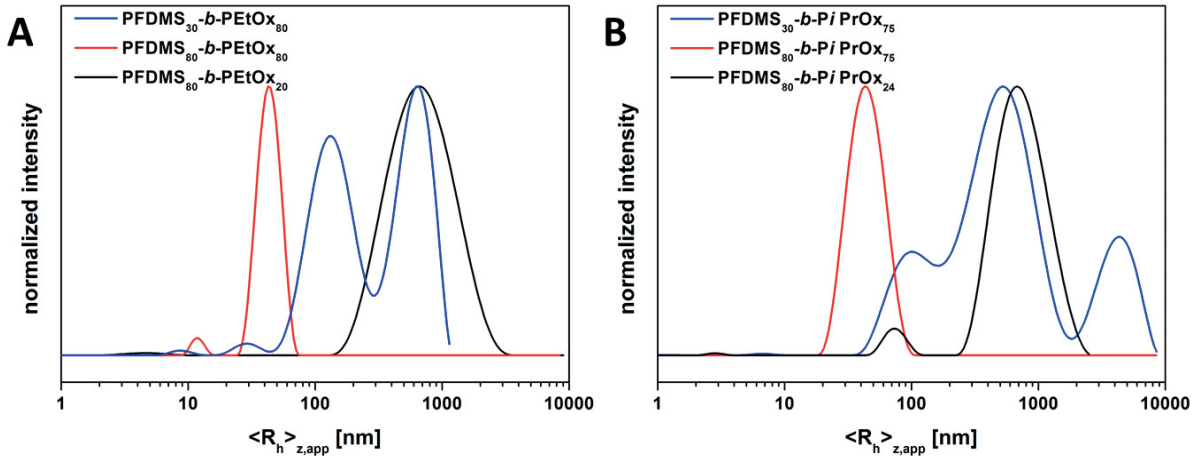

Figure S7: Comparison of DLS CONTIN plots for A) PFDMS$_{80}$-*b*-PEtOx$_{20}$ (92/8 wt. %; $<R_h>_{z,\,app}$ = 670 nm; black trace), PFDMS$_{80}$-*b*-PEtOx$_{80}$ (71/29 wt. %, $<R_h>_{z,\,app}$ = 12 and 43 nm; red trace), PFDMS$_{30}$-*b*-PEtOx$_{80}$ (47/53 wt. %; $<R_h>_{z,\,app}$ = 9, 30, 135 and 630 nm; blue trace); B) PFDMS$_{80}$-*b*-P*i*PrOx$_{24}$ (88/12 wt. %; $<R_h>_{z,\,app}$ = 73 and 680 nm; black trace); PFDMS$_{80}$-*b*-P*i*PrOx$_{75}$ (70/30 wt. %; $<R_h>_{z,\,app}$ = 45 nm; red trace); PFDMS$_{30}$-*b*-P*i*PrOx$_{75}$ (46/54 wt. %; $<R_h>_{z,\,app}$ = 100, 525 and 4300 nm; blue trace) at a constant concentration of 0.5 mg mL^{-1} in acetone.

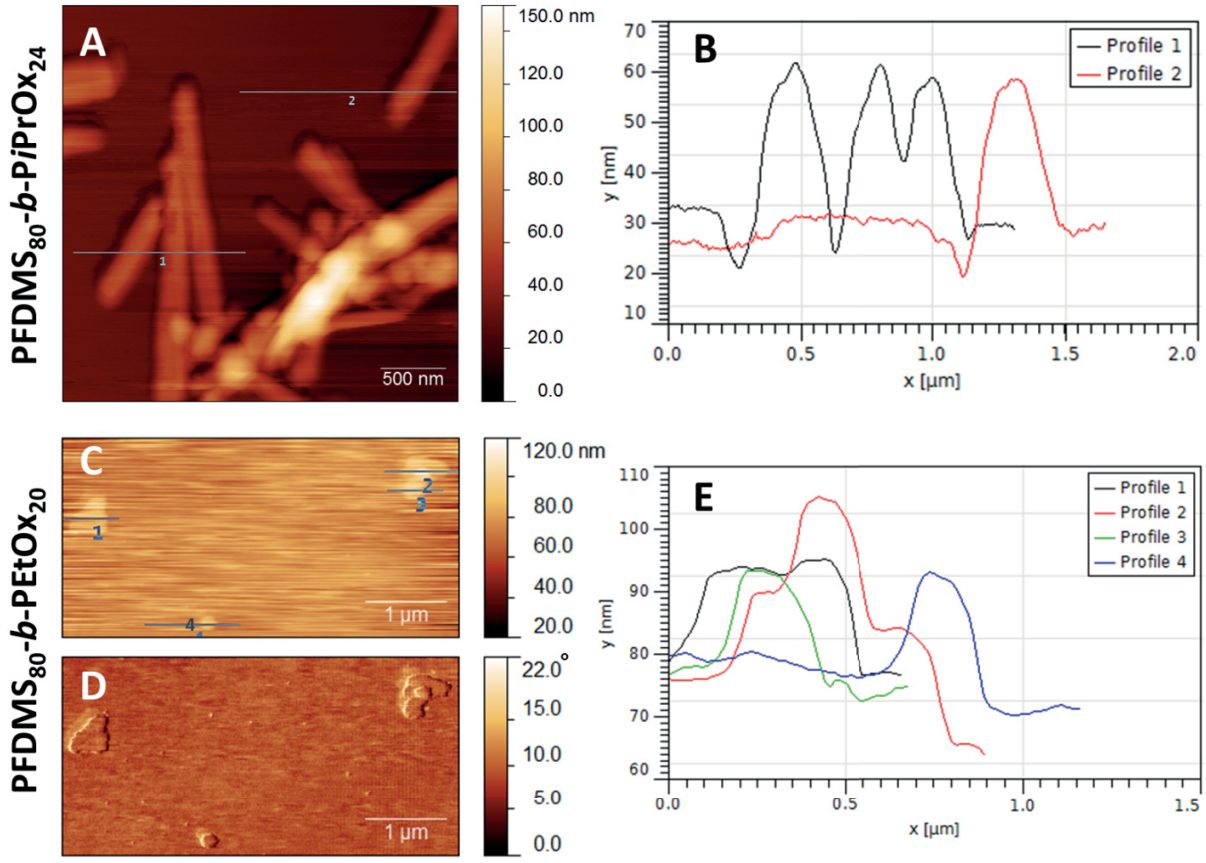

Figure S8: Comparison of AFM images for sheet forming block copolymers drop-casted from acetone: Height image (A) of PFDMS$_{80}$-*b*-PiPrOx$_{24}$ (88/12 wt. %) and the corresponding height profile (B, ~15-30 nm); height image (C) of PFDMS$_{80}$-*b*-PEtOx$_{20}$ (92/8 wt. %) and the corresponding phase image (D) and the height profile (E, ~15 nm).

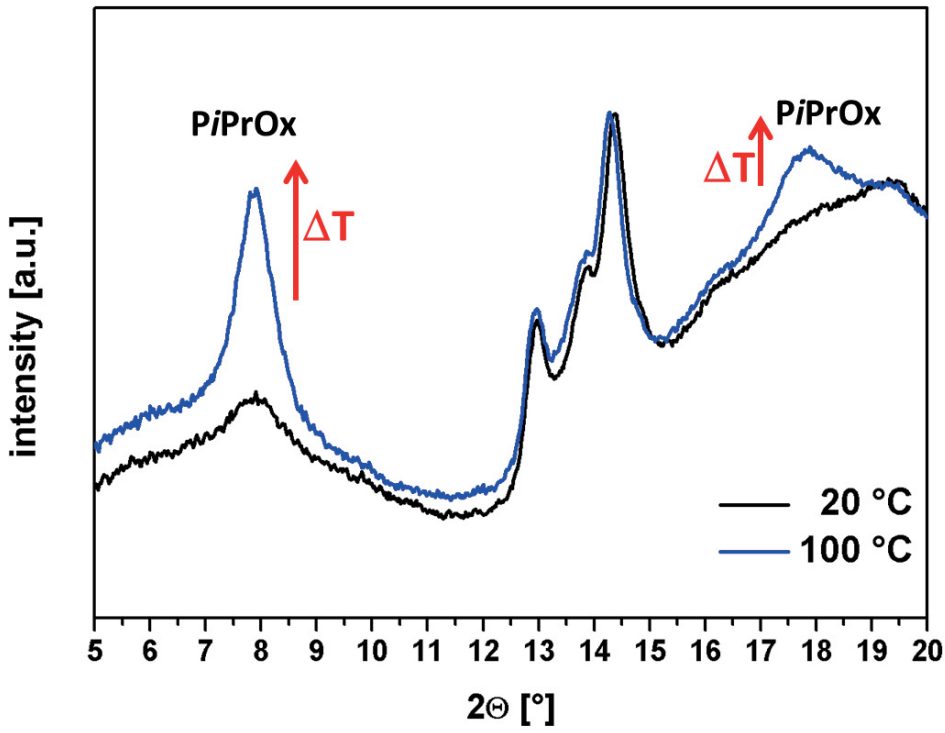

Figure S9: Wide angle x-ray scattering for $PFDMS_{30}$-*b*-P*i*$PrOx_{75}$ (46/54 wt.%) at different temperatures: 20 °C (black curve), and after heating to 100 °C (2 h@100 °C; blue curve).

Publication P5

“Hierarchical Self-Assembly of Double-Crystalline Poly(ferrocenyldimethylsilane)-*block*-poly(2-*iso*-propyl-2-oxazoline) (PFDMS-*b*-P*i*PrOx) Block Copolymers”

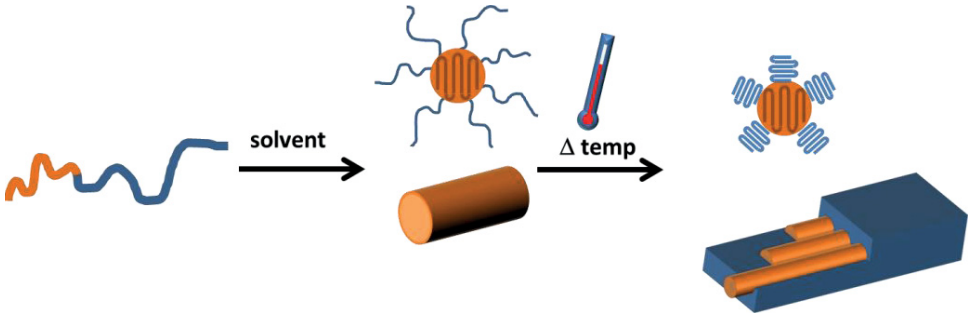

Tobias Rudolph, Adam Nunns, Steffi Stumpf, Christian Pietsch, Felix H. Schacher

Submitted, Submission date: 25.04.2015

Hierarchical Self-Assembly of Double-Crystalline Poly(ferrocenyldimethylsilane)-*block*-poly(2-*iso*-propyl-2-oxazoline) (PFDMS-*b*-P*i*PrOx) Block Copolymers

Tobias Rudolph,[1,2] Adam Nunns,[3] Steffi Stumpf,[1,2] Christian Pietsch,[1,2] Felix H. Schacher[1,2,*]

[1] Laboratory of Organic and Macromolecular Chemistry, Friedrich Schiller University Jena, Humboldtstr. 10, 07743 Jena, Germany

E-mail: felix.schacher@uni-jena.de

[2] Jena Center for Soft Matter (JCSM), Friedrich Schiller University Jena, Philosophenweg 7, 07743 Jena, Germany

[3] School of Chemistry, University of Bristol, Bristol BS8 1TS, U.K

Keywords: organometallic block copolymers, double crystalline block copolymers, cationic ring-opening polymerization, anionic ring-opening polymerization, self-assembly

Abstract

Herein, we demonstrate the synthesis of chain-end functionalized poly(ferrocenyldimethylsilane) (PFDMS), poly(2-*iso*-propyl-2-oxazoline)s (P*i*PrOx), and the subsequent macromolecular conjugation to double crystalline organometallic PFDMS-*b*-P*i*PrOx diblock copolymers. Two block copolymers were obtained by copper-catalyzed azide-alkyne cycloaddition (CuAAC), featuring PFDMS/P*i*PrOx weight fractions of 46/54 ($PFDMS_{30}$-*b*-P*i*$PrOx_{75}$) and 30/70 ($PFDMS_{30}$-*b*-P*i*$PrOx_{155}$). Non-solvent induced crystallization of PFDMS in acetone leads in both cases to cylindrical micelles with a PFDMS core. Afterwards, the structures were transferred into water for sequential temperature-induced crystallization of the P*i*PrOx corona, leading to hierarchical double crystalline superstructures, which were investigated using scanning electron microscopy (SEM), wide angle X-ray scattering (WAXS), and differential scanning calorimetry (DSC).

Introduction

During the last few decades, block copolymers have received increasing interest in various disciplines, including medicine, physics, and material science. This is in most cases due to the tremendous possibilities for the combination of different physical or chemical properties within one single material, as well as the fact that block copolymers typically undergo microphase separation in the bulk or in selective solvents. In that way, facile access to nanostructured materials with tunable (surface) chemistry can be realized.[1-5]

Recently, we demonstrated the synthesis of poly(ferrocenyldimethylsilane)-*block*-poly(2-alkyl-2-oxazoline) (PFDMS-*b*-POx) amphiphilic diblock copolymers *via* copper-catalyzed azide-alkyne cycloaddition (CuAAC). By varying the weight fraction of PFDMS, different morphologies like sheets, vesicular aggregates, and cylindrical micelles were formed *via* self-assembly in a selective solvent (acetone).[6] For these micelles, PFDMS represents the core-forming segment, while the POx corona stabilized the aggregates in solution. Both poly(2-ethyl-2-oxazoline) (PEtOx) and poly(2-*iso*-propyl-2-oxazoline) (P*i*PrOx) were studied as corona-forming block. In case of P*i*PrOx-based block copolymers, potentially double crystalline materials were obtained, as P*i*PrOx is known for crystallization from aqueous solution at elevated temperatures.[7-9] Non-specific hydrophobic interactions and oriented dipolar interactions are the main driving force for the formation of directional crystallization in this case.[7] Regarding PFDMS, solvent-induced crystallization in different selective solvents or solvent mixtures has been described by Manners and coworkers.[10-14] They showed the formation of hierarchical superstructures as well as crystallization-driven living self-assembly from size-tunable seed micelles obtained by sonication of pre-formed cylindrical micelles.[13, 14] This approach was meanwhile also adopted for other semi-crystalline polymers, *e.g.* polyethylene[15] or poly(3-hexylthiophene).[16] However, the synthesis of double crystalline diblock copolymers and, in particular, sequential crystallization of

both compartments has been frequently investigated in the bulk,[17-21] but the number of examples of sequential crystallization of diblock copolymers in solution is limited.[22, 23]

In this study we investigated the sequential crystallization in solution of two double crystalline diblock copolymers, poly(ferrocenyldimethylsilane)-*block*-poly(2-*iso*-propyl-2-oxazoline) ($PFDMS_x$-*b*-P*i*$PrOx_y$) featuring different volume fractions. The materials were synthesized by a combination of anionic and cationic ring-opening polymerization, followed by copper-catalyzed azide-alkyne cycloaddition (CuAAC). After purification and characterization by NMR, SEC and FT-IR, self-assembly in acetone (selective solvent) led to the formation of cylindrical micelles in both cases. These were then transferred into water, and the micellar solutions were subsequently heated to 65 °C for 24 hours, inducing the crystallization of P*i*PrOx. SEM, DSC and X-ray scattering indicated the formation of superstructures, presumably consisting of a semi-crystalline P*i*PrOx matrix embedding the originally formed PFDMS cylinders.

Materials and Instruments

Instruments

NMR: Proton nuclear magnetic resonance (^{1}H-NMR) spectra were recorded in $CDCl_3$ on a Bruker AC 300 MHz spectrometer at 298 K. Chemical shifts are given in parts per million (ppm, δ scale) relative to the residual signal of the deuterated solvent.

SEC: Size exclusion chromatography was measured on a Shimadzu system equipped with a SCL-10A system controller, a LC-10AD pump, and a RID-10A refractive index detector using a solvent mixture containing chloroform, triethylamine, and *iso*-propanol (94:4:2) at a flow rate of 1 mL min^{-1} on a PSS SDV linear M 5 μm column. The system was calibrated using PS (100 to 100 000 g mol^{-1}) and PEO (440 to 44 700 g mol^{-1}) standards.

Fourier Transform Infrared spectroscopy: Dry powders of the block copolymers were directly placed on the crystal of the ATR-FTIR (Affinity-1 FTIR, Shimadzu) for measurements in the range of 4 000 to 600 cm^{-1}.

Transmission Electron microscopy (TEM): The formed aggregates were analyzed using either a TEM (Zeiss-CEM 902A, Oberkochen, Germany) operated at 80 kV and images were recorded using a 1k TVIPS FastScan CCD camera, or on a FEI Tecnai G^2 20 (200 kV) equipped with a 4k x 4k Eagle HS CCD and a 1k x 1k Olympus MegaView camera for overview images. TEM samples were prepared by applying a drop of an aqueous sample solution onto the surface of a plasma-treated carbon coated copper grid (Quantifoil Micro-Tools GmbH, Jena, Germany). For samples from acetone the drop was applied directly to the TEM grid, without plasma treatment.

Scanning Electron microscopy (SEM): Gemini 1530 type LEO Field Emission scanning electron microscope (Carl-Zeiss AG, Germany) or on a Zeiss SIGMA VP Field Emission SEM

equipped with a GEMINI column (Carl-Zeiss AG, Germany) operating at 3 to 7 kV using the InLens or SE2 detector. Before the measurements the samples were coated with platinum (4 nm) using a BAL-TEC MED020 sputtering device (Bal-Tec AG, Lichtenstin).

Small and Wide Angle X-ray Scattering (SAXS/WAXS): SAXS/WAXS measurements on dried powders of the materials were performed on a Bruker AXS Nanostar (Bruker, Karlsruhe, Germany), equipped with a microfocus X-ray source (Incoatec IμSCu E025, Incoatec, Geesthacht, Germany), operating at $\lambda = 1.54$ Å. A pinhole setup with 750 mm, 400 mm, and 1000 mm (in the order from source to sample) was used and the sample-to-detector distance was 12 cm (WAXS) or 107 cm (SAXS). Samples were mounted on a metal rack and fixed using tape. The scattering patterns were corrected for the background (Scotch tape) prior to evaluations.

Materials:

Azide-modified poly(ferrocenyldimethylsilane) ($PFDMS_{30}$-N_3) was synthesized as described recently.[6, 24] Tetrahydrofuran (THF), acetonitrile (ACN) and dichloromethane (DCM) were purified using a Solvent Purification System (SPS, Innovative Technology, PM-400-3-MD) equipped with two activated alumina columns. Copper bromide (CuBr) and *N*,*N*,*N*′,*N*″,*N*″-pentamethyldiethylenetriamine (PMDETA) were purchased by Sigma Aldrich and used as received.

Synthesis of alkyne-modified poly(2-iso-propyl-2-oxazoline) (TB-PiPrOx$_y$)

Alkyne-modified poly(2-*iso*-propyl-2-oxazoline) (TB-P*i*PrOx) was synthesized as described previously.[6] Briefly, propargyl *p*-toluenesulfonate and 2-*iso*-propyl-2-oxazoline (*i*PrOx) were dissolved in acetonitrile at different monomer to initiator ratios ([M]/[I]) and a monomer concentration of 4M. The capped vials were placed in a microwave synthesizer at 140 °C. The

polymer was terminated *via* the addition of water and the final polymer obtained after extraction, by precipitation in cold diethyl ether.

SEC ($CHCl_3$/*i*-PrOH/TEA): TB-P*i*PrOx$_{75}$: M_n= 8800 g mol^{-1}; Đ = 1.07; TB-P*i*PrOx$_{155}$: M_n= 18000 g mol^{-1}; Đ = 1.06; **^{1}H NMR** (300 MHz, $CDCl_3$, δ): 3.6–3.2 (br, –N–C*H*2–C*H*2–), 2.5–2.2 (br, CO–C*H*–(CH3)$_2$), 1.2–0.9 (br, CO–CH–(C*H*3)$_2$) ppm.

Copper-catalyzed Alkyne-Azide Cycloaddition (CuAAC) click-reaction between PFDMS$_{30}$-N$_3$ and TB-PiPrOx$_y$.[6]

Poly(ferrocenyldimethylsilane)-*block*-poly(2-*iso*-propyl-2-oxazoline)s (PFDMS$_{30}$-*b*-P*i*PrOx$_y$) was synthesized as described previously by copper catalyzed azide-alkyne cycloaddition (CuAAC).[6, 24] Briefly, TB-P*i*PrOx$_y$ (2 eq.) and PFDMS$_{30}$-N_3 (1 eq.) were dissolved in a solvent mixture of THF and ethanol (1/1 vol.%) until a clear solution was observed and purged for 5 minutes with argon. CuBr and PMDETA (2 eq.) were added under argon flux, and the solution was purged with argon for additional 5 minutes. Afterwards the solution was heated to 80 °C for 15 minutes in an oil bath.

The resulting block copolymer solution was passed through a short AlOxN column to remove copper from the reaction mixture. The block copolymer was dissolved in DCM and added into acetone. The resulting acetone solution was stirred for 2 days, centrifuged (5000 rpm, 1 min), and the supernatant solution was removed (excess of P*i*PrOx soluble in acetone). The precipitate was dried under vacuum resulting in an orange product.

SEC ($CHCl_3$/*i*-PrOH/TEA): PFDMS$_{30}$-*b*-P*i*PrOx$_{75}$: M_n = 15000 g mol^{-1}; Đ = 1.22 (PS-calibration); PFDMS$_{30}$-*b*-P*i*PrOx$_{155}$: M_n = 27000 g mol^{-1}; Đ = 1.06; (PS-calibration).

^{1}H-NMR: (300 MHz, $CDCl_3$, δ): 4.3-4.1 (bs, Cp-H), 4.1-3.9 (Cp-H), 3.6-3.2 (br, –N–C*H*2–C*H*2–), 2.5–2.2 (br, CO–C*H*2–CH3), 1.2–0.9 (br, CO–CH2–C*H*3), 0.5-0.4 (Si-$(CH_3)_2$) ppm.

Transfer of the block copolymers into selective solvents

5 mg of the block copolymer was dissolved in 1 mL DCM and added under vigorous stirring to 5 mL acetone. The solution was stirred overnight to evaporate DCM from the solution while acetone was added subsequently to maintain a constant concentration of 1 g L^{-1}.

To transfer the pre-organized aggregates into aqueous solution, water was added dropwise to the acetone solution over several hours. The acetone was allowed to evaporate for 2 days afterwards.

Results and discussion

We synthesized two poly(ferrocenyldimethylsilane)-*block*-poly(2-*iso*-propyl-2-oxazoline) ($PFDMS_x$-*b*-P*i*$PrOx_y$) diblock copolymers with different composition using a modular approach. For this purpose, azide-modified PFDMS ($PFDMS_{30}$-N_3) was synthesized by anionic ring-opening polymerization (AROP) of dimethylsilaferrocenophane (FDMS), followed by introduction of an azide endgroup (Scheme S1; Table 1).[6, 24] As second macromolecular building block, 2-*iso*-propyl-2-oxazoline (*i*PrOx) was polymerized by cationic ring-opening polymerization (CROP) using propargyl *p*-toluenesulfonate as initiator (TB-P*i*$PrOx_y$, Scheme S2; Table 1). Hereby, TB represents the terminal triple bond present in TB-P*i*PrOx. The composition of the individual polymers was investigated by size exclusion chromatography (SEC), nuclear magnetic resonance spectroscopy (NMR), and fourier transform infrared spectrometry (FT-IR). Subsequently, CuAAC was used for covalent linkage of the two segments (Figure 1A, Scheme S3). Briefly, $PFDMS_{30}$-N_3 and TB-P*i*$PrOx_y$ were dissolved in THF/ethanol mixtures (1/1; v/v), and the mixture was purged with argon, while copper(I) bromide (Cu(I)Br) and *N*,*N*,*N*′,*N*″,*N*″-pentamethyldiethylenetriamine (PMDETA) were added under argon flux. The reaction solution was heated for 15 min to 80 °C. TB-P*i*$PrOx_y$ was used in excess (2 eq.) in comparison to the azide functionality to ensure full conversion of $PFDMS_{30}$-N_3. After purification, the diblock copolymers were investigated *via* SEC, NMR and FT-IR (Figures S1 and S2). By SEC, a shift to lower elution volume can be observed, indicating the successful linkage between the two building blocks. In case of $PFDMS_{30}$-*b*-P*i*$PrOx_{155}$, no homopolymer was observed by SEC (Figure S1), while for $PFDMS_{30}$-*b*-P*i*$PrOx_{75}$ a slight shoulder could be detected.[6] Subscripts denote the degree of polymerization (DP) of the corresponding block as determined by NMR. By FT-IR, the disappearance of the azide signal (2094 cm^{-1}) confirms full consumption of $PFDMS_{30}$-N_3 (Figure S2). Two compositions of 46/54 ($PFDMS_{30}$-*b*-P*i*$PrOx_{75}$) and 30/70 ($PFDMS_{30}$-*b*-P*i*$PrOx_{155}$) were

obtained (Table 1). Higher contents of P*i*PrOx were not investigated, as the degree of polymerization for the controlled CROP of 2-alkyl-2-oxazoline is limited due to undesirable side-reactions occurring upon using higher monomer to initiator ratios.[25, 26]

Table 1: Characterization data for the herein used homopolymers and diblock copolymers.

Polymer	**ratio PFDMS/POx[a]** [wt. %]	**M_n[b]** [g mol^{-1}]	**M_n[c]** **[g mol^{-1}]**	Đ[c]
$PFDMS_{30}$-N_3[d]	-	7 300	7 300	1.08
TB-P*i*$PrOx_{75}$[d]	-	8 600	8 000	1.08
TB-P*i*$PrOx_{155}$[d]	-	17 700	18 000	1.06
$PFDMS_{30}$-*b*-P*i*$PrOx_{75}$[d]	46 / 54	16 000	15 000	1.22
$PFDMS_{30}$-*b*-P*i*$PrOx_{155}$[d]	30 / 70	25 000	27 000	1.06

a) calculated according to the constituting building blocks; b) SEC ($CHCl_3$/TEA/*i*-PrOH) PS calibration; c) theoretical molar masses determined *via* NMR; d) subscripts denote the degree of polymerization for the corresponding block.

Initially, the bulk morphology of the diblock copolymers was investigated by small angle x-ray scattering (SAXS). The results indicate the presence of a lamellar structure in both cases with d-spacings of 19 nm for $PFDMS_{30}$-*b*-P*i*$PrOx_{75}$ and 21 nm for $PFDMS_{30}$-*b*-P*i*$PrOx_{155}$ (Figure 1B, Figure S3). In case of $PFDMS_{30}$-*b*-P*i*$PrOx_{75}$, earlier TEM micrographs from thin-films prepared using an ultramicrotome support this assumption.[6]

We also carried out temperature-dependent WAXS experiments for $PFDMS_{30}$-*b*-P*i*$PrOx_{75}$ in the bulk. Already at RT (20 °C), the presence of the characteristic reflections for PFDMS can be observed (Figure 1C).[11, 27] The corresponding reflections for P*i*PrOx at ≈ 8 and 21° start to appear upon annealing at higher temperatures. This clearly indicates crystallization of this domain upon

heating, while the PFDMS reflection intensity remains constant up to 100 °C. Additionally, by increasing the temperature above 100 °C, a decrease of the reflex intensity for PFDMS can be observed, presumably due to partial melting, which is also observed by DSC (Figure S4; first heating run).[28, 29]

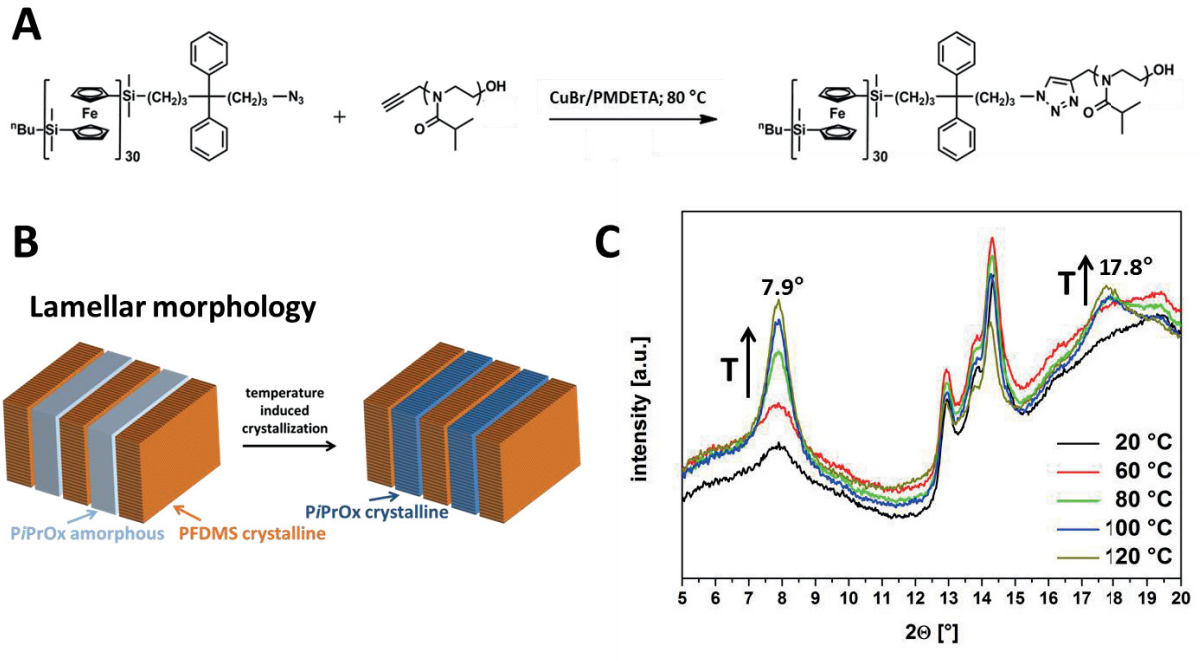

Figure 1: A) Synthesis of PFDMS-*b*-P*i*PrOx block copolymers; B) Temperature-induced crystallization of P*i*PrOx in the bulk; C) comparison of WAXS diffractograms for $PFDMS_{30}$-*b*-$PiPrOx_{75}$ at different temperatures: 20 (black trace), 60 (red trace), 80 (green trace), 100 (blue trace), and 120 (olive trace) °C.

After confirmation that the diblock copolymers are double crystalline in the bulk, we were interested in the self-assembly in selective solvents. For this purpose, the diblock copolymers were dissolved in a non-selective solvent, *e.g.* dichloromethane (DCM), and added to acetone, a selective solvent for the P*i*PrOx segment. The solutions were stirred for 24 hours, while DCM was allowed to evaporate and acetone was added to maintain a concentration of 1 mg mL^{-1}. The solutions turned slightly opaque with time, indicating the formation of micellar structures, which were investigated by transmission electron microscopy (TEM). In both cases, cylindrical micelles

featuring a PiPrOx corona and a PFDMS core of up to several µm length and 20 nm ($PFDMS_{30}$-*b*-P*i*$PrOx_{75}$) or 40-50 nm width ($PFDMS_{30}$-*b*-P*i*$PrOx_{155}$) were formed (Figures 2, S5 and S6). These dispersions had to be constantly agitated, otherwise partial precipitation occurred within several hours.

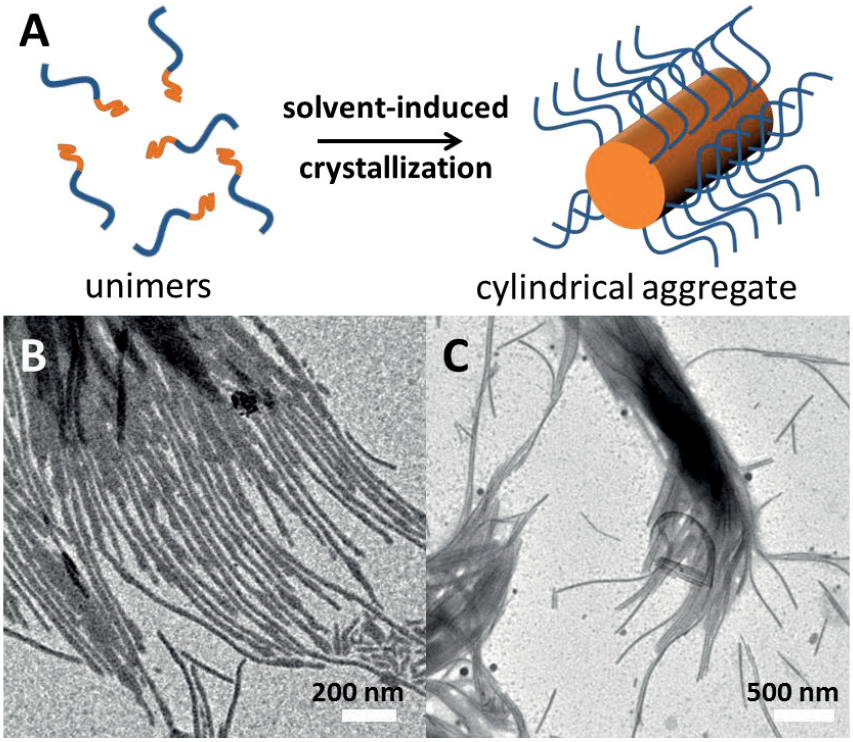

Figure 2: A) Formation of cylindrical core-corona micelles featuring a PFDMS core (orange) and a P*i*PrOx corona (blue); B) TEM micrographs of $PFDMS_{30}$-*b*-P*i*$PrOx_{155}$ and C) $PFDMS_{30}$-*b*-P*i*$PrOx_{75}$ from acetone (1 mg mL^{-1}).

Homopolymeric P*i*PrOx is known for its temperature-dependent solubility in water and the ability to undergo directional crystallization upon heating above the lower critical solution temperature (LCST) for several hours.[7-9] Hence, we anticipated that a subsequent crystallization step involving previously formed cylindrical micelles with a P*i*PrOx corona might be feasible. Therefore, we transferred the cylindrical micelles with a PFDMS core into aqueous media *via* slow addition of water, followed by evaporation of acetone (Figure 3A).

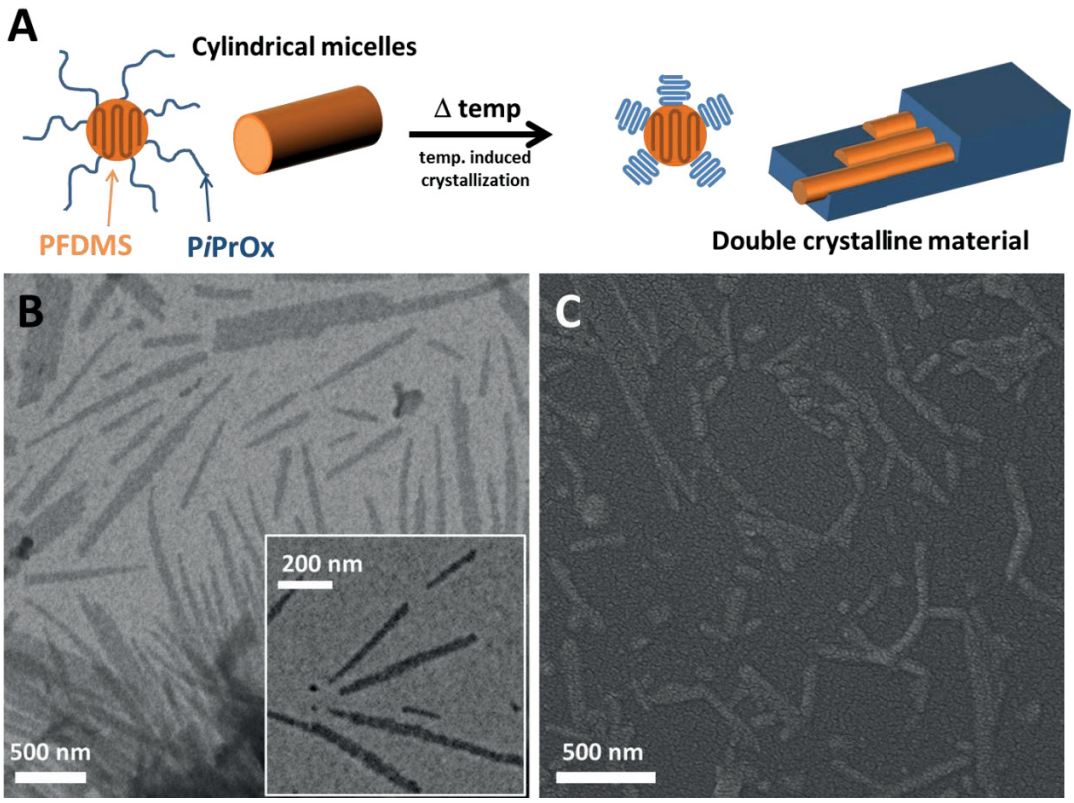

Figure 3: Temperature-induced crystallization of the P*i*PrOx corona in water upon heating above the LCST, embedding the PFDMS cylinders in a semi-crystalline P*i*PrOx matrix; B) TEM micrograph of cylindrical PFDMS$_{30}$-*b*-P*i*PrOx$_{155}$ micelles after transfer from acetone to water, the inset shows an enlargement; C) SEM micrograph of PFDMS$_{30}$-*b*-P*i*PrOx$_{155}$ after transfer from acetone to water.

The resulting turbid aqueous solutions were again investigated using TEM and SEM (Figures 3B and C), confirming the integrity of the initial cylindrical micelles. However, a certain broadening of some cylindrical micelles can be seen (from 30 to 60 nm), which at the moment we attribute to fusion processes occurring during solvent exchange. If block copolymers with a P*i*PrOx content below 50 wt.% were used, immediate precipitation from aqueous solutions was observed afterwards.

For the subsequent crystallization of the P*i*PrOx segment, the aqueous solutions were heated to 65 °C for up to 24 hours, and samples were freeze-dried for SEM, DSC and WAXS

measurements. During the heating procedure, the formation of larger aggregates and precipitation of macroscopic particles within a few hours can be observed (Figure S7). By SEM, aggregates of several μm in length and width were found. The fine structure can be observed at higher magnification, showing bundles of cylindrical micelles packed into giant fiber-like superstructures (Figure 4). We hypothesize that the slight morphological differences observed can be explained with the different segment length of the crystallizing P*i*PrOx.

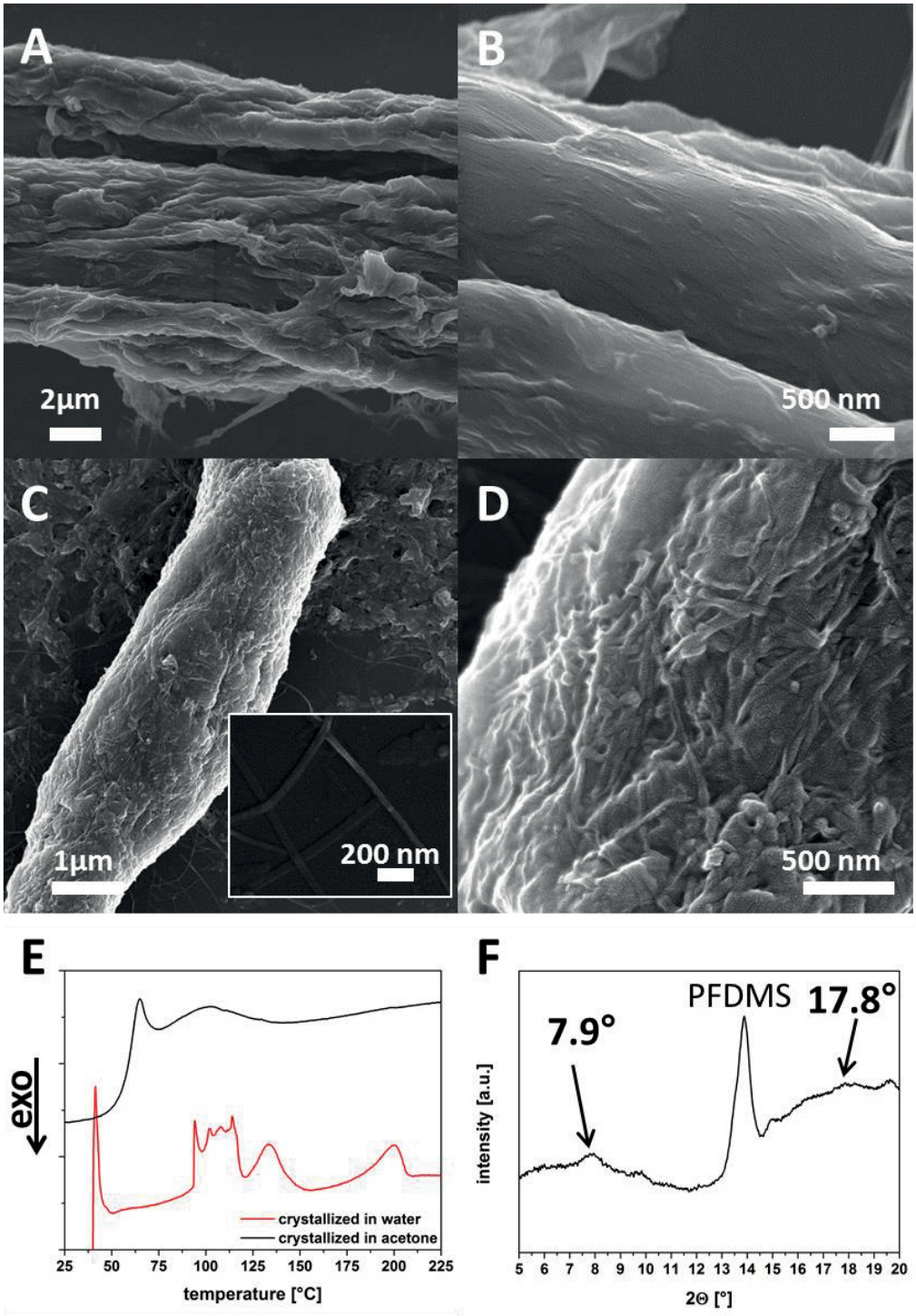

Figure 4: SEM micrographs after heating in water at 65 °C for24 h of PFDMS$_{30}$-*b*-P*i*PrOx$_{75}$ (A, B) and PFDMS$_{30}$-*b*-P*i*PrOx$_{155}$ (C, D); E) Comparison of DSC traces of the first heating run for samples obtained after solvent-induced crystallization of PFDMS$_{30}$-*b*-P*i*PrOx$_{155}$ in acetone (black trace) and after sequential crystallization of the P*i*PrOx segment at elevated temperatures in water (red trace); F) WAXS diffractogram of PFDMS$_{30}$-*b*-P*i*PrOx$_{155}$ after sequential crystallization in solution towards double crystalline hierarchical superstructures.

We were able to show the formation of double crystalline $PFDMS_{30}$-*b*-P*i*$PrOx_{75}$ in the bulk state (see above). While only very weak reflections for P*i*PrOx were found in WAXS experiments for solution crystallized samples of $PFDMS_{30}$-*b*-P*i*$PrOx_{75}$ (Figure S8), this changed upon increasing the weight fraction of P*i*PrOx in $PFDMS_{30}$-*b*-P*i*$PrOx_{155}$ (Figure 4F). The positions of the reflexes at 7.9 ° and 17.8 ° are comparable to the results discussed in detail by Schlaad, Winnik, and Dworak for homopolymers and our own investigations in the bulk.[7, 30, 31] The reflex corresponding to the PFDMS core (2 Θ ≈14 °) changed its shape in comparison to the material in the bulk (Figure 2B), which is also observed for solution cast samples of PFDMS micelles, the low reflex intensity for the P*i*PrOx segment might be due to a very thin crystalline domain around the cylindrical core.[27]

We also investigated solution-crystallized samples of $PFDMS_{30}$-*b*-P*i*$PrOx_{155}$ from acetone (after solution-induced crystallization of PFDMS) and after subsequent crystallization of $PFDMS_{30}$-*b*-P*i*$PrOx_{155}$ in water by differential scanning calorimetry (DSC). Figure 4E shows both DSC traces for the first heating run, indicating for the sample from acetone the presence of two signals corresponding to the glass transition temperature (T_g) of P*i*PrOx (≈ 68 °C) and a broad signal for the melting temperature (T_m) of crystalline PFDMS domains (T_m ≈ 90-140 °C). Depending on the treatment of PFDMS, the T_m of PFDMS domains varies in the range of 90 to 140 °C, which is in good agreement with our results.[28, 29] Also the shape of the melting peak depends on the temperature treatment and the molar mass of the PFDMS, therefore even more than one peak can be observed as described by Vancso *et al.*[28] For the second sample, the supposed double crystalline diblock copolymer ($PFDMS_{30}$-*b*-P*i*$PrOx_{155}$), no T_g for the P*i*PrOx is observed. In the range of 90-140 °C multiple signals corresponding to T_m of PFDMS and an additional signal between 170 to 210 °C is observed. The melting peak around 190 °C corresponds to the T_m of crystalline P*i*PrOx.[30]

Conclusion

We were able to study the sequential crystallization of double crystalline PFDMS-*b*-P*i*PrOx diblock copolymers with weight fractions of 54 and 70 % for for poly(2-*iso*-propyl-2-oxazoline) (P*i*PrOx) in the bulk and in solution. First, non-solvent-induced crystallization of PFDMS in acetone led to cylindrical core-crystalline micelles as observed by TEM. Afterwards, the micelles were transferred into aqueous media for the subsequent temperature-induced crystallization of the P*i*PrOx corona, leading to the formation of double crystalline aggregates. This was verified using a combination of WAXS, DSC, and electron microscopy (TEM, SEM).

Acknowledgements

We thank Frank Steiniger and Christine Kämnitz (Electron Microscope Center Jena) for help with the TEM measurements, and Renzo Paulus for DSC measurements. F. H. S. and T. R. are further grateful to the Thuringian Ministry for Education, Science, and Culture (TMBWK; #B515-10065, ChaPoNano; #B515-11028, SWAXS-JCSM) for financial support. F. H. S. thanks the VCI for a starting independent researcher fellowship and Ulrich S. Schubert for continuous support. T. R. acknowledges the Carl-Zeiss foundation for a PhD-scholarship. T. R. would also like to thank Helmut Schlaad for fruitful discussions concerning the crystallization of P*i*PrOx. The SEM (Zeiss Sigma VP) and TEM (FEI Tecnai G^2 20) facilities of the Jena Center for Soft Matter (JCSM) were established with a grant from the German Research Council (DFG) and the European Fonds for Regional Development (EFRE).

References

1. F. S. Bates and G. H. Fredrickson, *Physics Today*, 1999, **52**, 32-38.
2. N. S. Cemeron, M. K. Corbierre and A. Eisenberg, *Can. J. Chem.*, 1999, **77**, 1311-1326.
3. A. Choucair and A. Eisenberg, *Eur. Phys. J. E.*, 2003, **10**, 37-44.
4. Y. Mai and A. Eisenberg, *Chem. Soc. Rev.*, 2012, **41**, 5969-5985.
5. G. Riess, *Prog. Polym. Sci.*, 2003, **28**, 1107-1170.
6. T. Rudolph, A. Nunns, A. M. Schwenke and F. H. Schacher, *Polym. Chem.*, 2015, **6**, 1604-1612.
7. A. L. Demirel, M. Meyer and H. Schlaad, *Angew. Chem. Int. Ed.*, 2007, **46**, 8622-8624.
8. C. Diehl, P. Cernoch, I. Zenke, H. Runge, R. Pitschke, J. Hartmann, B. Tiersch and H. Schlaad, *Soft Matter*, 2010, **6**, 3784-3788.
9. M. Meyer, M. Antonietti and H. Schlaad, *Soft Matter*, 2007, **3**, 430-431.
10. J. Qian, G. Guerin, Y. Lu, G. Cambridge, I. Manners and M. A. Winnik, *Angew. Chem. Int. Ed.*, 2011, **50**, 1622-1625.
11. J. Rasburn, R. Petersen, T. Jahr, R. Rulkens, I. Manners and G. J. Vancso, *Chem. Mater.*, 1995, **7**, 871-877.
12. J. A. Massey, K. Temple, L. Cao, Y. Rharbi, J. Raez, M. A. Winnik and I. Manners, *J. Am. Chem. Soc.*, 2000, **122**, 11577-11584.
13. J. B. Gilroy, T. Gädt, G. R. Whittell, L. Chabanne, J. M. Mitchels, R. M. Richardson, M. A. Winnik and I. Manners, *Nat. Chem.*, 2010, **2**, 566-570.
14. X. Wang, G. Guerin, H. Wang, Y. Wang, I. Manners and M. A. Winnik, *Science*, 2007, **317**, 644-647.
15. J. Schmelz, A. E. Schedl, C. Steinlein, I. Manners and H. Schmalz, *J. Am. Chem. Soc.*, 2012, **134**, 14217-14225.
16. S. K. Patra, R. Ahmed, G. R. Whittell, D. J. Lunn, E. L. Dunphy, M. A. Winnik and I. Manners, *J. Am. Chem. Soc.*, 2011, **133**, 8842-8845.
17. R. V. Castillo and A. J. Müller, *Prog. Polym. Sci.*, 2009, **34**, 516-560.
18. L. Sun, Y. Liu, L. Zhu, B. S. Hsiao and C. A. Avila-Orta, *Polymer*, 2004, **45**, 8181-8193.
19. A. J. Müller, V. Balsamo and M. L. Arnal, *Adv. Polym. Sci.*, 2005, **190**, 1-63.
20. H. Takeshita, K. Fukumoto, T. Ohnishi, T. Ohkubo, M. Miya, K. Takenaka and T. Shiomi, *Polymer*, 2006, **47**, 8210-8218.
21. S. Li, S. B. Myers and R. A. Register, *Macromolecules*, 2011, **44**, 8835-8844.
22. T. Li, W. J. Wang, R. Liu, W. H. Liang, G. F. Zhao, Z. Li, Q. Wu and F. M. Zhu, *Macromolecules*, 2009, **42**, 3804-3810.
23. W. Wang, R. Liu, Z. Li, C. Meng, Q. Wu and F. Zhu, *Macromol. Chem. Phys.*, 2010, **211**, 1452-1459.
24. A. Nunns, C. A. Ross and I. Manners, *Macromolecules*, 2013, **46**, 2628-2635.
25. F. Wiesbrock, R. Hoogenboom, M. A. M. Leenen, M. A. R. Meier and U. S. Schubert, *Macromolecules*, 2005, **38**, 5025-5034.

26. J. M. Warakomski and B. P. Thill, *J. Polym. Sci. Part A: Polym. Chem.*, 1990, **28**, 3551-3563.

27. N. McGrath, F. H. Schacher, H. Qiu, S. Mann, M. A. Winnik and I. Manners, *Polym. Chem.*, 2014, **5**, 1923.

28. R. G. H. Lammertink, M. a. Hempenius, I. Manners and G. J. Vancso, *Macromolecules*, 1998, **31**, 795-800.

29. J. Xu, V. Bellas, B. Jungnickel, B. Stühn and M. Rehahn, *Macromol. Chem. Phys.*, 2010, **211**, 1261-1271.

30. N. Oleszko, A. Utrata-Wesołek, W. Wałach, M. Libera, A. Hercog, U. Szeluga, M. Domański, B. Trzebicka and A. Dworak, *Macromolecules*, 2015, **48**, 1852-1859.

31. Y. Katsumoto, A. Tsuchiizu, X. Qiu and F. M. Winnik, *Macromolecules*, 2012, **45**, 3531-3541.

Table of content

Hierarchical Self-Assembly of Double-Crystalline Poly(ferrocenyldimethylsilane)-*block*-poly(2-*iso*-propyl-2-oxazoline) (PFDMS-*b*-P*i*PrOx) Block Copolymers

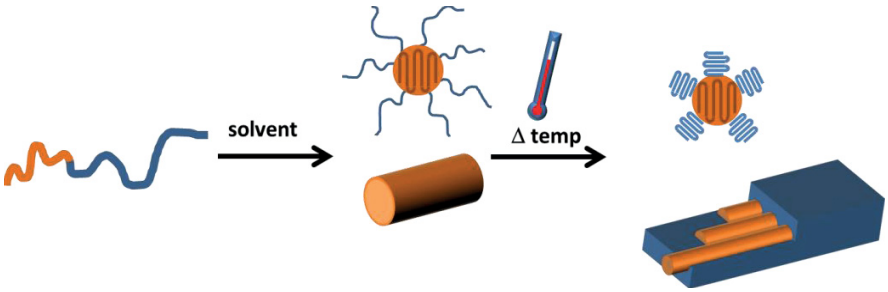

Supporting information

Hierarchical Self-Assembly of Double-Crystalline Poly(ferrocenyldimethylsilane)-*block*-poly(2-*iso*-propyl-2-oxazoline) (PFDMS-*b*-P*i*PrOx) Block Copolymers

Tobias Rudolph,[1,2] Adam Nunns,[3] Steffi Stumpf,[1,2] Christian Pietsch,[1,2] Felix H. Schacher[1,2,*]

[1] Laboratory of Organic and Macromolecular Chemistry, Friedrich Schiller University Jena, Humboldtstr. 10, 07743 Jena, Germany

E-mail: felix.schacher@uni-jena.de

[2] Jena Center for Soft Matter (JCSM), Friedrich Schiller University Jena, Philosophenweg 7, 07743 Jena, Germany

[3] School of Chemistry, University of Bristol, Bristol BS8 1TS, U.K

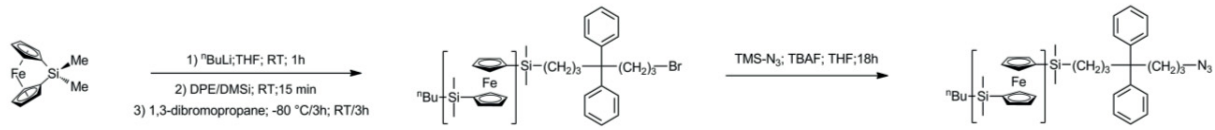

Scheme S1: Synthesis of azide-functionalized PFDMS-N_3 of different molar mass.

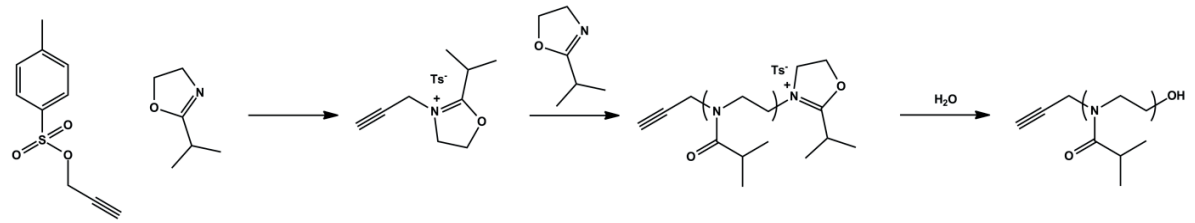

Scheme S2: Synthesis of alkyne-functionalized P*i*PrOx *via* CROP initiated by propargyl *p*-toluenesulfonate.

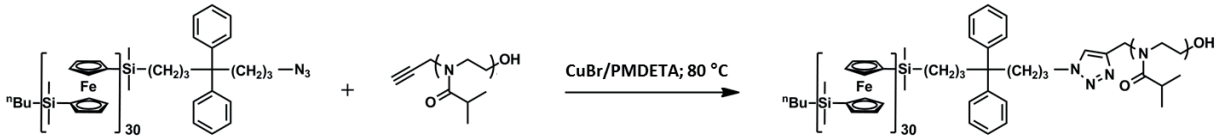

Scheme S3: Copper catalyzed azide-alkyne cycloaddition (CuAAC) between PFDMS$_{30}$-N_3 and TB-P*i*PrOx$_x$.

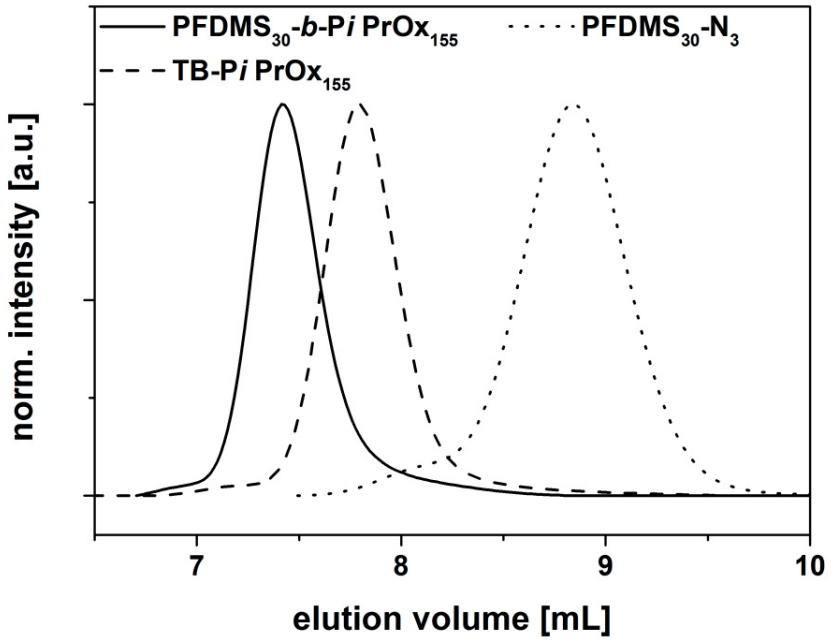

Figure S1: Comparison of SEC traces for PFDMS$_{30}$-N_3 (dotted line), TB-P*i*PrOx$_{155}$ (dashed line), and PFDMS$_{30}$-*b*-P*i*PrOx$_{155}$ (straight line).

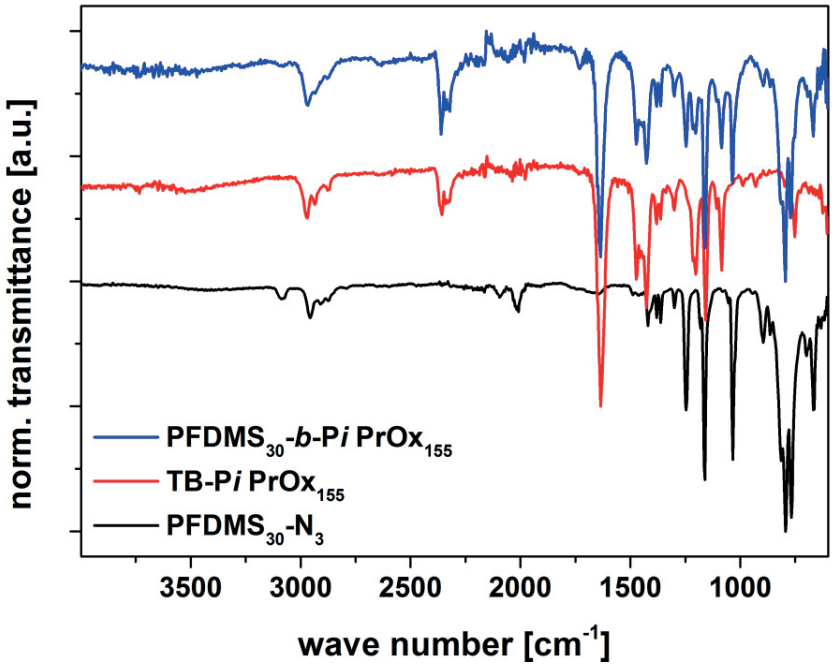

Figure S2: Comparison of FT-IR spectra for $PFDMS_{30}$-N_3 (black trace), TB-P*i*$PrOx_{155}$ (red trace), and $PFDMS_{30}$-*b*-P*i*$PrOx_{155}$ (blue trace).

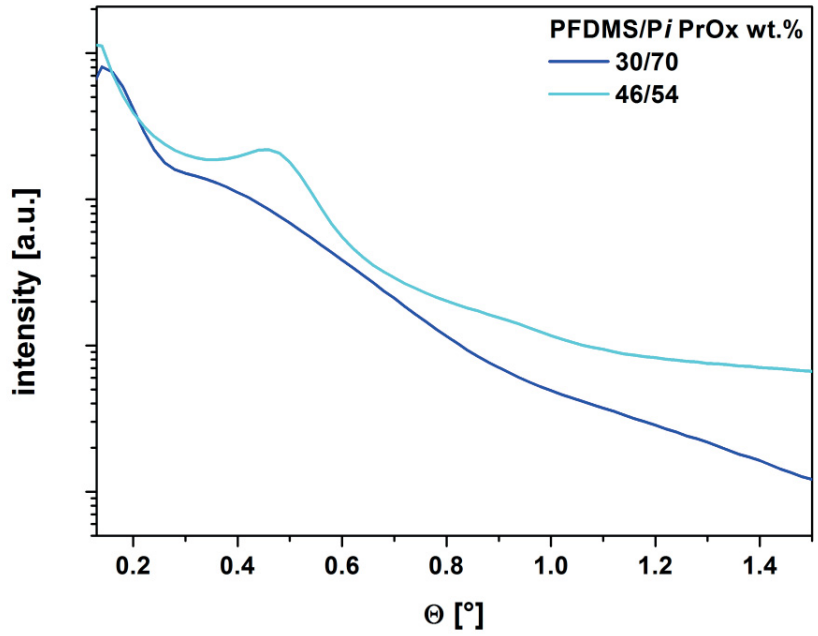

Figure S3: Comparison of SAXS data for $PFDMS_{30}$-*b*-P*i*$PrOx_{155}$ (cyan trace) and $PFDMS_{30}$-*b*-P*i*$PrOx_{75}$ (blue trace).

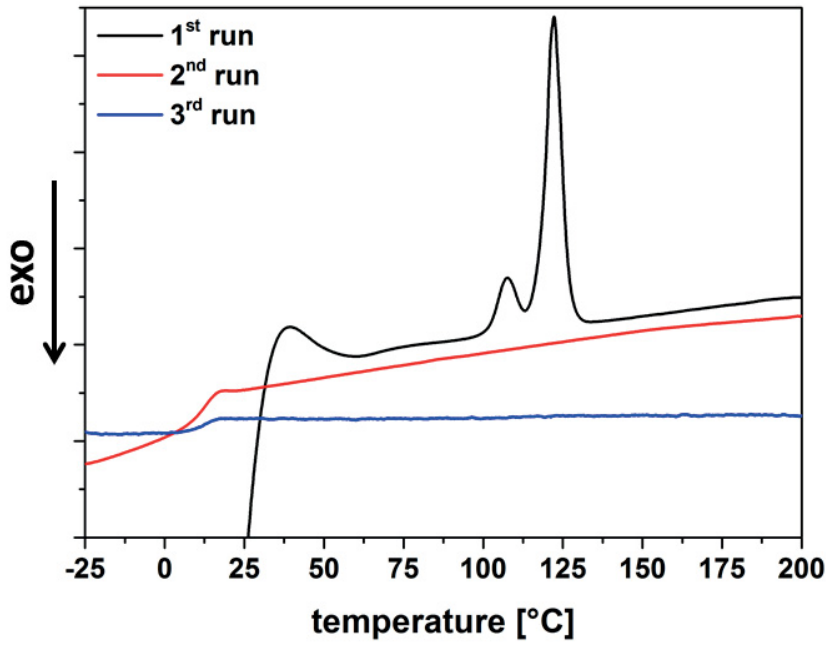

Figure S4: Comparison of DSC traces for $PFDMS_{30}$-N_3 first (20 K min^{-1}; black trace), second (20 K min^{-1}; black trace; T_g = 11 °C) and third (10 K min^{-1}; red trace; T_g = 12 °C) heating run in the range of -25 to 200 °C.

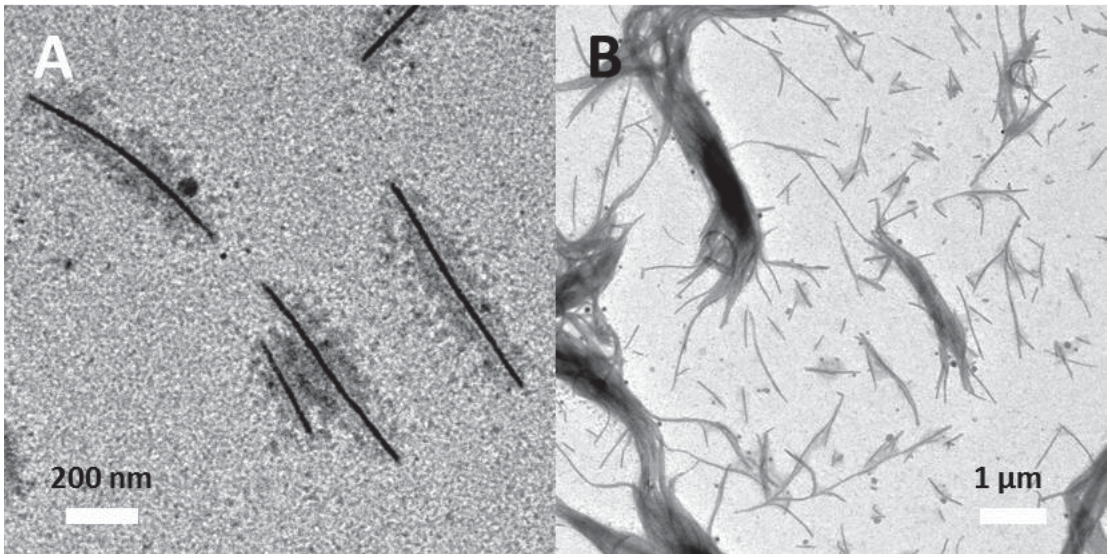

Figure S5: TEM micrographs of $PFDMS_{30}$-*b*-P*i*PrOx_{75} from acetone (1 mg mL^{-1}).

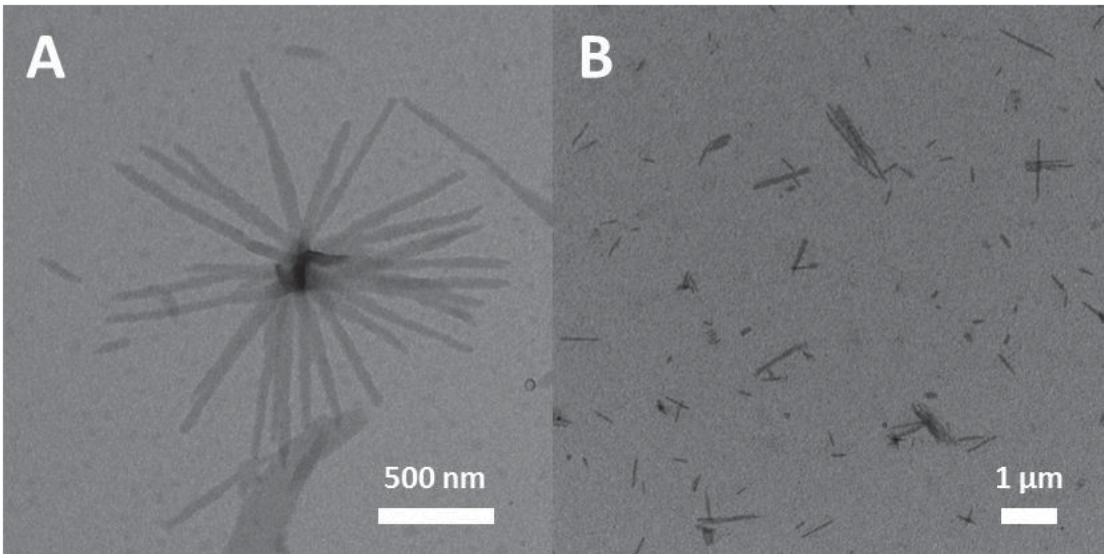

Figure S6: TEM micrographs of $PFDMS_{30}$-*b*-P*i*$PrOx_{155}$ from acetone (1 mg mL^{-1}).

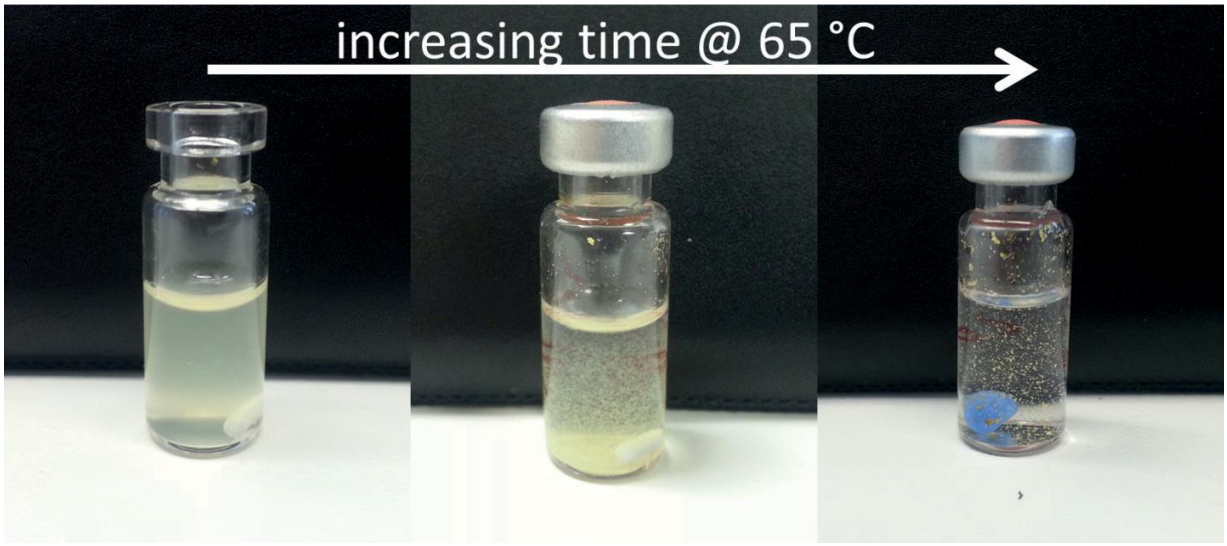

Figure S7: Photographs of micellar solutions upon heating and the formation of macroscopic aggregates for $PFDMS_{30}$-*b*-P*i*$PrOx_{75}$.

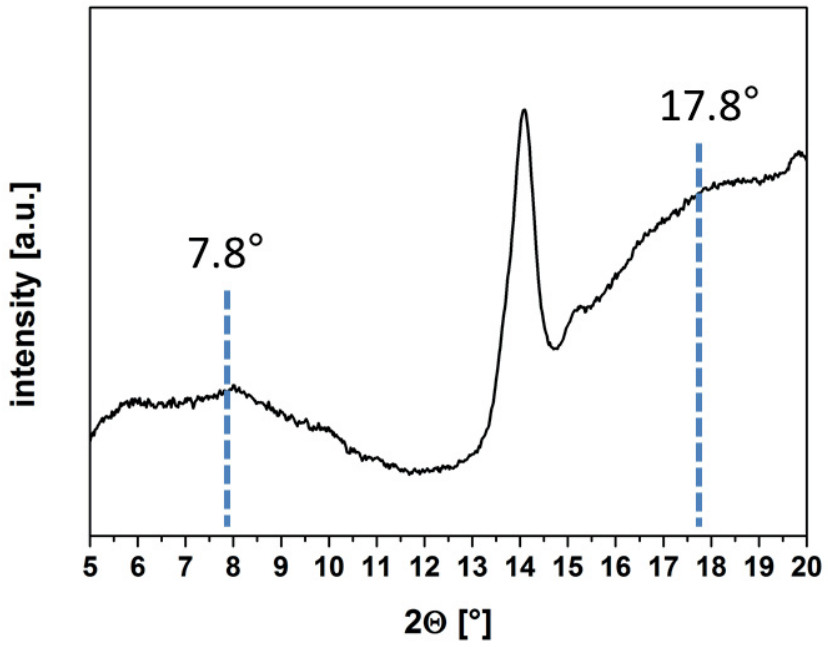

Figure S8: WAXS diffractogram of $PFDMS_{30}$-*b*-P*i*$PrOx_{75}$ after crystallization in water at 65 °C for 24 hours (lines indicates supposed position of reflexes for crystalline PiPrOx).

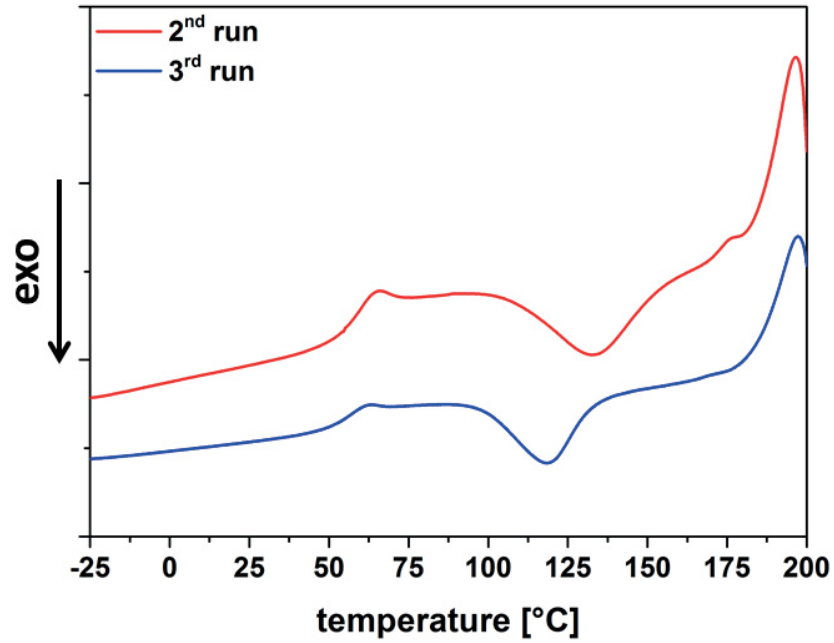

Figure S9: Comparison of DSC traces for P*i*$PrOx_{75}$ for the second (20 K min^{-1}; black trace; T_g = 57 °C) and third (10 K min^{-1}; red trace; T_g = 55 °C) heating run in the range of -25 to 200 °C.

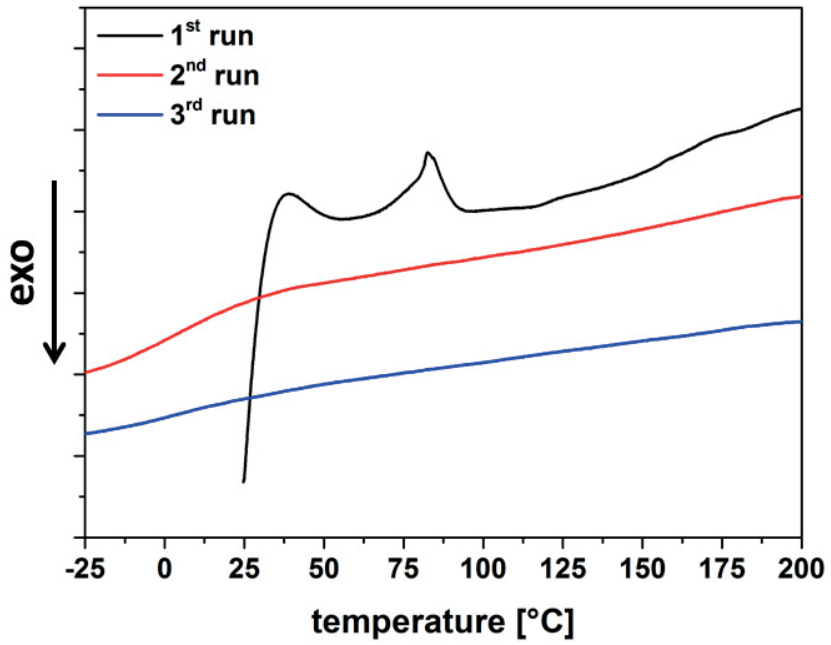

Figure S10: Comparison of DSC traces for PFDMS$_{30}$-*b*-P*i*PrOx$_{75}$ for the first (20 K min^{-1}; black trace), second (20 K min^{-1}; red trace) and third (10 K min^{-1}; blue trace) heating run in the range of -25 to 200 °C.

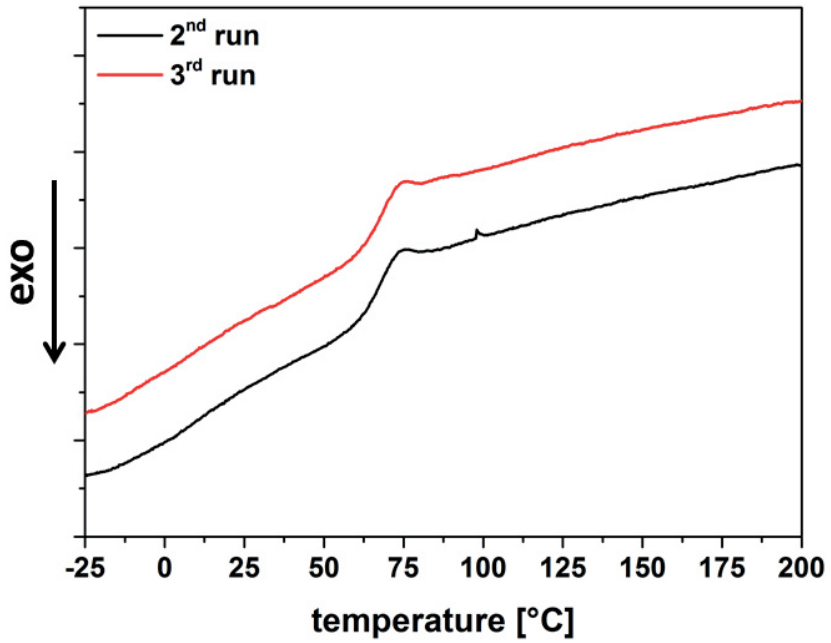

Figure S11: Comparison of DSC traces for PFDMS$_{30}$-*b*-P*i*PrOx$_{155}$ for the second (20 K min^{-1}; black trace; T_g = 68 °C) and third (10 K min^{-1}; red trace; T_g = 67 °C) heating run in the range of -25 to 200 °C.

Publication P6

“Towards Anisotropic Hybrid Materials: Solution Self-Assembly of Linear Polyethylene-*block*-poly(2-(4-((*tert*-butoxycarbonyl)amino)butyl-2-oxazoline)–*block*-poly(2-*iso*-propyl-2-oxazoline) Triblock Terpolymers”

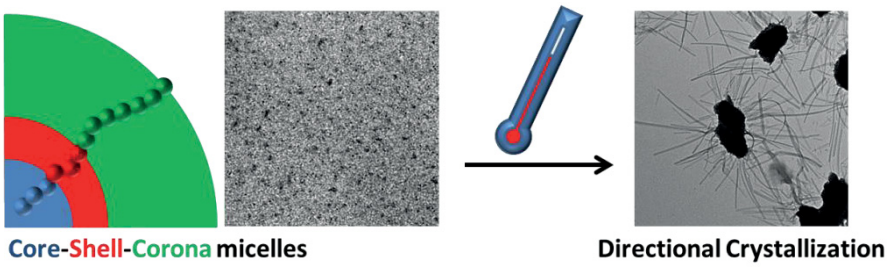

Tobias Rudolph, Matthias Hartlieb, Moritz von der Lühe, Ulrich S. Schubert, Franck DAgosto, Felix H. Schacher

in preparation

Towards Anisotropic Hybrid Materials: Solution Self-Assembly of Linear Polyethylene-*block*-poly(2-(4-((*tert*-butoxycarbonyl)amino)butyl-2-oxazoline)–*block*-poly(2-*iso*-propyl-2-oxazoline) Triblock Terpolymers

Tobias Rudolph,[1,2] Matthias Hartlieb,[1,2] Moritz von der Lühe,[1,2] Sebastien Norsic,[3] Ulrich S. Schubert,[1,2] Franck D´Agosto,[3] Felix H. Schacher[1,2,*]

[1] Laboratory of Organic and Macromolecular Chemistry, Friedrich Schiller University Jena, Humboldtstr. 10, D-07743 Jena, Germany

E-mail: felix.schacher@uni-jena.de

[2] Jena Center for Soft Matter (JCSM), Friedrich Schiller University Jena, Philosophenweg 7, D-07743 Jena, Germany

[3] Université de Lyon, Univ. Lyon 1, CPE Lyon, CNRS UMR 5265 Laboratoire de Chimie, Catalyse, Polyméres et Procédés (C2P2), Equipe LCPP, Bat 308F, 43 Bd du 11 novembre 1918, F-69616 Villeurbanne, France

Keywords: Triblock terpolymer, poly(2-alkyl-2-oxazoline)s, self-assembly, crystallization, fiber-like micelles

Abstract

We present the design and synthesis of a linear ABC triblock terpolymer for the bottom-up synthesis of anisotropic organic/inorganic hybrid materials: polyethylene-*block*-poly(2-(4-((*tert*-butoxycarbonyl)amino)butyl-2-oxazoline)–*block*-poly(2-*iso*-propyl-2-oxazoline) (PE-*b*-PBocAmOx-*b*-*i*PrOx). The synthesis was realized *via* the covalent linkage of azide-functionalized polyethylene and alkyne functionalized poly(2-alkyl-2-oxazoline)-based diblock copolymers exploiting copper-catalyzed azide-alkyne cycloaddition (CuAAC) chemistry. After purification of the resulting triblock terpolymer, the middle block was deprotected, resulting in a primary amine in the side-chain. In the next step, solution self-assembly into core-shell-corona micelles in aqueous solution was investigated by dynamic light scattering (DLS) and transmission electron microscopy (TEM). Subsequent directional crystallization of the corona-forming block, poly(2-*iso*-propyl-2-oxazoline), led to the formation of anisotropic superstructures as demonstrated by, e.g., electron microscopy (SEM and TEM). We present hypotheses concerning the aggregation mechanism as well as first promising results regarding the selective loading of such anisotropic nanostructures with metal nanoparticles (Au, Fe_3O_4).

Introduction

Block copolymers are an intriguing class of materials as they offer direct access to nanostructures of various morphologies and, depending on the choice of monomers, the individual blocks can be selectively functionalized. Owing to the covalent linkage between the constituting segments and the fact that most polymers are not miscible, phase separation occurs in the bulk or in selective solvents.[1-4] In both cases size, shape, and spatial arrangement of the involved segments can be precisely controlled by the monomer sequence and the corresponding weight fractions.

If possible, block copolymers are typically synthesized *via* sequential polymerization of the respective monomers - however, for certain monomer combinations this is not possible and alternative strategies need to be established. One elegant way is to introduce reactive endgroups and use such macromolecular building blocks in suitable conjugation reactions to form block copolymers of linear or other architectures. One frequently reported example is the combination of alkyne- and azide-functionalities in copper-catalyzed azide-alkyne cycloaddition (CuAAC) reactions.[5-12] Using this approach the "polymerization" of monomers,[13] the introduction of endgroups,[14] the synthesis of block copolymers,[15, 16] or the formation of different macromolecular architectures has been shown.[17-21] As mentioned above, block copolymers show depending on their composition the ability to form micelles with different morphology, e.g. spherical or cylindrical micelles, induced by solvophobic behavior, stacking or crystallization in solution. [2, 22] The introduction of a crystallizable segment in block copolymers allows using directional crystallization as driving force for the formation of anisotropic structures in solution. This has been shown for, e.g. ferrocenyl- and polyethylene-based materials in selective solvents.[23-27] In case of poly(ferrocenyldimethylsilane)s (PFDMS) concepts for control over micellar architecture, size, and corona compartmentalization were established by Manners and coworkers for a variety

of block copolymers. Moreover, micellar size could be tuned by ultrasonication, and sequential epitaxial growth of diblock copolymer unimers as a model system for living supramolecular polymerization could be achieved. Beside cylindrical micelles, recently multidimensional superstructures of amphiphilic PFDMS-based block copolymers have been described.[28] This concept could also be extended to polyethylene containing triblock terpolymers by Schmalz and coworkers.[26] In this context, another interesting semi-crystalline polymer is poly(2-*iso*-propyl-2-oxazoline) (P*i*PrOx), which shows directional growth into fiber-like structures upon heating above the LCST in aqueous media.[29-31]

Complexation of metals in polymers leads to the formation of new hybrid materials, which combine the physical properties of the polymer and inorganic material.[32-34] Beside the direct incorporation of metal ions into monomers like in case of PFDMS-based materials, certain polymers have the ability to attract or stabilize metal nanoparticles.[35, 36] Typically, polyelectrolytes such as poly(ethyleneimine) (PEI)[37] or poly(acrylic acid) (PAA) are used,[38] or non-ionic materials featuring nitrogen or oxygen atoms along the polymer chains.[36] The combination of both approaches, the formation of anisotropic superstructures by directed crystallization and the access to organic/inorganic hybrid materials *via* complexation of metal nanoparticles within block copolymer nanostructures, is particularly attractive. In that way, the synthesis of anisotropic hybrid materials with feature sizes typically not accessible by top-down approaches can be realized and prospective applications in nanoelectronics or as biochemical and optical sensors can be envisioned.[39-41]

Herein, we demonstrate the synthesis of polyethylene-*block*-poly(2-(4-((*tert*-butoxycarbonyl)amino)butyl-2-oxazoline)-*block*-poly(2-*iso*-propyl-2-oxazoline) (PE-*b*-PBocAmOx-*b*-*i*PrOx) using a combination of catalytic olefin polymerization, cationic ring-

opening polymerization, and copper-catalyzed azide-alkyne cycloaddition (CuAAC) click reactions. The middle block, PBocAmOx, can be selectively deprotected, introducing a primary amine in the side-chain (PAmOx). In the next step, we investigated the solution self-assembly in selective solvents and demonstrate the formation of core-shell-corona micelles by dynamic light scattering (DLS) and transmission electron microscopy (TEM). Subsequently, directional crystallization of the corona-forming block, poly(2-*iso*-propyl-2-oxazoline), can be used to form anisotropic superstructures of the initial spherical building blocks. Depending on whether PBocAmOx or PAmOx forms the middle segments, differences in the self-assembly mechanism or the resulting morphologies are highlighted. Further, selective introduction of gold and iron nanoparticles into the PAmOx domains shows the potential of the herein demonstrated approach for the formation of extended hybrid nanowires.

Results and Discussion

The aim was to use a two-step approach for the solution self-assembly of triblock terpolymers into anisotropic nanostructures, which can then be selectively loaded using metal ions or metal nanoparticles. For this, we designed a poly(ethylene)-*block*-poly(2-(4-((*tert*-butoxycarbonyl)amino)butyl-2-oxazoline)-*block*-poly(2-*iso*-propyl-2-oxazoline) (PE-*b*-PBocAmOx-*b*-P*i*PrOx) triblock terpolymer (Scheme 1). In a first step, self-assembly in water as selective solvent leads to the formation of core-shell-corona micelles with a PE core, a PBocAmOx shell and a P*i*PrOx corona. Subsequent heating above the LCST of P*i*PrOx is then supposed to induce directional crystallization and the formation of anisotropic superstructures. The middle block, PBocAmOx, can be transformed into poly(2-(4-amino)butyl-2-oxazoline) (PAmOx) and used for the complexation of metal ions afterwards. For the synthesis of PE-*b*-PBocAmOx-*b*-P*i*PrOx, we used an azide-functionalized PE in combination with alkyne-functionalized PBocAmOx-*block*-PiPrOx diblock copolymers in copper-catalyzed azide-alkyne cycloaddition (CuAAC) reactions.

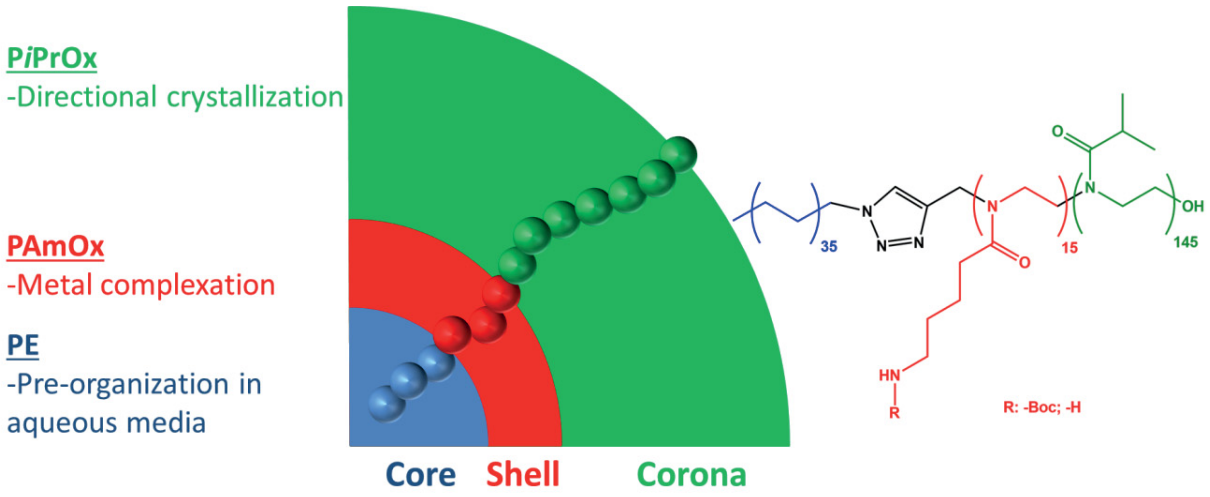

Scheme 1: Illustration of the designed PE-*b*-PBocAmOx-*b*-P*i*PrOx triblock terpolymer and brief task associated with each block.

Synthesis of azide functionalized polyethylene (PE-N_3)

Azide-functionalized poly(ethylene) (PE_{35}-N_3 – the subscript denotes the degree of polymerization) was synthesized *via* catalyzed chain shuttling polymerization of ethane using dipolyethylenylmagnesium compounds, followed by the introduction iodine. Afterwards, the iodide moiety is transferred into an azide endgroup using sodium azide (Scheme S1).[42] PE_{35}-N_3 was characterized by nuclear magnetic resonance spectroscopy (NMR), high temperature size exclusion chromatography (HT-SEC), and FT-IR (Figures S1-3). The degree of functionalization for PE-N_3 is in the range of 85%, while the molar mass was determined *via* NMR to be around 1000 g mol^{-1} (Figure S2). By FT-IR the characteristic azide peak at 2094 cm^{-1} was found, as well as CH_2 vibrations between 3000 - 2800 cm^{-1} (Figure S3).

Synthesis of alkyne-functionalized TB-PBocAmOx-b-PiPrOx diblock copolymer

The synthesis of the alkyne-functionalized poly(2-alkyl-2-oxazoline) counterpart was realized *via* sequential CROP of 2-(4-((*tert*-butoxycarbonyl)amino)butyl-2-oxazoline (BocAmOx)[43] and 2-*iso*-propyl-2-oxazoline (*i*PrOx) using established microwave-assisted techniques. For the introduction of an alkyne functionality propargyl *p*-toluenesulfonate (TB-Ts) was used as initiator in acetonitrile (ACN) at 140 °C. BocAmOx was polymerized at a concentration of 1M and a monomer to initiator ratio ([M]/[I]) of 15 (Scheme S2). Afterwards, an *i*PrOx stock solution (in ACN, [M]/[I] = 150) was added to the polymerization mixture (1M), and again placed in the microwave synthesizer at 140 °C. The polymerization was stopped by the addition of water, followed by precipitation in diethyl ether. The obtained materials were characterized *via* NMR, SEC, and FT-IR (Figure 1A; Figures S4 and S5). The degree of polymerization (DP) of the precursor (TB-PBocAmOx) was determined *via* NMR, confirming a DP of 15. For the block extension, SEC shows a shift of the elution trace for the block copolymer in comparison to TB-

PBocAmOx (Figure 1B). The composition of the block copolymer was determined in comparison to the characteristic BocAmOx signals in NMR, leading to TB-PBocAmOx$_{15}$-*b*-P*i*PrOx$_{145}$. The degree of polymerization for the second block is slightly lower compared to the [M]/[I] ratio of 150, presumably the monomer conversion was not quantitative as observed *via* NMR (Figure S4). Furthermore, the block copolymer was investigated *via* FT-IR, showing signals for the amide at 3300 cm^{-1}, for the carbonyl of the protective group at 1705 cm^{-1}, for the amide at 1516 cm^{-1}, and an increase in the region of methyl groups (1365 cm^{-1}; Figure S5).

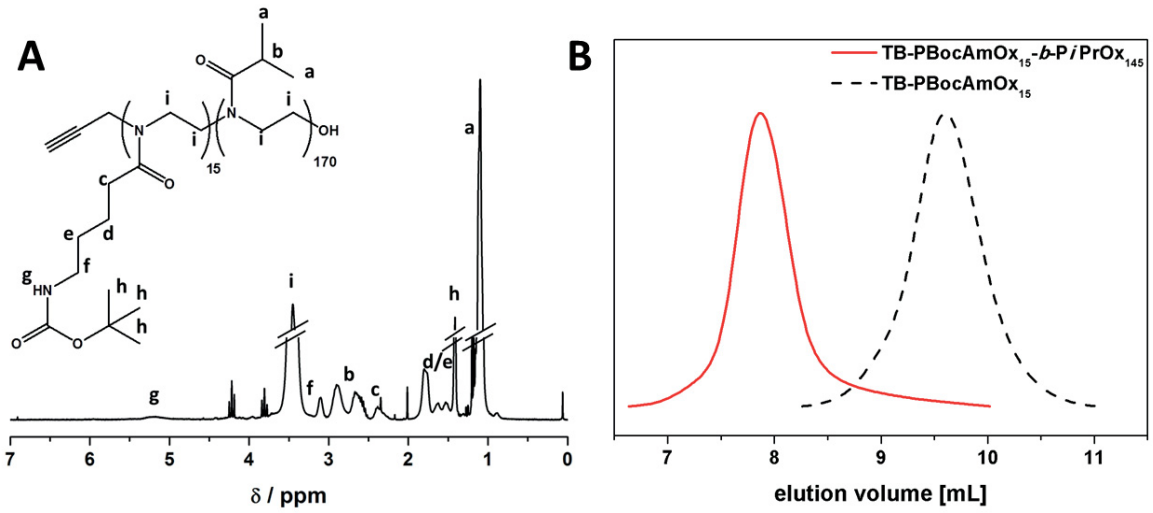

Figure 1: A) ^{1}H-NMR spectrum for TB-PBocAmOx$_{15}$-*b*-P*i*PrOx$_{145}$ and peak assignment (300 MHz; $CDCl_3$); B) comparison of SEC traces for TB-PBocAmOx$_{15}$ (dashed line) and TB-PBocAmOx$_{15}$-*b*-P*i*PrOx$_{145}$ (straight line).

CuAAC reaction between PE$_{35}$-N$_3$ and TB-PBocAmOx$_{15}$-b-PiPrOx$_{145}$

For the copper-catalyzed azide-alkyne cycloaddition (CuAAC) reaction between PE$_{35}$-N$_3$ and TB-PBocAmOx$_{15}$-*b*-P*i*PrOx$_{145}$ both components were dissolved in THF (Figure 2A). PE$_{35}$-N$_3$ was added in an excess of 3 equivalents in comparison to the alkyne functionalities to ensure full conversion. The solution was degassed with argon, and N,N,N′,N″,N″-

pentamethyldiethylenetriamine (PMDETA; 2 eq.) and copper bromide (CuBr; 2 eq.) were added under argon flux. The sealed vial was heated for 1 hour at 120 °C as at this temperature PE is fully molten, and a clear green solution was observed. Afterwards, the reaction was allowed to cool to RT, diluted with dichloromethane (DCM) and mixed with water. The aqueous solution turned blue due to the presence of Cu^{2+}, while the organic phase turned clear. The organic phase was removed and filtered twice using syringe filters (PTFE, 0.45 µm), and precipitated into diethyl ether. The excess of PE-N_3 forms large aggregates and was removed by filtration, while the generated triblock terpolymer is well soluble due to the high poly(2-alkyl-2-oxazoline) (POx) content. The resulting triblock terpolymer was investigated *via* FT-IR, NMR and SEC. By FT-IR the disappearance of the azide peak (2094 cm^{-1}) was observed and new signals at 2916 and 2846 cm^{-1} corresponding to PE appear (Figures S6 and 7). By ^{1}H-NMR the triblock terpolymer shows a new signal at 1.25 ppm, again corresponding to PE, whereas the comparison with signals for the POx backbone (around 3.6 ppm) indicates an equimolar incorporation of PE. This was used for the determination of the composition, yielding the triblock terpolymer PE_{35}-*click*-$PBocAmOx_{15}$-*b*-P*i*$PrOx_{145}$ (Figure 2C; Figure S9). Due to interactions of PBocAmOx and the column material of the HT-SEC used, it was not possible to study these materials by this technique. SEC of PE_{35}-*click*-$PBocAmOx_{15}$-*b*-P*i*$PrOx_{145}$ was performed using either dimethylacetamide (DMAC) or chloroform ($CHCl_3$) as eluent. In both cases, the SEC traces show comparable molar masses as observed for $PBocAmOx_{15}$-*b*-P*i*$PrOx_{145}$ (Table 1; Figure S8). Nevertheless, we assume this to result from the rather low DP of the PE_{35}-N_3 segment. Also, as in later TEM studies no characteristic trapezoid aggregates as reported for the crystallization of PE were found (Figure S17), at this point we assume that contamination of the samples with PE_{35}-N_3 is negligible.[44]

Table1: Characterization of the herein used diblock copolymers and triblock terpolymers.

Polymer	$M_n^{theo,a}$ [g mol^{-1}]	M_n^{b} [g mol^{-1}]	$Đ^{b}$	M_n^{c} [g mol^{-1}]	$Đ^{c}$	Ratio hydrohilic/ hydrophobic [wt.%/wt.%]
TB-PBocAmOx$_{15}$-*b*-P*i*PrOx$_{145}$	20000	23500	1.08	28000	1.09	82/18
TB-PAmOx$_{15}$-*b*-P*i*PrOx$_{145}$	18500	-[d]	-[d]	29000	1.07	100/-
PE-*click*-PBocAmOx$_{15}$-*b*-P*i*PrOx$_{145}$	21000	24000	1.09	27000	1.11	78/22
PE-*click*-PAmOx$_{15}$-*b*-P*i*PrOx$_{145}$	19500	-[d]	-[d]	25000	1.06	95/5

a) Calculated from NMR; b) SEC ($CHCl_3$/*i*-PrOH/TEA) (PS-calibration); c) SEC (DMAC/LiCl) (PS-calibration); d) not determined due to interactions with the column material.

The next step was to remove the Boc protective group of PBocAmOx. The deprotection of PBocAmOx$_{15}$-*b*-P*i*PrOx$_{145}$ and PE$_{35}$-*click*-PBocAmOx$_{15}$-*b*-P*i*PrOx$_{145}$ was performed using trifluoroacetic acid (TFA, Figure 2A). After purification using an Amberlyst® resin, the resulting materials revealed no differences by SEC for PAmOx$_{15}$-*b*-P*i*PrOx$_{145}$, while in the case of PE$_{35}$-*click*-PAmOx$_{15}$-*b*-P*i*PrOx$_{145}$ a shift to higher elution volume in comparison to PE$_{35}$-*click*-PBocAmOx$_{15}$-*b*-P*i*PrOx$_{145}$ was found (Figure 2B). Both NMR and FT-IR confirmed the successful deprotection through disappearance of the characteristic signals for the Boc-group (Figure 2C; Figures S9, 10, 11 and 12). FT-IR measurements indicated the presence of small amounts of residual TFA after deprotection due to signals in the range of 1700 to 1800 cm^{-1}. Additional signals corresponding to the free amine can be observed in the fingerprint region (Figures S11 and 12).

All important characteristics for PE_{35}-*click*-$PAmOx_{15}$-*b*-P*i*$PrOx_{145}$, PE_{35}-*click*-$PBocAmOx_{15}$-*b*-P*i*$PrOx_{145}$, $PBocAmOx_{15}$-*b*-P*i*$PrOx_{145}$, and $PBocAmOx_{15}$-*b*-P*i*$PrOx_{145}$, including the respective hydrophilic to hydrophobic ratio are summarized in Table 1.

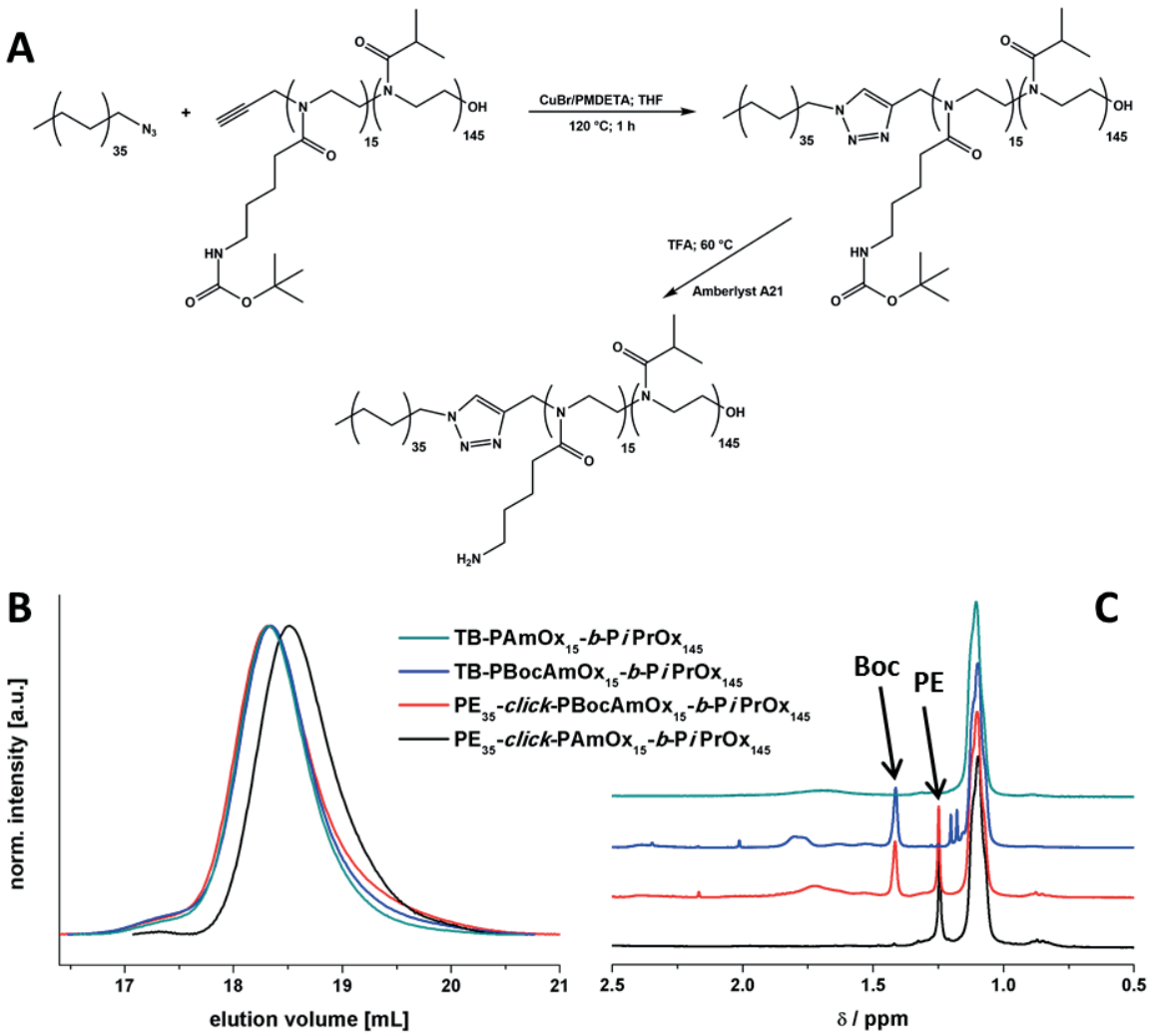

Figure 2: A) CuAAC cycloaddition reaction between PE_{35}-N_3 and TB-$PBocAmOx_{15}$-*b*-P*i*$PrOx_{145}$ toward PE_{35}-*click*-$PBocAmOx_{15}$-*b*-P*i*$PrOx_{145}$; sequential deprotection of the Boc group under acidic conditions; B) comparison of SEC traces for TB-$PBocAmOx_{15}$-*b*-P*i*$PrOx_{145}$ (cyan curve), TB-$PAmOx_{15}$-*b*-P*i*$PrOx_{145}$ (blue curve), PE_{35}-*click*-$PBocAmOx_{15}$-*b*-P*i*$PrOx_{145}$ (red curve), and PE_{35}-*click*-$PBocAmOx_{15}$-*b*-P*i*$PrOx_{145}$ (black curve); C) comparison of NMR spectra for TB-$PBocAmOx_{15}$-*b*-P*i*$PrOx_{145}$ (cyan curve), TB-$PAmOx_{15}$-*b*-P*i*$PrOx_{145}$ (blue curve), PE_{35}-*click*-$PBocAmOx_{15}$-*b*-P*i*$PrOx_{145}$ (red curve), and PE_{35}-*click*-$PBocAmOx_{15}$-*b*-P*i*$PrOx_{145}$ (black curve).

Solution behavior in water as selective solvent

We were now interested in the solution behavior of the materials in aqueous solution. Therefore, the materials were dissolved in a non-selective solvent, dimethylformamide (DMF), and heated for 10 minutes at 120 °C at a concentration of 1 mg mL^{-1} – at these conditions the triblock terpolymers exist as unimers as the PE block is above its melting point. After cooling the samples to room temperature, the solutions were dialyzed against water for 2 days (RC MWCO 1000 Da) to remove the DMF. We now anticipate the formation of core-shell-corona micelles featuring a PE core, a PBocAmOx or PAmOx shell, and a P*i*PrOx corona (Figure 3A). Both corresponding diblock copolymers could be directly dissolved in water. The resulting solutions were investigated *via* dynamic light scattering (DLS), transmission electron microscopy (TEM) and zeta-potential measurements. The hydrodynamic radius (R_h) according to DLS varies, depending on the copolymer composition. For PE_{35}-*click*-$PBocAmOx_{15}$-*b*-P*i*$PrOx_{145}$ and PE_{35}-*click*-$PAmOx_{15}$-*b*-P*i*$PrOx_{145}$, micelles with hydrodynamic radii of 17 nm (PE_{35}-*click*-$PBocAmOx_{15}$-*b*-P*i*$PrOx_{145}$) and 14 nm (PE_{35}-*click*-$PAmOx_{15}$-*b*-P*i*$PrOx_{145}$) are found. While $PAmOx_{15}$-*b*-P*i*$PrOx_{145}$ can be regarded as double hydrophilic and unimers with a R_h of 2 nm are found, $PBocAmOx_{15}$-*b*-P*i*$PrOx_{145}$ forms core-corona micelles with a R_h of 13 nm, where the core is formed by PBocAmOx and the corona consists of P*i*PrOx. TEM confirms the spherical shape of the core-shell-corona micelles in aqueous solution (Figure 3C). By zeta-potential measurements a value of -0.5 mV was found for PE_{35}-*click*-$PBocAmOx_{15}$-*b*-P*i*$PrOx_{145}$, while a slightly positive value of +8.5 mV was obtained for PE_{35}-*click*-$PAmOx_{15}$-*b*-P*i*$PrOx_{145}$ micelles (at pH7).

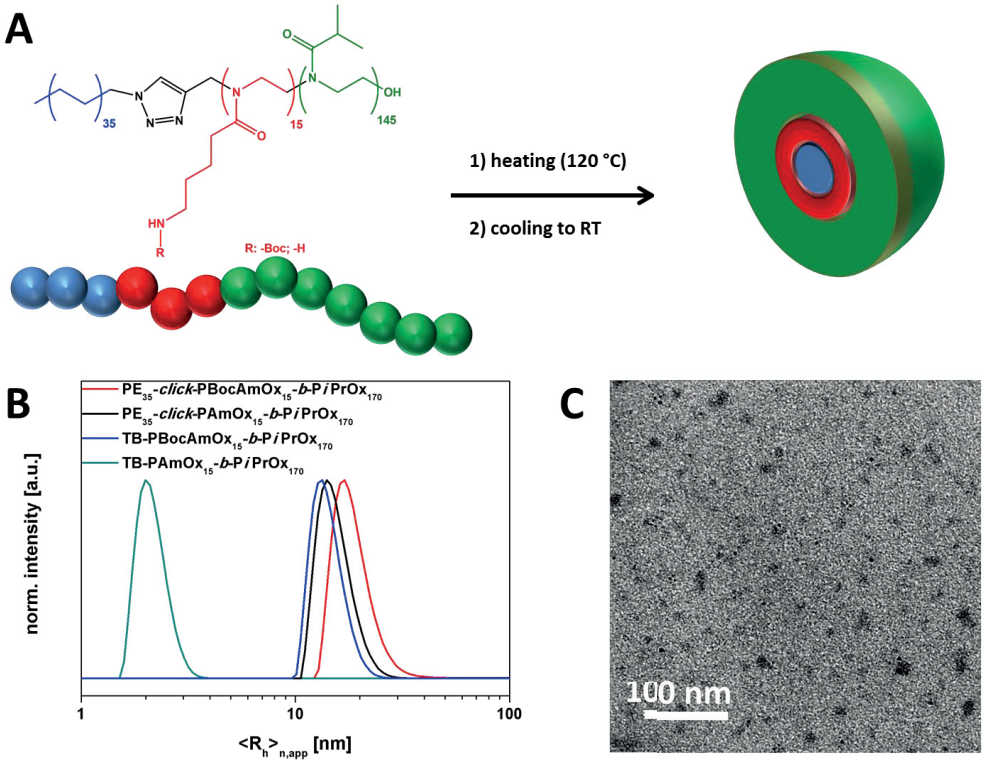

Figure 3: A) Illustration of micelle formation of PE_{35}-*click*-$PAmOx_{15}$-*b*-P*i*$PrOx_{145}$ or PE_{35}-*click*-$PBocAmOx_{15}$-*b*-P*i*$PrOx_{145}$ after heating and cooling in DMF;B) comparison of DLS size distributions for TB-$PBocAmOx_{15}$-*b*-P*i*$PrOx_{145}$ (blue curve; $<R_h>$ = 2 nm), TB-$PAmOx_{15}$-b-P*i*$PrOx_{145}$ (cyan curve; $<R_h>$ = 13 nm), PE_{35}-*click*-$PBocAmOx_{15}$-*b*-P*i*$PrOx_{145}$ (red curve; $<R_h>$ = 17 nm), and PE_{35}-*click*-$PAmOx_{15}$-*b*-P*i*$PrOx_{145}$ (black curve; $<R_h>$ = 14 nm); C) TEM micrograph for PE_{35}-*click*-$PAmOx_{15}$-*b*-P*i*$PrOx_{145}$ micelles in water (0.33 mg mL^{-1}).

Directional crystallization of PiPrOx

The crystallization of P*i*PrOx from aqueous solution upon heating above the cloud point temperature at 65 °C has been reported by Schlaad and coworkers. They proposed a combination of non-specific hydrophobic interactions and oriented dipolar interactions as main driving force.[29] Also, recent efforts by Dworak et al. have shown that P*i*PrOx crystallization can be achieved in organic media, such as acetonitrile or dimethylsulfoxide, as well.[45] Our aim was now to use the previously described core-shell-corona micelles with a P*i*PrOx corona as building blocks during directional crystallization.[29-31, 46] Initial investigations at concentrations of up to 20 mg mL^{-1}

resulted in rather rapid formation of a precipitate, and we therefore decreased the concentration to values between 0.33 and 0.1 mg mL^{-1} for all following investigations. The aqueous copolymer solutions were heated for 24 hours at 65 °C, and the scattering intensity of the micellar solutions was monitored by DLS. In all cases, the overall scattering intensity strongly increased within 1 minute, as 65 °C exceeds the cloud point temperature (T_{cp}) of P*i*PrOx. Afterwards, a further slight increase can be observed, followed by a sharp drop after 10 to 12 hours in case of PE_{35}-*click*-$PAmOx_{15}$-*b*-P*i*$PrOx_{145}$, while only a slight decrease can be seen for PE_{35}-*click*-$PAmOx_{15}$-*b*-P*i*$PrOx_{145}$ (Figure 4). The corresponding hydrodynamic radii for PE_{35}-*click*-$PAmOx_{15}$-*b*-P*i*$PrOx_{145}$ constantly increase until the respective correlation function shows more than one mode, leading to the assumption that two different aggregate populations coexist (Figure S13). Presumably, the P*i*PrOx chains initially collapse and form larger aggregates, which then start to crystallize until precipitation occurs. This observation has also been reported for linear P*i*PrOx upon crystallization within 10-12 hours, while afterwards the crystallization seems to "stop".[29-31, 46] On the other hand, for PE_{35}-*click*-$PBocAmOx_{15}$-*b*-P*i*$PrOx_{145}$, the aggregate size increases within 2 hours up to a plateau of ≈ 320 nm and no precipitation is observed. Similar behavior was observed for TB-$PAmOx_{15}$-*b*-P*i*$PrOx_{145}$, while in case of TB-$PBocAmOx_{15}$-*b*-P*i*$PrOx_{145}$ precipitation occurred within 10 hours (Figure S14).

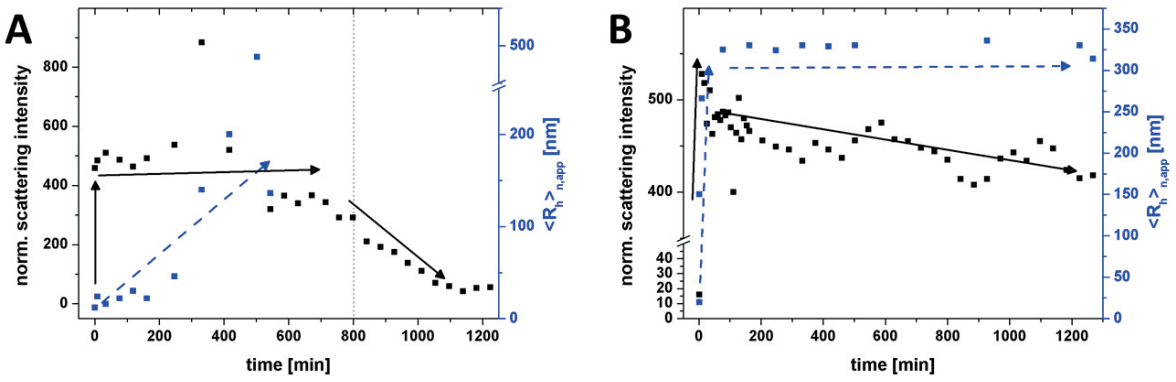

Figure 4: Normalized scattering intensity (black) and $<R_h>_{n,app}$ (blue) over time while the micellar solution was annealed at 65 °C (0.1 mg mL^{-1}) for PE$_{35}$-*click*-PAmOx$_{15}$-*b*-P*i*PrOx$_{145}$ (A) and PE$_{35}$-*click*-PBocAmOx$_{15}$-*b*-P*i*PrOx$_{145}$ (B).

From DLS results, a clear difference between the aggregates formed *via* crystallization of P*i*PrOx for the two investigated triblock terpolymers can be deduced. Therefore, samples after 24 hours at 65 °C in water were investigated *via* transmission electron microscopy (TEM). Depending on the colloidal stability of the solution, TEM samples were prepared by direct drop-casting from solution (PE$_{35}$-*click*-PBocAmOx$_{15}$-*b*-P*i*PrOx$_{145}$ and TB-PAmOx$_{15}$-*b*-P*i*PrOx$_{145}$) or by re-dispersing the precipitate (for PE$_{35}$-*click*-PAmOx$_{15}$-*b*-P*i*PrOx$_{145}$ and TB-PBocAmOx$_{15}$-*b*-P*i*PrOx$_{145}$) and subsequent drop-casting. In both cases, plasma treated carbon coated TEM grids were used.

For PE$_{35}$-*click*-PBocAmOx$_{15}$-*b*-P*i*PrOx$_{145}$, the material featuring the highest hydrophobic weight fraction, cylindrical micelles of several hundred nm length, also emanating from bigger agglomerates (Figures 5B and C) were found by TEM and scanning electron microscopy (SEM; Figure 5D). The average width of the aggregates was determined by grey scale analysis of 100 individual cylinders, leading to 27 +/- 4 nm (Figure 5E). Therefore, we assume a fusion of initially spherical micelles (R_h = 17 nm, diameter ~ 34 nm) upon heating. The annealing temperature of 65 °C is at the same time above the glass transition temperature (T_g) of PBocAmOx (≈40 °C)[43] and the melting temperature (T_m) of PE (≈50 °C), thereby increasing chain mobility for both hydrophobic blocks. Crystallization of the P*i*PrOx corona then leads to unidirectional growth of the aggregates (Figure 5A).

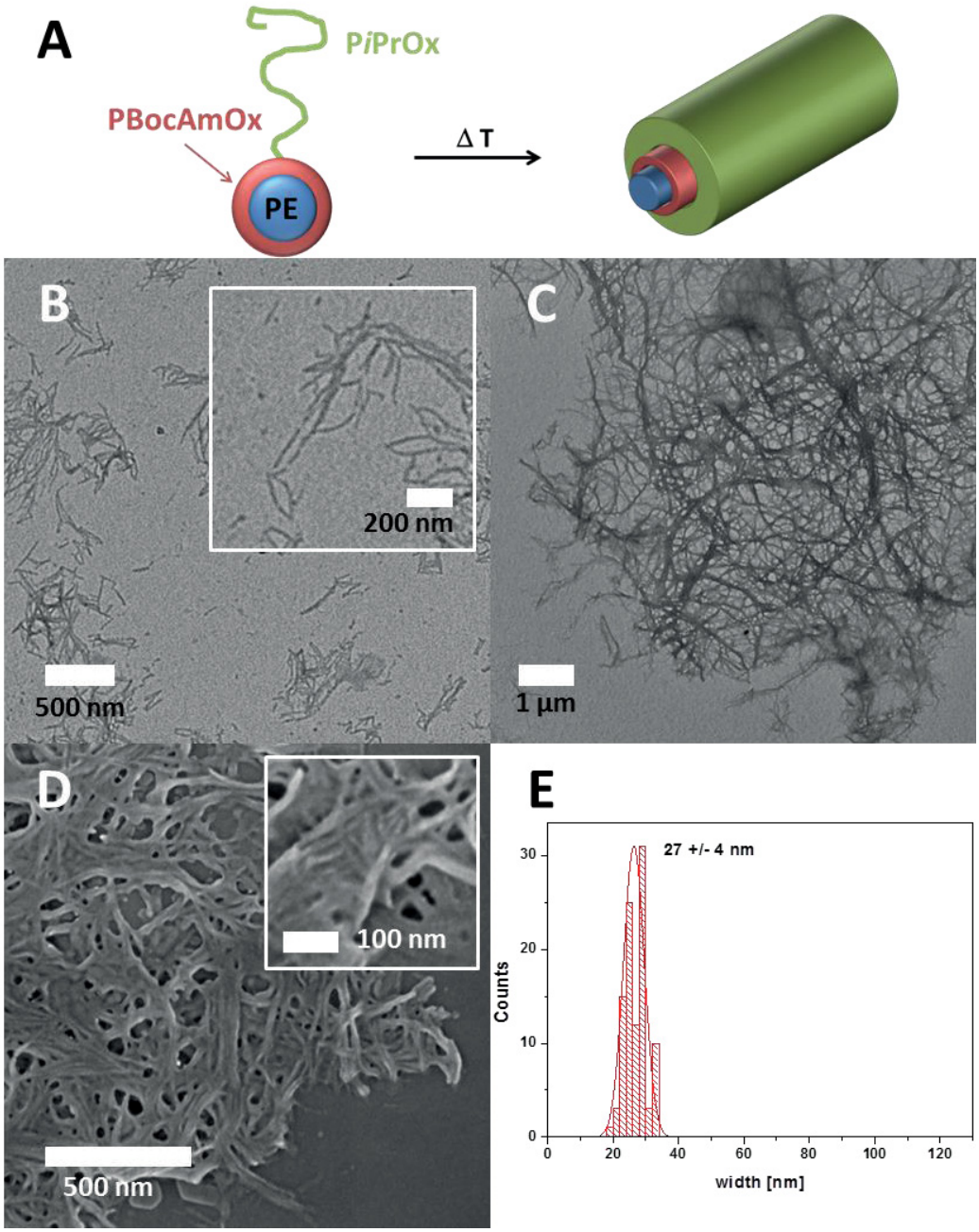

Figure 5: A) Illustration of the aggregation mechanism of PE_{35}-*click*-$PBocAmOx_{15}$-*b*-P*i*$PrOx_{145}$ after directional crystallization of P*i*PrOx; B) and C) TEM micrographs of PE_{35}-*click*-$PBocAmOx_{15}$-*b*-P*i*$PrOx_{145}$ from aqueous solution after heating to 65 °C for 24 hours; D) SEM micrograph of PE_{35}-*click*-$PBocAmOx_{15}$-*b*-P*i*$PrOx_{145}$ from aqueous solution after heating to 65 °C for 24 hours; E) histogram of width distribution determined for cylindrical micelles as determined by grey-scale analysis from TEM micrographs.

While for PE_{35}-*click*-$PBocAmOx_{15}$-*b*-P*i*$PrOx_{145}$ the cylinder length of the micelles was rather short (50 nm – 1000 nm) and mostly individual assemblies were found. PE_{35}-*click*-$PAmOx_{15}$-*b*-

P*i*PrOx$_{145}$ formed long crystalline fibers of several µm (Figure 6B and C). Beside the fiber-like structures, "wool" like aggregates (darker areas observed by TEM; Figure S15) with diameter of 0.5 to 4 µm were found.[30] These structures were investigated by TEM and SEM matching to the observations described by Schlaad and coworkers (Figures 6D, S15 and 16). Again, we used grey-scale analysis to determine the width distribution for the cylinders and found 71 +/- 15 nm and varies along the crystal (Figure 6D). Due to the differences observed in DLS and TEM, we assume a slightly different mechanism for the crystallization of P*i*PrOx. First, PE$_{35}$-*click*-PAmOx$_{15}$-*b*-P*i*PrOx$_{145}$, features a lower hydrophobic weight fraction (5 wt.%) in comparison to PE$_{35}$-*click*-PBocAmOx$_{15}$-*b*-P*i*PrOx$_{145}$ (22 wt.%) and, second, the positively charged PAmOx segment might lead to an inversion of the core-shell-corona micelle at higher temperatures. The predicted corresponding pK_a value of the 4-aminobutyl moiety should be ≈ 10, therefore should be protonated to a certain extent at pH 7.[47, 48] In this case, upon heating above the LCST P*i*PrOx forms the micellar core, partially incorporating the PE segment. PAmOx forms the corona, presumably as short loops (Figure 6A). Further heating then leads to crystallization of P*i*PrOx and the formation of cylindrical superstructures with a cationically charged outer layer.

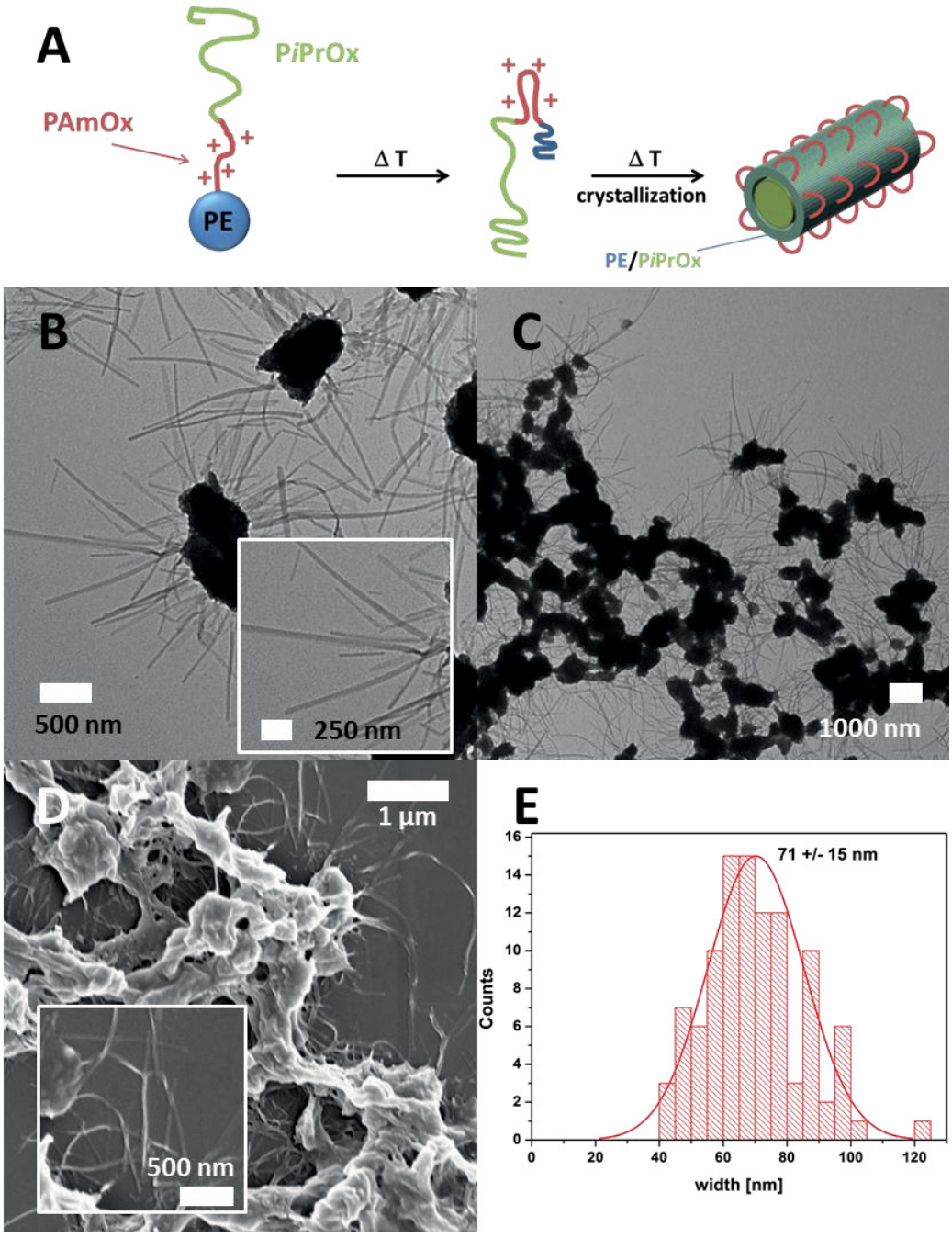

Figure 6: A) Illustration of the aggregation mechanism of PE_{35}-*click*-$PAmOx_{15}$-*b*-P*i*$PrOx_{145}$ after directional crystallization of P*i*PrOx; B) and C) TEM micrographs of PE_{35}-*click*-$PAmOx_{15}$-*b*-P*i*$PrOx_{145}$ from aqueous solution after heating to 65 °C for 24 hours; D) SEM micrograph of PE_{35}-*click*-$PAmOx_{15}$-*b*-P*i*$PrOx_{145}$ from aqueous solution after heating to 65 °C for 24 hours; E) histogram of width distribution determined for cylindrical micelles determined by grey-scale analysis from TEM micrographs.

To probe whether the pH plays a significant role for the aggregation mechanism, PE_{35}-*click*-$PAmOx_{15}$-*b*-P*i*$PrOx_{145}$ was heated to 65 °C for 24 h at pH 12. Afterwards, aggregates with

comparable size and shape as shown earlier at pH 7 can be observed (Figure S16). The width remains almost constant with 68 +/- 19 nm (Figure S17). It seems that the increased hydrophilicity of the PAmOx block is sufficient to influence the aggregation mechanism even at pH-values where the amino group is not in its protonated state.

For comparison, we also investigated the directional crystallization for both corresponding diblock copolymers, PBocAmOx$_{15}$-*b*-P*i*PrOx$_{145}$ and PAmOx$_{15}$-*b*-P*i*PrOx$_{145}$, under the same conditions. Whereas TB-PBocAmOx$_{15}$-*b*-P*i*PrOx$_{145}$ represents an amphiphilic material and a comparable aggregation mechanism can be assumed as discussed for PE$_{35}$-*click*-PAmOx$_{15}$-*b*-P*i*PrOx$_{145}$ earlier, in case of TB-PAmOx$_{15}$-*b*-P*i*PrOx$_{145}$ block copolymer unimers are initially present. In the latter case, directional crystallization of P*i*PrOx results in the formation of core-corona fibers with a polycationic outer layer (Figure 7A and B). The TEM micrographs show similar length and size distributions for the aggregates formed from TB-PBocAmOx$_{15}$-*b*-P*i*PrOx$_{145}$ and TB-PAmOx$_{15}$-*b*-P*i*PrOx$_{145}$. Grey-scale analysis revealed diameters of 64 +/- 13 nm and 52 +/- 12 nm, respectively (Figures 7C-F; Table 2).

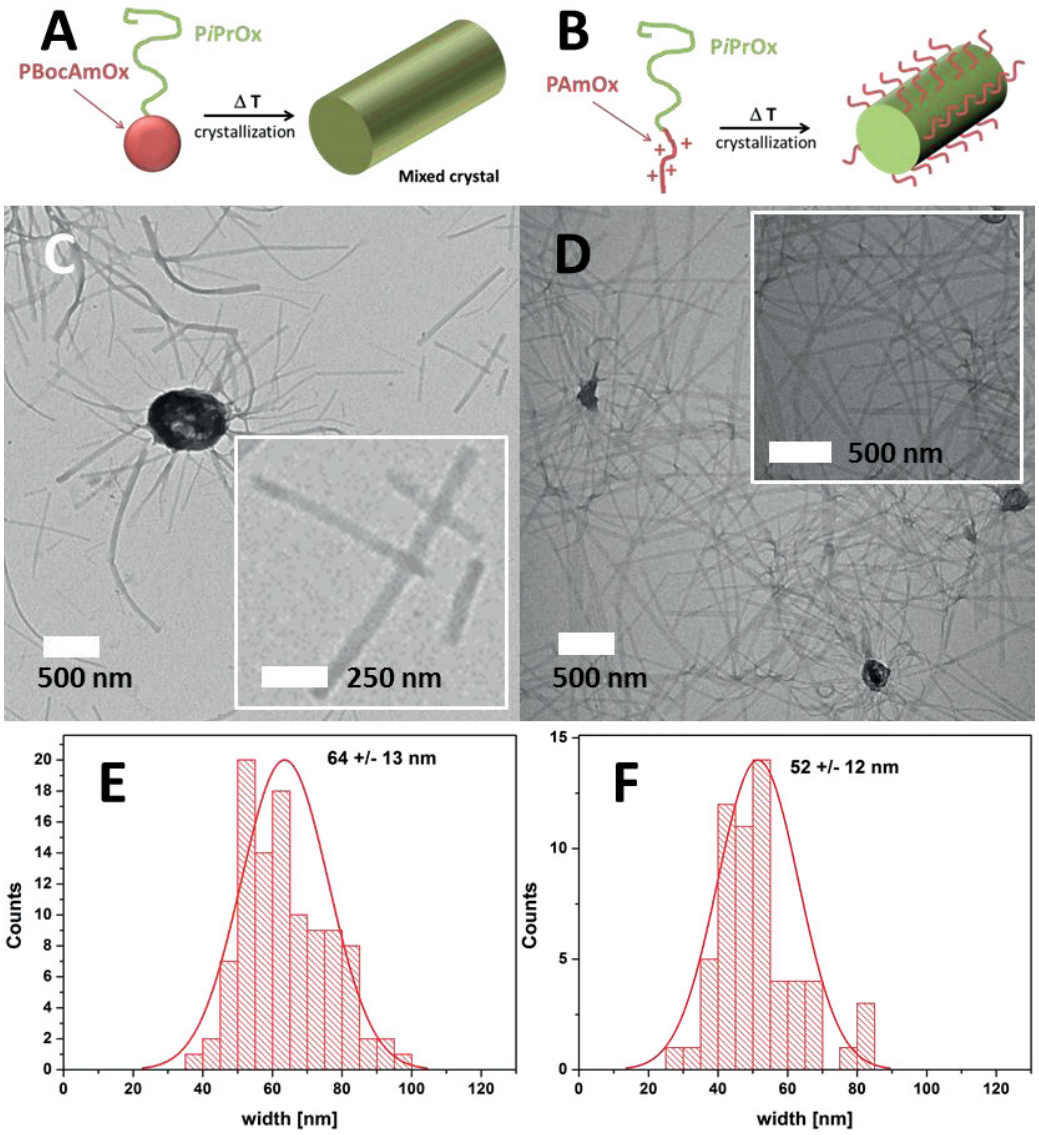

Figure 7: A) Proposed aggregation mechanism of PBocAmOx$_{15}$-*b*-P*i*PrOx$_{145}$ after directional crystallization of P*i*PrOx; B) proposed aggregation mechanism of PAmOx$_{15}$-*b*-P*i*PrOx$_{145}$ after directional crystallization of P*i*PrOx; C) TEM micrograph of PBocAmOx$_{15}$-*b*-P*i*PrOx$_{145}$ from aqueous solution after heating to 65 °C for 24 hours; D) TEM micrograph of PAmOx$_{15}$-*b*-P*i*PrOx$_{145}$ from aqueous solution after heating to 65 °C for 24 hours; histogram of width distribution determined for cylindrical micelles determined by grey-scale analysis from TEM micrographs for PBocAmOx$_{15}$-*b*-P*i*PrOx$_{145}$ (E) and PBocAmOx$_{15}$-*b*-P*i*PrOx$_{145}$ (F).

Table 2: Characteristics for the diblock copolymers and triblock terpolymers obtained by DLS before and TEM after directional crystallization of P*i*PrOx

Polymer	Hydrophilic	$\langle R_h \rangle_{n,app}$[b] [nm]	Crystal width[c] [nm]

	part[a] [wt.%]		
TB-PAmOx$_{15}$-*b*-P*i*PrOx$_{145}$	100	2	52 +/- 12
PE$_{35}$-*click*-PAmOx$_{15}$-*b*-P*i*PrOx$_{145}$	95	14	71 +/- 15
TB-PBocAmOx$_{15}$-*b*-P*i*PrOx$_{145}$	82	13	64 +/- 13
PE$_{35}$-*click*-PBocAmOx$_{15}$-*b*-P*i*PrOx$_{145}$	78	17	27 +/- 4

a) Calculated according to the block copolymer composition; b) DLS, CONTIN plot; 25 °C before heating; c) average width size determined from TEM micrographs by grey-scale analysis at 100 different positions after directional crystallization of P*i*PrOx.

We were now aiming at incorporating metal nanoparticles within the PAmOx part of the above described anisotropic superstructures. Therefore, we added either as-synthesized Fe_3O_4-nanocrystals with a diameter of 6 nm (obtained by an adopted literature protocol by pyrolyzing tris(acetylacetonato)iron(III) ($Fe(acac)_3$) in N-vinyl-2-pyrrolidone at 200 °C in the microwave, Figure S20)[49] or $HAuCl_4$ to micellar solutions of PE$_{35}$-*click*-PAmOx$_{15}$-*b*-P*i*PrOx$_{145}$ in water. After stirring for 12 hours (in the dark in case of $HAuCl_4$) the solutions were dialyzed against water for 2 days. In case of $HAuCl_4$, 0.1 and 10 equivalents of precursor/AmOx ratios (Au/AmOx) were tested. Afterwards, heating for 24 hours at 65 °C led to the formation of a precipitate as already discussed above. In case of $HAuCl_4$, subsequent reduction using sodium borohydride ($NaBH_4$) after the heating procedure resulted in the formation of Au NP. The hybrid structures from the coagulate were investigated *via* TEM by re-dispersing and drop-casting the solution onto TEM grids. As can be seen, anisotropic cylindrical superstructures were found in both cases. At higher magnification, increased attachment of the respective Au or Fe_3O_4 NPs to the fiber surface is visible. In case of Au NP, dark spots with a size of several nm can be found (Figure 8C; arrows indicate dark spots along the fiber; Figure S19). By UV-Vis, a slight absorption between 500-800 nm (absorbance maximum ≈ 555 nm) indicates the presence of Au

NP (Figure 8B).[37, 50] Similar results were observed, if $HAuCl_4$ was reduced before or after the directional crystallization of P*i*PrOx. For the Fe_3O_4 nanocrystals, again preferential location within the outer layer of the anisotropic superstructures can be observed in TEM (Figure 8D; arrows guide the eye to NP positions; Figure S20).

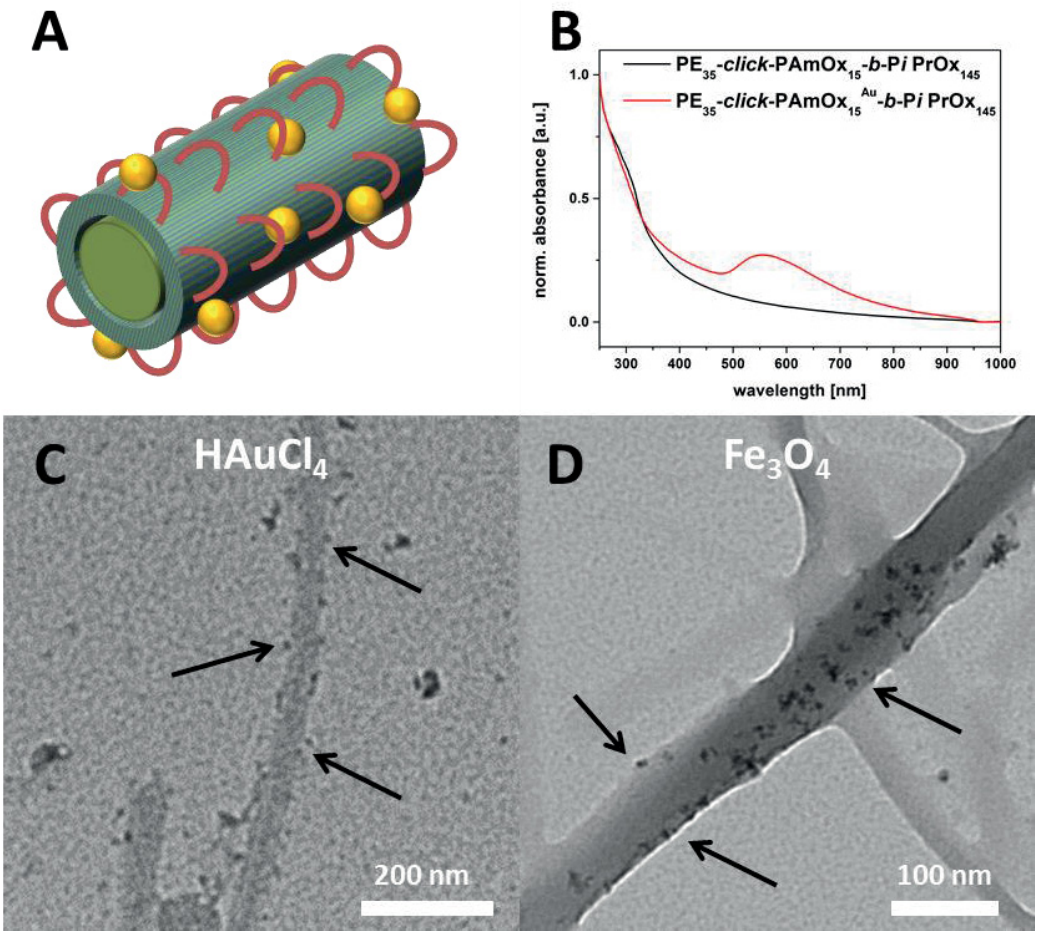

Figure 8: A) Anisotropic hybrid cylinders of PE_{35}-*click*-$PAmOx_{15}$-b-P*i*$PrOx_{145}$ and metal nanoparticles; B) comparison of UV-Vis spetra for PE_{35}-*click*-$PAmOx_{15}$-*b*-P*i*$PrOx_{145}$ (black trace) and PE_{35}-*click*-$PAmOx_{15}^{Au}$-*b*-P*i*$PrOx_{145}$ (red trace); TEM micrographs of PE_{35}-*click*-$PAmOx_{15}$-*b*-P*i*$PrOx_{145}$ fibers with: C) Au ions (reduced in-situ by $NaBH_4$), D) Fe-NP (arrows indicate position of complexed material).

In a further step, $HAuCl_4$ was also added to micellar solutions of PE_{35}-*click*-$PBocAmOx_{15}$-*b*-P*i*$PrOx_{145}$. After dialysis and directional crystallization, a weak signal could be detected in UV-Vis, indicating the presence of Au NPs (Figure S22). However, the localization of the Au NPs by

TEM was more or less randomly distributed (Figure S23), presumably due to the bulky protective groups shielding the amine moiety.

The position of either Au or Fe_3O_4 NPs confirms our hypothesis regarding the assembly mechanism of PE_{35}-*click*-$PAmOx_{15}$-*b*-P*i*$PrOx_{145}$ upon directional crystallization of PiPrOx. Both $HAuCl_4$ and the negatively charged Fe_3O_4 nanocrystals are attracted by a positively charged outer PAmOx layer.

Conclusion

We introduced a bottom-up strategy for the formation of anisotropic organic/inorganic hybrid fibers by directional crystallization of the poly(2-*iso*-porpyl-2-oxazoline) (P*i*PrOx) corona of spherical core-shell-corona micelles in aqueous solution. For this purpose we established the synthesis of a triblock terpolymer, polyethylene-*block*-poly(2-(4-((*tert*-butoxycarbonyl)amino)butyl)-2-oxazoline)-*block*-poly(2-iso-propyl-2-oxazoline) (PE-*b*-PBocAmOx-*b*-P*i*PrOx), by a combination of sequential polymerization and subsequent linkage by copper-catalyzed azide-alkyne cycloaddition (CuAAC). By deprotection of the middle block to PAmOx primary amine functionalities were generated. Due to the block sequence, the formation of spherical core-shell-corona micelles in solution was observed in both cases by dynamic light scattering (DLS) and transmission electron microscopy (TEM). In the next step, the directional crystallization of P*i*PrOx in water was investigated by heating the solution for 24 hours to 65 °C. The crystallization was monitored *in-situ* by DLS, while the resulting structures were investigated in detail by electron microscopy (TEM and SEM). Two different assembly mechanisms were identified for PE-*b*-PBocAmOx-*b*-P*i*PrOx and PE-*b*-PAmOx-*b*-P*i*PrOx, presumably owing to differences in the hydrophobic weight fraction of 22 and 5 wt.%, respectively. For PE-*b*-PBocAmOx-*b*-P*i*PrOx (22 wt.% hydrophobic) defined cylindrical micelles with a diameter of 27 nm were observed, while for the hydrophilic PE-*b*-PAmOx-*b*-P*i*PrOx (5 wt.%) fiber-like structures of several µm length and 60 nm width were formed. For PE-*b*-PBocAmOx-*b*-P*i*PrOx, we assume a fusion of initially spherical micelles into cylindrical superstructures, while in the case of PE-*b*-PAmOx-*b*-P*i*PrOx, P*i*PrOx fibers with a positively charged PAmOx corona are formed. This was confirmed by the selective incorporation of Au and Fe_3O_4 nanoparticles within the AmOx corona. These first results towards the formation of anisotropic hybrid material by linear triblock terpolymers with two crystalline segments

demonstrate the potential of materials for controlled assembly in solution into 2D or 3D structures. Optimization of loading efficiency and length control for these systems will be the subject of further investigations.

Experimental Section

Instruments

NMR: Proton nuclear magnetic resonance (^{1}H-NMR) spectra were recorded in $CDCl_3$ on a Bruker AC 300 MHz spectrometer at 298 K. Chemical shifts are given in parts per million (ppm, δ scale) relative to the residual signal of the deuterated solvent.

SEC: Size exclusion chromatography was measured on a Shimadzu system equipped with a SCL-10A system controller, a LC-10AD pump, a RID-10A refractive index detector, and both a PSS Gram30 and a PSS Gram1000 column in series, whereby *N,N*-dimethylacetamide (DMAC) with 5 mmol of LiCl was used as an eluent at 1 mL min^{-1} flow rate and the column oven was set to 60 °C. The system was calibrated with PS (100 to 1 000 000 g mol^{-1}) standards. Furthermore, a Shimadzu system equipped with an SCL-10A system controller, an LC-10AD pump and an RID-10A refractive index detector using a solvent mixture containing chloroform ($CHCl_3$), triethylamine (TEA) and *iso*-propanol (*i*-PrOH) (94:4:2) at a flow rate of 1 mL min^{-1} on a PSS SDV linear M 5 μm column at 40 °C. The system was calibrated using polystyrene (100 to 100 000 g mol^{-1}) standards.

FT-IR Infra-red spectroscopy: Dry powders of the materials were directly placed on the crystal of the ATR-FTIR (Affinity-1 FTIR, Shimadzu) for measurements in the range of 4000 to 600 cm^{-1}.

Microwave-assisted polymerizations were carried out utilizing an Initiator Sixty single-mode microwave synthesizer from Biotage, equipped with a non-invasive IR sensor (accuracy: 2%). Microwave vials (conical, 0.5 to 2 mL) were heated at 110 °C overnight and allowed to cool to room temperature under nitrogen atmosphere. All polymerizations were carried out using temperature control.

DLS: Dynamic light scattering was performed at a scattering angle of 90° on an ALV CGS-3 instrument equipped with a He-Ne laser operating at a wavelength of 633 nm at 25 °C. Micelle solutions were filtered before measurement (Nylon; 0.45 μm). The CONTIN algorithm was applied to analyze the obtained correlation functions. For temperature control, the DLS is equipped with a Lauda thermostat. Apparent hydrodynamic radii were calculated according to the Stokes-Einstein equation.

Transmission electron microscopy (TEM): The formed aggregates were analyzed using a TEM (Zeiss-CEM 902A, Oberkochen, Germany) operated at 80 kV. Images were recorded using a 1k TVIPS FastScan CCD camera. Or on a FEI Tecnai G^2 20 (200 kV) equipped with a 4k x 4k Eagle HS CCD and a 1k x 1k Olympus MegaView camera for overview images. TEM samples were prepared by applying a drop of an aqueous sample solution onto the surface of a plasma-treated carbon coated copper grid (Quantifoil Micro-Tools GmbH, Jena, Germany).

Scanning Electron microscopy (SEM): Zeiss SIGMA VP Field Emission SEM equipped with the GEMINI column (Carl-Zeiss AG, Germany) operating at 3 to 7 kV using the InLens or SE2 detector.

Materials

2-ethyl-2-oxazoline (EtOx), 2-*iso*-propyl-2-oxazoline (*i*PrOx) were distilled over barium oxide under vacuum and stored under nitrogen atmosphere in a glove box. 2-(4-((*tert*-butoxycarbonyl)amino)butyl-2-oxazoline (BocOx) was synthesized according to the literature[43] and distilled prior to usage and stored in a glove box. Tetrahydrofuran (THF), acetonitrile (ACN) and dichloromethane (DCM) were purified using a Solvent Purification System (SPS, Innovative Technology, PM-400-3-MD) equipped with two activated alumina columns. Copper bromide

(CuBr), *N*,*N*,*N*′,*N*″,*N*″-pentamethyldiethylenetriamine (PMDETA), were purchased from Aldrich and used as received. If not mentioned otherwise the educts were used as received. PE_{35}-N_3 was synthesized according to literature, and the degree of functionalization of 85% determined by NMR.[42]

Synthesis

Synthesis of alkyne-modified poly-(2-(4-((*tert*-butoxycarbonyl)amino)butyl)-2-oxazoline)-block-poly(2-*iso*-propyl-2-oxazoline) block copolymer (PBocAmOx$_{15}$-*b*-P*i*PrOx$_{145}$)

Propargyl *p*-toluenesulfonate and 2-(4-((*tert*-butoxycarbonyl)amino)butyl-2-oxazoline (BocAmOx) were dissolved in acetonitrile (ACN) a monomer to initiator ratios of 15 and a monomer concentration of 1M. The capped vials were placed in a microwave synthesizer at 140 °C. After the polymerization the vial was transferred into a glove box. A stock solution of 2-*iso*-propyl-2-oxazoline and ACN (1M) were added to the polymer solution. The vial was capped and placed in the microwave synthesizer at 140 °C again to form the block copolymer. A small amount of the first block was kept under the inert atmosphere at room temperature and was investigated together with the other polymers *via* SEC and NMR. The block copolymers were terminated *via* the addition of water, and removing the solvent under reduced pressure.
SEC ($CHCl_3$/TEA/*i*-PrOH): M_n = 23500 g mol^{-1}; Đ = 1.08; SEC (DMAC/LiCl): M_n = 28000g mol^{-1}; Đ = 1.09; NMR (300 MHz; $CDCl_3$): 5.5-4.8 (-NH), 3.9-3.1 (backbone), 3.1-3.0 (-CH_2-Boc), 3.0-2.5 (-CO-CH_2-$^{i\text{PrOx}}$), 2.5-2.2 (-CO-CH_2-$^{\text{BocAmOx}}$), 1.75-1.5 (-CH_2-CH_2-$^{\text{BocAmOx}}$), 1.42 (-CH_3^{BocAmOx}), 1.2-0.7 (-C$H_3^{i\text{PrOx}}$) ppm. FT-IR: 3300 (-NH), 1705 (C=O$^{\text{Boc}}$), 1630 (C=O$^{\text{POx}}$), 1516 (amide), 1365 (-CH_3^{Boc}) cm^{-1}.

Synthesis of triblock terpolymers *via* CuAAC between the azide-modified PE$_{35}$-N$_3$ and diblock copolymers (PE$_{35}$-*click*-PBocAmOx$_{15}$-*b*-P*i*PrOx$_{145}$)

100 mg (6 µmol) of the diblock copolymer were dissolved together with 20 mg PE$_{35}$-N$_3$ (20 µmol; 3 eq.) and copper bromide (CuBr; 2 eq.) in tetrahydrofuran (THF) at 120 °C in an oil bath.

Obtaining a clear solution *N*,*N*,*N*′,*N*′′,*N*′′-pentamethyldiethylenetriamine (PMDETA; 2 eq.) was added under stirring. The solution was allowed to stir at 120 °C for 1 hour. Afterwards the solution cooled to room temperature and diluted with water. The turbid solution was filtered and washed with acetone. The aqueous solution was vigorous stirred together with dichloromethane. The clear organic phase was filtered with a syringe filter (PTFE; 0.45 µm), twice, and dried under vacuum. The obtained polymer was precipitated in cold ether, filtered and dried under vacuum.

SEC ($CHCl_3$/TEA/*i*-PrOH): M_n = 24000 g mol^{-1}; Đ = 1.09; SEC (DMAC/LiCl): M_n = 27000 g mol^{-1}; Đ = 1.11; ^{1}H-NMR (300MHz; $CDCl_3$): 5.5-4.8 (-NH), 3.9-3.1 (backbone), 3.2-3.0 (-CH_2-Boc), 3.0-2.5 (-CO-CH_2-$^{i\text{PrOx}}$), 2.5-2.2 (-CO-CH_2-$^{\text{BocAmOx}}$), 1.75-1.5 (-CH_2-CH_2-$^{\text{BocAmOx}}$), 1.42 (-CH_3^{BocAmOx}), 1.25 (PE backbone), 1.3-0.7 (-C$H_3^{i\text{PrOx}}$) ppm. FT-IR: 3070-2785 (-CH_2-), 1701 (C=O$^{\text{Boc}}$), 1630 (C=O$^{\text{POx}}$), 1514 (amide), 1365 (-CH_3^{Boc}) cm^{-1}.

Deprotection of triblock terpolymers PE_{35}-*click*-$PBocAmOx_{15}$-*b*-P*i*$PrOx_{145}$

The triblock terpolymer PE_{35}-*click*-$PBocAmOx_{15}$-*b*-P*i*$PrOx_{145}$ (80 mg; 4 µmol) was dissolved in trifluoroacetic acid (TFA, 2 mL, 26 mmol), stirred for 1 h at 60 °C and for 20 h at room temperature. The solution was diluted with methanol (2 mL) and precipitated in cold diethyl ether (150 mL, -80 °C). The polymer was filtered off and dissolved in a mixture of methanol and chloroform (1/1; 200 mL), and, subsequently, stirred with Amberlyst A21 for 3 d. After filtration the solvents were evaporated and the product was dried under high vacuum.

SEC (DMAC/LiCl): M_n = 25000 g mol^{-1}; Đ = 1.06; NMR (300 MHz; $CDCl_3$): 3.9-3.1 (backbone), 3.0-2.5 (-CO-CH_2-$^{i\text{PrOx}}$), 2.0-1.5 (-CH_2-CH_2-$^{\text{AmOx}}$), 1.25 (PE backbone), 1.2-0.7 (-C$H_3^{i\text{PrOx}}$) ppm. FT-IR: 3070-2785 (-CH_2-), 1630 (C=O$^{\text{POx}}$) 1162, 824, 800, 717 (amine) cm^{-1}.

Synthesis of alkyne-modified poly-(2-(4-(amino)butyl)-2-oxazoline)-*block*-poly(2-*iso*-propyl-2-oxazoline) block copolymer (TB-PAmOx$_{15}$-*b*-P*i*PrOx$_{145}$)

The diblock copolymer PBocAmOx$_{15}$-*b*-P*i*PrOx$_{145}$ (80 mg; 4 µmol) was dissolved in trifluoroacetic acid (TFA, 2 mL, 26 mmol), stirred for 1 h at 60 °C and for 20 h at room temperature. The solution was diluted with methanol (2 mL) and precipitated in cold diethyl ether (150 mL, -80 °C). The polymer was filtered off and dissolved in a mixture of methanol and chloroform (1:1, 200 mL), and, subsequently, stirred with Amberlyst A21 for 3 d. After filtration the solvents were evaporated and the product was dried under high vacuum.

SEC (DMAC/LiCl): M_n = 29000 g mol^{-1}; Đ = 1.07; NMR (300 MHz; $CDCl_3$): 3.9-3.1 (backbone), 3.0-2.5 (-CO-CH_2-^{iPrOx}), 2.0-1.5 (-CH_2-CH_2-^{AmOx}), 1.2-0.7 (-CH_3^{iPrOx}) ppm. FT-IR: 3070-2785 (-CH_2-), 1630 (C=O^{POx}) 1150, 824, 800, 717 (amine) cm^{-1}.

Synthesis of Fe_3O_4 nanocrystals[49]

For the preparation of Fe_3O_4 nanocrystals, tris(acetylacetonato)iron(III) ((Fe(acac)$_3$); 283 mg, 0.8 mmol) was dissolved in 2 mL *N*-vinyl-2-pyrrolidon (NVP) in a microwave vial and heated to 200 °C for 20 min under microwave irradiation. The mixture was diluted with deionized water (300 mL) and centrifuged at 11,000 rpm for 15 min. The washing procedure was repeated until the supernatant of the nanocrystals remained colorless.

Transfer of triblock terpolymer into water

10 mg of the respective triblock terpolymer were dissolved in 10 mL DMF (1 mg mL^{-1}) and heated in an oil bath to 120 °C for 10 minutes under stirring, afterwards the solution was allowed to cool down to room temperature. The solution was dialyzed against water for 2 days (RC, MWCO 1000).

Incorporation of nanoparticles in PE_{35}-*click*-$PAmOx_{15}$-*b*-P*i*$PrOx_{145}$

10 mg of the respective triblock terpolymer were dissolved in 10 mL DMF (1 mg mL^{-1}) and heated in an oil bath to 120 °C for 10 minutes under stirring, afterwards the solution was allowed to cool down to room temperature. 1 mL of a stock solution of $HAuCl_4$ (1 mg mL^{-1}) or Fe_3O_4 nanocrystals (1 mg mL^{-1}) was added to the micellar solution at room temperature. Afterwards the solutions were stirred for 12 hours (in the dark in case of gold precursor), and subsequently dialyzed against water for 2 days (RC, MWCO 1000; in the dark in case of gold precursor), before the solutions were heated up for 24 hours at 65 °C. In case of the gold precursor solution, the dialysis bag turned red due to the reduction of un-complexed gold salt. For the reduction of the complexed gold precursor, sodium borohydride ($NaBH_4$) was added to the solution, which turned slightly red.

Acknowledgement

The authors would like to thank Stefanie Rudolph for help with the grey-scale analysis of TEM micrographs, Christian Pietsch for SEM measurements, and Grit Festag for taking care of the SEC. F. H. S. and T. R. are further grateful to the Thuringian Ministry for Education, Science, and Culture (TMBWK; #B515-10065, ChaPoNano; #B515-11028, SWAXS-JCSM) for financial support. F. H. S. thanks the VCI for a starting independent researcher fellowship. T. R. acknowledges the Carl-Zeiss foundation for a PhD-scholarship.

References

1. F. S. Bates and G. H. Fredrickson, *Physics Today*, 1999, **52**, 32-38.
2. Y. Mai and A. Eisenberg, *Chem. Soc. Rev.*, 2012, **41**, 5969-5985.
3. V. Abetz and P. Simon, ed. V. Abetz, Springer Berlin / Heidelberg, 2005, vol. 189, pp. 125-212.
4. F. H. Schacher, P. A. Rupar and I. Manners, *Angew. Chem. Int. Ed.*, 2012, **51**, 7898-7921.
5. W. Xi, T. F. Scott, C. J. Kloxin and C. N. Bowman, *Adv. Funct. Mater.*, 2014, **24**, 2572-2590.
6. H. C. Kolb, M. G. Finn and K. B. Sharpless, *Angew. Chem. Int. Ed.*, 2001, **40**, 2004-2021.
7. R. K. Iha, K. L. Wooley, A. M. Nyström, D. J. Burke, M. J. Kade and C. J. Hawker, *Chem. Rev.*, 2009, **109**, 5620-5686.
8. K. Kempe, A. Krieg, C. R. Becer and U. S. Schubert, *Chem. Soc. Rev.*, 2012, **41**, 176-191.
9. L. Liang and D. Astruc, *Coord. Chem. Rev.*, 2011, **255**, 2933-2945.
10. W. H. Binder and R. Sachsenhofer, *Macromol. Rapid Commun.*, 2007, **28**, 15-54.
11. P. Espeel and F. E. Du Prez, *Macromolecules*, 2015, **48**, 2-14.
12. C. Barner-Kowollik, F. E. Du Prez, P. Espeel, C. J. Hawker, T. Junkers, H. Schlaad and W. Van Camp, *Angew. Chem. Int. Ed.*, 2011, **50**, 60-62.
13. C. Lang, D. Voll, A. J. Inglis, N. Dingenouts, A. S. Goldmann, L. Barner and C. Barner-Kowollik, *Macromol. Rapid Commun.*, 2011, **212**, 831-839.
14. O. Altintas, T. Rudolph and C. Barner-Kowollik, *J. Polym. Sci. Part A: Polym. Chem.*, 2011, **49**, 2566-2576.
15. T. Rudolph, A. Nunns, A. M. Schwenke and F. H. Schacher, *Polym. Chem.*, 2015, **6**, 1604-1612.
16. M. Zhang, P. A. Rupar, C. Feng, K. Lin, D. J. Lunn, A. Oliver, A. Nunns, G. R. Whittell, I. Manners and M. A. Winnik, *Macromolecules*, 2013, **46**, 1296-1304.
17. D. Fournier, R. Hoogenboom and U. S. Schubert, *Chem. Soc. Rev.*, 2007, **36**, 1369-1380.
18. A. Hanisch, H. Schmalz and A. H. E. Müller, *Macromolecules*, 2012, **45**, 8300-8309.
19. T. Rudolph, S. Crotty, M. v. d. Lühe, D. Pretzel, U. S. Schubert and F. H. Schacher, *Polymers*, 2013, **5**, 1081-1101.
20. O. Altintas, A. P. Vogt, C. Barner-Kowollik and U. Tunca, *Polym. Chem.*, 2012, **3**, 34-45.
21. H. Durmaz, A. Sanyal, G. Hizal and U. Tunca, *Polym. Chem.*, 2012, **3**, 825-835.
22. X. Wang, G. Guerin, H. Wang, Y. Wang, I. Manners and M. A. Winnik, *Science*, 2007, **317**, 644-647.
23. T. Gädt, N. S. Ieong, G. Cambridge, M. A. Winnik and I. Manners, *Nat. Mater.*, 2009, **8**, 144-150.
24. J. B. Gilroy, T. Gädt, G. R. Whittell, L. Chabanne, J. M. Mitchels, R. M. Richardson, M. A. Winnik and I. Manners, *Nat. Chem.*, 2010, **2**, 566-570.
25. J. A. Massey, K. Temple, L. Cao, Y. Rharbi, J. Raez, M. A. Winnik and I. Manners, *J. Am. Chem. Soc.*, 2000, **122**, 11577-11584.
26. J. Schmelz, A. E. Schedl, C. Steinlein, I. Manners and H. Schmalz, *J. Am. Chem. Soc.*, 2012, **134**, 14217-14225.
27. J. Schmelz, F. H. Schacher and H. Schmalz, *Soft Matter*, 2013, **9**, 2101.
28. H. Qiu, Z. M. Hudson, M. a. Winnik and I. Manners, *Science*, 2015, **347**, 1329-1332.
29. A. L. Demirel, M. Meyer and H. Schlaad, *Angew. Chem. Int. Ed.*, 2007, **46**, 8622-8624.
30. C. Diehl, P. Cernoch, I. Zenke, H. Runge, R. Pitschke, J. Hartmann, B. Tiersch and H. Schlaad, *Soft Matter*, 2010, **6**, 3784-3788.
31. M. Meyer, M. Antonietti and H. Schlaad, *Soft Matter*, 2007, **3**, 430-431.
32. S. Förster and M. Antonietti, *Adv. Mater.*, 1998, **10**, 195-217.
33. J. Yuan, Y. Xu and A. H. E. Müller, *Chem. Rev.*, 2011, **40**, 640-655.
34. C. Sanchez, B. Julian, P. Belleville and M. Popall, *J. Mater. Chem.*, 2005, **15**, 3559-3592.
35. F. H. Schacher, T. Rudolph, M. Drechsler and A. H. E. Müller, *Nanoscale*, 2011, **3**, 288-297.

36. B. L. Rivas, E. D. Pereira and I. Moreno-Villoslada, *Prog. Polym. Sci.*, 2003, **28**, 173-208.
37. F. Kretschmer, U. Mansfeld, S. Hoeppener, M. Hager and U. S. Schubert, *Chem. Commun.*, 2013, **50**, 88-90.
38. Y. Lu, Y. Mei, M. Schrinner, M. Ballauff, M. W. Möller and J. Breu, *J. Phys. Chem. C*, 2007, **111**, 7676-7681.
39. W. Lu and C. M. Lieber, *Nat. Mater.*, 2007, **4**, 841-850.
40. E. Katz and I. Willner, *Angew Chem Int Ed Engl*, 2004, **43**, 6042-6108.
41. M. M. Cheng, G. Cuda, Y. L. Bunimovich, M. Gaspari, J. R. Heath, H. D. Hill, C. A. Mirkin, A. J. Nijdam, R. Terracciano, T. Thundat and M. Ferrari, *Curr. Opin. Chem. Biol.*, 2006, **10**, 11-19.
42. R. Briquel, J. Mazzolini, T. Le Bris, O. Boyron, F. Boisson, F. Delolme, F. D'Agosto, C. Boisson and R. Spitz, *Angew. Chem. Int. Ed.*, 2008, **47**, 9311-9313.
43. M. Hartlieb, D. Pretzel, K. Kempe, C. Fritzsche, R. M. Paulus, M. Gottschaldt and U. S. Schubert, *Soft Matter*, 2013, **9**, 4693.
44. M. Bieligmeyer, S. M. Taheri, I. German, C. Boisson, C. Probst, W. Milius, V. Altstadt, J. Breu, H. W. Schmidt, F. D'Agosto and S. Forster, *J. Am. Chem. Soc.*, 2012, **134**, 18157-18160.
45. N. Oleszko, A. Utrata-Wesołek, W. Wałach, M. Libera, A. Hercog, U. Szeluga, M. Domański, B. Trzebicka and A. Dworak, *Macromolecules*, 2015, **48**, 1852-1859.
46. R. Hoogenboom and H. Schlaad, *Polymers*, 2011, **3**, 467-488.
47. H. K. H. Jr., *JACS*, 1957, **79**, 5441-5444.
48. J. M. Geurts, C. M. Göttgens, M. A. I. V. Graefschepe, R. W. A. Welland, J. J. G. S. V. Es and A. L. German, *J. Appl. Polym. Sci.*, 2001, **80**, 1401-1415.
49. X. Lu, M. Niu, R. Qiao and M. Gao, *J. Phys. Chem. B*, 2008, **112**, 14390-14394.
50. C. Hoerenz, T. Rudolph, M. J. Barthel, U. Guenther and F. H. Schacher, *Polym. Chem.*, 2015, DOI: 10.1039/C1034PY01434K.

Table of content

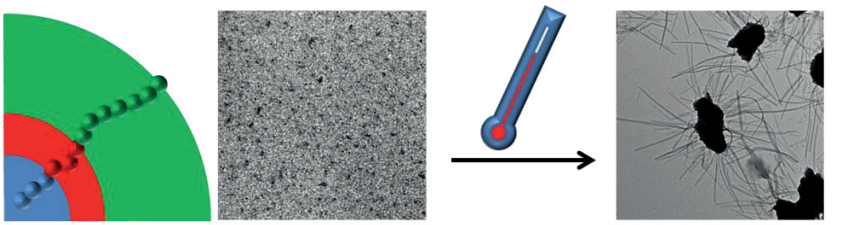

Supporting Information

Towards Anisotropic Hybrid Materials: Solution Self-Assembly of Linear Polyethylene-*block*-poly(2-(4-((*tert*-butoxycarbonyl)amino)butyl-2-oxazoline)–*block*-poly(2-*iso*-propyl-2-oxazoline) Triblock Terpolymers

Tobias Rudolph;[1,2] Matthias Hartlieb;[1,2] Moritz von der Lühe;[1,2] Sebastien Norsic;[3] Ulrich S. Schubert;[1,2,4] Franck D´Agosto;[3] Felix H. Schacher[1,2,*]

Affiliation

[1] Laboratory of Organic and Macromolecular Chemistry, Friedrich Schiller University Jena, Humboldtstr. 10, 07743 Jena, Germany

E-mail: felix.schacher@uni-jena.de

[2] Jena Center for Soft Matter (JCSM), Friedrich Schiller University Jena, Philosophenweg 7, 07743 Jena, Germany

[3]

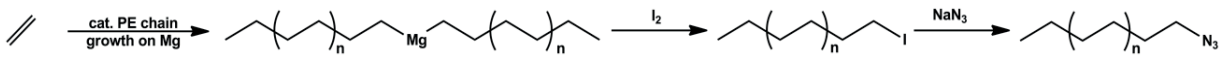

Scheme S1: Catalyzed polyethylene chain growth on Mg and subsequent conversion via iodide and sodium azide (NaN_3), leading to azide functionalized PE-N_3.

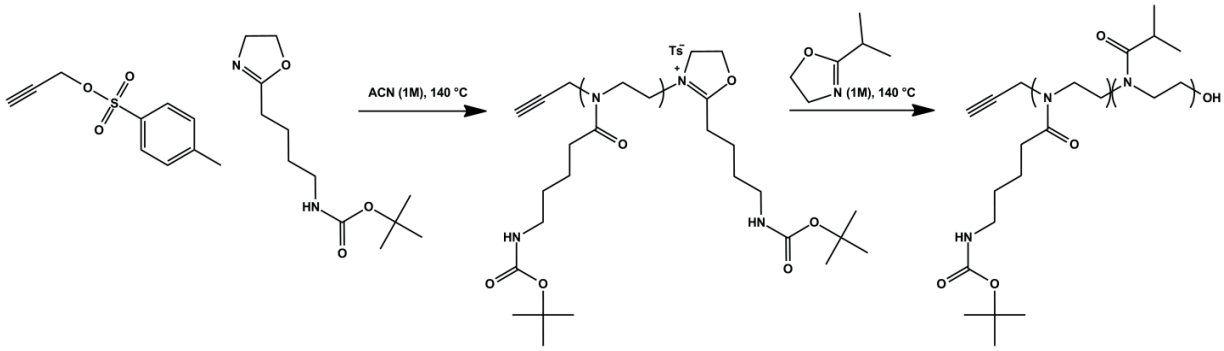

Scheme S2: Microwave-assisted CROP of alkyne functionalized diblock copolymers of poly-(2-(4-((*tert*-butoxycarbonyl)amino)butyl)-2-oxazoline)-*block*-poly(2-*iso*-propyl-2-oxazoline) (PBocAmOx-*b*-P*i*PrOx) initiated by propargyl p-toluenesulfonate.

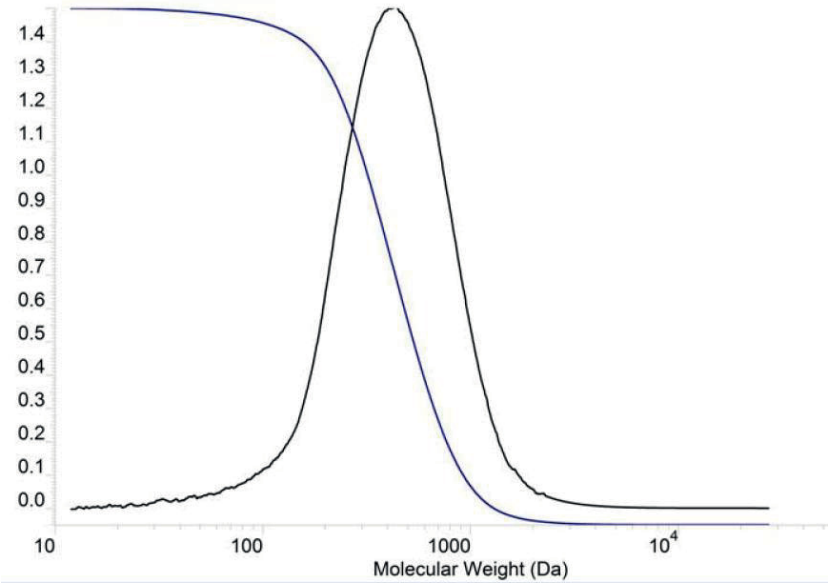

Figure S1: Molar mass distribution of PE_{35}-N_3 determined *via* high temperature SEC (column temperature: 150 °C; solvent: trichlorobenzene; M_n = 318 g mol^{-1}; Đ = 1.6).

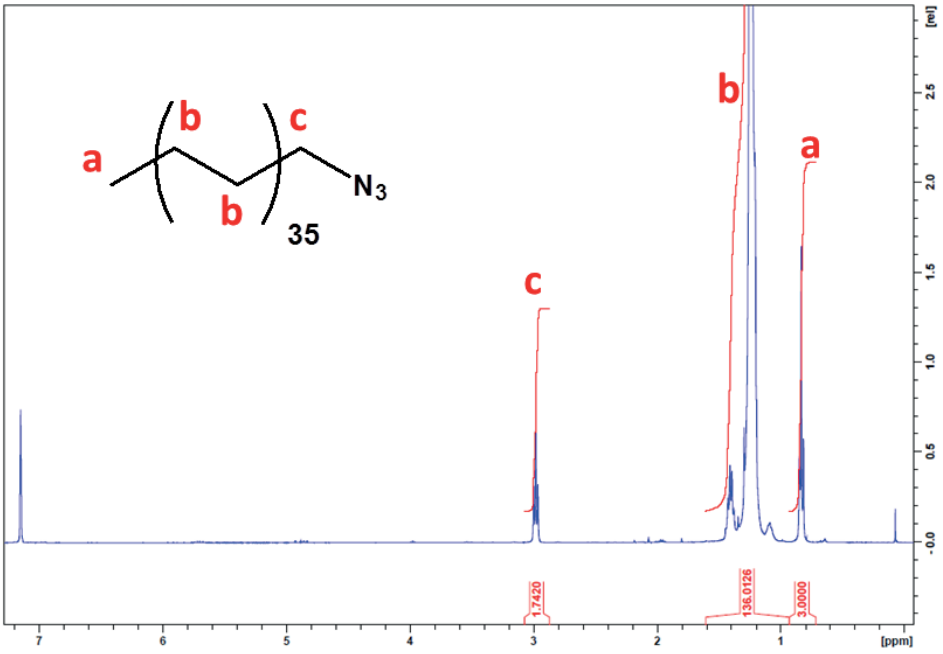

Figure S2: ^{1}H-NMR spectrum for PE_{35}-N_3 ; degree of azide-functionality of ≈87% ($CDCl_3$).

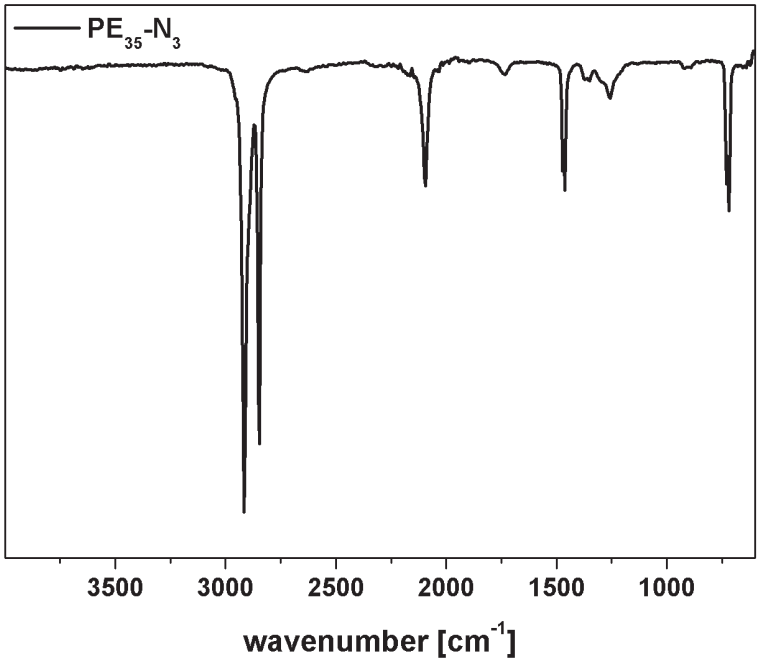

Figure S3: FT-IR spectrum for PE_{35}-N_3 and the characteristic peak for the azide at 2094 cm^{-1}.

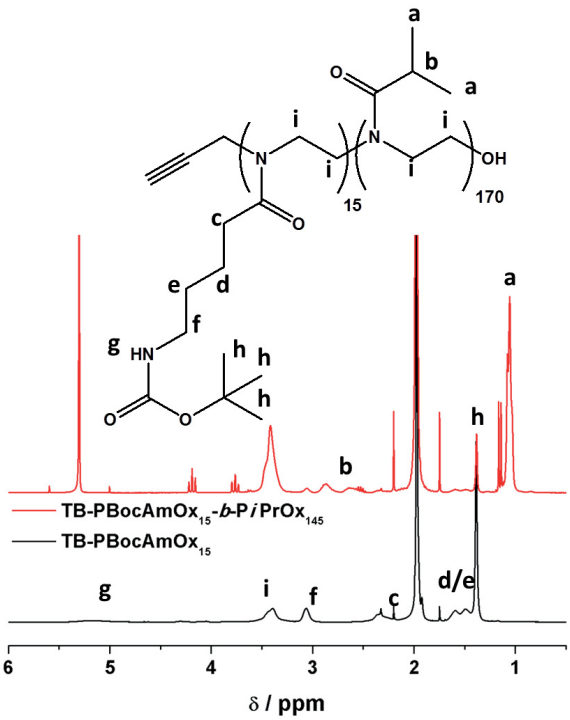

Figure S4: Comparison of NMR spectra for the block copolymerization of BocAmOx and *i*PrOx: TB-PBocAmOx$_{15}$ (black trace) and TB-PBocAmOx$_{15}$-*b*-P*i*PrOx$_{145}$ (red trace, 300 MHz; $CDCl_3$).

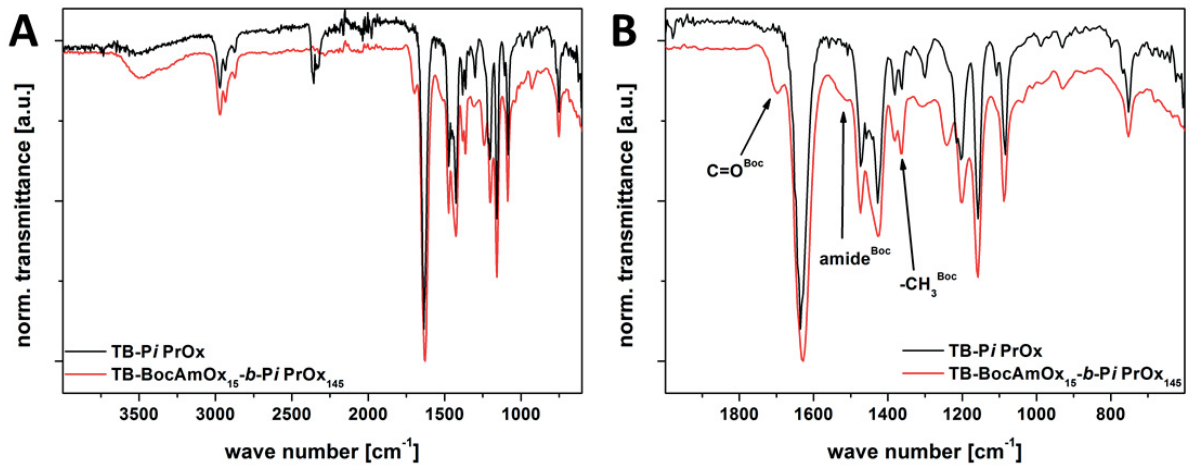

Figure S5: A) Comparison of FT-IR spectra for TB-P*i*PrOx$_x$ (black trace; not mentioned in this manuscript) and TB-PBocAmOx$_{15}$-*b*-P*i*PrOx$_{145}$ (red trace) and an inset of the spectra (B).

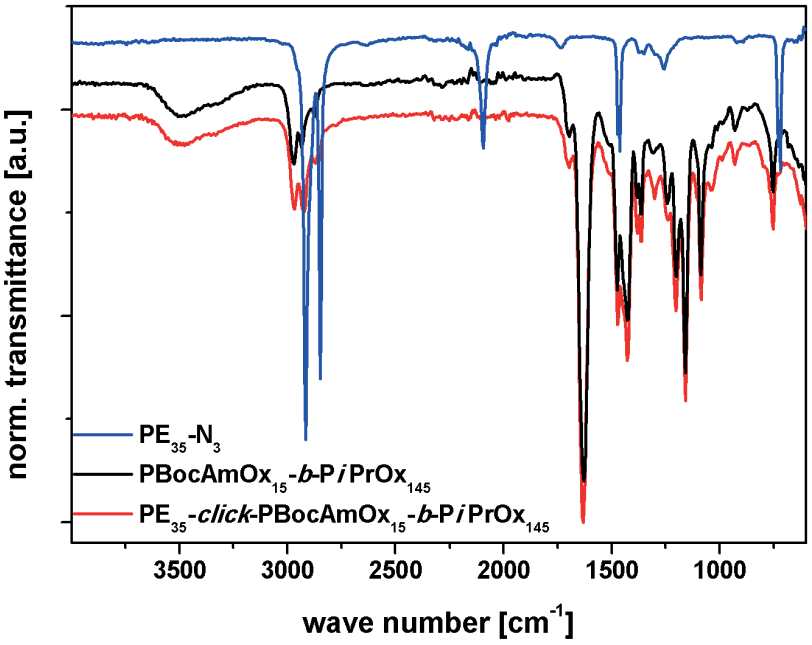

Figure S6: Comparison of FT-IR spectra for PE_{35}-N_3 (blue trace), PBocAmOx$_{15}$-*b*-P*i*PrOx$_{145}$ (black trace), PE_{35}-*click*-PBocAmOx$_{15}$-*b*-P*i*PrOx145 (red trace).

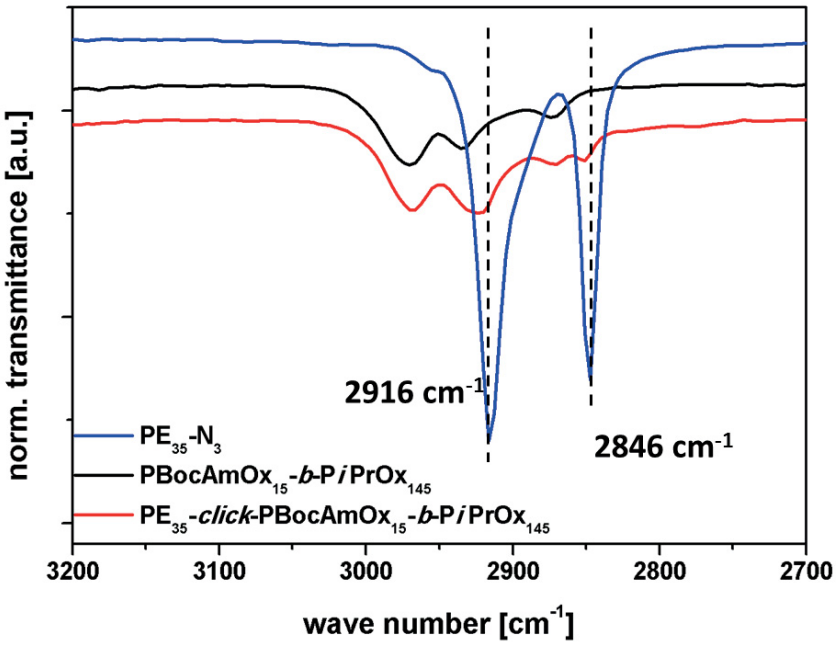

Figure S7: Comparison of FT-IR spectra in the range of 3200 to 2700 cm^{-1} for PE_{35}-N_3 (blue trace), PBocAmOx$_{15}$-*b*-P*i*PrOx$_{145}$ (black trace), PE_{35}-*click*-PBocAmOx$_{15}$-*b*-P*i*PrOx$_{145}$ (red trace).

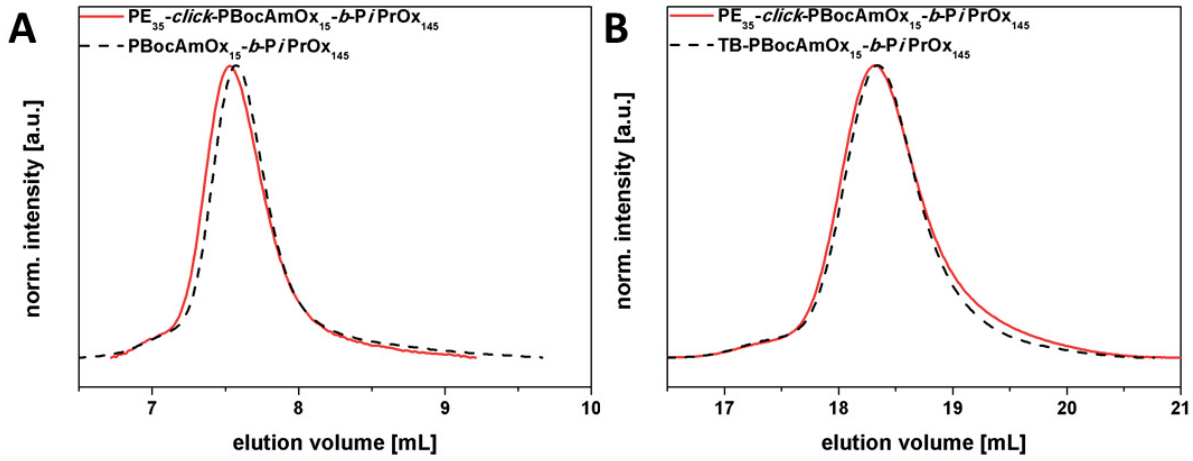

Figure S8: Comparison of SEC traces for PBocAmOx$_{15}$-*b*-P*i*PrOx$_{145}$ (black dashed line) and PE$_{35}$-*click*-PBocAmOx$_{15}$-*b*-P*i*PrOx$_{145}$ (red straight line) with different eluents: A) chloroform; B) dimethylacetamide.

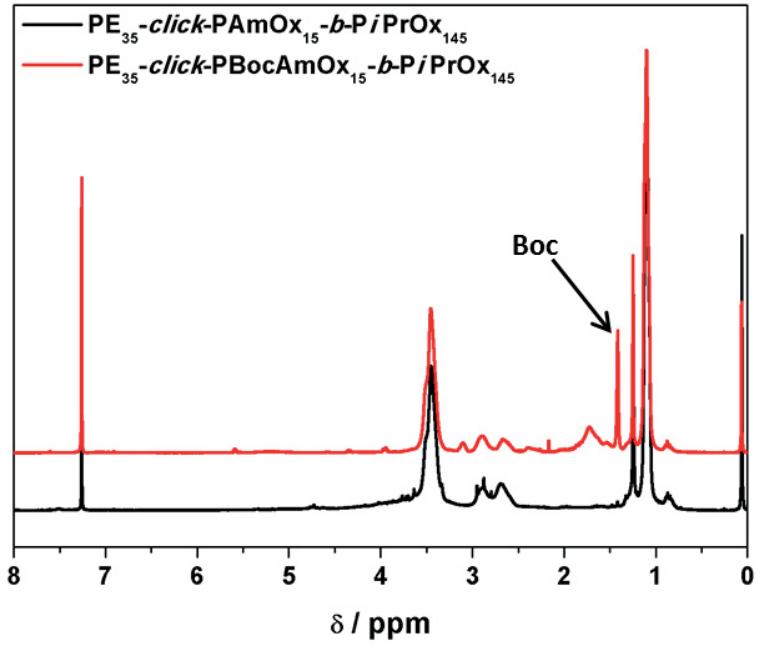

Figure S9: Comparison of NMR spectra before (red trace) and after (black trace) deprotection of PE$_{35}$-*click*-PBocAmOx$_{15}$-*b*-P*i*PrOx$_{145}$.

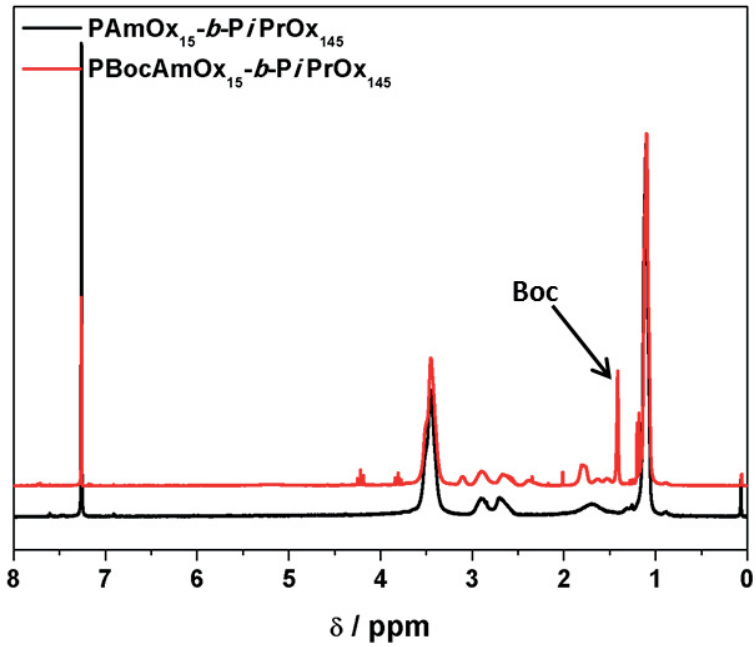

Figure S10: Comparison of ^{1}H-NMR spectra before (red trace) and after (black trace) deprotection of PBocAmOx$_{15}$-*b*-P*i*PrOx$_{145}$.

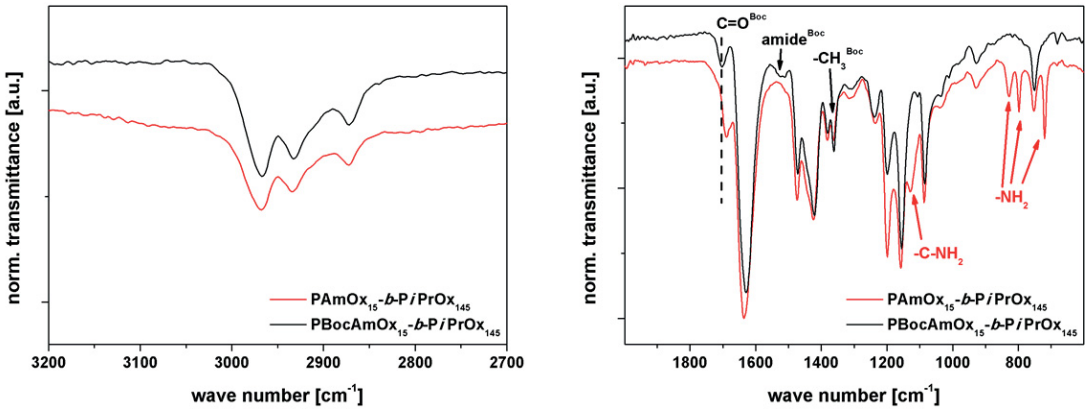

Figure S11: Comparison of FT-IR spectra before (black trace) and after (red trace) deprotection of PE$_{35}$-*click*-PBocAmOx$_{15}$-*b*-P*i*PrOx$_{145}$.

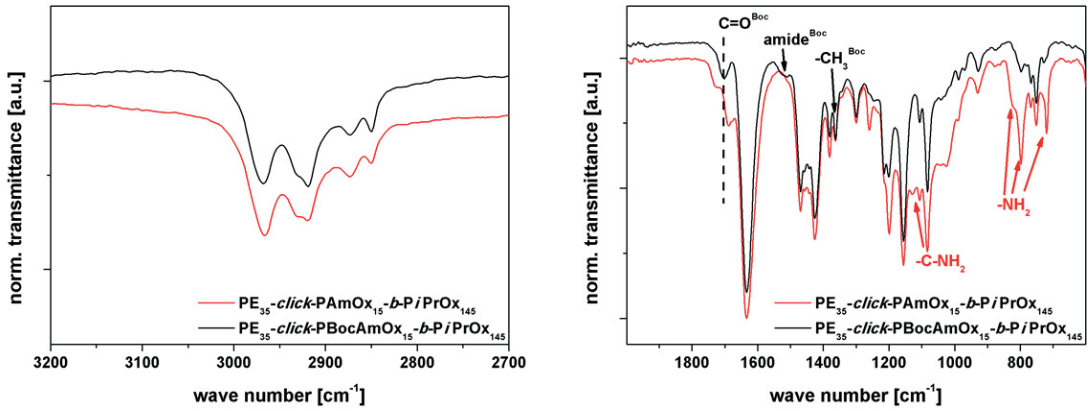

Figure S12: Comparison of FT-IR spectra before (black trace) and after (red trace) deprotection of PBocAmOx$_{15}$-*b*-P*i*PrOx$_{145}$.

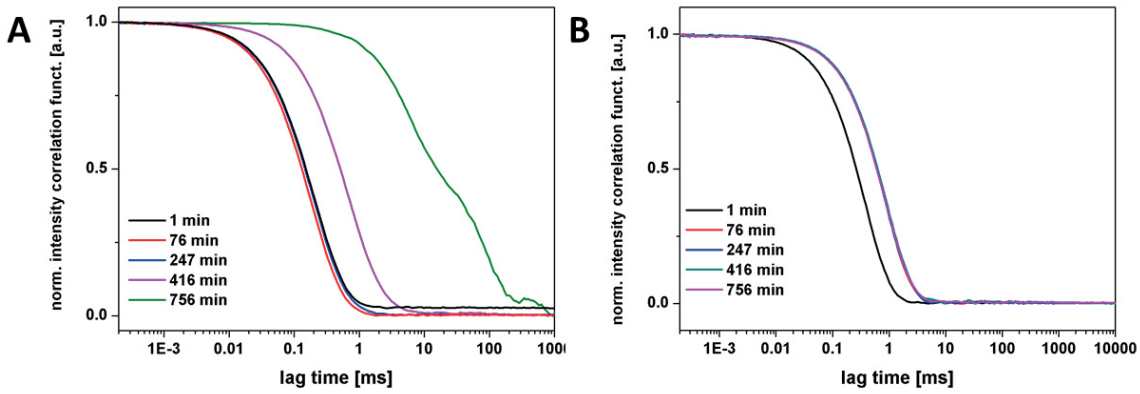

Figure S13: Time-dependent normalized intensity autocorrelation functions for PE$_{35}$-*click*-PAmOx$_{15}$-*b*-P*i*PrOx$_{145}$ (A) and PE$_{35}$-*click*-PBocAmOx$_{15}$-*b*-P*i*PrOx$_{145}$ (B) after: 1 (black line), 76 (red line), 247 (blue line), 416 (pink line) and 756 (green line) minutes.

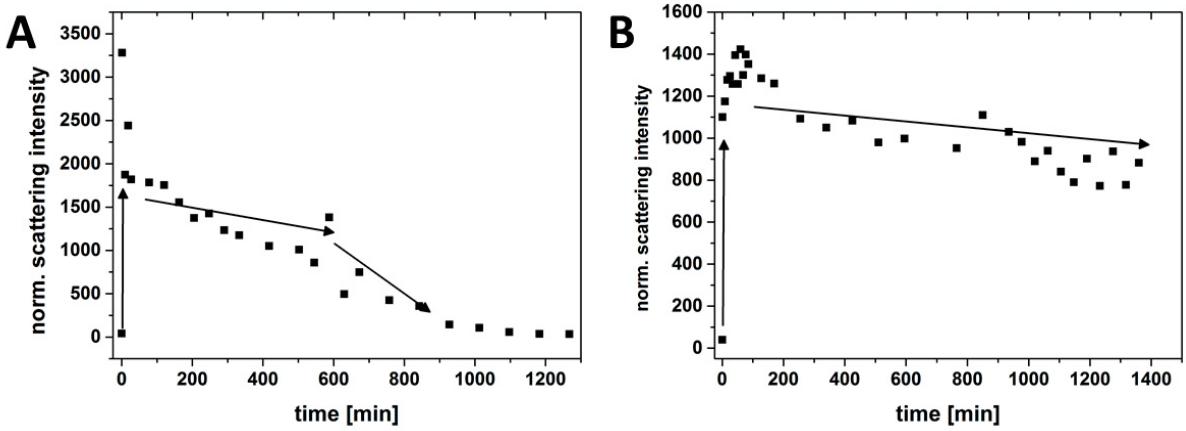

Figure S14: Normalized scattering intensity (black) over time annealed at 65 °C (0.1 mg mL^{-1}) for TB-PBocAmOx$_{15}$-*b*-P*i*PrOx$_{145}$ (A) and TB-PAmOx$_{15}$-*b*-P*i*PrOx$_{145}$ (B) diblock copolymers.

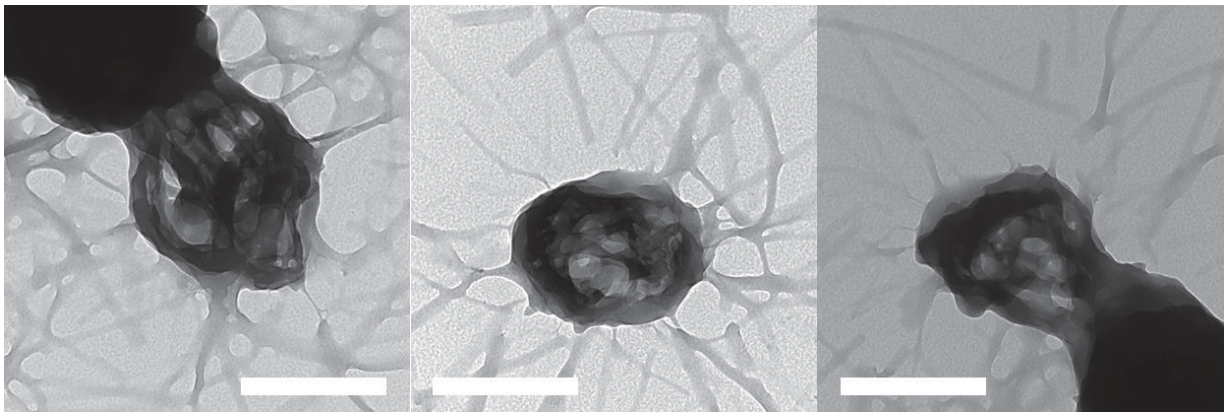

Figure S15: TEM micrographs for PBocAmOx$_{15}$-*b*-P*i*PrOx$_{145}$ after 24 hours at 65 °C in water (0.33 mg mL^{-1}).

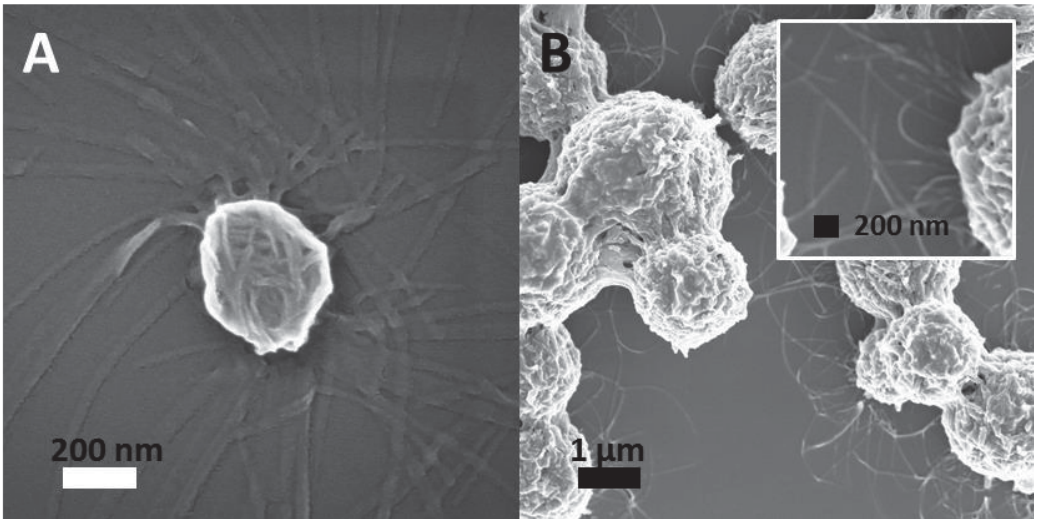

Figure S16: SEM micrographs for PAmOx$_{15}$-*b*-P*i*PrOx$_{145}$ (A) PBocAmOx$_{15}$-*b*-P*i*PrOx$_{145}$ (B) and after 24 hours at 65 °C in water (0.33 mg mL^{-1}).

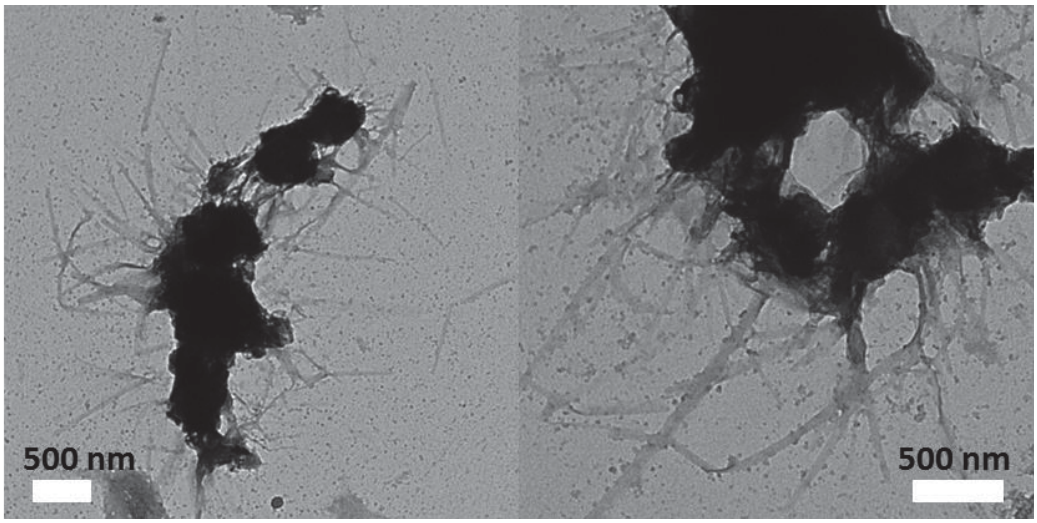

Figure S17: TEM micrographs for PE_{35}-*click*-$PAmOx_{15}$-*b*-P*i*$PrOx_{145}$ after 24 hours at 65 °C in water (0.33 mg mL^{-1}) at pH 12 (adjusted by NaOH).

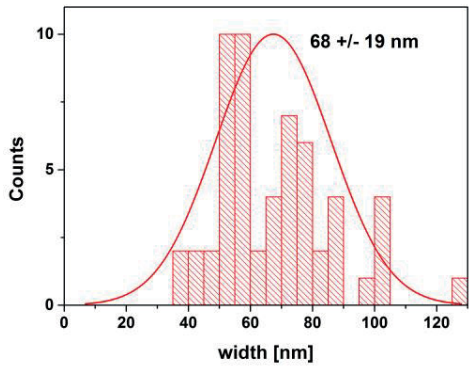

Figure S17: Histogram of width distribution determined for PE_{35}-*click*-$PAmOx_{15}$-*b*-P*i*$PrOx_{145}$ after directional crystallization of PiPrOx at pH 12 determined by grey-scale analysis from TEM micrographs (for 57 positions).

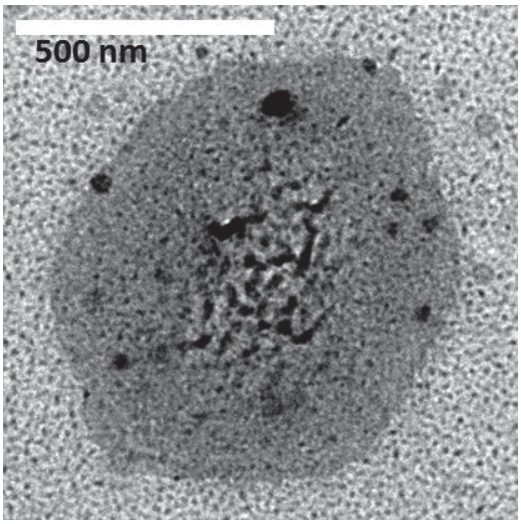

Figure S18: TEM micrograph for kite-like PE_{35}-N_3 aggregate obtained after heating in DMF to 120 °C and cooling to room temperature.

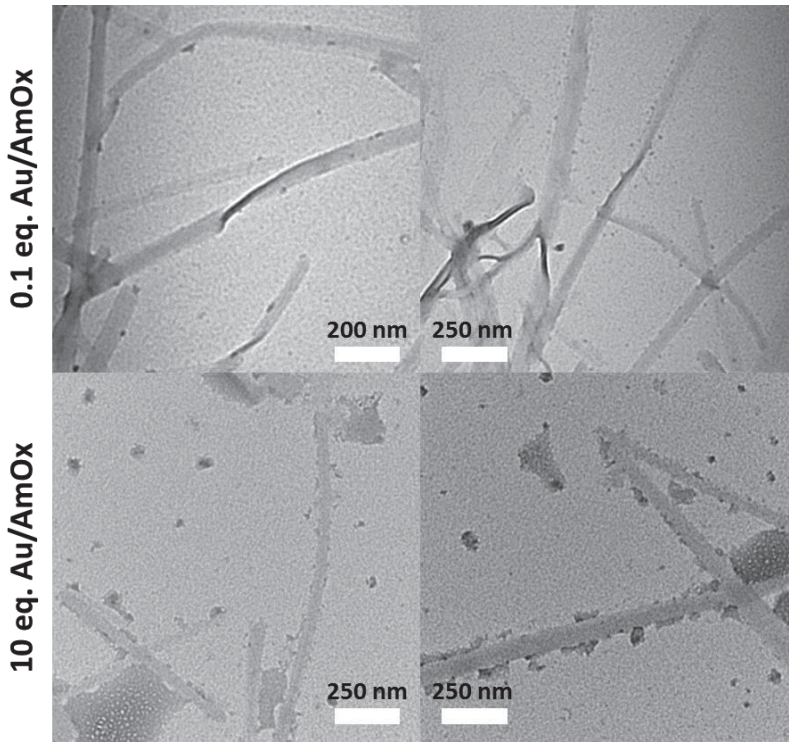

Figure S19: TEM micrographs for PE_{35}-*click*-$PAmOx_{15}$-*b*-P*i*$PrOx_{145}$ after 24 hours at 65 °C in water (0.33 mg mL^{-1}) and *in-situ* reduced $HAuCl_4$ with different equivalent equivalents of gold precursor to AmOx: 0.1 eq. Au/AmOx (top micrographs) and 10 eq. Au/AmOx (bottom micrographs).

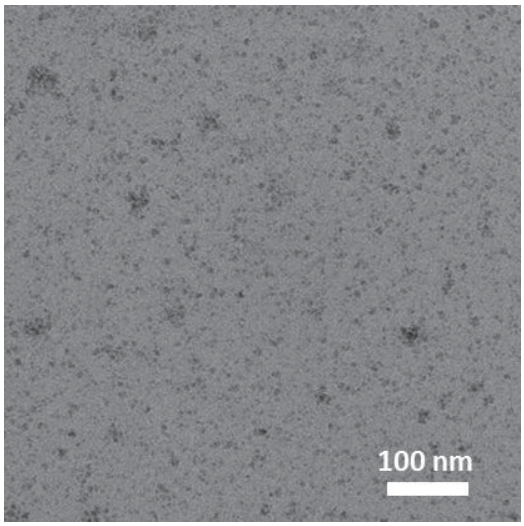

Figure S20: TEM micrograph for as-synthesized Fe_3O_4 -nanocrystals.

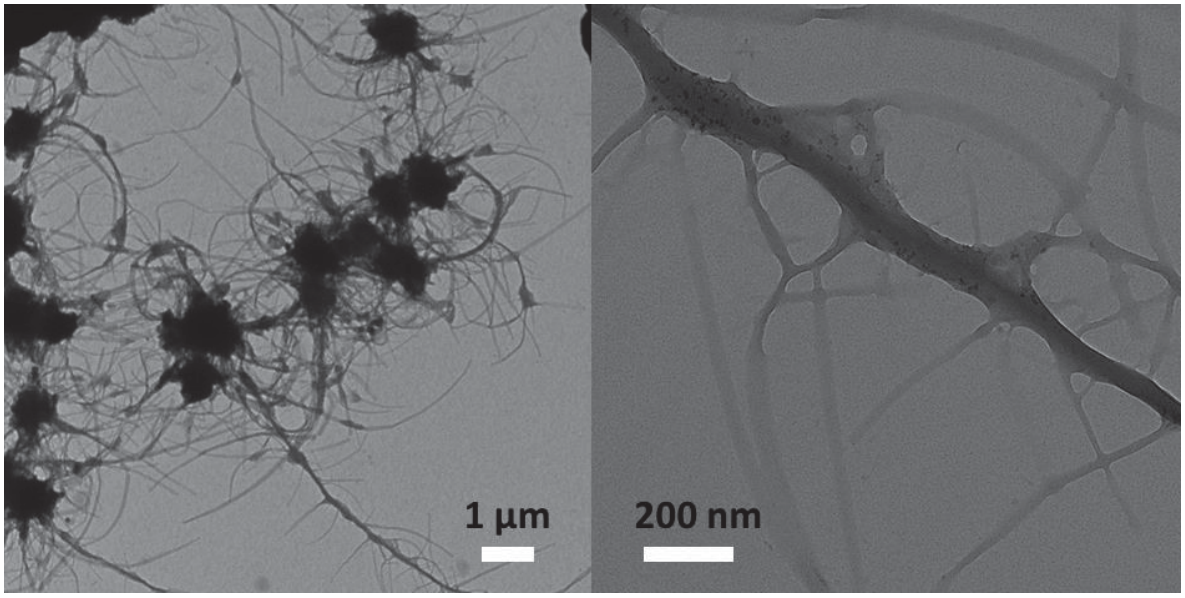

Figure S21: TEM micrographs for PE_{35}-*click*-$PAmOx_{15}$-*b*-P*i*$PrOx_{145}$ after 24 hours at 65 °C in water (0.33 mg mL^{-1}) and Fe_3O_4 nanocrystals.

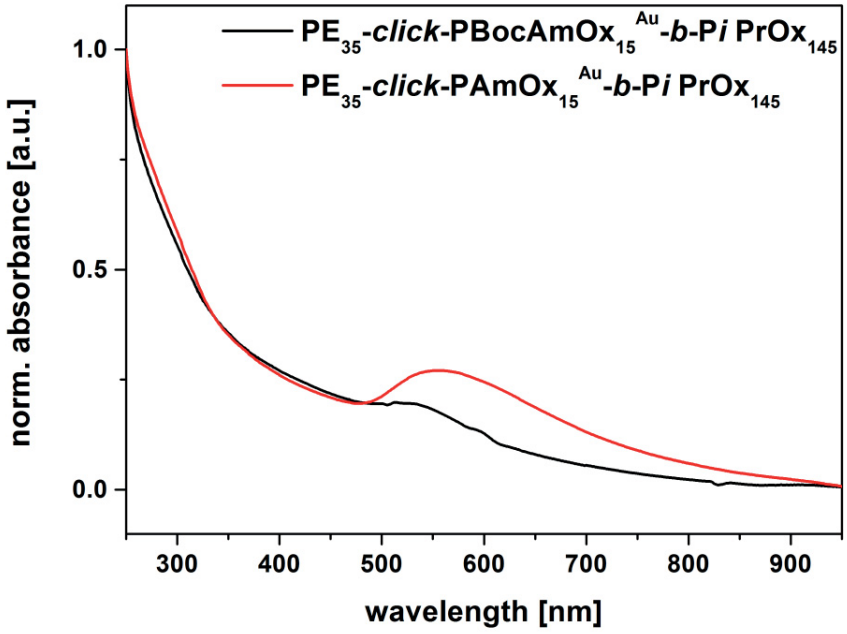

Figure S22: Comparison of UV-Vis spectra for PE_{35}-*click*-$PAmOx_{15}$-*b*-P*i*$PrOx_{145}$ (red trace) and PE_{35}-*click*-$PAmOx_{15}$-*b*-P*i*$PrOx_{145}$ (black trace) after reduction of $HAuCl_4$ (0.1 eq. Au/AmOx).

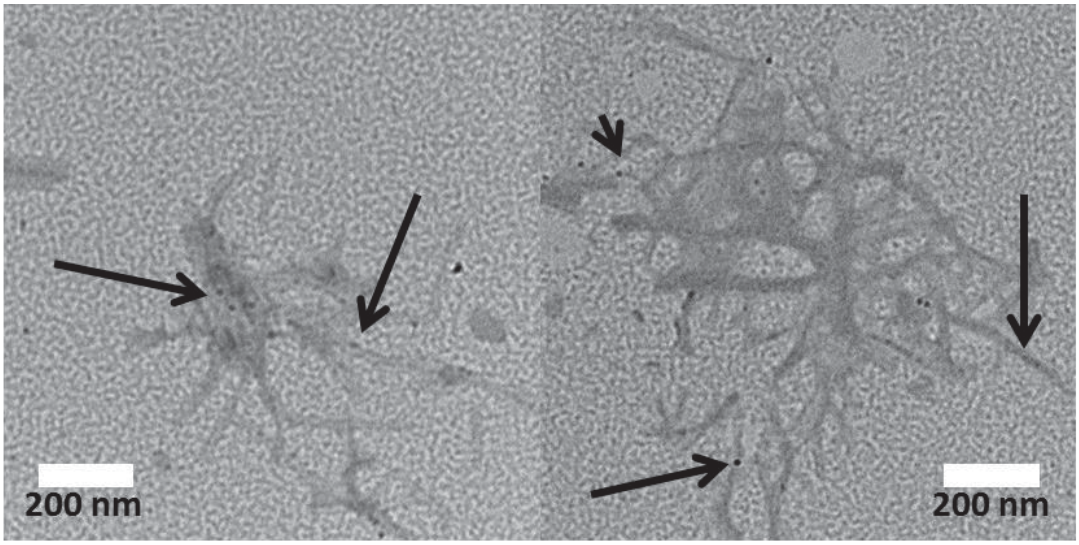

Figure S23: TEM micrographs for PE_{35}-*click*-$PBocAmOx_{15}$-*b*-P*i*$PrOx_{145}$ after 24 hours at 65 °C in water (0.33 mg mL^{-1}) and *in-situ* reduced $HAuCl_4$.

Publication P7

"Homo- and Block Copolymers of Poly(furfuryl glycidyl ether) by Living Anionic Polymerization: Towards Reversibly Core-Crosslinked Micelles"

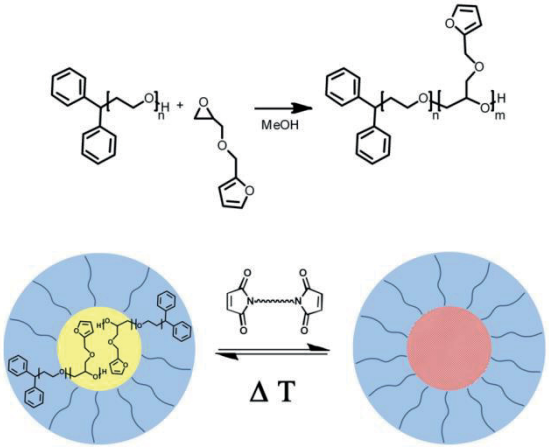

Markus J. Barthel,[#] Tobias Rudolph,[#,] Sarah Crotty, Felix H. Schacher, Ulrich S. Schubert

[#]Both authors contributed equally to this publication.

J. Polym. Sci., Part A: Polym. Chem., **2012**, *50*, 4958-4965

Homo- and Diblock Copolymers of Poly(furfuryl glycidyl ether) by Living Anionic Polymerization: Toward Reversibly Core-Crosslinked Micelles

Markus J. Barthel,[1,2,3]* Tobias Rudolph,[1,2]* Sarah Crotty,[1,2,3] Felix H. Schacher,[1,2] Ulrich S. Schubert[1,2,3]

[1]Laboratory of Organic and Macromolecular Chemistry (IOMC), Friedrich-Schiller-University Jena, Humboldtstr 10, 07743 Jena, Germany
[2]Jena Center for Soft Matter (JCSM), Friedrich-Schiller-University Jena, Humboldtstr. 10, 07743 Jena, Germany
[3]Dutch Polymer Institute (DPI), John F. Kennedylaan 2, 5612 AB Eindhoven, The Netherlands
Correspondence to: U. S. Schubert (E-mail: ulrich.schubert@uni-jena.de) or F. H. Schacher (E-mail: felix.schacher@uni-jena.de)

Received 26 July 2012; accepted 6 August 2012; published online 29 August 2012
DOI: 10.1002/pola.26327

ABSTRACT: We report the synthesis and characterization of well-defined homo- and diblock copolymers containing poly(furfuryl glycidyl ether) (PFGE) via living anionic ring-opening polymerization using different initiators. The obtained materials were characterized by SEC, MALDI-TOF MS, and ^{1}H NMR spectroscopy and molar masses of up to 9400 g/mol were obtained for PFGE homopolymers. If the amphiphilic diblock copolymer PEG-*block*-PFGE was dissolved in water, micelles with a PFGE core and a PEG corona were formed. Hereby, the hydrophobic PFGE core domains were used for the incorporation of a suitable bismaleimide and heating to 60 °C induced the crosslinking of the micellar core via Diels-Alder chemistry. This process was further shown to be reversible. © 2012 Wiley Periodicals, Inc. J Polym Sci Part A: Polym Chem 50: 4958–4965, 2012

KEYWORDS: anionic polymerization; block copolymers; cross-linking; furfuryl glycidyl ether; poly(ethylene glycol); ring-opening polymerization; self-assembly; self-healing

INTRODUCTION The preparation of micellar structures with controlled size, solubility, and surface chemistry for example, the controlled uptake and/or delivery of guest substances in selected compartments has rapidly increased over the last years.[1,2] Quite often, poly(ethylene glycol) (PEG) has been employed as the hydrophilic block, as PEG is non-toxic, chemically inert and highly water-soluble.[3,4]

For the preparation of well-defined, functionalized PEG and related poly(glycidyl ethers) with controlled molar masses, low polydispersity indices (PDIs), and predictable architectures, living anionic ring-opening polymerization (ROP) represents a powerful tool. Poly(glycidyl ethers) offer the possibility to introduce additional side-chain functionality into polyether-based polymers and block copolymers. This has been shown for example, PEG-*block*-poly(allyl glycidyl ether) block copolymers and their self-assembly into micelles in aqueous solution.[5] The PAGE segment enables post-polymerization modifications using thiol-ene chemistry and, therefore, the covalent attachment of drugs or bioactive moieties.[6–10] In that respect, Hrubý reported the attachment of doxorubicin, a drug commonly used in cancer therapy, to the PAGE compartment featuring a pH-sensitive linker to enable the selective cleavage of the drug at the target.[11] Besides PAGE, ethoxy ethyl glycidyl ether (EEGE),[12,13] or isopropyliden glyceryl glycidyl ether can be used for the synthesis of functional polyethers.[14]

An additional possibility for a (reversible) post-polymerization functionalization is the introduction of furfuryl groups. Kavita et al. used furfuryl methacrylate as a comonomer in the ATRP of methacrylates.[15] After polymerization, the furfuryl groups could be used in a subsequent Diels-Alder reaction for example, cross-linking and network formation.[16,17] Further heating above a certain temperature can be used to induce a retro-Diels-Alder reaction, resulting in a cleavage of the network junctions. Subsequent cooling restores the network and the process was shown to be fully reversible. One possible application field for these systems are self-healing materials, as recently demonstrated for PEG-based networks.[18,19] As an example for polyethers carrying furfuryl moieties in the side-chain, poly(furfuryl glycidyl ether) (PFGE) has been prepared using condensation reactions but with limited control over molar mass, molecular architecture, and PDI values.[20]

*Author Markus J. Barthel and Author Tobias Rudolph contributed equally to this work.

Additional Supporting Information may be found in the online version of this article.

Here, we report the synthesis of well-defined PFGE homopolymers and the corresponding poly(ethylene glycol)-*block*-poly(furfuryl glycidyl ether) (PEG_{139}-*b*-$PFGE_{12}$) diblock copolymer by living anionic ROP using different initiators [Diphenylmethyl potassium DPMK, sodium hydride (NaH), cesium hydroxide monohydrate (CsOH), and potassium *t*-butanolate (*t*-BuOK)]. Due to the hydrophobic nature of the PFGE block, poly(ethylene glycol)-*block*-PFGE (PEG-*b*-PFGE) diblock copolymers undergoes self-assembly in dilute aqueous solution into micelles with a PFGE core and a PEG corona. We show that a suitable crosslinker, 1-1′-(methylenedi-4,1-phenylene)bismaleimide (BMA), can be successfully encapsulated within the PFGE core domains and used for core-crosslinking upon heating of the micellar solution to 60 °C. This could be verified by dialysis of the aggregates into non-selective solvents (THF, DMF) where the micellar structure could be retained. We further demonstrate that the crosslinking process is reversible to a certain extent.

EXPERIMENTAL

Instruments

^{1}H NMR spectra were recorded on a Bruker AC 300 MHz. Size exclusion chromatography was performed on either a Shimadzu SCL-10 A system (with a LC-10AD pump, a RID-10 A refractive index detector, and a PL gel 5 μm mixed-D column at 25 °C) where the eluent was a mixture of chloroform:triethylamine:isopropanol (94:4:2) with a flow rate of 1 mL/min or on an Agilent Technologies 1200 Series SEC system equipped with a G131A isocratic pump, a G1329A autosampler, a G1362A refractive index detector, and both a PSS Gram 30 and a PSS Gram 1000 columns in series. 2.1% LiCl solution in DMA was used as eluent at 1 mL/min flow rate at a column oven temperature of 40 °C. Both systems were calibrated with PEG standards from PSS (M_n = 1470–42000 g/mol).

MALDI-TOF mass spectra were obtained using an Ultraflex III TOF/TOF mass spectrometer (Bruker Daltonics) with *trans*-2-[3-(4-*tert*-butylphenyl)-2-methyl-2-propenylidene] malononitrile or 2,5-dihydroxybenzoic acid as matrix in reflector as well as in linear mode. The instrument was calibrated prior to each measurement with an external PMMA standard from PSS Polymer Standards Services GmbH.

DLS was performed at a scattering angle of 90° on an ALV CGS-3 instrument and a He–Ne laser operating at a wavelength of λ = 633 nm at 25 °C. The CONTIN algorithm was applied to analyze the correlation functions obtained. Apparent hydrodynamic radii were calculated according to the Stokes–Einstein equation. All CONTIN plots are number-weighted.

Transmission electron microscopy (TEM) was performed on a Zeiss-CEM 902A, Oberkochen, Germany operating at 80 kV. Images were recorded using a 1k TVIPS FastScan CCD camera. No staining of the samples was necessary. For sample preparation, a drop of the micellar solution was cast onto carbon-coated TEM grids, the solvent was blotted away using filter paper, and the structures were imaged after drying.

Materials

Ethylene oxide (EO), furfuryl glycidyl ether (FGE), sodium hydride in mineral oil, potassium *t*-butanolate, cesium hydroxide monohydrate, *N, N*-dimethylformamide (DMF), tetrahydrofuran (THF), and toluene were purchased from Aldrich. Toluene was used directly from a solvent purification system (PureSolv, Innovative Technology). THF was distilled from sodium/benzophenone. EO was distilled from sodium. FGE was purified by column chromatography (eluent: ethylacetate/*n*-hexane 5/1) and vacuum drying before usage. Diphenylmethyl potassium (DPMK) was synthesized as reported previously.[1] Sodium hydride was washed with dry cyclohexane to remove the mineral oil and stored under argon. Cesium hydroxide was suspended in dry toluene and the solvent was removed under vacuum at 90 °C to dry the cesium hydroxide. The PEG precursor was synthesized via living anionic ROP of EO with DPMK in THF in a BüchiGlasUster PicoClave and dried via azeotropic distillation under vacuum from dry toluene. *t*-BuOK was used as received.

Polymerization of FGE in the Bulk

t-BuOK (5.6 mg, 0.05 mmol) were transferred into a Schlenk flask under inert conditions and 0.45 mL FGE (3.24 mmol, the ratio M:I was 65:1, $M_{n,theo}$ = 10,000 g/mol) were added. The mixture was kept for 24 h at 45 °C under vigorous stirring. The reaction was terminated by the addition of 0.1 mL methanol and the product was dried under vacuum. SEC: M_n = 5500 g/mol, PDI = 1.18. The synthesis of PFGE using NaH, CsOH, and DPMK as initiators was carried out using the same procedure.

Polymerization of FGE in Solution

Four milliliter of freshly prepared THF were transferred into a Schlenk flask and 0.071 mL DPMK (0.05 mmol) were added. Afterwards, 0.45 mL (FGE, 3.24 mmol, ratio of M:I was 65:1, and $M_{n,theo}$ = 10,000 g/mol) were introduced and the reaction was allowed to stir for 24 h at 45 °C. The reaction was terminated by the addition of 0.5 mL methanol and the product was dried under vacuum.

^{1}H NMR (300 MHz, DMSO-d_6, δ, ppm): 3.6–3.2 (br, 5H), 3.9 (t, 1H), 4.42 (s, 2H), 6.28 (m, 2H), 7.26–7.1 (m, 10H), and 7.36 (s, 1H). SEC: M_n = 2900 g/mol, PDI = 1.09; MALDI-TOF MS: M_p = 8200 g/mol.

The synthesis of PFGE using NaH, CsOH, and DPMK as initiators was carried out using the same procedure.

Synthesis of PEG-*b*-PFGE

One gram monohydroxy-functionalized PEG ($M_{p,MALDI}$ = 6100 g/mol, 0.16 mmol) was dried under vacuum at 75 °C for 2 h and dissolved in 10 mL freshly prepared THF. To activate the hydroxyl group, a stoichiometric amount of DPMK was added until the solution remained slightly red. FGE (0.73 mL, 5.3 mmol) were added and the reaction mixture was stirred for 24 h at 45 °C. The reaction was terminated by the addition of 0.5 mL methanol and the crude polymer was purified by precipitation in cold diethyl ether and dried under vacuum.

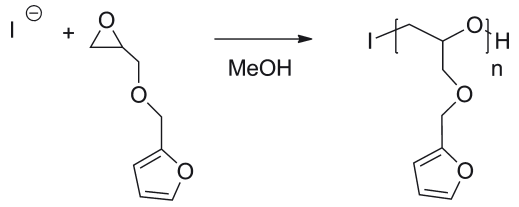

FIGURE 1 Schematic representation of the homopolymerization of FGE.

^{1}H NMR (300 MHz, DMSO-d_6, δ, ppm): 3.65–3.15 (br, PEG-backbone), 3.95 (t, 1H), 4.3 (s, 2H), 6.3 (m, 2H), 7.2–7.05 (m, 10H), 7.5 (s, 1H). SEC: M_n = 6000 g/mol, PDI = 1.06; MALDI-TOF MS: M_p = 8050 g/mol

RESULTS AND DISCUSSION

Synthesis of PFGE

The living anionic ring-opening polymerization (AROP) of allyl glycidyl ether (AGE) or EEGE represents a facile strategy for the introduction of functional groups into polyether-based materials, thus enabling post-polymerization functionalizations.[14] In most cases, click chemistry is used to modify the polymer and to adjust its properties, either in solution or in the bulk. FGE is another promising monomer for anionic ROP and subsequent post-polymerization functionalization via the pendant furane ring by, for example, Diels-Alder reactions. However, FGE was up to now only used in condensation reactions, exhibiting limited control over molar masses or PDI values.[20]

FGE was purified by column chromatography, followed by vacuum drying before usage in anionic ROP reactions. The homopolymerization in THF was first studied using DPMK as initiator, synthesized according to literature procedures.[21] For this system lower molar masses than expected were observed, even if longer reaction times (48 h) were used. Therefore, a general study of the FGE homopolymerization was performed. Hereby, we focused on different initiators for the AROP [DPMK, sodium hydride (NaH), cesium hydroxide monohydrate (CsOH), and potassium *t*-butanolate (*t*-BuOK)] (Fig. 1).

TABLE 1 Characterization Data for the PFGE Homopolymers Initiated Using Different Initiators in Bulk and in Solution

	In Bulk			In THF		
Initiator	M_n[a]	M_w[a]	PDI[a]	M_n[a]	M_w[a]	PDI[a]
NaH	2700	3200	1.18	–	–	–
CsOH	2800	3300	1.18	865	900	1.06
DPMK	3100	3500	1.11	2800	3150	1.09
t-BuOK	5500	7000	1.28	2900	3100	1.10

[a] Obtained by SEC ($CHCl_3$:*i*-Prop.:TEA 94:4:2, using PEG standards).

In addition, to study the influence of THF as solvent, the reactions were performed in solution as well as in the bulk. It can be clearly seen from the SEC traces [Fig. 2(a); Table 1] that *t*-BuOK (solid black line, $M_{n,app}$ = 5500 g/mol) lead to (apparently) higher molar masses than DPMK (dashed black line, $M_{n,app}$ = 3100 g/mol) under bulk conditions. CsOH (dotted black line, $M_{n,app}$ = 2800 g/mol), and NaH (black line with alternating dots and dashes, $M_{n,app}$ = 2700 g/mol) lead to even lower molar masses. However, coupling products were observed in case of *t*-BuOK, DPMK, and CsOH (bimodal distributions), as well as a broadening of the molar mass distribution using NaH as initiator.

To obtain a full picture, all initiators for the anionic ROP were also tested in THF. The results are displayed in Figure 2(b) and Table 1. The best results were obtained in case of *t*-BuOK (solid black line, $M_{n,app}$ = 2900 g/mol), leading to well-defined PFGE with higher molar masses as DPMK (dotted black line, $M_{n,app}$ = 2800 g/mol). No polymer was obtained for NaH, whereas CsOH (dashed black line, $M_{n,app}$ = 865 g/mol) again yielded lower molar masses.

For a detailed characterization of the obtained homopolymers, the DPMK initiated sample was studied using MALDI-TOF MS and ^{1}H NMR spectroscopy [Fig. 3(a,b)].

In this case, a molar mass (M_p) of 8200 g/mol could be determined by MALDI-TOF MS. The observed isotopic pattern in MALDI-TOF MS [Fig. 3(a), inset] corresponds well to

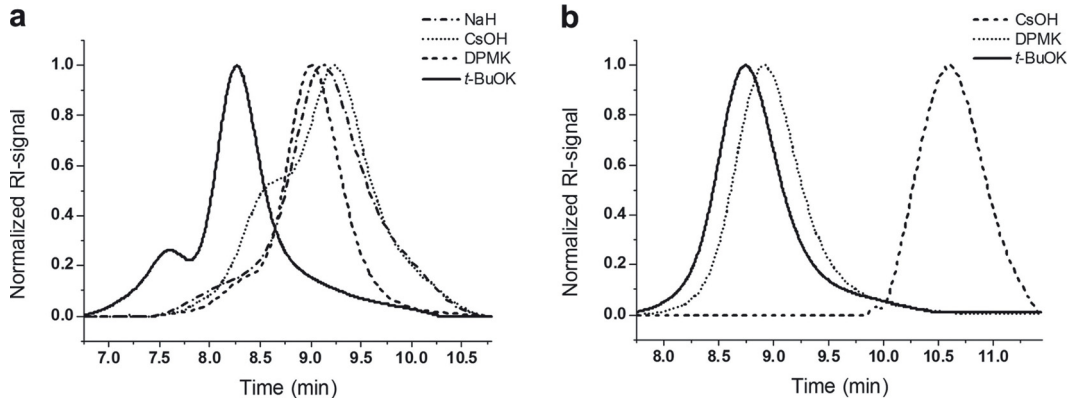

FIGURE 2 SEC traces for PFGE obtained by homopolymerization in bulk (a) and in THF (b) using different initiators for living anionic ROP.

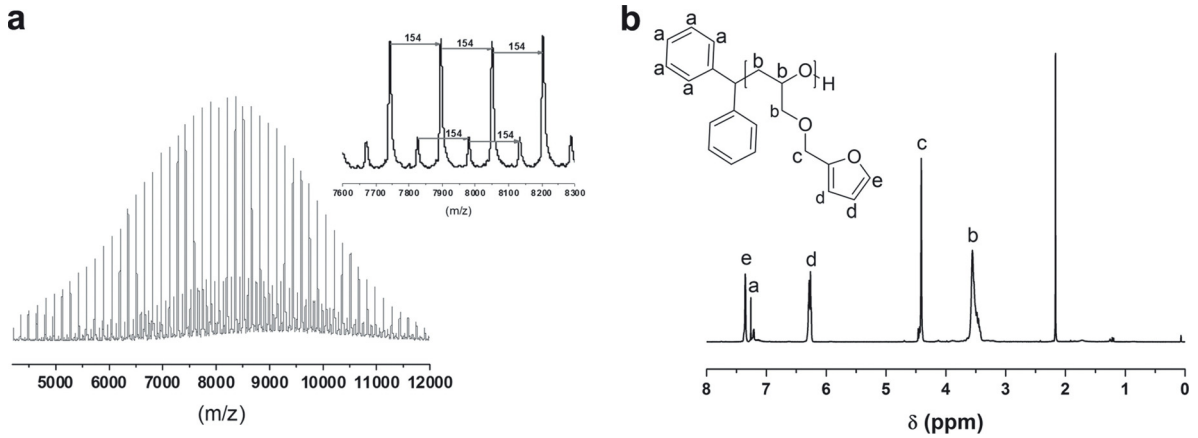

FIGURE 3 MADLI-TOF MS spectrum (a) and ^{1}H NMR (DMSO-d_6, 300 MHz) spectrum (b) of PFGE.

the calculated mass distribution with a repeating unit of 154 g/mol. The small second distribution can be attributed to side-reactions occurring during the measurement. In the ^{1}H NMR spectrum [Fig. 3(b)], the characteristic peaks for the furane ring at 7.36 and 6.26 ppm (e and d), as well as the signals for the phenyl groups of the initiator at 7.26 ppm (a) could be detected. It could be observed that the polymer shows significantly lower molar masses in the SEC measurements in comparison to the values determined by NMR and MALDI-TOF MS.

To probe the reaction kinetics for FGE, a polymerization aiming at a molar mass (M_n) of 10,000 g/mol (ratio of M:I was 65:1) using *t*-BuOK as initiator was performed in THF and monitored by a combination of SEC and ^{1}H NMR measurements. The results are displayed in Figure 4 and Table 2.

As shown in Figure 4(a) in the SEC measurements, almost no increase in the molar mass can be seen after 12 h. The conversion of the monomer was simultaneously monitored by ^{1}H NMR spectroscopy (Supporting Information Figure S1a) via the decrease of the characteristic signal of the proton next to the oxirane ring at 3.05 ppm. The signal of the two protons of the furane ring [Fig. 2(d)] was used as an internal standard. For the T24 sample ($M_{n,app}$ = 3450 g/mol) a monomer conversion of ~100% could be obtained, whereas T12 ($M_{n,app}$ = 3450 g/mol) yielded 90% FGE consumption. The living character of the polymerization is demonstrated by the semilogarithmic plot of the monomer concentration at t = 0 (M_0) divided by the concentration at $t = n$ (M_n) as displayed in Supporting Information Figure S1b. As shown in Figure 4(b), MALDI-TOF MS measurements yielded a molar mass (M_p) of 9400 g/mol for T24, being in good agreement with the targeted value of 10,000 g/mol. The small differences can be attributed to the handling of the initiator in very small amounts (6 mg *t*-BuOK) in the glovebox.

Synthesis of PEG-*b*-PFGE

For the synthesis of an AB diblock copolymer, PEG-*b*-PFGE, sequential anionic ROP of EO and FGE, respectively [Fig. 5(a)] was performed. As initiator, DPMK was used due to the possibility of an exact titration of the hydroxyl groups of the PEG macroinitiator, presumably avoiding the formation of homopolymer due to an excess of initiator. The PEG

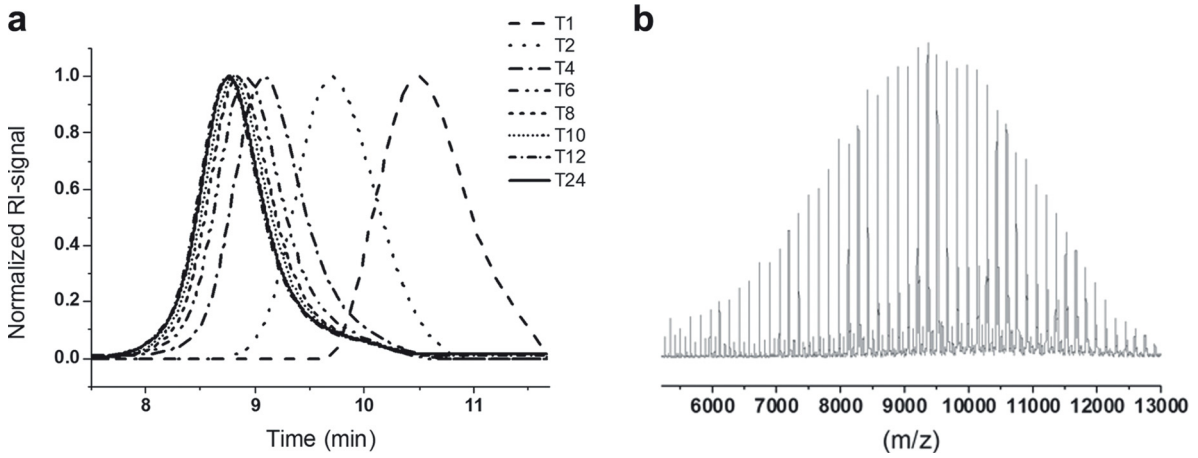

FIGURE 4 SEC traces for a kinetic study of the PFGE homopolymerization (a) and the corresponding MALDI-TOF MS spectrum of the final product (b, M_p = 9400 g/mol).

TABLE 2 Characterization Data for the Kinetic Study of the PFGE Homopolymerization

Sample	M_n[a]	M_w[a]	PDI[a]	Conversion[b] (%)
PFGE T1	900	1000	1.11	11
PFGE T2	1800	1900	1.07	30
PFGE T4	2750	3050	1.11	45
PFGE T6	3150	3500	1.10	64
PFGE T8	3300	3700	1.11	77
PFGE T10	3400	3800	1.12	82
PFGE T12	3450	3850	1.12	90
PFGE T24	3450	3850	1.12	100

[a] Obtained by SEC ($CHCl_3$:*i*-Prop.:TEA 94:4:2, using PEG standards).
[b] Determined by ^{1}H NMR.

precursor was prepared using DPMK as initiator for EO in THF.[21] The corresponding macroinitiator, PEG-OH with a molar mass (M_n) of 6100 g/mol and a PDI value of 1.05, was subsequently reactivated using DPMK, followed by the addition of FGE. MALDI-TOF MS [Fig. 5(b)] revealed a molar mass (M_n) of 8050 g/mol for the obtained PEG-*b*-PFGE diblock copolymer. Both PEG-OH and PEG-*b*-PFGE were further analyzed by SEC [Fig. 5(c)] and a shift to lower elution volume as well as a narrow PDI of 1.06 was obtained for the diblock copolymer.

The characteristic signals of the PEG backbone (3.5–3.2 ppm) and the furfuryl groups in the side-chain (7.5, 6.3, and 4.3 ppm) are also visible in the ^{1}H NMR spectrum (Supporting Information Fig. S2), resulting in a composition of PEG_{139}-*b*-$PFGE_{12}$, where the subscripts denote the degrees of polymerization of the respective segment.

As shown in Table 3 for PEG-*b*-PFGE, the obtained molar mass (M_n) of 8200 g/mol is significantly lower than the calculated one with 10,000 g/mol. One possible explanation for this could be the formation of aggregates during the polymerization in THF, thus limiting the molar mass. If the diblock copolymer is directly dissolved in THF, dynamic light scattering (DLS) yields mainly unimolecular polymer chains ($R_{h,app}$ = 4 nm), but also larger aggregates ($R_{h,app}$ = 300 nm) after 24 h (Supporting Information Fig. S3). This confirms the results obtained for the homopolymerization of FGE using different initiators, that is, that the ROP of FGE in THF does not reach full conversion if DPMK is used as an initiating system. Nevertheless, THF remained the solvent of choice due the even larger aggregates (~100 nm) formed immediately after dissolving PEG-*b*-PFGE in toluene and the insolubility of PEG-*b*-PFGE in cyclohexane or ethylbenzene.

Self-Assembly of PEG-*b*-PFGE in Water

Due to its amphiphilic nature, PEG_{139}-*b*-$PFGE_{12}$ forms micelles in dilute aqueous solution, as demonstrated using DLS experiments. The structures presumably consist of a hydrophobic PFGE core and a hydrophilic PEG corona [Fig. 6(a)] and we assume a spherical shape of the particles.

Directly after dissolution in water, micelles of $R_{h,app}$ = 10 nm and with a rather narrow size-distribution were obtained

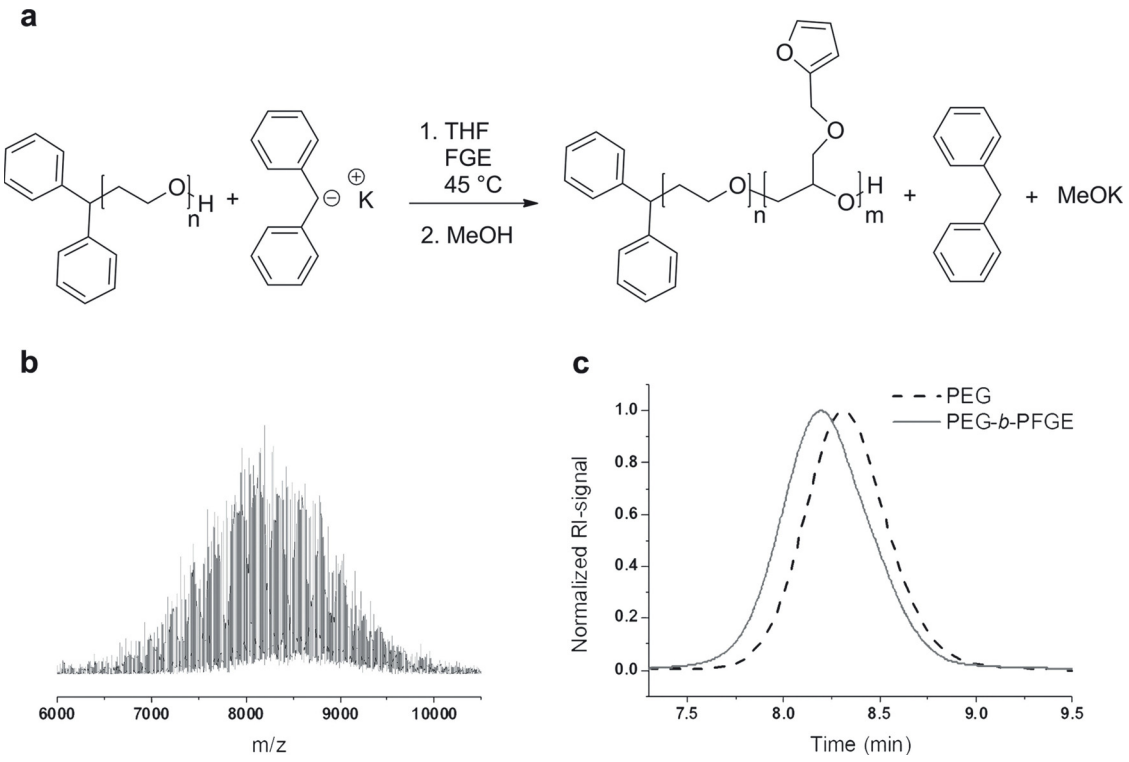

FIGURE 5 Synthesis of PEG-*b*-PFGE using sequential living anionic ROP (a), MALDI-TOF MS spectrum (b), and SEC traces for the PEG precursor (dashed black line) and PEG-*b*-PFGE (c, solid gray line).

TABLE 3 Characterization Data for Homopolymers and Block Copolymers

Sample	$M_{n,theo}$ (g/mol)	$M_{n,SEC}$ (g/mol)	$M_{p,MALDI}$ (g/mol)	PDI
PEG[a]	5000	5100[b]	6100	1.05[b]
PEG_{139}-*b*-$PFGE_{12}$[c]	10,000	6000[b]	8050	1.06[b]

[a] Precursor.
[b] Obtained by SEC ($CHCl_3$:*i*-Prop.:TEA 94:4:2, using PEG standards).
[c] Subscripts denote the degrees of polymerization of the corresponding block determined by ^1H NMR spectroscopy.

(Supporting Information Fig. S3a). The core-forming block, PFGE, can now be crosslinked via a Diels-Alder reaction, using a bisfunctional crosslinker, for example, a bismaleimide [Reaction scheme in Fig. 6(a)]. The controlled crosslinking of selected domains in micellar structures is desirable and can be used to enhance their resistance against degradation, limit the diffusion of guest molecules into or out of the core domains, or ensure the stability within desired environments.[22–24]

In our case, crosslinking of the micellar core was achieved by a [4 + 2] cycloaddition reaction [Fig. 6(a)]. For this purpose, PEG_{139}-*b*-$PFGE_{12}$ and a bisfunctional crosslinker, 1-1′-(methylenedi-4,1-phenylene)bismaleimide (BMA), were dissolved in DMF at a concentration of 15 g/L and a molar ratio crosslinker/PFGE of 50/1. To encapsulate the BMA linker within the hydrophobic PFGE core domains, water was slowly added until a turbid solution was obtained (water:DMF = 2:1). The remaining DMF was then removed by dialysis against water and the resulting aqueous solution was analyzed by DLS. The exact amount of encapsulated material is difficult to estimate, as BMA is insoluble in water and partially precipitated during dialysis. For the PEG_{139}-*b*-$PFGE_{12}$ micelles containing BMA in the core, a radius of $R_{h,app}$ = 6 nm was detected in water afterwards. To induce crosslinking of the core domains, the solution was subsequently heated to 60 °C for several hours. According to DLS, the micellar size did not change significantly upon the crosslinking procedure [Fig. 6(b)]. To prove the successful crosslinking of the PFGE core, the micelles were transferred to nonselective solvents for both blocks, THF and DMF. Therefore, the aqueous micellar solution was poured into an excess of, for example, THF so that the ratio was THF:H_2O = 6:1 (concentration = 0.8 g/L), dialyzed against THF and again analyzed by DLS [Fig. 6(c)]. Here, micelles with a radius of $R_{h,app}$ = 15 nm could be detected. The increase in size can be explained by a certain swelling of the crosslinked PFGE core in THF as a nonselective solvent. In a next step, the solvent was removed under vacuum and DMF as an alternative nonselective solvent was added (concentration = 1.6 g/L). Again, DLS studies revealed micelles with a solvent-swollen PFGE core and a radius of $R_{h,app}$ = 10 nm even after several days [Fig. 6(d)]. These results clearly indicate a successful crosslinking of the PFGE core. The structure of the PEG-*b*-PFGE micelles was also investigated using TEM (Fig. 7). As can be seen, spherical structures with diameters of ~20 nm but also larger species, most probably due to aggregation occurring during the drying process, can be

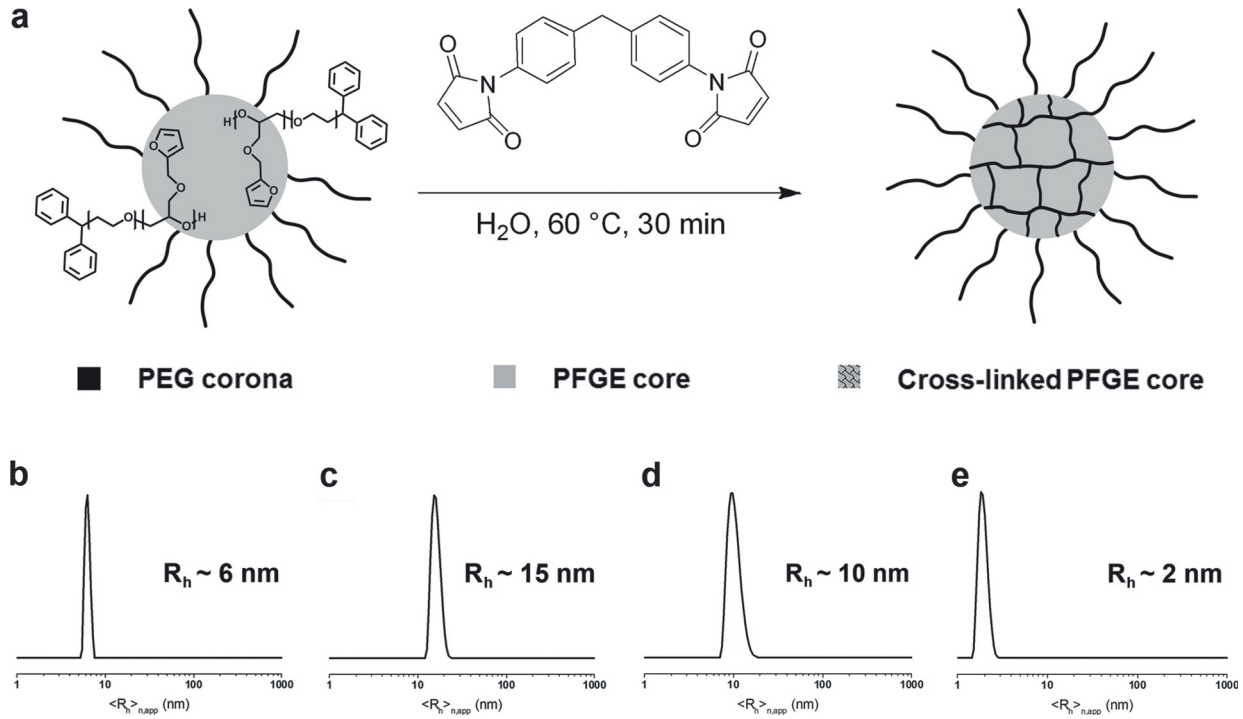

FIGURE 6 Crosslinking of the micellar core (a), number-weighted DLS CONTIN plots for PEG-*b*-PFGE micelles in water after crosslinking (b), in THF (c), and DMF (d), and after the retro-Diels-Alder reaction in DMF (e).

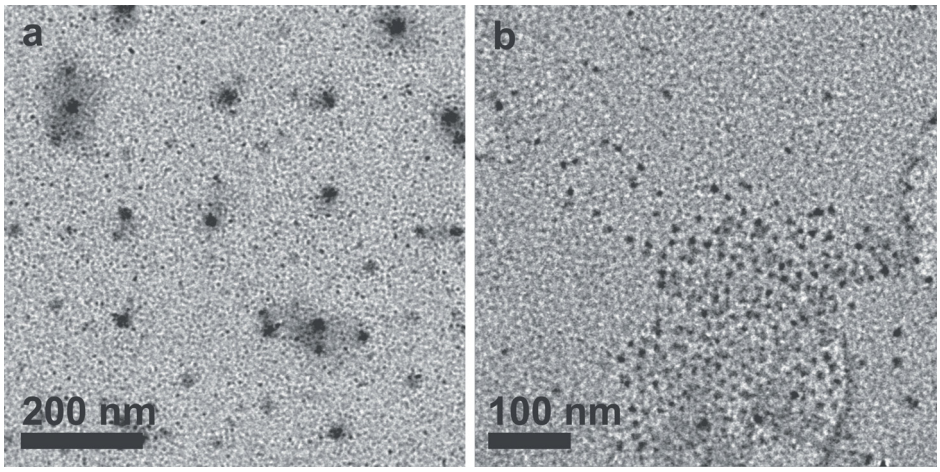

FIGURE 7 TEM micrographs of PEG_{139}-*b*-$PFGE_{12}$ micelles cast from aqueous solution (a) or after crosslinking of the PFGE core and subsequent dialysis to THF (b) onto carbon-coated TEM grids.

observed directly after dissolution of PEG_{139}-*b*-$PFGE_{12}$ in water [Fig. 7(a)]. The dark spots represent the PFGE core; the PEG corona is not visible under these conditions. After crosslinking of the PFGE core and subsequent dialysis into THF, again spherical micelles can be observed [Fig. 7(b)]. Here, core sizes of 10–20 nm are observed, again proving a successful crosslinking of the PFGE core domains.

Additionally, the crosslinking could be proven by the disappearance of the furan signals (6.3 and 4.3 ppm, Fig. 8) in ^{1}H NMR after prolonged heating at 60 °C (Fig. 8). Moreover, a new signal (5.3 ppm) appears which can be assigned to the double bond formed during the DA reaction. Although this indicates complete consumption of the furan moieties, the exact amount of encapsulated BMA is unknown and the presence of unreacted PFGE cannot be excluded. As the crosslinking via Diels-Alder chemistry should be reversible, the micellar solution was further heated to higher temperatures (150 °C) for 30 min in DMSO. As shown in Figure 8, the signals for the furan ring reappear, but also the signal for the cross-linked species is still present. Integration suggests that ~50% of the core undergo retro-DA reactions under these conditions, also for longer reaction times (6 h). Nevertheless, DLS after 2 h shows that unimolecular block copolymer chains are present [$R_{h,app}$ = 2 nm, Fig. 6(e)]. Presumably, the dissolution of the micellar core leads increases the conformational freedom of the polymer chains and decreases the concentration of reaction sites, which might explain the incomplete retro-DA reaction.

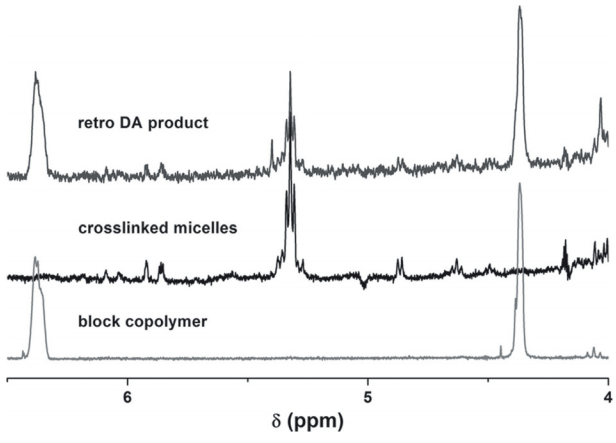

FIGURE 8 Characteristic region of the ^{1}H NMR (DMSO, 300 MHz) spectrum of PEG-*b*-PFGE, core-crosslinked micelles, and the retro-Diels-Alder product.

CONCLUSION

In summary, we synthesized well-defined homo- and diblock copolymers containing FGE with a narrow molar mass distribution (PDI < 1.1), molar masses (M_p) of up to 9400 g/mol for PFGE, and studied the influence of different initiators and the reaction kinetics in detail. For the PEG_{139}-*b*-$PFGE_{12}$ diblock copolymer, self-assembly in aqueous solution resulted in the formation of well-defined spherical micelles with a PFGE core and a PEG corona. One intriguing feature of the herein employed hydrophobic domain, PFGE, is that it can be reversibly crosslinked using Diels-Alder chemistry. The core-crosslinked micelles retain their structure in nonselective solvents like THF or DMF. For the retro-DA process, however, high temperatures are necessary and only a conversion of 50% could be observed. Nevertheless, the micellar cores were shown to disassemble into unimolecular chains. One possible improvement regarding the crosslinking process could be the use of a bismaleimide linker with a less rigid or pH-labile spacer, improving either the solubility or a triggered dissolution of the micellar cores. Although the initial results reported here describe only one single diblock copolymer (PEG_{139}-*b*-$PFGE_{12}$), the concept could be convincingly demonstrated. In the future, we will extend this to block copolymers with different weight fractions, giving access to other and also more complex morphologies in solution.[25] Whereas the reversible crosslinking of the core in spherical core-corona systems might be interesting for controlled release or surface patterning from non-selective solvents, such processes would be very

appealing if applied to vesicular,[26] tubular, or cylindrical structures.[27]

ACKNOWLEDGMENTS

The authors wish to acknowledge the Dutch Polymer Institute (DPI, technology area high-throughput-experimentation, project #690) and the Thuringian Ministry for Education, Science and Culture (grant #B514-09051, NanoConSens) for financial support of this study. F. H. S. and T. R. are grateful to the Thuringian Ministry for Education, Science, and Culture (TMBWK; #B515-10065, ChaPoNano) for financial support.

REFERENCES AND NOTES

1 Tyrrell, Z. L.; Shen, Y. Q.; Radosz, M. *Prog. Polym. Sci.* **2010**, *35*, 1128–1143.

2 Schacher, F. H.; Rupar, P. A.; Manners, I. *Angew. Chem. Int. Ed.* **2012**, *51*, 7898–7921.

3 Harris, J. M.; Chess, R. B. *Nat. Rev. Drug. Discov.* **2003**, *2*, 214–221.

4 Knop, K.; Hoogenboom, R.; Fischer, D.; Schubert, U. S. *Angew. Chem. Int. Ed.* **2010**, *49*, 6288–6308.

5 Hruby, M.; Konak, C.; Ulbrich, K. *J. Appl. Polym. Sci.* **2005**, *95*, 201–211.

6 Koyama, Y.; Umehara, M.; Mizuno, A.; Itaba, M.; Yasukouchi, T.; Natsume, K.; Suginaka, A.; Watanabe, K. *Bioconjugate Chem.* **1996**, *7*, 298–301.

7 Obermeier, B.; Frey, H. *Bioconjugate Chem.* **2011**, *22*, 436–444.

8 Ozdemir, F.; Keul, H.; Mourran, A.; Möller, M. *Macromol. Rapid. Commun.* **2011**, *32*, 1007–1013.

9 Hunt, J. N.; Feldman, K. E.; Lynd, N. A.; Deek, J.; Campos, L. M.; Spruell, J. M.; Hernandez, B. M.; Kramer, E. J.; Hawker, C. J. *Adv. Mater.* **2011**, *23*, 2327–2331.

10 Barthel, M. J.; Babiuch, K.; Rudolph, T.; Vitz, J.; Hoeppener, S.; Gottschaldt, M.; Hager, M. D.; Schacher, F. H.; Schubert, U. S. *J. Polym. Sci. Part A: Polym. Chem.* **2012**, *50*, 2914–2923.

11 Hruby, M.; Konak, C.; Ulbrich, K. *J. Controlled Release* **2005**, *103*, 137–148.

12 Reinicke, S.; Schmelz, J.; Lapp, A.; Karg, M.; Hellweg, T.; Schmalz, H. *Soft Matter* **2009**, *5*, 2648–2657.

13 Toy, A. A.; Reinicke, S.; Müller, A. H. E.; Schmalz, H. *Macromolecules* **2007**, *40*, 5241–5244.

14 Obermeier, B.; Wurm, F.; Mangold, C.; Frey, H. *Angew. Chem. Int. Ed.* **2011**, *50*, 7988–7997.

15 Kavitha, A. A.; Singha, N. K. *J. Polym. Sci. Part A: Polym. Chem.* **2007**, *45*, 4441–4449.

16 Kavitha, A. A.; Singha, N. K. *Macromolecules* **2010**, *43*, 3193–3205.

17 Bergman, S. D.; Wudl, F. *J. Mater. Chem.* **2008**, *18*, 41–62.

18 Imbesi, P. M.; Fidge, C.; Raymond, J. E.; Cauet, S. I.; Wooley, K. L. *ACS Macro Lett.* **2012**, *1*, 473–477.

19 Tian, Q. A.; Rong, M. Z.; Zhang, M. Q.; Yuan, Y. C. *Polym. Int.* **2010**, *59*, 1339–1345.

20 Pratama, P. A.; Peterson, A. M.; Palmese, G. R. *Macromol. Chem. Phys.* **2012**, *213*, 173–181.

21 Normant, H.; Angelo, B. *Bull. Soc. Chim. Fr.* **1960**, *2*, 354–359.

22 Kim, Y.; Pourgholami, M. H.; Morris, D. L.; Stenzel, M. H. *Biomacromolecules* **2012**, *13*, 814–825.

23 Schacher, F.; Walther, A.; Ruppel, M.; Drechsler, M.; Müller, A. H. E. *Macromolecules* **2009**, *42*, 3540–3548.

24 O'Reilly, R. K.; Hawker, C. J.; Wooley, K. L. *Chem. Soc. Rev.* **2006**, *35*, 1068–1083.

25 Percec, V.; Wilson, D. A.; Leowanawat, P.; Wilson, C. J.; Hughes, A. D.; Kaucher, M. S.; Hammer, D. A.; Levine, D. H.; Kim, A. J.; Bates, F. S.; Davis, K. P.; Lodge, T. P.; Klein, M. L.; DeVane, R. H.; Aqad, E.; Rosen, B. M.; Argintaru, A. O.; Sienkowska, M. J.; Rissanen, K.; Nummelin, S.; Ropponen, J. *Science* **2010**, *328*, 1009–1014.

26 Discher, B. M.; Won, Y.-Y.; Ege, D. S.; Lee, J. C.-M.; Bates, F. S.; Discher, D. E.; Hammer, D. A. *Science* **1999**, *284*, 1143–1146.

27 Zhang, X.; Tanner, P.; Graff, A.; Palivan, C. G.; Meier, W. *J. Polym. Sci. Part A: Polym. Chem.* **2012**, *50*, 2293–2318.

Supporting information for

"Homo- and Block Copolymers of Poly(furfuryl glycidyl ether) by Living Anionic Polymerization: Towards Reversibly Core-Crosslinked Micelles"

Markus J. Barthel,[1,2,3§] Tobias Rudolph,[1,2§] Sarah Crotty,[1,2] Felix H. Schacher[1,2]* and Ulrich S. Schubert[1,2,3]*

[1] Laboratory of Organic and Macromolecular Chemistry (IOMC), Friedrich-Schiller-University Jena, Humboldtstr. 10, 07743 Jena, Germany.

[2] Jena Center for Soft Matter (JCSM), Friedrich-Schiller-University Jena, Philospophenweg, 07743 Jena, Germany.

[3] Dutch Polymer Institute (DPI), John F. Kennedylaan 2, 5612 AB Eindhoven, The Netherlands.

§ These authors contributed equally to this work.

Materials and methods:

^{1}H NMR spectra were recorded on a Bruker AC 300 MHz using the residual solvent signal as an internal standard.

DLS was performed at a scattering angle of 90° on an ALV CGS-3 instrument and a He–Ne laser operating at a wavelength of λ = 633 nm at 25 °C. The CONTIN algorithm was applied to analyze the correlation functions obtained. Apparent hydrodynamic radii were calculated according to the Stokes–Einstein equation. All CONTIN plots are number-weighted.

Kinetic study of PFGE:

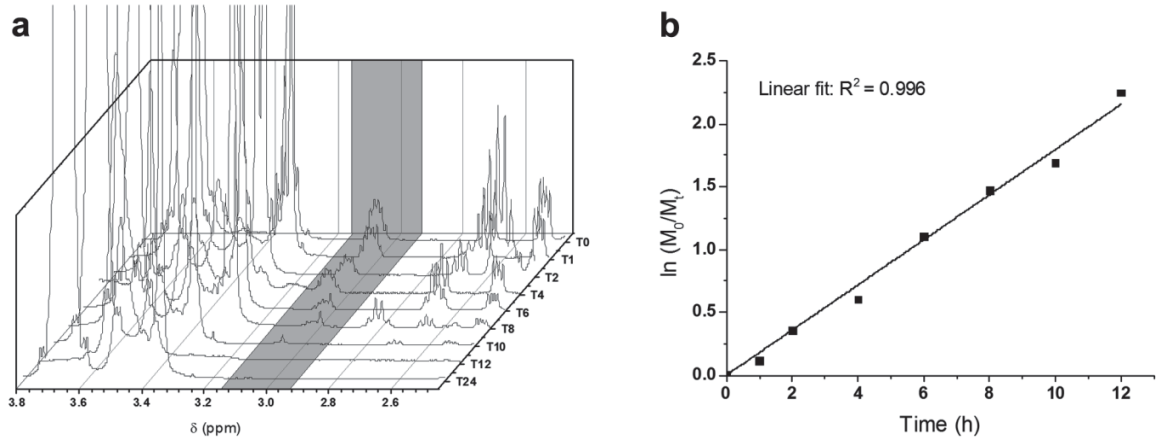

Figure S1. ^{1}H NMR traces of the kinetic study of the PFGE homopolymerization (a) and logarithmic plot of conversion against time (b).

PEG-*b*-PFGE:

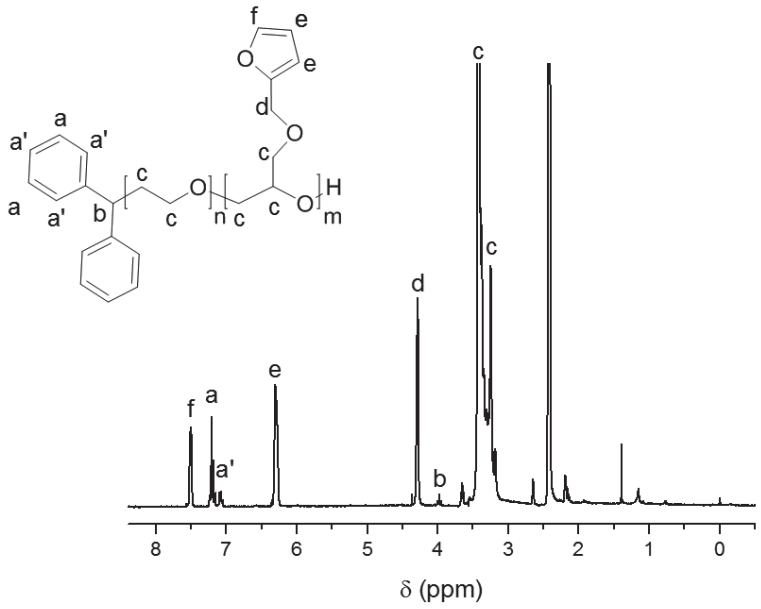

Figure S2: ^{1}H NMR (DMSO-d_6, 300 MHz) spectrum of PEG-*b*-PFGE.

DLS investigations of the diblock copolymer:

For DLS investigations 5 mg of the diblock copolymer PEG-*b*-PFGE were directly dissolved in 1 mL of a selective (H_2O), a non-selective solvent (DMF), as well as in the reaction solvent (THF). The corresponding behavior in solution was investigated and depicted in **Figure S2**. In water the amphiphilic block copolymer forms spherical micelles with a radius of $R_{h,app}$ = 10 nm.

For the reaction solvent, THF, particles with a radius of $R_{h,app}$ = 4 nm were obtained directly after dissolution. Over 24 h, this size increased up to several hundreds of nm and the solution turned slightly turbid, which indicates the formation of large agglomerates/micelles, which might also be an explanation for the lower degree of polymerization for PFGE during the polymerization.

As a non-selective solvent DMF was further used for the investigation of the diblock copolymer in solution showing a monomodal size distribution of $R_{h,app}$ = 2 nm.

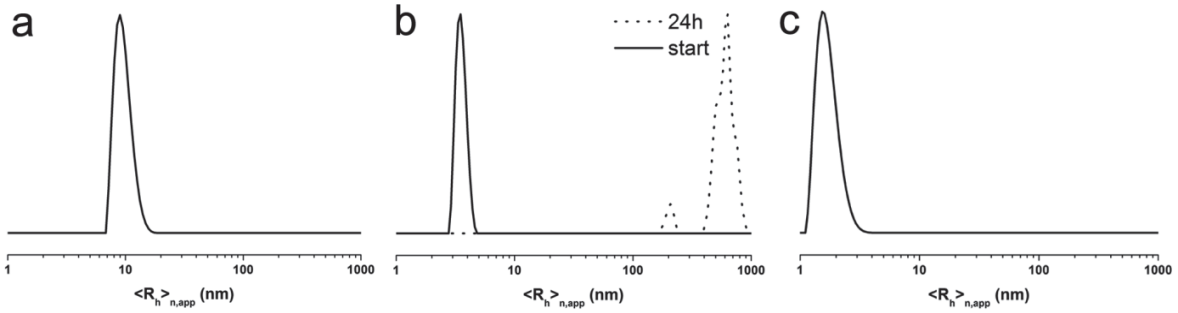

Figure S3: Number-weighted DLS CONTIN plots for PEG-*b*-PFGE in water (a), as well as directly after dissolving in THF and after 24 h in THF (b) or DMF (c).

1. H. Normant, B. Angelo, B. *Bull. Soc. Chim. Fr.* **1960**, 354.

Publication P8

"Self-Healing Materials via Reversible Crosslinking of Poly(ethylene oxide)-*block*-poly(furfuryl glycidyl ether) (PEO-*b*-PFGE) Block Copolymer Films"

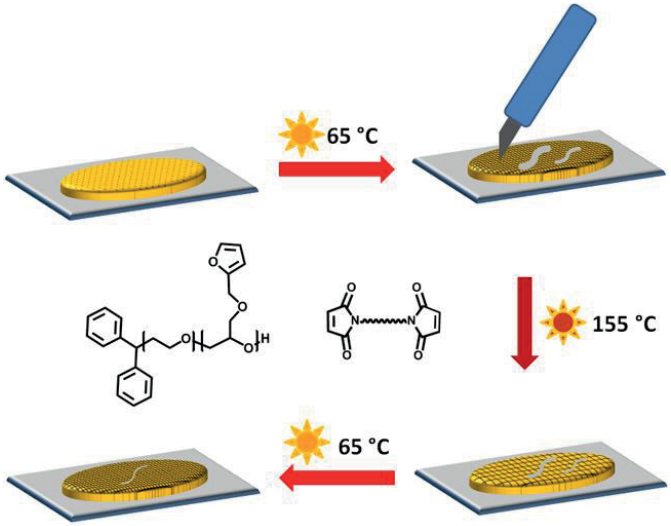

Markus J. Barthel, Tobias Rudolph, Anke Teichler, Renzo M. Paulus, Jürgen Vitz, Stephanie Hoeppener, Martin D. Hager, Felix H. Schacher, Ulrich S. Schubert

Adv. Funct. Mater., **2013**, *23*, 4921-4932

ADVANCED FUNCTIONAL MATERIALS
www.afm-journal.de

Self-Healing Materials via Reversible Crosslinking of Poly(ethylene oxide)-*Block*-Poly(furfuryl glycidyl ether) (PEO-*b*-PFGE) Block Copolymer Films

*Markus J. Barthel, Tobias Rudolph, Anke Teichler, Renzo M. Paulus, Jürgen Vitz, Stephanie Hoeppener, Martin D. Hager, Felix H. Schacher * and Ulrich S. Schubert**

The application of well-defined poly(furfuryl glycidyl ether) (PFGE) homopolymers and poly(ethylene oxide)-*b*-poly(furfuryl glycidyl ether) (PEO-*b*-PFGE) block copolymers synthesized by living anionic polymerization as self-healing materials is demonstrated. This is achieved by thermo-reversible network formation via (retro) Diels-Alder chemistry between the furan groups in the side-chain of the PFGE segments and a bifunctional maleimide crosslinker within drop-cast polymer films. The process is studied in detail by differential scanning calorimetry (DSC), depth-sensing indentation, and profilometry. It is shown that such materials are capable of healing complex scratch patterns, also multiple times. Furthermore, microphase separation within PEO-*b*-PFGE block copolymer films is indicated by small angle X-ray scattering (lamellar morphology with a domain spacing of approximately 19 nm), differential scanning calorimetry, and contact angle measurements.

1. Introduction

The capability to heal inflicted damage is ubiquitous in nature as, e.g., shown via the merging of broken bones, the closure of injured blood vessels,[1–3] or the healing of byssal threads of marine mussels.[4] The present awareness that the availability of raw materials will decrease, accompanied by increasing material and production costs, renders self-healing approaches an attractive research field in polymer chemistry and materials science. Particular interest is devoted to the facile introduction of such features into mechanically robust polymeric systems whilst maintaining synthetic feasibility and, even more important, processability of the resulting materials.

Different methods have been reported to introduce self-healing properties to a polymeric material.[5–7] One possibility is the encapsulation of reactive ingredients (a polymerizable healing agent and an initiator) within the desired material. Scratching or crack formation leads to a release of the embedded substances (e.g., by rupture of microcapsules), followed by mixing of both ingredients and resulting in a healing process of the damaged material.[8] This approach was also extended by the introduction of vascular networks containing a healing agent, which was released upon rupture.[9] Therefore, multiple healing processes are possible. A second approach represents the use of intermolecular forces. For this purpose, reversible interactions (i.e., crosslinks) of polymer chains with, e.g., hydrogen bonds represent a widely used strategy. After being damaged, these bonds allow a healing due to the reformation of bonds without any external stimuli such as heating or irradiation being necessary. This has been achieved using highly specific donor-acceptor systems,[10–15] and could recently be also applied for "hard" epoxy networks.[16] Another example of this approach are metal-ligand interactions. Thereby, materials consisting of polymers or oligomers comprising reversible non-covalent metal-ligand interactions (e.g., 2,6-bis(1′-methylbenzimidazolyl)pyridine or terpyridine, as well as corresponding metal ions) can heal inflicted damage.[17,18] Also, this ability represents an inherent material characteristic (i.e. intrinsic self-healing materials) and does not require the encapsulation of external healing agents. Moreover, the application of π–π interactions in self-healing processes has also been demonstrated for, e.g., pyrenyl units which interact with naphthalene diimide oligomers to reversibly crosslinked polymeric networks.[19,20]

M. J. Barthel, T. Rudolph, A. Teichler, R. M. Paulus, Dr. J. Vitz, Dr. S. Hoeppener, Dr. M. D. Hager, Prof. F. H. Schacher, Prof. U. S. Schubert
Laboratory of Organic and Macromolecular Chemistry (IOMC)
Friedrich Schiller University Jena
Humboldtstr. 10, 07743 Jena, Germany
E-mail: felix.schacher@uni-jena.de; ulrich.schubert@uni-jena.de
M. J. Barthel, T. Rudolph, A. Teichler, R. M. Paulus, Dr. J. Vitz, Dr. S. Hoeppener, Dr. M. D. Hager, Prof. F. H. Schacher, Prof. U. S. Schubert
Jena Center for Soft Matter (JCSM)
Friedrich-Schiller-University Jena
Philosophenweg 7, 07743 Jena, Germany
M. J. Barthel, A. Teichler, Dr. J. Vitz, Dr. S. Hoeppener, Prof. U. S. Schubert
Dutch Polymer Institute (DPI)
John F. Kennedylaan 2, 5612 AB Eindhoven, The Netherlands

DOI: 10.1002/adfm.201300469

The temperature-dependent reversible covalent crosslinking of polymers or block copolymers represents another interesting concept for the implementation of intrinsic self-healing into a material. Hereby, the Diels-Alder reaction represents a powerful tool.[21–27] One well-known example is the combination of furan and maleimide functionalities.[28–30] In this context, we have recently reported that furfuryl glycidyl ether can be used as a monomer for living anionic polymerization and the preparation of well-defined poly(ethylene oxide)-*b*-poly(furfuryl glycidyl ether) (PEO-*b*-PFGE) block copolymers comprising furan units in the side chain.[31] Subsequently, the furan units were used for the reversible core-crosslinking of the micelles formed by these block copolymers in selective solvents for the PEO segment. The application of polymer networks bearing free furan groups with a suitable linker (e.g., bismaleimides) in reversible Diels-Alder reactions represents a powerful system for potential self-healing applications.[21–24,28–30,32–34] This has been recently reported in the case of furfuryl glycidyl ether,[35,36] where the epoxy-ring was used in a condensation reaction with amino groups to create polymeric materials. These polymers can be turned into a network structure by reacting them with a bismaleimide compound.

We were now interested in exploiting the features of PEO-*b*-PFGE block copolymers for the generation of self-healing materials, in particular of nanostructured polymer films. Apart from the use of PEO-related materials in biological and medical context for PEG-ylation or drug-delivery approaches, PEO is widely used in the field of coatings. Here, antifouling properties, proliferated cell adhesion, or the coating of food supplement products have been described.[37–42] Moreover, the employment of block copolymers in self-healing applications represents an attractive approach. Such materials undergo microphase separation in bulk into a variety of well-documented morphologies.[43] In the case of AB diblock copolymers, this might be one way to solve a fundamental problem related to self-healing materials: the combination of strong reversible interactions between individual polymer chains together with dynamic properties (low glass transition temperature segments). However, such approaches have been rarely described,[44–48] as mostly statistical or random copolymers have been used for such purposes.

We herein describe the synthesis of well-defined PEO-*b*-PFGE block copolymers via living anionic ring-opening polymerization. Films of these materials were reversibly crosslinked using Diels-Alder (DA)/retro Diels-Alder (rDA) chemistry and investigated with regard to possible self-healing behavior. Multiple healing cycles as well as even complex damage patterns can be recovered, and the extent of the healing process (length, width of scratches as well as the time frame) were carefully investigated with a combination of differential scanning calorimetry (DSC), depth-sensing indentation, and profilometry studies. We further show that PEO-*b*-PFGE block copolymers undergo phase separation in the bulk, as indicated by small angle X-ray scattering, differential scanning calorimetry, and contact angle measurements.

2. Experimental Section

2.1. Instruments

^{1}H NMR spectra were recorded on a Bruker AC 300 MHz spectrometer in chloroform. Size exclusion chromatography (SEC) was performed on a Shimadzu SCL-10A system (with a LC-10AD pump, a RID-10A refractive index detector, and a PL gel 5 μm mixed-D column at RT), the eluent was a mixture of chloroform:triethylamine:*iso*-propanol (94:4:2) with a flow rate of 1 mL min^{-1}. The system was calibrated with poly(ethylene glycol) standards from PSS (M_n = 1470 g mol^{-1} to 42 000 g mol^{-1}). MALDI–ToF mass spectra were obtained using an Ultraflex III ToF/ToF mass spectrometer (Bruker Daltonics) with *trans*-2-[3-(4-*tert*-butylphenyl)-2-methyl-2-propenylidene] malononitrile (DCTB) or 2,5-dihydroxybenzoic acid (DHB) as matrix in reflector as well as in linear mode. The instrument was calibrated prior to each measurement with an external PMMA standard from PSS Polymer Standards Services GmbH. Surface topography as well as film thicknesses were measured using an optical interferometric profiler Wyko NT9100 (Veeco, Germany). The instrument is equipped with three objectives (2.5×, 5× and 20×), which enable effective magnifications between 1× to 40×. Differential scanning calorimetry (DSC) was performed on a Netzsch DSC 204 F1 equipped with a liquid nitrogen dewar. Dried samples were weighed into aluminum crucibles in amounts ranging from 5 to 20 mg, and an empty aluminum crucible was used as reference. The samples were measured with a temperature program consisting of three heating runs ranging from –150 to 150 °C with a heating rate of 20 K min^{-1} for the first heating run and 10 K min^{-1} for the second and third heating runs. The glass transition temperatures (T_g) were determined from the second and third heating runs (onset value). All thermograms were exported in graphs with exo down.

Mechanical Properties: The elastic moduli of the materials were characterized via depth-sensing indentation (DSI) using a TriboIndenter TI 900 (Hysitron Inc., Minneapolis, MN) with a NanoDMA 06 transducer, equipped with a conospherical diamond indenter tip of ≈4.7 μm radius. The polymer films were prepared by drop casting and dried afterwards under air. The measurements were conducted at ambient conditions, at 23 ± 1 °C and 31 ± 6% relative humidity (RH) for $PFGE_{55}$ and at 23 ± 1 °C and 30.0 ± 3% RH for PEO_{330}-*b*-$PFGE_{20}$, as measured with a Voltcraft DL–141TH data logger. For quasi-static testing, an open loop load function with 1 s loading, 2 s hold at maximum load, and 1 s unloading profile was applied.[49] All measurements were performed in a single automated run in less than 3 h for one sample. The reduced modulus E_r was determined from the unloading response using the analysis method proposed by Oliver and Pharr.[50] Measurements were repeated at sixteen maximum loads in a 4 × 4 array, for $PFGE_{55}$ increasing in steps of 120 μN from 100 to 1900 μN or in steps of 140 μN from 100 to 2200 μN, respectively. PEO_{330}-*b*-$PFGE_{20}$ was measured in steps of 100 μN from 100 to 1600 for the film and in steps of 120 μN from 100 to 1900 μN for the crosslinked sample. Values are averaged from at least ten measurements each. From the reduced modulus E_r, the indentation modulus

E_i was calculated using the elastic modulus and Poisson's ratio of the diamond indenter, 1140 GPa and 0.07, respectively, and a Poisson's ratio of 0.4 for the polymeric material, according to

$$E_{i,\text{sample}} = \frac{1 - v^2_{\text{sample}}}{\frac{1}{E_{r,\text{sample}}} - \frac{1-v^2_{\text{indenter}}}{E_{\text{indenter}}}} \quad (1)$$

The hardness is defined as:

$$H = \frac{P_{\max}}{A} \quad (2)$$

Small and Wide Angle X-Ray Scattering: SWAXS measurements on dried samples of $PFGE_{55}$ and PEO_{330}-*b*-$PFGE_{20}$ were performed on a Bruker AXS Nanostar (Bruker, Karlsruhe, Germany), equipped with a microfocus X-ray source (Incoatec IμSCu E025, Incoatec, Geesthacht, Germany), operating at λ = 1.54 Å. A pinhole setup with 750 μm, 400 μm, and 1000 μm (in the order from source to sample) was used and the sample-to-detector distance was 107 cm (SAXS) and 12 cm (WAXS). Samples were mounted on a metal rack and fixed using tape. The scattering patterns were corrected for the beam stop and the background (Scotch tape) prior to evaluations.

Transmission Electron Microscopy: performed using a TEM (Zeiss-CEM 902A, Oberkochen, Germany) operating at 80 kV. Images were recorded using a 1 k TVIPS FastScan CCD camera. The TEM samples were prepared by applying a drop of the sample solutions onto the surface of a carbon coated copper grid (Quantifoil Micro-Tools GmbH, Jena, Germany).

2.2. Materials

Ethylene oxide (EO) was purchased from Linde and Aldrich. Furfuryl glycidyl ether (FGE), *t*-BuOK, tetrahydrofuran (THF), *n*-hexane and toluene were purchased from Aldrich. Toluene and THF were used from a solvent purification system (PureSolv, Innovative Technology) and distilled over sodium/benzophenone. Ethylene oxide was distilled over sodium. Furfuryl glycidyl ether was purified by column chromatography (eluent: ethylacetate/*n*-hexane 5/1) and vacuum drying before usage. Diphenylmethyl potassium (DPMK) was synthesized as reported previously.[51] The PEO precursor was prepared via living anionic ring-opening polymerization of ethylene oxide with DPMK in THF in a BüchiGlasUster PicoClave and dried by azeotropic distillation under vacuum from dry toluene. *t*-BuOK was used as received.

Polymerization of FGE: 4 mL of freshly distilled THF were transferred into a Schlenk flask and 5.61 mg potassium *t*-butanolate (0.05 mmol) were added. Subsequently, 0.45 mL furfuryl glycidyl ether (FGE, 3.24 mmol, ratio of M:I was 65:1, $M_{n,\text{ theo}}$ = 10 000 g mol^{-1}) was introduced and the reaction was allowed to stir for 24 h at 45 °C. The reaction was terminated by adding 0.5 mL methanol and the product was washed with *n*-hexane and dried under vacuum.

^{1}H NMR (300 MHz, $CDCl_3$–d_6, δ): 7.27 (d, 1H, CH), 6.24–6.17 (m, 2H, CH), 4.35 (s, 2H, CH_2), 3.55–3.29 (br, 5H, backbone), 1.18 (s, 9H, *t*-Bu CH_3).

SEC: M_n = 2900 g mol^{-1}, M_w = 3100 g mol^{-1}, PDI = 1.07; MALDI–ToF MS: M_p = 8400 g mol^{-1}

Synthesis of PEO-b-PFGE Block Copolymers: PEO_{330}-*b*-$PFGE_{10}$: 3.45 g monohydroxy-functionalized PEO ($M_{n,SEC}$ = 14 000 g mol^{-1}, PDI = 1.05, $M_{p,MALDI}$ = 14 500 g mol^{-1}, 0.24 mmol) was dried under vacuum at 75 °C for 2 h and dissolved in 30 mL freshly distilled THF. To activate the hydroxyl group, a stoichiometric amount of DPMK was added until the solution remained slightly red. 0.33 mL (2.4 mmol) FGE was added and the reaction mixture was allowed to stir for 24 h at 45 °C under inert conditions. The reaction was terminated by the addition of 0.5 mL methanol and the crude polymer was purified by precipitation in cold diethyl ether and dried under vacuum.

^{1}H NMR (300 MHz, DMSO–d_6, δ): 7.5 (s, 1H, CH), 7.2–7.05 (m, 10H, Ar H), 6.3 (m, 2H, CH), 4.3 (s, 2H, CH_2), 3.95 (t, 1H, CH), 3.65–3.15 (br, PEO-backbone).

SEC: M_n = 15 200 g mol^{-1}, M_w = 16 100 g mol^{-1}, PDI = 1.06; MALDI–ToF MS: M_p = 16 000 g mol^{-1}

PEO_{330}-*b*-$PFGE_{20}$ was synthesized according the same procedure with regard to stoichiometry.

SEC: M_n = 17 600 g mol^{-1}, M_w = 18 100 g mol^{-1}, PDI = 1.04; MALDI–ToF MS: M_p = 17 000 g mol^{-1}

3. Results and Discussion

We have recently prepared well-defined PFGE homo- and PEO-*b*-PFGE block copolymers via living anionic ring-opening polymerization (AROP).[31] Herein, PEO-*b*-PFGE materials will be used for temperature-mediated self-healing of films after the controlled application of scratches. For this purpose two PEO-*b*-PFGE block copolymers, PEO_{330}-*b*-$PFGE_{10}$ and PEO_{330}-*b*-$PFGE_{20}$, were synthesized by sequential AROP and, for comparison, a $PFGE_{55}$ homopolymer (**Figure 1** and **Table 1**). Both PEO-*b*-PFGE block copolymers were prepared starting from a monohydroxy-PEO precursor by activation with diphenylmethyl potassium (DPMK), followed by the addition of FGE.[31]

3.1. Structural and Thermal Characterization of $PFGE_{55}$ and PEO_{330}-*b*-$PFGE_X$ Films

Both PFGE and PEO-*b*-PFGE block copolymers were investigated using differential scanning calorimetry (DSC, **Figure 2**).

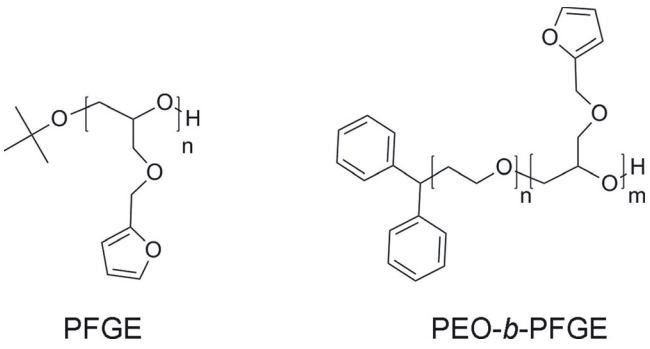

Figure 1. Schematic representation of the materials used in this study: PFGE and PEO-*b*-PFGE block copolymers.

Table 1. Characterization data of the used homo- and block copolymers.

Sample	$M_{n,theo}$ [g mol^{-1}]	$M_{n,SEC}$ [g mol^{-1}][b)]	$M_{p,MALDI}$ [g mol^{-1}]	PDI[b)]
$PFGE_{55}$	10 000	2900	8400	1.07
PEO_{330}[a)]	14 000	14 800	14 500	1.05
PEO_{330}-*b*-$PFGE_{10}$[c)]	16 000	15 200	16 000	1.06
PEO_{330}-*b*-$PFGE_{20}$[c)]	17 600	17 400	17 000	1.04

[a)]Precursor; [b)]Obtained by SEC ($CHCl_3$:TEA:i-Prop. 94:4:2, using PEO standards); [c)] Subscripts denote the degrees of polymerization of the corresponding block determined by ^{1}H NMR spectroscopy. The corresponding SEC traces, NMR spectra and MALDI-ToF MS pattern can be found in the Supporting Information, Figures S1–S3.

In addition, material degradation during the heating cycles, as well as the healing experiments discussed later, can be excluded, as thermogravimetric analysis (TGA) demonstrated thermal stability of the materials up to approximately 170 °C under air and 335 °C under nitrogen atmosphere (Supporting Information Figure S4).

As can be seen, the homopolymer $PFGE_{55}$ exhibits a T_g at approximately –40 °C (Figure 2a). PEO_{330}-*b*-$PFGE_{20}$ shows a strong melting peak at T_m = 59 °C, which can be attributed to the PEO segments (Figure 2b). The inset in Figure 2b shows the regime below 0 °C at higher resolution and reveals two separated glass transition temperatures at –79 and –40 °C, respectively. The first value can be assigned to PEO[52] whereas –40 °C reflects the PFGE segments. Both separate glass transition temperatures were also observed in case of PEO_{330}-*b*-$PFGE_{10}$ (data not shown here). The presence of two separated T_g's hints towards phase separation, although the overall molar mass of both PEO_{330}-*b*-$PFGE_X$ block copolymers is rather low. To confirm this assumption, additional SAXS experiments were performed on films which were annealed at 70 °C for 30 min and afterwards cooled to room temperature (Figure 2c).

Reflections could be observed for PEO_{330}-b-$PFGE_{20}$ at 0.46°, 0.92°, and 1.36°, corresponding to the [100]:[200]:[300] positions of a potential lamellar pattern, and the most intense [100] signal corresponds to a domain size of d_{lam} = 19 ± 2 nm. The formation of lamellae is rather surprising, as the volume fraction of PFGE in PEO_{330}-*b*-$PFGE_{20}$ is of about 17.5 wt%, rather hinting towards the formation of cylindrical domains. To probe the surface properties of the investigated films, water contact angle measurements were performed on PEO_{330}, $PFGE_{55}$, and PEO_{330}-*b*-$PFGE_{20}$ surfaces (Figure 2d). As expected, PEO_{330} shows a contact angle of 34.5°, which is characteristic for a hydrophilic surface, whereas this increases to 83.6° for $PFGE_{55}$. In case of PEO_{330}-*b*-$PFGE_{20}$, a value of 64.5° was obtained, showing surface characteristics in between the two corresponding homopolymers. At this point, we assume the

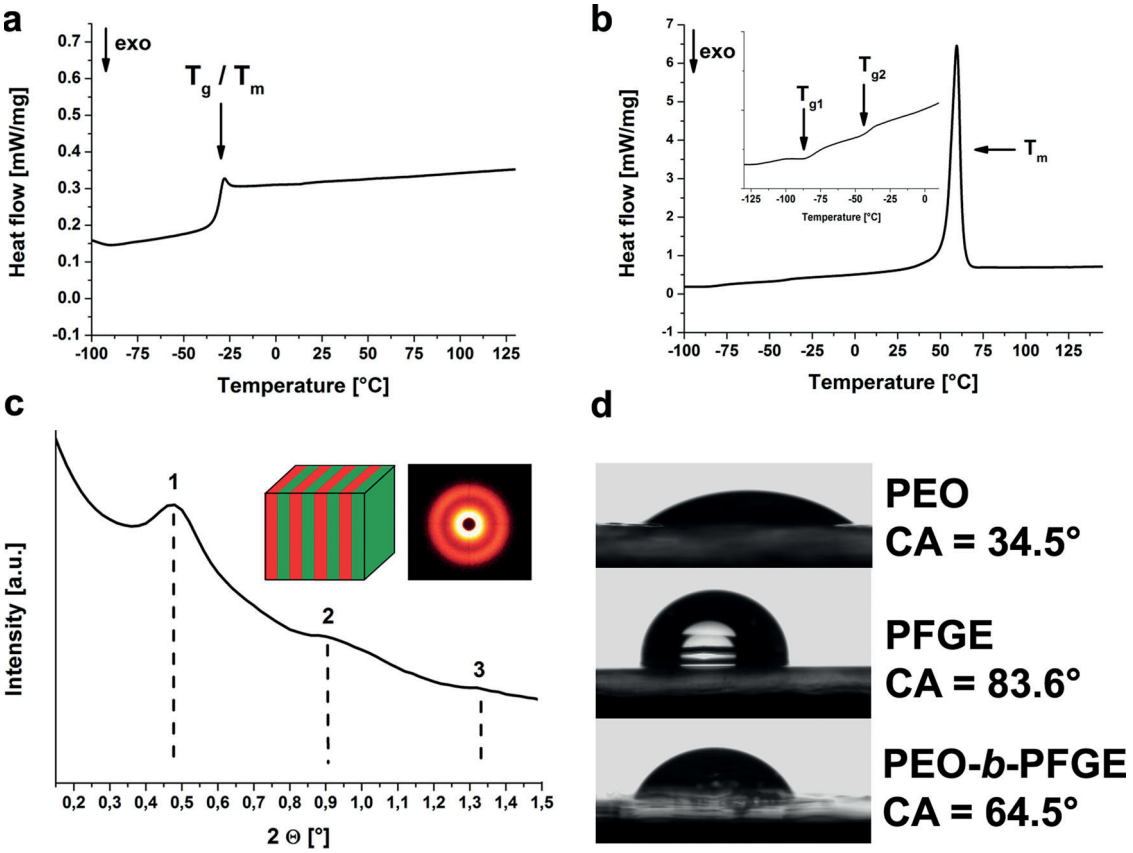

Figure 2. DSC thermograms of a) PFGE and b) PEO_{330}-*b*-$PFGE_{20}$. c) Zoom-in for PEO_{330}-*b*-$PFGE_{20}$. SAXS measurements of PEO_{330}-*b*-$PFGE_{20}$ and schematic representation of the proposed block copolymer bulk morphology. d) Contact angle measurements for PEO_{330}, $PFGE_{55}$ and PEO_{330}-*b*-$PFGE_{20}$.

formation of a lamellar bulk morphology in the case of PEO_{330}-*b*-$PFGE_{20}$. For PEO_{330}-*b*-$PFGE_{10}$, the obtained SAXS pattern (Supporting Information Figure S5a) was different, and the volume fraction of approximately 10% for PFGE hints towards the formation of PFGE spheres within a PEO matrix. This was confirmed by sonication-assisted dissolution of a crosslinked PEO_{330}-*b*-$PFGE_{10}$ block copolymer film in DMF, resulting in micellar structures with a crosslinked PFGE core of about 10 nm in diameter and a PEO corona, as observed via TEM measurements (Supporting Information, Figure S5b). Unfortunately, we were not able to distinguish between both domains in case of PEO_{330}-*b*-$PFGE_{20}$ block copolymers via atomic force microscopy (AFM) or TEM. In the latter case, thin samples (≈80 nm) were prepared from a crosslinked block copolymer film using a microtome. We observed rather rapid electron beam damage and the formation of sheet-like fragments. Even staining with OsO_4 (addressing any remaining double bonds in the PFGE domains) did not result in an improved phase contrast. As a consequence, the assumption of lamellar structures within films from PEO_{330}-*b*-$PFGE_{20}$ relies on the SAXS data, as well as contact angle measurements and the DSC results.

To exclude that the SAXS pattern in Figure 2c is merely caused by crystalline PEO domains, small (SAXS) and wide angle X-ray (WAXS) measurements at different temperatures were carried out (**Figure 3**). As it is clearly shown, the most intense reflection in SAXS at 0.46° is still present even above the melting point of PEO and after 16 h at 70 °C (Figure 3a). The fact that here only the [100] reflection is visible can be ascribed to shorter measurement times (≈30 min if compared to 4 h in Figure 2c), resulting in a decreasing signal-to-noise ratio. If this is combined with WAXS measurements of the same sample under comparable conditions (Figure 3b), very intense reflections at 18.6° and 22.8° (among other less intense signals) can be assigned to semicrystalline PEO domains.[53] Upon heating, these disappear at about 64 °C (inset in Figure 3b) and a broad amorphous halo can be observed.

3.2. Reversible Crosslinking of PFGE-Based Materials

For self-healing studies, films were prepared from $PFGE_{55}$, PEO_{330}-*b*-$PFGE_{10}$ and PEO_{330}-*b*-$PFGE_{20}$ via drop-casting onto polished glass slides. Typically, 20 mg of the polymer and a stoichiometric amount of the crosslinker, 1,1-diphenylmethyl bismaleimide (BMA), were dissolved in 0.2 mL dichloromethane (DCM). The solution was applied to a glass slide using a syringe and the solvent was allowed to evaporate.

Due to the presence of BMA, slightly yellow films (depending on the amount of crosslinker) were obtained. In case of the PFGE homopolymer, the amount of BMA was reduced to 0.8 equivalents, otherwise demixing and crystallization of the crosslinker was observed. For crosslinking, the polymer films were heated to 65 °C in an oven (**Figure 4**a). To ensure full crosslinking, the samples were kept at this temperature for 14 h. Subsequent network formation via crosslinking of the furan groups led to a significant change in the material properties, accompanied by a color change in case of the block copolymer films from slightly yellow to red. This was not the case for films from $PFGE_{55}$. We tentatively propose an aggregation of the crosslinker within the PEO domains, possibly due to the formation of π-complexes. This color change can also be monitored by time-dependent UV–Vis spectroscopy at 50 °C in solution (Supporting Information, Figure S6). However, the color change also depends on the temperature or the time during sample preparation. A detailed study of this phenomenon is, however, beyond the scope of this work. In all cases an increase of the film hardness was observed during crosslinking using depth sensing indentation measurements (Figure 4). We have to point out that films of PEO_{330}-*b*-$PFGE_{10}$ visibly melted at 59 °C even after crosslinking. As melting of crosslinked PEO_{330}-*b*-$PFGE_x$ films during the heating cycles would lead to film deformations, we focused on $PFGE_{55}$ and PEO_{330}-*b*-$PFGE_{20}$ for further studies.

First, the mechanical properties of PFGE-based films prior to and after crosslinking with BMA were investigated. As pristine films from $PFGE_{55}$ were liquid (highly viscous) at room-temperature, no indentation measurements were possible. PEO_{330}-*b*-$PFGE_{20}$ shows a hardness (H, defined as load/indentation area) of 0.038 GPa and a stiffness (E_i, Young modulus) of 0.46 GPa. All H values provided refer to a displacement of 150 nm. The E_i values represent average values of the obtained data in the linear range. After crosslinking, $PFGE_{55}$ shows a hardness of 0.6 GPa and a stiffness of E_i = 5.13 GPa (Figure 4b,d), the values being slightly higher as reported for "hard" polymers, like poly(methyl methacrylate) (PMMA, 0.32 GPa, 4.8 GPa) as well as polystyrene (PS, 0.34 GPa,

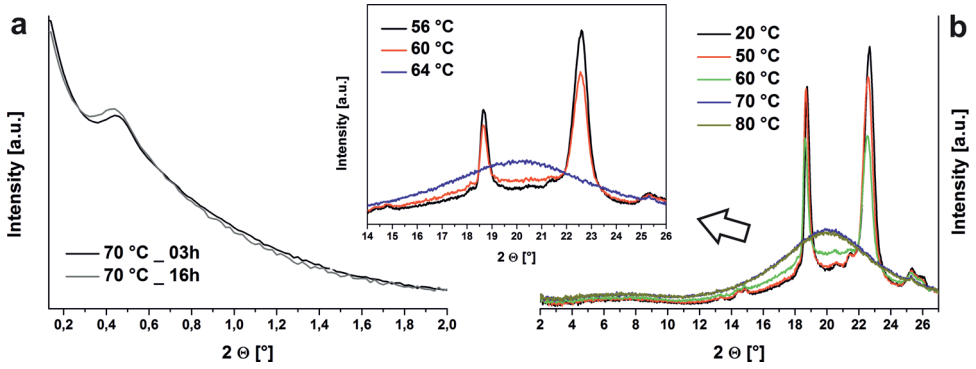

Figure 3. a) Small and b) wide angle X-ray patterns for PEO_{330}-*b*-$PFGE_{20}$ at different temperatures; the inset in (b) shows the enlarged region containing the reflexes for semicrystalline PEO.

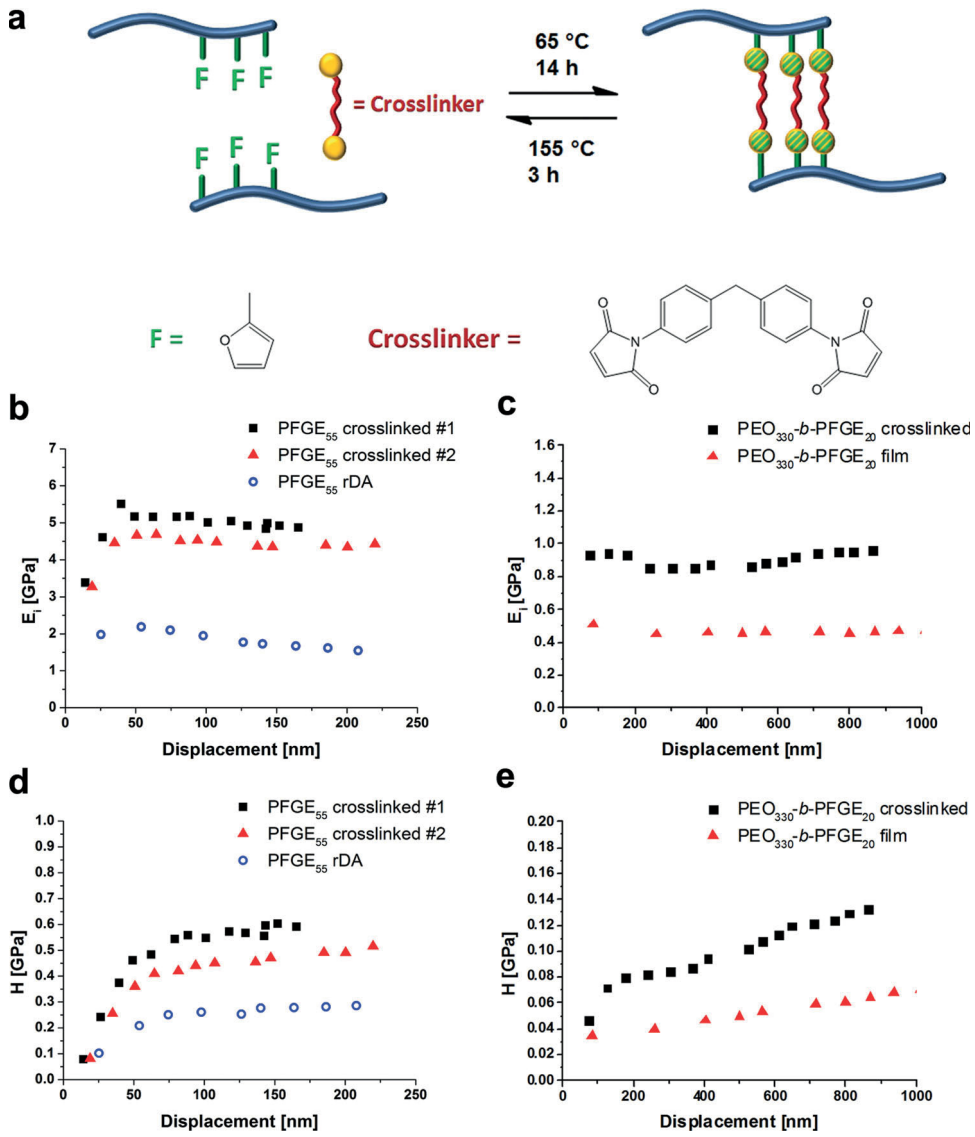

Figure 4. a) Schematic representation of the crosslinking of PFGE with a bifunctional maleimide BMA crosslinker. Depth-sensing indentation measurements for b,d) $PFGE_{55}$ and c,e) PEO_{330}-*b*-$PFGE_{20}$ films before and after crosslinking.

4.8 GPa).[54] This can be explained by a rather high degree of crosslinking, as each monomer unit carries a furan group in the side chain. For PEO_{330}-*b*-$PFGE_{20}$, significantly lower values of $H = 0.071$ GPa and $E_i = 0.91$ GPa compared to $PFGE_{55}$, but increased by a factor of two compared to the non-crosslinked state were obtained (Figure 4c,e). This can be rationalized by the presence of only 17 wt% PFGE and, hence, a lower overall degree of crosslinking.

According to the load displacement results, the block copolymer films showed visco-elastic behavior (Supporting Information, Figure S7), which is one prerequisite/driving force for a self-healing process. The PEO segments seemed to act as a softening material, whereas an increasing hardness at higher displacements was observed as well. The increase of both hardness and stiffness can be attributed to the crosslinking of $PFGE_{55}$ and PEO_{330}-*b*-$PFGE_{20}$ and, therefore, the rDA reaction is expected to invert this process. The films were therefore heated to 155 °C for 3 h and subjected to additional depth-sensing-indentation measurements at RT. At this point, a color change of the diblock copolymer film from red to brown was observed. Nevertheless, the block copolymer was shown to withstand these conditions.[31]

As expected, the E_i-modulus decreased to 1.76 GPa after the treatment at 155 °C, and the hardness was reduced to 0.26 GPa for $PFGE_{55}$ (Figure 4b,d). Subsequent re-crosslinking by heating to 65 °C for 14 h led to an increase to 4.51 GPa (E-modulus) and 0.45 GPa (hardness), although the values are slightly lower than after the first crosslinking procedure. We attribute this to an incomplete DA reaction. For the PEO_{330}-*b*-$PFGE_{20}$ block copolymer film, no significant changes after the rDA reaction were observed, which can be attributed to the rather low weight fraction of the PFGE segment.

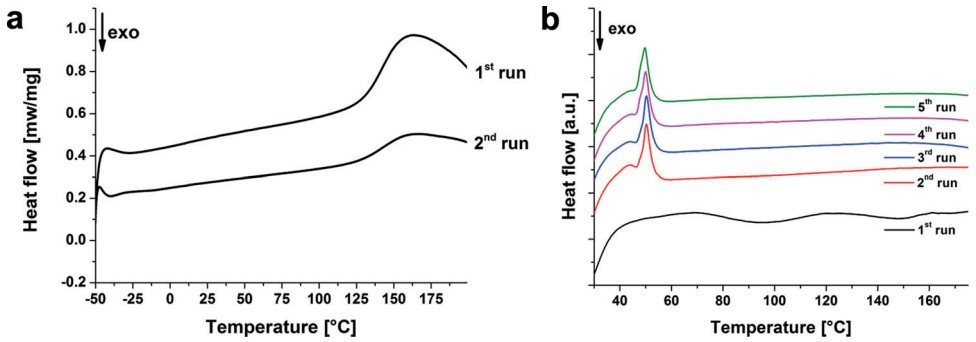

Figure 5. a) DSC measurements of a crosslinked $PFGE_{55}$ film with a heating rate of 20 K min^{-1} for the first run and 10 K min^{-1} for the second run. b) Multiple measurements of a crosslinked PEO_{330}-*b*-$PFGE_{20}$ block copolymer film.

As the rDA is the key for a successful reversible network formation, we studied a crosslinked $PFGE_{55}$ film in more detail by DSC measurements (**Figure 5**). As shown in Figure 5a for $PFGE_{55}$, the rDA reaction occurs within a temperature range of 135 to 160 °C. We attribute the fact that this is not visible for PEO_{330}-*b*-$PFGE_{20}$ to the limited sensitivity of the DSC and the low content of crosslinked furan rings. Heating of a crosslinked PEO_{330}-*b*-$PFGE_{20}$ does not reveal any signal during the first heating run (Figure 5b). However, after heating above the rDA temperature, subsequent cooling, and repeated heating a slight melting peak at 50 °C can be detected, which we ascribe to partial crystallization of the PEO domains.

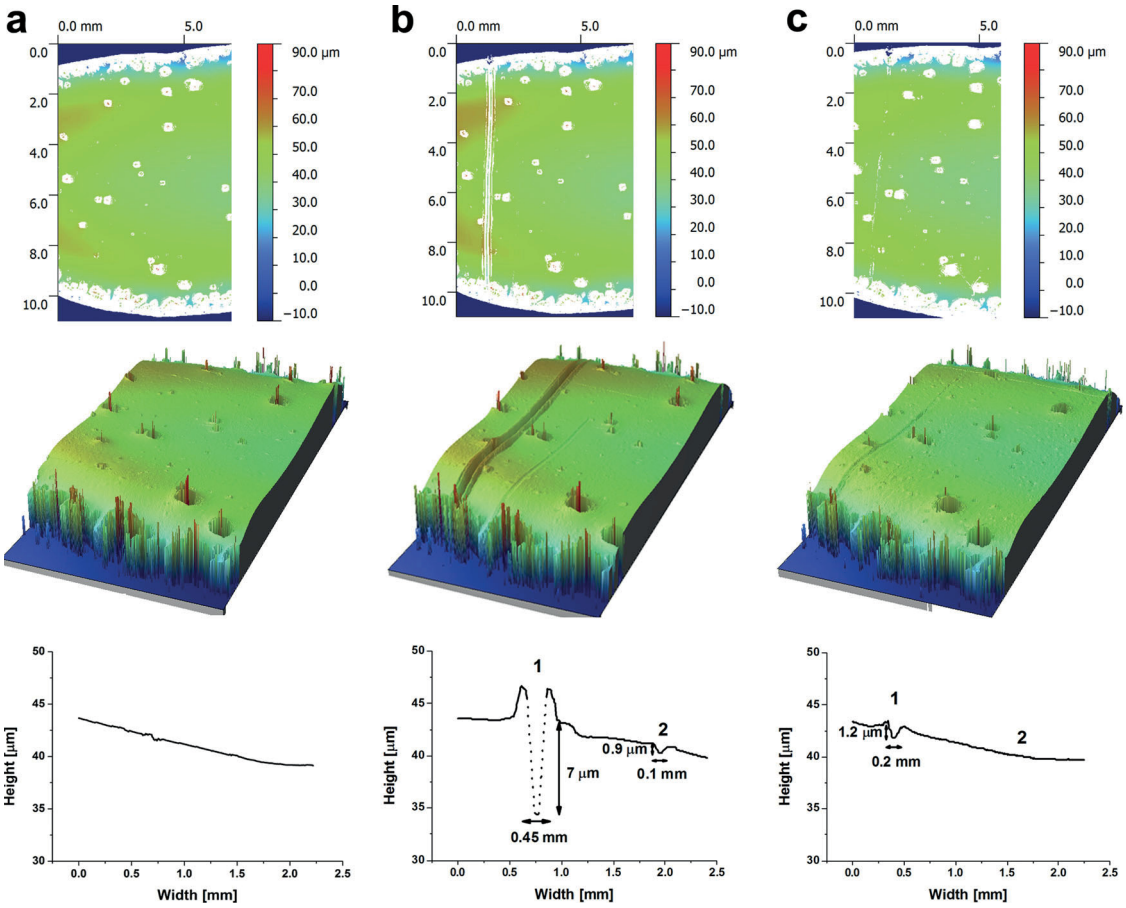

Figure 6. Profilometry measurements of PEO_{330}-*b*-$PFGE_{20}$ block copolymer films after a) crosslinking, b) scratching with a spatula, and c) the healing process at 155 °C.

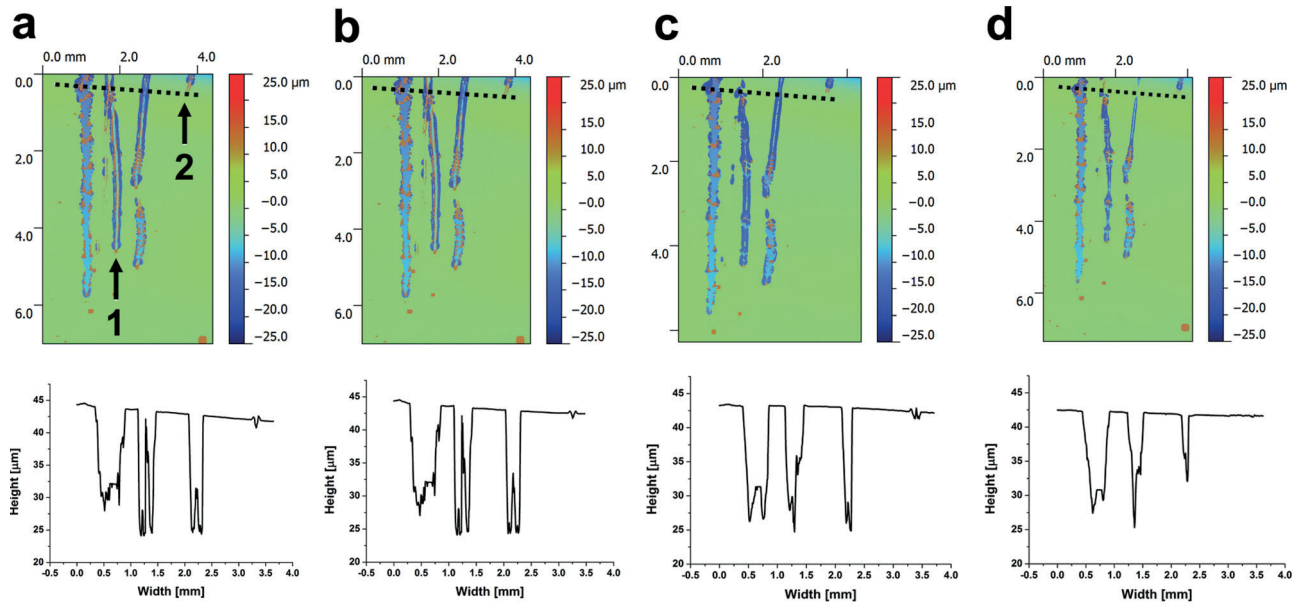

Figure 7. Profilometry measurements of a) a crosslinked PEO_{330}-*b*-$PFGE_{20}$ film, b) after heating for 4 h at 65 °C, c) subsequent heating for 4 h at 100 °C, and d) heating for 3 h at 155 °C.

3.3. Self-Healing Properties of PEO_{330}-*b*-$PFGE_{20}$

In order to introduce controlled surface defects, the respective films were treated with a spatula, resulting in scratches of varying depth, length and width. At this point, it can be noticed that such films from $PFGE_{55}$ were very brittle and scratching led to film breakage. Therefore, it was concluded that "pure" films from $PFGE_{55}$ are not suitable, at least as thin films, and we focused on PEO_{330}-*b*-$PFGE_{20}$ films, which were stable upon scratching.

Films containing PEO_{330}-*b*-$PFGE_{20}$ and the BMA crosslinker (molar ratio was 1:1) were prepared and crosslinked at 65 °C for 14 h. In the literature, values between 50 and 70 °C were determined for this procedure by DSC.[28,29,55,56] After crosslinking, the film surface was analyzed using an optical profilometer (**Figure 6**) and subsequently scratched with a spatula. As it can be seen, defined scratches (Scratch 1: 7 µm depth, 0.45 mm width, length 8 mm; Scratch 2: 0.9 µm depth, 0.1 mm width, length of 3.5 mm) were created (Figure 6b, the dashed lines are a guide to the eye as the instrument is not able to resolve the steep walls of this particular scratch). Afterwards, the block copolymer film was heated for 3 h at 155 °C, allowed to cool down slowly to 65 °C, and re-crosslinked for 14 h at 65 °C.

After the rDA reaction at 155 °C and subsequent crosslinking at 65 °C, profilometry revealed that Scratch 2 disappeared completely and Scratch 1 decreased to 1.2 µm depth and 0.2 mm width. Repetition of the heating process and increasing of the heating time did not lead to a further reduction of the scratch size. During all steps of this process, the overall thickness of the PEO_{330}-*b*-$PFGE_{20}$ film was monitored and shown to be constant (height ≈54 µm) (Supporting Information, Figure S8). Furthermore, defects within the block copolymer film remained unchanged, which would not be the case if the sample would undergo melting.

To ensure that the rDA reaction, followed by crosslinking at 65 °C, is responsible for the healing process, a film (**Figure 7**a) with defined scratches was heated for 4 h at 65 °C (over the melting temperature of the pristine block copolymer) and the surface was investigated by profilometry (Figure 7b). At this temperature, no changes were observed whereas subsequent heating to 100 °C for additional 4 h led to slight changes of the film surface (Figure 7c). In case of small scratches (max. depth 1 µm, Figure 7a,2), the depth was reduced by approximately 0.5 µm whereas deeper scratches (depth ≈6 µm or higher Figure 7a,1) remained unchanged. At this point we assume that heating to 100 °C leads to an increase of the chain mobility and possibly to the rDA reaction of small parts of the crosslinked units, which can be regarded as a kind of "pre-healing" process. Only if the film was heated to 155 °C for 3 h (Figure 7d), significant changes were observed (complete disappearance of smaller scratches as well as the decrease in length and width of larger defects). The fact that rather small gashes can already be repaired at lower temperatures has also been observed for networks from hyperbranched fluorinated polyethers created via DA chemistry.[57] Tentatively, the following mechanism is proposed to be responsible for the self-healing process: the incorporation of BMA and subsequent crosslinking leads to increasing hardness and decreasing chain mobility. At this point, the block copolymer film is damaged by mechanical force. Heating to 155 °C induces a rDA reaction and a partial decrosslinking of the network, accompanied by an increase in chain mobility leading to a kind of a reflow and, therefore, closure of the crack. The crosslinks are then partially reformed upon cooling.

We were also interested in the maximum number of possible self-healing cycles. For this purpose, a PEO_{330}-*b*-$PFGE_{20}$ block copolymer film was subjected to several cycles of crosslinking-scratching-rDA-crosslinking (**Figure 8**).

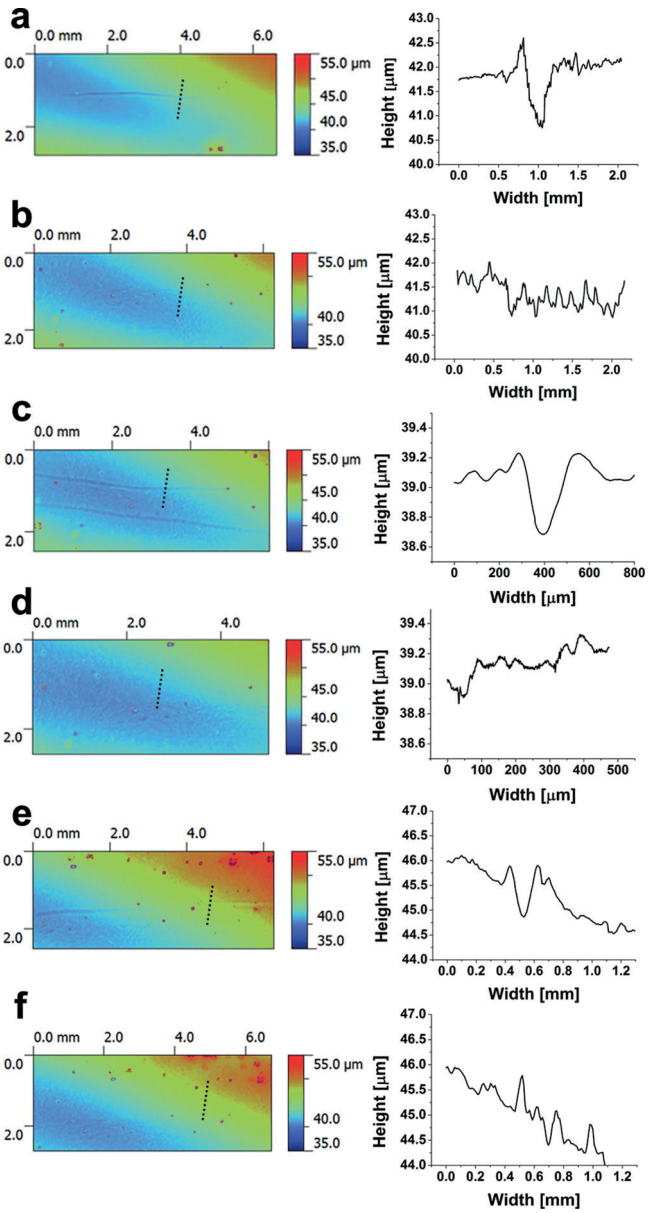

Figure 8. Repeated scratch healing of a PEO_{330}-*b*-$PFGE_{20}$ block copolymer film: 1st cycle a) after scratching; b) after healing, c,d) 2nd cycle, and e,f) 4th cycle.

In the first cycle, a scratch of 0.13 mm width, 0.82 µm depth and 4.4 mm length was inflicted (Figure 8a), and heating to 155 °C for 3 h, followed by subsequent crosslinking for 14 h at 65 °C lead to a disappearance of the scratch (Figure 8b). This procedure was repeated 4 times, and the 2nd healing cycle (a scratch of 0.14 mm, 0.42 µm depth and 5.4 mm length) is shown in Figure 8c before and Figure 8d afterwards. Already here, it can be noticed that the film surface increases in roughness, particularly visible in the surface profile in Figure 8d. Nevertheless, in the fourth healing cycle, a 0.13 mm wide, 0.68 µm deep and 5.2 mm long scratch (Figure 8e) can be still removed (Figure 8f). Whereas this can be applied to rather small scratches, the efficiency of the healing process for the

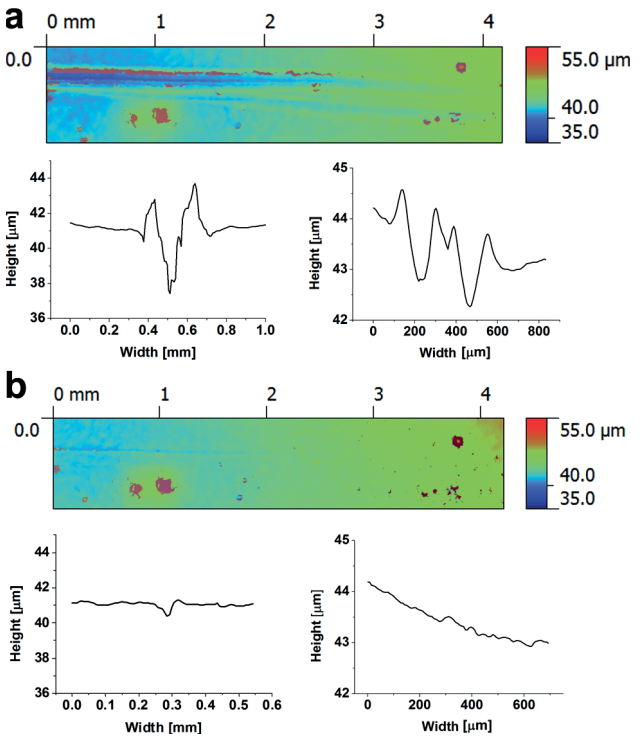

Figure 9. 5th scratch healing cycle of a PEO_{330}-*b*-$PFGE_{20}$ block copolymer film comprising a scratch with a gradient depth and width before (a) and after self-healing (b).

block copolymer films regarding larger surface defects seems to decrease with increasing cycle number. To demonstrate this, a scratch with a depth (3.8 to 1.3 µm) and width (3.4 to 1.7 mm) gradient was applied to a film after 4 healing cycles (**Figure 9**a). After heating to 155 °C for 3 h and subsequent crosslinking, the scratch depth decreased to 0.66 µm on the left side of the sample (Figure 9b). Also the width was reduced to 1.2 mm, whereas the thinner parts of the scratch completely disappeared. If compared to block copolymer films during the first healing cycles, where the depth of scratches could be reduced by up to 6–7 µm, this decreased after 5 healing cycles to approx. 2 to 3 µm.

Our explanation for this phenomenon is that with increasing number of heating cycles the amount of thermodynamically stable exo-product during the Diels-Alder reaction increases, which lead to a shift of the rDA process to higher temperatures.[58,59] As severe broadening of the signals in ^{1}H NMR spectroscopy hints towards (at least partial) material degradation when films were heated above 170 °C in air, a complete cleavage of the DA adducts is not possible under these conditions. As this currently limits the process, the films were heated under an inert atmosphere in a glovebox as an alternative. After 30 min at temperatures of 175 to 215 °C, a color change from brownish to dark brown was visible. Nevertheless, the network structure still seemed to be intact as the PEO_{330}-*b*-$PFGE_{20}$ film remained insoluble in different organic solvents (e.g., THF, DMF). To identify the origin of the color change, we heated pure PEO_{330}, $PFGE_{55}$ (pristine as well as crosslinked) and the BMA crosslinker was heated to 215 °C.

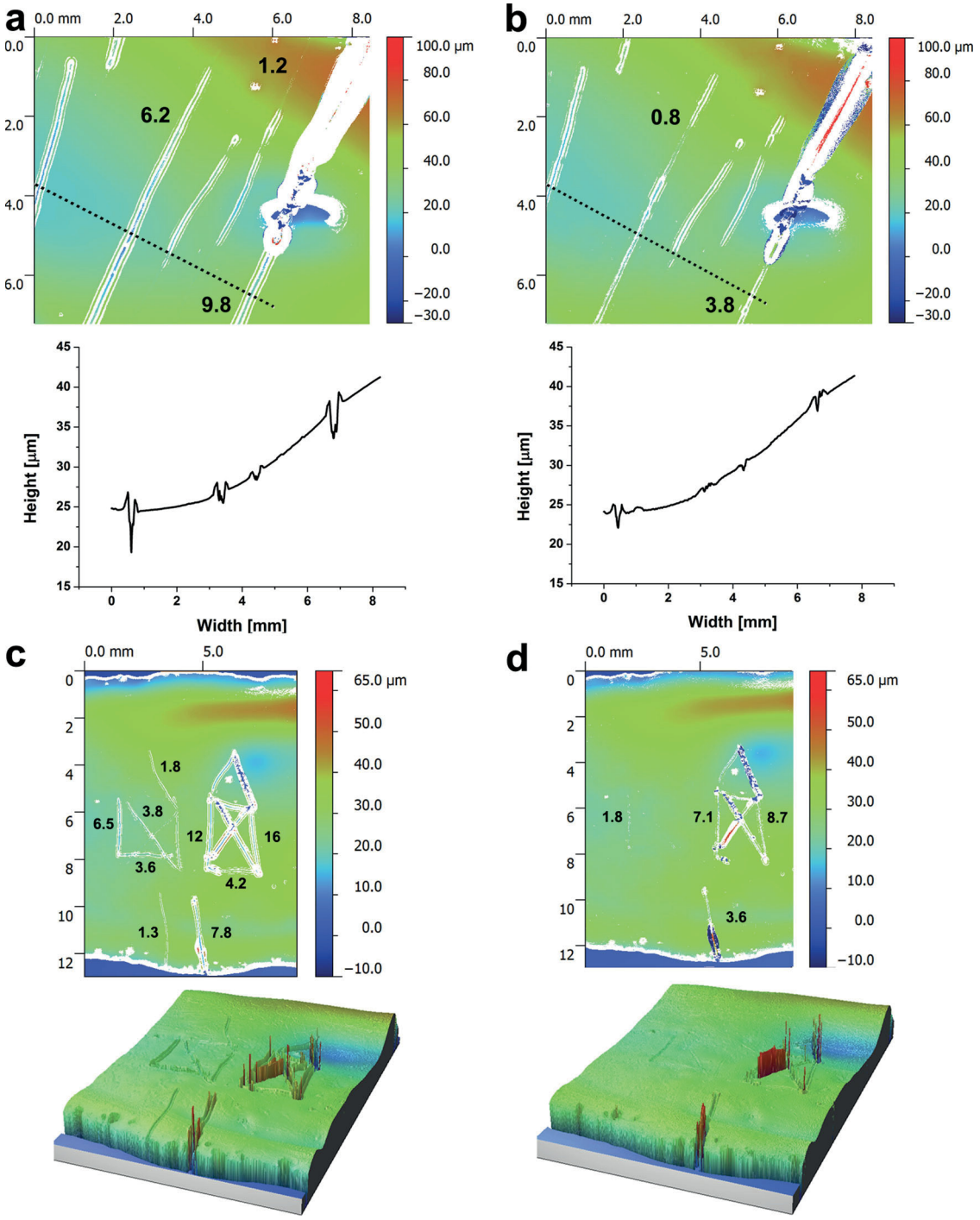

Figure 10. Self-healing process of a multi-scratch pattern (a) before, and b) after) as well as a complex pattern within a crosslinked PEO_{330}-*b*-$PFGE_{20}$ block copolymer film (c) before, and d) after heating to 155 °C).

Both PEO_{330} and BMA melted, whereas both PFGE samples revealed a rapid color change to dark brown, presumably due to the thermal instability of the furan moieties.[60] According to SEC measurements, no degradation occurred for $PFGE_{55}$ as a comparable elution trace was observed afterwards (Supporting Information, Figure S9). Nevertheless, we found that under these rather harsh conditions the surface roughness increased rapidly. This might be explained by a fast cooling of the sample and partial breakage of the film due to mechanical stress. Even after this heat treatment, the block copolymer films exhibited self-healing abilities (a scratch of 2.9 µm depth decreased to 0.3 µm).

3.4. Multiple Scratches and Complex Scratch Patterns

We also applied complex scratch patterns to crosslinked PEO_{330}-*b*-$PFGE_{20}$ block copolymer films (**Figure 10**). As shown in Figure 10b, small scratches with, e.g., a depth of 1.2 µm and a width of 0.16 mm disappeared completely, whereas deeper scratches with a depth of 6.2 or 9.8 µm and widths of 0.45 and 0.5 mm only decreased in size. The depths could be reduced to 0.8 and 3.8 µm, respectively, as well as the scratch width to 0.23 and 0.3 mm.

Figure 10c depicts a rather challenging scratch pattern, two "Santa's houses" with depths of approximately 1.8 to 6.8 µm and 4.2 to 16 µm. As shown in Figure 10d, the left (less deep) pattern vanished nearly completely. Only in case of the deeper scratch (6.5 µm), the depth was reduced to 1.8 µm, whereas the right-hand pattern comprising deeper scratches (12 to 16 µm) can still be seen afterwards (remaining scratches with 7.1 and 8.7 µm depth).

Finally, the comparison of the healing efficiency of the system presented here with literature examples was targeted. As shown before, it is possible to heal scratches of up to 6 µm depth and 1.7 mm width at elevated temperatures and on a time scale of 17 h (3 h at 155 °C and 14 h at 65 °C). One of the next targets for future studies is to reduce the required annealing times. For the initial investigation of the system the focus was placed on the complete crosslinking of the polymer films. However, self-healing approaches exploiting Diels-Alder chemistry will be necessarily limited to this temperature range in order to induce network formation or cleavage. This has also been demonstrated for comparable systems using this approach.[29,35] Self-healing processes based on π–π interactions have been shown to operate at 90 °C and were able to cure scratches of up to 75 µm width within minutes.[20] In the case of systems based on hydrogen bonding it could be shown that previously cut pieces reconnect by simple surface contact at ambient temperatures, but this ability decreased the longer the pieces were kept separate (which we did not observed in the current example).[15,61] Comparable materials based on reversible metal-ligand-interactions were also healed at elevated temperatures (>100 °C) and the BMA crosslinker to 215 °C.[17,18,62]

4. Conclusion

We demonstrate one of the first examples for self-healing materials based on block copolymers. Films from PEO_{330}-*b*-$PFGE_{20}$ diblock copolymers were shown to exhibit a smooth surface and a lamellar bulk morphology with a domain size of approximately 19 nm. The materials are capable of undergoing reversible (up to five times shown here) crosslinking/de-crosslinking and, hence, healing of inflicted damage at elevated temperatures. Comparison with $PFGE_{55}$ homopolymers via depth-sensing indentation revealed that this is accompanied by changes in hardness of the PFGE minority fraction. The results clearly show that PEO-*b*-PFGE block copolymers are promising candidates for self-healing surfaces (possible healing of scratches of up to 6 µm depth and 1.7 mm width), although still rather long cycles (up to 17 h) and high temperatures (155 °C) are required, and the employed BMA crosslinker is rather toxic. In addition, the efficiency of the rDA process decreases with increasing cycle number, presumably due to the formation of the exo-product during the DA reaction. Nevertheless, our approach addresses one of the inherent problems in self-healing materials: the combination of smooth and dynamic segments with the capability of strong and reversible network formation via, here, Diels-Alder chemistry.

It will be the subject of further studies to purposefully vary the weight fraction of PFGE to access different bulk morphologies for such block copolymers as well as to identify superior crosslinking agents. Also, the use of PFGE-*b*-PEO-*b*-PFGE triblock copolymers might be advantageous.

Supporting Information

Supporting Information is available from the Wiley Online Library or from the author.

Acknowledgements

The authors thank Steffi Stumpf for help with AFM measurements, Sarah Crotty for MALDI-ToF-MS measurements and Ulrike Günther for help with the sample preparation for TEM measurements. We also wish to acknowledge the Dutch Polymer Institute (DPI, technology area high-throughput-experimentation, project #690) and the Thuringian Ministry for Education, Science and Culture (grants #B514-09051, NanoConSens and #B515-11028, SWAXS-JCSM) for financial support of this study. F. H. S. and T. R. are further grateful to the Thuringian Ministry for Education, Science, and Culture (TMBWK; #B515-10065, ChaPoNano). T. R. acknowledges the Carl-Zeiss foundation for a PhD-scholarship. U. S. S. and M. D. H. thank the DFG for financial support within the framework of SPP 1568.

Received: February 4, 2013
Revised: February 26, 2013
Published online: April 19, 2013

[1] M. D. Hager, P. Greil, C. Leyens, S. van der Zwaag, U. S. Schubert, *Adv. Mater.* **2010**, *22*, 5424–5430.
[2] R. S. Trask, H. RWilliams, I. P. Bond, *Bioinspir. Biomim.* **2007**, *2*, P1–P9.
[3] E. W. Davie, O. D. Ratnoff, *Science* **1964**, *145*, 1310-&.
[4] E. Vaccaro, J. H. Waite, *Biomacromolecules* **2001**, *2*, 906–911.
[5] B. J. Blaiszik, S. L. B. Kramer, S. C. Olugebefola, J. S. Moore, N. R. Sottos, S. R. White, *Annu. Rev. Mater. Res.* **2010**, *40*, 179–211.
[6] N. K. Guimard, K. K. Oehlenschlaeger, J. W. Zhou, S. Hilf, F. G. Schmidt, C. Barner-Kowollik, *Macromol. Chem. Phys.* **2012**, *213*, 131–143.
[7] S. Bode, B. Sandmann, M. D. Hager, U. S. Schubert, *Metal-Complex based Self-healing Polymers* in *Self-Healing Polymers: From Principles to Applications* (Ed. W. Binder), Wiley-VCH, Weinheim **2013**.
[8] S. R. White, N. R. Sottos, P. H. Geubelle, J. S. Moore, M. R. Kessler, S. R. Sriram, E. N. Brown, S. Viswanathan, *Nature* **2001**, *409*, 794–797.
[9] H. R. Williams, R. S. Trask, P. M. Weaver, I. P. Bond, *J. R. Soc. Interface* **2008**, *5*, 55–65.
[10] V. Berl, M. Schmutz, M. J. Krische, R. G. Khoury, J. M. Lehn, *Chem-Eur. J.* **2002**, *8*, 1227–1244.
[11] J. L. Wietor, A. Dimopoulos, L. E. Govaert, R. A. T. M. van Benthem, G. de With, R. P. Sijbesma, *Macromolecules* **2009**, *42*, 6640–6646.

[12] R. P. Sijbesma, F. H. Beijer, L. Brunsveld, B. J. B. Folmer, J. H. K. K. Hirschberg, R. F. M. Lange, J. K. L. Lowe, E. W. Meijer, *Science* **1997**, *278*, 1601–1604.
[13] O. A. Scherman, G. B. W. L. Ligthart, R. P. Sijbesma, E. W. Meijer, *Angew. Chem. Int. Ed.* **2006**, *45*, 2072–2076.
[14] H. Ohkawa, G. B. W. L. Ligthart, R. P. Sijbesma, E. W. Meijer, *Macromolecules* **2007**, *40*, 1453–1459.
[15] P. Cordier, F. Tournilhac, C. Soulie-Ziakovic, L. Leibler, *Nature* **2008**, *451*, 977–980.
[16] D. Montarnal, M. Capelot, F. Tournilhac, L. Leibler, *Science* **2011**, *334*, 965–968.
[17] S. Bode, L. Zedler, F. H. Schacher, B. Dietzek, M. Schmitt, J. Popp, M. D. Hager, U. S. Schubert, *Adv. Mater.* **2013**, *25*, 1634–1638.
[18] M. Burnworth, L. M. Tang, J. R. Kumpfer, A. J. Duncan, F. L. Beyer, G. L. Fiore, S. J. Rowan, C. Weder, *Nature* **2011**, *472*, 334–337.
[19] S. Burattini, B. W. Greenland, W. Hayes, M. E. Mackay, S. J. Rowan, H. M. Colquhoun, *Chem. Mater.* **2011**, *23*, 6–8.
[20] S. Burattini, H. M. Colquhoun, J. D. Fox, D. Friedmann, B. W. Greenland, P. J. F. Harris, W. Hayes, M. E. Mackay, S. J. Rowan, *Chem. Commun.* **2009**, 6717–6719.
[21] X. X. Chen, M. A. Dam, K. Ono, A. Mal, H. B. Shen, S. R. Nutt, K. Sheran, F. Wudl, *Science* **2002**, *295*, 1698–1702.
[22] X. X. Chen, F. Wudl, A. K. Mal, H. B. Shen, S. R. Nutt, *Macromolecules* **2003**, *36*, 1802–1807.
[23] Y. L. Liu, C. Y. Hsieh, *J. Polym. Sci. Part A: Polym. Chem.* **2006**, *44*, 905–913.
[24] M. Wouters, E. Craenmehr, K. Tempelaars, H. Fischer, N. Stroeks, J. van Zanten, *Prog. Org. Coat.* **2009**, *64*, 156–162.
[25] J. Zhou, N. K. Guimard, A. J. Inglis, M. Namazian, C. Y. Lin, M. L. Coote, E. Spyrou, S. Hilf, F. G. Schmidt, C. Barner-Kowollik, *Polym. Chem.* **2012**, *3*, 628–639.
[26] A. J. Inglis, L. Nebhani, O. Altintas, F. G. Schmidt, C. Barner-Kowollik, *Macromolecules* **2010**, *43*, 5515–5520.
[27] J. Kötteritzsch, S. Stumpf, S. Hoeppener, J. Vitz, M. D. Hager, U. S. Schubert, *Macromol. Chem. Phys.* **2013**, DOI: 10.1002/macp.201200712.
[28] A. Gandini, *Prog. Polym. Sci.* **2013**, *38*, 1–29.
[29] Y. Zhang, A. A. Broekhuis, F. Picchioni, *Macromolecules* **2009**, *42*, 1906–1912.
[30] J. A. Syrett, C. R. Becer, D. M. Haddleton, *Polym. Chem.* **2010**, *1*, 978–987.
[31] M. J. Barthel, T. Rudolph, S. Crotty, F. H. Schacher, U. S. Schubert, *J. Polym. Sci. Part A: Polym. Chem.* **2012**, *50*, 4958–4965.
[32] R. Gheneim, C. Perez-Berumen, A. Gandini, *Macromolecules* **2002**, *35*, 7246–7253.
[33] Q. Tian, Y. C. Yuan, M. Z. Rong, M. Q. Zhang, *J. Mater. Chem.* **2009**, *19*, 1289–1296.
[34] C. Gousse, A. Gandini, P. Hodge, *Macromolecules* **1998**, *31*, 314–321.
[35] P. A. Pratama, A. M. Peterson, G. R. Palmese, *Macromol. Chem. Phys.* **2012**, *213*, 173–181.
[36] A. M. Peterson, R. E. Jensen, G. R. Palmese, *ACS Appl. Mater. Interfaces* **2010**, *2*, 1141–1149.
[37] T. Ekblad, G. Bergstroem, T. Ederth, S. L. Conlan, R. Mutton, A. S. Clare, S. Wang, Y. L. Liu, Q. Zhao, F. D'Souza, G. T. Donnelly, P. R. Willemsen, M. E. Pettitt, M. E. Callow, J. A. Callow, B. Liedberg, *Biomacromolecules* **2008**, *9*, 2775–2783.
[38] H. Xu, F. Yan, E. E. Monson, R. Kopelman, *J. Biomed. Mater. Res. A* **2003**, *66A*, 870–879.
[39] *EFSA J.* **2006**, *4*, 414–415.
[40] I. Banerjee, R. C. Pangule, R. S. Kane, *Adv. Mater.* **2011**, *23*, 690–718.
[41] P. Kim, D. H. Kim, B. Kim, S. K. Choi, S. H. Lee, A. Khademhosseini, R. Langer, K. Y. Suh, *Nanotechnology* **2005**, *16*, 2420–2426.
[42] N. A. Peppas, J. Z. Hilt, A. Khademhosseini, R. Langer, *Adv. Mater.* **2006**, *18*, 1345–1360.
[43] F. H. Schacher, P. A. Rupar, I. Manners, *Angew. Chem. Int. Ed.* **2012**, *51*, 7898–7921.
[44] P. Tyagi, A. Deratani, D. Bouyer, D. Cot, V. Gence, M. Barboiu, T. N. T. Phan, D. Bertin, D. Gigmes, D. Quemener, *Angew. Chem. Int. Ed.* **2012**, *51*, 7166–7170.
[45] K. J. Henderson, T. C. Zhou, K. J. Otim, K. R. Shull, *Macromolecules* **2010**, *43*, 6193–6201.
[46] M. D. Chipara, M. Chipara, E. Shansky, J. M. Zaleski, *Polym. Adv. Technol.* **2009**, *20*, 427–431.
[47] J. Hentschel, A. M. Kushner, J. Ziller, Z. Guan, *Angew. Chem.* **2012**, *51*, 10561.
[48] A. A. Kavitha, N. K. Singha, *Macromolecules* **2010**, *43*, 3193–3205.
[49] E. F. J. Rettler, J. M. Kranenburg, H. M. L. Lambermont-Thijs, R. Hoogenboom, U. S. Schubert, *Macromol. Chem. Phys.* **2010**, *211*, 2443–2448.
[50] W. C. Oliver, G. M. Pharr, *J. Mater. Res.* **1992**, *7*, 1564–1583.
[51] H. Normant, B. Angelo, *B. Soc. Chim. Fr.* **1960**, 354–359.
[52] E. Araneda, A. Leiva, L. Gargallo, N. Hadjichristidis, I. Mondragon, D. Radic, *Polym. Eng. Sci.* **2012**, *52*, 1128–1136.
[53] F. H. Schacher, J. Elbert, S. K. Patra, S. F. M. Yusoff, M. A. Winnik, I. Manners, *Chem-Eur. J.* **2012**, *18*, 517–525.
[54] B. J. Briscoe, L. Fiori, E. Pelillo, *J. Phys. D. Appl. Phys.* **1998**, *31*, 2395–2405.
[55] J. A. Syrett, G. Mantovani, W. R. S. Barton, D. Price, D. M. Haddleton, *Polym. Chem.* **2010**, *1*, 102–106.
[56] C. Toncelli, D. C. De Reus, F. Picchioni, A. A. Broekhuis, *Macromol. Chem. Phys.* **2012**, *213*, 157–165.
[57] P. M. Imbesi, C. Fidge, J. E. Raymond, S. I. Cauët, K. L. Wooley, *ACS Macro Lett.* **2012**, *1*, 473–477.
[58] J. Canadell, H. Fischer, G. De With, R. A. T. M. Van Benthem, *J. Polym. Sci. Part A: Polym. Chem.* **2010**, *48*, 3456–3467.
[59] L. Rulisek, P. Sebek, Z. Havlas, R. Hrabal, P. Capek, A. Svatos, *J. Org. Chem.* **2005**, *70*, 6295–6302.
[60] S. D. Bergman, F. Wudl, *J. Mater. Chem.* **2008**, *18*, 41–62.
[61] G. M. L. van Gemert, J. W. Peeters, S. H. M. Sontjens, H. M. Janssen, A. W. Bosman, *Macromol. Chem. Phys.* **2012**, *213*, 234–242.
[62] J. Yuan, X. Fang, L. Zhang, G. Hong, Y. Lin, Q. Zheng, Y. Xu, Y. Ruan, W. Weng, H. Xia, G. Chen, *J. Mater. Chem.* **2012**, *22*, 11515–11522.

ADVANCED FUNCTIONAL MATERIALS

Supporting Information

for *Adv. Funct. Mater.*, DOI: 10.1002/adfm.201300469

Self-Healing Materials via Reversible Crosslinking of Poly(ethylene oxide)- Block -Poly(furfuryl glycidyl ether) (PEO- b -PFGE) Block Copolymer Films

*Markus J. Barthel, Tobias Rudolph, Anke Teichler, Renzo M. Paulus, Jürgen Vitz, Stephanie Hoeppener, Martin D. Hager, Felix H. Schacher * and Ulrich S. Schubert**

Supporting information for

Self-Healing Materials via Reversible Crosslinking of Poly(ethylene oxide)-*block*-poly(furfuryl glycidyl ether) (PEO-*b*-PFGE) Block Copolymer Films

Markus J. Barthel,[1,2,3] Tobias Rudolph,[1,2] Anke Teichler,[1,2,3] Renzo M. Paulus,[1,2] Jürgen Vitz,[1,2,3] Stephanie Hoeppener,[1,2,3] Martin D. Hager,[1,2] Felix H. Schacher,[1,2]* and Ulrich S. Schubert[1,2,3]*

[1] Laboratory of Organic and Macromolecular Chemistry (IOMC), Friedrich-Schiller-University Jena, Humboldtstr. 10, 07743 Jena, Germany.

[2] Jena Center for Soft Matter (JCSM), Friedrich-Schiller-University Jena, Philosophenweg 7, 07743 Jena, Germany.

[3] Dutch Polymer Institute (DPI), John F. Kennedylaan 2, 5612 AB Eindhoven, The Netherlands.

Email: ulrich.schubert@uni-jena.de; felix.schacher@uni-jena.de;

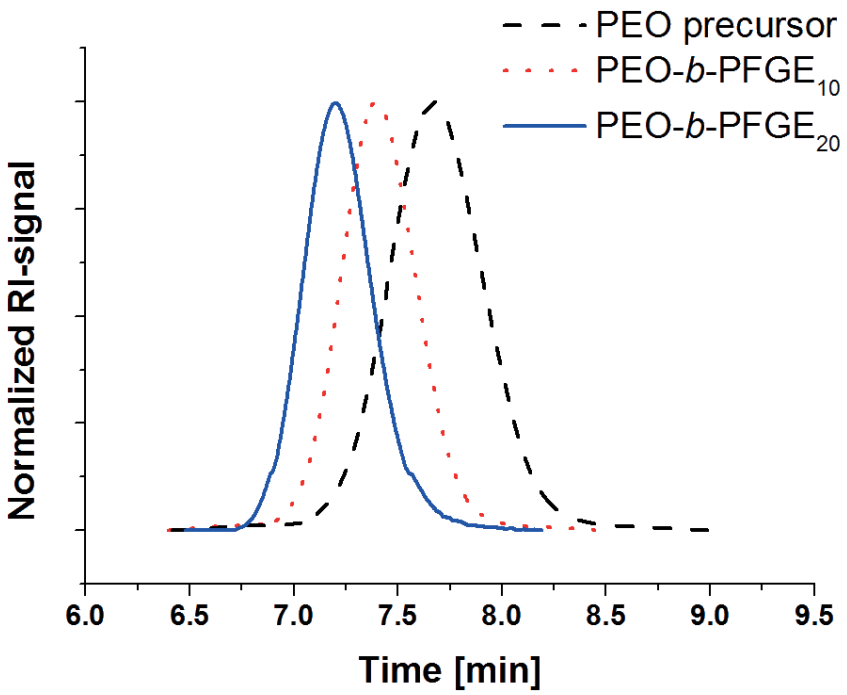

Figure S1. SEC traces for the PEO_{330} precursor (dashed black line), PEO_{330}-*b*-$PFGE_{10}$ (dotted red line), and PEO_{330}-*b*-$PFGE_{20}$ (solid blue line) block copolymers (eluent: $CHCl_3$ / *i*-propanol / triethylamine).

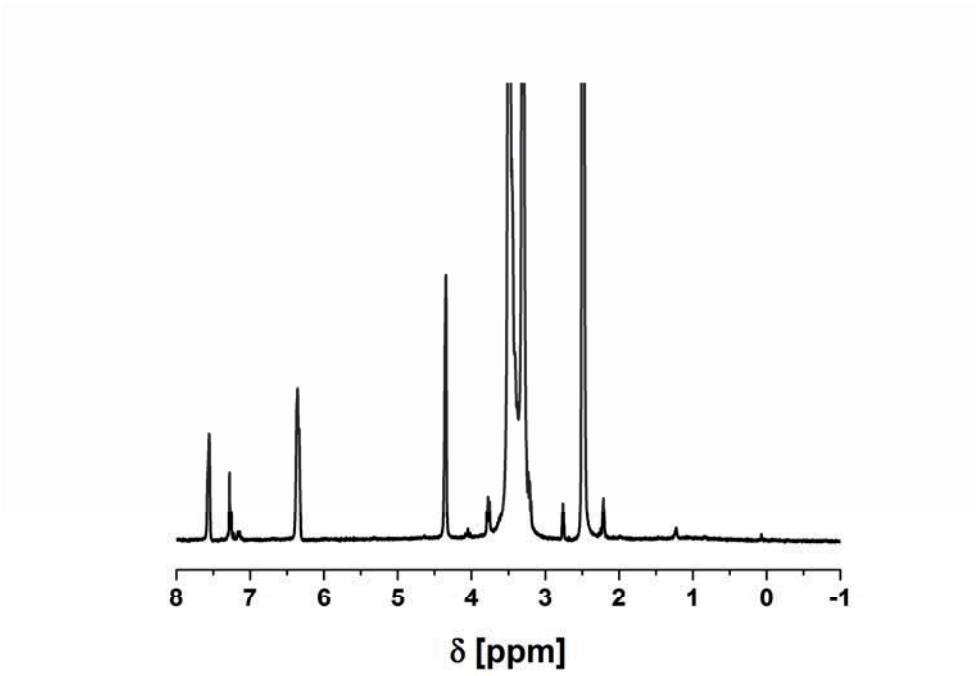

Figure S2. ^{1}H NMR spectrum (300 MHz) of PEO_{330}-*b*-$PFGE_{20}$ in DMSO–*d6*.

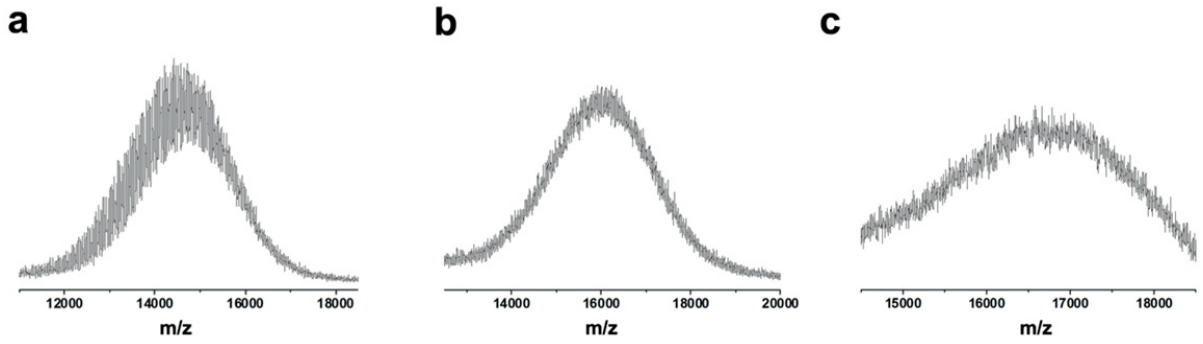

Figure S3. MALDI-ToF MS measurements of the PEO_{330} precursor (a), and of PEO_{330}-*b*-$PFGE_{10}$ (b) and PEO_{330}-*b*-$PFGE_{20}$ (c) block copolymers.

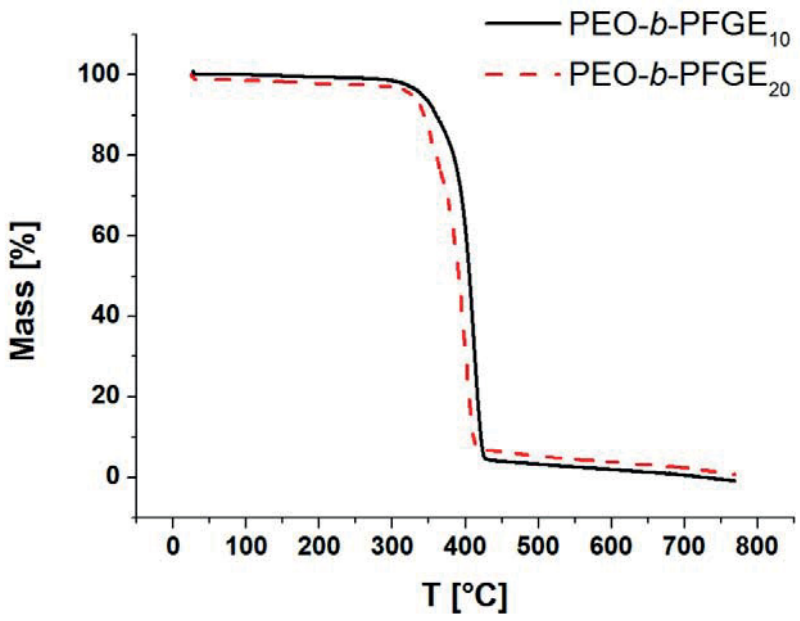

Figure S4. TGA measurements for PEO_{330}-*b*-$PFGE_{10}$ and PEO_{330}-*b*-$PFGE_{20}$ block copolymers under nitrogen atmosphere.

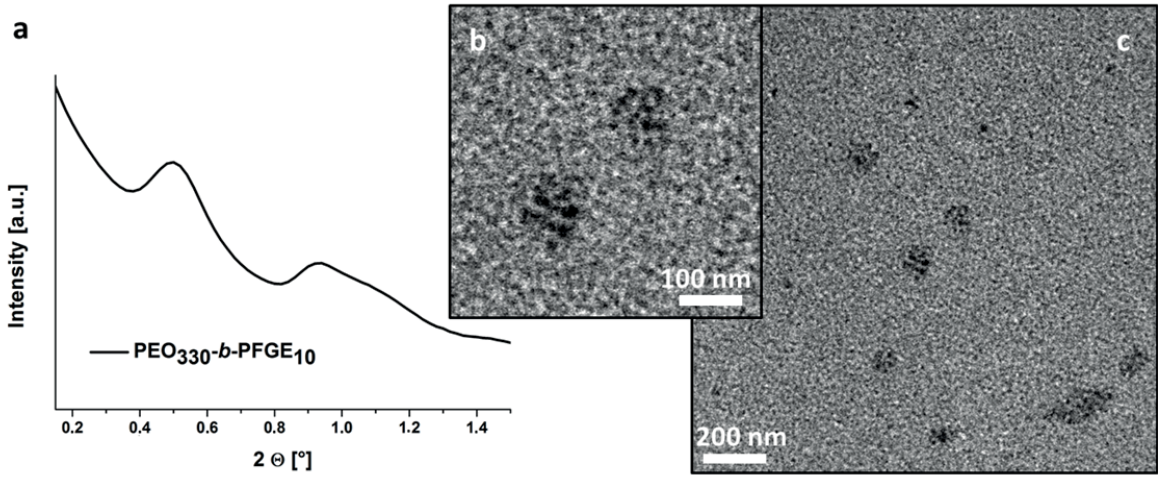

Figure S5. SAXS measurement for a crosslinked PEO_{330}-*b*-$PFGE_{10}$ film (a) and TEM micrograph for core-crosslinked PEO_{330}-*b*-$PFGE_{10}$ micelles after bulk crosslinking and sonication-assisted dissolution (b, higher magnification and c presents an overview).

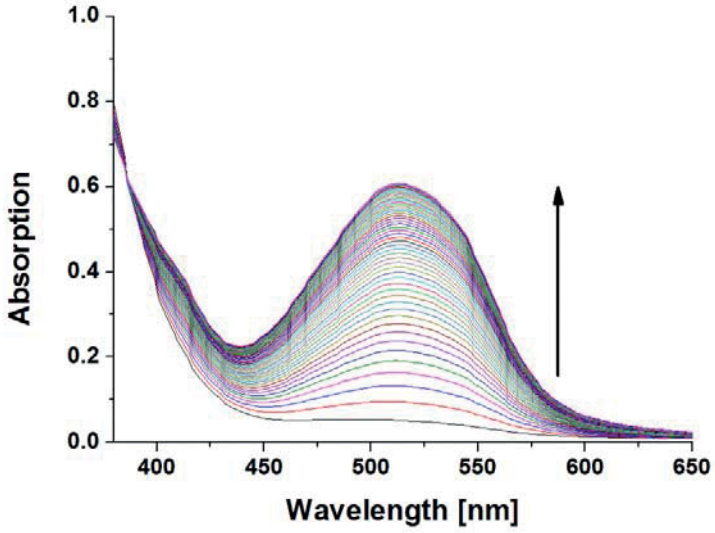

Figure S6. Time depending UV/Vis measurements of a PEO_{330}-*b*-$PFGE_{20}$ / BMA linker mixture in DMF.

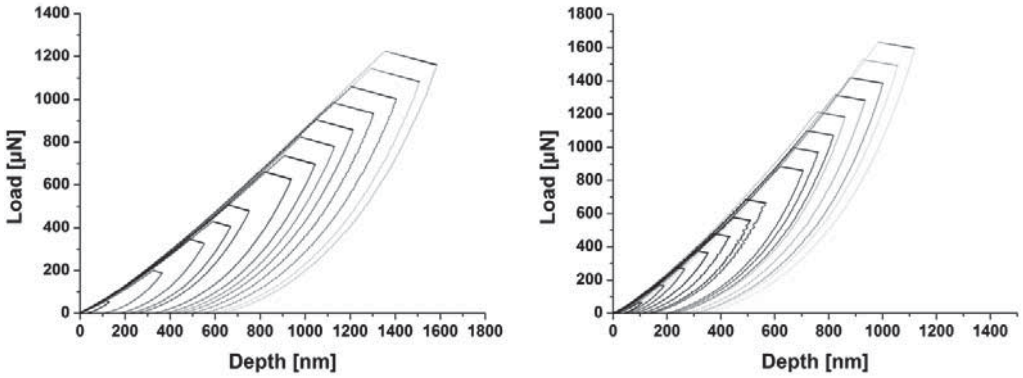

Figure S7. Load-depth curves of a pristine (left) and crosslinked (right) PEO_{330}-*b*-$PFGE_{20}$ sample at different loadings.

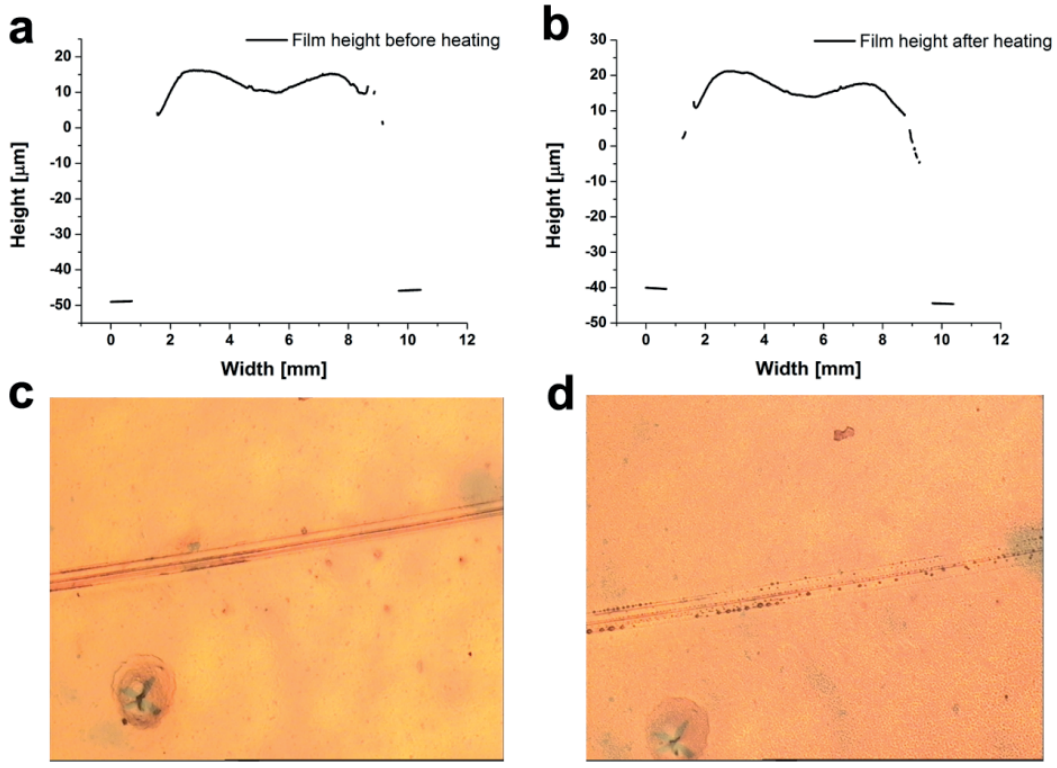

Figure S8. Height profiles of a PEO_{330}-*b*-$PFGE_{20}$ block copolymer film before (a) and after heating (b) as well as optical microscopy images of the polymer film at room-temperature (c) and at 155 °C (d). The slight variation of the axis values in Figure 8a and b originate from a tilt of the sample during the measurement process.

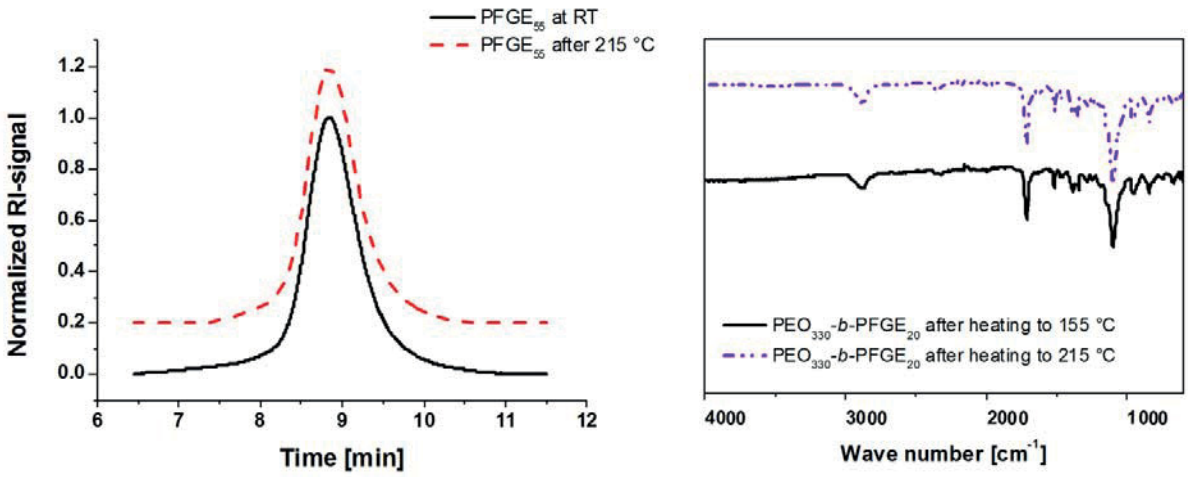

Figure S9. SEC traces of $PFGE_{55}$ before (solid black line) and after heating to 215 °C (dashed red line) (left) as well as IR spectroscopy measurements of a PEO_{330}-*b*-$PFGE_{20}$ sample heated to 155 °C (solid line) and 215 °C (dashed line) (right).

Publication P9

Poly(2-vinyl pyridine)-*block*-Poly(ethylene oxide) featuring a Furan Group at the Block Junction – Synthesis and Functionalization

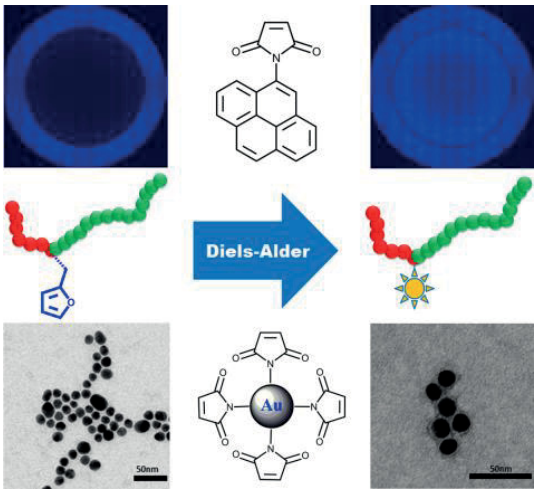

Tobias Rudolph,[#] Markus J. Barthel,[#] Florian Kretschmer, Ulrich Mansfeld, Stephanie Hoeppener, Martin D. Hager, Ulrich S. Schubert, Felix H. Schacher

[#] Both authors contributed equally to this publication.

Macromol. Rapid Commun., **2014**, 35, 916-921

Poly(2-vinyl pyridine)-*block*-Poly(ethylene oxide) Featuring a Furan Group at the Block Junction—Synthesis and Functionalization

Tobias Rudolph, Markus J. Barthel, Florian Kretschmer, Ulrich Mansfeld, Stephanie Hoeppener, Martin D. Hager, Ulrich S. Schubert, Felix H. Schacher*

Furfuryl glycidyl ether (FGE) represents a highly versatile monomer for the preparation of reversibly cross-linkable nanostructured materials via Diels–Alder reactions. Here, the use of FGE for the mid-chain functionalization of a P2VP-*b*-PEO diblock copolymer is reported. The material features one furan moiety at the block junction, $P2VP_{68}$-FGE-*b*-PEO_{390}, which can be subsequently addressed in Diels–Alder reactions using maleimide-functionalized counterparts. The presence of the FGE moiety enables the introduction of dyes as model labels or the formation of hetero-grafted brushes as shell on hybrid Au@Polymer nanoparticles. This renders $P2VP_{68}$-FGE-*b*-PEO_{390}, a powerful tool for selective functionalization reactions, including the modification of surfaces.

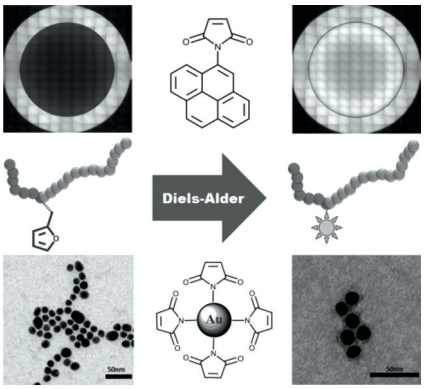

1. Introduction

During the last decades, well-defined block copolymers revealed high potential for a broad range of applications, mainly driven by the possibility to combine different properties within one single material and to introduce the ability to undergo self-assembly into nanostructured materials in various environments.[1–5] The preparation of block copolymers is usually achieved by sequential polymerization of different monomers or via post-polymerization modification using suitable macromolecular conjugation reactions [e.g., 1,3-dipolar cycloadditions or (hetero) Diels–Alder (DA) reactions].[6–10] Thereby, the precise positioning of functional groups within polymer chains is crucial for the synthesis of linear block copolymers or materials of different architectures, e.g., star-shaped structures.[11–13] Although more and more examples are found where polymeric building blocks are functionalized at one or both chain ends, examples for addressing the mid-chain junction point, i.e., the covalent linkage of blocks A and B of diblock copolymers, are scarce.[14–17] Such functional mid-chain junctions can be introduced by functional initiators[18–20] or end-capping of an active polymer chain and the subsequent polymerization of the second block.[21] The resulting functionalized polymers were used in surface coatings (e.g., on glass)[22] as well as for the preparation

T. Rudolph,[+] M. J. Barthel,[+] F. Kretschmer, U. Mansfeld, Dr. S. Hoeppener, Dr. M. D. Hager, Prof. U. S. Schubert, Prof. F. H. Schacher
Laboratory of Organic and Macromolecular Chemistry, Friedrich Schiller University Jena, Humboldtstr. 10, 07743 Jena, Germany
E-mail: felix.schacher@uni-jena.de
T. Rudolph,[+] M. J. Barthel,[+] F. Kretschmer, U. Mansfeld, Dr. S. Hoeppener, Dr. M. D. Hager, Prof. U. S. Schubert, Prof. F. H. Schacher
Jena Center for Soft Matter (JCSM), Friedrich Schiller University Jena, Philosophenweg 7, 07743 Jena, Germany
M. J. Barthel,[+] Prof. U. S. Schubert
Dutch Polymer Institute, P.O. Box 902, Eindhoven 5600 AX, The Netherlands
[+]These authors contributed equally to this work.

DOI: 10.1002/marc.201300875

of different architectures (e.g., H-shaped polymers[23] and miktoarm stars).[14] Current examples most commonly feature a new initiating group or a clickable moiety. In that respect, epoxides can be used as straightforward and highly efficient end-capping agents during living anionic polymerization using lithium counter ions. Here, due to the strong coordination of lithium toward the alkoxide chain-end, further polymerization of epoxides is prevented and the attachment of one single molecule can be realized. Potential functionalized epoxides such as allyl glycidyl ether (AGE) or ethoxy ethyl glycidyl ether (EEGE) are commercially available and transform this substance class into an interesting tool for the selective mid-chain functionalization of polymer chains.

Recently, furfuryl glycidyl ether (FGE) has been established as a versatile and functional monomer for anionic ring-opening polymerization (AROP) and the subsequent use of the furan moiety for controlled and reversible crosslinking of micellar cores or individual domains within nanostructured films via the DA reaction using a bismaleimide.[24,25] In the latter case, the potential application of poly(ethylene oxide)-*block*-poly(furfuryl glycidyl ether) (PEO-*b*-PFGE) diblock copolymers as self-healing coatings was proposed.

Here, we use FGE as functional end-capping agent for the living anionic polymerization of poly(2-vinyl pyridine) (P2VP), followed by the subsequent polymerization of ethylene oxide (EO) and the formation of mid-chain-functionalized P2VP-*b*-PEO. After characterization via size-exclusion chromatography (SEC), nuclear magnetic resonance (NMR) spectroscopy, and MALDI-TOF MS, the furan moiety in between the two blocks was used for selective DA reactions with maleimide-functionalized model dyes and gold nanoparticles (AuNPs).

2. Results and Discussion

Mid-chain-functionalized block copolymers represent interesting materials when it comes to the modification of surfaces such as on planar substrates or on (nano) particles. The introduction of a furan group at the junction point of diblock copolymers in turn is motivated by the broad accessibility of functional groups and architectures by the DA chemistry. Therefore, the synthesis of poly(2-vinyl pyridine)-*block*-poly(ethylene oxide) (P2VP-FGE-*b*-PEO), featuring a FGE moiety in between the P2VP and the PEO segment, was carried out in two steps. First, 2-vinylpyridine was polymerized after initiation via *sec*-butyl lithium (*sec*-BuLi). After full conversion, 1,1-diphenylethylene was added to the reaction mixture to decrease the nucleophilicity of the active chain end,[16] and the living P2VP chains were end-capped with FGE (Figure 1A). Afterward, the reaction was quenched by the addition of methanol and the crude product was precipitated into cold hexane. P2VP-FGE-OH was characterized via SEC, ^{1}H NMR, and MALDI-TOF MS (Figure 1; Table S1 and Figure S2, Supporting Information). The degree of polymerization (DP) was determined to be 68, resulting in P2VP$_{68}$-FGE-OH. The end-group fidelity was assessed via MALDI-TOF MS and NMR and was found to be 100% within the error of the measurement. MALDI-TOF MS also revealed the presence of the lithium counterion (Figure S2, Supporting Information), which however had to be removed prior to the polymerization of ethylene oxide. For this purpose, the material was intensively washed with water and precipitated into cold hexane several times (Figure S3, Supporting Information). As second step, P2VP$_{68}$-FGE-OH was dissolved in THF and the hydroxyl end-group was activated by the addition of an excess of diphenylmethyl potassium (DPMK), until a deep red color could be observed (Figure 1A). Under vigorous stirring, ethylene oxide was added to the reaction at –20 °C, the reaction mixture was slowly heated to 40 °C, and the polymerization was terminated via the addition of methanol after 24 h, followed by precipitation of the block copolymer into cold diethyl ether. The obtained material was again investigated via SEC, ^{1}H NMR, and MALDI-TOF MS (Figure S4, Supporting Information). The SEC trace shows a clear shift to lower elution volume in comparison to P2VP$_{68}$-FGE-OH (Figure 1B; Table S1, Supporting Information), and a new peak around 3.6 ppm for the PEO backbone appears in the ^{1}H NMR spectrum. The exact molar mass of the block copolymer was determined by MALDI-TOF MS, leading to 24 500 g mol^{-1}, and a composition of P2VP$_{68}$-FGE-PEO$_{390}$ (Figure S4, Supporting Information), which was also confirmed via ^{1}H NMR spectroscopy.

As a first proof of successful functionalization, P2VP$_{68}$-FGE-*b*-PEO$_{390}$ was used in DA reactions with two different maleimide-functionalized dyes [*N*-(1-pyrenyl)maleimide and 4-phenylazomaleinanil]. Therefore, the block copolymer and the respective dye (20 equiv.) were dissolved in 2 mL DMF separately in two vials and heated to 75 °C for 24 h. Afterward, the dye-functionalized materials were purified via size exclusion column chromatography (BioBeads SX1) to remove any excess of the dyes. In both cases, successful functionalization with the azobenzene-, P2VP$_{68}$-azo-*b*-PEO$_{390}$, and the pyrene-moiety, P2VP$_{68}$-pyr-*b*-PEO$_{390}$, was proven by UV–vis measurements (Figure 2B,C). The UV–vis spectra display that the initial P2VP$_{68}$-FGE-*b*-PEO$_{390}$ shows no characteristic absorption band (triangles), whereas the characteristic patterns of the individual molecules [spheres, 331 nm for 4-phenylazomaleinanil and 313, 326, and 342 nm for *N*-(1-pyrenyl) maleimide] can be found for the block copolymers after successful functionalization (squares).

Pyrene is known as a hydrophobic, fluorescent dye suitable for the determination of the critical

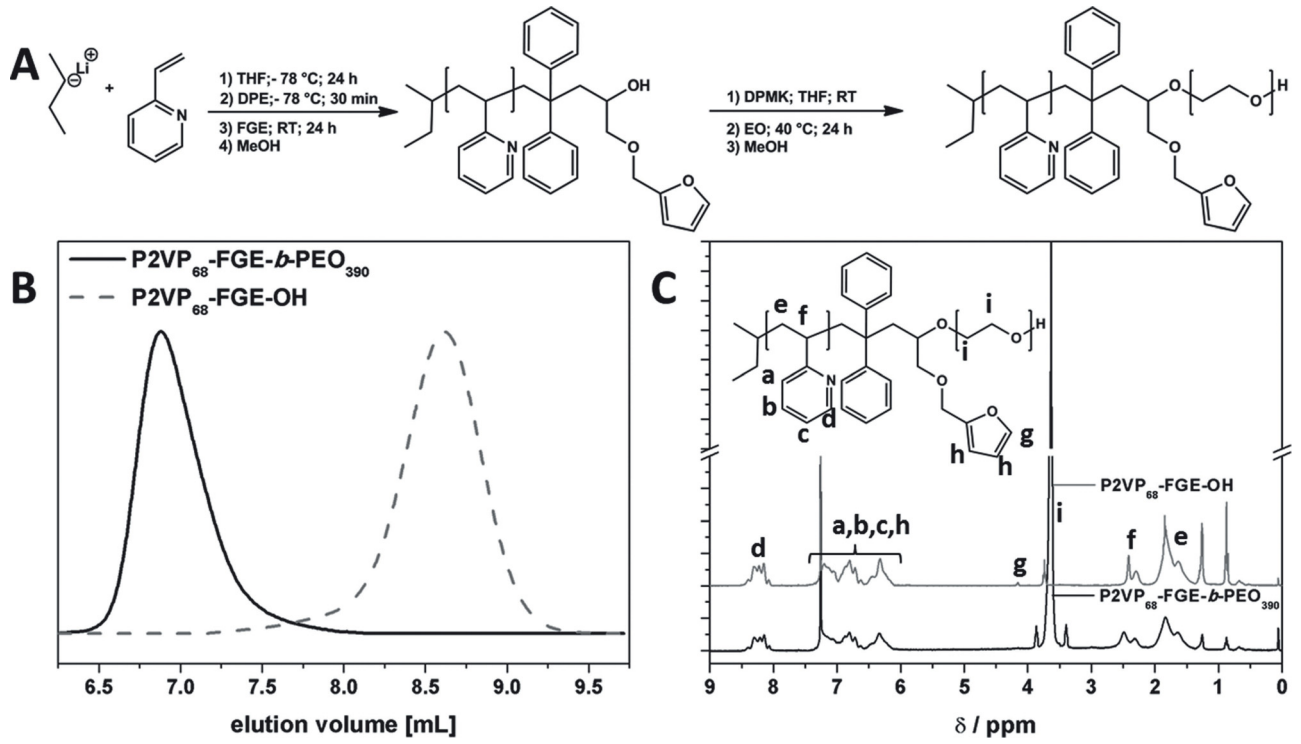

Figure 1. A) Block copolymer synthesis via sequential polymerization of 2-vinylpyridine and ethylene oxide, B) comparison of SEC traces for $P2VP_{68}$-FGE-OH (dashed gray line) and $P2VP_{68}$-FGE-*b*-PEO_{390} (black straight line), and C) the NMR spectra for $P2VP_{68}$-FGE-OH (gray line) and $P2VP_{68}$-FGE-*b*-PEO_{390} (black line).

micellization concentration (cmc) of amphiphilic block copolymers.[26–29] In case of *N*-(1-pyrenyl)maleimide, no fluorescence is described in the literature for the pristine dye in water, only after nucleophilic attack by thiols.[30] This can also be observed for our system after functionalization with *N*-(1-pyrenyl)maleimide and this was investigated via fluorescence microscopy (excitation wavelength = 357 nm; emission filter = 460 nm, Figure 3). Using this setup, no fluorescence could be detected for the pure dye in MilliQ water, whereas pyrene itself showed clear fluorescence under these conditions (Figure S6C, Supporting Information). Both $P2VP_{68}$-pyr-*b*-PEO_{390} and $P2VP_{68}$-FGE-*b*-PEO_{390} were transferred from THF into MilliQ water (pH7) by evaporation of the organic solvent (concentration was 5 mg mL^{-1} in both cases). In Figure 3, the circle originates from the fluorescence of the well-plate itself, while in the center the sample solution is located. As P2VP is known to exhibit a weak autofluorescence,[31] some fluorescence was also observed for $P2VP_{68}$-FGE-*b*-PEO_{390}, whereas $P2VP_{68}$-pyr-*b*-PEO_{390} shows a twofold increase in fluorescence in comparison to the pristine block copolymer (Figure 3; Figures S6 and S7, Supporting Information). This strong increase in fluorescence can be explained by electronic changes after the covalent attachment to the block copolymer chain by DA chemistry.

We were also interested in using $P2VP_{68}$-FGE-*b*-PEO_{390} for the functionalization of AuNPs. In that way, a hetero-brush could be generated in analogy to poly(styrene)-*block*-poly(ethylene oxide) (PS-*b*-PEO) brushes on planar surfaces.[22] Therefore, a maleimide-functionalized tri-thioacetate was synthesized (Figure S1, Supporting Information) and used for the synthesis of maleimide-functionalized AuNPs.[32–35] Possible excess of the maleimide-linker was removed by centrifugation of the particles (60 min at 5000 rpm), followed by resuspension in DMF (three cycles). The protective group was removed by heating the functionalized NP for 1 h at 140 °C. Both size and shape of the NPs were confirmed via DLS, TEM, and UV–vis (Figure 4). Spherical AuNPs with a $\langle R_h \rangle_{z,app}$ of 8 nm were obtained according to DLS (Figure 4D) and TEM (Figure 4A). For the attachment of $P2VP_{68}$-FGE-*b*-PEO_{390} to the NP surface, AuNP and $P2VP_{68}$-FGE-*b*-PEO_{390} were suspended together in DMF and heated for 2 d at 75 °C. After this treatment, the solution was centrifuged and washed with DMF to remove any unreacted $P2VP_{68}$-FGE-*b*-PEO_{390}. After resuspension, the particles ($P2VP_{68}$-DA_{Au}-*b*-PEO_{390}) were investigated using UV–vis spectroscopy and DLS, showing a slight red-shift in the UV–vis spectra from 527 to 538 nm (Figure 4C) and an increase in hydrodynamic radius ($\langle R_h \rangle_{z,app}$ = 12 nm)

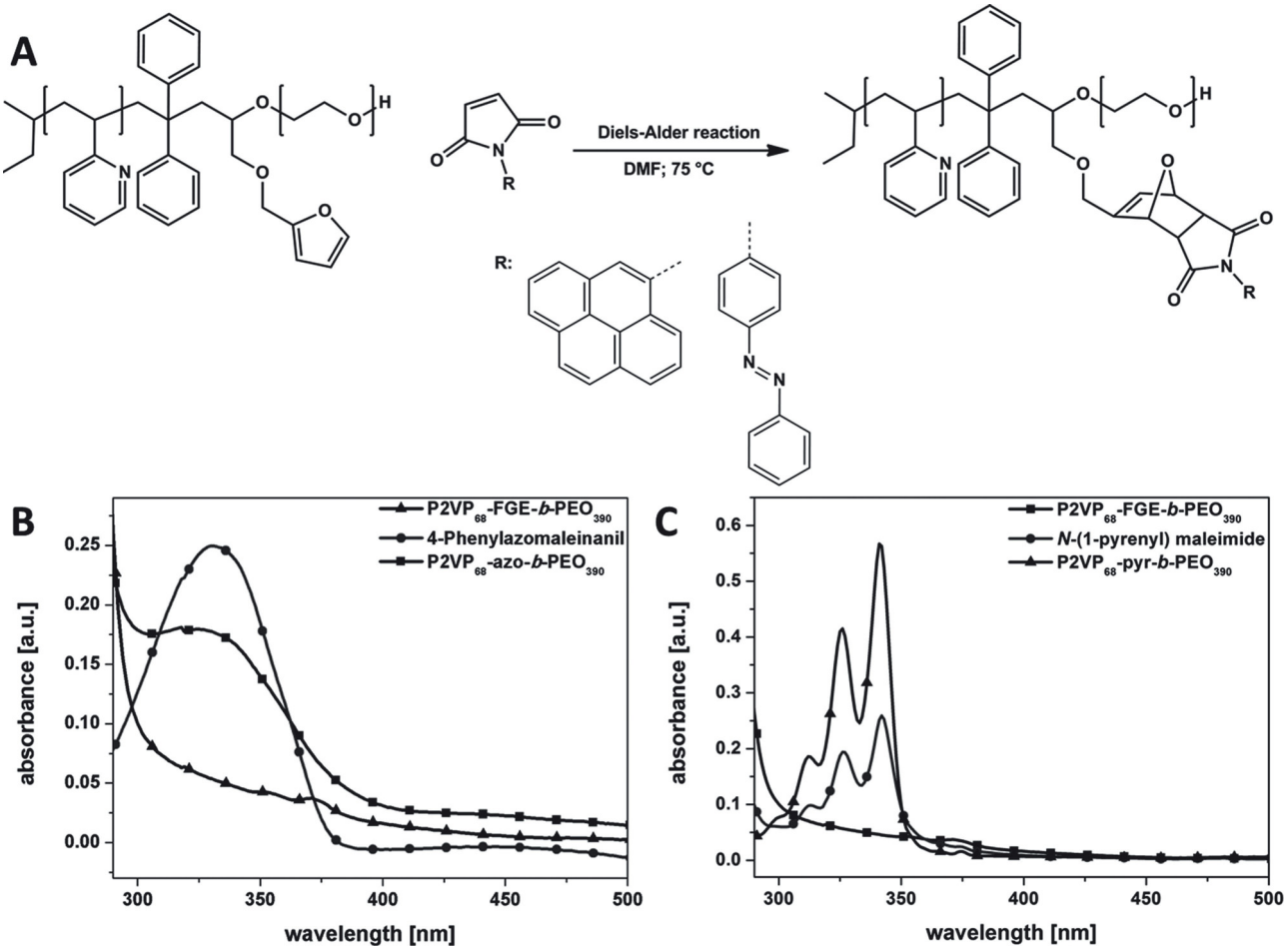

Figure 2. A) DA reaction between $P2VP_{68}$-FGE-*b*-PEO_{390} and maleimide-functionalized dyes; comparison of UV–vis spectra for B) $P2VP_{68}$-FGE-*b*-PEO_{390} (triangles), 4-phenylazomaleinanil (spheres), and $P2VP_{68}$-azo-*b*-PEO_{390} (squares); C) $P2VP_{68}$-FGE-*b*-PEO_{390} (squares), *N*-(1-pyrenyl) maleimide (spheres), and $P2VP_{68}$-azo-*b*-PEO_{390} (triangles) in THF.

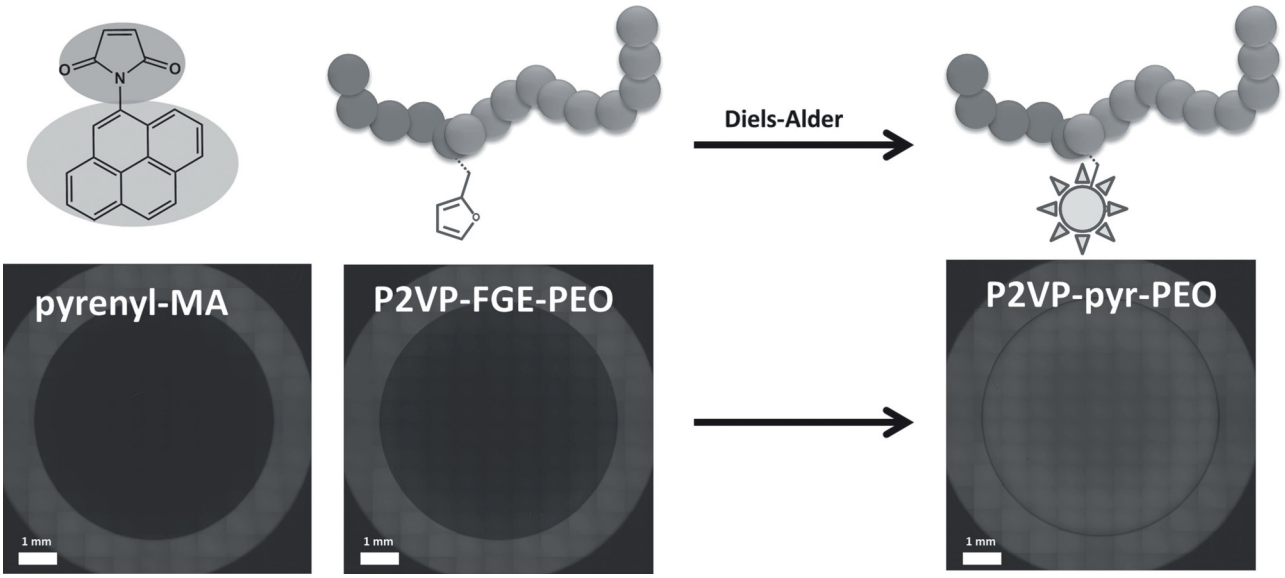

Figure 3. Functionalization of $P2VP_{68}$-FGE-*b*-PEO_{390}; comparison of fluorescence microscope images of *N*-(1-pyrenyl)maleimide (left), $P2VP_{68}$-FGE-*b*-PEO_{390} (5 mg mL^{-1}, middle), and $P2VP_{68}$-pyr-*b*-PEO_{390} (5 mg mL^{-1}, right) in water.

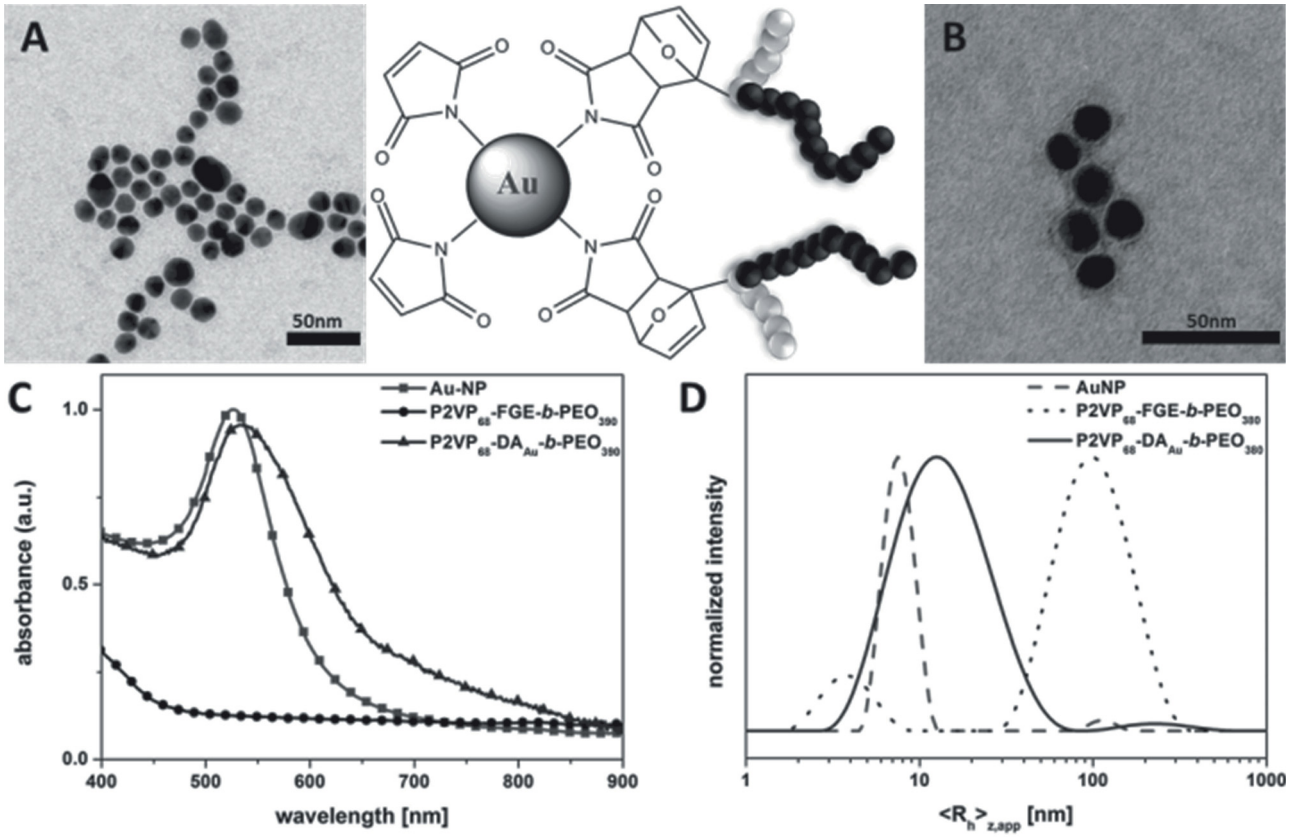

Figure 4. Comparison of TEM images for the pristine (A, unstained) and block copolymer-coated AuNP (B, stained with uranyl acetate); C) comparison of UV–vis spectra for $P2VP_{68}$-FGE-*b*-PEO_{390} (spheres), maleimide-functionalized AuNP (squares), and $P2VP_{68}$-DA_{Au}-*b*-PEO_{390} (triangles); D) comparison of intensity-weighted DLS CONTIN plots for $P2VP_{68}$-FGE-*b*-PEO_{390} (dotted curve; $<R_h>_{z,app}$ = 4 nm and 100 nm; 2 mg mL^{-1}), maleimide-functionalized AuNP (dashed curve; $<R_h>_{z,app}$ = 8 nm; 1 mg mL^{-1}), and $P2VP_{68}$-DA_{Au}-*b*-PEO_{390} (straight curve; $<R_h>_{z,app}$ = 12 nm; 1 mg mL^{-1}) in DMF.

compared with the pristine block copolymer ($<R_h>_{z,app}$ = 4 nm), and the maleimide-functionalized AuNP ($<R_h>_{z,app}$ = 8 nm, Figure 4D).

According to DLS, the size distribution of $P2VP_{68}$-DA_{Au}-*b*-PEO_{390} slightly broadens, which might be due to a certain amount of aggregation of the hybrid particles in solution. If the structures are subjected to TEM analysis, the freshly prepared AuNPs feature sharp edges whereas this seems not to be the case after DA reaction with $P2VP_{68}$-FGE-*b*-PEO_{390}, indicating the attachment of a polymeric shell (Figure S8, Supporting Information). Staining with uranyl acetate was applied to the NP both before and after surface modification. As expected, no changes were observed for the pristine AuNP, except for a slight decrease of the overall contrast within the corresponding TEM images due to an increase of the electron density on the underlying carbon support on the whole TEM grid (Figure S8, Supporting Information). For $P2VP_{68}$-DA_{Au}-*b*-PEO_{390}, a continuous dark ring of a few nanometers thickness is observed and this further supports the assumption of the successful formation of a P2VP/PEO shell. $P2VP_{68}$-DA_{Au}-*b*-PEO_{390} was also transferred into DMF-d_7 and was investigated via ^{1}H NMR, but the signal intensity of the obtained spectrum was rather low (Figure S9, Supporting Information). However, both the characteristic signals for P2VP and PEO could be assigned.

As a further proof for the successful particle coating, both $P2VP_{68}$-DA_{Au}-*b*-PEO_{390} and the pristine AuNP were transferred from DMF into water (pH 7). While the solution containing $P2VP_{68}$-DA_{Au}-*b*-PEO_{390} showed a red color (hinting toward well-dispersed hybrid particles), the pristine NP aggregated, indicated by a bluish color (Figure S10A, Supporting Information). Under acidic conditions (pH ≤ 4), P2VP becomes protonated and positively charged. Therefore, zeta-potential measurements were performed for the block copolymer and the NPs, respectively (Figure S10B, Supporting Information). While the pristine AuNP show a zeta potential of ≈–33 mV at pH 7, precipitation was observed at pH 4. After coating, a zeta potential of –3 mV at pH 7 and +22 mV at pH 4 was found, following the trend observed for

$P2VP_{68}$-FGE-*b*-PEO_{390} under this conditions (Figure S10B, Supporting Information).

3. Conclusion

We successfully synthesized a mid-chain-functionalized block copolymer featuring one furan moiety, $P2VP_{68}$-FGE-*b*-PEO_{390}, by sequential living anionic polymerization. The furan moiety was subsequently used in DA reactions with maleimide-functionalized counterparts to introduce dyes as model labels to the block copolymer or to create a hetero-grafted shell on AuNP. Our results convincingly demonstrate that $P2VP_{68}$-FGE-*b*-PEO_{390} is a versatile example for (surface) functionalization and the introduction of hetero-brushes. Our results may also be used in the future for the stabilization of carbon nanotubes via $P2VP_{68}$-pyr-*b*-PEO_{390}, surface modification of NPs different from Au, or the preparation of ABC miktoarm star terpolymers.

Supporting Information

Supporting Information is available from the Wiley Online Library or from the author.

Acknowledgements: The authors thank Sarah Crotty for MALDI-TOF MS, Ulrike Günther for zeta-potential measurements, David Pretzel for fluorescence microscopy measurements, and Jürgen Vitz for technical support regarding the ethylene oxide polymerization. F.H.S. thanks the VCI for an independent researcher fellowship, and T.R. acknowledges the Carl-Zeiss foundation for a PhD scholarship. The work of M.J.B. forms part of the research program of the Dutch Polymer Institute (DPI), project #690. The authors also acknowledge the Thuringian Ministry for Education, Science and Culture (grants #B514–09051, NanoConSens, #B515–10065, ChaPoNano, #B515–11028, BASIS, and #B515–07008) for financial support of this study. U.S.S., M.D.H., F.K. and S.H. thank the Federal Ministry of Education and Research (Spitzencluster PHONA) for financial support.

Received: November 27, 2013; Revised: December 30, 2013; Published online: February 24, 2014; DOI: 10.1002/marc.201300875

Keywords: anionic polymerization; block copolymer; Diels–Alder reaction; furfuryl glycidyl ether; mid-chain junction; poly(ethylene oxide)

[1] F. H. Schacher, P. A. Rupar, I. Manners, *Angew. Chem Int. Ed.* **2012**, *51*, 7898.
[2] A. H. Gröschel, F. H. Schacher, H. Schmalz, O. V. Borisov, E. B. Zhulina, A. Walther, A. H. E. Müller, *Nat. Commun.* **2012**, *3*, 710.
[3] H.-C. Kim, S.-M. Park, W. D. Hinsberg, *Chem. Rev.* **2009**, *110*, 146.
[4] A. Nunns, J. Gwyther, I. Manners, *Polymer* **2013**, *54*, 1269.
[5] S. B. Darling, *Prog. Polym. Sci.* **2007**, *32*, 1152.
[6] M. A. Tasdelen, M. U. Kahveci, Y. Yagci, *Prog. Polym. Sci.* **2011**, *36*, 455.
[7] C. Barner-Kowollik, F. E. Du Prez, P. Espeel, C. J. Hawker, T. Junkers, H. Schlaad, W. Van Camp, *Angew. Chem Int. Ed.* **2011**, *50*, 60.
[8] K. Kempe, A. Krieg, C. R. Becer, U. S. Schubert, *Chem. Soc. Rev.* **2012**, *41*, 176.
[9] A. S. Goldmann, M. Glassner, A. J. Inglis, C. Barner-Kowollik, *Macromol. Rapid Commun.* **2013**, *34*, 810.
[10] T. T. T. N'Guyen, H. T. T. Duong, J. Basuki, V. Montembault, S. Pascual, C. Guibert, J. Fresnais, C. Boyer, M. R. Whittaker, T. P. Davis, L. Fontaine, *Angew. Chem Int. Ed.* **2013**, *52*, 14152.
[11] T. Rudolph, S. Crotty, M. v. d. Lühe, D. Pretzel, U. S. Schubert, F. Schacher, *Polymers* **2013**, *5*, 1081.
[12] D. Fournier, R. Hoogenboom, U. S. Schubert, *Chem. Soc. Rev.* **2007**, *36*, 1369.
[13] H. Durmaz, A. Sanyal, G. Hizal, U. Tunca, *Polym. Chem.* **2012**, *3*, 825.
[14] A. Hanisch, H. Schmalz, A. H. E. Müller, *Macromolecules* **2012**, *45*, 8300.
[15] C. Tonhauser, H. Frey, *Macromol. Rapid Commun.* **2010**, *31*, 1938.
[16] A. Natalello, C. Tonhauser, E. Berger-Nicoletti, H. Frey, *Macromolecules* **2011**, *44*, 9887.
[17] X.-S. Feng, C.-Y. Pan, *Macromolecules* **2002**, *35*, 4888.
[18] O. Altintas, U. Tunca, C. Barner-Kowollik, *Polym. Chem.* **2011**, *2*, 1146.
[19] O. Altintas, B. Yankul, G. Hizal, U. Tunca, *J. Polym. Sci., Part A: Polym. Chem.* **2007**, *45*, 3588.
[20] Z. L. Wang, J. T. Xu, B. Y. Du, Z. Q. Fan, *J. Colloid Interface Sci.* **2011**, *360*, 350.
[21] C. Tonhauser, B. Obermeier, C. Mangold, H. Lowe, H. Frey, *Chem. Commun.* **2011**, *47*, 8964.
[22] C. Tonhauser, A. A. Golriz, C. Moers, R. Klein, H. J. Butt, H. Frey, *Adv. Mater.* **2012**, *24*, 5559.
[23] O. Altintas, D. Schulze-Suenninghausen, B. Luy, C. Barner-Kowollik, *ACS Macro Lett.* **2013**, *2*, 211.
[24] M. J. Barthel, T. Rudolph, S. Crotty, F. H. Schacher, U. S. Schubert, *J. Polym. Sci., Part A: Polym. Chem.* **2012**, *50*, 4958.
[25] M. J. Barthel, T. Rudolph, A. Teichler, R. M. Paulus, J. Vitz, S. Hoeppener, M. D. Hager, F. H. Schacher, U. S. Schubert, *Adv. Funct. Mater.* **2013**, *23*, 4921.
[26] K. Knop, G. M. Pavlov, T. Rudolph, K. Martin, D. Pretzel, B. O. Jahn, D. H. Scharf, A. A. Brakhage, V. Makarov, U. Mollmann, F. H. Schacher, U. S. Schubert, *Soft Matter* **2013**, *9*, 715.
[27] K. Kalyanasundaram, J. K. Thomas, *J. Am. Chem. Soc.* **1977**, *99*, 2039.
[28] M. Wilhelm, C. L. Zhao, Y. Wang, R. Xu, M. A. Winnik, J. L. Mura, G. Riess, M. D. Croucher, *Macromolecules* **1991**, *24*, 1033.
[29] G. Kwon, M. Naito, M. Yokoyama, T. Okano, Y. Sakurai, K. Kataoka, *Langmuir* **1993**, *9*, 945.
[30] C.-W. Wu, L. R. Yarbrough, F. Y. H. Wu, *Biochemistry* **1976**, *15*, 2863.
[31] D. Vyprachtický, K. W. Sung, Y. Okamoto, *J. Polym. Sci., Part A: Polym. Chem.* **1999**, *37*, 1341.
[32] F. Kretschmer, U. Mansfeld, S. Hoeppener, M. Hager, U. S. Schubert, *Chem. Commun.* **2013**, *50*, 88.
[33] H. Y. Song, M. H. Ngai, Z. Y. Song, P. A. MacAry, J. Hobley, M. J. Lear, *Org. Biomol. Chem.* **2009**, *7*, 3400.
[34] M. G. Badin, A. Bashir, S. Krakert, T. Strunskus, A. Terfort, C. Woll, *Angew. Chem Int. Ed.* **2007**, *46*, 3762.
[35] Y. K. Kang, D. J. Won, S. R. Kim, K. J. Seo, H. S. Choi, G. H. Lee, Z. S. Noh, T. S. Lee, C. J. Lee, *Mater. Sci. Eng. C* **2004**, *24*, 43.

Supporting Information

for *Macromol. Rapid Commun.,* DOI: 10.1002/marc.201300875

Poly(2-vinyl pyridine)-*block*-Poly(ethylene oxide) Featuring a Furan Group at the Block Junction—Synthesis and Functionalization

*Tobias Rudolph, Markus J. Barthel, Florian Kretschmer, Ulrich Mansfeld, Stephanie Hoeppener, Martin D. Hager, Ulrich S. Schubert, and Felix H. Schacher**

Supporting Information

Poly(2-vinyl pyridine)-*block*-Poly(ethylene oxide) featuring a Furan Group at the Block Junction – Synthesis and Functionalization

Tobias Rudolph,[1,2,#] Markus J. Barthel,[1,2,3,#] Florian Kretschmer,[1,2] Ulrich Mannsfeld,[1,2] Stephanie Hoeppener,[1,2] Martin D. Hager,[1,2] Ulrich S. Schubert,[1,2,3] and Felix H. Schacher[1,2,*]

[1] Laboratory of Organic and Macromolecular Chemistry, Friedrich Schiller University Jena, Humboldtstr. 10, 07743 Jena, Germany

E-mail: felix.schacher@uni-jena.de

[2] Jena Center for Soft Matter (JCSM), Friedrich Schiller University Jena, Philosophenweg 7, 07743 Jena, Germany

[3] Dutch Polymer Institute, P.O. Box 902, Eindhoven 5600 AX, The Netherlands

# These authors contributed equally to this work.

Instruments

NMR: Proton nuclear magnetic resonance (^{1}H-NMR) spectra were recorded in $CDCl_3$ on a Bruker AC 300 MHz spectrometer at 298 K. Chemical shifts are given in parts per million (ppm, δ scale) relative to the residual signal of the deuterated solvent.

SEC: Size exclusion chromatography was measured on a system equipped with a SCL-10A system controller, a LC-10AD pump and a RID-10A refractive index detector using a solvent mixture containing chloroform ($CHCl_3$), triethylamine (TEA) and *iso*-propanol (*i*-PrOH) (94:4:2) at a flow rate of 1 mL min^{-1} on a PSS SDV linear M 5 μm column. The system was calibrated using PS (100 to 100,000 g mol^{-1}) and PEO (440 to 44,700 g mol^{-1}) standards.

MALDI-ToF MS: Matrix-assisted laser desorption/ionization time of flight mass spectrometry was performed on an Ultraflex III TOF/TOF (Bruker Daltonics, Bremen, Germany), equipped with a Nd:YAG laser and with *trans*-2-[3-(4-*tert*-butylphenyl)-2-methyl-2-propenylidene] malononitrile (DCTB) as the matrix and NaCl as the doping agent in reflector and linear mode. The instrument was calibrated prior to each measurement with an external poly(methyl methacrylate) (PMMA) standard from PSS Polymer Standards Services GmbH (Mainz, Germany).

DLS: Dynamic light scattering was performed at a scattering angle of 90° on an ALV CGS-3 instrument equipped with a He-Ne laser operating at a wavelength of 633 nm at 25 °C. The CONTIN algorithm was applied to analyze the obtained correlation functions. For temperature control, the DLS is equipped with a Lauda thermostat. Apparent hydrodynamic radii were calculated according to the Stokes-Einstein equation.

Transmission electron microscopy (TEM): TEM measurements were performed on a Philips CM-120. 15 μL of the sample solution were blotted onto clean carbon coated TEM

grids (Mesh 400, Quantifoil, Jena) and excess material was removed by a filter paper (Whatman No. 1); the samples were allowed to dry prior to the transfer to the microscope. Grid cleaning was performed by UV-ozone treatment for 40 s. For staining purpose a drop of uranyl acetate (3 mg ml^{-1}) was applied to the grid, the supernatant solution was removed via filter paper and the sample washed with water to remove the excess of uranyl acetate.

Centrifugation was performed with a Heraeus Biofuge Primo with a fixed angle rotor in 1.5 mL Eppendorf tubes.

UV-Vis spectroscopy: UV-Vis absorption spectra were recorded with a Specord 250 spectrometer (Analytik Jena) or a Lambda 750 UV/VIS/NIR spectrometer (PerkinElmer) in Suprasil quartz glass cuvettes 104-QS (Hellma Analytics) with a thickness of 10 mm at room temperature.

Fluorescence microscope: Fluorescence images were measured on a fluorescence microscope (Cell Observer Z1, Carl Zeiss, Jena, Germany) equipped with a mercury arc UV lamp and the appropriate filter combinations for excitation and detection of emission. In this case the sample was irradiated with 357 nm and an emission filter of 460 nm. All images were measured using identical instrument settings (e.g. UV lamp power, integration time, camera gain) and spots of the well plate were addressed using an automated XY table.

Zeta Potential Measurements: The ζ-potentials were measured on a ZetaSizer Nano ZS from Malvern *via* the M3-PALS technique with a laser beam at 633 nm. The detection angle was 13°. The electrophoretic mobilities (*u*) were converted into ζ –potentials *via* the Henry equation in the Smoluchowski approximation, $z = u\ \eta/\varepsilon_0\ \varepsilon$, where η denotes the viscosity and $\varepsilon_0\ \varepsilon$ the permittivity of the solution.

Experimental section

Materials

Sec-butyl lithium, tetrahydrofuran, dimethylformamide, 2-vinyl pyridine, ethylene oxide, DPMK was synthesized as described in the literature.[1] Furfuryl glycidyl ether was purified *via* column chromatography as described in literature.[2] 4-Phenylazomaleinanil and N-(1-pyrenyl)-maleimide were purchased from Sigma Aldrich and used as received. DMF (anhydrous, amine free, 99.9%) was purchased from Alfa Aesar. Dicylcohexylcarbodiimide (DCC), furane, 4-dimethylaminopyridine (DMAP) and potassium thioacetate were purchased from Sigma-Aldrich. Pentaerythritol tribromide was received from TCI Europe. Water (< 0.1µS/cm) was purchased from ELGA Purelab Prima. All chemicals were used as received.

Compound **1**[3] and citrate stabilized nanoparticles[4] were synthesized as reported in the literature.

Anionic polymerization of 2-vinylpyridine and end-capping with furfuryl glycidyl ether

In a Schlenk flask 80 mL freshly prepared THF were cooled to –78 °C with an *iso*-propanol/dry ice bath and 0.71 mL (1 mmol) of *s*-BuLi was added and stirred for 10 min. Afterwards 5.1 mL (47 mmol) of freshly distilled 2-vinyl pyridine were added quickly to the reaction solution and stirred for 1 hours. Afterwards, 0.4 mL diphenylethylene (2.3 mmol) were added to the reaction mixture to decrease the nucleophilicity of the active chain end. After addition of 0.27 mL of furfuryl glycidyl ether (2.3 mmol) the solution was allowed to warm to RT and stirred overnight at 25 °C. The reaction was terminated afterwards by the addition of methanol.

The polymer was precipitated in cold hexane and the crude product was purified by dissolving in chloroform and washing with water. The solvent was removed under reduced pressure and the product was dried under vacuum.

SEC ($CHCl_3$/*i*-PrOH/Et_3N): M_n = 8 700 g mol^{-1}; Đ = 1.08 (PS-calibration); **^{1}H NMR** (300 MHz, $CDCl_3$, δ): 8.5-8.0 (br, arom. *H*), 7.4-7.1 (br, arom. *H*), 4.15 (s, C*H*$_2$-furan), 3.74 (t, C*H*$_2$), 2.55-2.15 (br, -C*H*-P2VP); **MALDI-TOF MS**: M_p = 7 200 g mol^{-1}.

Anionic polymerization of ethylene oxide (EO) via P2VP$_{68}$-FGE-OH-macro initiator

2.0 g of P2VP$_{68}$-FGE-OH (0.28 mmol) were dissolved in 100 mL freshly distilled THF and transferred into a Büchi GlasUster PicoClave reactor. The hydroxyl-end group was activated *via* the addition of an excess of DPMK (~10 eq.) until a black color was observed. The reaction mixture was cooled to –20 °C and ethylene oxide (EO; 5.3 mL; 107 mmol) were introduced into the reaction vessel. The solution was slowly heated to 40 °C and stirred for 24 hours. The remaining pressure was released from the reactor system and the polymerization was terminated by the addition of methanol.

The desired block copolymer was obtained after precipitation into cold ether, filtering, and drying under vacuum.

SEC ($CHCl_3$/*i*-PrOH/Et_3N): M_n = 20 000 g mol^{-1}; Đ = 1.11 (-calibration); **^{1}H NMR** (300 MHz, $CDCl_3$, δ): 8.5-8.0 (br, arom. *H*), 7.4-7.1 (br, arom. *H*), 3.8-3.4 (PEO-backbone), 2.55-2.15 (br, -C*H*-P2VP); **MALDI-TOF MS**: M_p= 24 500 g mol^{-1}.

Synthesis of the thiol-linker

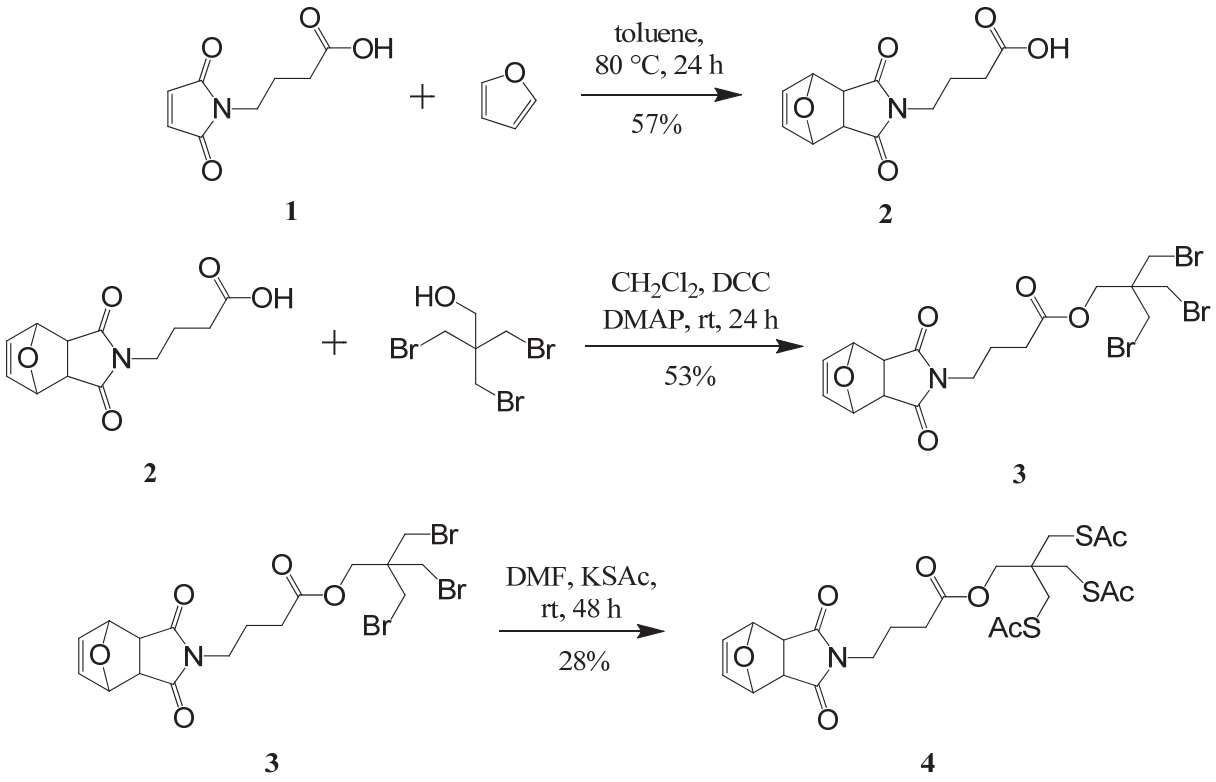

Figure S1: Synthetic strategy for the preparation of the maleimide-functionalized thiol-linker.

4-(1,3-Dioxo-3a,4,7,7a-tetrahydro-1H-4,7-epoxyisoindol-2(3H)-yl)butanoic acid (2)

1 (1.4 g, 7.64 mmol) and furane (5.2 g, 76.40 mmol) were dissolved in 20 mL toluene and the solution was heated to 80 °C for 24 h. Subsequently, the reaction was cooled to 4 °C in the fridge. The formed precipitated was filtered off and dried to obtain **2** as white crystals. Yield 1.1 g (57% of theory).

^{1}H NMR (300 MHz, $CDCl_3$): δ = 6.52 (s, 2 H, 2 CH), 5.28 (s, 2 H, 2 CH), 3.58 (t, J = 6.8 Hz, 2 H, CH_2), 2.86 (s, 2 H, 2 CH), 2.37 (t, J = 7.42 Hz, 2 H, CH_2), 1.93 (m, J = 7.22 Hz, 2 H,

CH_2) ppm. **^{13}C NMR** (250 MHz, $CDCl_3$): *d* = 177.31, 176.28, 136.50, 80.94, 47.40, 37.95, 30.78, 22.59 ppm.

3-Bromo-2,2-bis(bromomethyl)propyl-4-(1,3-dioxo-3a,4,7,7a-tetrahydro-1H-4,7-epoxy-isoindol-2(3H)-yl)butanoate (3)

2 (1.1 g, 4.38 mmol), pentaerythritol tribromide (1.7 g, 5.23 mmol), DCC (1.36 g, 6.59 mmol) and DMAP (82 mg, 0.67 mmol) were dissolved in 50 mL methylene chloride and stirred at room temperature under nitrogen for 24 h. Afterwards the mixture was filtered and the clear solution was washed with 50 mL water. The organic phase was dried over sodium sulfate and the solvent was removed under reduced pressure. Subsequently the crude product was purified *via* column chromatography (silica gel 60, methylene chloride: ethyl acetate 95:5) and **3** was obtained as a colorless solid. Yield 1.3g (53% of theory).

^{1}H NMR (300 MHz, $CDCl_3$): δ = 6.52 (s, 2 H, 2 CH), 5.27 (s, 2 H, 2 CH), 4.21 (s, 2 H, CH_2), 3.56 (s, 6 H, 3 CH_2), 3.55 (t, 2 H, CH_2), 2.86 (s, 2 H, 2 CH), 2.35 (t, *J* = 7.31 Hz, 2 H, CH_2), 1.92 (m, *J* = 7.08 Hz, 2 H, CH_2) ppm. **^{13}C NMR** (75 MHz, $CDCl_3$): δ = 176.22, 171.53, 136.49, 80.94, 63.71, 47.39, 42.73, 37.88, 34.11, 30.89, 22.71 ppm. **MS (HR-ESI)**: *m/z* calculated for $[C_{17}H_{20}Br_3NO_5]^{Na+}$: 577.8784; found: 577.8776 [M + Na].

3-(Acetylthio)-2,2-bis((acetylthio)methyl)propyl 4-(1,3-dioxo-3a,4,7,7a-tetrahydro-1H-4,7-epoxyisoindol-2(3H)-yl)butanoate (4)

3 (1 g, 1.79 mmol) and potassium thioacetate (1.22 g, 10.68 mmol) were dissolved in 10 mL DMF and stirred in a closed vial at room temperature for 48 h. Subsequently, 50 mL diethyl ether were added and the formed precipitate was filtered off. The organic solution was washed five times with 50 mL water followed by drying over sodium sulfate. Afterwards the solvent was removed under reduced pressure. The crude product was purified *via* column

chromatography (silica gel 60, methylene chloride: acetonitrile 38:2) to obtain **4** as a yellow oil which solidifies upon standing. Yield 290 mg (28% of theory).

^{1}H NMR (300 MHz, $CDCl_3$): δ = 6.52 (s, 2 H, 2 CH), 5.29 (s, 2 H, 2 CH), 3.95 (s, 2 H, CH_2), 3.57 (t, J = 6.85, 2 H, CH_2), 3.07 (s, 6 H, 3 CH_2), 2.86 (s, 2 H, CH_2) 2.36 (s, 9 H, 3 CH_3), 2.35 (t, 2 H, CH_2), 1.93 (m, J = 7.08 Hz, 2 H, CH_2) ppm. **^{13}C NMR** (75 MHz, $CDCl_3$): δ = 194.14, 176.20, 171.97, 136.53, 80.94, 66.09, 47.43, 42.16, 37.99, 32.94, 30.99, 30.58, 22.68 ppm. **MS (HR-ESI)**: *m/z* calculated for $[C_{23}H_{29}NO_8S_3]^{Na+}$: 566.0948; found: 566.0900 [M + Na].

Synthesis of maleimide stabilized gold nanoparticles (Au-NP)

10 × 1 mL citrate stabilized gold nanoparticles were pipetted in Eppendorf tubes and centrifuged at 5000 rpm for 90 minutes. Respectively, 950 µL of the supernatant solution were taken off, subsequently, a solution of **4** (100 µL, 1 mg/mL DMF) and 850 µL DMF were added. The particles were redispersed by simple shaking. The solution was centrifuged at 5000 rpm for 90 minutes, afterwards, 900 µL of the supernatant solution were taken off and the remaining 100 µL solution of the ten tubes were combined and pipetted in a glass vial. Finally, a solution of **4** (46 µL, 1 mg/mL DMF) was added and the mixture was heated to 130 °C for 1 h in order to cleave off the furan unit.

Diels-Alder reaction with maleimide-functionalized gold-nanoparticle

$P2VP_{68}$-FGE-*b*-PEO_{390} (5 mg) and 1 mg AuNP (46 µg of **4**) were dissolved in 1.5 mL DMF and heated to 75 °C for 2 days. The excess of block copolymer was removed by centrifugation at 5000 rpm for 90 minutes. The supernatant solution was removed and the particles re-suspended in DMF.

Diels-Alder reaction $P2VP_{68}$-FGE-b-PEO_{390} and N-(1-pyrenyl)maleimide

$P2VP_{68}$-FGE-*b*-PEO_{390} (100 mg; 4 µmol) and *N*-(1-pyrenyl)maleimide (24 mg; 0.08 mmol) were dissolved in 2 mL DMF. The solution was heated to 75 °C overnight. The desired product was received after size exclusion column chromatography (BioBeads SX1) with THF as eluent.

SEC ($CHCl_3$/*i*-PrOH/Et_3N): M_n = 17 000 g mol^{-1}; Đ = 1.22 (PEO-calibration)

Diels-Alder reaction $P2VP_{68}$-FGE-b-PEO_{390} and 4-phenylazomaleinanil

$P2VP_{68}$-FGE-*b*-PEO_{390} (100 mg; 4 µmol) and 4-phenylazomaleinanil (24 mg; 0.08 mmol) were dissolved in 2 mL DMF. The solution was heated to 75 °C overnight. The desired product was received after size exclusion column chromatography (BioBeads SX1) with THF as eluent.

SEC ($CHCl_3$/*i*-PrOH/Et_3N): M_n = 16 000 g mol^{-1}; Đ = 1.24 (PEO-calibration)

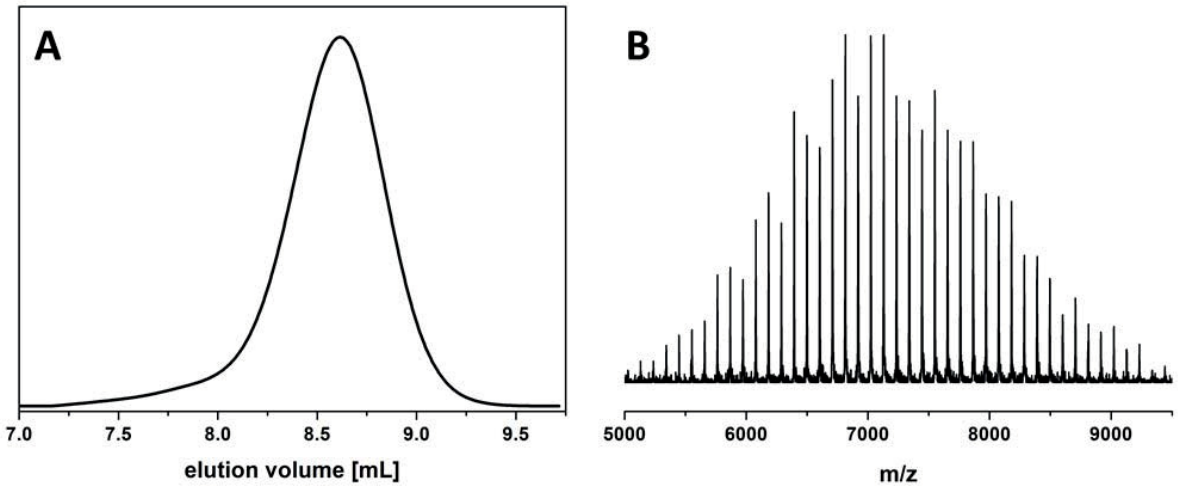

Figure S2: SEC trace (A) and MALDI-TOF MS spectra (B) for P2VP$_{68}$-FGE-OH.

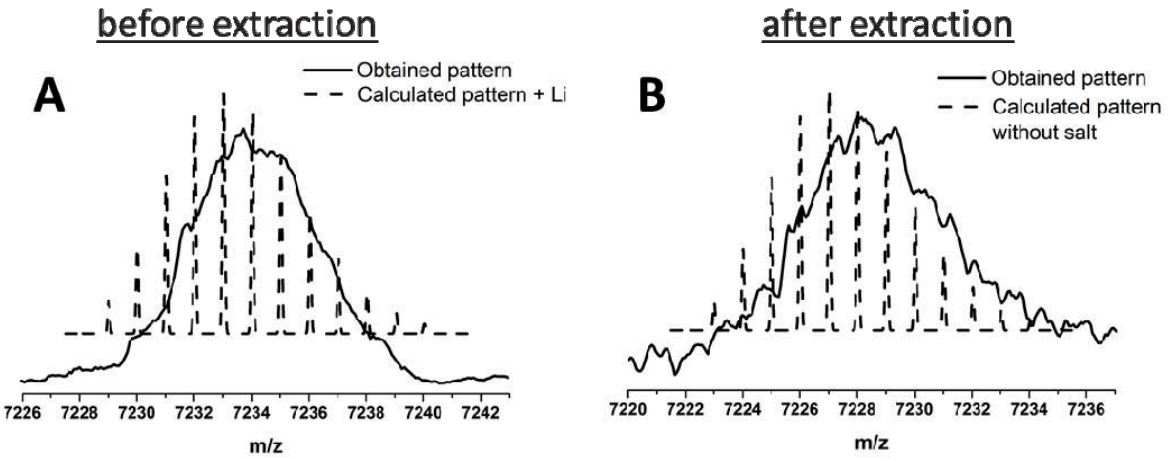

Figure S3: Comparison of the measured and the calculated MALDI-TOF MS spectra for P2VP$_{68}$-FGE-OH before (A) and after (B) extraction to remove the lithium counterion.

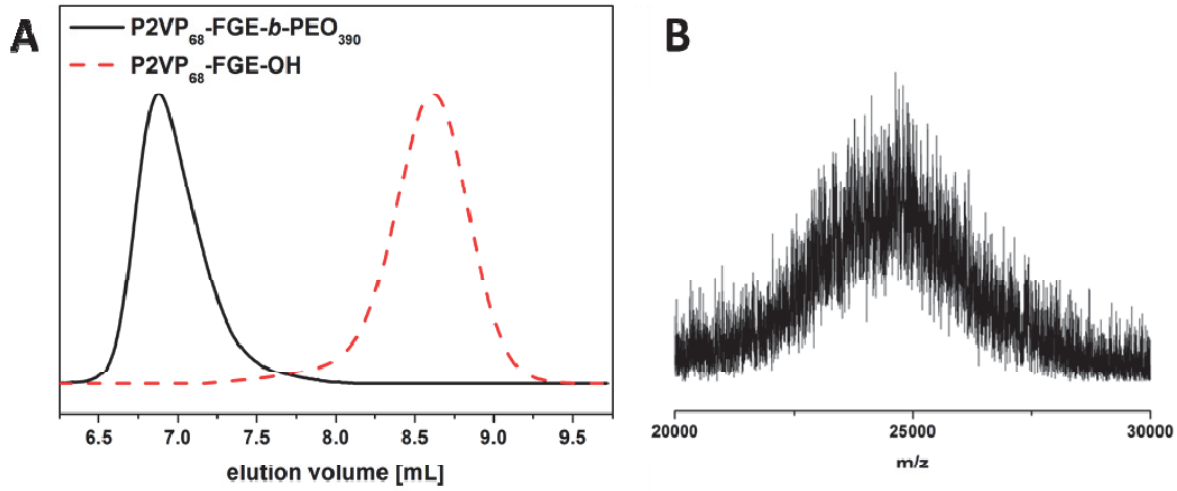

Figure S4: Comparison of the SEC traces for for $P2VP_{68}$-FGE-OH (dashed line) and for $P2VP_{68}$-FGE-*b*-PEO_{390} (A) and MALDI-TOF MS spectra of $P2VP_{68}$-FGE-*b*-PEO_{390}.

Table S1: Characterization of the functionalized homopolymer ($P2VP_{68}$-FGE-OH), block copolymer ($P2VP_{68}$-FGE-*b*-PEO_{390}) and the functionalized $P2VP_{68}$-FGE-*b*-PEO_{390}.

Polymer	M_n[a] [g mol^{-1}]	PDI[a]	M_p[d] [g mol^{-1}]
$P2VP_{68}$-FGE-OH[b]	8 700[c]	1.08[c]	7 200
$P2VP_{68}$-FGE-*b*-PEO_{390}[b]	19 000	1.11	24 500
$P2VP_{68}$-azo-*b*-PEO_{390}	16 000	1.24	-
$P2VP_{68}$-pyr-*b*-PEO_{390}	17 000	1.22	-

a) SEC ($CHCl_3$/*iso*-propanol/triethylamine) (PEO-calibration)
b) Determination by a combination of ^{1}H-NMR and MALDI-TOF MS
c) SEC ($CHCl_3$/*iso*-propanol/triethylamine) (PS-calibration)
d) MALDI-TOF MS

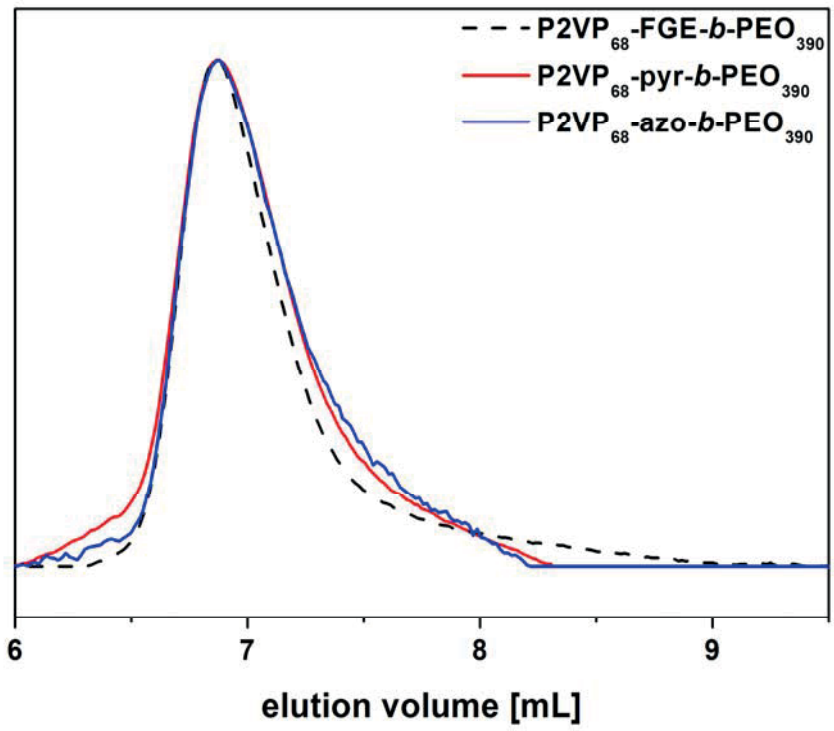

Figure S5: Comparison of SEC traces for the $P2VP_{68}$-FGE-*b*-PEO_{390} (black dashed curve), $P2VP_{68}$-pyr-*b*-PEO_{390} (red curve), and $P2VP_{68}$-azo-*b*-PEO_{390} (blue curve).

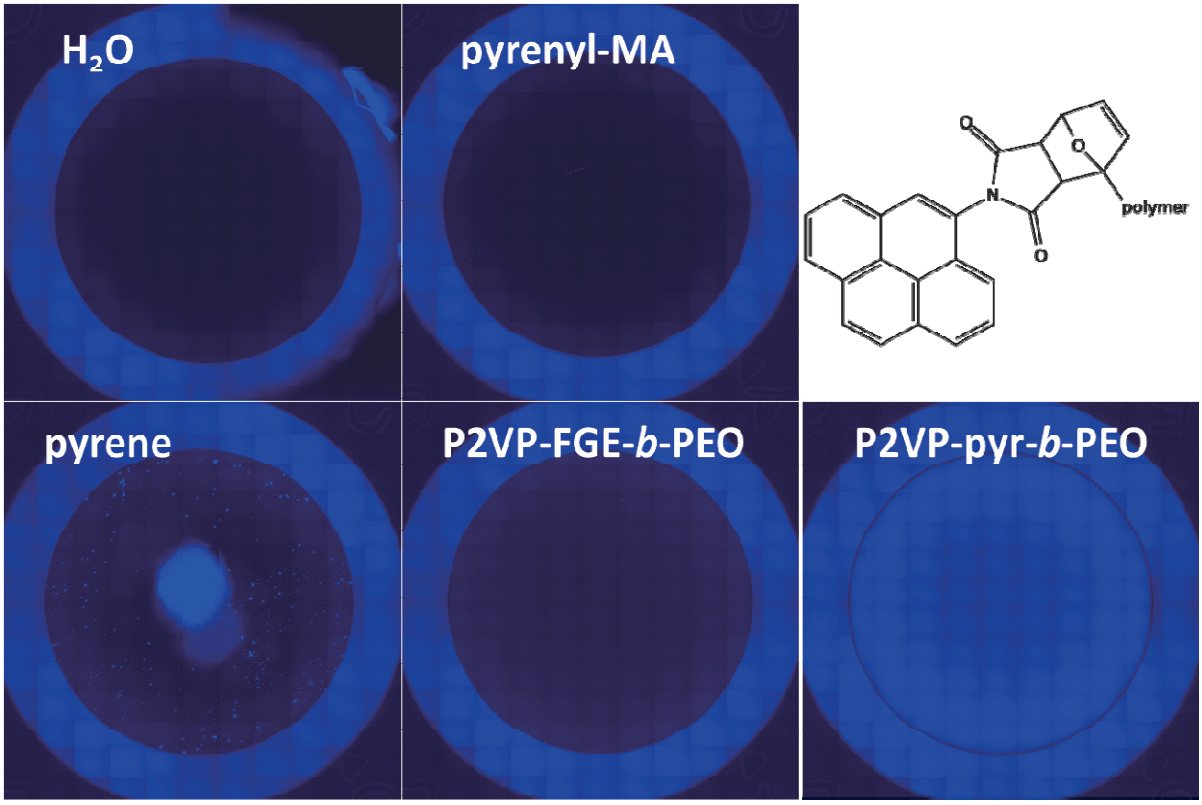

Figure S6: Comparison of fluorescence micrographs for water (A), pristine *N*-(1-pyrenyl)maleimide (B), pyrene (C), $P2VP_{70}$-FGE-*b*-PEO_{380} (5 mg mL^{-1}), and $P2VP_{70}$-pyr-*b*-PEO_{380} (5 mg mL^{-1}) in water (at pH 7) under comparable conditions (same gain, excitation 357 nm; emission filter 460 nm).

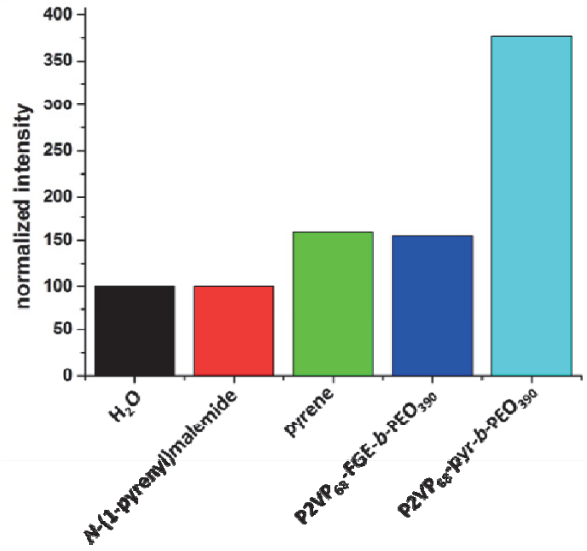

Figure S7: Comparison of the fluorescence measurements normalized in comparison to H_2O (black) for *N*-(1-pyrenyl)-maleimide (red), pyrene (green), $P2VP_{68}$-FGE-*b*-PEO_{390} (blue, 5 mg mL^{-1}) and $P2VP_{68}$-pyr-*b*-PEO_{390} (cyan, 5 mg mL^{-1}) in water (at pH 7) under comparable conditions (same gain, excitation 357 nm; emission filter 460 nm).

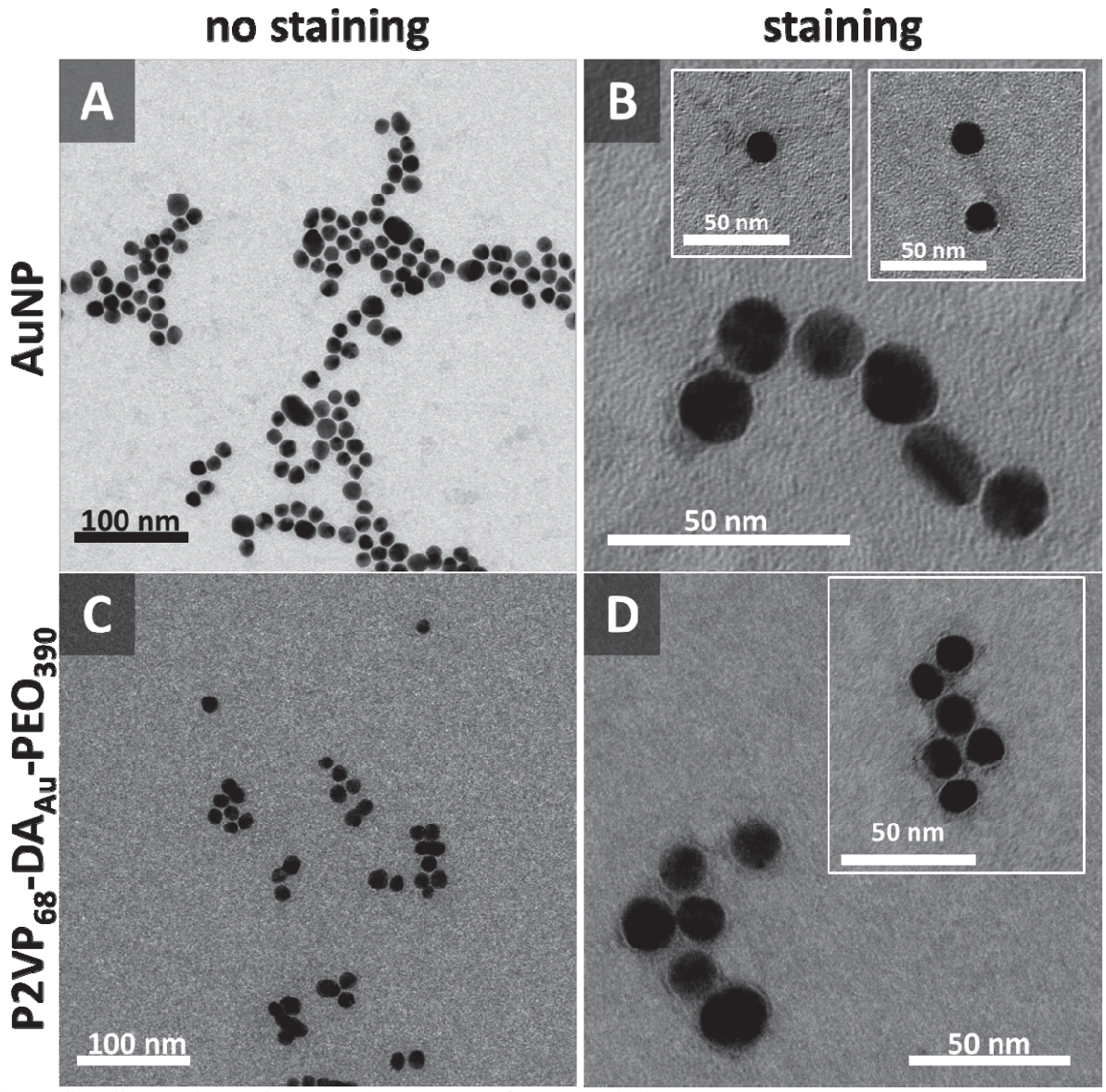

Figure S8: Comparison of TEM micrographs of the maleimide-coated AuNPs (A and B) and $P2VP_{68}$-DA_{Au}-*b*-PEO_{390} (C and D): before (A and C) and after (B and D) staining with uranyl acetate.

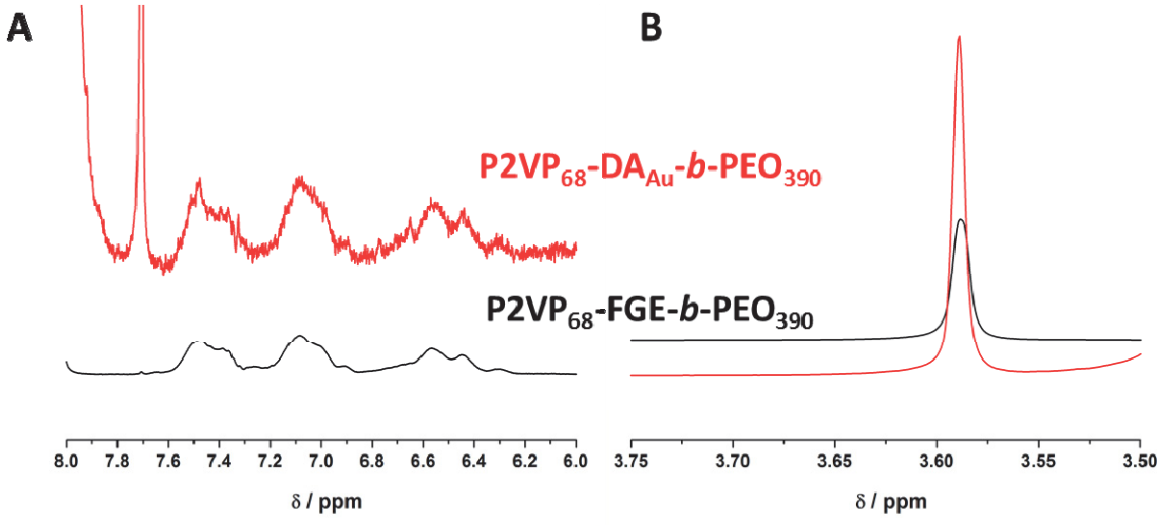

Figure S9: Comparison of NMR spectra for P2VP$_{68}$-FGE-*b*-PEO$_{390}$ (black curve) and P2VP$_{68}$-DA$_{Au}$-*b*-PEO$_{390}$ (black curve) in the characteristic regions for P2VP (A) and PEO (B).

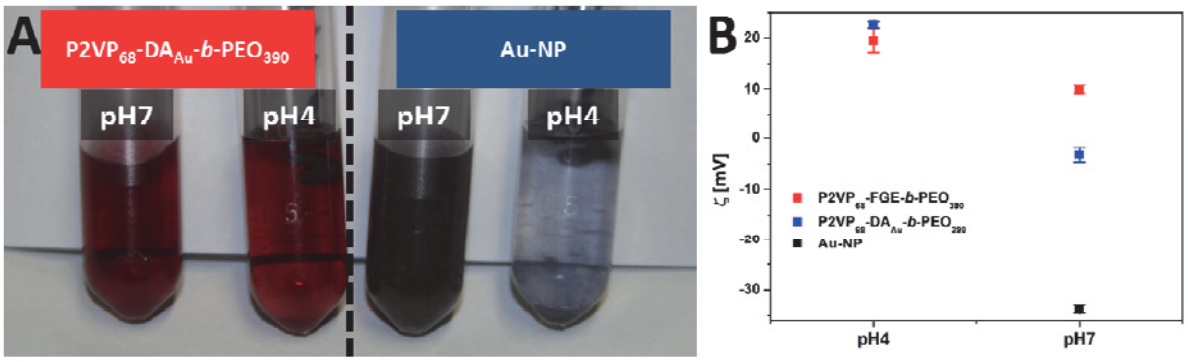

Figure S10: A) Comparison of images for P2VP$_{68}$-DA$_{Au}$-*b*-PEO$_{390}$ (left) and AuNP (right); B) Zeta potential measurements for P2VP$_{68}$-DA$_{Au}$-*b*-PEO$_{390}$ (blue dots; ~0.2 mg mL^{-1} polymer), P2VP$_{68}$-FGE-*b*-PEO$_{390}$ (red dots; 0.5 mg mL^{-1}) and Au-NP (black dot) after transfer into water at different pH 4 and 7.

References

1 H. Normant, B. Angelo; *B. Soc. Chim. Fr.,* 1960, 354.

2 M. J. Barthel, T. Rudolph, S. Crotty, F. H. Schacher, U. S. Schubert; *J. Polym. Sci. Part A: Polym. Chem.*, 2012, 50, 4958-4965.

3 H. Y. Song, M. H. Ngai, Z. Y. Song, P. A. MacAry, J. Hobley, M. J. Lear, *Org. Biomol. Chem.*, 2009, **7**, 3400-3406.

4 F. Kretschmer, U. Mansfeld, S. Hoeppener, M. Hager and U. S. Schubert, *Chem. Commun.*, 2013, **50**, 88-90.

Publication P10

"A Strong Cationic Brønsted Acid, $[H(OEt_2)_2][Al\{OC(CF_3)_3\}_4]$, as an Efficient Initiator for the Cationic Ring-Opening Polymerization of 2-Alkyl-2-Oxazolines"

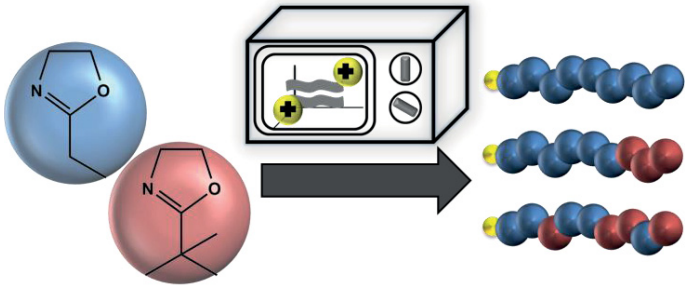

Tobias Rudolph, Kristian Kempe, Sarah Crotty, Renzo M. Paulus, Ulrich S. Schubert, Ingo Krossing, Felix H. Schacher

Polym. Chem., **2013**, *4,* 495-505

Polymer Chemistry

RSC Publishing

PAPER

A strong cationic Brønsted acid, $[H(OEt_2)_2]$-$[Al\{OC(CF_3)_3\}_4]$, as an efficient initiator for the cationic ring-opening polymerization of 2-alkyl-2-oxazolines

Cite this: *Polym. Chem.*, 2013, **4**, 495

Tobias Rudolph,[ab] Kristian Kempe,†[ab] Sarah Crotty,[abc] Renzo M. Paulus,[ab] Ulrich S. Schubert,[abc] Ingo Krossing[d] and Felix H. Schacher*[ab]

Received 3rd August 2012
Accepted 7th September 2012

DOI: 10.1039/c2py20598j

www.rsc.org/polymers

In this contribution, the cationic ring-opening polymerization (CROP) and copolymerization of 2-ethyl-2-oxazoline and 2-*tert*-butyl-2-oxazoline using a strong cationic Brønsted acid, $[H(OEt_2)_2][Al\{OC(CF_3)_3\}_4]$, as an initiator are described. First, various poly(2-ethyl-2-oxazoline) (PEtOx) samples are prepared and the living/controlled character of the reaction is demonstrated. We could show that the microwave-assisted CROP of EtOx using this initiator system proceeds faster if compared to classical initiators such as methyl tosylate. These results were then extended to the CROP of poly(2-*tert*-butyl-2-oxazoline) (P*t*ButOx) and to PEtOx/P*t*ButOx random and block copolymers of different compositions. The resulting materials were characterized using spectroscopic (^{1}H-NMR, FT-IR), chromatographic (SEC), and thermoanalytic techniques (DSC, TGA). Although samples containing more than 13 wt% P*t*ButOx were insoluble in common organic solvents, thermogravimetric (TGA, DSC), spectroscopic (IR), scattering methods (wide-angle X-ray scattering, WAXS), and SEC in hexafluoro-*iso*-propanol (HFIP) hinted at the successful formation of block copolymers. In particular, WAXS revealed increasing crystallinity for samples containing higher weight fractions of P*t*ButOx.

Introduction

Over the last few decades a variety of controlled/living polymerization techniques[1] such as atom transfer radical polymerization (ATRP),[2] reversible addition fragmentation transfer (RAFT) polymerizations,[3,4] nitroxide mediated polymerization (NMP),[5] and ring-opening methodologies, *e.g.* cationic (CROP),[6] have been developed and optimized. Significant progress concerning possible monomers (*i.e.* the tolerance of the respective method towards functional groups being present), the control over molar mass, chain end functionality, or the usage of functional initiators has been made and broadened the applicability of such techniques. Not only homopolymers, but also copolymers of various types (random,[7] statistical,[8] gradient,[9] block-type[10]) or advanced macromolecular structures like star-shaped,[11,12] graft,[13,14] or cyclic structures[15] can be prepared in this way. Especially for block copolymers, the range of possible applications is continuously expanding and spans over different scientific disciplines like biology, medicine, chemistry, materials science, and physics.[16,17]

Poly(2-oxazoline)s represent an interesting polymer class accessible *via* cationic ring-opening polymerization (CROP). They can be regarded as pseudo-peptides and, for poly(2-ethyl-2-oxazoline) (PEtOx), it has been demonstrated that the resulting water-soluble materials are biocompatible and possess similar properties as polyethylene glycol.[18,19] As for oxazolines the easy access in the C-2 position of the ring enables the attachment of a wide variety of substituents and, hence, a library of functional monomers.[20] The physical properties of the resulting polymeric materials, *e.g.* solubility or glass transition temperatures, can thus be tuned in a wide range by simply preparing copolymers of different 2-oxazoline monomers.[18] One further advantage of 2-alkyl-2-oxazolines is that the polymerization can be performed both by conventional- and microwave-assisted heating in a controlled fashion.[21,22]

There are a few prevailing drawbacks concerning the CROP of 2-alkyl-2-oxazolines, for example the rather low reactivities of certain monomers carrying sterically demanding substituents,[23] chain transfer reactions related to impurities within the initiator leading to proton-initiated polymer chains,[24,25] side reactions occurring if molar masses above 25 000 g mol^{-1} are targeted (loss of control),[25] or a slight yellowish color of the final materials (in particular for near-quantitative conversions).[26]

[a]*Laboratory of Organic and Macromolecular Chemistry (IOMC), Friedrich Schiller University Jena, Humboldtstr. 10, 07743 Jena, Germany. E-mail: felix.schacher@uni-jena.de*

[b]*Jena Center for Soft Matter (JCSM), Friedrich Schiller University Jena, Philosophenweg 7, 07743 Jena, Germany*

[c]*Dutch Polymer Institute, P.O. Box 902, 5600 AX Eindhoven, The Netherlands*

[d]*Institute of Inorganic and Analytic Chemistry, University of Freiburg, Albertstr. 21, D-79104 Freiburg i. Br., Germany*

† Current address: Department of Chemical and Biomolecular Engineering, The University of Melbourne, Victoria 3010, Australia.

$[H(OEt_2)_2][Al\{OC(CF_3)_3\}_4]$, a strong cationic Brønsted acid with $[Al\{OC(CF_3)_3\}_4]$ as a non-oxidizing and weakly coordinating anion,[27,28] can be prepared from the lithium salt by reaction with HCl gas and diethyl ether in CH_2Cl_2 solution and yields the corresponding oxonium acid ($[H(OEt_2)_2]^+$) in multi-gram scale and the product (as a solid powder) can be stored for years under inert conditions without degradation, enabling easy handling.[29] Due to the rather weakly bound oxonium acid,[30] $[H(OEt_2)_2][Al\{OC(CF_3)_3\}_4]$ represents a possible initiator system for the proton-initiated CROP of 2-alkyl-2-oxazolines. In the case of super acid esters, the influence of the respective substituent concerning the CROP of tetrahydrofuran has been already investigated intensively.[31,32] Here, higher propagation and initiation rates were found for fluorinated esters in such reactions.[31] This has been attributed to an improved stabilization of the intermediate protonated species and a better accessibility of the latter for the addition of further monomers.

Herein, we describe the investigation of $[H(OEt_2)_2][Al\{OC(CF_3)_3\}_4]$ as an initiator-system for the homo- and copolymerization of 2-alkyl-2-oxazolines. First, various poly(2-ethyl-2-oxazoline)s (PEtOx) are prepared and the living/controlled character of the microwave-assisted CROP is demonstrated. Further, poly(2-*tert*-butyl-2-oxazoline) (P*t*ButOx) as an example for a more demanding oxazoline-type material is prepared and characterized using differential scanning calorimetry (DSC) and wide angle X-ray scattering (WAXS). Finally, the random and block copolymerization of EtOx and *t*ButOx was investigated and the resulting materials were characterized using spectroscopic (^{1}H-NMR, FT-IR), chromatographic (SEC), and thermoanalytic techniques (DSC, TGA).

Experimental section

Chemicals

$[H(OEt_2)_2][Al\{OC(CF_3)_3\}_4]$ was synthesized as described in the literature[29] and stored in a sealed vial under an inert atmosphere in a glove box. 2-Ethyl-2-oxazoline (EtOx) was distilled over barium oxide before polymerization and stored under argon. CH_3CN was purified using a Solvent Purification System (SPS, Innovative Technology, PM-400-3-MD) equipped with 2 activated alumina columns. Trimethylacetonitrile (Sigma Aldrich, 98%), ethanolamine (ABCR), and zinc acetate were used without further purification.

Instruments

^{1}H-Nuclear magnetic resonance (^{1}H-NMR) spectra were recorded on a Bruker AC 300 MHz using the residual solvent resonance as an internal standard.

Size exclusion chromatography (SEC) was performed on two systems: a Shimadzu SCL-10A system (a controller with a LC-10AD pump, a RID-10A refractive index detector, and a PSS SDV column, which was kept at room temperature). The eluent was a mixture of chloroform–triethylamine–*iso*-propanol (94 : 4 : 2) with a flow rate of 1 mL min^{-1}. All copolymers (except for the P*t*ButOx homopolymer) containing P*t*ButOx were soluble in hexafluoro-*iso*-propanol (HFIP) and were measured on a PSS System (equipped with a controller with a SECcurity 1100 pump, a SECcurity 1200 refractive index and an UV (230 nm) detector, and PSS PFG (7 μm, 100 Å and 7 μm, 1000 Å) columns, which were kept at room temperature).

Infra-red spectroscopy: Dry powders of the copolymers were directly placed on the crystal of the ATR-FTIR (Affinity-1 FT-IR, Shimadzu) for measurements in the range of 4000 to 600 cm^{-1}.

Differential scanning calorimetry (DSC) thermograms were recorded on a Netzsch DSC 204 F1 instrument. For the sample annealing the sample was first heated up to 200 °C, cooled and heated in a second run with 20 K min^{-1}, cooled and measured for a third time with 10 K min^{-1} in a temperature range of −50 to 200 °C. The glass transition temperatures were determined from the third heating cycle. Midpoint values have been used for the evaluation.

Thermo-gravimetric analyses (TGA) were performed under nitrogen atmosphere in a Netzsch TG 209 F1 Iris in the range from room temperature to 800 °C with a heating rate of 10 K min^{-1}. The corresponding decomposition temperatures were determined at the decay point of the curves.

Wide angle X-ray scattering (WAXS) measurements on dried powders of P*t*BuOx were performed on a Bruker AXS Nanostar (Bruker, Karlsruhe, Germany), equipped with a microfocus X-ray source (Incoatec IμSCu E025, Incoatec, Geesthacht, Germany), operating at $\lambda = 1.54$ Å. A pinhole setup with 750 μm, 400 μm, and 1000 μm (in the order from source to sample) was used and the sample-to-detector distance was 27 cm. Samples were mounted on a metal rack and fixed using tape. The scattering patterns were corrected for the beam stop and the background (Scotch tape) prior to evaluations.

Microwave-assisted polymerizations

Microwave-assisted polymerizations were carried out utilizing an Initiator Sixty single-mode microwave synthesizer from Biotage, equipped with a noninvasive IR sensor (accuracy: 2%). Microwave vials (conical, 0.5 to 2 mL) were heated at 130 °C overnight, allowed to cool to room temperature under reduced pressure, and subsequently transferred to the glove box. All polymerizations were carried out with temperature control.

Synthesis of 2-*tert*-butyl-2-oxazoline (*t*ButOx)

2-*tert*-Butyl-2-oxazoline was synthesized using a standard procedure described in the literature.[20,33] Trimethylacetonitrile (1 eq.) and catalytic amounts of zinc acetate (0.025 eq.) were heated to 130 °C under reflux. Subsequently, 1.1 eq. of ethanolamine were added under vigorous stirring. After 24 hours the reaction mixture was cooled to ambient temperatures, diluted with chloroform and extracted three times with water and once with brine. The organic layer was dried over magnesium sulfate ($MgSO_4$) and the solvent removed under reduced pressure. The purified *t*ButOx was obtained by distillation over barium oxide with a yield of 40%.

^{1}H-NMR (300 MHz, DMSO-d_6, δ): 4.16 (t, 2H), 3.67 (t, 2H), 1.14 (s, 9H).

Kinetic investigations of the microwave-assisted polymerization of 2-ethyl-2-oxazoline (EtOx) using ($[H(OEt_2)_2][Al\{OC(CF_3)_3\}_4]$) as initiator

A stock solution of EtOx, ($[H(OEt_2)_2][Al\{OC(CF3)_3\}_4]$), and acetonitrile ([M]/[I] = 60) with a monomer concentration of 4 M was prepared under inert conditions. The solution was added to different microwave vials, which were capped and separately heated in the microwave synthesizer at 80 °C or 140 °C for different times, respectively. Afterwards the reaction mixture was cooled to room temperature and 50 μL were removed for ^{1}H NMR and SEC measurements. The pure polymers were obtained after extraction with $NaHCO_3$ solution, brine, and dried under vacuum. After precipitation in cold diethyl ether the polymer was filtered and dried under vacuum.

^{1}H-NMR (300 MHz, $CDCl_3$, δ): 3.6–3.2 (br, –N–CH_2–CH_2–), 2.5–2.2 (br, CO–CH_2–CH_3), 1.2–0.9 (br, CO–CH_2–CH_3).

General procedure for the copolymerization of 2-*tert*-butyl-2-oxazoline (*t*ButOx) and 2-ethyl-2-oxazoline (EtOx) using ($[H(OEt_2)_2][Al\{OC(CF_3)_3\}_4]$) as initiator

Different ratios of *t*ButOx and EtOx with a total number of repeating units of 60 (DP60) were prepared under inert conditions. The monomer–initiator mixture was diluted with CH_3CN to reach a total monomer concentration of 4 M. The polymerization was performed in a microwave synthesizer at 140 °C until an almost full (>90%) conversion of the monomer was observed in the polymerization solution *via* NMR. After precipitation in cold diethyl ether the polymer was filtered and dried under vacuum.

$PEtOx_{50}$-*co*-P*t*$ButOx_6$: ^{1}H-NMR (300 MHz, $CDCl_3$, δ): 3.6–3.2 (br, –N–CH_2–CH_2–), 2.5–2.2 (br, CO–CH_2–CH_3), 1.4–1.2 (s, C–$(CH_3)_3$) 1.2–0.9 (br, CO–CH_2–CH_3).

Exemplarily: $PEtOx_{50}$-*co*-P*t*$ButOx_6$ – SEC ($CHCl_3$/*i*-PrOH/TEA): M_n = 8100 g mol^{-1}; PDI 1.19 (PS-calib.).

General procedure for the block copolymerization of 2-*tert*-butyl-2-oxazoline (*t*ButOx) and 2-ethyl-2-oxazoline (EtOx) using ($[H(OEt_2)_2][Al\{OC(CF_3)_3\}_4]$) as initiator

A mixture of EtOx and the initiator ([M]/[I] = 50) was diluted with CH_3CN to reach a total monomer concentration of 4 M. The polymerization was performed in a microwave synthesizer at 140 °C. After full conversion of EtOx, the vial was transferred to the glove box and *t*ButOx was added under inert conditions, followed by additional time in the microwave synthesizer at 140 °C. The block copolymer was precipitated in cold diethyl ether, filtered, and dried under vacuum.

Block copolymer ($PEtOx_{50}$-*b*-P*t*$ButOx_6$): SEC ($CHCl_3$/*i*-PrOH/TEA): M_n = 10 000 g mol^{-1}; PDI 1.06 (PS-calib.).

Results and discussion

Since its discovery, the cationic ring-opening polymerization (CROP) has been used for a variety of monomers (*e.g.* tetrahydrofuran,[31,32,34] 2-alkyl-2-oxazolines[35–38]). In the case of oxazolines, both conventional- and microwave-assisted heating have been shown to be highly efficient (Scheme 1). However, if microwave heating is employed, one clear advantage is distinctly higher polymerization rates.[39] Depending on the reaction temperature, such polymerizations can be conducted in a controlled manner and reach full conversion within a few minutes while maintaining a controlled/living character shown by, *e.g.*, a high end group fidelity.

Typical initiators for the CROP of 2-alkyl-2-oxazolines are alkyl halides,[40,41] tosylates,[42] and triflates,[43] enabling a controlled polymerization and the introduction of different functionalities to the resulting polymeric materials.[44] The proton-initiated CROP of oxazolines can either be achieved using suitable initiators such as, *e.g.*, *para*-toluenesulfonic acid,[45] or occur as a side-product due to impurities included in different initiators (*e.g.* methyl tosylate[23]). In most cases these are unwanted side-products, in particular when functional groups are to be introduced.

The initiating system presented here, $[H(OEt_2)_2][Al\{OC(CF_3)_3\}_4]$, consists of a strong cationic Brønsted acid $[H(OEt_2)_2]^+$ and $[Al\{OC(CF_3)_3\}_4]^-$ as a weakly coordinating and non-oxidizing anion. This compound can be easily synthesized on a multi-gram scale, in high purity and handled easily as a powder under inert conditions in a glove box. Due to the high acidity of $[H(OEt_2)_2]^+$ and the absence of side-products we considered this system as a fast and promising potential initiator for the CROP of 2-alkyl-2-oxazolines. We therefore first investigated the polymerization of 2-ethyl-2-oxazoline (EtOx) using a standard literature protocol, with a monomer concentration of 4 M (396 mg mL^{-1}) and a monomer-to-initiator ratio of 60 : 1 in acetonitrile (CH_3CN).[21]

Kinetic investigations of the microwave-assisted polymerization of 2-ethyl-2-oxazoline (EtOx)

A stock solution of the initiator ($[H(OEt_2)_2][Al\{OC(CF_3)_3\}_4]$) and the monomer (EtOx) with a monomer-to-initiator ratio of 60 was

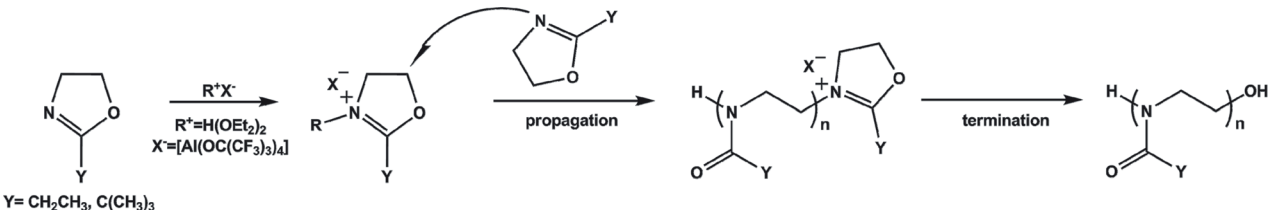

Scheme 1 Mechanism for the proton-initiated cationic ring-opening polymerization (CROP) of 2-alkyl-2-oxazolines using $[H(OEt_2)_2][Al\{OC(CF3)_3\}_4]$ as the initiating system.

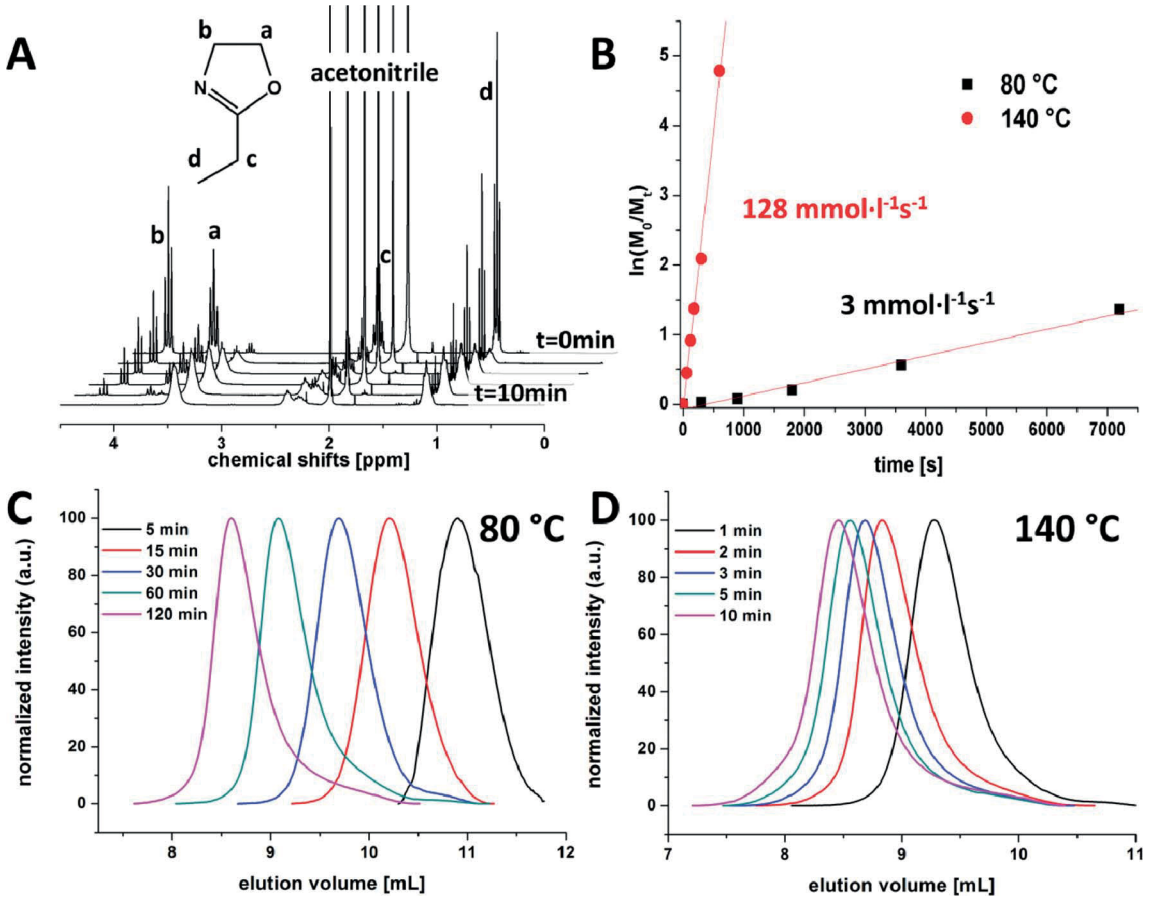

Fig. 1 NMR spectra for the polymerization of EtOx at 140 °C at different reaction times. (A) First order time–conversion plots for the kinetic investigation of the microwave assisted polymerization of EtOx with $[H(OEt_2)_2][Al\{OC(CF_3)_3\}_4]$ as initiator at different temperatures, 80 °C (black squares) and 140 °C (red dots); the polymerization rate has been determined (B); comparison of the time dependent SEC traces for the polymerization of EtOx at 80 °C (C) and 140 °C (D).

prepared and diluted with acetonitrile (CH_3CN) to reach a monomer concentration of 4 M (396 mg mL^{-1}). This stock solution was then added to separate microwave-vials under inert conditions in a glove box at room temperature.

The polymerization rate was determined for two different temperatures, 80 and 140 °C, and the resulting kinetic plots are shown in Fig. 1B. In both cases a linear pseudo first-order kinetic was obtained. In the case of 140 °C, full conversion (~99%) was observed according to ^{1}H-NMR measurements within a few minutes. A polymerization rate of 128 mmol L^{-1} s^{-1} can be calculated (Fig. 1B, red dots), being slightly higher if compared to initiators such as *e.g.* methyl tosylate in CH_3CN.[21,41] At 80 °C, also a linear slope is obtained but with a distinctly lower propagation rate of 3 mmol L^{-1} s^{-1} (Fig. 1B, black squares).

The obtained polymers were also investigated *via* size exclusion chromatography (SEC). A steady increase of the molar mass and polydispersity index (PDI) values below 1.15 for all polymers were obtained, which is in good agreement with other initiator systems (Fig. 1C and D, Table 1). The theoretical molar masses were calculated using the monomer conversion as determined *via* ^{1}H-NMR spectroscopy. The values from the SEC measurements and the PDI values were determined against PS standards and are higher compared to the expected molar masses, which might be explained due to the presence of the $[Al\{OC(CF_3)_3\}_4]^-$ counter ion, possibly influencing the elution behavior on the SEC column. For the polymers obtained after 120 min (80 °C) and 3 min (140 °C), comparable monomer conversions of ~75% were found. In both cases, also comparable molar masses of 9200/9300 g mol^{-1} and PDIs around 1.1 were observed (Table 1).

Unfortunately, an additional characterization *via* MALDI-TOF mass spectrometry was not possible, even though different matrices/doping agents combination or purification steps (solvent extraction, dialysis) and different delayed ion extractions were tested despite the rather low PDI values. We attribute this to the presence of traces of the initiator, preventing an efficient ionization of the materials. Therefore, the molar masses reported here were determined using SEC and the feed [M]/[I]-ratios used in the polymerization reactions (in combination with the observed monomer conversion by ^{1}H-NMR).

In summary, these observations support the controlled character of the CROP of EtOx using $[H(OEt_2)_2][Al\{OC(CF_3)_3\}_4]$ as an initiator in CH_3CN at different temperatures under microwave irradiation.

Table 1 Details for the kinetic investigation of the microwave-assisted polymerization of EtOx *via* $[H(OEt_2)_2][Al\{OC(CF_3)_3\}_4]$ at 80 and 140 °C ([M]/[I] = 60)

Time [min]	Temperature [°C]	Conv.[a] [%]	$M_{n,theo}$[a] [g mol^{-1}]	M_n[b] [g mol^{-1}]	PDI
5	80	2.4	144	1200	1.10
15	80	7.5	450	2600	1.08
30	80	18.5	1110	4100	1.08
60	80	42.7	2560	6300	1.11
120	80	74.2	4450	9300	1.11
1	140	35.9	2150	5700	1.09
2	140	60	3600	8000	1.09
3	140	74.5	4470	9200	1.09
5	140	87.6	5250	10 200	1.10
10	140	99	5940	10 800	1.13
10 days[c]	45		25 000	17 000	1.32

[a] Obtained by ^{1}H-NMR (300 MHz; $CDCl_3$). [b] SEC ($CHCl_3$/*i*-PrOH/TEA) PS-calibration. [c] Bulk polymerization with a [M]/[I] = 250.

For comparison, also conventional heating in an oil bath was used for the CROP of EtOx in the bulk ([M] : [I] = 250, same initiating system) around 45 °C,[9,46] leading to a highly viscous polymerization mixture after 10 days. The resulting polymer exhibited a molar mass of 17 000 g mol^{-1} and a PDI value of 1.32 (Table 1).

Homo- and copolymerization of *t*ButOx

In addition to EtOx, we also investigated the CROP of 2-*tert*-butyl-2-oxazoline (*t*ButOx) using $[H(OEt_2)_2][Al\{OC(CF_3)_3\}_4]$ as an initiator. Litt *et al.* already described the synthesis of the monomer in 1967, and the polymerization of *t*ButOx using dimethyl sulfate as an initiator in the bulk at temperatures between 160 and 200 °C.[38,47] Due to solubility issues, the resulting polymers were only characterized by DSC (no T_g observed, melting point $T_m \sim 320$ °C) and wide-angle X-ray scattering (WAXS). Only a few more examples are known in the literature, where polymerization of *t*ButOx was tried in a more controlled way *via* tosylates or triflates under different conditions.[20,48] The difficulties in obtaining well-defined materials based on P*t*ButOx were attributed to the steric demand of the *tert*-butyl substituent during the CROP process, leading to very slow propagation rates. As $[H(OEt_2)_2][Al\{OC(CF_3)_3\}_4]$ was demonstrated to be a highly efficient initiator for PEtOx, we hypothesized that this might also represent a suitable system for the preparation of P*t*ButOx.[48]

Regarding the material properties of P*t*ButOx, a decrease of the glass transition temperature (T_g) would be supposed within the row of butyl isomers and in the increase of further carbon atoms in the substituent in 2-alkyl-2-oxazolines.[49] In the case of further methyl-groups in the side-chain an increase is observed from PEtOx ($T_g \sim 59$ °C) to poly(2-iso-propyl-2-oxazoline) (P*i*PrOx, $T_g \sim 67$ °C), and a further increase might be anticipated due to the lower flexibility of the side chain for P*t*ButOx.

The monomer, *t*ButOx, was synthesized according to literature procedures in 40% yield. Both the homopolymerization as well as the copolymerization with EtOx using $[H(OEt_2)_2][Al\{OC(CF_3)_3\}_4]$ as an initiator were investigated. For the homopolymerization of *t*ButOx in CH_3CN ([M] : [I] = 60), oligomers were found after 1 h reaction time (11% conversion according to ^{1}H-NMR). After about 5 h at 140 °C, a white precipitate was observed. ^{1}H-NMR measurements of the supernatant solution revealed no residual monomer, hinting at full monomer consumption. The resulting P*t*ButOx was insoluble in common organic solvents, polar and unpolar (to list a few: THF, DMF, DMAc, hexane, toluene, acetone). Nevertheless, the material could be characterized using DSC ($T_g \sim 38$ °C) and TGA (a detailed description will follow later in the manuscript).

To improve the solubility of the resulting materials and to probe the incorporation of *t*ButOx into random and block copolymers, the copolymerization with EtOx was investigated. Different ratios of EtOx/*t*ButOx (44/56, 61/39, and 87/13 wt%) with a constant overall [M] : [I] ratio of 60 were used. Due to the lower reactivity of *t*ButOx, the polymerization time was increased to 10 hours. The respective compositions and the results from the SEC in hexafluoro-iso-propanol (HFIP) are listed in Table 2.

$PEtOx_{50}$-*co*-P*t*BuOx_6 (87/13 vol%) was soluble in chloroform and could therefore be further characterized by SEC and NMR (Fig. 2A, Table 3). For the copolymers, the subscripts denote the degree of polymerization of the corresponding segment. The other two compositions, $PEtOx_{40}$-*co*-P*t*BuOx_{20} and $PEtOx_{30}$-*co*-P*t*BuOx_{30}, were further characterized using DSC and WAXS measurements (see discussion below).

Both random and block copolymers (except P*t*BuOx_{60}) were soluble in hexafluoro-iso-propanol (HFIP) and were characterized *via* HFIP-SEC. The results are listed in Table 2. Rather high PDI values between 1.5 and 1.9 were observed, which we attribute to the high viscosity of the solvent and slight interactions of the materials with the column, visible through a certain tailing towards higher elution volumes for $PEtOx_{40}$-*co*-P*t*BuOx_{20} and $PEtOx_{30}$-*co*-P*t*BuOx_{30} (Fig. 2D). This is also the case for $PEtOx_{60}$ (PDI = 1.85), which was also previously analyzed using a $CHCl_3$-SEC (10 800 g mol^{-1}; PDI 1.13). Nevertheless, monomodal elution traces are obtained in all cases, hinting at a successful copolymerization. The corresponding values for the molar mass of the different copolymers are higher in comparison to $PEtOx_{60}$, which confirms the expected trend in the elution behavior.

Table 2 Theoretical compositions and SEC (HFIP) results for homopolymers, random, and block copolymers of EtOx and *t*ButOx using $[H(OEt_2)_2][Al\{OC(CF_3)_3\}_4]$ as initiator in CH_3CN at 140 °C ([M]/[I] = 60)

Polymers	DP[a] (EtOx)	DP[a] (*t*ButOx)	wt%[a] EtOx	wt%[a] *t*ButOx	$M_{n,theo}$[a] [g mol^{-1}]	M_n[c] [g mol^{-1}]	PDI[c]
$PEtOx_{60}$	60	—	100	—	5940	4500	1.85
$PEtOx_{50}$-*b*-P*t*$ButOx_6$	50	6[b]	87	13	5710	8000	1.68
$PEtOx_{50}$-*co*-P*t*$ButOx_6$	50	6[b]	87	13	5710	7600	1.66
$PEtOx_{40}$-*co*-P*t*$ButOx_{20}$	40	20	61	39	6500	6000	1.46
$PEtOx_{30}$-*co*-P*t*$ButOx_{30}$	30	30	44	56	6780	6700	1.65
P*t*$ButOx_{60}$	—	60	—	100	7620	—	—

[a] Theoretical values through the ratio of [EtOx]/[*t*ButOx]/[I]. [b] Obtained by ^{1}H-NMR (300 MHz; $CDCl_3$). [c] Obtained *via* SEC (hexafluoro-*iso*-propanol).

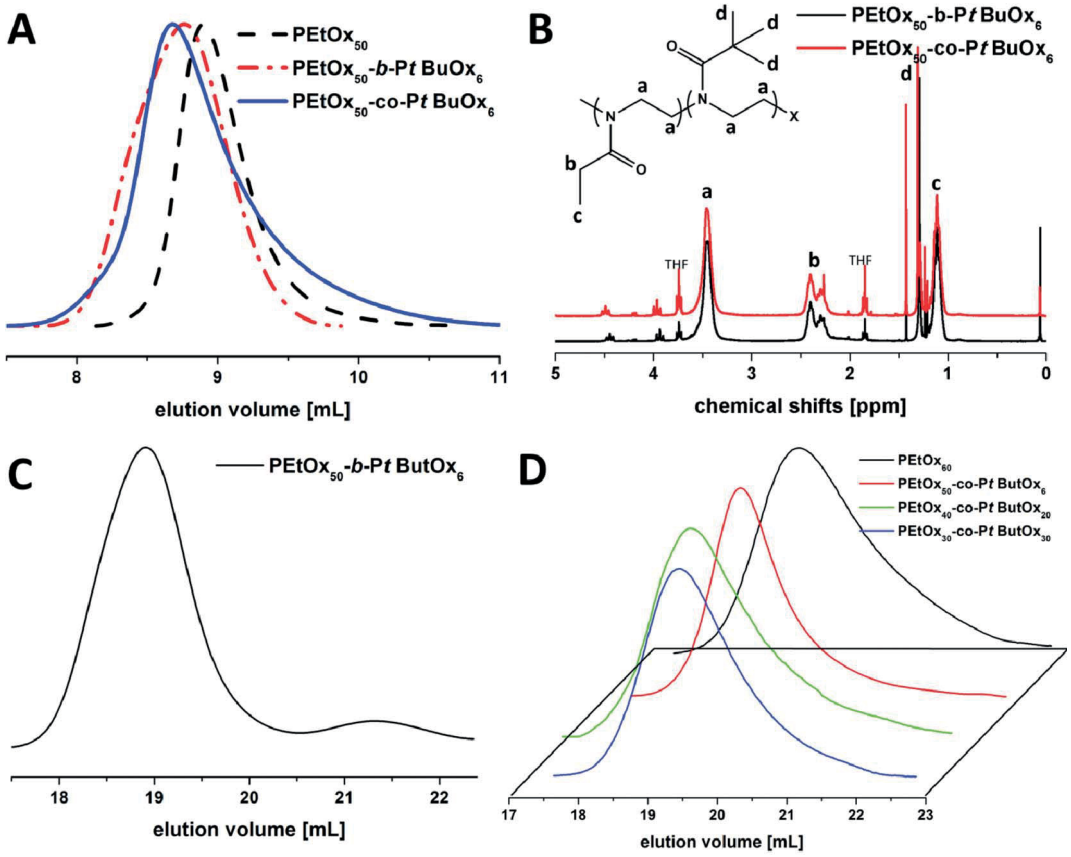

Fig. 2 Comparison of the SEC (chloroform) traces (A) $PEtOx_{50}$ (dashed black line), $PEtOx_{50}$-*b*-P*t*$ButOx_6$ (dashed red line), and $PEtOx_{50}$-*co*-P*t*$ButOx_6$ (blue line); corresponding NMR spectra (B) of the block (black line) and the random (red line) copolymer $PEtOx_{50}$-*co*-P*t*$ButOx_6$; SEC (HFIP) trace for $PEtOx_{50}$-*b*-P*t*$ButOx_6$ (C); SEC (HFIP) traces (D) for $PEtOx_{60}$ (solid black line), $PEtOx_{50}$-*co*-P*t*$ButOx_6$ (solid red line), $PEtOx_{40}$-*co*-P*t*$ButOx_{20}$ (solid green line) and $PEtOx_{30}$-*co*-P*t*$ButOx_{30}$ (solid blue line).

Due to its solubility in, *e.g.* $CHCl_3$, a composition of EtOx/*t*ButOx of 50 : 6 was chosen for further studies, *i.e.* the synthesis of a $PEtOx_{50}$-*b*-P*t*$ButOx_6$ block copolymer. For this purpose, a stock solution of the initiator and EtOx ([M]/[I] = 50) was diluted with CH_3CN and added to three separate microwave vials. One vial was used as a control reaction without additional *t*ButOx, to the second vial the respective amount of *t*ButOx ($PEtOx_{50}$-*co*-P*t*$ButOx_6$) was added, and the third vial was used for the sequential CROP of EtOx and *t*ButOx, respectively, yielding $PEtOx_{50}$-*b*-P*t*$ButOx_6$. Both the first and the third vials for the block copolymer were heated to 140 °C in the microwave-synthesizer for 15 minutes to ensure full conversion of EtOx. Afterwards, the control reaction was investigated using SEC and ^{1}H-NMR to check both the molar mass distribution and the conversion. *t*ButOx was added to the third vial for the block copolymer under inert conditions in the glove box. Both copolymerizations (random and block) were then allowed to react at 140 °C for 6 hours in the microwave. The products were afterwards investigated using SEC and ^{1}H-NMR (Table 3). In addition, HFIP-SEC for $PEtOx_{50}$-*b*-P*t*$ButOx_6$ revealed a small second distribution at higher elution volume, which we attribute to transfer reactions occurring (Fig. 2C).

Table 3 Copolymerization of EtOx and *t*ButOx in CH_3CN at 140 °C ([M]/[I] = 60)

Polymers	$Ratio_{theo}$[a] (EtOx/*t*ButOx)	$Ratio_{NMR}$[b] (EtOx/*t*ButOx)	$M_{n,theo}$[a] [g mol^{-1}]	M_n[c] [g mol^{-1}]	PDI[c]
$PEtOx_{50}$	50/0	50/0	5000	8000	1.06
$PEtOx_{50}$-*b*-P*t*BuOx$_6$	50/10	50/6	5760	10 000	1.07
$PEtOx_{50}$-*co*-P*t*BuOx$_6$	50/10	50/6	5760	8100	1.19

[a] Feed ratio. [b] Obtained by ^{1}H-NMR (300 MHz; $CDCl_3$). [c] SEC ($CHCl_3$/*i*-PrOH/TEA) PS-calibration.

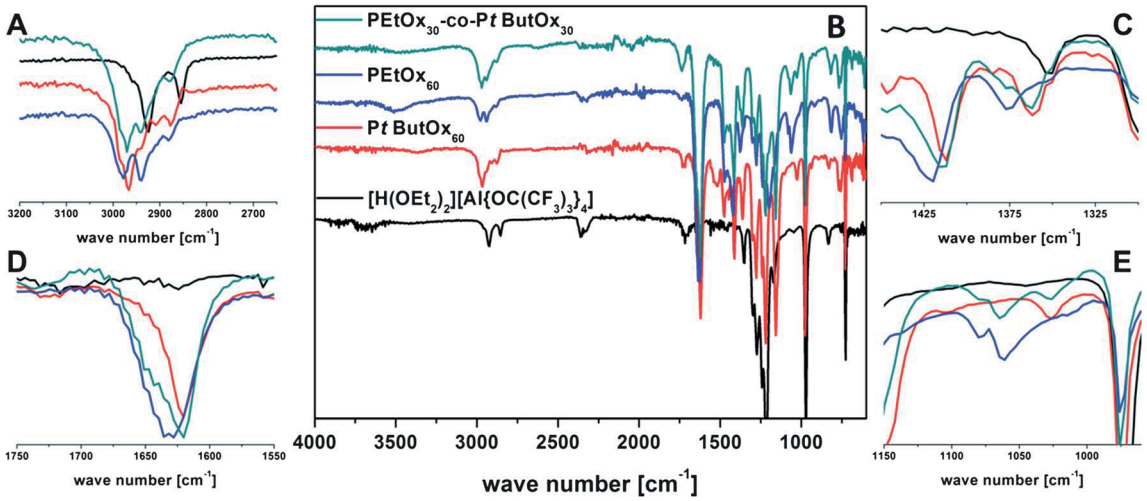

Fig. 3 Fourier transform infrared (FT-IR) spectra for $PEtOx_{60}$ (blue line), P*t*BuOx$_{60}$ (red line), $PEtOx_{30}$-*co*-P*t*BuOx$_{30}$ (cyan line), and $[H(OEt_2)_2][Al\{OC(CF_3)_3\}_4]$ (black line) (B) and the enlargements for the important regions: (A) polymer-backbone, (C) region of α-carbon next to the carbonyl group, (D) carbonyl vibration, and (E) methyl vibration.

The SEC traces for the copolymers show a distinct shift towards lower elution volumes in comparison to the precursor curve (Fig. 2A, dashed black line; Table 3). For $PEtOx_{50}$-*co*-P*t*BuOx$_6$ (solid blue line), a slightly broader size distribution (PDI value of 1.19) is observed, probably related to the lower propagation rate of *t*ButOx if compared to EtOx. On the other hand, for $PEtOx_{50}$-*b*-P*t*BuOx$_6$ (dashed red line) a parallel shift of the elution curve is observed, indicating almost quantitative crossover during the sequential CROP. Nevertheless, a small shoulder can be seen at lower elution volumes and no second distribution at higher elution volumes like in the HFIP-SEC (discussed above) is observed, which might be due to the low solubility of the homopolymer in chloroform.

Assuming full conversion of EtOx during the polymerization, compositions of $PEtOx_{50}$-*co*-P*t*BuOx$_6$ and $PEtOx_{50}$-*b*-P*t*BuOx$_6$ could be calculated according to ^{1}H-NMR measurements (Fig. 2B).

Another method for the (qualitative) analysis of the generated compounds and to prove the incorporation of *t*ButOx is Fourier transform infrared spectroscopy (FT-IR).[50–52] Fig. 3 shows a comparison of the FT-IR spectra for $PEtOx_{60}$ (blue line), P*t*BuOx$_{60}$ (red line), and $PEtOx_{30}$-*co*-P*t*BuOx$_{30}$ (cyan line). In all three cases, the specific peaks for the amine backbone (~3000 cm^{-1}), the carbonyl vibration (~1650 cm^{-1}), the α-carbon next to the carbonyl group (~1360 cm^{-1}), and the methyl groups in the side chain (~1050 cm^{-1}) are shown and insets in Fig. 3 provide a higher resolution of the respective area. In addition, the IR spectrum for $[H(OEt_2)_2][Al\{OC(CF_3)_3\}_4]$ has been recorded (black curve, Fig. 3) as well.

For the polyoxazoline backbone two individual signals (2980 and 2940 cm^{-1}, Fig. 3A) are observed for $PEtOx_{60}$, while for P*t*BuOx$_{60}$ and $PEtOx_{30}$-*co*-P*t*BuOx$_{30}$ only one vibration (2960 cm^{-1}) can be found. We explain this by changes in size and, hence, rotational freedom of the substituent attached to the polymer main chain. The carbonyl vibration around (~1650 cm^{-1}, Fig. 3D) is rather narrowly defined for P*t*BuOx$_{60}$ at 1620 cm^{-1} (1650–1580 cm^{-1}) and distinctly broader (at 1635 cm^{-1}, 1680–1580 cm^{-1}) for $PEtOx_{60}$. For $PEtOx_{30}$-*co*-P*t*BuOx$_{30}$ (1680–1580 cm^{-1}) a peak maximum again at 1620 cm^{-1} is observed. In the case of the methyl groups in the side chain, the peak maxima for $PEtOx_{60}$ (1377 cm^{-1}) and P*t*BuOx (1360 cm^{-1}) are also observed for the copolymer at the consistent positions (Fig. 3C). The absorption bands corresponding to the α-C in the side-chain for $PEtOx_{60}$ and P*t*BuOx$_{60}$ are observed around 1050 cm^{-1} (Fig. 3E). For the homopolymers single peak maxima at 1050 ($PEtOx_{60}$) and 1060 cm^{-1} (P*t*BuOx$_{60}$) are observed, while for the copolymer two different peak maxima at the associated positions were detected.

In summary, the FT-IR spectra hint at the incorporation of *t*ButOx and the successful formation of $PEtOx_m$-*co*-P*t*BuOx$_n$ copolymers of different compositions.

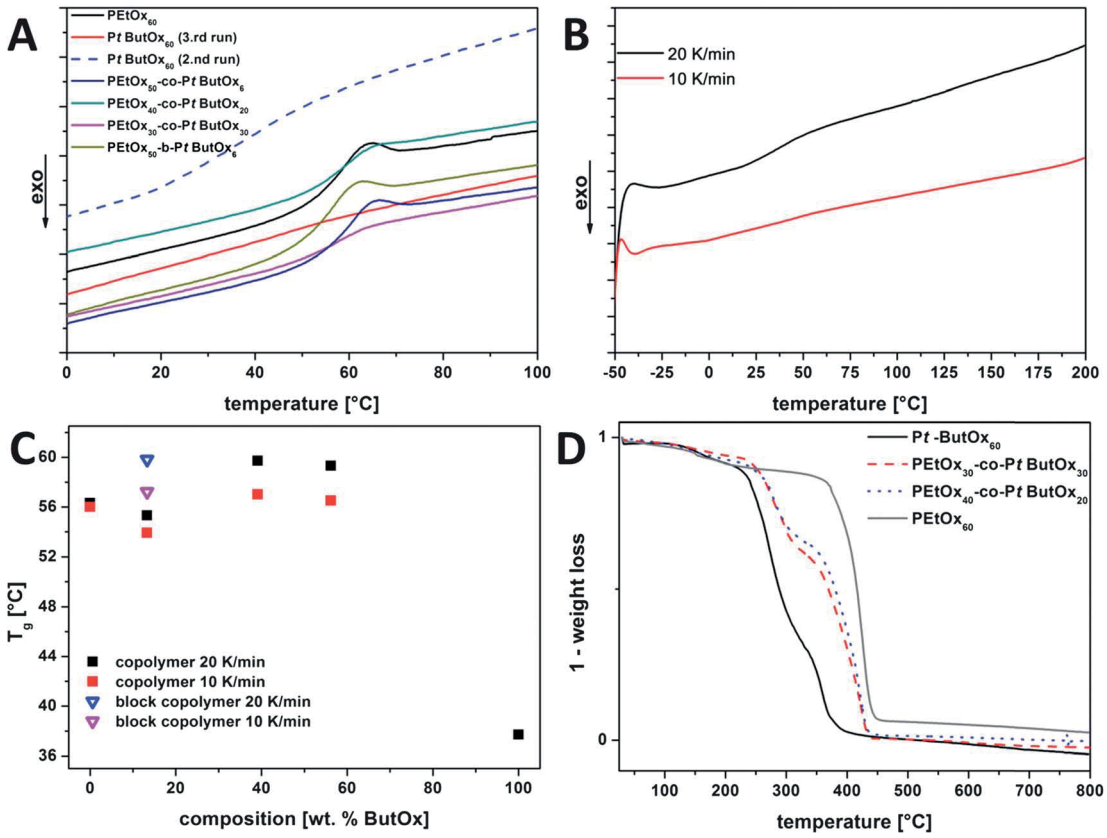

Fig. 4 DSC measurements for $PEtOx_{60}$ (black), $PtButOx_{60}$ (third run, solid red line; second run, dashed blue line), $PEtOx_{50}$-*co*-$PtButOx_6$ (blue line), $PEtOx_{40}$-*co*-$PtButOx_{20}$ (turquoise line), $PEtOx_{30}$-*co*-$PtButOx_{30}$ (pink line), $PEtOx_{50}$-*b*-$PtButOx_6$ (brown line) (A); two individual DSC runs for $PtButOx_{60}$ at different heating rates: 20 K min^{-1} (black line) and 10 K min^{-1} (red line) (B); dependence of the T_g values with regard to the composition of the block copolymers (C); and TGA measurements for the $PEtOx_{60}$ (grey line), $PtButOx_{60}$ (black line), $PEtOx_{40}$-*co*-$PtButOx_{20}$ (dotted blue line), and $PEtOx_{30}$-*co*-$PtButOx_{30}$ (dashed red line).

Table 4 Comparison of the temperature dependency of the different homo- and copolymers analyzed *via* DSC and TGA

Polymers	wt% P*t*ButOx[a]	$M_{n,theo}$[a] [g mol^{-1}]	T_g[b] [°C]	Theo. weight loss[a] [wt%]	Weight loss[c] [wt%]
$PEtOx_{60}$	0	5960	56.0		
$PtButOx_{60}$	100	7620	37.7[e]	69	71
$PEtOx_{50}$-*co*-$PtButOx_6$[d]	13.3	5710	53.9	9.2	15
$PEtOx_{40}$-*co*-$PtButOx_{20}$	39.1	6500	57.0	26.9	30
$PEtOx_{30}$-*co*-$PtButOx_{30}$	56.2	6780	56.5	38.8	38
$PEtOx_{50}$-*b*-$PtButOx_6$[d]	13.3	5710	57.2	9.2	14

[a] Feed ratio. [b] Determined *via* the mid-value obtained by DSC from the third run. [c] Determined *via* TGA. [d] Consumption determined *via* ^{1}H-NMR. [e] Determined from the second DSC run.

Thermal analysis of homo- and copolymers containing P*t*ButOx

Owing to the low solubility of the obtained copolymers with a P*t*ButOx content of more than six repeating units (*i.e.*, $PEtOx_{40}$-*co*-$PtButOx_{20}$ and $PEtOx_{30}$-*co*-$PtButOx_{30}$), additional characterization using differential scanning calorimetry (DSC) and thermogravimetric analysis (TGA) was performed. To exclude any influence of the counter ion from the initiator on the measurements, PEtOx with a similar DP and synthesized using a different initiator was investigated as well.[21] With increasing length of the alkyl chain in the side chain of poly-2-alkyl-2-oxazolines, the glass transition temperature (T_g) decreases (*e.g.*, from methyl- to pentyl-oxazoline (DP = 60) the values decrease from 72 to 21 °C).[49] The corresponding polymers obtained from 2-*n*-butyl- and 2-*i*-butyl-2-oxazoline exhibit T_g-values of 23 and 53 °C, respectively.[49] In our case, for $PtButOx_{60}$, a T_g of 38 °C was determined (Fig. 4A, blue dashed curve, 2nd heating run), whereas no such transition was observed in the third heating run (red curve). We attribute this to partial cleavage of the side-chain (release of isobutylene) at elevated temperatures during the measurement, as already the signal observed in the second heating run is rather weak. All measured T_g values for the different homo- and copolymers are summarized in Table 4 – as

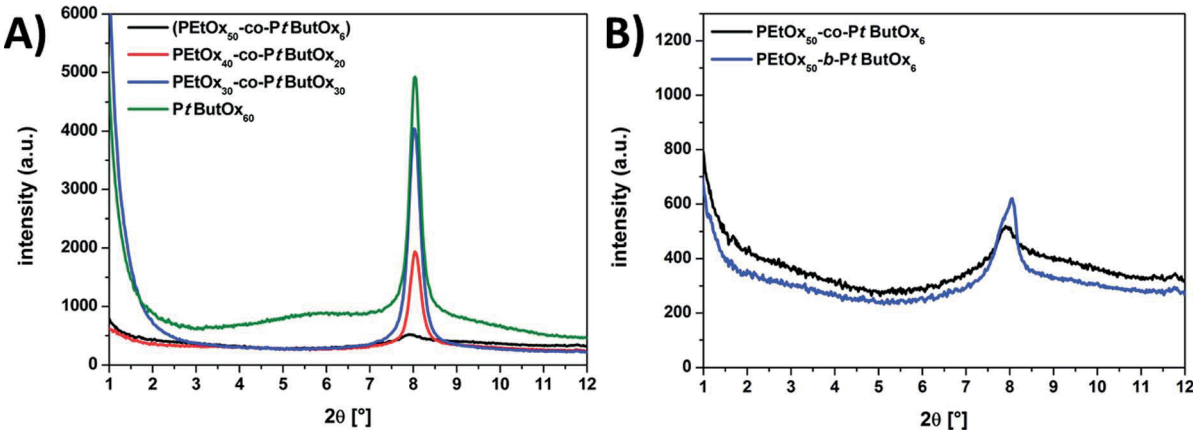

Fig. 5 WAXS diffractograms for PEtOx$_{50}$-*co*-P*t*-ButOx$_6$ (black line), PEtOx$_{40}$-*co*-P*t*ButOx$_{20}$ (red line), PEtOx$_{30}$-*co*-P*t*ButOx$_{30}$ (blue line), and P*t*ButOx$_{60}$ (green line, A); comparison of the WAXS data for PEtOx$_{50}$-*co*-P*t*ButOx$_6$ (black line) and PEtOx$_{50}$-*b*-P*t*ButOx$_6$ (blue line, B).

can be seen, the expected T_g of PEtOx with approximately 56 to 57 °C remains unchanged in all cases (Fig. 4A and C, Table 4). The T_g of P*t*ButOx, however, is not visible for both homo- and block copolymers, even for higher weight fractions, *e.g.* PEtOx$_{30}$-*co*-P*t*ButOx$_{30}$.

Thermogravimetric analysis (TGA) of P*t*ButOx$_{60}$ revealed two decomposition temperatures (T_{decomp}) around 240 and 340 °C (Fig. 4D). Presumably, at 240 °C the cleavage of the side chain results in the formation of isobutylene and carbon monoxide (loss of 85 g mol^{-1}; 69 wt% of the repeating unit), like has been already observed for *tert*-butyl aziridine polymers[53–55] or *tert*-butyl methacrylate polymers in the literature.[56,57] This might well represent a very promising approach for the synthesis of linear poly(ethylene imine), if compared to the controlled hydrolysis in a multi-step reaction.[42] Very recently, Schlaad *et al.* investigated 2-*iso*-propyl-2-oxazoline polymers regarding the decomposition mechanism of the polymer chains at elevated temperatures (~420 °C).[58] The authors also reported the occurrence of a cleavage of the side chain, followed by the decomposition of the main chain into mixtures of protonated monomers and oligomers. In our case, this can be assumed as the second T_{decomp}, leading to the degradation of the backbone.

For the different copolymers TGA traces with characteristics in between both homopolymers (PEtOx and P*t*ButOx) were observed, showing a similar two-step decomposition of the materials. Depending on the composition, the decay can be used for a rough estimation of the P*t*ButOx content (Table 4). We attribute the weight loss observed up to 200 °C to the evaporation of residual solvent and the degradation of the initiator, $[H(OEt_2)_2][Al\{OC(CF_3)_3\}_4]$ (Fig. 4D).[29]

The weight loss observed in the TGA measurements is in good agreement with the theoretical calculated values according to the experimental calculated compositions (Table 4).

Wide-angle X-ray scattering (WAXS) of P*t*ButOx$_{60}$ and the corresponding block copolymers

We further subjected P*t*ButOx$_{60}$ and the different copolymers (PEtOx$_{30}$-*co*-P*t*ButOx$_{30}$, PEtOx$_{40}$-*co*-P*t*ButOx$_{20}$, and PEtOx$_{50}$-*co*-P*t*ButOx$_6$) to wide-angle X-ray scattering (WAXS, Fig. 5A). In all cases, a distinct reflection at $2\theta = 8°$ is observed, corresponding to a *d*-spacing of 11.01 Å, which is in good agreement with the value reported by Litt *et al.* (11.2 Å).[37] For identical measurement times of 2 h, the displayed peak intensity decreases with decreasing amount of incorporated *t*ButOx. In all cases displaying a sufficient signal-to-noise ratio (P*t*ButOx$_{60}$, PEtOx$_{30}$-*co*-P*t*ButOx$_{30}$, and PEtOx$_{40}$-*co*-P*t*ButOx$_{20}$), a degree of crystallinity of approximately 65 ± 2% could be deduced from the WAXS data. We further compared the diffractograms of PEtOx$_{50}$-*co*-P*t*ButOx$_6$ and PEtOx$_{50}$-*b*-P*t*ButOx$_6$ (Fig. 5B). In this case, the signal intensity is higher for the block copolymer, hinting at an improved crystallization of the respective P*t*ButOx segments, whereas the reflection obtained for PEtOx$_{50}$-*co*-P*t*ButOx$_6$ is rather weak, in particular if compared to the intensities depicted in Fig. 5A. This can be explained by the low weight fraction of P*t*ButOx of 13 wt%. For the block copolymer with the same weight fraction of P*t*ButOx, PEtOx$_{50}$-*b*-P*t*ButOx$_6$, the improved crystallization behavior might be a hint of the occurrence of microphase separation. We, therefore, also dissolved PEtOx$_{50}$-*b*-P*t*ButOx$_6$ in water, which is a selective solvent for the PEtOx segment. A slightly turbid solution was obtained, showing micelles with an apparent R_h of 20 nm (data not shown here). These measurements further support the successful formation of random and block copolymers of PEtOx and P*t*ButOx.

Conclusion

We have shown that $[H(OEt_2)_2][Al\{OC(CF_3)_3\}_4]$, a strong cationic Brønsted acid, represents an efficient initiator for the cationic ring-opening polymerization of 2-alkyl-2-oxazolines. A rather high propagation rate (128 mmol L^{-1} s^{-1}) was found for 2-ethyl-2-oxazoline under microwave irradiation at 140 °C in CH_3CN, exceeding reported values for, *e.g.*, methyl tosylate.[21] This was then extended to a more demanding member of the oxazoline class, 2-*tert*-butyl-2-oxazoline, and first examples of random and block copolymers of EtOx and *t*ButOx were synthesized and characterized using different techniques. Owing to the rather low solubility of P*t*ButOx containing materials in common

organic solvents, SEC in hexafluoro-*iso*-propanol (HFIP) was employed and the increasing content of P*t*ButOx in different copolymers was qualitatively proven by FT-IR, TGA, and WAXS data. The fact that P*t*ButOx seems to degrade in a two-step procedure during heating at elevated temperatures and that the first step might represent a cleavage of the side chain will be investigated in more detail in the near future. This might enable a facile protocol for the synthesis of linear poly(ethylene imine) segments in homo- and block copolymers.

Acknowledgements

F.H.S., T.R. and U.S.S. are grateful to the Thuringian Ministry for Education, Science, and Culture (TMBWK; grants #B514-09051, NanoConSens, #B515-11028, SWAXS-JCSM, and #B515-10065, ChaPoNano) for financial support. The authors further thank Polymer Standard Service (PSS, Mainz) for help with the HFIP-SEC measurements. I.K. thanks Petra Klose for preparing samples of $[H(OEt_2)_2]^+[Al\{OC(CF_3)_3\}_4]^-$ and acknowledges the ERC-UniChem project for support. In addition, F.H.S. is indebted to the ChemikerSpassGesellschaft (CSG e.V.).

References

1 C. Barner-Kowollik, J.-F. Lutz and S. Perrier, *Polym. Chem.*, 2012, **3**, 1677–1679.
2 W. A. Braunecker and K. Matyjaszewski, *Prog. Polym. Sci.*, 2007, **32**, 93–146.
3 L. Barner, T. P. Davis, M. H. Stenzel and C. Barner-Kowollik, *Macromol. Rapid Commun.*, 2007, **28**, 539–559.
4 G. Moad, E. Rizzardo and S. H. Thang, *Aust. J. Chem.*, 2005, **58**, 379–410.
5 C. J. Hawker, A. W. Bosman and E. Harth, *Chem. Rev.*, 2001, **101**, 3661–3688.
6 A. Makino and S. Kobayashi, *J. Polym. Sci., Part A: Polym. Chem.*, 2010, **48**, 1251–1270.
7 M. W. M. Fijten, J. M. Kranenburg, H. M. L. Thijs, R. M. Paulus, B. M. van Lankvelt, J. de Hullu, M. Springintveld, D. J. G. Thielen, C. A. Tweedie, R. Hoogenboom, K. J. Van Vliet and U. S. Schubert, *Macromolecules*, 2007, **40**, 5879–5886.
8 K. Matyjaszewski and K. Davis, in *Advances in Polymer Science*, Springer, Berlin/Heidelberg, 2002, vol. 159, pp. 1–13.
9 J.-S. Park and K. Kataoka, *Macromolecules*, 2007, **40**, 3599–3609.
10 F. Schacher, J. Yuan, H. G. Schoberth and A. H. E. Müller, *Polymer*, 2010, **51**, 2021–2032.
11 N. Hadjichristidis, M. Pitsikalis, S. Pispas and H. Iatrou, *Chem. Rev.*, 2001, **101**, 3747–3792.
12 A. Schmalz, H. Schmalz and A. H. E. Müller, *Soft Matter*, 2012, **8**, 9436–9445.
13 K. Matyjaszewski and J. H. Xia, *Chem. Rev.*, 2001, **101**, 2921–2990.
14 J. Yuan, A. H. E. Müller, K. Matyjaszewski and S. S. Sheiko, in *Polymer Science: A Comprehensive Reference*, ed. K. Matyjaszewski and M. Martin, Elsevier, Amsterdam, 2012, pp. 199–264.
15 A. S. Goldmann, D. Quémener, P.-E. Millard, T. P. Davis, M. H. Stenzel, C. Barner-Kowollik and A. H. E. Müller, *Polymer*, 2008, **49**, 2274–2281.
16 F. H. Schacher, P. A. Rupar and I. Manners, *Angew. Chem., Int. Ed.*, 2012, **51**, 7898–7921.
17 F. H. Schacher, P. A. Rupar and I. Manners, *Angew. Chem.*, 2012, **124**, 8020–8044.
18 H. Schlaad, C. Diehl, A. Gress, M. Meyer, A. L. Demirel, Y. Nur and A. Bertin, *Macromol. Rapid Commun.*, 2010, **31**, 511–525.
19 K. Knop, R. Hoogenboom, D. Fischer and U. S. Schubert, *Angew. Chem., Int. Ed.*, 2010, **49**, 6288–6308.
20 K. Kempe, M. Lobert, R. Hoogenboom and U. S. Schubert, *J. Comb. Chem.*, 2009, **11**, 274–280.
21 R. Hoogenboom, M. W. M. Fijten, H. M. L. Thijs, B. M. van Lankvelt and U. S. Schubert, *Des. Monomers Polym.*, 2005, **8**, 659–671.
22 F. Wiesbrock, R. Hoogenboom, M. Leenen, S. F. G. M. van Nispen, M. van der Loop, C. H. Abeln, A. M. J. van den Berg and U. S. Schubert, *Macromolecules*, 2005, **38**, 7957–7966.
23 K. Kempe, M. Lobert, R. Hoogenboom and U. S. Schubert, *J. Polym. Sci., Part A: Polym. Chem.*, 2009, **47**, 3829–3838.
24 P. Appukkuttan, W. Dehaen, V. V. Fokin and E. Van der Eycken, *Org. Lett.*, 2004, **6**, 4223–4225.
25 J. P. Collman, N. K. Devaraj and C. E. D. Chidsey, *Langmuir*, 2004, **20**, 1051–1053.
26 L. T. T. Trinh, H. M. L. Lambermont-Thijs, U. S. Schubert, R. Hoogenboom and A.-L. Kjøniksen, *Macromolecules*, 2012, **45**, 4337–4345.
27 I. Krossing and I. Raabe, *Angew. Chem., Int. Ed.*, 2004, **43**, 2066–2090.
28 I. Krossing, *Chem.–Eur. J.*, 2001, **7**, 490–502.
29 I. Krossing and A. Reisinger, *Eur. J. Inorg. Chem.*, 2005, **2005**, 1979–1989.
30 R. Luxenhofer and R. Jordan, *Macromolecules*, 2006, **39**, 3509–3516.
31 S. Kobayashi, H. Danda and T. Saegusa, *Bull. Chem. Soc. Jpn.*, 1973, **46**, 3214–3220.
32 K. Matyjaszewski, P. Kubisa and S. Penczek, *J. Polym. Sci., Polym. Chem. Ed.*, 1974, **12**, 1333–1336.
33 H. Witte and W. Seeliger, *Justus Liebigs Ann. Chem.*, 1974, 996–1009.
34 S. Penczek, M. Cypryk, A. Duda, P. Kubisa and S. Słomkowski, *Prog. Polym. Sci.*, 2007, **32**, 247–282.
35 T. Kagiya, S. Narisawa, T. Maeda and K. Fukui, *J. Polym. Sci., Part B: Polym. Lett.*, 1966, **4**, 441–445.
36 W. Seeliger and W. Thier, *Angew. Chem., Int. Ed.*, 1966, **5**, 612–617.
37 D. A. Tomalia and D. P. Sheetz, *J. Polym. Sci., Part A: Polym. Chem.*, 1966, **4**, 2253–2265.
38 T. G. Bassiri, A. Levy and M. Litt, *J. Polym. Sci., Part B: Polym. Lett.*, 1967, **5**, 871–879.
39 K. Kempe, C. R. Becer and U. S. Schubert, *Macromolecules*, 2011, **44**, 5825–5842.

40 S. Kobayashi, H. Uyama, Y. Narita and J. Ishiyama, *Macromolecules*, 1992, **25**, 3232–3236.
41 R. Hoogenboom, M. W. M. Fijten and U. S. Schubert, *J. Polym. Sci., Part A: Polym. Chem.*, 2004, **42**, 1830–1840.
42 M. W. M. Fijten, C. Haensch, B. M. van Lankvelt, R. Hoogenboom and U. S. Schubert, *Macromol. Chem. Phys.*, 2008, **209**, 1887–1895.
43 R. Luxenhofer, M. Bezen and R. Jordan, *Macromol. Rapid Commun.*, 2008, **29**, 1509–1513.
44 K. Aoi and M. Okada, *Prog. Polym. Sci.*, 1996, **21**, 151–208.
45 L. Tauhardt, K. Kempe, K. Knop, E. Altuntaş, M. Jäger, S. Schubert, D. Fischer and U. S. Schubert, *Macromol. Chem. Phys.*, 2011, **212**, 1918–1924.
46 J.-S. Park and K. Kataoka, *Macromolecules*, 2006, **39**, 6622–6630.
47 M. Litt, F. Rahl and L. G. Roldan, *J. Polym. Sci., Part A-2*, 1969, **7**, 463–473.
48 S. Huber and R. Jordan, *Colloid Polym.Sci.*, 2008, **286**, 395–402.
49 E. F. J. Rettler, J. M. Kranenburg, H. M. L. Lambermont-Thijs, R. Hoogenboom and U. S. Schubert, *Macromol. Chem. Phys.*, 2010, **211**, 2443–2448.
50 Y. Katsumoto, A. Tsuchiizu, X. Qiu and F. M. Winnik, *Macromolecules*, 2012, **45**, 3531–3541.
51 R. Jordan, K. Martin, H. J. Räder and K. K. Unger, *Macromolecules*, 2001, **34**, 8858–8865.
52 N. A. Hutter, A. Reitinger, N. Zhang, M. Steenackers, O. A. Williams, J. A. Garrido and R. Jordan, *Phys. Chem. Chem. Phys.*, 2010, **12**, 4360–4366.
53 S. Zulfiqar, M. Zafar-ur-Zaman, A. Munir and I. C. McNeill, *Polym. Degrad. Stab.*, 1995, **50**, 33–37.
54 S. Zulfiqar, M. Zafar-uz-Zaman, A. Munir and I. C. McNeill, *Polym. Degrad. Stab.*, 1997, **55**, 89–94.
55 S. Zulfiqar, M. Zafar-uz-Zaman, A. Munir and I. C. McNeill, *Polym. Degrad. Stab.*, 1995, **47**, 59–65.
56 J. H. Lai, *Macromolecules*, 1984, **17**, 1010–1012.
57 H. Ito and M. Ueda, *Macromolecules*, 1988, **21**, 1475–1482.
58 N. Atılkan, Y. Nur, J. Hacaloglu and H. Schlaad, *Macromol. Chem. Phys.*, 2012, **213**, 945–951.

Publication P11

“Poly(thiolactone) Homo- and Copolymers from Maleimide Thiolactone: Synthesis and Functionalization”

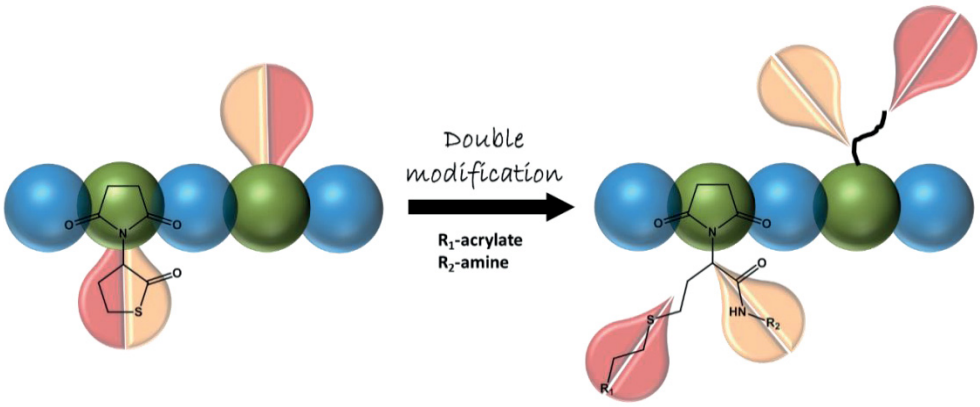

Tobias Rudolph, Pieter Espeel, Filip E. Du Prez, Felix H. Schacher

Polym. Chem., in press (DOI: 10.1039/C5PY00329F)

Polymer Chemistry

PAPER

Poly(thiolactone) homo- and copolymers from maleimide thiolactone: synthesis and functionalization†

Cite this: DOI: 10.1039/c5py00329f

Tobias Rudolph,[a,b] Pieter Espeel,[c] Filip E. Du Prez*[c] and Felix H. Schacher*[a,b]

Received 6th March 2015,
Accepted 29th April 2015

DOI: 10.1039/c5py00329f

www.rsc.org/polymers

We describe the synthesis of a thiolactone-functionalized maleimide (MITla), and its (co)polymerization into poly(thiolactone) homo- and copolymers *via* controlled or free radical polymerization (CRP or FRP) techniques. Homopolymers were synthesized using FRP whereas MITla was copolymerized with styrene and *N*-iso-propylacrylamide (NIPAAm) *via* RAFT. In that way, we were able to combine the properties of a maleimide with the possibility to use the thiolactone side chain functionality in subsequent double modification reactions. Thiolactones are susceptible to nucleophilic ring-opening in the presence of primary amines, releasing a thiol moiety that can be used for conjugate addition (nucleophilic thiol–ene) reactions afterwards. We synthesized and characterized copolymers of different compositions, followed by site-specific double modification reactions with a combination of *n*-butylamine and methyl acrylate.

Introduction

The controlled copolymerization of different monomers is of increasing interest in polymer and material science, as the physical properties of the resulting copolymers can be easily varied by changing the composition or distribution of the constituting building blocks. In this respect various polymerization techniques, including ionic and radical methodologies, can be used for the preparation of well-defined polymers and copolymers.[1,2] The distribution of the monomers along a copolymer chain can be random, gradient, alternating, or block-like – often depending on the method used or on the reactivity of the monomers. A special case are block copolymers, where the immiscibility of unlike polymeric segments often induces phase separation in the bulk or in solution.[3,4] A prominent example for strictly alternating copolymers is a combination of donor and acceptor monomers, *e.g.* a combination of styrene and maleimides.[5] The incorporation of maleic anhydride or functionalized maleimides was used for the facile synthesis of functionalized copolymers and for the precise introduction of maleimides at certain positions along the copolymer chain.[5–16] *Via* this approach, mostly styrene-containing copolymers with an additional functionality present in the side-chain, *e.g.* alkynes, were synthesized.[8,17] Such materials can be used in subsequent post polymerization modification reactions, like (for the case of alkynes) copper-catalyzed alkyne azide cycloaddition (CuAAC) click reactions.[8] Post polymerization modifications (PPM) are used for the introduction of further functionalities, the macromolecular conjugation of polymer chains, or selective crosslinking.[18,19] Besides CuAAC, also thiol–ene and Diels–Alder reactions between complementary motifs have been reported.[18,20–24]

Thiolactones are reactive functional handles of increasing interest in the field of synthetic polymer science.[25] Indeed, thiolactone chemistry is a valuable synthetic tool, in addition to established thiol-X conjugation reactions and has been used for polymer synthesis,[26–30] post-polymerization modification,[31–35] hydrogel formation,[36] solid-supported, sequence-controlled chain elongation,[37] and the decoration of metal surfaces.[38] It is generally accepted that amines attack the thiolactone ring, forming an amide between with the carbonyl of the thiolactone, while the released thiol moiety subsequently can react with acrylates, present in the same reaction mixture (one-pot, nucleophilic amine-thiol–ene conjugation).[27,32] By this approach, a site specific double modification and the introduction of two new substituents in a one-pot reaction on a polymeric chain can be realized.

Therefore, the aim of this study was the combination of a maleimide as straightforward approach for the controlled incorporation into alternating copolymers with a thiolactone as versatile platform for post-polymerization modifications of

[a]*Laboratory of Organic and Macromolecular Chemistry, Friedrich Schiller University Jena, Humboldtstr. 10, 07743 Jena, Germany. E-mail: felix.schacher@uni-jena.de*
[b]*Jena Center for Soft Matter (JCSM), Friedrich Schiller University Jena, Philosophenweg 7, 07743 Jena, Germany*
[c]*Polymer Chemistry Research Group, Department of Organic and Macromolecular Chemistry, Ghent University, Krijgslaan 281 S4-bis, B-9000 Gent, Belgium. E-mail: filip.duprez@ugent.be*

†Electronic supplementary information (ESI) available. See DOI: 10.1039/c5py00329f

(co)polymers. The synthesis of the maleimide thiolactone monomer (MITla) can be achieved from bio-based, sustainable resources such as maleic anhydride (MAN) and D,L-homocysteine thiolactone hydrochloride (Tla*HCl), respectively, both of which are available in large quantities. The monomer identity and purity were investigated using nuclear magnetic resonance (NMR), Fourier Transform infrared spectroscopy (FT-IR), and elemental analysis (EA). We further demonstrate the homo- and copolymerization with styrene or *N*-iso-propylacrylamide (NIPAAm), respectively. In all cases, the composition and the integrity of the thiolactone moiety in the resulting homo- and copolymers was verified afterwards. Subsequently, we address the thiolactone in a simultaneous double modification with *n*-butylamine and methyl acrylate for both homo- and copolymers. In case of the homopolymer (PMITla) and the copolymer with NIPAAm (P(MITla-*co*-NIPAAm)$_x$), quantitative double modification could be achieved, while for the styrene-based copolymer (P(MITla-*alt*-S)$_x$) this was only partially possible.

Experimental section

Materials

Maleic anhydride (MAN) was purchased from Sigma Aldrich and used as received. Styrene (Sigma Aldrich) was passed over an aluminum oxide column before usage to remove any inhibitor. *N*-Iso-propylacrylamide (NIPAAm) (Aldrich, 97%) was recrystallized from a mixture of toluene/*n*-hexane (1/1 v/v). 2,2′-Azobis(2-methylpropionitrile) (AIBN) was crystalized from methanol, twice, and stored in the fridge. If not further mentioned the chemicals were used as received. D,L-Homocysteine thiolactone hydrochloride (Tla*HCl) was purchased from Haihang Industry (Jinan City, China). 2,4,6-Trimethylbenzoyldiphenylphosphine oxide (Lucirin TPO©) was kindly donated by BASF. 2-(((Butylthio)carbonothioyl)thio)propanoic acid (BuPAT) was synthesized according to literature procedures.[39] If not further mentioned the chemicals were used as received.

Synthesis of maleimide thiolactone (IUPAC-name: 1-(2-oxotetrahydrothiophen-3-yl)-1*H*-pyrrole-2,5-dione; MITla)

Maleic anhydride (51 mmol, 5 g) was dissolved together with D,L-homocysteine thiolactone hydrochloride (51 mmol, 7.84 g) in dimethylsulfoxide (DMSO; 20 mL). Anhydrous sodium sulfate (Na_2SO_4) was suspended in the resulting clear solution and heated up to 70 °C in an oil bath for 3 hours. The reaction solution was diluted with 200 mL dichloromethane, and extracted with 1 L water. The organic phase was dried under vacuum. The desired product was obtained as slightly yellow crystals by crystallization from *n*-hexane. Yield: 33% (3.3 g). ^{1}H-NMR (300 MHz; $CDCl_3$): 6.76 (s, –C*H*=C*H*–), 4.85–4.75 (dd, –N–C*H*), 3.45–3.30 (m, –CH–CH_2), 2.90–2.70 (m, –CH_2–S–), 2.55–2.39 (m, –CH_2–S–) ppm. ^{13}C-NMR (75 MHz; $CDCl_3$): 201.5 (–CH–*C*O–S–), 169.6 (–N–*C*O–CH–), 134.5 (–*C*H=*C*H–), 58.0 (–N–*C*H–), 27.7 (–CH_2–*C*H_2–S–), 27.2 (–CH–*C*H_2–CH_2–) ppm. ^{1}H-NMR (300 MHz; DMSO-d_6): 7.11 (s, –C*H*=C*H*–), 5.08–4.93 (dd, –N–C*H*), 3.58–3.30 (m, –CH–CH_2; below the water peak), 2.60–2.30 (m, –CH_2–S–; under the DMSO peak) ppm. ^{13}C-NMR (75 MHz; DMSO-d_6): 203.1 (–CH–*C*O–S–), 170.1 (–N–*C*O–CH–), 134.9 (–*C*H=*C*H–), 57.4 (–N–*C*H–), 27.6 (–CH_2–*C*H_2–S–), 26.9 (–*C*H_2–CH_2–S–) ppm. FT-IR: 1697 (maleimide C=O), 1685 (thiolactone C=O), 1400 (C–N–C), 833 (H–C=C) and 690 (C=C) cm^{-1}. EA: calc. C 48.72%; H 3.58%; N 7.10%; S 16.26%; meas. C 48.45%; H 3.52%; N 6.96%; S 16.50%. T_{mp} = 128 °C.

Homopolymerization of MITla using 2,2′-azobis(2-methylpropionitrile) (AIBN) as initiator in THF

MITla (200 mg; 1.02 mmol) was dissolved together with different amounts of 2,2′-azobis(2-methylpropionitrile) (AIBN) (5, 10, and 20 wt%) in 2 mL tetrahydrofuran (THF; 100 mg mL^{-1}). The solution is purged with argon for 5 minutes and heated afterwards for 24 hours in an oil bath at 70 °C. The reaction solution was diluted with chloroform and precipitated into methanol. ^{1}H-NMR (300 MHz; $CDCl_3$): 4.9–4.6 (–N–C*H*), 4.4–4.0 (polymer backbone), 3.9–3.6 (furan), 3.6–3.1 (–S–CH_2), 3.1–2.9 (polymer backbone), 2.9–2.3 (–CH–CH_2), 2.3–1.6 (furan) ppm. ^{1}H-NMR (300 MHz; DMSO-d_6): 5.3–4.8 (–N–C*H*), 4.4–2.8 (polymer backbone, furan, –S–CH_2), 2.7–2.1 (–CH–CH_2), 2.1–1.6 (furan) ppm. ^{13}C-NMR (75 MHz; DMSO-d_6): 203–200 (thiolactone *C*=O), 177–174 (maleimide *C*=O), 77 (furan), 68 (furan), 58 (–N–*C*H–), 46–39 (backbone), 29–26 (CH_2–CH_2–S–) ppm. ^{13}C-NMR (75 MHz; $CDCl_3$): 203–200 (thiolactone *C*=O), 177–173 (maleimide *C*=O), 68 (furan), 59 (–N–*C*H–), 49–37 (backbone), 28–25 (CH_2–CH_2–S–) ppm. FT-IR: 1700 (C=O), 1500–900 (thiolactone) cm^{-1}. SEC (DMAC/LiCl): 10 wt%: M_n = 1500 g mol^{-1}; $Đ$ = 1.22 (PS calibration).

Homopolymerization of MITla using Lucirin TPO© as initiator in DCM

MITla (200 mg; 1.02 mmol) was dissolved together with different amounts of 2,4,6-trimethylbenzoyldiphenylphosphine oxide (Lucirin TPO©; 5, 10, and 20 wt%) in 2 mL dichloromethane (DCM; 100 mg mL^{-1}) in a capped vial. The solution is purged with argon for 5 minutes and irradiated under a UV lamp (250 W) for 30 minutes. The reaction solution was diluted with chloroform and precipitated into methanol. SEC (DMAC/LiCl): 5 wt%: M_n = 5100 g mol^{-1}; $Đ$ = 1.40; 10 wt%: M_n = 4700 g mol^{-1}; $Đ$ = 1.36; 20 wt%: M_n = 4400 g mol^{-1}; $Đ$ = 1.34 (PS calibration).

Homopolymerization of MITla using Lucirin TPO© as initiator in the bulk

MITla (200 mg; 1.02 mmol) was dissolved together with different amounts of 2,4,6-trimethylbenzoyldiphenylphosphine oxide (Lucirin TPO©) (5, 10, and 20 wt%) in 2 mL dichloromethane (DCM; 100 mg mL^{-1}) and spread over a glass slide. DCM was allowed to evaporate in the dark, afterwards the film was irradiated using a UV lamp (250 W) for 30 minutes. The product was dissolved in chloroform and precipitated into methanol. ^{1}H-NMR (300 MHz; DMSO-d_6): 8.2–7.3 (TPO), 7.95–7.72 (TPO), 5.3–4.7 (–N–C*H*), 4.3–1.7 (polymer backbone, thiolactone signals) ppm. ^{13}C-NMR (75 MHz; DMSO-d_6):

203–200 (thiolactone *C*=O), 177–173 (maleimide *C*=O), 132–127 (TPO), 58 (–N–*C*H–), 46–39 (backbone), 29–25 (CH_2–CH_2–S–) ppm. FT-IR: 1700 (C=O), 1500–900 (thiolactone) cm^{-1}. SEC (DMAC/LiCl): 5 wt%: M_n = 7000 g mol^{-1}; $Đ$ = 1.55; 10 wt%: M_n = 5500 g mol^{-1}; $Đ$ = 1.33; 20 wt%: M_n = 4700 g mol^{-1}; $Đ$ = 1.29 (PS calibration).

Kinetic studies for the copolymerization of MITla and styrene

MITla (3 g; 15.22 mmol; 100 eq.) and styrene (1.584 g; 15.22 mmol; 100 eq.) were dissolved in 20 mL dioxane together with 150 mg trioxane (as internal standard) and degassed with argon for 20 min. CTA (145 mg; 4 eq.) and AIBN (10 mg; 0.4 eq.) were added under argon flux and the solution was further degassed and divided into different vials. The reaction vials were placed in an oil bath at 65 °C, and removed after certain times, cooled to room temperature (a small amount was removed for the determination of the monomer conversion), and precipitated twice in ethanol. The resulting precipitate was filtered, dried, and the resulting polymers were investigated using ^{1}H-NMR.

Alternating copolymerization of styrene (S) and maleimide–thiolactone (MITla) (P(MITla-*alt*-S)) *via* RAFT

Exemplarily described for P(MITls-*alt*-S)$_{23}$: 2-(((butylthio)carbonothioyl)thio)propanoic acid (BuPAT, CTA; 125 mg; 1 eq.), 2,2′-azobis(2-methylpropionitrile) (AIBN; 9 mg; 0.1 eq.), styrene (1.365 g; 25 eq.), MITla (2.586 g; 25 eq.), and trioxane (50 mg, as internal standard) were dissolved in 10 mL dioxane. The reaction solution was degassed *via* three "freeze–pump–thaw" cycles. The reaction was heated up to 70 °C in an oil bath and stirred overnight (for 15 hours) and the conversion was determined *via* NMR. The solution was allowed to cool down to room temperature, diluted with chloroform and precipitated twice into methanol. The yellow precipitate was filtered and dried under vacuum. ^{1}H-NMR (300 MHz; $CDCl_3$): 7.7–5.9 (arom. C*H*), 5.0–4.3 (–N–C*H*), 4.3–1.7 (polymer backbone, thiolactone signals) ppm. FT-IR: 1700 (C=O), 1500–900 (thiolactone), 700 (aromatic) cm^{-1}. SEC ($CHCl_3$/i-PrOH/TEA): P(MITls-*alt*-S)$_{10}$: M_n = 3300 g mol^{-1}; $Đ$ = 1.26; P(MITls-*alt*-S)$_{23}$: M_n = 5300 g mol^{-1}; $Đ$ = 1.34; P(MITls-*alt*-S)$_{36}$: M_n = 7800 g mol^{-1}; $Đ$ = 1.39 (PS calibration).

Copolymerization of *N*-iso-propylacrylamide (NIPAAm) and maleimide-thiolactone (MITla) (P(MITla-*co*-NIPAAm)$_x$) *via* RAFT

Exemplarily described for P(MITla-*co*-NIPAAm)$_{23}$: BuPAT (125 mg; 1 eq.), AIBN (9 mg; 0.1 eq.), *N*-iso-propylacrylamide (NIPAAm; 1.480 g; 25 eq.), MITla (2.586 g; 25 eq.), and trioxane (50 mg, internal standard) were dissolved in 10 mL dioxane. The reaction solution was degassed *via* three "freeze–pump–thaw" cycles. The reaction was stirred in an oil bath at 70 °C until the desired conversion was reached as determined *via* NMR. The solution was allowed to cool to room temperature, diluted with chloroform and precipitated twice into diethyl ether. The yellow precipitate was filtered, and dried under vacuum. ^{1}H-NMR (300 MHz; $CDCl_3$): 7.7–5.9 (–N*H*–), 5.0–4.5 (–N–C*H*–), 4.0–3.7 (–C*H*-$(CH_3)_2$), 3.7–0.7 (polymer backbone and thiolactone) ppm. FT-IR: 1700 (C=O), 1650 and 1530 NIPAAm), 1500–900 (thiolactone) cm^{-1}. SEC ($CHCl_3$/i-PrOH/TEA): P(MITla-*co*-NIPAAm)$_{10}$: M_n = 1800 g mol^{-1}; $Đ$ = 1.11; P(MITla-*co*-NIPAAm)$_{23}$: M_n = 3300 g mol^{-1}; $Đ$ = 1.21; P(MITla-*co*-NIPAAm)$_{35}$: M_n = 4300 g mol^{-1}; $Đ$ = 1.31 (PS calibration).

Double modification of the thiolactone moiety

Exemplary described for P(MITla-*co*-NIPAAm)$_{23}$: P(MITla-*co*-NIPAAm)$_{23}$ (100 mg) was dissolved together with methyl acrylate (250 eq.) in 3 mL chloroform and stirred at room temperature. Afterwards, *n*-butylamine was added under vigorous stirring. The solution turned immediately pink, while the color vanished over time. After 24 hours, the solution was precipitated twice into cold diethyl ether, filtered and dried under vacuum. SEC (DMAC/LiCl): P(MITla-*co*-NIPAAm)$_{23}^{DM}$: M_n = 10 200 g mol^{-1}; $Đ$ = 1.11; P(MITla-*alt*-S)$_{36}^{DM}$: M_n = 13 200 g mol^{-1}; $Đ$ = 1.32; PMITla^{AIBN,DM}: M_n = 3700 g mol^{-1}; $Đ$ = 1.26.

Characterization

NMR: Nuclear magnetic resonance (^{1}H- and ^{13}C-NMR) spectra were recorded in $CDCl_3$ or DMSO-d_6 on a Bruker AC 300/75 MHz spectrometer at 298 K. Chemical shifts are given in parts per million (ppm, δ scale), relative to the residual signal of the deuterated solvent.

SEC: Size exclusion chromatography was measured on a Shimadzu system equipped with a SCL-10A system controller, a LC-10AD pump, a RID-10A refractive index detector, and both a PSS Gram30 and a PSS Gram1000 column in series, whereby *N*,*N*-dimethylacetamide (DMAC) with 5 mmol of LiCl was used as an eluent at 1 mL min^{-1} flow rate and the column oven was set to 60 °C. The system was calibrated with PS (100 to 1 000 000 g mol^{-1}) standards. Furthermore, a Shimadzu system equipped with an SCL-10A system controller, an LC-10AD pump and an RID-10A refractive index detector using a solvent mixture containing chloroform ($CHCl_3$), triethylamine (TEA) and iso-propanol (i-PrOH) (94 : 4 : 2) at a flow rate of 1 mL min^{-1} on a PSS SDV linear M 5 μm column at 40 °C. The system was calibrated using polystyrene (100 to 100 000 g mol^{-1}) standards.

Elemental analysis (EA) was measured on a CHN(S) analyzer Euro EA3000 by HekaTech.

Fourier-transform infra-red spectroscopy: Dry powders of the copolymers were directly placed on the crystal of the ATR-FTIR (Affinity-1 FTIR, Shimadzu) or ATR-FT-IR (ALPHA's Platinum ATR, Bruker) for measurements in the range of 4000 to 600 cm^{-1}.

Differential scanning calorimetry (DSC) thermograms were recorded on a Netzsch DSC 204 F1 instrument. For the sample annealing the sample was first heated up to 200 °C, cooled and heated in a second run with 20 K min^{-1}, cooled and measured for a third time with 10 K min^{-1} in a temperature range of −50 to 200 °C. The glass transition temperatures were determined from the third heating cycle. Midpoint values have been used for the evaluation.

Thermo-gravimetric analyses (TGA) were performed under nitrogen atmosphere in a Netzsch TG 209 F1 Iris in the range from room temperature to 800 °C with a heating rate of 10 K min^{-1}. The corresponding decomposition temperatures were determined at the decay point of the curves.

UV-Irradiations were carried out using a Hoehnle UVACUBE 100 equipped with a 250 W lamp. *Melting temperatures* of MITla were determined on a melting point apparatus SMP3 (Stuart, UK) with a heating rate of 5 K min^{-1}.

Results and discussion

Monomer synthesis

Maleimides are well established in chemistry, material science and bioscience, and are mostly used in Diels–Alder reactions or Michael-additions.[19,40,41] Thiolactones, on the other hand, are of interest as platform for simultaneous double modification reactions, *e.g. via* ring-opening induced nucleophilic substitutions by amines, and subsequent thiol-X reactions involving the released thiol moiety.[25,27,32] Therefore, the synthesis of a molecule combining both functionalities, maleimide and thiolactone, and its incorporation into homopolymers and copolymers of controlled composition is particularly interesting.

The synthesis was realized from maleic anhydride (MAN) and D,L-homocysteine thiolactone hydrochloride (Tla*HCl) as starting materials, both bio-based and available in large quantities. The desired molecule, maleimide thiolactone (1-(2-oxotetrahydrothiophen-3-yl)-1*H*-pyrrole-2,5-dione, MITla, Fig. 1A) was prepared by dissolving MAN and Tla*HCl in DMSO in an equimolar ratio together with anhydrous sodium sulfate (Na_2SO_4) as *in situ* drying agent, followed by heating to 70 °C in an oil bath. The reaction progress was determined *via* NMR, comparing the appearance of a new signal at 5.0 ppm to trioxane as internal standard over time (Fig. S1†). During the first 3 hours an almost linear increase of the conversion up to roughly 50% was obtained. Afterwards the reaction rate decreases and reaches a plateau at ≈75% during 24 hours. During the reaction the clear solution turns first yellow (within the first hour) and further from brownish (after 3 hours) to dark brown. At this point we assume that undesired side-reactions limit the conversion and consequently stopped the reaction after 3 hours. After extraction, the desired product was obtained by crystallization from *n*-hexane as slightly yellowish crystals in an overall yield of 33%. In Fig. 1B, the maleimide protons can be observed in the ^{1}H-NMR spectrum at 6.9 ppm, while the characteristic thiolactone protons are found at 4.7, 3.4 and between 2.8 to 2.3 ppm.

By ATR-FT-IR (Fig. 1C; Fig. S2 and 3†) the molecule was analyzed in comparison to the educts, showing bands at 3093, 833 and 690 cm^{-1} for the maleimide stretching vibration,[42,43] 1697 cm^{-1} for the carbonyl vibrations of maleimide and thiolactone, 1400 cm^{-1} for the C–N–C– band, and peaks between 1300 and 900 cm^{-1} correspond to the thiolactone ring. The melting temperature (T_m) for MITla was determined to 128 °C, which is in between the melting points for the two starting compounds, ≈50 °C for MAN and ≈200 °C for Tla*HCl, respectively. ^{1}H-, ^{13}C-NMR, FT-IR, ESI-MS, elemental analysis (EA), and melting temperature (T_m), confirm the successful

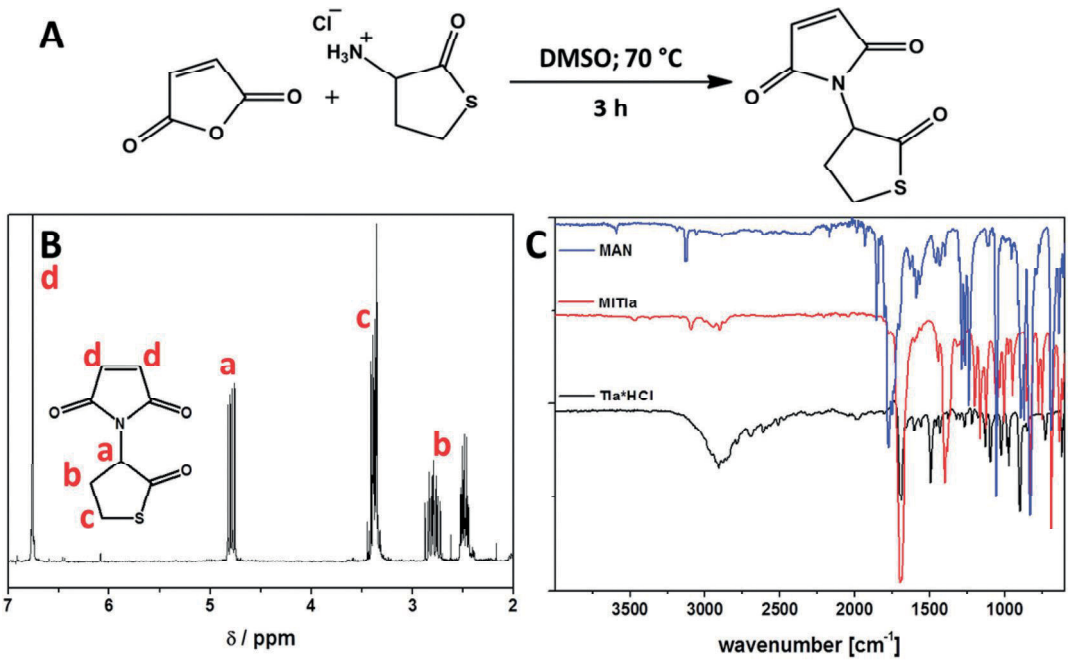

Fig. 1 Synthesis of 1-(2-oxotetrahydrothiophen-3-yl)-1*H*-pyrrole-2,5-dione (MITla) from maleic anhydride (MAN) and D,L-homocysteine thiolactone hydrochloride (Tla*HCl) (A); characterization *via* ^{1}H-NMR ($CDCl_3$, 300 MHz) (B); comparison of FT-IR spectra for MAN (blue curve), Tla*HCl (black curve), and MITla (red curve).

synthesis of the desired maleimide thiolactone, 1-(2-oxotetrahydrothiophen-3-yl)-1*H*-pyrrole-2,5-dione (MITla, Fig. S2–S6†).

Homopolymerization

Maleimides are known to undergo polymerization as homopolymers or alternating copolymers with, *e.g.*, styrenic comonomers.[5,44] We anticipated that MITla, would enable the synthesis of a new class of poly(thiolactone)s, both homo- and copolymers. Typically, maleimides equipped with one functional group, *e.g.* alkynes, are found,[5] while thiolactones in the side-chain of polymers would allow for simultaneous double modifications with a broad range of nucleophiles in combination with subsequent thiol-X reactions.[25]

First, the ability to polymerize MITla *via* free-radical polymerization (FRP), initiated *via* 2,2′-azobis(2-methylpropionitrile (AIBN) and a photo-initiator (2,4,6-trimethylbenzoyldiphenylphosphine oxide; Lucirin TPO©, a commonly used photo-initiator in our group) was tested. Different ratios of initiator to monomer (5, 10, 20 wt% initiator) were tested for the polymerization in the bulk and in solution for TPO. The amount of initiator was chosen to prepare polymers of lower molecular weight, as first attempts using higher [M]/[I] showed increased dispersities and suffered from precipitation during polymerization. In case of the polymerization in solution the monomer was dissolved together with the initiator in dichloromethane (DCM; 100 mg mL^{-1}) and irradiated with an UV lamp (250 W) for 30 minutes. The reaction solutions were precipitated into cold methanol and investigated *via* SEC. A decrease of the amount of initiator leads to higher molar masses (Fig. S7,† Table 1), indicated by a shift to lower elution volume in the chromatograms. The monomer conversions for the solution polymerizations were 80 to 90% as determined gravimetrically by weighing the resulting polymers after precipitation. The same reactions were also performed in the bulk, therefore the monomer and the respective amount of TPO were dissolved in DCM, spread on a glass slide, and the DCM was allowed to evaporate (in the dark) for several hours. Afterwards the glass slides with the monomer films were irradiated for 30 min. The films were dissolved afterwards, precipitated into cold methanol, and the obtained PMITla was investigated *via* SEC (Table 1; Fig. 2A). The molar masses obtained from SEC for 10 and 20 wt% of TPO in the bulk are comparable to the results obtained in solution. For 5 wt% the molar mass in the bulk is higher if compared to the reaction in solution (Fig. 2B). In case of the bulk polymerization, lower monomer conversions of 30 to 50% were found, which can be explained by lower chain mobility.

As control, the monomer was dissolved in DCM and heated to 70 °C in a pressure tube without any initiator being present. Here, no polymerization was observed within 24 h.

The obtained PMITla shows low solubility in chloroform, DCM or acetone after precipitation, and was only well soluble in DMSO or DMF. We do not attribute this to crosslinking at this point as the molar mass distributions are still moderate (<1.6). As the solubility might depend on the chain length, we were also interested in the synthesis of an oligomer of MITla. It is known that THF can act as initiator for the radical polymerization of maleimides in the presence of AIBN.[44] Therefore, the use of THF as solvent for the AIBN-initiated FRP of MITla might represent an easy access to oligomers. The polymerization was carried out in THF (100 mg mL^{-1}) at 70 °C for 24 hours and the obtained molar masses were indeed much lower in comparison to the TPO-initiated polymerizations, independent of the used monomer to initiator ratio (Fig. 2B; Table 1; Fig. S8†). The molar mass was only 1500 g mol^{-1} (Fig. 2B, dotted line) and the materials were still soluble in chloroform and THF.

Beside the characterization *via* SEC, the homopolymers initiated by TPO (10 wt% in the bulk, $PMITla^{TPO}$) and AIBN (10 wt% in THF, $PMITla^{AIBN}$), were further investigated *via* NMR, FT-IR, DSC and TGA. The superscripts for these polymers denote the initiator used for polymerization of MITla.

For the ^{1}H-NMR spectra for $PMITla^{TPO}$ (Fig. 2C), the aromatic TPO signals are observed in the range of 7.3 to 8.2 ppm, while at 5 ppm the single proton of the thiolactone ring is found, confirming the integrity of the thiolactone. The maleimide backbone signals can be found in the range of 4.5 to 2.8 ppm,[45] while the CH_2 protons for the thiolactone are observed between 1.8 to 2.8 ppm in DMSO-d_6. *Via* ^{13}C-NMR of $PMITla^{TPO}$, a disappearance of the maleimide carbon atoms at 135 ppm (Fig. S9†) and a shift of the maleimide carbonyl-groups in comparison to the monomer from 170 ppm to 175 ppm is observed, indicating a change in the chemical environment. The carbonyl peak at 205 ppm for the thiolactone remains, while the shape of the peak broadens, indicating the presence of the thiolactone in the polymeric side chain. As well as for $PMITla^{TPO}$, $PMITla^{AIBN}$ was investigated *via* ^{1}H- and ^{13}C-NMR concerning the presence of the THF starting group and the peak assignment for PMITla (Fig. S10–14†). By 2D NMR spectroscopy the presence of the THF unit in the polymer chain was confirmed and the corresponding signals assigned to the different groups of the polymer chain.[44]

Table 1 Characterization of PMITla homopolymers initiated *via* AIBN or TPO in solution (S) or in the bulk (B), depending on the amount (wt%) of initiator used in comparison to the monomer

Initiator	Conditions[a]	wt% initiator[b]	Monomer conv.[c] [%]	M_n[d] [g mol^{-1}]	$Đ$[d]
TPO	S	5	82	5100	1.40
TPO	S	10	85	4700	1.36
TPO	S	20	90	4400	1.34
TPO	B	5	45	7000	1.55
TPO	B	10	33	5500	1.33
TPO	B	20	50	4700	1.29
AIBN	S[e]	10	n.d.[f]	1500	1.22

[a] Reaction conditions: S in solution (100 mg mL^{-1} monomer in DCM; UV (250 W); 30 min); B in the bulk (as monomer film casted from DCM solution; UV (250 W); 30 min). [b] Feed ratio. [c] Determined gravimetrically by weighing the obtained polymers after precipitation. [d] SEC (DMAC/LiCl): PS-calib. [e] Reaction conditions: S in solution (100 mg mL^{-1} in THF; 70 °C; 24 hours). [f] Not determined.

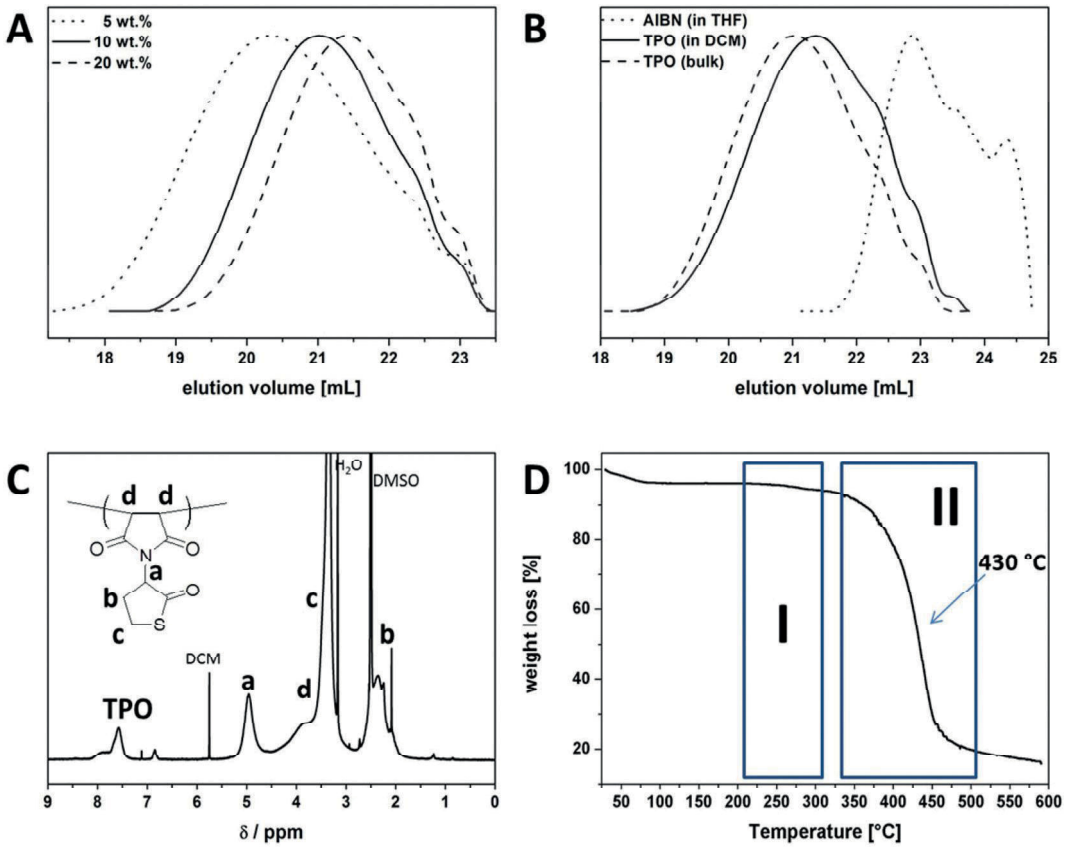

Fig. 2 (A) Comparison of SEC traces for the homopolymerization of MITla with different amounts of TPO in the bulk: 5 wt% (dotted line), 10 wt% (straight line) and 20 wt% (dashed line); (B) comparison of SEC traces for the homopolymerization of MITla *via* AIBN in solution (dotted line), TPO in solution (straight line) and in the bulk (dashed line); (C) NMR spectrum for PMITla initiated *via* TPO in the bulk (10 wt%; DMSO-d_6); (D) TGA trace for PMITla^{TPO} (10 wt% TPO, bulk).

In Fig. 2D the TGA for PMITla^{TPO} shows the beginning of polymer decomposition at 310 °C, and loss of half of the weight at 430 °C (Fig. 2D; area II). Before degradation, a weight loss between 210 to 310 °C is observed, which indicates the release of carbon dioxide in accordance with literature (Fig. 2D; area I).[16] The TGA curve, furthermore, shows only one clear step for the decomposition of the polymer, leading to the assumption that no thiolactone cleavage or ring-opening and partial decomposition is observed until 310 °C. The glass transition temperature (T_g) for polymers containing a high degree of maleic anhydride or maleimides is mostly reported above 200 °C in the literature.[16,46] As a first change in the polymer structure is observed at 210 °C *via* TGA, differential scanning calorimetry (DSC) was measured in a temperature range of −50 to 200 °C. In the corresponding thermograms no glass transition temperature (T_g) could be observed (Fig. S15†).

Via FT-IR it was shown that the corresponding maleimide double bond bands (830 and 690 cm^{-1}) disappear during polymerization, while the carbonyl signal for MITla and PMITla remains at the same position of 1700 cm^{-1} (Fig. S16†) and also the thiolactone ring signals still can be found. No difference was observed in between PMITla^{TPO} and PMITla^{AIBN}, leading to the conclusion that in both cases comparable products were obtained. In summary, the homopolymerization of maleimide thiolactone (MITla) was shown *via* FRP, leading to poly(thiolactone) homopolymers with molar masses below 10 000 g mol^{-1}. It was also shown that the molar mass can be regulated by changing the [M]/[I] in case of TPO, while for AIBN only oligomers were observed if the polymerization was carried out in THF as solvent.

Copolymerization

We also investigated the copolymerization of MITla with styrene and NIPAAm as comonomers. It is known that maleimides have a strong tendency to copolymerize in an alternating fashion with several comonomers, including styrene, vinyl ethers, or some acrylates.[5,10,11,47–50]

For copolymerization, reversible addition-fragmentation chain transfer polymerization (RAFT) was applied as controlled radical polymerization (CRP) technique. The alternating copolymerization of styrene and maleimide is well-known,[5,51] while in case of NIPAAm only the copolymerization with maleic anhydride has been described so far.[47,52,53] Another reason for the choice of these monomer combinations is that styrene-

and NIPAAm-based copolymers with other thiolactone derivatives have been already described.[31,32] However, for these examples the content of thiolactone was limited to a maximum of 30 mol% due to solubility problems, while an alternating copolymerization would allow for the incorporation of up to 50 mol%.

Different molar masses between 3000 and 12 000 g mol^{-1} were targeted by changing the monomer to chain transfer agent (CTA) ratio, keeping an equimolar ratio between MITla and styrene (Fig. 3A). The composition of the reaction solution was determined *via* NMR before and after the polymerization in comparison to an internal standard (1,3,5-trioxane). The monomer conversion was determined after the reaction to be 75–90%, respectively, and degrees of polymerization (DP) of 10, 23 and 36 (Table 2, Fig. S17†) were found. A similar procedure was applied for the copolymerization of MITla and NIPAAm and comparable DPs were achieved (Table 2, Fig. 3B).

The copolymers were investigated *via* SEC concerning molar mass and dispersity ($Đ$). With increasing DP, an increase in the molar mass was obtained for all copolymers (Table 2). Due to the different solution behavior and different interactions with the SEC column material, the samples were measured on two different SEC systems, with different eluents – chloroform ($CHCl_3$) and dimethylacetamide (DMAC), leading to a similar trend but different values for $Đ$. The observed molar masses are in good agreement with the theoretical values as deduced from the [M]/[I] ratios.

The obtained copolymers were further investigated *via* NMR (Fig. 3C; Fig. S18–20†). For styrene the aromatic signals (7–8 ppm) can be compared to the thiolactone signal (4.6 ppm), resulting in a 5 : 1 ratio (in DMSO-d_6; Fig. S19†) and confirming the synthesis of alternating copolymers of MITla and styrene with different chain length P(MITla-*alt*-S)$_{10}$, P(MITla-*alt*-S)$_{23}$, and P(MITla-*alt*-S)$_{36}$. Hereby, subscripts denote the DP calculated for the corresponding copolymer. We also investigated the copolymerization kinetics for MITla and styrene. The styrene conversion shows a linear increase up to 80% (Fig. S21A†). Beside monomer conversion, also the copolymer composition was analyzed by NMR after different reaction times. The ratio of signals for styrene (5 protons, 5.9–7.7 ppm) and MITla (1 proton, 4.6 ppm) was 4.9/1 for all samples up to monomer conversions of 80%, confirming our initial assumption of an alternating copolymerization. SEC data also depicts a constant increase in molar mass, indicated by a shift to lower elution volumes (Fig. S21B†).

For the NIPAAm copolymers, the determination of the composition was slightly different as in this case the NIPAAm signals are included in the quite broad signal between 4.2 to 0.8 ppm, including all signals for NIPAAm, the thiolactone, as well as the copolymer backbone. We nevertheless compared the integrals for the thiolactone signal at 4.8 ppm with the NIPAAm signal at 3.9 ppm, expecting a 1 : 1 ratio (Fig. S20†). Instead, we observed a ratio of 1 : 1.15 – however, we are aware that the baseline of the NIPAAm signal is not completely separated. As up to now only the copolymerization of NIPAAm and maleic anhydride or citraconic acid has been described in an alternating fashion,[47,52,53] and a detailed mechanistic investigation was beyond the scope of this study, we denote the

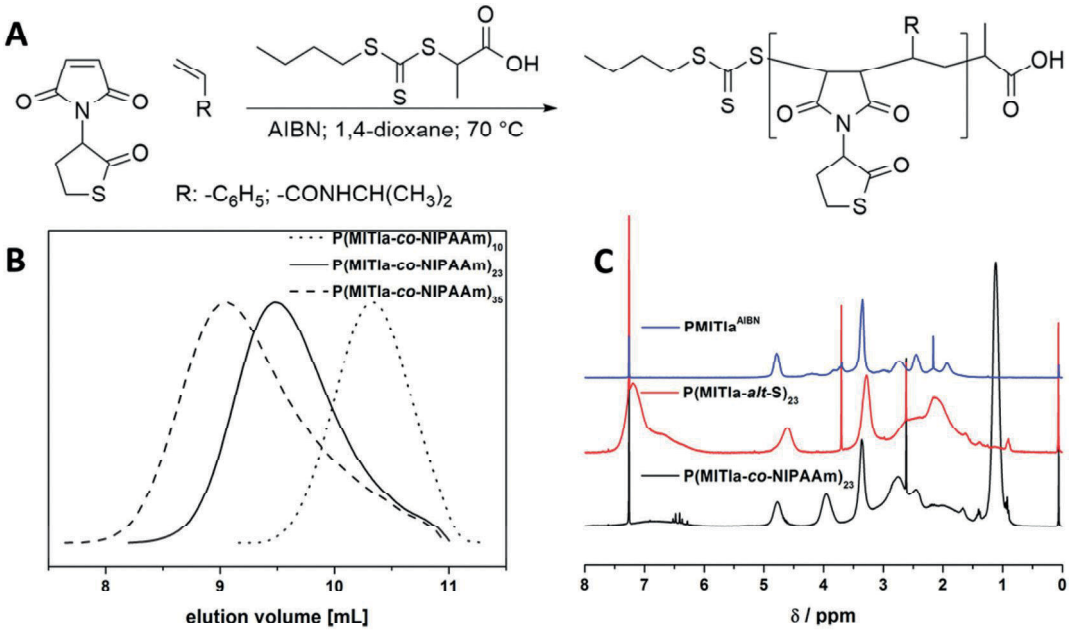

Fig. 3 (A) RAFT copolymerization of MITla and styrene/NIPAAm with 2-(((butylthio)carbonothioyl)thio)propanoic acid (BuPAT) as chain transfer agent; (B) comparison of SEC traces for different molar masses for P(MITla-*co*-NIPAAm) copolymers: DP 10 (dotted line), 23 (straight line), and 35 (dashed line); (C) comparison of ^{1}H-NMR spectra ($CDCl_3$, 300 MHz) for PMITla^{AIBN} (blue line), P(MITla-*alt*-S)$_{23}$ (red line), P(MITla-*co*-NIPAAm)$_{23}$ (black line).

Table 2 Characterization of copolymers of MITla and styrene or NIPAAm prepared *via* RAFT

Sample	$DP_{theo.}$ [a]	Conv. [b,c] [%]	$DP_{meas.}$ [b,c]	M_n [d] [g mol^{-1}]	$Đ$ [d]	M_n [e] [g mol^{-1}]	$Đ$ [e]
P(MITla-*alt*-S)$_{10}$	13	75	9.75	3300	1.26	3100	1.39
P(MITla-*alt*-S)$_{23}$	25	90	22.5	5300	1.34	4800	1.58
P(MITla-*alt*-S)$_{36}$	40	90	36	7800	1.39	8900	1.51
P(MITla-*co*-NIPAAm)$_{10}$	13	80	10.4	1800	1.11	3500	1.17
P(MITla-*co*-NIPAAm)$_{23}$	25	90	22.5	3300	1.21	6900	1.20
P(MITla-*co*-NIPAAm)$_{35}$	40	86	34.4	4300	1.31	9400	1.29

[a] [M]/[I] ratio. [b] NMR (300 MHz, $CDCl_3$) in comparison to trioxane as internal standard. [c] NMR (300 MHz, DMSO-d_6) in comparison to trioxane as internal standard. [d] SEC ($CHCl_3$/i-PrOH/TEA): PS-calib. [e] SEC (DMAC/LiCl): PS-calib.

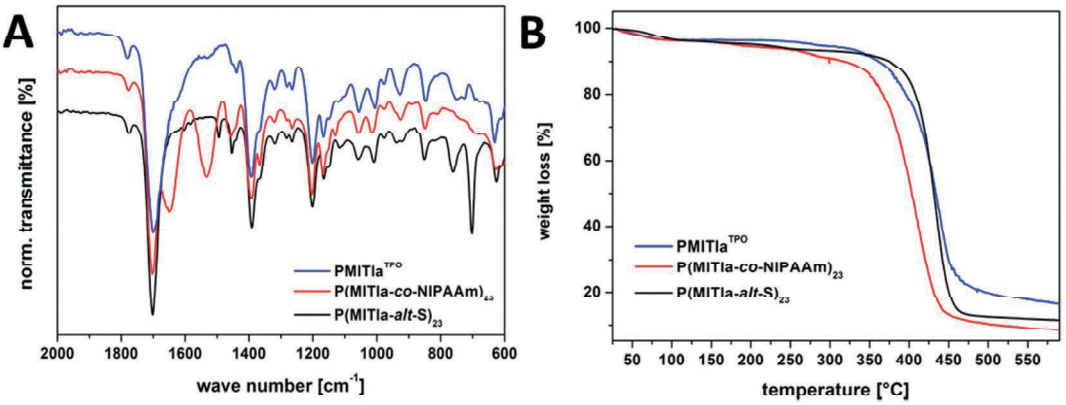

Fig. 4 (A) Comparison of FT-IR spectra for PMITla^{TPO} (blue curve), P(MITla-*co*-NIPAAm)$_{23}$ (red curve) and P(MITla-*alt*-S)$_{23}$ (black curve); (B) TGA traces for PMITla^{TPO} (blue curve), P(MITla-*co*-NIPAAm)$_{23}$ (red curve) and P(MITla-*alt*-S)$_{23}$ (black curve).

resulting copolymers as P(MITla-*co*-NIPAAm)$_x$, where the subscript refers to the assumed DP.

Beside SEC and NMR, the copolymers were also investigated *via* FT-IR. For P(MITla-*alt*-S)$_{23}$, PMITla^{TPO}, and P(MITla-*co*-NIPAAm)$_{23}$ the carbonyl band at 1700 cm^{-1} and the thiolactone bands between 1500–900 cm^{-1} (Fig. 4A) can be observed. In case of P(MITla-*alt*-S)$_{23}$, a characteristic signal at 700 cm^{-1} can be found for the aromatic ring, while for P(MITla-*co*-NIPAAm)$_{23}$ further characteristic signals at 1650 and 1530 cm^{-1} additionally corresponding to the incorporation of NIPAAm are observed.

The TGA traces for the copolymers of styrene or NIPAAm show no significant change in the decomposition temperature in comparison to the respective homopolymers (Fig. 4B).[54–56] Again, a first step between 210 and 300 °C is observed for both copolymers and decomposition takes place at comparable temperatures. DSC traces for the copolymers were also measured in the range of −50 to 200 °C (Fig. S22†). PS and PNIPAAm homopolymers feature T_g values at 100 and 135 °C, while for P(MITla-*alt*-S)$_{23}$ and P(MITla-*co*-NIPAAm)$_{23}$ no T_g was observed within the investigated temperature range. As already discussed above, T_g values above 200 °C are expected, but due to the first degradation step at 200 °C these temperatures were not investigated.

Site-specific double modification

We were interested in addressing the thiolactone functionalities of the herein discussed homo- and copolymers by simultaneous double modification reactions. Therefore, PMITla^{AIBN}, P(MITla-*alt*-S)$_{36}$, and P(MITla-*co*-NIPAAm)$_{23}$, were chosen. The reason for PMITla^{AIBN} was that its solubility in chloroform was higher in comparison to PMITla^{TPO}, which is a common solvent for such reactions. As proof of concept, we used *n*-butylamine as nucleophile for the thiolactone ring-opening, and methyl acrylate for the subsequent thiol–ene reaction (Fig. 5A).

For the reaction the (co)polymers were dissolved together with methyl acrylate (10 eq. in comparison to the thiolactone units present) in chloroform (50 mg mL^{-1}; in case of P(MITla-*alt*-S)$_{36}$-25 mg mL^{-1}) under vigorous stirring. The *n*-butylamine (10 eq. in comparison to thiolactone) was added afterwards, which led to a color change from slightly yellow, presumably due to the RAFT endgroup in case of the copolymers, to slightly pink (P(MITla-*co*-NIPAAm)$_{23}$), dark red (PMITla^{AIBN}), or remained yellow (P(MITla-*alt*-S)$_{36}$). After 24 hours the reaction solutions were precipitated into cold diethyl ether, filtered and dried under vacuum. White powders were obtained for P(MITla-*co*-NIPAAm)$_{23}^{DM}$ and P(MITla-*alt*-S)$_{36}^{DM}$, while the homopolymer formed a red precipitate. The obtained (co)poly-

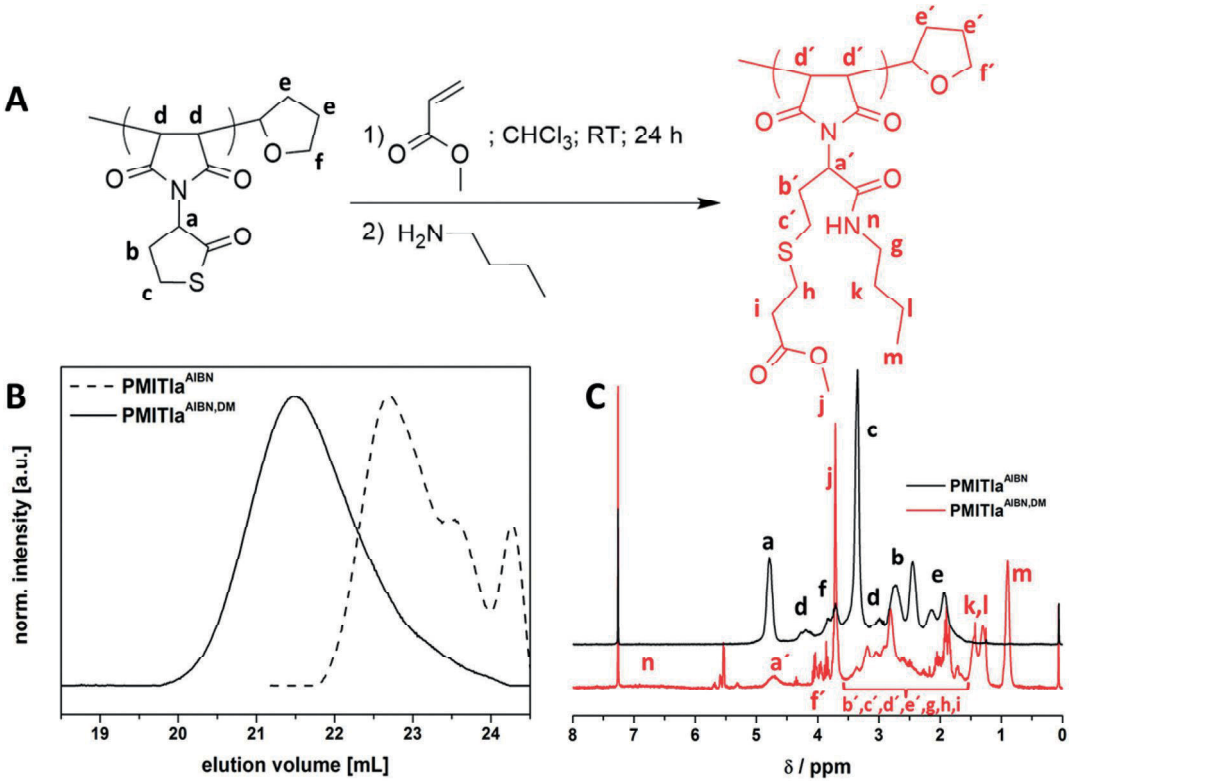

Fig. 5 (A) Simultaneous double modification of (PMITla^{AIBN} by methyl acrylate and *n*-butylamine; (B) comparison of SEC traces before (dashed line) and after (straight line; PMITla^{AIBN,DM}) double modification; (C) comparison of NMR spectra for PMITla^{AIBN} before (black trace) and after (red trace) double modification with peak assignment (300 MHz; $CDCl_3$).

mers are denoted as "DM" after this double modification and were investigated *via* SEC, NMR and FT-IR concerning the final composition and the degree of functionalization according to the thiolactone moiety. Due to the disappearance of the yellow color of the resulting copolymers, we assume full aminolysis of the RAFT endgroup.

For all (co)polymers a shift to lower elution volume was observed in SEC (Fig. 5B and 6B; Table 3). The obtained molar masses for the copolymers increase, while $Đ$ and the shape of the SEC traces do not change significantly, indicating the absence of possible crosslinking due to S–S coupling reactions.

In case of PMITLA^{AIBN}, the modification can be easily monitored by ^{1}H-NMR as the shape of the signal of the thiolactone C–H proton, at 4.7 ppm, broadens and shifts after modification and the signal c, at 3.4 ppm, for the thiolactone ring disappears completely. In Fig. 6A, the ^{13}C-NMR shows the complete disappearance of the thiolactone signals at 203 (C═O), 58 (tertiary C), and 28 ppm (secondary C) fully, while new signals for the modified polymer (PMITla^{AIBN,DM}) corresponding to the acrylate and amine arise – *e.g.* methyl groups (at 3.6 ppm for $CH_3^{acrylate}$ and 0.8 ppm for CH_3^{amine}) (Fig. 5C; Fig. S23 and S24†). We therefore assume a quantitative modification of PMITla^{AIBN} according to NMR.

For P(MITla-*co*-NIPAAm)$_{23}$ and P(MITla-*alt*-S)$_{36}$ the assignment of the different signals and the determination of the composition is slightly more challenging as many signals overlap in ^{1}H-NMR in the region of 1 to 4.5 ppm (Fig. S25 and 26†). Therefore, these copolymers were investigated *via* ^{13}C-NMR to confirm the successful modification. For P(MITla-*co*-NIPAAm)$_{23}$ the signals at 58 ppm for the tertiary carbon and the carbonyl signal in the thiolactone at 203 ppm completely disappeared after the double modification, again indicating full conversion of the thiolactone in the side chain (Fig. S27†). Beside the aminolysis of the thiolactone, also the RAFT endgroup can participate in both aminolysis and subsequent thiol-en reactions. In case of P(MITla-*alt*-S)$_{23}$, however, these signals are still present afterwards, hinting towards an incomplete modification. This observation can be confirmed from ^{1}H-NMR spectra, as still signals for the intact thiolactone ring can be found. From NMR, a degree functionalization of ≈60% can be assumed for P(MITla-*alt*-S)$_{23}$ (Fig. S26†). We therefore varied the solvent, the reaction time, and the amount of amine/acrylate for the modification of P(MITla-*alt*-S)$_{23}$. Beside chloroform, also THF, dioxane, and dimethylformamide (DMF) were tested to increase the degree of functionalization, but only small changes in the elution behavior of the obtained copolymers were observed and functionalization degrees between 40% and 60% were found according to NMR (Fig. S29, Table S1†). Further, the amount of amine and acrylate was increased to ensure the presence of unreacted amine over the whole duration of the reaction as these compounds

Table 3 Characterization data for the double modification with methyl acrylate and *n*-butylamine of MITla homo- and copolymers before and after *via* SEC

	Before double modification		After double modification	
Sample	M_n[a] [g mol^{-1}]	$Đ$[a]	M_n[a] [g mol^{-1}]	$Đ$[a]
PMITla^{AIBN}	1500	1.22	3700	1.26
P(MITla-*co*-NIPAAm)$_{23}$	6900	1.20	10 200	1.11
P(MITla-*alt*-S)$_{36}$	8900	1.51	13 200	1.32

[a] SEC (DMAC/LiCl): PS-calib.

can also undergo Michael-additions (different reaction conditions are listed in Table S1†). Nevertheless, in all resulting ^{13}C-NMR spectra still unreacted thiolactone could be detected (Fig. S29†). If the modification was carried out in DMF, a broadening of the SEC trace can be observed, hinting towards disulfide crosslinking as side reaction (Fig. S28†).[36] At this point, we speculate that solubility issues are the main reason for incomplete double modification as partial precipitation occurs in $CHCl_3$, THF and dioxane. Nevertheless, the product remains soluble in DMF. Another possible reason might be steric hindrance, although this has not been observed for P(MITla-*co*-NIPAAm)$_{23}$ or PMITLA^{AIBN}. The reaction temperature was not increased as elevated temperatures would probably favor the Michael-addition between amine and acrylate.

Additionally, the obtained (co)polymers were investigated *via* FT-IR (Fig. 6C). In all cases a shoulder in the peak for the carbonyl group (at 1700 cm^{-1}) at 1750 cm^{-1} is observed and new signals at 1640 and 1580 cm^{-1} appear (Fig. 6C; direct comparison in Fig. S30–32†). Also, the peaks in the range of 1400 to 900 cm^{-1} change in shape, hinting towards changes for the environment of the thiolactone ring.

In summary, both for PMITla^{AIBN} and P(MITla-*co*-NIPAAm)$_{23}$ a complete double modification with methyl acrylate and *n*-butylamine was possible, while for P(MITla-*alt*-S)$_{36}$ only a degree of functionalization of up to 60% in THF or chloroform could be reached.

Conclusion

We described the synthesis of a thiolactone-functionalized maleimide, 1-(2-oxotetrahydrothiophen-3-yl)-1*H*-pyrrole-2,5-dione (MITla), and its polymerization to poly(thiolactone) homo- and copolymers *via* (controlled) radical polymerization techniques. Homopolymerization was achieved *via* FRP, while the RAFT methodology was chosen for the copolymerization of MITla with styrene or *N*-iso-propylacrylamide. Different copolymers were synthesized and a thiolactone content of 50 mol% could be obtained.

Thiolactones are known for nucleophilic ring-opening in the presence of, *e.g.*, amines, enabling subsequent thiol-X reaction with acrylates – a facile strategy for simultaneous double modification of polymeric materials. We exploited this for the double modification of PMITla^{AIBN}, P(MITla-*co*-NIPAAm)$_{23}$, and P(MITla-*alt*-S)$_{36}$ with *n*-butylamine and methyl acrylate and reached full conversion for PMITla^{AIBN} and P(MITla-*co*-NIPAAm)$_{23}$ whereas only up to 60% conversion of the thio-

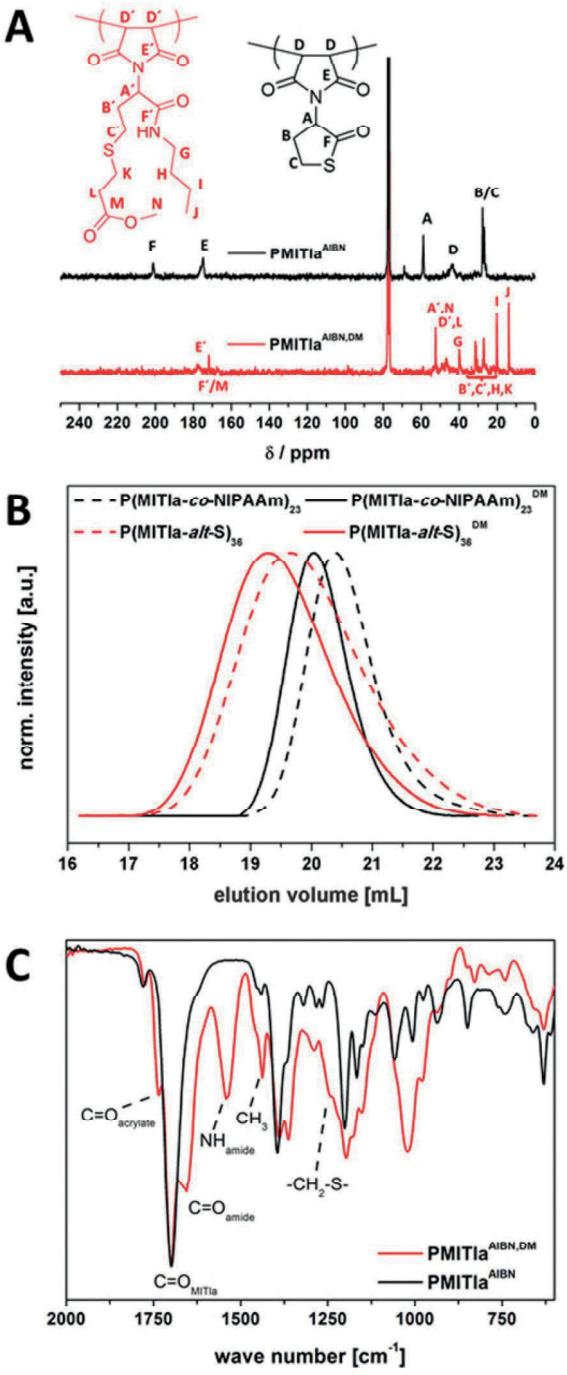

Fig. 6 (A) Comparison of ^{13}C-NMR spectra for PMITla^{AIBN} (black trace) and PMITla^{AIBN,DM}; (B) comparison of SEC traces for P(MITla-*alt*-S)$_{36}$ (red dashed line), P(MITla-*alt*-S)$_{36}^{DM}$ (red straight line), P(MITla-*co*-NIPAAm)$_{23}$ (black dashed line), and P(MITla-*co*-NIPAAm)$_{23}^{DM}$ (black straight line); (C) comparison of FT-IR spectra for PMITla^{AIBN} (black traces), and PMITla^{AIBN,DM} (red traces).

lactone could be achieved for P(MITla-*alt*-S)$_{36}$. We currently attribute the latter to differences in solubility between P(MITla-*alt*-S)$_{36}$ and P(MITla-*co*-NIPAAm)$_{23}$ – also, lower molar masses might improve this modification reaction in the future.

We think that such materials will be of further interest concerning their functionalization with different combinations of amines/acrylates, their introduction into block copolymers, and their use in selective (reversible) crosslinking of polymeric materials.

Acknowledgements

T.R. would like to thank the whole PCR group (especially Daniel, Steven, Sophie L., Bernhard and Fabienne) for help during his stay in Ghent and is also grateful to Renzo Paulus for DSC and TGA measurements, Sven Krieck for FT-IR, and Sandra Köhn for elemental analysis. F.H.S. thanks the VCI for an independent researcher fellowship, and T.R. the Carl-Zeiss foundation for a PhD scholarship, as well as the European Science Foundation (ESF) within the framework of the ESF activity entitled 'Precision Polymer Materials'. F.H.S. and T.R. also acknowledge the Thuringian Ministry for Education, Science and Culture (TMBWK, grants #B514-09051, NanoConSens and #B515-10065, ChaPoNano) for financial support. P.E. and F.D.P. are thankful to Ghent University and the Belgian program on Interuniversity Attraction Poles initiated by the Belgian State, the Prime Minister's office (P7/05).

References

1 C. Barner-Kowollik, J.-F. Lutz and S. Perrier, *Polym. Chem.*, 2012, **3**, 1677–1679.
2 K. Matyjaszewski and A. H. E. Müller, *Prog. Polym. Sci.*, 2006, **31**, 1039–1040.
3 F. S. Bates and G. H. Fredrickson, *Phys. Today*, 1999, **52**, 32–38.
4 Y. Mai and A. Eisenberg, *Chem. Soc. Rev.*, 2012, **41**, 5969–5985.
5 M. Zamfir and J.-F. Lutz, *Nat. Commun.*, 2012, **3**, 1138.
6 J. F. Lutz, *Acc. Chem. Res.*, 2013, **26**, 2696–2705.
7 S. Srichan, L. Oswald, M. Zamfir and J. F. Lutz, *Chem. Commun.*, 2012, **48**, 1517–1519.
8 B. V. K. J. Schmidt, N. Fechler, J. Falkenhagen and J.-F. Lutz, *Nat. Chem.*, 2011, **3**, 234–238.
9 J. Jiang, X. Jia, Y. Pang and J. Huang, *J. Macromol. Sci., Pure Appl. Chem.*, 1998, **35**, 781–792.
10 P. Kohli, A. B. Scranton and G. J. Blanchard, *Macromolecules*, 1998, **31**, 5681–5689.
11 Y. Ren, Z. Zhu and J. Huang, *J. Polym. Sci., Part A: Polym. Chem.*, 2004, **42**, 3828–3835.
12 S. G. Fenimore, L. Abezgauz, D. Danino, C.-C. Ho and C. C. Co, *Macromolecules*, 2009, **42**, 2702–2707.
13 D. J. Hall, H. M. Van Den Berghe and A. P. Dove, *Polym. Int.*, 2011, **60**, 1149–1157.
14 J. F. Lutz, B. V. Schmidt and S. Pfeifer, *Macromol. Rapid Commun.*, 2011, **32**, 127–135.
15 S. Srichan, H. Mutlu and J.-F. Lutz, *Eur. Polym. J.*, 2015, **62**, 338–346.
16 L. Häußler, U. Wienhold, V. Albrecht and S. Zschoche, *Thermochim. Acta*, 1996, **277**, 17–27.
17 S. Pfeifer and J. F. Lutz, *Chemistry*, 2008, **14**, 10949–10957.
18 A. S. Goldmann, M. Glassner, A. J. Inglis and C. Barner-Kowollik, *Macromol. Rapid Commun.*, 2013, **34**, 810–849.
19 M. A. Gauthier, M. I. Gibson and H. A. Klok, *Angew. Chem., Int. Ed.*, 2009, **48**, 48–58.
20 H. C. Kolb, M. G. Finn and K. B. Sharpless, *Angew. Chem., Int. Ed.*, 2001, **40**, 2004–2021.
21 W. H. Binder and R. Sachsenhofer, *Macromol. Rapid Commun.*, 2007, **28**, 15–54.
22 C. Barner-Kowollik, F. E. Du Prez, P. Espeel, C. J. Hawker, T. Junkers, H. Schlaad and W. Van Camp, *Angew. Chem., Int. Ed.*, 2011, **50**, 60–62.
23 P. Espeel and F. E. Du Prez, *Macromolecules*, 2015, **48**, 2–14.
24 W. Xi, T. F. Scott, C. J. Kloxin and C. N. Bowman, *Adv. Funct. Mater.*, 2014, **24**, 2572–2590.
25 P. Espeel and F. E. Du Prez, *Eur. Polym. J.*, 2015, **62**, 247–272.
26 P. Espeel, F. Goethals and F. E. Du Prez, *J. Am. Chem. Soc.*, 2011, **133**, 1678–1681.
27 P. Espeel, F. Goethals, F. Driessen, L.-T. T. Nguyen and F. E. Du Prez, *Polym. Chem.*, 2013, **4**, 2449–2456.
28 F. Goethals, S. Martens, P. Espeel, O. van den Berg and F. E. Du Prez, *Macromolecules*, 2014, **47**, 61–69.
29 S. Mommer, H. Keul and M. Moller, *Macromol. Rapid Commun.*, 2014, **35**, 1986–1993.
30 J. J. Yan, J. T. Sun, Y. Z. You, D. C. Wu and C. Y. Hong, *Sci. Rep.*, 2013, **3**, 2841.
31 P. Espeel, F. Goethals, M. M. Stamenović, L. Petton and F. E. Du Prez, *Polym. Chem.*, 2012, **3**, 1007–1015.
32 S. Reinicke, P. Espeel, M. M. Stamenović and F. E. Du Prez, *ACS Macro Lett.*, 2013, **2**, 539–543.
33 M. M. Stamenovic, P. Espeel, E. Baba, T. Yamamoto, Y. Tezuka and F. E. Du Prez, *Polym. Chem.*, 2013, **4**, 184–193.
34 Y. Chen, P. Espeel, S. Reinicke, F. E. Du Prez and M. H. Stenzel, *Macromol. Rapid Commun.*, 2014, **35**, 1128–1134.
35 C. Ferris, M. Casas, M. J. Lucero, M. V. de Paz and M. R. Jimenez-Castellanos, *Carbohydr. Polym.*, 2014, **111**, 125–132.
36 S. Reinicke, P. Espeel, M. Stamenovic and F. Du Prez, *Polym. Chem.*, 2014, **5**, 5461–5470.
37 P. Espeel, L. L. G. Carrette, K. Bury, S. Capenberghs, J. C. Martins, F. E. Du Prez and A. Madder, *Angew. Chem., Int. Ed.*, 2013, **52**, 13261–13264.
38 S. Belbekhouche, S. Reinicke, P. Espeel, F. E. Du Prez, P. Eloy, C. Dupont-Gillain, A. M. Jonas, S. Demoustier-Champagne and K. Glinel, *ACS Appl. Mater. Interfaces*, 2014, **6**, 22457–22466.

39 C. J. Ferguson, R. J. Hughes, D. Nguyen, B. T. T. Pham, R. G. Gilbert, A. K. Serelis, C. H. Such and B. S. Hawkett, *Macromolecules*, 2005, **38**, 2191–2204.

40 B. D. Mather, K. Viswanathan, K. M. Miller and T. E. Long, *Prog. Polym. Sci.*, 2006, **31**, 487–531.

41 G.-Z. Li, R. K. Randev, A. H. Soeriyadi, G. Rees, C. Boyer, Z. Tong, T. P. Davis, C. R. Becer and D. M. Haddleton, *Polym. Chem.*, 2010, **1**, 1196–1204.

42 X. Zeng, S. Yu, M. Lai, R. Sun and C.-P. Wong, *Sci. Technol. Adv. Mater.*, 2013, **14**, 065001.

43 M.-F. Grenier-Loustalot and N. Aycaguer, *Eur. Polym. J.*, 1998, **34**, 1705–1714.

44 D. J. T. Hill, L. Y. Shao, P. J. Pomery and A. K. Whittaker, *Polymer*, 2001, 4791–4802.

45 T. Oishi, K. Kagawa and H. Nagata, *Polymer*, 1997, **38**, 1461–1469.

46 S. Krishnamoorthy, M. Haria, B. E. Fortier-McGill, M. A. Jafar Mazumder, E. I. Robinson, Y. Xia, N. A. D. Burke and H. D. H. Stöver, *J. Polym. Sci., Part A: Polym. Chem.*, 2011, **49**, 192–202.

47 S. Dinçer, V. Köseli, H. Kesim, Z. M. O. Rzaev and E. Pişkin, *Eur. Polym. J.*, 2002, **38**, 2143–2152.

48 F. Morel, C. Decker, S. Jönsson, S. C. Clark and C. E. Hoyle, *Polymer*, 1999, **40**, 2447–2454.

49 S. Srichan, D. Chan-Seng and J.-F. Lutz, *ACS Macro Lett.*, 2012, **1**, 589–592.

50 E. Zhao, J. W. Y. Lam, L. Meng, Y. Hong, H. Deng, G. Bai, X. Huang, J. Hao and B. Z. Tang, *Macromolecules*, 2014, DOI: 10.1021/ma502160w. Q4

51 J.-F. Lutz, M. Ouchi, D. R. Liu and M. Sawamoto, *Science*, 2013, **341**, 1238149.

52 A. Okudan and A. Karasakal, *Int. J. Polym. Sci.*, 2013, **2013**, 1–9.

53 D. Demircan, G. Kibarer, A. Güner, Z. M. O. Rzaev and E. Ersoy, *Carbohydr. Polym.*, 2008, **72**, 682–694.

54 A. Saeed, D. M. R. Georget and A. G. Mayes, *J. Polym. Sci., Part A: Polym. Chem.*, 2010, **48**, 5848–5855.

55 H. G. Schild, *Prog. Polym. Sci.*, 1992, **17**, 163–249.

56 S. L. Malhotra, J. Hesse and L.-P. Blanchard, *Polymer*, 1975, **16**, 81–93.

Supporting information

Poly(thiolactone) Homo- and Copolymers from Maleimide Thiolactone: Synthesis and Functionalization

Tobias Rudolph,[1,2] Pieter Espeel,[3] Filip E. Du Prez,[3,*] Felix H. Schacher[1,2,*]

[1] Laboratory of Organic and Macromolecular Chemistry, Friedrich Schiller University Jena, Humboldtstr. 10, 07743 Jena, Germany

E-mail: felix.schacher@uni-jena.de

[2] Jena Center for Soft Matter (JCSM), Friedrich Schiller University Jena, Philosophenweg 7, 07743 Jena, Germany

[3] Polymer Chemistry Research Group, Department of Organic and Macromolecular Chemistry, Ghent University, Krijgslaan 281 S4-bis, B-9000 Gent, Belgium

E-mail: filip.duprez@ugent.be

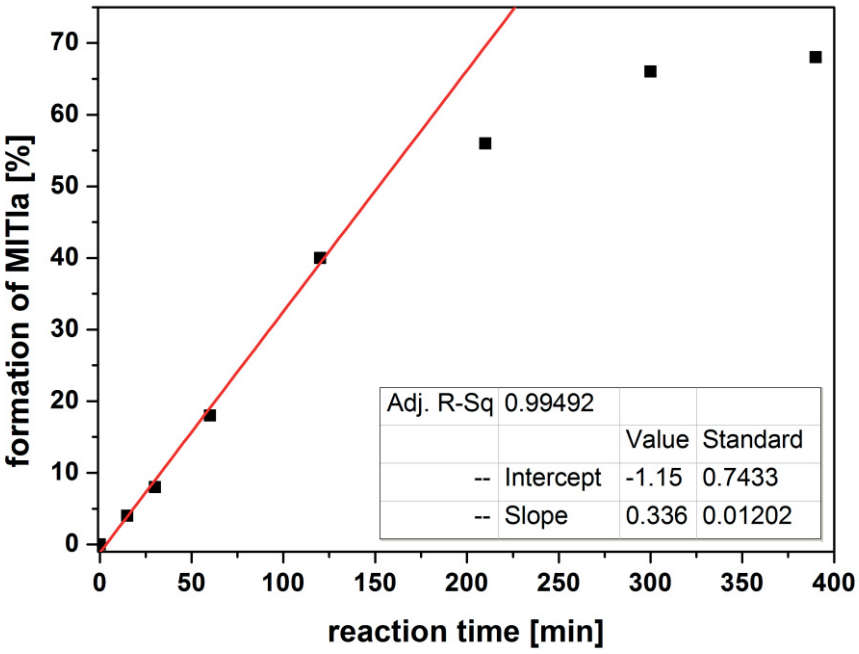

Figure S1: Kinetic investigation of the synthesis of MITla comparing the newly formed thiolactone signal at 4.95 ppm (DMSO- d_6) to trioxane as internal standard at 70 °C.

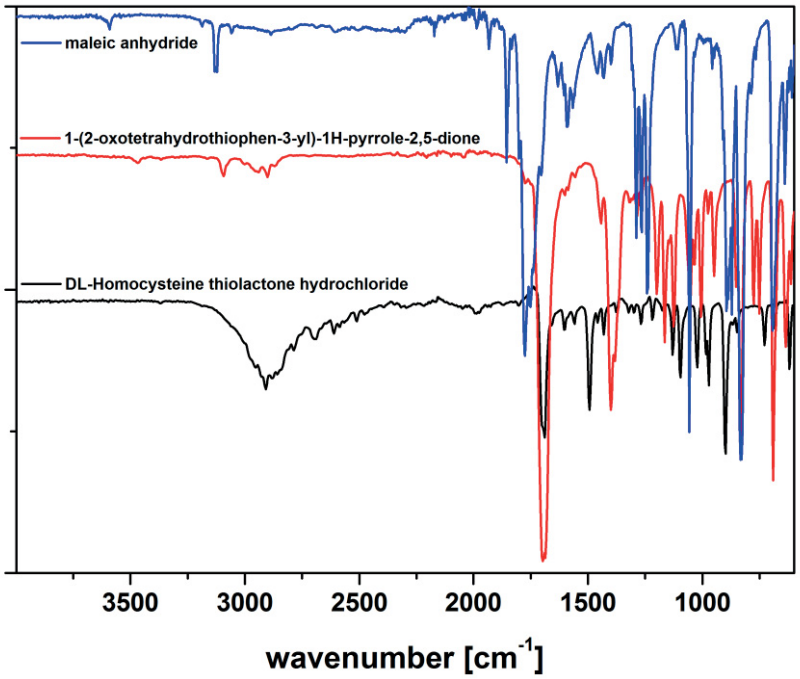

Figure S2: Comparison of FT-IR spectra for maleic anhydride (blue trace-), D,L-homocysteine thiolactone hydrochloride (black trace), and the desired maleimide thiolactone (IUPAC: 1-(2-oxotetrahdrothiophen-3-yl)-1H-pyrrole-2,5-dione; MITla, red trace).

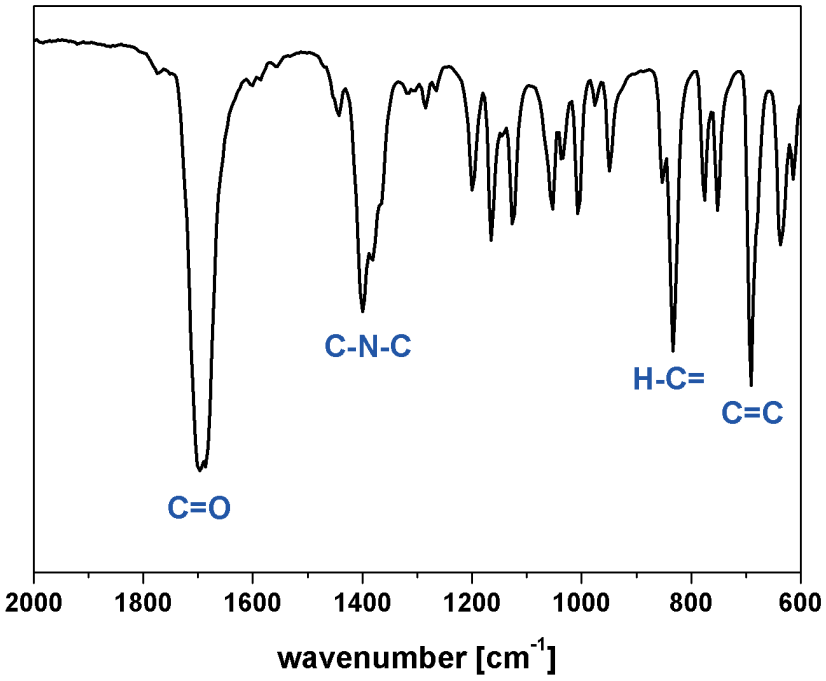

Figure S3: Enlarged FT-IR spectrum for MITla and the important signals for: carbonyls at 1689, C-N-C at 1400, and the maleimide double bond at 830 and 690 cm^{-1}.

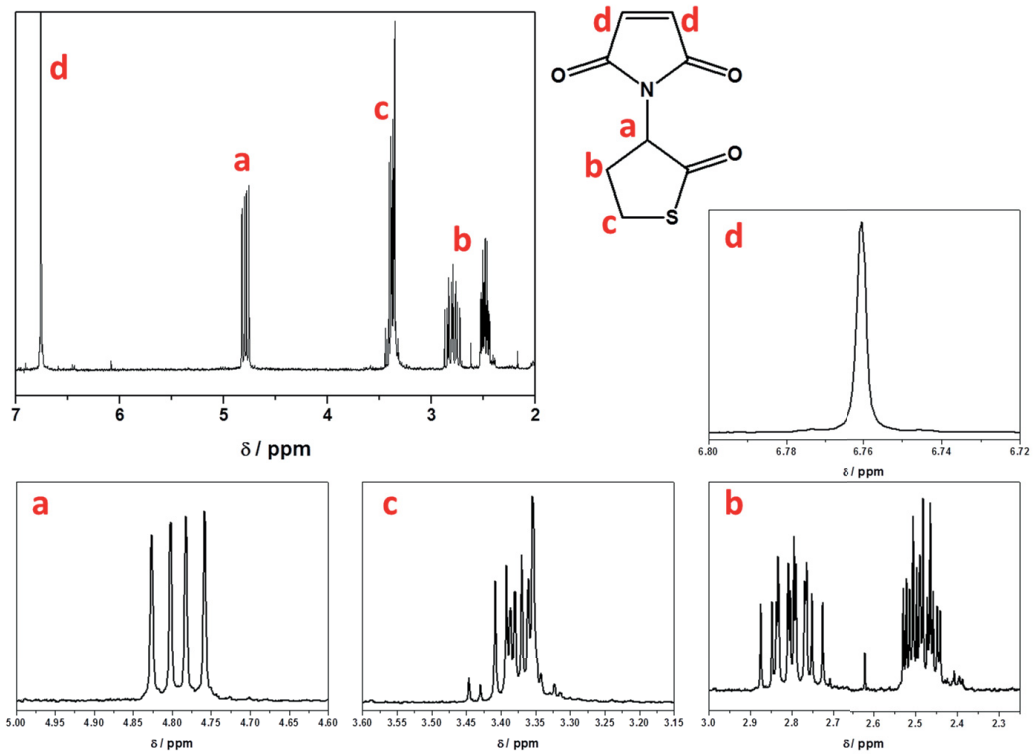

Figure S4: ^{1}H-NMR spectra of maleimide thiolactone (MITla) and peak assignment ($CDCl_3$, 300 MHz).

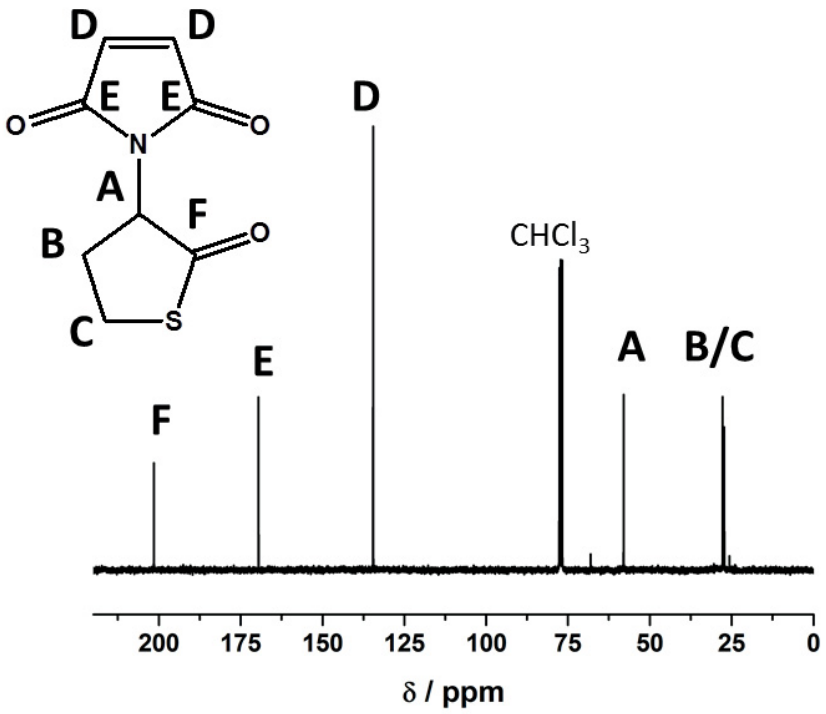

Figure S5: ^{13}C-NMR spectrum of maleimide thiolactone (MITla) ($CDCl_3$, 75 MHz).

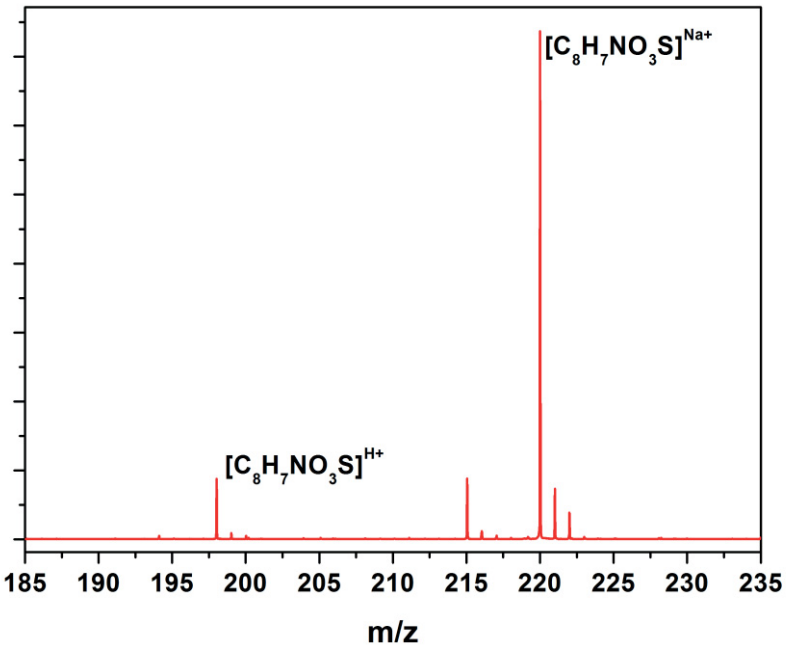

Figure S6: ESI-MS spectrum for MITla.

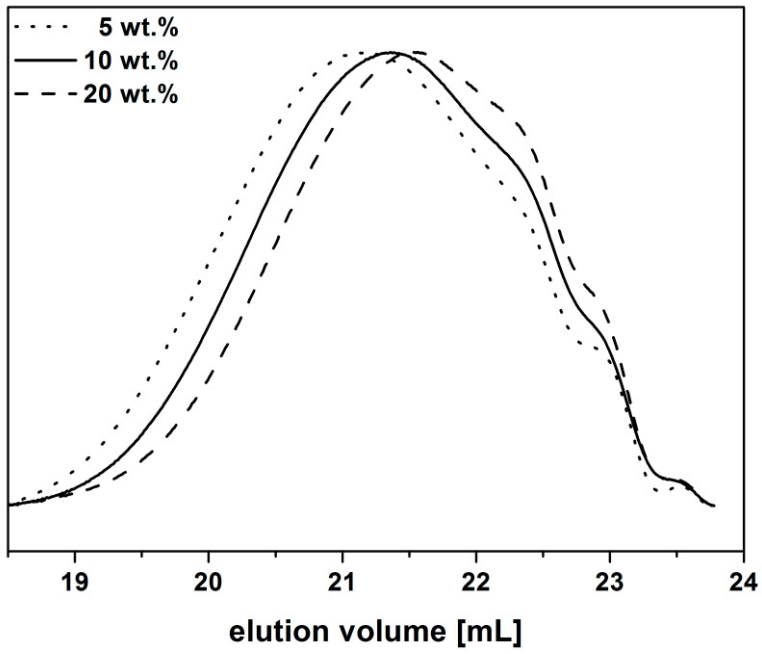

Figure S7: Comparison of SEC traces for the homopolymerization of MITla initiated by different amounts of TPO in solution (100 mg mL^{-1} DCM): 5 wt.% (dotted line), 10 wt.% (straight line), and 20 wt.% (dashed line).

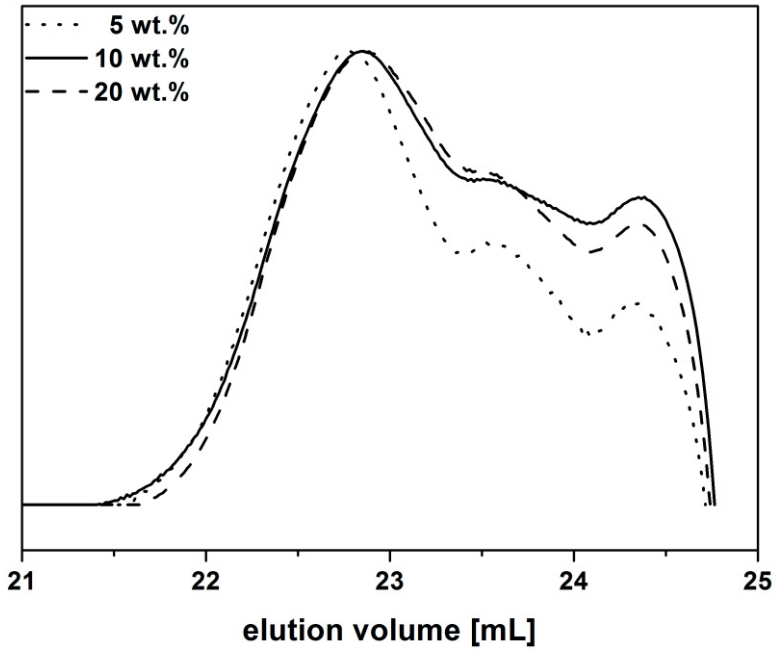

Figure S8: Comparison of SEC traces for the homopolymerization of MITla initiated by different amounts of AIBN in solution (100 mg mL^{-1} THF): 5 wt.% (dotted line), 10 wt.% (straight line), and 20 wt.% (dashed line).

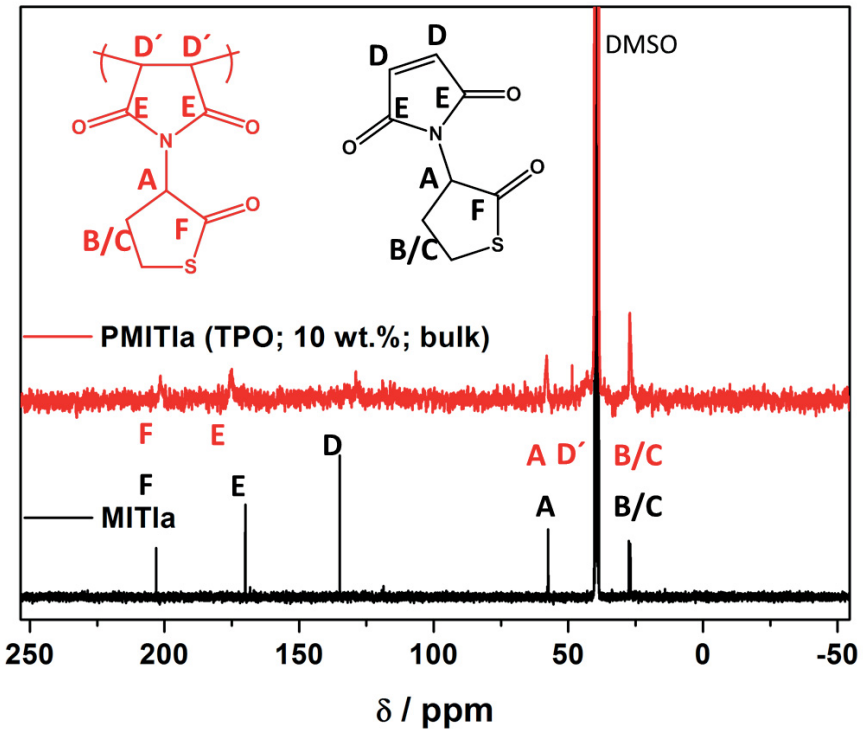

Figure S9: Comparison of ^{13}C-NMR traces for MITla (black trace) and PMITla (10 wt.% TPO, bulk; red trace) (DMSO-d_6 , 75 MHz).

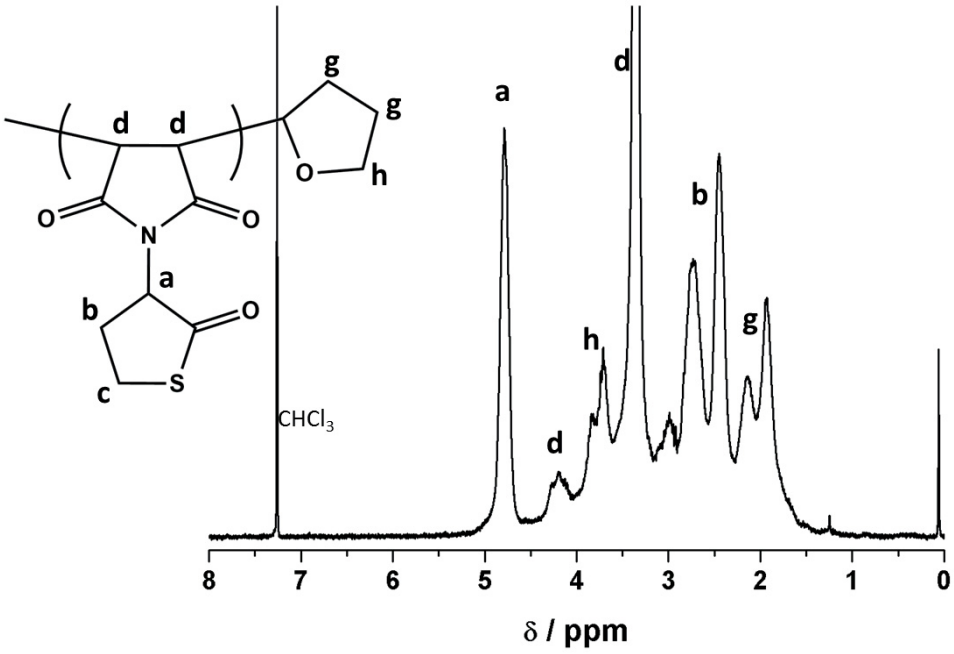

Figure S10: NMR spectrum for PMITla^{AIBN} initiated by AIBN in THF ($CDCl_3$, 300 MHz).

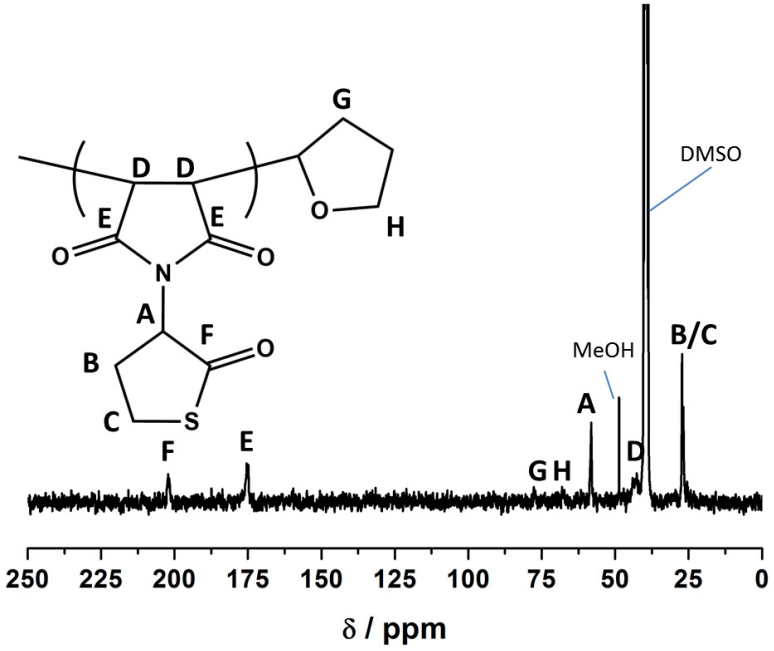

Figure S11: ^{13}C-NMR spectrum for PMITla^{AIBN} (DMSO-d_6 , 75 MHz).

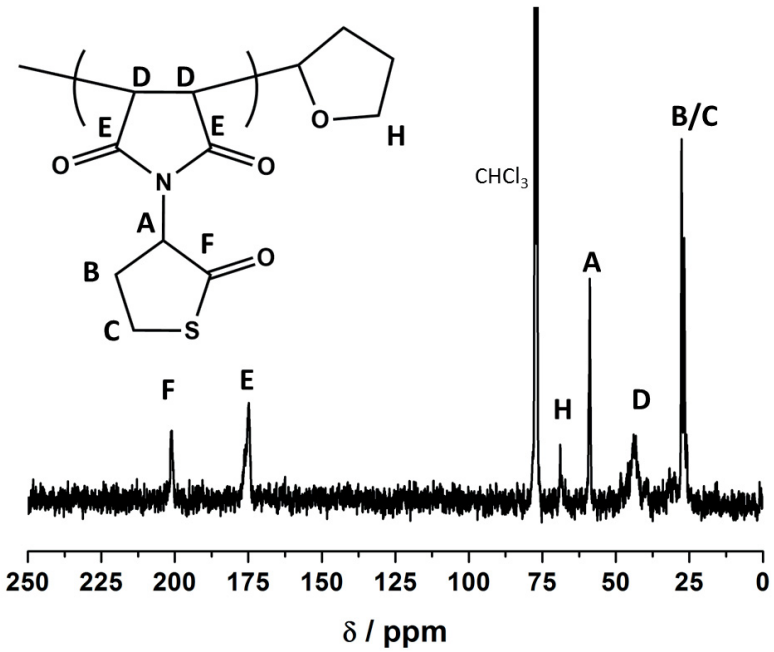

Figure S12: ^{13}C-NMR spectrum for PMITla^{AIBN} ($CDCl_3$, 75 MHz).

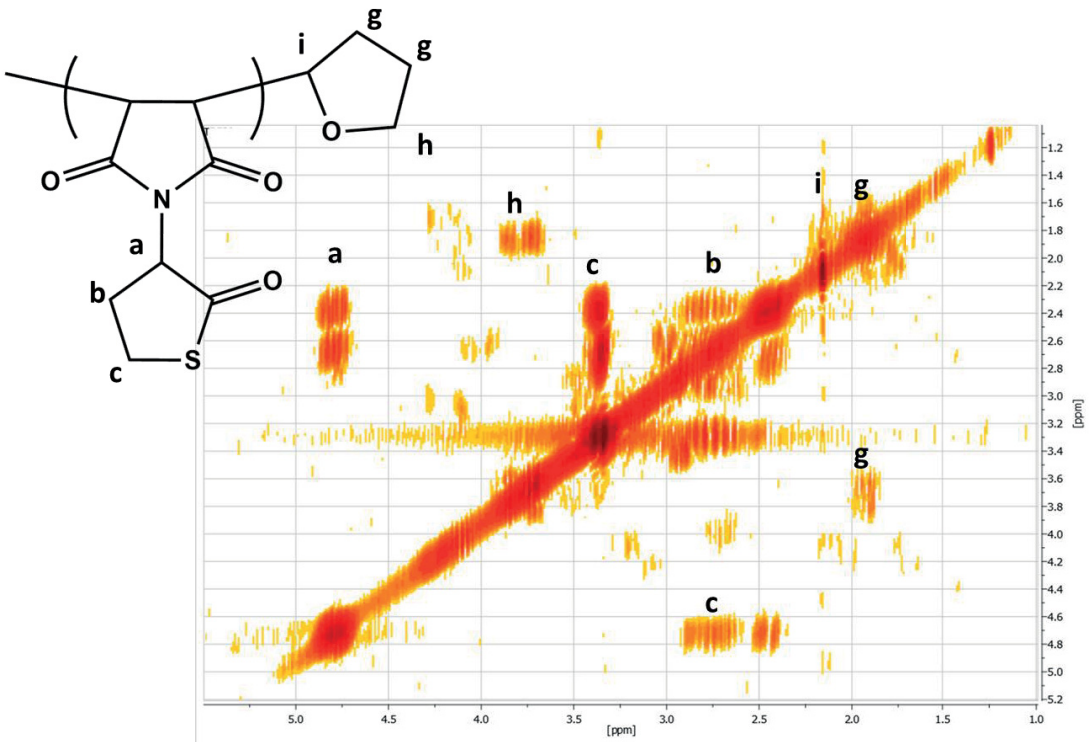

Figure S13: COSY spectrum for PMITla^{AIBN} initiated *via* AIBN in THF (300 MHz; $CDCl_3$).

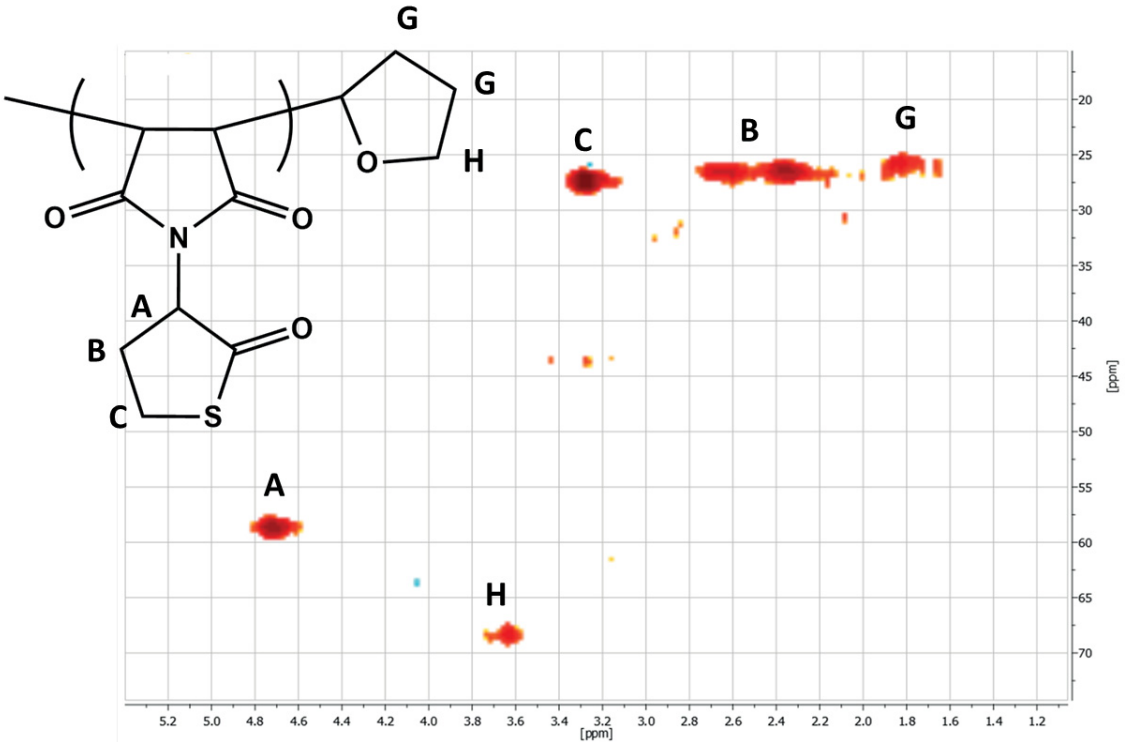

Figure S14: HSQC NMR spectrum for PMITla^{AIBN} initiated *via* AIBN in THF (300 MHz; $CDCl_3$).

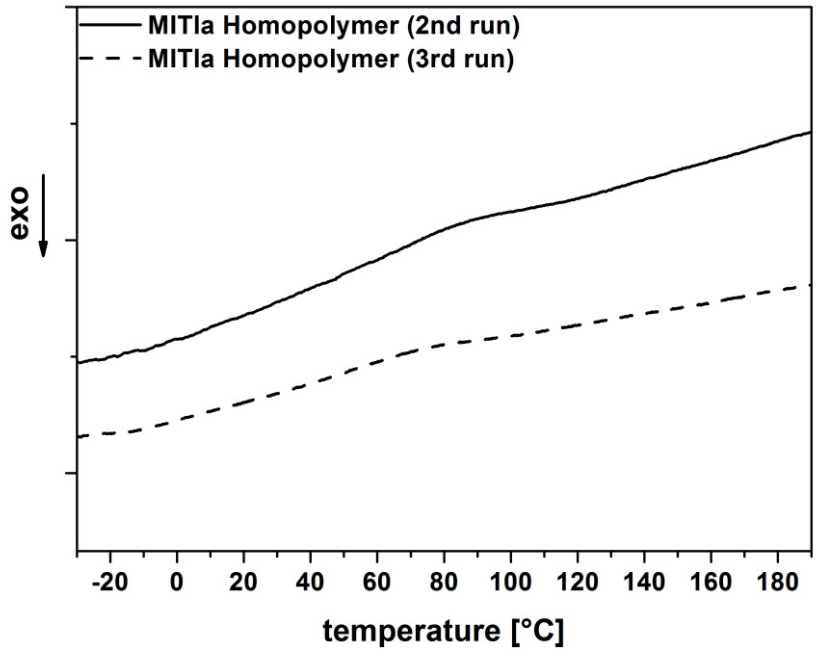

Figure S15: DSC thermogram for PMITIa^{TPO} in the temperature range of -30 to 200°C.

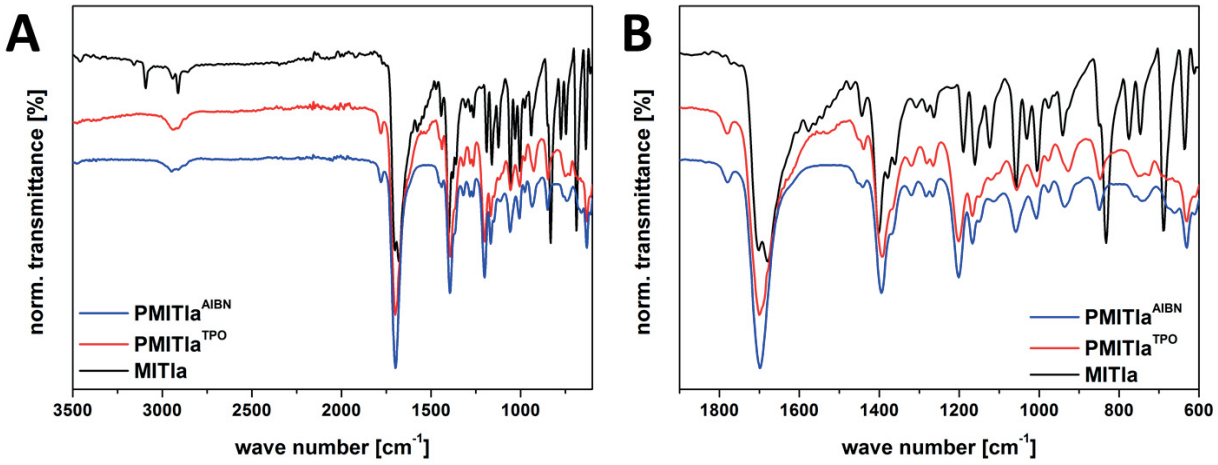

Figure S16: Comparison of FT-IR traces for PMITIa^{AIBN} (red trace) and PMITIa^{TPO} (black trace) (A) and an enlargement of the fingerprint region (B).

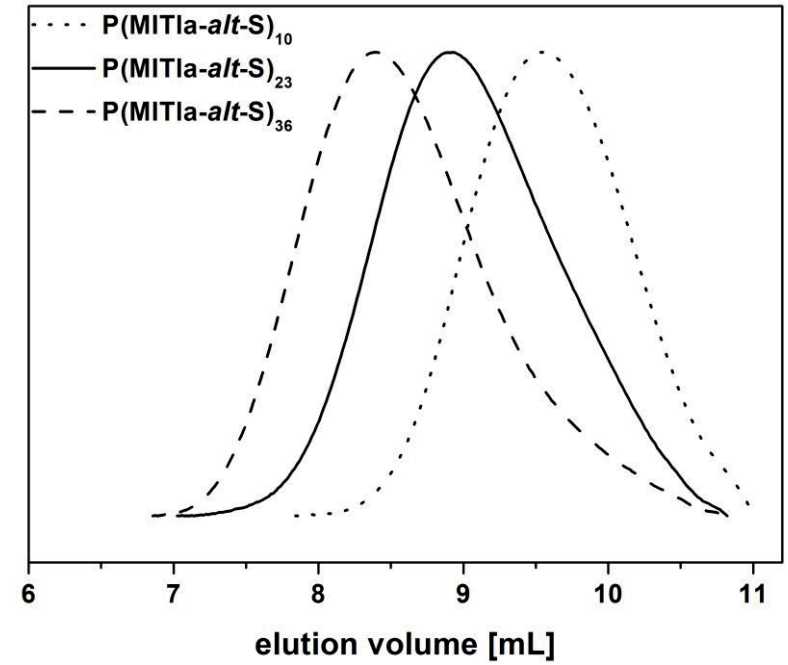

Figure S17: Comparison of SEC traces for P(MITla-*alt*-S)$_{10}$ (dotted line), P(MITla-*alt*-S)$_{23}$ (straight line), and P(MITla-*alt*-S)$_{36}$ (dashed line).

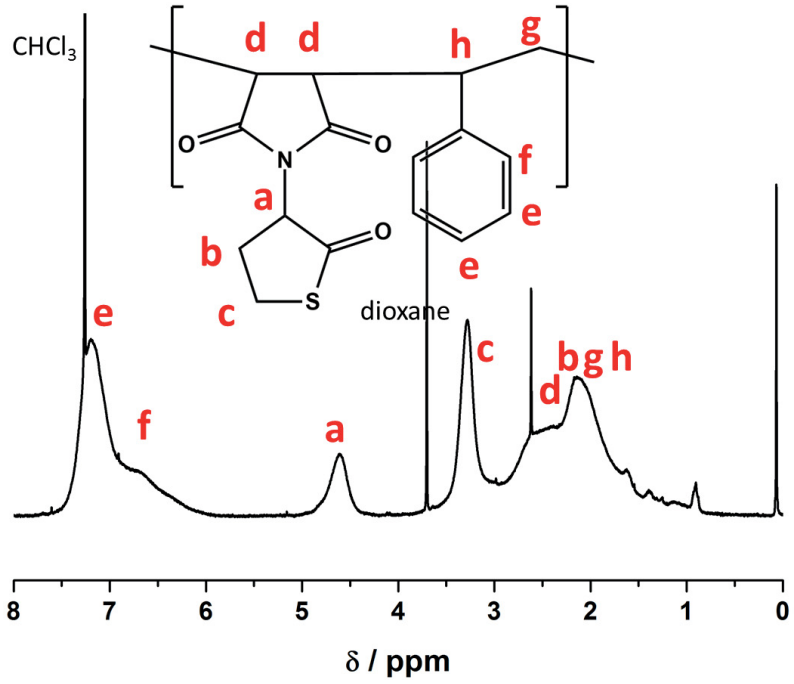

Figure S18: ^{1}H-NMR spectrum for P(MITla-*alt*-S)$_{23}$ and peak assignment (300 MHz; $CDCl_3$).

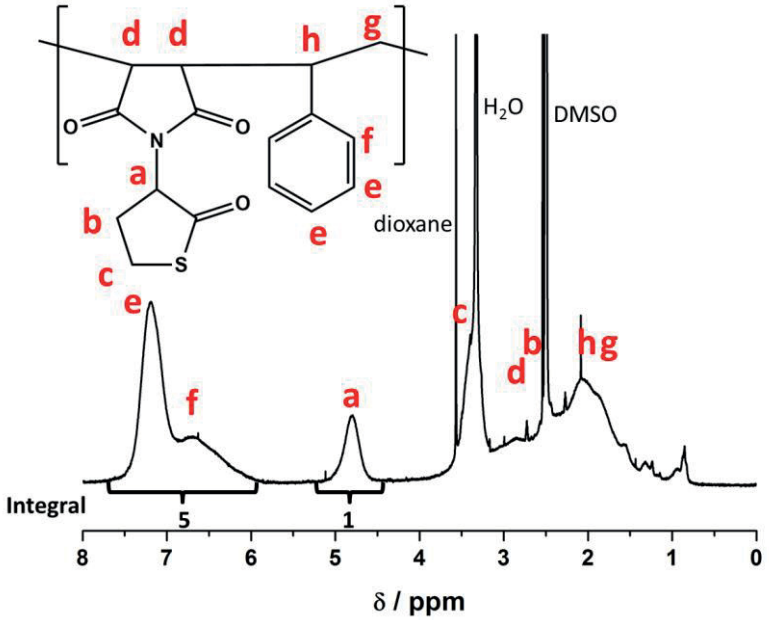

Figure S19: ^{1}H-NMR spectrum for P(MITla-*alt*-S)$_{23}$ and peak assignment (300 MHz; DMSO-d_6).

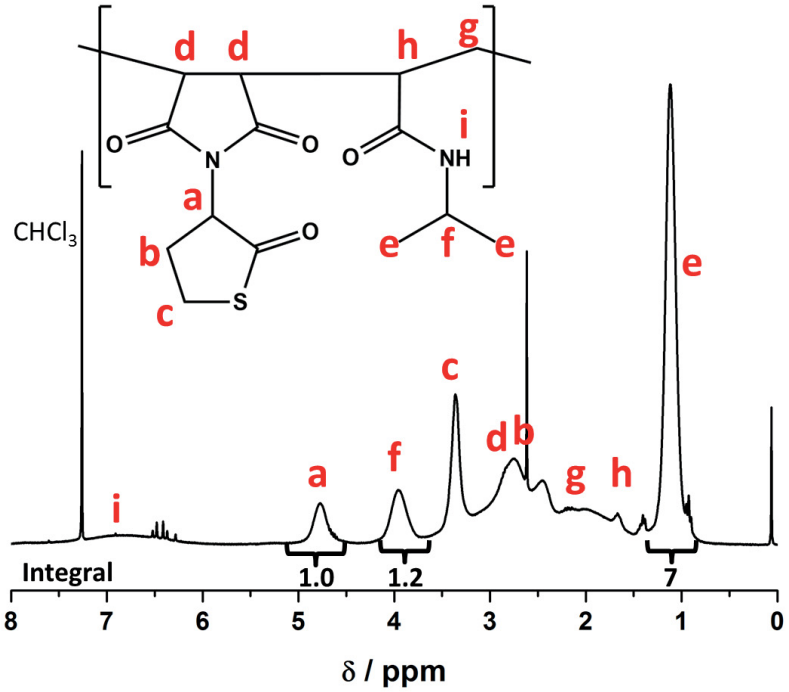

Figure S20: ^{1}H-NMR spectrum for P(MITla-*co*-NIPAAm)$_{23}$ and peak assignment (300 MHz; $CDCl_3$).

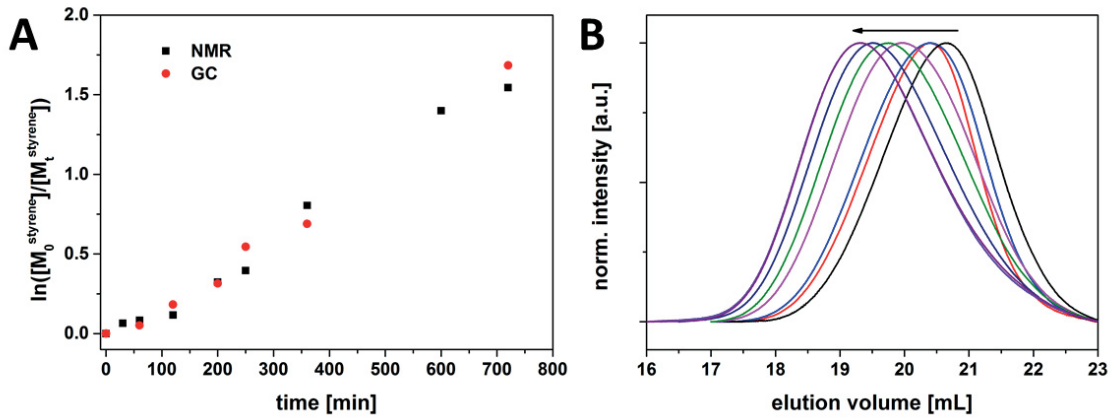

Figure S21: A) Time vs. styrene monomer conversion plot determined by NMR (black square) and GC (red dot) for the copolymerization of MITla and styrene; B) comparison of SEC traces for the kinetic investigation of the copolymerization of MITla and styrene using RAFT.

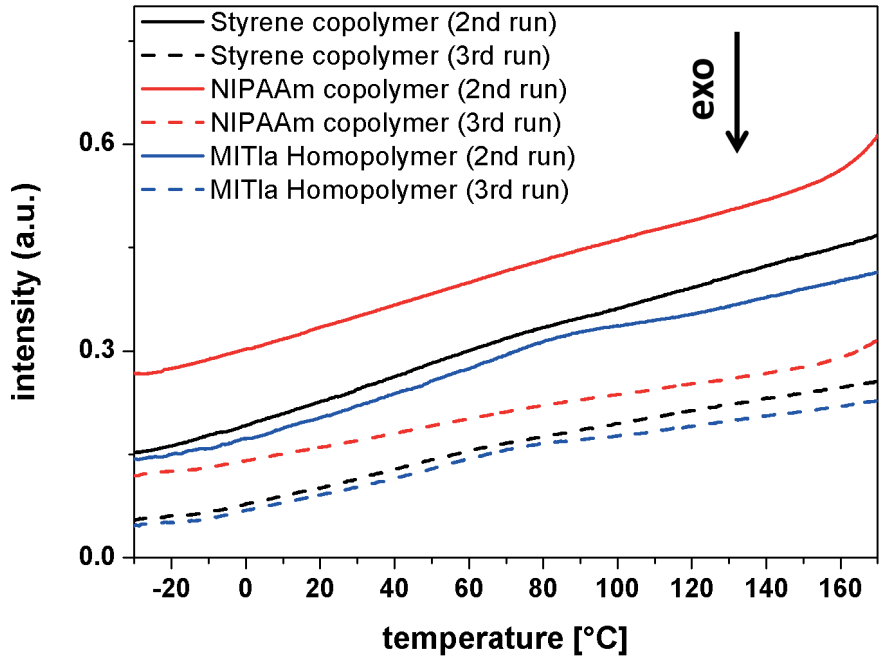

Figure S22: Comparison of DSC traces for P(MITla-*alt*-S)$_{23}$ (black lines), P(MITla-*co*-NIPAAm)$_{23}$ (red lines) and PMITla^{TPO} (blue lines) in the second (straight lines) and third (dashed lines) heating run.

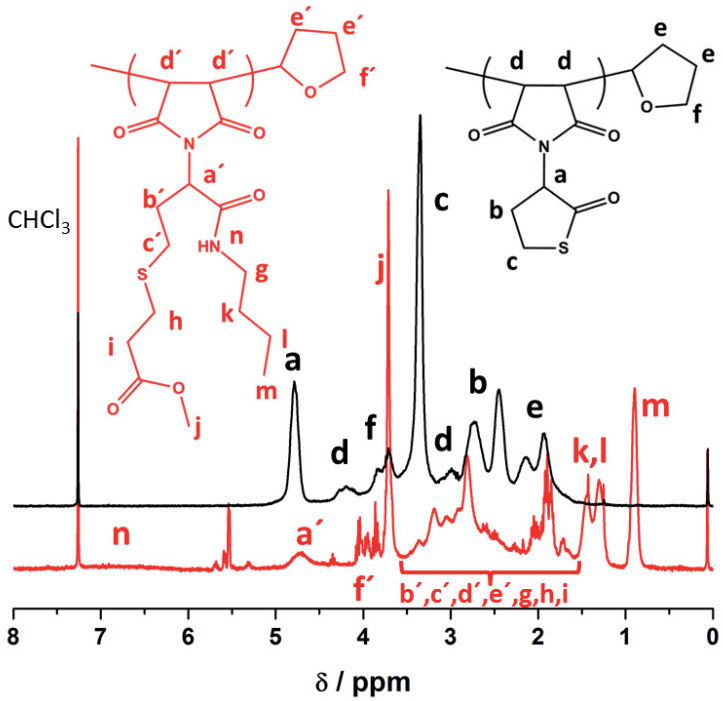

Figure S23: Comparison of NMR spectra for PMITla^{AIBN} before (black trace) and after (red trace) double modification *via n*-butylamine and methyl acrylate (300 MHz; $CDCl_3$).

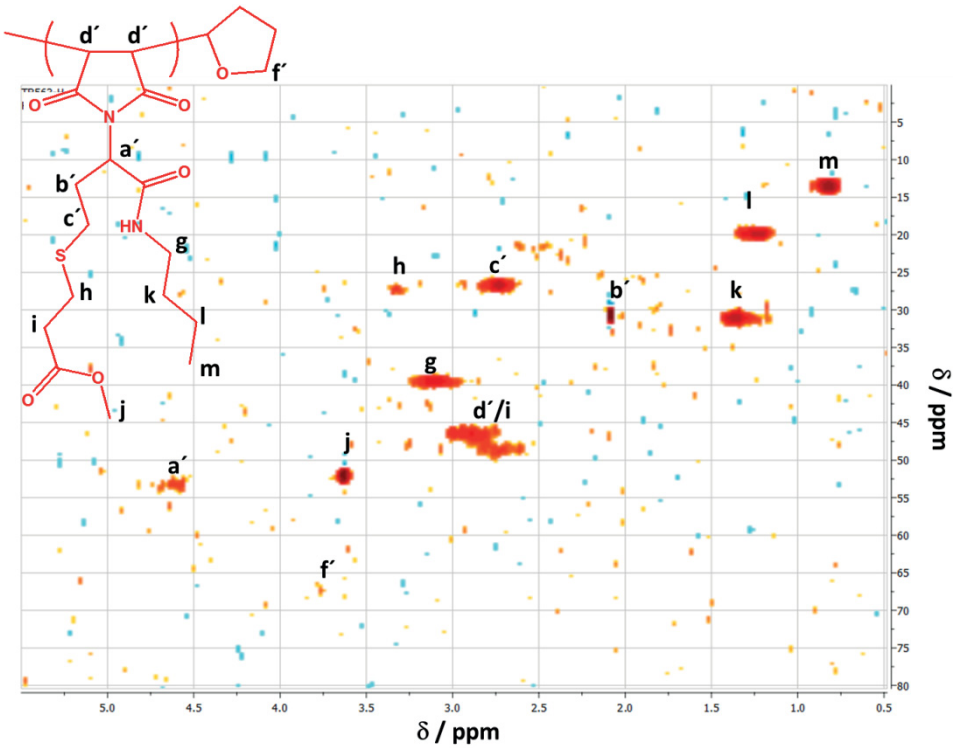

Figure S24: HSQC NMR spectra for PMITla^{AIBN,DM} initiated *via* AIBN in $CHCl_3$ by methyl acrylate and *n*-butylamine and peak assignment (300 MHz; $CDCl_3$).

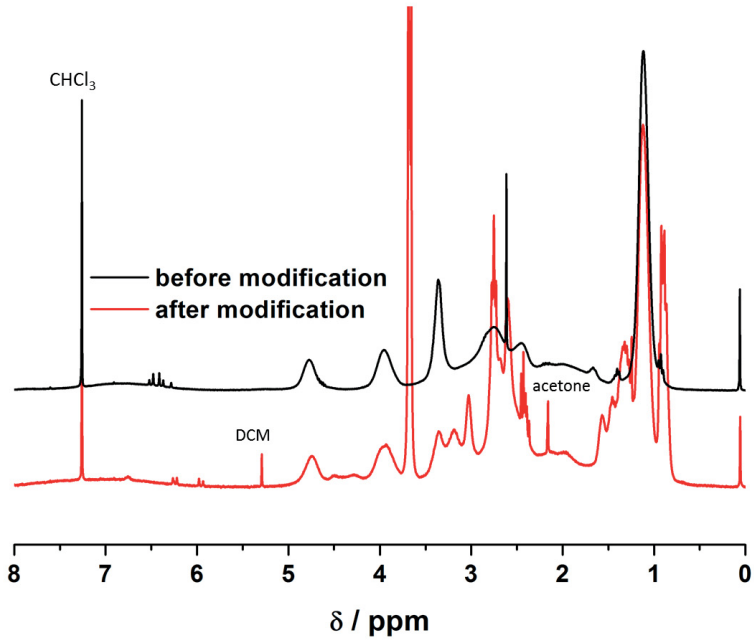

Figure S25: Comparison of NMR traces for P(MITla-*co*-NIPAAm)$_{23}$ before (black trace) and after (red trace) double modification *via n*-butylamine and methyl acrylate (300 MHz; $CDCl_3$).

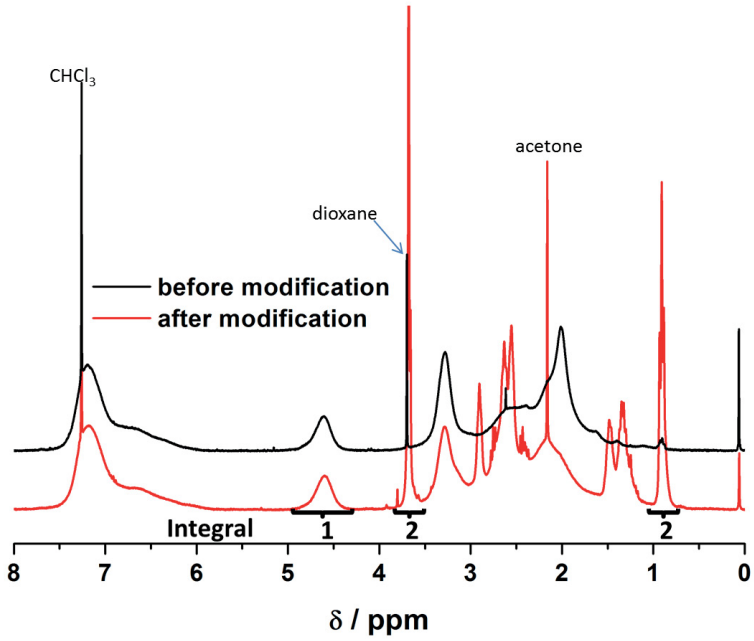

Figure S26: Comparison of NMR traces for P(MITla-*alt*-S)$_{36}$ before (black trace) and after (red trace) double modification *via n*-butylamine and methyl acrylate (300 MHz; $CDCl_3$).

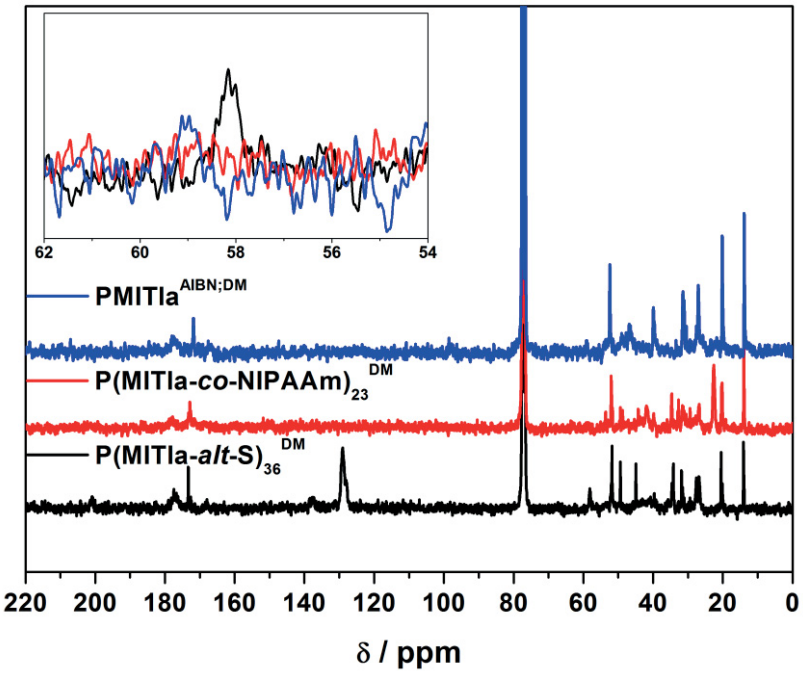

Figure S27: Comparison of ^{13}C-NMR traces for PMITIa^{AIBN,DM} (blue trace), P(MITIa-*co*-NIPAAm)$_{23}^{DM}$ (red trace), and P(MITIa-*alt*-S)$_{36}^{DM}$ (black trace); inset shows the signal at 58 ppm.

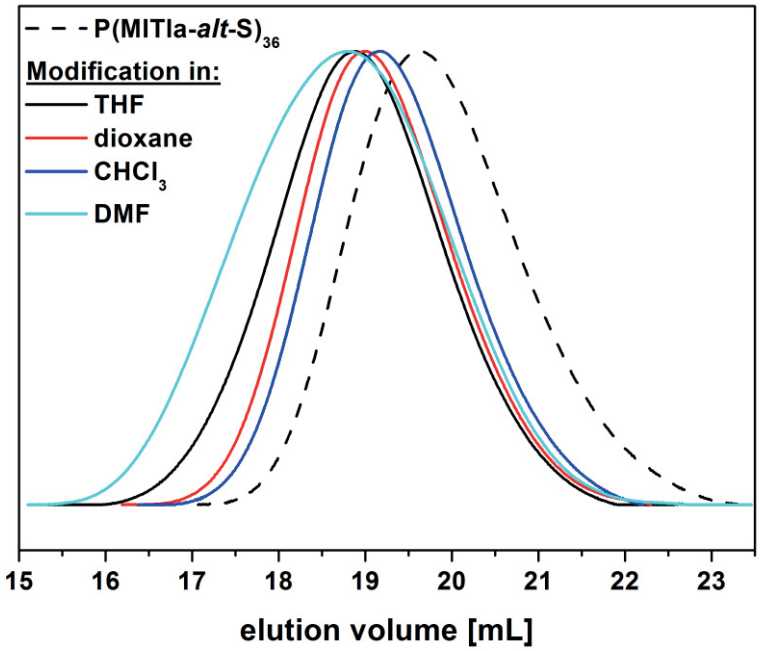

Figure S28: Comparison of SEC traces for the double modification by methyl acrylate and *n*-butylamine for P(MITIa-*alt*-S)$_{36}$ in different solvents: pristine P(MITIa-*alt*-S)$_{36}$ (dashed line), in THF (black line), in dioxane (red line), chloroform (blue line), DMF (blue line).

Table S1: Double modification of P(MITla-*co*-S)$_{36}$ by *n*-butylamine and methyl acrylate at different conditions (25 mg mL^{-1}).

Solvent	Reaction Time [h]	Further educt addition after	Estimated degree of functionalization [%][a]	M_n[b] [g mol^{-1}]	Đ[b]
DMF	48	24 h	40	19 600	1.55
THF	48	24 h	60	18 600	1.37
Dioxane	48	24 h	50	16 600	1.30
Chloroform	48	24 h	60	15 000	1.29

a) Degree of functionalization is estimated *via* ^{1}H-NMR (300 MHz; $CDCl_3$)
b) SEC (DMAC/LiCl): PS-calib.

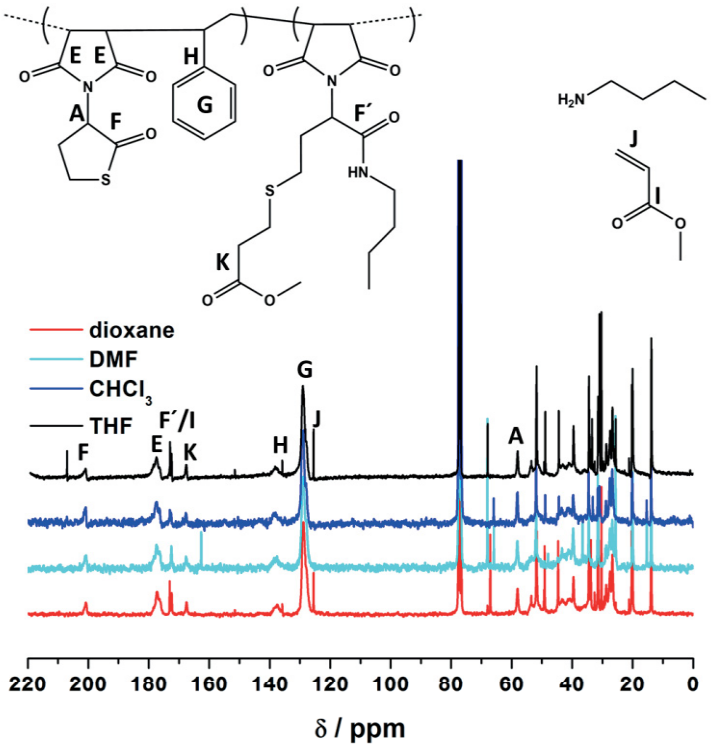

Figure S29: Comparison of ^{13}C-NMR spectra for double modification by methyl acrylate and *n*-butylamine for P(MITla-*alt*-S)$_{36}$ in different solvents: in THF (black line), in dioxane (red line), chloroform (blue line), DMF (blue line) (75 MHz; $CDCl_3$); (As polymers were only precipitated once before measuring NMR, educt signals are still observed).

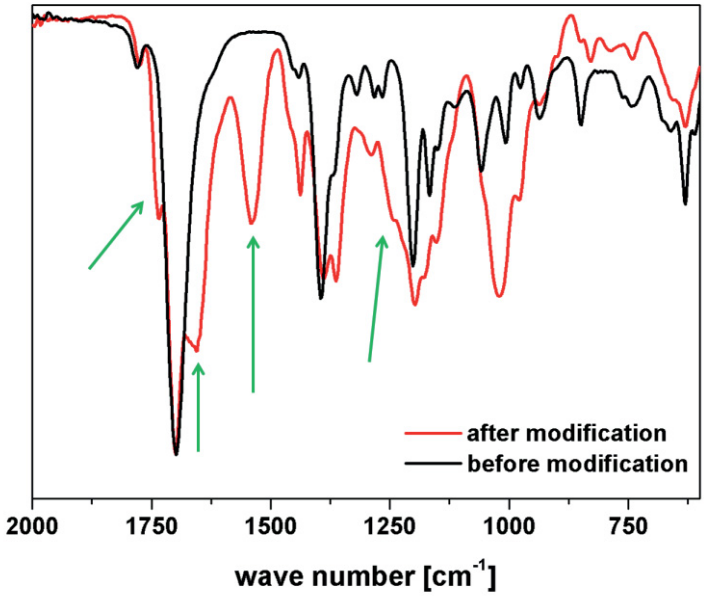

Figure S30: Comparison of FT-IR spectra for PMITla^{AIBN} before (black trace) and after (red trace) modification by methyl acrylate and *n*-butylamine.

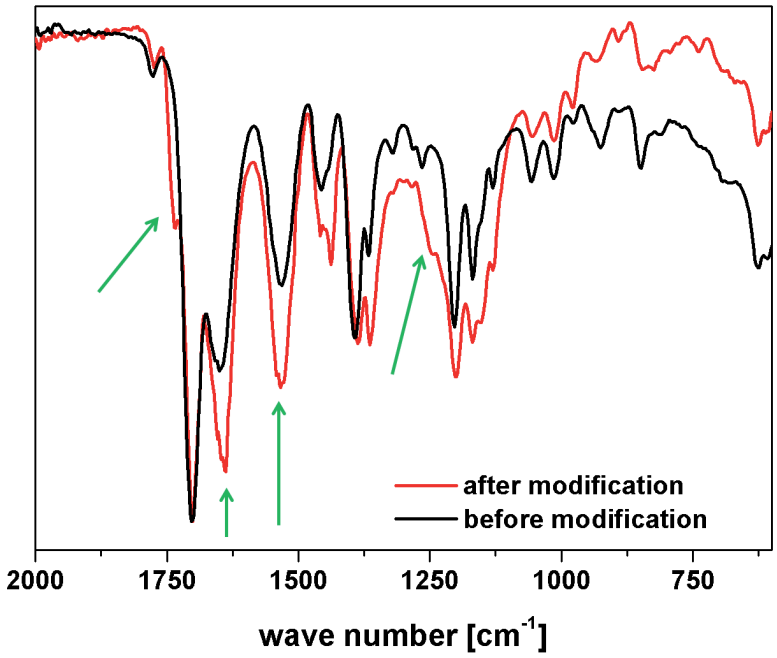

Figure S31: Comparison of FT-IR spectra for P(MITla-*co*-NIPAAm)$_{23}$ before (black trace) and after (red trace) modification by methyl acrylate and *n*-butylamine.

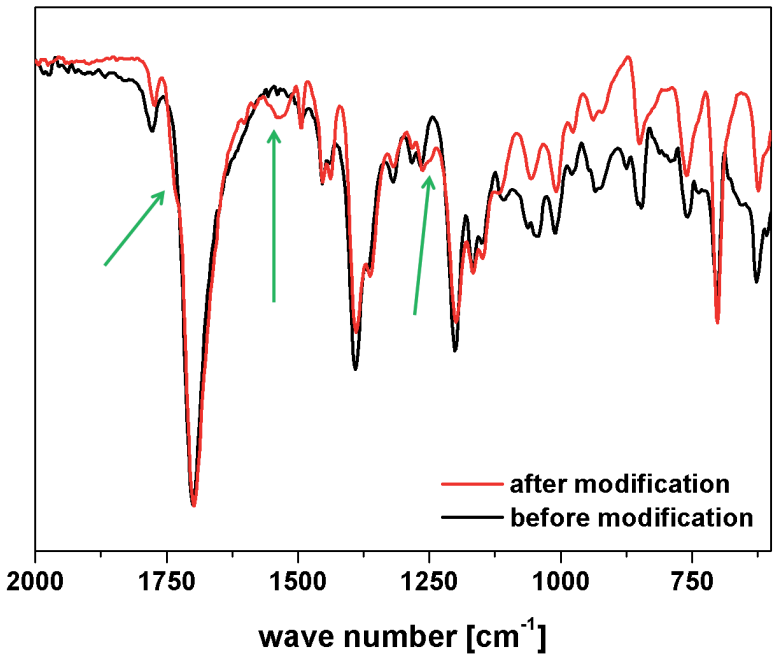

Figure S32: Comparison of FT-IR spectra for P(MITla-*co*-S)$_{36}$ before (black trace) and after (red trace) modification by methyl acrylate and *n*-butylamine.

Publication P12

"Hybrid Fe_3O_4@Amino Cellulose Nanoparticles in Organic Media: Heterogeneous Ligands for Atom Transfer Radical Polymerizations"

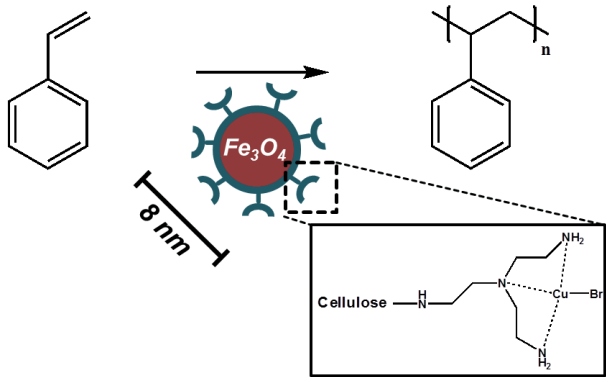

Ludmila C. Fidale, Melanie Nikolasjski, Tobias Rudolph, Felix H. Schacher, Thomas Heinze

J. Coll. Inter. Sci., **2013**, 390, 25-33

Journal of Colloid and Interface Science xxx (2012) xxx–xxx

Contents lists available at SciVerse ScienceDirect

Journal of Colloid and Interface Science

www.elsevier.com/locate/jcis

Hybrid Fe_3O_4@amino cellulose nanoparticles in organic media – Heterogeneous ligands for atom transfer radical polymerizations

Ludmila C. Fidale [a], Melanie Nikolajski [a], Tobias Rudolph [b,c], Silvio Dutz [d], Felix H. Schacher [b,c,*], Thomas Heinze [a,*]

[a] Friedrich-Schiller University Jena, Institute of Organic Chemistry and Macromolecular Chemistry, Center of Excellence for Polysaccharide Research, Humboldtstraße 10, D-07743 Jena, Germany
[b] Friedrich-Schiller University Jena, Institute of Organic Chemistry and Macromolecular Chemistry, Humboldtstraße 10, D-07743 Jena, Germany
[c] Jena Center for Soft Matter (JCSM), Friedrich-Schiller University Jena, Philosophenweg 7, D-07743 Jena, Germany
[d] Institute of Photonic Technology, Department of Nano Biophotonics, A.-Einstein-Straße 9, D-07745 Jena, Germany

ARTICLE INFO

Article history:
Received 8 June 2012
Accepted 11 September 2012
Available online xxxx

Keywords:
Hybrid particles
Magnetic nanoparticles
Amino cellulose
ATRP

ABSTRACT

We demonstrate an efficient strategy for the preparation of well-dispersed hybrid particles in organic media *via* a combination of the solution-based formation of magnetic nanoparticles (MNPs) and subsequent coating with amino celluloses of different degrees of polymerization. The coating process was verified by a combination of light scattering, thermogravimetry, and magnetic techniques. Further, the hybrid particles exhibit an average diameter of roughly 8 nm, as demonstrated by electron microscopy and light scattering. The stability of the so-called MNP@AC_x hybrid particles (x represents the average degree of polymerization of the amino cellulose) in polar organic solvents such as DMAc was exploited by using the materials as heterogeneous ligands in the atom transfer radical polymerization (ATRP) of styrene. We could show that PS with a near-narrow molecular weight distribution (PDIs < 1.3) and low Cu contents (5 ppm) can be prepared. The MNP@AC_x particles could be separated from the reaction mixture afterwards by an external magnetic field and reused in further polymerizations.

1. Introduction

During the last decades, the field of nanotechnology, in particular the synthesis and characterization of metal nanoparticles (NPs), has gained considerable interest in a variety of disciplines, including chemistry, physics, biology, biotechnology, and medicine. The development of efficient routes for the preparation of functional nanomaterials represents one current research focus [1]. Due to their size, nanoparticles exhibit unique properties, for example, a large surface-to-volume ratio and highly active surface sites, which renders them promising candidates for a wide range of applications [2–4]. More specific, metal NPs have already been applied as carriers for drug targeting [5–7], contrast enhancement [8,9], chromatographic separations [10], or for the encapsulation of enzymes [11], Among those, magnetic nanoparticles (MNP, e.g., Fe_3O_4) have been widely employed for cell labeling and separation [12], as contrast agents during magnetic resonance imaging (MRI) [13], as magnetic ferrofluids for hyperthermia treatment [14], and for the separation of enzymes and proteins [15]. The physical background for all these applications is the response of these MNPs to external magnetic fields.

The coating of MNPs or, in general, inorganic NPs with potentially biocompatible polymeric materials is a facile way to improve the solution stability for such hybrid structures, prevent agglomeration, aid the in vivo distribution, or even target specific microenvironments. Therefore, simple and economical routes for the preparation of MNP@polymer hybrids are an important topic. Current approaches include MNPs coated with amino acids (L-glutamic acid and L-lysine monohydrochloride) [16], silica shells [17], polydiacetylene [18], poly(vinyl alcohol) [19], or polysaccharides, such as dextran [20], carboxymethyl dextran, -pullulan, and carboxymethylated cellulose [21].

Further applications of MNP@polymer hybrid particles include the removal of traces of heavy metal ions in solution, for example, for water purification, as has been shown for MNP@SiO_2 where Bismuthiol II could be immobilized. The resulting nanoparticles could be used as a solid-phase extraction adsorbent for the removal of traces of Cr, Cu, and Pb from environmental aqueous samples [22]. The selective complexation of immobilized ligands on MNPs has also been used in heterogeneous atom transfer radical polymerizations (ATRPs), where *N,N,N′,N″*-tetraethyldiethylenetriamine-grafted MNPs were shown to be suitable ligands for the controlled radical polymerization of methyl methacrylate [23].

* Corresponding authors. Address: Jena Center for Soft Matter (JCSM), Friedrich-Schiller University Jena, Philosophenweg 7, D-07743 Jena, Germany (F.H. Schacher).
E-mail addresses: felix.schacher@uni-jena.de (F.H. Schacher), thomas.heinze@uni-jena.de (T. Heinze).

0021-9797/$ - see front matter © 2012 Elsevier Inc. All rights reserved.
http://dx.doi.org/10.1016/j.jcis.2012.09.019

The atom transfer radical polymerization (ATRP) process is among the most effective and versatile methods for controlled/living radical polymerizations (CRPs) [24–26]. ATRP has been investigated extensively and a huge variety of polymers with well-defined properties or topologies are accessible, as well as the modification of surfaces, or the preparation of block copolymers [27–30]. One drawback of ATRP is the presence of a transition metal catalyst, typically Cu, in the order of 0.1–1 mol% relative to the used monomer. This may cause environmental problems and therefore limits an industrial application. Further, depending on the synthesized polymers, it can be difficult to remove the catalyst afterwards from the polymeric materials generated. Several approaches have been developed to circumvent these problems: for example, reducing agents can be used to continuously regenerate the active Cu(I) in activators regenerated by electron transfer (ARGET) ATRP processes [31]. The immobilization of the catalyst on a solid support, for example, silica and crosslinked polystyrene beads, is another strategy for the regeneration and the recycling of Cu [32]. Other approaches include the use of ionic liquids [33,34] or solvent mixtures [35] during the polymerization, the catalyst removal using ion exchange resins [36], or ligands containing alkoxysilyl groups which also complex Cu [37].

Polysaccharides are unique biopolymers with an enormous structural diversity. Cellulose is a renewable, biodegradable, and non-fossile polysaccharide most abundant in nature, which has attracted great interest in academic and industrial life. In addition, cellulose can be easily derivatized to produce industrial products, which are used in different fields, like shown for pharmaceutical products, or the food, textile, and paper industry [38]. Moreover, studies revealed that films formed by aliphatic amino celluloses can be used for the immobilization of biomolecules, creating opportunities for the preparation of biosensors, bioreactors, and immunoassays [39].

In this work, we demonstrate an efficient strategy for the formation of Fe_3O_4@aminocellulose hybrid nanoparticles. The materials are well-dispersed in DMAC afterwards and can be used as heterogeneous ligands in the Cu-mediated controlled radical polymerization of styrene (Fig. 1). The so-called amino cellulose used for the coating of MNPs was 6-deoxy-6-(2-(bis(2-aminoethyl) aminoethylamino) cellulose (AC). The material has been synthesized using established techniques and with different degrees of polymerization, DP (Avicel, DP = 250, AC250; degraded cellulose fiber, DP = 50, AC50).

The coating process was carried out in dilute solution at elevated temperatures, and the hybrid particles were characterized using X-ray diffraction (XRD), magnetization measurements, transmission electron microscopy (TEM), and dynamic light scattering (DLS) afterwards. The MNP, coated and uncoated, proved to be stable in aqueous media, even after a long period. Further, the coating with amino cellulose rendered well-dispersed hybrid nanoparticles in polar organic solvents, such as *N*,*N*-dimethylacetamide (DMAc) or dimethylsulfoxide (DMSO). The structure of the amino-moieties of AC50 and AC250 is similar to commonly used ligands in atom transfer radical polymerizations, such as *N*,*N*,*N*′,*N*′,*N*″-pentamethyldiethylenetriamine (PMDETA), as shown in Fig. 1. We therefore used such Fe_3O_4 @amino cellulose hybrid NPs (MNP@AC_x, where the subscript corresponds to the estimated degree of polymerization of the amino cellulose) as heterogeneous ligands in the ATRP of styrene and near-narrow molecular weight distributions with polydispersities lower than 1.3 could be accomplished. Even more, the hybrid particles could be easily removed after the polymerization by an external magnetic field and reused in further reactions. The polymers generated via this approach showed very low Cu contents (~5 ppm), comparable to those reported for state-of-the-art ARGET methodologies.

2. Experimental

2.1. Materials

Microcrystalline cellulose, Avicel PH 101, was purchased from Fluka with DP = 250, and cellulose with DP = 50 was achieved after degradation of the regenerated fibers [40]. All solvents and reagents were purchased from Acros or Sigma–Aldrich and were purified as recommended elsewhere [41]. $FeCl_3 \cdot 6 \times H_2O$ and $FeCl_2 \cdot 4 \times H_2O$ (Sigma) were used as received. Styrene was

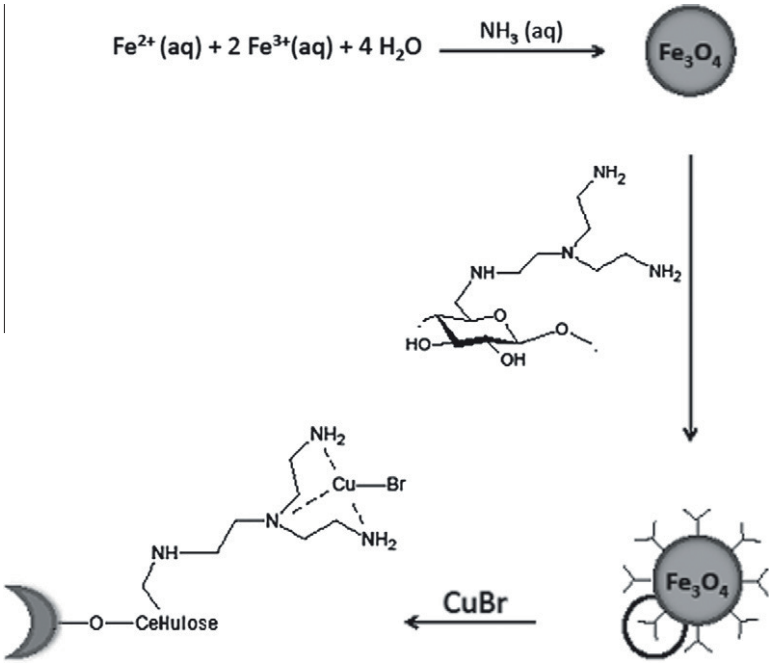

Fig. 1. Synthesis of the Fe_3O_4 nanoparticles, coating with amino cellulose, and complexation of CuBr during heterogeneous ATRP procedures.

filtered over aluminum oxide to remove any inhibitors prior to polymerization.

2.2. Synthesis of 6(2)-O-tosyl cellulose (TC)

6(2)-O-tosyl cellulose was synthesized by reacting celluloses (DP, 50 and 250) with tosyl chloride (TosCl) and triethylamine, TEA in *N*,*N*-dimethylacetamide/lithium chloride (DMAc/LiCl) under homogeneous conditions according to Rahn [42]. The molar ratio of the anhydroglucose unit (AGU) and reagents was 1:2:4 (AGU/TosCl/TEA), yielding a product with a degree of substitution (DS) of 1.0. The DS was determined by elemental analysis (sulfur content).

Elemental analysis: C 48.77, H 4.98, S 10.60.

FTIR (KBr): 3550 ν(OH), 3074 ν(=CH), 2030 ν(CH), 1598 ν(C=C), 1367 δ(CH) and $\nu_{as}(SO_2)$, 1119 ν(C—O—C), 814 δ(C=H) cm^{-1}.

^{13}C NMR (DMSO-d_6): δ 144.7–127.4 (tosylate aromatics), δ 105–65 (cellulose backbone), 20.7 (CH_3) ppm.

2.3. Synthesis of 6-deoxy-6-(2-(bis(2-aminoethyl)aminoethylamino) cellulose (AC)

The samples of AC were synthesized via 6(2)-O-tosyl cellulose (DS = 1.0) with tris(2-aminoethyl)amine according to a method described elsewhere [43]. 2 g of TC was dissolved in 20 mL DMSO and heated to 100 °C, under an inert atmosphere. The amine was added as a 25-fold excess compared to the amount of AGU units present. The solution was stirred for 6 h at 100 °C. The product was precipitated in acetone and washed several times with isopropanol. The sample was dried under reduced pressure for analysis. For our purpose, 2% w/w stock aqueous solutions was prepared. The AC was obtained with a DS of 0.80, as determined from the elemental analysis, and the product was characterized by ^1H NMR and ^{13}C NMR spectroscopy (Table S1). The remaining amount of tosylate moieties (DS_{Tos}) was around 0.05. The tosylate anion was exchanged against chloride afterward.

Elemental analysis: C 50.27, H 8.92, N 15.31, S 1.27.

2.4. Preparation and coating of magnetic nanoparticles (MNPs)

MNPs were obtained by alkaline hydrolysis of iron(II) and iron(III) chloride (molar ratio 1:2) in aqueous solution according to the co-precipitation method described previously [44]. The pH value of the resulting suspension was 2.2, and the conductivity was 1.2 mS/cm.

The surface modification was carried out by adding a solution of 6-deoxy-6-(2-(bis(2-aminoethyl)aminoethylamino) cellulose (2 wt.%) to an aqueous solution of the MNP (10 mg/mL). The resulting mixture (1:1 v/v) was heated at 70 °C for 2 h. MNP@AC_{50} and MNP@AC_{250} were isolated by applying an external magnetic field and washed five times with 20 mL of deionized water. One part of the product was frozen and freeze-dried for further analysis. The MNP-AC were stored in water and treated with ultrasound. For the transfer of the particles into DMAc, washing was performed for five times with 30 mL of DMAc.

2.5. ATRP of styrene

Polymerizations were carried out in DMAc as the solvent, and each entry in Table 2 represents an individual experiment. Therefore, the coated MNPs were transferred from water to DMAc. Both MNP@AC_{50} and MNP@AC_{250} were stored in 5 ml of DMAc (40 mg/mL) and treated with ultrasound prior to the experiments.

The experiments were performed using sealed flasks (Schott) under an inert atmosphere. Initially, stock solutions were prepared, and from those stock solutions, portions were taken to ensure the exact concentration of the reagents. In a typical reaction, MNP@AC_x stored in 5 mL of DMA, monomer (styrene, 22 mg, 0.21 mmol), and 1,3,5-trioxane (46 mg, 0.51 mmol), an internal standard for the control of the conversion via NMR spectroscopy, were added to a dry flask. The mixture was degassed for 15 min with nitrogen and afterwards CuBr (0.30 mg, 2.13 μmol) was added under nitrogen flux. In a second sealed flask, the initiator, methyl α-bromoisobutyrate (0.38 mg, 2.11 μmol) in 1 mL of DMA was degassed and transferred to the reaction flask *via* syringe subsequently. The sealed flask was placed in a shaker set to a temperature of 70 °C for 3 days. The ratio of reagents was 100: 1.01: 1.0: 1.3 for monomer, CuBr, initiator, and ligand, respectively.

In order to compare the results of the polymerization with MNP@AC_x, a standard reaction was performed using *N*,*N*,*N*′,*N*′,*N*″-pentamethyldiethylenetriamine, PMDETA, as a ligand. The reaction was carried out under the same experimental conditions and with the same ratio of reagents (M/Cu/I/L = 100:1.01:1:1.3).

2.6. Separation and reuse of the heterogeneous ligands

The MNP@AC_x were separated from the polymerization solution using an external magnetic field gradient afterwards. The remaining solution containing the polymer and eventually unreacted monomer was removed from the flask *via* syringe, and the MNP@AC_x were washed (1 × 5 mL) with degassed DMAc. Then, further 5 mL of degassed DMAc was added and the MNP@AC_x solution subjected to ultrasound. The same concentration of reagents as used during the first run and additional ascorbic acid (0.17 mg, 1.0 μmol) were added and the mixture was degassed for 15 min. The initiator, methyl α-bromoisobutyrate in 1 mL of DMAc was degassed, and transferred to the reaction flask *via* syringe. The second run was carried out at 70 °C for 3 days, as described earlier.

3. Characterization of MNP and MNP@AC_x

3.1. X-ray diffraction (XRD)

XRD measurements were performed with an X'Pert-Twin diffractometer (Philips, Eindhoven, Netherlands), using Cu Kα radiation.

3.2. Thermogravimetrical analysis (TGA)

Thermogravimetric analysis (Netzsch STA409, Selb, Germany) was used to determine the amount of adsorbed amino cellulose. The measurement was carried out under nitrogen atmosphere from 30 °C to 500 °C, with a heating rate of 10 °C/min.

3.3. Magnetization measurements

The magnetic properties of MNP and MNP@AC_x were determined using a Micromag vibrating sample magnetometer model Micromag 3900 (Princeton, USA). The measurements were carried out at room temperature.

3.4. Transmission electron microscopy (TEM)

The morphology and size of the MNP and MNP@AC_x were analyzed using a TEM (Zeiss-CEM 902A, Oberkochen, Germany) operating at 80 kV. Images were recorded using a 1 k TVIPS FastScan CCD camera. The TEM samples were prepared by applying a drop of the sample solutions onto the surface of a carbon coated copper grid (Quantifoil Micro-Tools GmbH, Jena, Germany).

Please cite this article in press as: L.C. Fidale et al., J. Colloid Interface Sci. (2012), http://dx.doi.org/10.1016/j.jcis.2012.09.019

3.5. Dynamic light scattering (DLS)

DLS measurements were performed on an ALV CGS-3 setup equipped with a He–Ne laser operating at a wavelength of $\lambda = 632.8$ nm and at a scattering angle of 90°. The CONTIN algorithm was applied to analyze the obtained correlation functions. Apparent hydrodynamic radii were calculated according to the Stokes–Einstein equation.

Further DLS and zeta potential measurements of the MNP and MNP@AC_x in solution were performed using a Zetasizer Nano ZS (Malvern Instrument, Worcestershire, UK), equipped with a He–Ne Laser operating at 633 nm and at a scattering angle of 173°. The obtained hydrodynamic diameters are sizes by intensity. The polydispersity index (PDI) was obtained using the cumulant method, assuming a spherical shape. Data were averaged from at least three runs.

In all cases, the samples were diluted with deionized water or DMAc to final concentrations of about 0.05 mg/ml, and ultrasound was applied for 10 min prior to the experiments where necessary.

3.6. Elemental analysis (EA)

Elemental analysis was conducted using a CHNS 932 Analyzer (Leco).

4. Polymer characterization

4.1. ^{1}H NMR spectroscopy

^{1}H NMR spectra were recorded on a Bruker Advance 250 MHz spectrometer using $CDCl_3$ as solvent and TMS as internal standard. The monomer conversions were determined gravimetrically and by ^{1}H NMR spectroscopy using 1,3,5-trioxane as reference.

4.2. Size exclusion chromatography (SEC)

The molecular weight and molecular weight distribution of the synthesized polymers were determined by a Shimadzu system, equipped with a SCL-10A system controller, a LC-10AD pump, and a RID-10A refractive index detector. A solvent mixture containing chloroform, triethylamine, and isopropanol (94:4:2) was used as eluent at a flow rate of 1 mL min^{-1} on a PSS-SDV-linear M 5 μm column at room temperature. The system was calibrated with polystyrene (100–150 000 Da) standards.

4.3. Copper and iron content

Residual copper and iron were determined by atomic absorption spectroscopy (AAS), using an Analytik Jena, model Nova 400, atomic absorption spectrophotometer (Jena, Germany). Samples of 300 μg of PS were dissolved in THF and used for each AAS measurement. The analysis was performed in 1% HNO_3/H_2O. The quantification was done by comparison with a standard curve.

5. Results and discussion

5.1. Synthesis and characterization of Fe_3O_4@amino cellulose hybrid NPs

The synthesis of the Fe_3O_4 nanoparticles (MNPs) was carried out according to literature protocols [44]. The as-synthesized MNPs show a hydrodynamic diameter (DLS) of 56 nm in water. This can mainly be attributed to agglomeration and the individual particles show a diameter of 8 ± 2 nm, as will be demonstrated by TEM measurements (Fig. 4A). Fig. 1 illustrates the synthesis of the Fe_3O_4 nanoparticles, followed by the coating with AC and subsequent complexation with CuBr. The so-generated Fe_3O_4@amino cellulose hybrid NPs can then be used as heterogeneous ligands in the ATRP of styrene.

Due to the amino groups, the MNPs exhibit a positive surface charge in ζ-potential measurements, +48 mV (pH 2). Coating of the Fe_3O_4 nanoparticles with amino cellulose of different average degrees of polymerization (AC_{50}, AC_{250}) was performed in dilute aqueous solution (pH 6). Afterwards, the values obtained for the ζ-potential were +41 and +40 mV for MNP@AC_{50} and MNP@AC_{250}, respectively. The prevailing positive ζ-potential values can be explained due to the presence of amino groups on the surface of the modified nanoparticles, which are protonated under these conditions. The difference between the DS of amino celluloses samples did not lead to a significant change in the ζ-potential values [16,45].

Another possibility to prove the formation of hybrid structures is the monitoring of the temperature-dependent weight loss during thermogravimetry (TGA). Therefore, we dried both MNP@AC_{50} and MNP@AC_{250}, and TGA measurements were performed on samples of 10 mg quantity (Fig. S1, solid black line). The decomposition process can be divided into two stages within a temperature range from 35 to 500 °C. Between 35 and 150 °C, the initial weight loss of the samples was below 5%, presumably due to the evaporation of adsorbed water. At higher temperatures (150–400 °C), a weight loss of approximately 28% can be seen, indicating the degradation of organic material, that is, amino cellulose. If this is compared to the as-synthesized MNP, almost no weight loss is observed up to a temperature of 500 °C (Fig. S1, solid gray line). According to the TGA measurements, the DP of the used AC had no significant influence on the adsorbed amount of polysaccharide onto the preformed MNPs. The thickness of the amino cellulose shell can be roughly calculated according to the determined weight loss during TGA experiments (taking into account, the respective densities of $\rho_{Fe3O4} = 5.2$ g/cm^3 and $\rho_{AC} \sim 1.7$ g/cm^3) and leads to values of approximately 4 nm. Although these values are relatively high for particles with a diameter of roughly 8 nm, such shell thicknesses are in good agreement with literature data on amino cellulose monolayers on planar surfaces [46]. Please note that although the main fraction is individual MNP (see Fig. 3), the presence of some aggregates and, hence, coating of multiple particles by amino cellulose cannot be excluded at this point.

5.2. XRD characterization of the as-synthesized Fe_3O_4 MNPs

Fig. 2 shows the XRD powder diffraction pattern of the as-synthesized particles, characteristic for spinel iron oxide (maghemite/magnetite) [47]. By XRD, the mean crystallite size of the synthesized MNP was determined to be 8 nm, as calculated according to the width of the (4 4 0) XRD peak at half height, using the Scherrer equation:

$$D = K\lambda / b\cos\theta \quad (1)$$

Here, K is the Scherrer constant (0.9 for magnetite); λ the X-ray wavelength (1.54 Å); b the corrected width of the XRD peak at half height (radian), and θ the Bragg diffraction angle [48].

5.3. Solution characterization of Fe_3O_4@amino cellulose hybrid NPs

Another indication for the successful formation of MNP@AC_x hybrid structures is a significant change of the solution properties: after coating with amino cellulose, the resulting hybrid particles were stable in polar organic media such as DMAc, whereas this was not the case for the uncoated MNPs under these conditions. This was further investigated using dynamic light scattering, both before and after coating with amino cellulose. All sample solutions

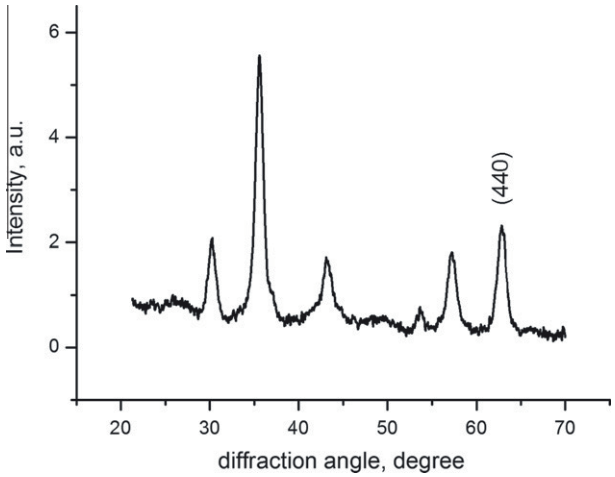

Fig. 2. XRD pattern of the as-synthesized Fe_3O_4 MNPs, the reflection used for the size determination [440] is highlighted.

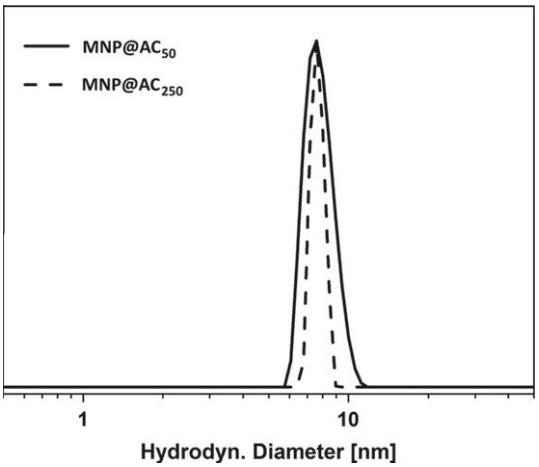

Fig. 3. number-weighted CONTIN plots for diluted solutions (0.1 mg/mL) of MNP@AC_{50} ($D_{h,app}$ = 7.6 nm; solid black line) and MNP@AC_{250} ($D_{h,app}$ = 7.8 nm; dashed black line).

were treated with ultrasound to reduce aggregate formation prior to the measurements and diluted to a final concentration of 0.05 mg/mL. To allow for an estimation of the long-term stability, the hydrodynamic diameters were determined after 10 min, 5, 24, 48, 72, and 168 h in water and DMAc (Fig. S2). The size distribution of MNP in water and DMAc is shown in Fig. S3. All samples analyzed showed a monomodal size distribution and hydrodynamic diameters larger than expected for the individual particles according to other techniques, for example, XRD and TEM. This can be attributed to agglomeration of the individual particles [49,50]. Nevertheless, the results demonstrate that the uncoated MNP form stable dispersions in aqueous media. If dispersed directly in DMAc, precipitation could be observed within several minutes.

After coating, the MNP@AC_x hybrid particles are well-dispersed in DMAc, as demonstrated by constant hydrodynamic diameters (Fig. S3) and the absence of precipitation. We attribute this to the structure of the amino cellulose coating present on the surface of the particles. The fact that such MNP@AC_x hybrid particles are stable both in aqueous and organic media renders this approach quite attractive.

Whereas Fig. S2 depicts the long-term stability of the hybrid structures, further DLS experiments and the corresponding number-weighted size distributions are shown in Fig. 3. Number-weighted hydrodynamic diameters of 7.6 nm (MNP@AC_{50}) and 7.8 nm (MNP@AC_{250}) were observed, which is in relatively good agreement with the DLS (6.8 nm) and the XRD (8 nm) results of the as-synthesized MNP.

5.4. TEM analysis

The size and the morphology of MNP@AC_{250}, both before and after the coating process, were also characterized by TEM (Fig. 4, similar results were obtained for MNP@AC_{50}). The as-synthesized MNPs are shown in Fig. 4A and B, after drop-casting from water and DMAc, respectively.

As can be seen in Fig. 4A, the as-synthesized MNPs exhibit a spherical shape with an average diameter of 8 ± 2 nm, which is in good agreement with DLS and XRD measurements. In contrast, in DMAc (Fig. 4B), larger agglomerates were formed, leading to precipitation. This can also be observed in TEM, where large particle clusters are found.

After coating with amino cellulose, the MNP@AC_{250} particles are well-dispersed both in DMAc and in aqueous media. In both cases, (Fig. 4C for water and 4D for DMAc), individual particles and also smaller clusters were found in TEM. The individual particles revealed similar average diameters as observed earlier for the as-synthesized MNP. The amino cellulose shell could not be visualized in TEM, even after staining with uranyl acetate. Also, attempts to detect the shell using cryo-TEM were unsuccessful, even after staining with uranyl acetate or quaternization of the amino groups using methyl iodide. However, the solution properties and the TGA measurements do support a successful coating with either AC_{50} or AC_{250}. We attribute the formation of smaller clusters to agglomeration in solution, as also observed during DLS studies. Nonetheless, constant hydrodynamic diameter values indicate a long-term stability of these hybrid particles. We conclude that the morphology and the size of the individual MNPs are retained during the coating process, and similar results were found for particles after coating with AC_{50} (micrographs not shown here).

5.5. Magnetic properties of MNP@AC_x

The magnetic behavior of the as-synthesized MNP, MNP@AC_{50}, and MNPqAC_{250} was investigated by vibrating sample magnetometry (VSM). The magnetization curves recorded at room temperature are shown in Fig. 5. Both the particle size and a low coercivity visible in their magnetic profile are an evidence for predominantly superparamagnetic behavior of the MNP [51]. The saturation magnetization of the uncoated MNP is 59 $Am^2\,kg^{-1}$ which is typically for maghemite nanoparticles. Due to the nonmagnetic properties of amino cellulose on the particle surface, mean saturation magnetization decreases after the coating process. The here investigated samples MNP@AC_{50} and MNP@AC_{250} have a saturation magnetization of 50 and 47 $Am^2\,kg^{-1}$, respectively. Within the accuracy of the measurements, both MNP@AC_{50} and MNP@AC_{250} seem to have the same shell thickness. The slight difference in saturation magnetization in our case might also be related to rather small sample amounts, which have been available for investigation. Further, another effect – the substantial decrease in the relative Fe_3O_4 magnetic core content in MNP@AC_x also leads to a decrease in saturation magnetization. This behavior has already been described in other studies, for example, a significant decrease of 58% in saturation magnetization has been found after coating MNP with ethylcellulose [52]. Detailed studies of the magnetic behavior of polymer-coated magnetic ferrites have also been reported by other authors [53].

The coercivity increases in the sample order MNP, MNP@AC_{50}, and MNP@AC_{250} from 0.9 Oe, 2.6 Oe, to 8.1 Oe, respectively. This

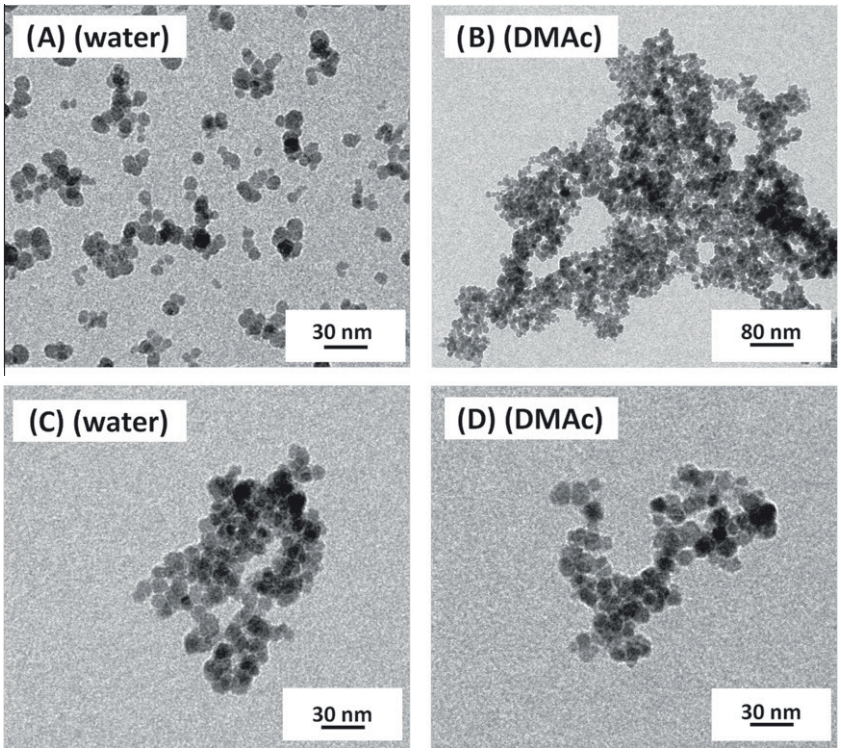

Fig. 4. TEM micrographs for MNP and MNP@AC_{250}; as-synthesized MNP from water (A) and DMAc (B); MNP@AC_{250} from water (C) and DMAc (D).

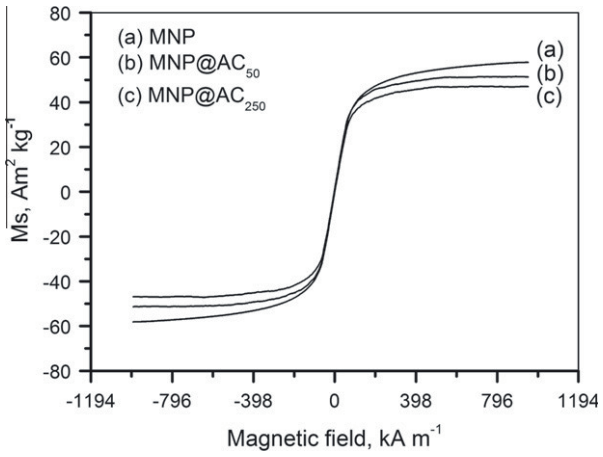

Fig. 5. Magnetic hysteresis curves for the as-synthesized MNP (a), MNP@AC_{50} (b), and MNP@AC_{250} (c).

could be caused by slight differences in shell thickness for MNP@AC_{50} and MNP@AC_{250}, leading to changes in the effective distance between adjacent magnetic cores and an increase in coercivity and remanence due to decreasing particle–particle interactions with increasing distance [54,55]. But as other measurements (DLS, TEM, and TGA) suggest that both shell thicknesses are comparable, we tentatively attribute this finding to the agglomeration of the MNP@AC_x to larger clusters. An increasing size of the agglomerates (as observed in DLS measurements) can also cause an increase in these parameters [56].

From the shape of the magnetization curve, the effective magnetic core diameter was determined to be 8.1 nm following the Chantrell method [49], which is in good accordance to the results obtained from the other characterization methods (DLS, TEM, and XRD). The obtained characterizations for the different MNP suspensions are summarized in Table 1.

Table 1
Summary of characterization data for the as-synthesized MNP and MNP@AC_x.

Entry	Sample	XRD (nm)	DLS (nm)	TEM (nm)	VSM (nm)	M_s ($Am^2\ kg^{-1}$)
1	MNP	8	6.8	≈8	8.1	59
2	MNP@AC_{50}	–	7.6	≈8	8.1	50
3	MNP@AC_{250}	–	7.8	≈8	8.1	47

5.6. Heterogeneous ATRP of styrene

The ATRP of styrene was carried out in DMAc, a medium in which the MNP@AC_x particles proved to be stable. Previous studies have shown that the ATRP of styrene can be performed in DMAc [57,58]. For example, styrene chains were grafted from silica beads (as a colloidal sol in DMAc) [57]. Moreover, the ATRP of styrene and

Table 2
Conditions and results employed for the polymerization of styrene in DMAc at 70 °C.

Entry	Sample	Time (h)	M_n ($g\ mol^{-1}$)	M_n, theorical	PS conversion (%)	M_w/M_n
1	MNP@AC_{50}	48	2300	2900	29	1.27
2	MNP@AC_{50}	60	4800	4700	47	1.26
3	MNP@AC_{50}[a]	72	8000	6800	68	1.20
4	MNP@AC_{50}	96	9200	7800	78	2.36
5	MNP@AC_{50} 2nd run	72	8400	6900	69	1.22
6	MNP@AC_{250}[a]	72	8000	6700	67	1.23
7	MNP@AC_{250} 2nd run	72	8400	6900	69	1.20
8	Control[a]	72	9900	5100	51	1.23
9	MNP@AC_{50} 2nd run[b]	72	4500	4200	42	1.90

[a] Experiments carried out at least in duplicates.
[b] Without additional ascorbic acid.

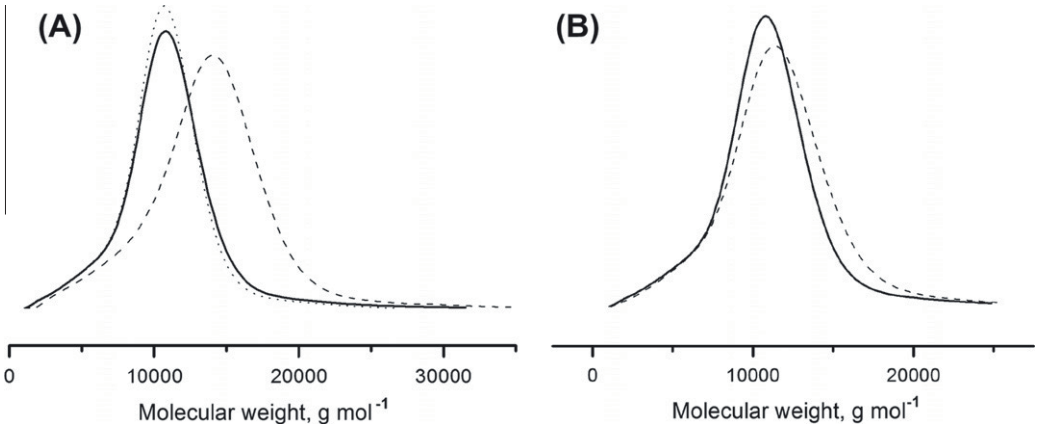

Fig. 6. SEC traces for polystyrene (PS) generated via ATRP reactions: Part A, control reaction with PMDETA as ligand (dotted line), and using MNP@AC_{50} (dashed line) or MNP@AC_{250} (solid line); Part B, using MNP@AC_{250} in a first (solid line) and second (dashed line) polymerization procedure.

methyl methacrylate using initiators for continuous activator regeneration (ICAR) and with $Ru(Cp^*)Cl(PPh_3)_2$ as the catalyst was conducted in a mixture of DMAc and anisole [57]. In our case, MNP@AC_x hybrid particles serve as a heterogeneous ligand during the ATRP procedure.

For comparison, one experiment was performed using PMDETA as ligand and this will be referred to as the *control* reaction. PMDETA represents one of the most widely employed ligands in ATRP [26], and the structure is similar if compared to the amino-substitution present on the surface of the coated particles. All experiments were conducted in a heatable shaker, and the monomer conversion was determined both gravimetrically and by ^1H NMR spectroscopy, using the signal for the vinyl protons of styrene in comparison with an internal standard (1,3,5-trioxane) (Fig. S4).

The evolution of M_n and the polydispersity index (PDI) with increasing monomer conversion for different reaction times is shown in Table 2. The experimental conditions were optimized using MNP@AC_{50}. The molecular weight increases with increasing conversion and near-narrow molecular weight distributions of around 1.2 (Table 2, entries 1–3) were obtained. The polymerization is rather slow, as demonstrated by a conversion of only 29% after 48 h (entry 1). After 72 h, a conversion of 68% could be achieved (entry 3). A further increase in polymerization time resulted in a less controlled process, indicated by a drastic increase in polydispersity (entry 4), which we tentatively attribute to a higher tendency for termination reactions with decreasing monomer concentration at such high dilutions. Using the same experimental conditions and MNP@AC_{250}, comparable results concerning reaction speed and polydispersity were obtained (entry 6). In most cases, the molecular weight obtained was slightly higher if compared to the theoretical values, indicating an initiator efficiency below 100%. In all cases except entry 4 and 9, a monomodal elution trace was obtained, indicating a good control over the ATRP process. The results are comparable with those obtained for the control reaction using PMDETA (entry 8). The SEC traces for PS, using MNP@AC_{50}, MNP@AC_{250}, and PMDETA as ligand, are shown in Fig. 6A. Within this study, no effect of the molecular weight of the amino cellulose used for the coating process on the use as heterogeneous ligand in ATRP could be observed.

5.7. MNP@AC_x recycling and reuse

In comparison with other methods (e.g., ARGET ATRP) used for the preparation of polymers with a reduced Cu-content, one clear advantage of this approach using magnetic hybrid nanoparticles as heterogeneous ligands is that the material can be isolated easily afterwards and, even more important, potentially reused for further reactions. We therefore isolated the MNP@AC_x particles using an external magnetic field after 72 h and used them as ligands in a second polymerization (Table 2, entries 5 + 7; Fig. 6B). More precise, MNP@AC_x were washed with degassed DMAc and treated with ultrasound. Initial attempts targeting a direct reuse unfortunately lead to less controlled polymerizations (M_n = 4500 g/mol and a PDI of 1.9) (Table 2, entry 9), although all steps were carried out under oxygen-free conditions. We therefore added small amounts of ascorbic acid to reactivate any Cu(II) generated. The presence of a reducing agent during the second polymerization proved to be extremely important and, also here, conversions of 69 % and near-narrow molecular weight distributions were achieved (Table 2, entries 5 + 7). Exemplarily, SEC traces for polymers generated with MNP@AC_{250} as heterogeneous ligands in a first and second run are shown in Fig. 6B.

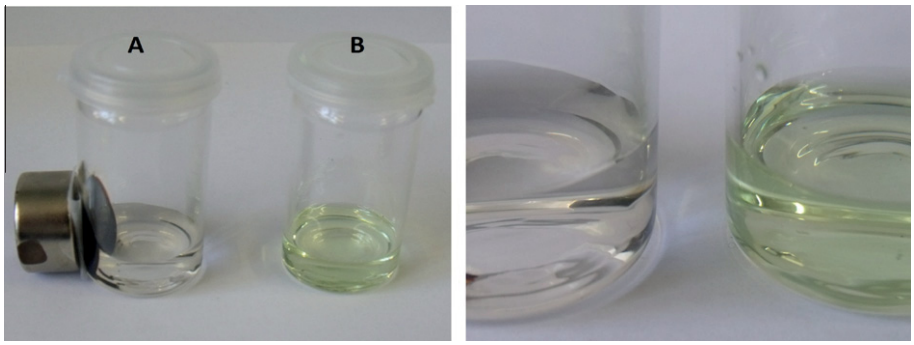

Fig. 7. Images of PS solutions after ATRP using MNP@AC_{50} (A) and PMDETA (B) as ligands.

5.8. Determination of residual Cu

In ATRP polymerizations, the efficient removal of any transition metals afterwards can cause problems. In our case, the MNP@AC$_x$ hybrid particles could be easily isolated after the polymerization using an external magnetic field to afford a clear, colorless polymer solution. This is shown in Fig. 7 (Tube A). In case of the control reaction (Tube B), a greenish solution is obtained afterwards.

The residual amount of Cu in the final polymer (PS) was determined using atomic absorption spectroscopy (AAS), resulting in >10.000 ppm for the control reaction using PMDETA and only 4.9 ppm for the heterogeneous procedure employing MNP@AC$_{50}$. If the reaction mixture with PMDETA as a ligand was filtrated over an aluminum oxide column after the polymerization, the amount of residual Cu could be reduced to about 17 ppm. In another approach, where the ligand was immobilized on a Merrifield resin, approximately 15 ppm of residual Cu was obtained [59]. In case of ARGET ATRP under batch, semibatch, and continuous reactor conditions, different methacrylate- and acrylate-based materials with Cu levels below 50 ppm could be generated [60]. In this context, our strategy to use heterogeneous Fe_3O_4@amino cellulose hybrid ligands and the subsequent separation with an external magnetic field represents an efficient way for the preparation of almost Cu-free polystyrene. Moreover, no residual Fe and hence, no remaining hybrid particles, could be detected by AAS.

6. Conclusion

We demonstrated an efficient strategy for the formation of MNP@AC$_x$ hybrid nanoparticles. The successful coating process can be proven by a decrease in the values of both ζ-potential and magnetization. In addition, TGA measurements revealed a weight loss below 400 °C, which can be attributed to the deterioration of the amino cellulose. According to a combination of XRD, VSM, TEM, and DLS measurements, the hybrid particles exhibit an average diameter of roughly 8 nm. Most important, after coating, the MNP@AC$_x$ can be dispersed both in aqueous media and in DMAc, which renders this approach promising for the fabrication of hybrid particles with a broad solubility range.

As one possible application field, we used MNP@AC$_x$ hybrid particles as heterogeneous ligands in the ATRP of styrene and near-narrow molecular weight distributions with polydispersities lower than 1.3 could be accomplished. Even more, the hybrid particles could be easily removed after polymerization by an external magnetic field and reused in further polymerization reactions. The so-generated polymeric materials showed low Cu contents, comparable to established procedures such as ARGET-ATRP.

Future improvements of the presented approach will focus on the scalability of the particle preparation and also the effective magnetization (separation time after the polymerization procedure) of the particles used. The latter might be improved in the future by using multi-core particles of slightly larger diameter, whereas the current preparation route should be feasible on a multi-gram scale.

Acknowledgments

L.C. Fidale and T. Heinze thank the European Community Seventh Framework program [FP7/2007-2013] for funding through STEP – ITN, agreement no. 214015. The authors thank Sandra Koehn and Prof. Ulrich S. Schubert (both FSU Jena) for the atomic absorption spectroscopy measurements. F. H. Schacher is grateful to the FCI for a fellowship and also to the Thuringian Ministry for Education, Science and Culture (TMBWK, Grant #B515-10065, ChaPoNano) for financial support. F.H. Schacher and T. Heinze gratefully acknowledge financial support of the TMBWK (Grant #B514-09051, NanoConSens).

Appendix A. Supplementary material

Supplementary data associated with this article can be found, in the online version, at http://dx.doi.org/10.1016/j.jcis.2012.09.019.

References

[1] B.L. Cushing, V.L. Kolesnichenko, C.J. O'Connor, Chem. Rev. 104 (2004) 3893.
[2] L. Trahms, Lect. Notes Phys. 763 (2009) 327.
[3] L. Dykman, N. Khlebtsov, Chem. Soc. Rev. 41 (2012) 2256.
[4] N.A. Frey, S. Peng, K. Cheng, Chem. Soc. Rev. 38 (2009) 2532.
[5] J.J. Kreuter, J. Controlled Release 16 (1991) 169.
[6] R. Gref, Y. Minamitake, M.T. Peracchia, V. Trubetskoy, V. Torchilin, R. Langer, Science 263 (1994) 1600.
[7] Y.-I. Jeong, J.B. Cheon, S.-H. Kim, J.W. Nah, Y.M. Lee, Y.K. Sung, T. Akaite, C.S.J. Cho, J. Controlled Release 51 (1998) 169.
[8] S.A. Anderson, R.K. Rader, W.F. Westlin, C. Null, D. Jackson, G.M. Lanza, S.A. Wickline, J. Kotyk, J. Magn. Reson. Med. 44 (2000) 433.
[9] V.S. Zaitsev, D.S. Filimonov, I.A. Presnyakov, R.J. Gambino, B. Chu, J. Colloid Interface Sci. 212 (1999) 49.
[10] J.G. Hou, Q. Ma, X.Z. Du, H.L. Deng, J.Z. Gao, Talanta 62 (2004) 241.
[11] T.K. Jain, I. Roy, T.K. De, A. Maitra, J. Am. Chem. Soc. 120 (1998) 11092.
[12] R.S. Faye, S. Aamdal, H.K. Hoifodt, Clin. Cancer Res. 10 (2004) 4134.
[13] J.C. Frias, Y.Q. Ma, K.J. Williams, Nano Lett. 6 (2006) 2220.
[14] R. Hergt, R. Hiergeist, I. Hilger, J. Magn. Magn. Mater. 27 (2004) 345.
[15] H.H. Yang, S.Q. Zhang, X.L. Chen, Z.X. Zhuang, J.G. Xu, X.R. Wang, Anal. Chem. 76 (2004) 1316.
[16] J.Y. Park, E.S. Choi, M.J. Baek, G.H. Lee, Mater. Lett. 63 (2009) 379.
[17] R.-Y. Hong, J.-H. Li, S.-Z. Zhang, H.-Z. Li, Y. Zheng, J.-M. Ding, D.-G. Wei, Appl. Surf. Sci. 255 (2009) 3485.
[18] X. Chen, L. Li, X. Sun, Y. Liu, B. Luo, C. Wang, Y. Bao, H. Xu, H. Peng, Angew. Chem. Int. Ed. 50 (2011) 5486.
[19] M. Chastellain, A. Petri, H. Hofmann, J. Colloid Interface Sci. 278 (2004) 353.
[20] S. Dutz, W. Andra, R. Hergt, R. Müller, C. Oestreich, C. Schmidt, J. Töpfer, M. Zeisberger, M.E. Bellemann, J. Magn. Magn. Mater. 311 (2007) 51.
[21] J. Wotschadlo, T. Liebert, T. Heinze, K. Wagner, M. Schnabelrauch, S. Dutz, R. Müller, F. Steiniger, M. Schwalbe, T. Kroll, K. Höffken, N. Buske, J. Clement, J. Magn. Magn. Mater. 321 (2009) 1469.
[22] J.S. Suleiman, B. Hu, H. Peng, C. Huang, Talanta 77 (2009) 1579.
[23] S. Ding, Y. Xing, M. Radosz, Y. Shen, Macromolecules 39 (2006) 6399.
[24] J.S. Wang, K. Matyjaszewski, J. Am. Chem. Soc. 117 (1995) 5614.
[25] K. Matyjaszewski, J. Xia, Chem. Rev. 101 (2001) 2921.
[26] N.V. Tsarevsky, K. Matyjaszewski, Chem. Rev. 107 (2007) 2270.
[27] V. Coessens, T. Pintauer, K. Matyjaszewski, Prog. Polym. Sci. 26 (2001) 337.
[28] K. Matyjaszewski, Chem. Eur. J. 5 (1999) 3095.
[29] A.J.D. Magenau, N.C. Strandwitz, A. Gennaro, K. Matyjaszewski, Science 332 (2011) 81.
[30] K. Matyjaszewski, N.V. Tsarevsky, Nat. Chem. 1 (2009) 276.
[31] K. Matyjaszewski, W. Jakubowski, K. Min, W. Tang, J. Huang, W.A. Braunecker, N.V. Tsarevsky, Proc. Natl. Acad. Sci. USA 103 (2006) 15309.
[32] G. Kickelbick, H.-J. Paik, K. Matyjaszewski, Macromolecules 32 (1999) 2941.
[33] A.J. Carmichael, D.M. Haddleton, S.A.F. Bon, K.R. Seddon, Chem. Commun. (2000) 1237.
[34] H. Ziqiang, H. Fang, Q.I.U. Huayu, L.A.I. Guoqiao, W.U. Jirong, L.I. Wenqing, J. Wuhan Univ. Technol. – Mater. Sci. Ed. 25 (2010) 785.
[35] T. Sarbu, T. Pintauer, B. McKenzie, K. Matyjaszewski, J. Polym. Sci., Polym. Chem. 40 (2002) 3153.
[36] K. Matyjaszewski, T. Pintauer, S. Gaynor, Macromolecules 33 (2000) 1476.
[37] J. Gromada, J. Spanswick, K. Matyjaszewski, Macromol. Chem. Phys. 205 (2004) 551.
[38] D. Klemm, F. Kramer, S. Moritz, T. Lindström, M. Ankerfors, D. Gray, A. Dorris, Angew. Chem. Int. Ed. 50 (2011) 5438.
[39] J. Tiller, D. Klemm, P. Berlin, Des. Monomers Polym. 4 (2001) 315.
[40] M. Meiland, T. Liebert, T. Heinze, Macromol. Mater. Eng. 296 (2011) 802.
[41] W.F.L. Armarego, C.L.L. Chai, Purification of Laboratory Chemicals, Elsevier, New York, 2009.
[42] K. Rahn, M. Diamantoglou, D. Klemm, H. Berghmans, T. Heinze, Angew. Makromol. Chem. 238 (1996) 143.
[43] A. Jung, P. Berlin, Cellulose 12 (2005) 67.
[44] R. Massart, V. Cabuil, J. Chem. Phys. 84 (1987) 967.
[45] X.M. Guo, B. Guo, Q. Zhangc, X. Sund, Dalton Trans. 40 (2011) 3039.
[46] A. Jung, B. Wolters, P. Berlin, Thin Solid Films 515 (2007) 6867.
[47] N.O. Dudchenko, Mat.-wiss. U. Werkstofftech 42 (2011) 89.
[48] Y. Sun, M. Ma, Y. Zhang, N. Gu, Colloid Surf. A. 245 (2004) 15.
[49] R.W. Chantrell, A. Bradbury, J. Popplewell, S.W. Charles, J. Appl. Phys. 53 (1982) 2742.
[50] D. Maity, D.C. Agrawal, J. Magn. Magn. Mater. 308 (2007) 46.
[51] G.C. Xi, C. Wang, X. Wang, Eur. J. Inorg. Chem. (2008) 425.
[52] J.L. Arias, M. López-Viota, A.V. Delgado, M.A. Ruiz, Colloids Surf. B 77 (2010) 111.

[53] B.D. Cullity, Element of X-ray Diffraction, Addison Wesley, Reading, MA, 1974.
[54] S. Dutz, R. Hergt, J. Nano- Electron. Phys. 4/2 (2012) 20101.
[55] A. Lapresta-Fernández, T. Doussineau, S. Dutz, F. Steiniger, A.J. Moro, G.J. Mohr, Nanotechnology 22 (2011) 415.
[56] S. Dutz, J.H. Clement, D. Eberbeck, T. Gelbrich, R. Hergt, R. Müller, J. Wotschadlo, M. Zeisberger, J. Magn. Magn. Mater. 321 (2009) 1501.
[57] A. El Harrak, G. Carrot, J. Oberdisse, J. Jestin, F. Boué, Polymer 46 (2005) 1095.
[58] A. Plichta, W. Li, K. Matyjaszewski, Macromolecules 42 (2009) 2330.
[59] S.C. Hong, H.-J. Paik, K. Matyjaszewski, Macromolecules 34 (2001) 5099.
[60] N. Chan, M.F. Cunningham, R.A. Hutchinson, Macromol. React. Eng. 4 (2010) 369.

Publication P13

"Porous NiOx Nanostructures Templated by Polystyrene-*block*-poly(2-vinylpyridine) Diblock Copolymer Micelles"

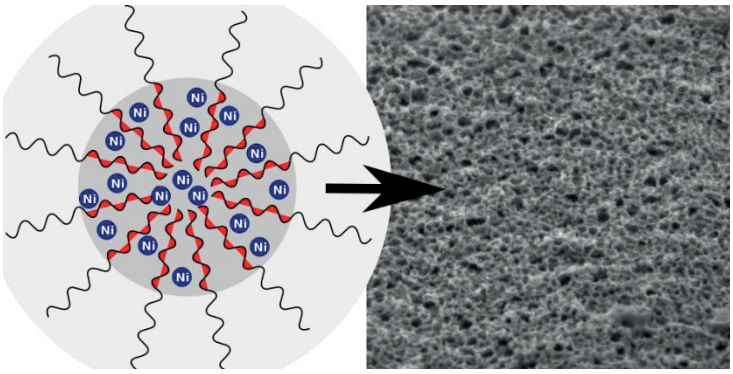

Maximilian Bräutigam, Peter Weyell, Tobias Rudolph, Jan Dellith, Sven Krieck, Holger Schmalz, Felix H. Schacher, Benjamin Dietzek

J. Mater. Chem. A, **2014**, 2, 6158-6166

Journal of Materials Chemistry A

PAPER

Porous NiO_x nanostructures templated by polystyrene-*block*-poly(2-vinylpyridine) diblock copolymer micelles

Cite this: *J. Mater. Chem. A*, 2014, **2**, 6158

Maximilian Bräutigam,[ab] Peter Weyell,[b] Tobias Rudolph,[c] Jan Dellith,[a] Sven Krieck,[d] Holger Schmalz,[e] Felix H. Schacher*[c] and Benjamin Dietzek*[ab]

Received 25th November 2013
Accepted 11th December 2013

DOI: 10.1039/c3ta14890d

www.rsc.org/MaterialsA

A facile synthetic route to NiO_x nanostructures using various amphiphilic polystyrene-*block*-poly-(2-vinylpyridine) (PS-*b*-P2VP) diblock copolymers as templates was investigated. The synthesis targets NiO_x nanostructures with a large surface area in order to allow an efficient functionalization, *e.g.*, through loading with dyes to enable photo-induced hole injection for use in dye-sensitized solar cells or in (photo-) catalytic systems. The complete synthetic process to NiO_x contains several steps: (i) the dissolution of the diblock copolymer, (ii) the subsequent addition of Ni^{2+}, followed by the formation of core–corona micelles and eventually, (iii) further addition of Ni^{2+}, resulting in the formation of a macroscopic precipitate. In all cases, (iv) deposition onto different substrates and calcination yielded NiO_x films. All intermediates were thoroughly investigated using scanning or transmission electron microscopy, dynamic light scattering, and UV-vis spectroscopy. In contrast to the well-established synthetic route *via* the commercially available Pluronic F108 triblock copolymer, in our case a variety of different morphologies was found, *i.e.* spherical particles, toroid structures, or networks. Furthermore, the obtained BET area of about 50 $m^2\ g^{-1}$ is comparable to the value for conventionally obtained NiO_x surfaces. First dye sensitization experiments with coumarine 343 confirm that the dye binds to the surface, which is a prerequisite for using the material as a photo-electrode. The presented route to porous NiO_x is easy and provides superior control over the morphology of the intermediates involved in nanostructure formation.

Introduction

Several NiO_x semiconductor syntheses are known to provide NiO_x for various applications.[1,2] For example, NiO_x has been used as a photo-catalyst to deposit organic substances,[3] for water splitting,[4–8] in lithium batteries, and in supercapacitor applications.[9–11] One of the most promising applications of NiO_x nanoparticles is to sensitize the nanoparticle films for improved light harvesting of the *p*-type NiO_x semiconductor. Here, an example is their use in dye-sensitized solar cells (DSSCs) where it had been tested for the first time by He *et al.* in 1999.[12] State-of-the-art dye-sensitized solar cells, however, use TiO_2 as an *n*-type semi-conductive material.[13] Attempts were made to combine both semiconductors within one solar cell, which leads to the concept of dye-sensitized tandem solar cells[1,14,15] that increase the Shockley–Queisser limit[16] to about 43% compared to a single junction cell with a limit of 31%.[13] Another example for the use of dye-sensitized NiO_x nanoparticles is their use as catalyst or support for the grafting of molecular catalysts.[17]

A wide variety of techniques for the production of NiO_x surfaces was developed, *e.g.*, scalable microwave sintering,[18,19] spray pyrolysis,[20] plasma-enhanced chemical vapor deposition,[21] pulsed laser deposition,[22] chemical bath deposition,[23] magnetron sputtering,[24,25] and sol–gel[26,27] or polymer template synthesis.[28–30] The most commonly used method is based on block copolymer micelles in selective solvents for one of the two blocks.[31] Of particular interest are systems featuring one segment to which Ni^{2+} can be selectively coordinated. These micelles then serve as templates for NiO_x nanoparticles. The Ni^{2+}–block copolymer complex micelles can be deposited onto a substrate and calcined in a furnace to yield NiO_x nanoparticles.[28] The most widely used polymeric material for this approach is the commercially available triblock copolymer Pluronic F108 (poly(ethylene oxide)-*block*-poly(propylene oxide)-*block*-poly(ethylene oxide)). This synthetic route *via* triblock

[a]*Leibniz Institute of Photonic Technology (IPHT) Jena e. V., Albert-Einstein-Str. 9, 07745 Jena, Germany*

[b]*Institute for Physical Chemistry and Abbe Center of Photonics, Friedrich Schiller University Jena, Helmholtzweg 4, 07743 Jena, Germany. E-mail: benjamin.dietzek@ipht-jena.de*

[c]*Institute of Organic Chemistry and Macromolecular Chemistry and Jena Center for Soft Matter (JCSM), Friedrich Schiller University Jena, Lessingstr. 8, 07743 Jena, Germany. E-mail: felix.schacher@uni-jena.de*

[d]*Institute for Inorganic and Analytical Chemistry, Friedrich Schiller University Jena, Humboldtstr. 8, 07743 Jena, Germany*

[e]*Macromolecular Chemistry II, University Bayreuth, Universitätsstr. 30, 95447 Bayreuth, Germany*

copolymer micellization is straightforward, cheap, reliable, and yields spherical particles with an average size of about 12 nm and the BET surface of the resulting NiO_x is in the 40 m^2 g^{-1} range. Furthermore, repeated deposition gives access to thicker multilayer films.[28,29]

The route described here was designed to provide control over the intermediates involved in such a multi-step synthetic process (block copolymer unimers, Ni^{2+}–block copolymer hybrid structures, mono- or multi-layer films, final NiO_x morphology). Furthermore, the protocols reported in the literature typically operate using spherical nanoparticles. Herein, we demonstrate an approach which allows fine-tuning of the intermediate particle morphology during preparation of NiO_x nanostructures, building on synthetic strategies that have already resulted in other metal oxide nanoparticles.[32,33] We used well-defined micelles formed by the addition of defined portions of Ni^{2+} to solutions of polystyrene-*block*-poly(2-vinylpyridine) (PS-*b*-P2VP) diblock copolymers in non-selective solvents. Hence, the micellar core will consist of a complex formed between Ni^{2+} and poly(2-vinylpyridine) (P2VP), which is well known to complex Ni^{2+}.[34,35] After loading, such micelles can be calcinated, resulting in NiO_x nanoparticles. Unlike the synthetic route *via* F108, the film thickness that can be reached for the presented route is determined by the block copolymer concentration, which, in turn, often has drastic effects on the micellar size distribution or homogeneity. We present a thorough investigation on the formation of block copolymer–Ni^{2+} hybrid micelles, their solution behavior, and the preparation of porous NiO_x nanostructures utilizing dynamic light scattering (DLS), UV-vis spectroscopy, or electron microscopy. We further use sonication to tune the size of the intermediates and, hence, the resultant NiO_x nanoparticles. Finally, it is demonstrated that spin coating of the mixture onto the substrate yields very homogeneous films.

The paper is organized as follows: first, three PS-*b*-P2VP diblock copolymers with different composition are compared with regard to micellar size and loading with Ni^{2+}. After identification of the most promising combination using dynamic light scattering and electron microscopic techniques, different deposition techniques, more precisely doctor blading and spin coating, were compared with regard to the preparation of block copolymer–Ni^{2+} films of varying thicknesses. After calcination, cyclic voltammetry (CV) measurements and NiO_x surface dye-sensitization experiments using coumarine 343 are described.

Experimental section

Materials

Tetrahydrofuran (Merck, p.a.) was purified by successive distillation over CaH_2 and potassium and kept under dry nitrogen before usage. Styrene (BASF, p.a.) was degassed three times *via* freeze pump thaw cycles using a high vacuum line. After degassing, styrene was stirred over Bu_2Mg and condensed under a high vacuum into storage ampoules and kept frozen under N_2 until use. 2-Vinylpyridine (Acros, 97%) was distilled from CaH_2 under nitrogen, stirred over Et_3Al for 2 h and condensed into storage ampoules. 1,1-Diphenylethylene (Aldrich, 97%) was purified by stirring with *sec*-BuLi under N_2 followed by distillation. *sec*-BuLi (Acros, 1.3 M in cyclohexane/hexane: 92/8), Bu_2Mg (Aldrich, 1 M in heptane), and Et_3Al (Aldrich, 1 M in hexanes) were used as received. Solvents used for the preparation of hybrid micelles were of spectroscopic grade.

Polystyrene-*block*-poly(2-vinylpyridine) (PS-*b*-P2VP) diblock copolymers with different compositions were synthesized *via* sequential anionic polymerization using a procedure adopted from the literature.[36] Polymerization was carried out in a thermostatted laboratory autoclave (Büchi) under dry nitrogen atmosphere using tetrahydrofuran (THF) as the solvent and *sec*-BuLi as the initiator. First, styrene was polymerized at −70 °C for 30 min. Subsequently, 1,1-diphenylethylene (DPE, [*sec*-BuLi]/[DPE] = 1/1.1) was injected to adjust the nucleophilicity of the living chain end followed by stirring for 1 h. Afterwards, 2-vinylpyridine was added and allowed to react for 1 h before being terminated with degassed methanol. The resulting PS-*b*-P2VP diblock copolymers were isolated by precipitation in water followed by drying in a vacuum oven.

Preparation of diblock copolymer–Ni^{2+} hybrid structures

A saturated, ethanolic $NiCl_2$ solution (abs. ethanol) was prepared at room temperature. This solution was added to a solution of polystyrene-*block*-poly(2-vinylpyridine) (PS-*b*-P2VP) in THF, toluene, or chloroform. Upon addition of the $NiCl_2$ solution to the diblock copolymer the solution turns blue and for high Ni^{2+} concentrations, *i.e.* more than one equivalent of Ni^{2+} per 2-vinylpyridine unit, precipitation is observed. Best results regarding homogeneity, porosity and thickness were obtained after sonicating the sample with a Sonics VibraCell VC505 for 10 s with a power of 500 W at a frequency of 20 kHz.

Preparation of NiO_x films

The block copolymer–Ni^{2+} mixture was deposited on Menzel microscope slides either *via* spin coating or *via* doctor blading. For the electrochemical investigation, conductive ITO glass substrates were used. Subsequently, the surface was burnt in a furnace with a temperature program starting at 300 °C and increased to 450 °C within 20 min. Afterwards, the sample was kept in the furnace at 450 °C for additional 10 min. In the last step, the surface of the NiO_x film was thoroughly rinsed with pure water to remove remaining $NiCl_2$.

Dye sensitization

Sensitization of the surface with a dye as needed for the use of the NiO_x films in dye-sensitized solar cells was performed by soaking the films in a 1 mM coumarine 343 solution in acetonitrile. The success of the sensitization process was confirmed by UV-vis spectroscopy.

Scanning electron microscopy (SEM) and energy dispersive X-ray microanalysis (EDX)

Electron microscopic examinations were performed by using a JSM-6300F (JEOL, Tokyo, Japan) field-emission microscope

(FE-SEM). The lateral resolving power of that system is specified to be approximately 3 nm at 15 keV electron energy. Detectors for secondary (SE; Everhardt–Thornley type) as well as back-scattered electrons (BSE; YAG- and semiconductor type) were used for imaging. In some cases the specimen stage was tilted (up to 60°) to enhance the topographic visibility. The Ni^{2+}-loaded material was deposited onto glass substrates. In order to avoid charging effects all samples were coated with approximately 20 nm carbon. Cross-sectional preparations were performed after short-term LN_2-cooling in order to reduce the degree of ductility and to achieve plain true edge fracture patterns.

Analytical studies were carried out simultaneously by energy dispersive X-ray spectrometry (EDX). For this purpose a 30 mm^2 Si(Li) type detector from Oxford Instruments (Abingdon, UK) in combination with the INCA-Energy evaluation software package was used. The energy resolution of the used detector amounts to 133 eV at 5.9 keV (Mn-KL_3 (α_1) radiation).

Transmission electron microscopy (TEM)

The formed aggregates were analyzed using a TEM (Zeiss-CEM 902A, Oberkochen, Germany) operated at 80 kV. Images were recorded using a 1k TVIPS FastScan CCD camera. TEM samples were prepared by applying a drop of the sample solution onto the surface of a carbon coated copper grid (Quantifoil Micro-Tools GmbH, Jena, Germany) directly after sonication and the excess liquid was removed with a filter paper.

Dynamic light scattering (DLS)

Dynamic light scattering was performed at a scattering angle of 90° on an ALV CGS-3 instrument equipped with a He–Ne laser operating at a wavelength of 633 nm at 25 °C. The CONTIN algorithm was applied to analyze the obtained correlation functions. For temperature dependent measurements the DLS is equipped with a Lauda thermostat. Apparent hydrodynamic diameters were calculated according to the Stokes–Einstein equation. All CONTIN plots shown are number-weighted.

UV-vis spectroscopy

All UV-vis spectra were measured on a Vario Cary 5000 UV-vis spectrometer.

BET

The specific surface area was determined *via* the BET method[37] by multipoint nitrogen adsorption measurements at 77 K utilizing an Autosorb-1, Quantachrome Corporation. Prior to the measurements, the sample was evacuated at 300 °C to remove remaining water from the surface.

Cyclic voltammetry (CV)

Electrochemical data were obtained by cyclic voltammetry using a conventional single-compartment three electrode cell arrangement in combination with a potentiostat AUTOLAB®, *eco chemie*. For the measurements a 0.196 cm^2 Pt disk was used as the working electrode, glassy carbon as the auxiliary electrode and Ag/AgCl (3 M KCl) as the reference electrode. Measurements were carried out in nitrogen purged water with 0.2 M KCl as the supporting electrolyte and 0.01 M KH_2PO_4 and 0.01 M K_2HPO_4 as the buffer.

Results and discussion

The aim of the work described was to establish a versatile and straightforward synthetic route toward nanostructured and porous NiO_x surfaces using amphiphilic diblock copolymers as templates for micellar intermediates. All steps involved were monitored using various techniques, *e.g.* light scattering and UV-vis measurements. It is well-known that amine-containing block copolymers can be used to complex metal ions, as has been demonstrated for poly(2-vinylpyridine) and Zn^{2+},[33] poly((2-dimethylamino)ethyl methacrylate),[38] poly(ethylene imine),[39] or for the formation of noble metal nanoparticles within distinct domains of block copolymer nanostructures.[31,40,41]

Here, we used three different polystyrene-*block*-poly(2-vinylpyridine) (PS-*b*-P2VP) diblock copolymers. The molecular parameters (block weight fractions, molecular weights, dispersity indices) are summarized in Table 1. The process employed for the formation of NiO_x nanostructures including all intermediate steps is depicted in Fig. 1. Starting with a block copolymer solution of PS-*b*-P2VP in a non-selective solvent (unimers are present), the subsequent addition of Ni^{2+} and the Ni^{2+}–P2VP complex formation leads to a collapse of the P2VP segment and the formation of micelles (see Fig. 1, step i). These structures then feature a PS corona and a hybrid Ni^{2+}–P2VP complex coacervate core. For these structures, we were aiming at diameters of about 100 nm to later yield NiO_x nanoparticles in the sub-100 nm range after calcination. An excess of Ni^{2+} eventually leads to further agglomeration of the structures and to a macroscopic precipitate (step ii). Both individual micelles in solution (step iv) and the precipitate (step iii) can then be deposited onto suitable substrates and used for subsequent calcination to yield nanostructured NiO_x nanoparticle surfaces.

We first started by investigating solutions of the different PS-*b*-P2VP block copolymers in toluene of varying polymer concentrations by dynamic light scattering (DLS, Fig. 2A). As shown in Table 1, we used three different compositions, PS_{65}-*b*-$P2VP_{35}$, PS_{68}-*b*-$P2VP_{32}$, and PS_{75}-*b*-$P2VP_{25}$. The subscripts denote the weight fraction (wt%) of the corresponding block. The DLS results shown in Fig. 2A confirm the presence of unimers ($\langle D_h \rangle_{n,app} < 20$ nm) for PS_{68}-*b*-$P2VP_{32}$ and PS_{75}-*b*-$P2VP_{25}$ in toluene at all concentrations investigated (up to 10 g L^{-1}). Only in the case of PS_{65}-*b*-$P2VP_{35}$ larger structures with hydrodynamic diameters of up to 200 nm were found when using concentrations higher than 5 g L^{-1} (red spheres in Fig. 2A). This might be due to the high content of P2VP in this block copolymer and this sample features the highest molar mass of all diblock copolymers used. For PS_{75}-*b*-$P2VP_{25}$ the corresponding CONTIN plots are shown in Fig. 2B, depicting hydrodynamic diameters of $\langle D_h \rangle_{n,app} = 14$–18 nm for the entire concentration range.

In all cases (PS_{65}-*b*-$P2VP_{35}$, PS_{68}-*b*-$P2VP_{32}$, and PS_{75}-*b*-$P2VP_{25}$) micellization can be induced upon addition of a saturated ethanolic $NiCl_2$ solution, indicated by a color shift of the

Table 1 Molecular characteristics of the three different polystyrene-*block*-poly(2-vinylpyridine) diblock copolymers used

Diblock copolymer	M_n[b] [kg mol^{-1}]	PDI[c]
PS_{65}-*b*-$P2VP_{35}$[a]	230	1.03
PS_{68}-*b*-$P2VP_{32}$	66	1.02
PS_{75}-*b*-$P2VP_{25}$	146	1.04

[a] The subscripts denote the weight fraction (%) of the corresponding segment and were determined *via* ^{1}H-NMR in $CDCl_3$. [b] The molecular weight of the first block (PS) was determined using THF–SEC with PS calibration; the length of the P2VP segment was then calculated by ^{1}H-NMR spectroscopy using the M_n of the PS block for signal calibration. [c] Determined by THF–SEC applying a PS calibration.

reaction mixture from colorless to green or blue. This color change is attributed to the formation of Ni^{2+} complexes with heterocyclic aromatic amines, which show a characteristic blue coloring.[35] The complexation can be induced by $NiCl_2$ in ethanol, while $Ni(acac)_2$ complexes were found to be not labile enough to enable complex formation with the 2-vinylpyridine moiety. Thereby, the micellar size depends on the Ni^{2+}/2VP ratio (Fig. 2C). While PS_{65}-*b*-$P2VP_{35}$ and PS_{68}-*b*-$P2VP_{32}$ strongly agglomerate starting from 0.5 and 0.7 equivalents of Ni^{2+}/2VP, as evidenced by the apparent hydrodynamic diameter of more than 2000 nm (data not shown), PS_{75}-*b*-$P2VP_{25}$ only shows a moderate size increase from 40 nm at 0.6 eq. to 80 nm when 1 eq. of Ni^{2+}/2VP was used. The subsequent addition of more than 1 eq. of Ni^{2+} leads to the formation of a blue precipitate (photograph shown in Fig. 2D), indicating further aggregation and, finally, precipitation. As will be shown later in the UV-vis spectra, the supernatant solution does not exhibit the characteristic absorption for Ni^{2+}–pyridine complexes and, hence, we expect the precipitation to be almost quantitative.

The comparison of the micellar sizes of the three PS-*b*-P2VP block copolymers revealed that micelles formed by PS_{75}-*b*-$P2VP_{25}$ match the desired size range of 40–80 nm diameter and, in addition, here the highest loading capacity with Ni^{2+} with respect to 2VP while maintaining colloidal stability was found. Both other block copolymer samples showed significant

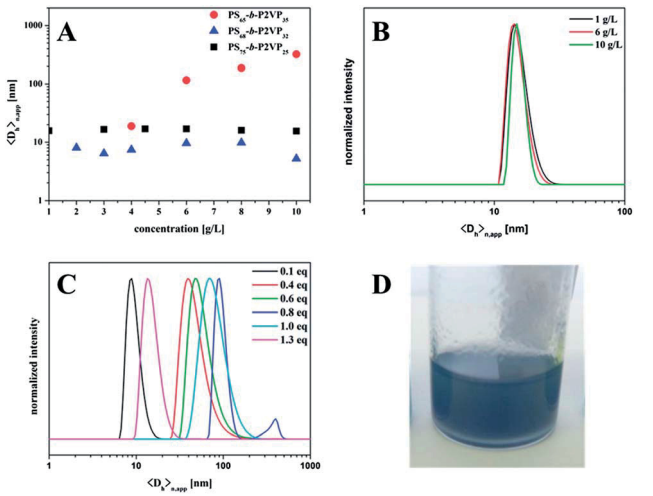

Fig. 2 (A) Hydrodynamic diameter of PS_{65}-*b*-$P2VP_{35}$ (red spheres), PS_{68}-*b*-$P2VP_{32}$ (blue triangles), and PS_{75}-*b*-$P2VP_{25}$ (black squares) in toluene at different concentrations. (B) DLS CONTIN plots of PS_{75}-*b*-$P2VP_{25}$ at different concentrations in toluene; (C) DLS CONTIN plots for PS_{75}-*b*-$P2VP_{25}$ after the addition of different amounts of Ni^{2+}: 0.1 eq. (8 nm), 0.4 eq. (40 nm), 0.6 eq. (48 nm), 0.8 eq. (90 nm), 1.0 eq. (68 nm), and 1.3 eq. (14 nm, also a macroscopic precipitate was formed) at a constant block copolymer concentration of 10 g L^{-1}; (D) photograph of a vial containing a Ni^{2+}–block copolymer mixture with 1.3 eq. Ni^{2+}/VP.

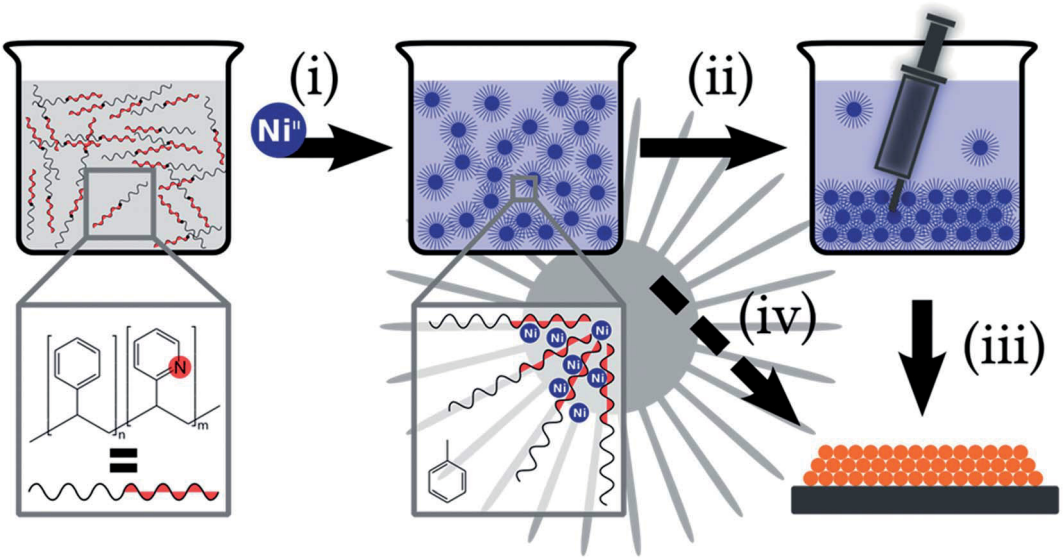

Fig. 1 Schematic representation of the synthetic route towards nanostructured NiO_x; the addition of Ni^{2+} to a PS-*b*-P2VP block copolymer solution leads to the formation of micelles (i); increasing the Ni^{2+} concentration above a critical threshold leads to precipitation (ii); this precipitate is then spin coated onto a glass substrate and calcined at 450 °C (iii); alternatively, the initial micellar solution after step (i) can be directly applied to a suitable substrate *via* spin coating (iv).

aggregation at comparable loading. Therefore, further experiments exclusively focused on the use of PS_{75}-*b*-$P2VP_{25}$.

After having identified a suitable block copolymer for templating, besides toluene also chloroform and THF were tested regarding the formation of Ni^{2+}–PS_{75}-*b*-$P2VP_{25}$ hybrid micelles. As shown in Fig. 2, hydrodynamic diameters in the desired sub-100 nm range could be obtained when using toluene. According to TEM, for the addition of 0.8 equivalents of Ni^{2+} micelles, a core of 20–30 nm in size can be found (Fig. 3A). This corresponds quite well to the results obtained earlier using DLS ($\langle D_h \rangle_{n,app} = 90$ nm) and the particles are of spherical shape. They thus fit the prerequisites we postulated above for the synthesis of a homogeneous nanostructured NiO_x surface. For comparison, micelles formed in chloroform and THF were rather ill-defined and exhibited – especially in the case of THF – a rather inhomogeneous size distribution (Fig. 3B). Furthermore, the micelles deposited from chloroform formed interconnected networks according to TEM (Fig. 3C) and the inner part of the structures appeared brighter than the surrounding, which hints towards the localization of the heavier Ni^{2+} ions within the corona of the micelle (collapses when deposited onto the TEM grid). We therefore focused on the use of Ni^{2+}/PS_{75}-*b*-$P2VP_{25}$ hybrid micelles prepared in toluene.

In toluene, the aforementioned blue color of the Ni^{2+}-loaded micelles is highly dependent on the Ni^{2+}/2VP ratio. This color change can be monitored by UV-vis spectroscopy in order to get more insight into the loading of the micellar core and, eventually, precipitation. The pure ethanolic solution of $NiCl_2$ exhibits an absorption band at 420 nm (Fig. 4). Solutions with low Ni^{2+}/2VP ratios of 0.4 eq. show decreasing intensity of this band at 420 nm, indicating low concentrations of free Ni^{2+}, *i.e.*, almost all nickel ions are complexed by P2VP. These solutions strongly absorb at around 620 nm, indicating the presence of the blue Ni^{2+}–2VP complex. Further increase of the amount of Ni^{2+} leads to a decrease of the band at 620 nm. These findings are supported by DLS measurements, which show a distinct decrease in particle size as the Ni^{2+}/2VP ratio approaches unity (Fig. 2). Besides precipitation occurring for the Ni^{2+}–block copolymer hybrid micelles, which simultaneously decreases the concentration of the blue Ni^{2+}–2VP complexes, also free Ni^{2+} remains in the supernatant solution as shown by an increase in the band at 420 nm.

The PS_{75}-*b*-$P2VP_{25}$ micelles with a Ni^{2+}/2VP ratio of 0.8 were further investigated using scanning electron microscopy (SEM) after deposition onto a carbon-coated copper grid (Fig. 5A). Here, an average micellar diameter of roughly 60 to 100 nm was found, which is slightly larger than the size estimated by TEM. This can be explained by the fact that by TEM only the micellar core could be visualized and the less densely packed corona is spread onto the TEM grid and not visible. The size is comparable to that obtained by DLS ($\langle D_h \rangle_{n,app} = 90$ nm). After calcination utilizing a temperature program raising the temperature from 300 °C to 450 °C in 20 min and holding at 450 °C for further 10 min, ellipsoidal toroids of 100 to 150 nm diameter were found on the substrate (Fig. 5B). These structures might have resulted from the fusion of several spherical micelles during the calcination process. A broadened size distribution of the tempered nanoparticles compared to the Ni^{2+}-loaded block copolymer micelles probably results from the sintering of adjacent precursor structures during the temperature program. This phenomenon was also observed for the synthesis of *e.g.* ZnO nanoparticles templated by PS-*b*-P2VP.[33] However, sample preparation from dilute but colloidally stable solutions bears one main disadvantage: we are interested in rather thick NiO_x films and this is difficult to realize due to the rather low nickel concentration in the mixture used here. The resultant material would feature a low optical density after dye sensitization and this would prohibit its use in, *e.g.*, dye-sensitized solar cells. The

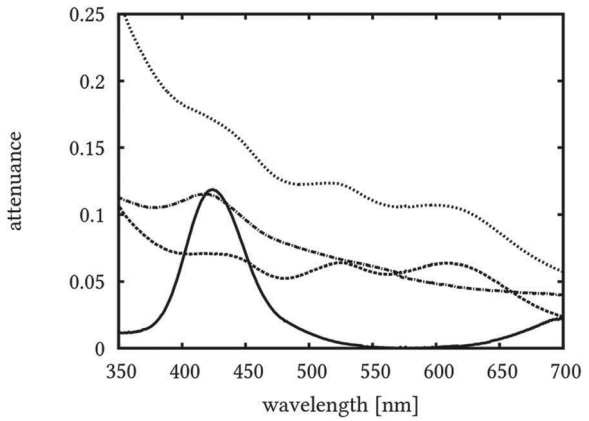

Fig. 4 UV-vis spectra of $NiCl_2$ in ethanol (solid line, saturated solution), micellar solutions (10 g L^{-1} in toluene) of PS_{75}-*b*-$P2VP_{25}$ with 0.4 equivalents (dashed line) and 0.8 equivalents (dotted line) of Ni^{2+}, and the supernatant solution of the reaction mixture with 1.6 equivalents (dash-dotted line) of Ni^{2+}.

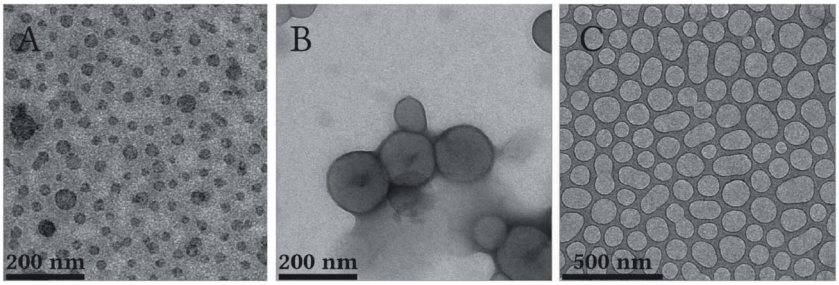

Fig. 3 TEM micrographs of Ni^{2+}-loaded block copolymer micelles of PS_{75}-*b*-$P2VP_{25}$ deposited from toluene (A), THF (B), and chloroform (C). Dark regions indicate the presence of Ni.

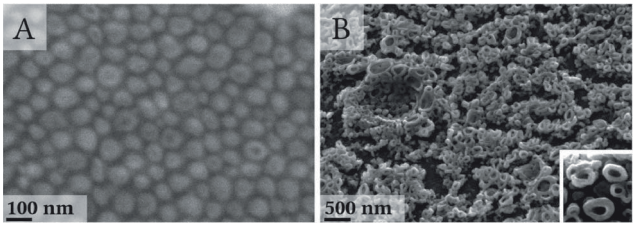

Fig. 5 (A) Backscattered electrons (BSE). SEM micrographs of PS_{75}-*b*-$P2VP_{25}$ block copolymer micelles with 0.8 equivalents of Ni^{2+}/2VP. (B) Secondary electron imaging (SEI). After depositing the micelle solution onto a glass substrate and calcination the remaining NiO_x forms ellipsoidal nano-toroids. The edge size of the inset is 500 nm.

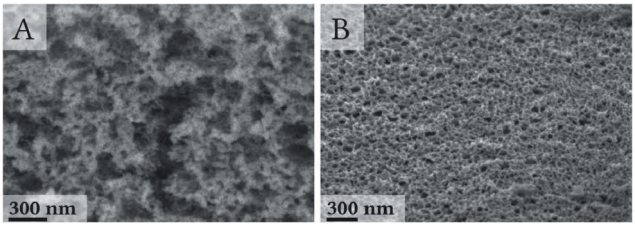

Fig. 6 (A) BSE. Calcination of the precipitate yields a fine-structured porous NiO_x film (1.3 eq. Ni^{2+}/2VP). (B) SEI, tilting 60°. Another nanostructured NiO_x surface produced *via* spin coating of a sonicated suspension of the precipitate (1.6 eq. Ni^{2+}/2VP).

overall film thickness, if multi-layer films are targeted, should exceed one μm. The thickness of the film and the nanoporosity present a high internal surface area and enable a high loading of dyes onto the electrodes, which are desirable for use in dye-sensitized NiO_x applications.

If a Ni^{2+}/2VP ratio of 1.3 is used, a macroscopic precipitate is formed (Fig. 2C and D). This is an attractive alternative as this precipitate most probably consists of agglomerated Ni^{2+}–block copolymer hybrid micelles. Therefore, the mixture with the precipitate was centrifuged and the supernatant solution was discarded. The wet precipitate was re-suspended by sonication using a Sonics Vibracall VC505 with a power of 500 W for 10 s with a frequency of 20 kHz to form a pasty suspension. This suspension can be deposited onto a glass substrate *via* spin coating or doctor blading. After calcination, an entirely different NiO_x morphology compared to the toroids and nanoparticles was found (Fig. 6; Fig. 6A represents the precipitate without additional sonication treatment). The structure can be best described as a nanostructured, highly porous NiO_x film. Depending on how the precipitate is treated before calcination, interlinked NiO_x nanoparticles (Fig. 7A, spin coating) or fine porous NiO_x network films (Fig. 6) are formed after calcination.

Generally, doctor blading yields thicker films if compared to spin coating, while the films prepared by spin coating typically are more homogeneous. In order to compare both techniques regarding the surface morphology, a suspension of the precipitate formed from a Ni^{2+}–block copolymer mixture at a ratio of 1.6 was prepared. At this point, the ratio was slightly increased in order to ensure quantitative precipitation. While stirring, this reaction mixture was deposited onto glass substrates by both spin coating and doctor blading. At this point no sonication was used. After calcination, the EDX spectra of the NiO_x surfaces resulting from spin coating exhibited a less intense Ni–L signal at 0.85 keV than the sample obtained by doctor blading. At the same time, the weaker Ni–K signal at 7.47 keV completely vanished, which was not the case when the sample was prepared by doctor blading (Fig. 8). Nevertheless, the background consisting of contributions from Na, Mg, Al, Si, Ca, and K from the glass substrate was comparable in both cases.

The SEM comparison of a thin and homogeneous film produced by spin coating and a thicker film produced by doctor blading is shown in Fig. 7A (spin coating) and 7B (doctor blading). The images reveal that doctor blading produces surfaces with crates (Fig. 7B) and spin coating yields very homogeneous surfaces compared to the surfaces produced by doctor blading with an average particle size of ~60 nm (Fig. 7A). In order to prohibit the formation of crates, the following experiments utilize sonication to yield more homogeneous films.

As an attempt to combine the benefits of spin coating and the use of larger agglomerates (formed in the precipitate separated by centrifugation) to gain more homogeneous NiO_x films, we partially re-dispersed the precipitate by sonication at high concentrations of 1.6 eq. Ni^{2+}/2VP prior to spin coating of this viscous, paste-like suspension. After subsequent deposition *via* spin coating very homogeneous surfaces were found by SEM (Fig. 6B). For producing thick NiO_x films of more than one μm, this procedure was repeated to form double and triple layers.[29,30] The procedure is straightforward since after calcination of the first film the second layer can be added using the same conditions. After repeating this procedure three times, a NiO_x triple layer of 1.4 μm thickness according to SEM was formed (Fig. 9). Interestingly, a homogeneous cross-section can be seen, *i.e.* the three different layers cannot be differentiated afterwards. We therefore regard this procedure as a facile and straightforward synthetic route to nanoporous and homogeneous NiO_x films of a thickness which is comparable to literature values for NiO_x films.[12,18,19,29,42]

To further investigate these films, the BET surface area against nitrogen has been determined to be approx. 50 $m^2\ g^{-1}$ (1.6 eq. Ni^{2+}/2VP). This value, which lies slightly below the expected range of 60 $m^2\ g^{-1}$ as measured for surfaces synthesized in our labs according to the literature using the triblock copolymer F108,[30] needs to be carefully interpreted as for the BET experiments at least 10 mg of the material have to be used.

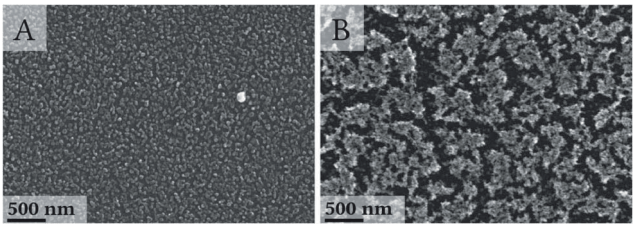

Fig. 7 SEM comparison of a NiO_x nanostructured surface produced by ((A) SEI) spin coating and ((B) SEI) doctor blading.

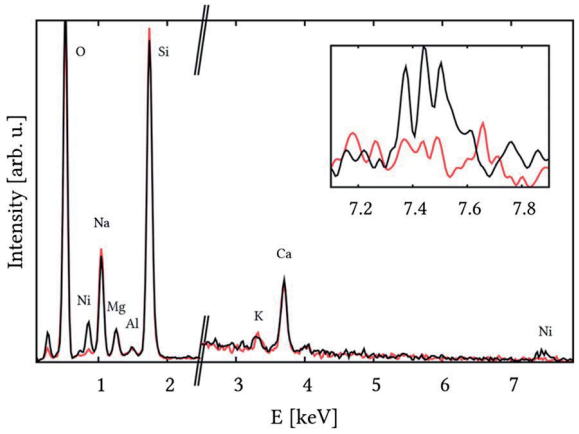

Fig. 8 Comparison of energy-dispersive X-ray spectra of NiO_x surfaces produced by doctor blading (black) and spin coating (red) using PS_{75}-*b*-$P2VP_{25}$ as a template for the nanoparticle formation. The intensities of the spectra greater than 2.5 keV are multiplied by a factor of 5. The inset highlights the region in the range of 7–8 keV including the Ni-Kα line ($K\alpha_1$: 7470 eV).

As a consequence, the corresponding sample was prepared in the bulk and not on a comparable glass substrate where the NiO_x nanoparticles can be scraped off – as it has been done with the reference value from the synthesis *via* F108. The consequence is that slightly different agglomeration and sintering might occur during the procedure and calcination. On the other hand, the BET surface areas reported by Sumikura *et al.* also using F108 were about 40 $m^2\ g^{-1}$. Compared with these results, our synthetic route presented here leads to about 25% higher surface areas, but it has to be taken into account that the preparation conditions might also be different.[28]

To further compare our approach with established routes,[26] cyclic voltammetry (CV) measurements were performed. The cyclic voltammograms obtained from the double film are shown in Fig. 10A. Here, the distinct double peak structure in both anodic and cathodic cycles can be seen, which originates from the oxidation of Ni^{II} to Ni^{III} and Ni^{IV}. The half peak potentials E_p(I) and E_p(II) are 0.38 V and 0.73 V, respectively. These CV measurements reveal that the NiO_x surfaces produced here behave comparably to NiO_x surfaces reported in the literature (E_p(I) = 0.32 V and E_p(II) = 0.69 V).[26] Furthermore, no changes in the cyclic voltammograms become visible upon the fourfold cycling of each scan rate (10, 20, 50, and 100 mV s^{-1}). Therefore, the surface appears to be stable under electrochemical conditions in the potential range. The CVs of the NiO_x nanostructures templated by polystyrene-*block*-poly(2-vinylpyridine) block copolymer micelles recorded at different scan rates suggest a surface-confined redox system.

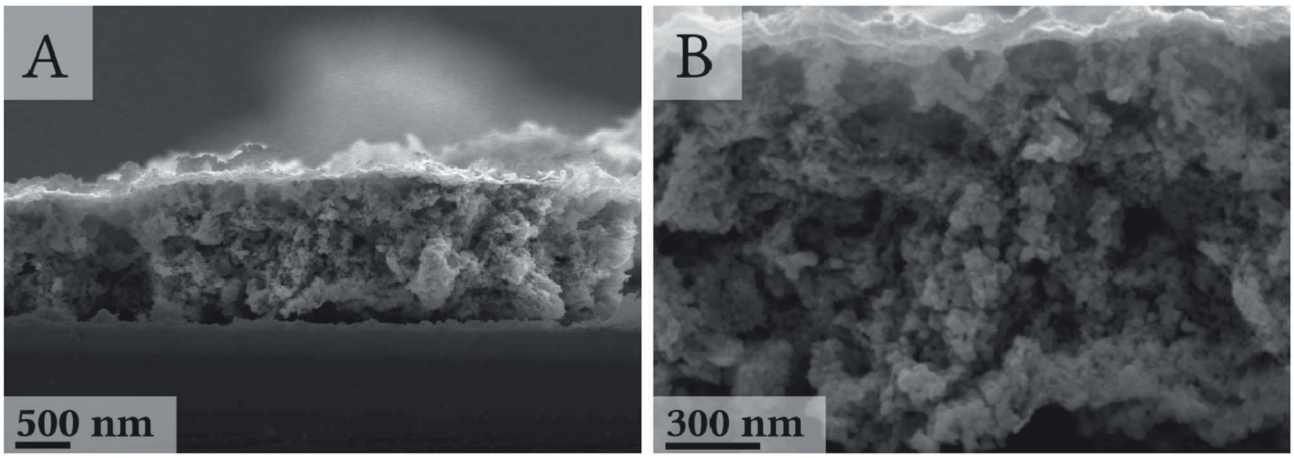

Fig. 9 SEM (SEI) images of a NiO_x edge after breaking a triple film under cryoscopic conditions. The film was produced by using the centrifuged and sonicated precipitate. The deposition step was repeated three times.

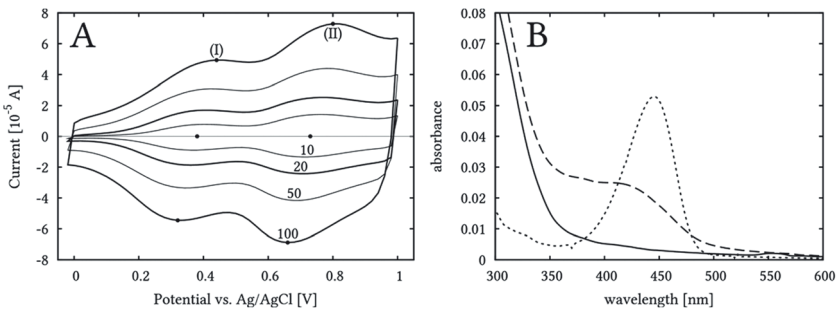

Fig. 10 (A) Comparison of cyclic voltammograms of a NiO_x double film at four scan rates: 10, 20, 50, and 100 mV s^{-1}. (B) UV-vis spectra of coumarine 343 (dotted), of a blank NiO_x surface (solid), and the dye-sensitized NiO_x surface (dashed).

To further elucidate the capabilities of the synthesized NiO_x film as dye-sensitized electrodes, the surfaces were loaded with coumarine 343 (C343), thoroughly washed with acetonitrile and investigated by UV-vis spectroscopy. As can be seen in Fig. 10B, the absorption spectrum of the pure NiO_x surface differs from the spectrum of the C343-sensitized surface by the formation of an absorption shoulder at about 430 nm, which matches the shape of the pure C343 solution. Hence, it is concluded that the dye C343 successfully binds to the surface. Therefore, the NiO_x nanostructured films discussed here might serve as the basis for photoelectrodes of dye-sensitized solar cells or (photo-) catalytic cells.

The experiments and results described above introduce a new synthetic route towards NiO_x nanostructured films (see Fig. 1), which, in contrast to established methods, can be easily tuned. If colloidally stable micellar solutions are used for the preparation of NiO_x layers onto glass substrates, toroidal aggregates are obtained. However, the applicability of these might be limited as rather dilute solutions hamper the production of thicker layers. However, if the precipitate of PS-*b*-P2VP micelles at higher Ni^{2+} loadings is used, thicker and more homogeneous networks are formed, rendering a promising material for various applications.

Conclusion

A new synthetic route to homogeneous and nanoporous NiO_x films is presented. Our approach is straightforward, flexible, and provides access to different NiO_x nanostructures. Three different block copolymers (PS_{65}-*b*-$P2VP_{35}$, PS_{68}-*b*-$P2VP_{32}$, and PS_{75}-*b*-$P2VP_{25}$) were investigated, and for PS_{75}-*b*-$P2VP_{25}$ well-defined Ni^{2+} containing hybrid micelles in the size range of 60–90 nm could be obtained. If a critical threshold regarding the content in Ni^{2+} is reached, the Ni^{2+}–block copolymer hybrid particles further agglomerate and a macroscopic precipitate is formed. Both colloidally stable micellar solutions and a macroscopic precipitate were tested to prepare NiO_x films by, at first, deposition on a glass substrate, followed by calcination. It is shown that very homogeneous and thick (up to 1.4 μm) nanostructured films can be produced by using thick suspensions of the precipitate after sonication as samples for spin coating. The resulting calcinated NiO_x films showed promising first results as parts in *p*-type dye-sensitized semiconductor modules for solar cells or (photo-)catalytic cells after sensitization with coumarine 343. UV-vis investigation shows that coumarine 343 is successfully adsorbed to the surface, which is a crucial prerequisite for this application. The measured surface area of the presented NiO_x films is comparable to literature values from attempts with Pluronic F108 as the block copolymer template. Future experiments, *e.g.*, transient absorption spectroscopy will prove if the NiO_x is able to inject electrons into the excited dyes.

Acknowledgements

Financial support from the Studienstiftung des deutschen Volkes (M.B.) and the Fonds der Chemischen Industrie (B.D.) is gratefully acknowledged. F. H. S. and T. R. are further grateful to the Thuringian Ministry for Education, Science, and Culture (TMBWK; #B515-10065, ChaPoNano). T. R. acknowledges the Carl-Zeiss foundation for a PhD-scholarship. F. H. S. thanks the VCI for a starting independent researcher fellowship and Ulrich S. Schubert for continuous support.

References

1 F. Odobel, L. Le Pleux, Y. Pellegrin and E. Blart, *Acc. Chem. Res.*, 2010, **43**, 1063–1071.
2 F. Odobel, Y. Pellegrin, E. A. Gibson, A. Hagfeldt, A. L. Smeigh and L. Hammarström, *Coord. Chem. Rev.*, 2012, **256**, 2414–2423.
3 F. A. Harraz, R. M. Mohamed, A. Shawky and I. A. Ibrahim, *J. Alloys Compd.*, 2010, **508**, 133–140.
4 K. Maeda and K. Domen, *J. Phys. Chem. Lett.*, 2010, **1**, 2655–2661.
5 K. Maeda, N. Sakamoto, T. Ikeda, H. Ohtsuka, A. Xiong, D. Lu, M. Kanehara, T. Teranishi and K. Domen, *Chem.–Eur. J.*, 2010, **16**, 7750–7759.
6 N. Hondow, Y.-H. Chou, K. Sader, R. Brydson and R. E. Douthwaite, *J. Phys. Chem. C*, 2010, **114**, 22758–22762.
7 X. Tang, H. Ye, H. Liu, C. Ma and Z. Zhao, *J. Solid State Chem.*, 2010, **183**, 192–197.
8 Y.-C. Chiou, U. Kumar and J. C. S. Wu, *Appl. Catal., A*, 2009, **357**, 73–78.
9 V. S. R. Channu, R. Holze and B. Rambabu, *Colloids Surf., A*, 2012, **414**, 204–208.
10 A. Kumar Rai, L. Tuan Anh, C.-J. Park and J. Kim, *Ceram. Int.*, 2013, **39**, 6611–6618.
11 G. H. Jeong, H.-B. Bae, D. Choi, Y. H. Kim, S. Yoon and S.-W. Kim, *J. Phys. Chem. C*, 2012, **116**, 23851–23857.
12 J. He, H. Lindström, A. Hagfeldt and S.-E. Lindquist, *J. Phys. Chem. B*, 1999, **103**, 8940–8943.
13 A. Hagfeldt, G. Boschloo, L. Sun, L. Kloo and H. Pettersson, *Chem. Rev.*, 2010, **110**, 6595–6663.
14 J. He, H. Lindström, A. Hagfeldt and S.-E. Lindquist, *Sol. Energy Mater. Sol. Cells*, 2000, **62**, 265–273.
15 A. Nattestad, M. Ferguson, R. Kerr, Y.-B. Cheng and U. Bach, *Nanotechnology*, 2008, **19**, 295304.
16 W. Shockley and H. J. Queisser, *J. Appl. Phys.*, 1961, **32**, 510–519.
17 L. Li, L. Duan, F. Wen, C. Li, M. Wang, A. Hagfeldt and L. Sun, *Chem. Commun.*, 2012, **48**, 988–990.
18 M. Awais, D. D. Dowling, M. Rahman, J. G. Vos, F. Decker and D. Dini, *J. Appl. Electrochem.*, 2013, **43**, 191–197.
19 E. A. Gibson, M. Awais, D. Dini, D. P. Dowling, M. T. Pryce, J. G. Vos, G. Boschloo and A. Hagfeldt, *Phys. Chem. Chem. Phys.*, 2013, **15**, 2411–2420.
20 B. A. Reguig, A. Khelil, L. Cattin, M. Morsli and J. C. Bernède, *Appl. Surf. Sci.*, 2007, **253**, 4330–4334.
21 E. Fujii, A. Tomozawa, S. Fujii, H. Torii, M. Hattori and R. Takayama, *Jpn. J. Appl. Phys.*, 1993, **32**, L1448–L1450.
22 M. Tachiki, T. Hosomi and T. Kobayashi, *Jpn. J. Appl. Phys.*, 2000, **39**, 1817–1820.
23 L. Berkat, L. Cattin, A. Reguig, M. Regragui and J. C. Bernède, *Mater. Chem. Phys.*, 2005, **89**, 11–20.

24 J. S. E. M. Svensson and C. G. Granqvist, *Appl. Phys. Lett.*, 1986, **49**, 1566–1568.
25 H.-L. Chen, Y.-M. Lu and W.-S. Hwang, *Surf. Coat. Technol.*, 2005, **198**, 138–142.
26 G. Boschloo and A. Hagfeldt, *J. Phys. Chem. B*, 2001, **105**, 3039–3044.
27 P. Qin, H. Zhu, T. Edvinsson, G. Boschloo, A. Hagfeldt and L. Sun, *J. Am. Chem. Soc.*, 2008, **130**, 8570–8571.
28 S. Sumikura, S. Mori, S. Shimizu, H. Usami and E. Suzuki, *J. Photochem. Photobiol., A*, 2008, **199**, 1–7.
29 L. Li, E. A. Gibson, P. Qin, G. Boschloo, M. Gorlov, A. Hagfeldt and L. Sun, *Adv. Mater.*, 2010, **22**, 1759–1762.
30 M. Bräutigam, M. Schulz, J. Inglis, J. Popp, J. G. Vos and B. Dietzek, *Phys. Chem. Chem. Phys.*, 2012, **14**, 15185–15190.
31 F. H. Schacher, P. A. Rupar and I. Manners, *Angew. Chem., Int. Ed.*, 2012, **51**, 7898–7921.
32 A. Sikora and Z. Tuzar, *Makromol. Chem.*, 1983, **184**, 2049–2059.
33 C. H. Braun, T. V. Richter, F. Schacher, A. H. E. Müller, E. J. W. Crossland and S. Ludwigs, *Macromol. Rapid Commun.*, 2010, **31**, 729–734.
34 H.-G. Biedermann, E. Griessl and K. Wichmann, *Makromol. Chem.*, 1973, **172**, 49–55.
35 H. Köhler, H. Hartung and B. Seifert, *Z. Anorg. Allg. Chem.*, 1966, **347**, 30–38.
36 E. Giebeler and R. Stadler, *Macromol. Chem. Phys.*, 1997, **198**, 3815–3825.
37 S. Brunauer, P. H. Emmett and E. Teller, *J. Am. Chem. Soc.*, 1938, **60**, 309–319.
38 J. Yuan, F. Schacher, M. Drechsler, A. Hanisch, Y. Lu, M. Ballauff and A. H. E. Müller, *Chem. Mater.*, 2010, **22**, 2626–2634.
39 L. Bai, H. Zhu, J. S. Thrasher and S. C. Street, *ACS Appl. Mater. Interfaces*, 2009, **1**, 2304–2311.
40 F. Schacher, E. Betthausen, A. Walther, H. Schmalz, D. V. Pergushov and A. H. E. Müller, *ACS Nano*, 2009, **3**, 2095–2102.
41 F. H. Schacher, T. Rudolph, M. Drechsler and A. H. E. Müller, *Nanoscale*, 2011, **3**, 288–297.
42 M. Awais, M. Rahman, J. M. Don MacElroy, D. Dini, J. G. Vos and D. P. Dowling, *Surf. Coat. Technol.*, 2011, **205**, S245–S249.

Publication P14

“Star-Shaped Poly-(2-ethyl-2-oxazoline) Featuring a Porphyrin Core: Synthesis, and Metal Complexation”

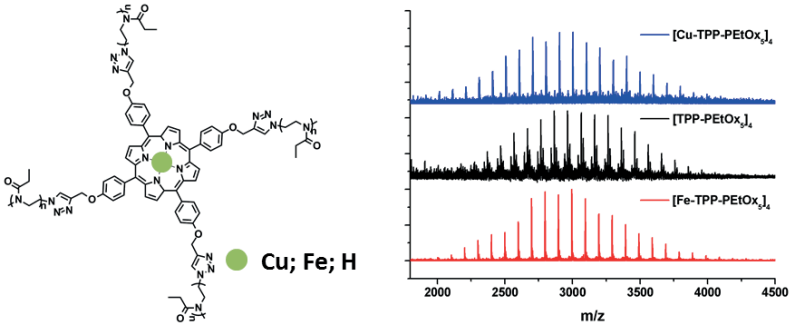

Tobias Rudolph, Sarah Crotty, Ulrich S. Schubert, Felix H. Schacher

e-Polymers, **2015**, in press (DOI: 10.1515/epoly-2015-0041)

Tobias Rudolph, Sarah Crotty, Ulrich S. Schubert and Felix H. Schacher*

Star-shaped poly(2-ethyl-2-oxazoline) featuring a porphyrin core: synthesis and metal complexation

Abstract: We demonstrate the synthesis of star-shaped poly(2-ethyl-2-oxazoline) featuring a porphyrin core starting from alkyne-functionalized porphyrin ($[TPP\text{-}TB]_4$) and azide-functionalized poly(2-ethyl-2-oxazoline) (PEtOx-N_3) via copper-catalyzed azide-alkyne cycloaddition (CuAAC). The porphyrin core was further utilized for the complexation of either copper or iron within the central cavity. The obtained materials were investigated using a combination of nuclear magnetic resonance spectroscopy, fourier transform infrared spectroscopy, ultraviolet-visible spectroscopy, size-exclusion chromatography, and matrix assisted laser desorption/ionization time-of-flight mass spectrometry. In the case of copper, the inclusion of the metal ion was achieved in a one-pot reaction during the CuAAC reaction for attaching the PEtOx-N_3 arms.

Keywords: metal-containing polymers; poly(2-ethyl-2-oxazoline); porphyrins; star-shaped polymers.

DOI 10.1515/epoly-2015-0041
Received February 17, 2015; accepted March 16, 2015

1 Introduction

For the synthesis of star-shaped polymers, typically two different approaches are used, either core first or arm first (1–3). In the case of core-first strategies, a core molecule or a multifunctional initiator is synthesized or modified with initiating groups applicable for controlled polymerization reactions. In the literature, different examples of atom transfer radical polymerization (4, 5), reversible addition fragmentation chain transfer (6), anionic ring-opening polymerization (7, 8), or cationic ring-opening polymerization (CROP) (9, 10) are reported. One clear disadvantage of the core-first approach is that complete initiation is often difficult to verify and lower arm numbers are found when compared to initiation sites. This can be avoided in the arm-first approach, as each building block can be separately characterized and the degree of functionalization can be quantitatively determined for each step. In that respect, efficient macromolecular conjugation reactions have been extensively investigated for an efficient linkage between two complementary motifs, leading to different possibilities for the synthesis of new materials (11–16). Among these possibilities, one versatile platform are copper-catalyzed azide-alkyne cycloaddition (CuAAC) reactions, which have already been used for the formation of networks (17, 18), block copolymers (19–21), or other polymer architectures (13, 22, 23).

Porphyrins show potential for use in applications such as photosensitizers (24) and catalysts (25), and, owing to an inherent high affinity for metal complexation within the porphyrin cavity, the resulting materials have attractive optical properties that render them suitable precursors for hybrid materials (6, 26–32). Moreover, polymers based on porphyrins have been studied with regard to hierarchical self-assembly processes (6, 33, 34) and to their use in selective ion complexation (4).

We were interested in the combination of functionalized porphyrins and CuAAC of suitably modified polymeric building blocks for the synthesis of symmetrical, star-shaped, porphyrin-centered polymers. For this purpose, 5,10,15,20-tetrakis(4-hydroxyphenyl)-21H,23H-porphyrin ($[TPP\text{-}OH]_4$) was equipped with alkyne functionalities, and azide-functionalized poly(2-ethyl-2-oxazoline) (PEtOx-N_3) was covalently attached via subsequent CuAAC chemistry. We present a detailed study of the obtained materials through a combination of nuclear magnetic resonance spectroscopy (NMR), Fourier transform infrared spectroscopy (FTIR), size exclusion chromatography (SEC), ultraviolet-visible spectroscopy (UV-Vis) and matrix assisted laser desorption/ionization time-of-flight mass spectrometry (MALDI-ToF MS). Regarding the introduction of metal ions into the porphyrin cavity, this could be achieved in a

***Corresponding author: Felix H. Schacher,** Institute of Organic Chemistry and Macromolecular Chemistry (IOMC), Friedrich Schiller University Jena, Humboldtstr. 10, 07743 Jena, Germany; and Jena Center for Soft Matter (JCSM), Friedrich Schiller University Jena, Philosophenweg 7, 07743 Jena, Germany,
e-mail: felix.schacher@uni-jena.de
Tobias Rudolph, Sarah Crotty and Ulrich S. Schubert: Institute of Organic Chemistry and Macromolecular Chemistry (IOMC), Friedrich Schiller University Jena, Humboldtstr. 10, 07743 Jena, Germany; and Jena Center for Soft Matter (JCSM), Friedrich Schiller University Jena, Philosophenweg 7, 07743 Jena, Germany

one-pot synthesis for copper, whereas the introduction of iron (III) was realized in two steps.

2 Results and discussion

Herein, we focus on the synthesis of star-shaped poly(2-ethyl-2-oxazoline) (PEtOx) featuring a porphyrin core and four PEtOx arms via the arm-first approach. After the synthesis of azide-functionalized PEtOx building blocks, subsequent CuAAC reactions were used for the formation of star-shaped polymers. Our motivation is that well-defined porphyrin-centered building blocks with side chains of different lengths might be used as unimolecular sensors or in self-assembly studies owing to the planar nature of the porphyrin core. In that respect, we have already shown that the self-assembly mechanism for ABA bolaamphiphiles can be controlled by adjusting the length of the solubilizing PEtOx side chain in oligophenyleneethylene-based materials (35).

Commercially available $[TPP\text{-}OH]_4$ was used as a starting material for the preparation of an alkyne-functionalized core ($[TPP\text{-}TB]_4$). By etherification of the four hydroxyl groups, alkyne-functionalized $[TPP\text{-}TB]_4$ could be synthesized, where TB refers to the alkyne moieties (Figure 1A; Scheme S1). Briefly, $[TPP\text{-}OH]_4$ was dissolved in a tetrahydrofuran/methanol mixture (THF/MeOH; 5:1; v/v) together with potassium carbonate (K_2CO_3) and propargyl bromide and stirred at 45°C overnight. After the purification, $[TPP\text{-}TB]_4$ was obtained and investigated via NMR and FTIR, confirming the formation of the desired product in an overall yield of 95% (Figures S1 and S2). Full conversion of the hydroxyl group was proven by ^1H NMR through the disappearance of the corresponding signal at ≈10 ppm, whereas the aromatic signals for the phenyl ring were shifted by 0.1 ppm to lower field (Figure S1). The pyrrole NH signal of the porphyrin appeared at -2.8 ppm, which remained constant, and new signals corresponding to the alkyne functionality appeared at 5.1 and 3.8 ppm. Through FTIR, the disappearance of a broad peak for the hydroxyl group in the range above ≈3000 cm^{-1} and the appearance of a new signal corresponding to alkyne C-H (at 3290 cm^{-1}) and at 1025 cm^{-1} for a C-O stretching vibration could be observed (Figure S2). The characterization via NMR and FTIR confirmed the successful synthesis of $[TPP\text{-}TB]_4$. The solution properties of the pristine $[TPP\text{-}OH]_4$ and $[TPP\text{-}TB]_4$ were investigated via UV-Vis in THF. As can be seen in Figure S3, the shape, distribution, and intensity ratio of the absorption maxima remained

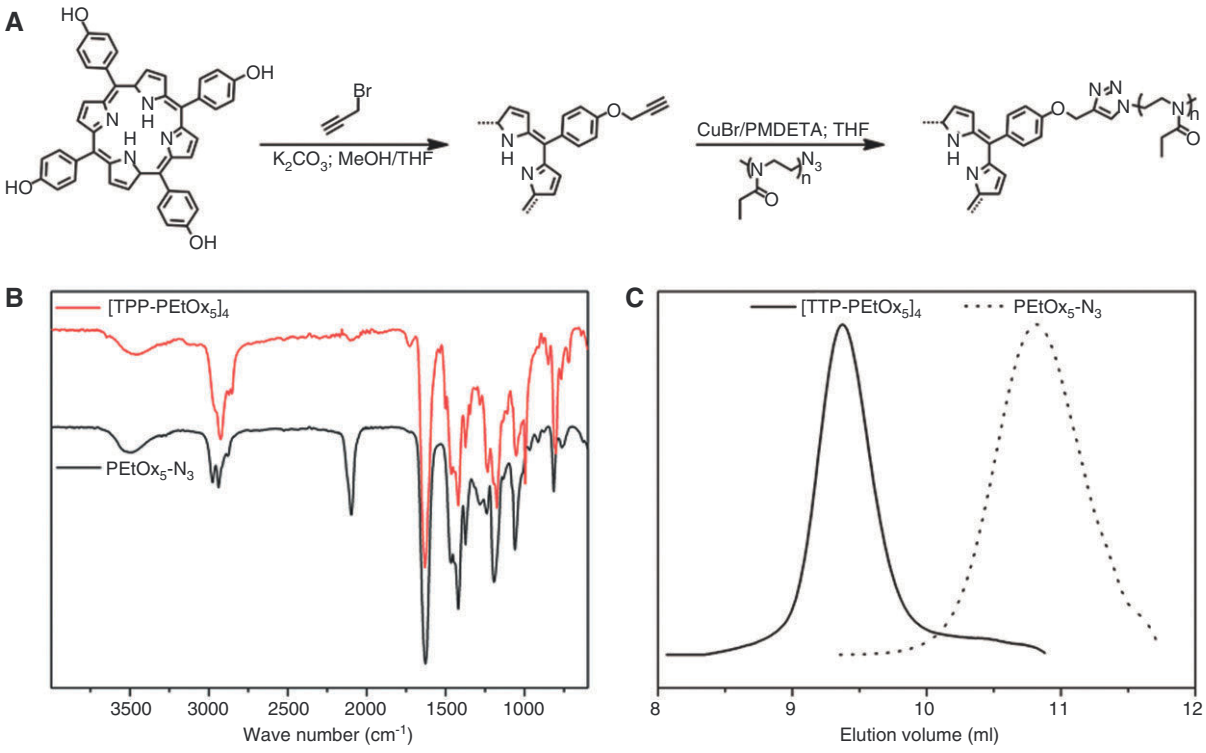

Figure 1: (A) Alkyne modification of $[TPP\text{-}OH]_4$ via etherification with propargyl bromide and subsequent CuAAC chemistry with $PEtOx_5\text{-}N_3$, forming porphyrin-centered star-shaped $[TPP\text{-}PEtOx_5]_4$; (B) comparison of FT-IR spectra for $PEtOx_5\text{-}N_3$ (black trace) and $[TPP\text{-}PEtOx_5]_4$ after purification (red trace); (C) comparison of SEC traces for $PEtOx_5\text{-}N_3$ (dotted line) and $[TPP\text{-}PEtOx_5]_4$ after precipitation (straight line).

constant before and after the modification, showing an intensive Soret band at 421 nm, whereas further bands were observed at 549, 554, 595, and 653 nm, respectively. This observation led us to the assumption that the optical properties were not changed during this modification step and that the integrity of the functionalized porphyrin unit was confirmed.

For the synthesis of azide-functionalized PEtOx oligomers, 2-ethyl-2-oxazoline (EtOx) was polymerized via microwave-assisted CROP initiated via methyl *p*-toluenesulfonate (MeTos) in acetonitrile (ACN). The reaction was terminated by the addition of sodium azide (NaN_3), leading to a substitution reaction introducing an azide end group (Scheme S2) (35). For the polymerization, a monomer-to-initiator ratio ([M]/[I]) of 5 at a constant monomer concentration of 4 mol l^{-1} was placed in the microwave synthesizer at 140°C. The obtained oligomer was investigated via NMR, SEC, and FTIR, to determine the degree of functionalization and molar mass (Figures S4–S6), and was found to be $PEtOx_5$-N_3 (the subscript denotes the degree of polymerization). The degree of functionalization seems to be quantitatively as no aromatic signals, corresponding to the tosyl group, were observed via ^1H NMR after azide modification (Figure S4).

For the synthesis of a symmetrical, star-shaped, porphyrin-centered $[TPP\text{-}PEtOx_5]_4$, CuAAC reactions were chosen as a versatile platform (Figure 1A). For this purpose, 1.5 eq. of $PEtOx_5$-N_3 in comparison to the alkyne functionalities of core ($[TPP\text{-}TB]_4$) was dissolved in THF. $PEtOx_5$-N_3 was used in a slight excess to ensure full conversion of the alkyne functionalities. The solution was purged with argon for 5 min, while copper bromide (CuBr; 1.5 eq.) and *N*,*N*,*N*′,*N*″,*N*″-pentamethyldiethylenetriamine (PMDETA; 1.5 eq.) were added under an argon stream. The solution was heated to 80°C in an oil bath for 10 min, passed over an aluminum oxide (AlOx N) column to remove the copper, and precipitated into diethyl ether. The purple precipitate was filtered and dried under vacuum, obtaining $[TPP\text{-}PEtOx_5]_4$ as a purple polymer, while any excess of $PEtOx_5$-N_3 remained in solution.

$[TPP\text{-}PEtOx_5]_4$ was investigated via SEC, FTIR, UV-Vis, NMR, and MALDI-ToF MS. Through SEC, a clear shift of the elution trace (straight line) to lower elution volume in comparison to $PEtOx_5$-N_3 (dashed line) could be observed (Figure 1C), indicating the absence of free linear polymer after purification. Through FTIR, a complete disappearance of the azide signal (≈2100 cm^{-1}) confirmed full conversion of $PEtOx_5$-N_3 (Figure 1B).

UV-Vis spectra (Figure 2B; Figure S7) of $[TPP\text{-}TB]_4$ and $[TPP\text{-}PEtOx_5]_4$ in THF showed differences in the Q-band region, whereas the Soret band remained at the same position. The individual signals at 519 and 554 nm ($[TPP\text{-}TB]_4$) collapsed into one signal at 542 nm, which has been described for the complexation of metal ions in the center of the phthalocyanine cavity (36). This led to the assumption that, during the CuAAC reaction, a copper complex with porphyrin was formed ($[Cu\text{-}TPP\text{-}PEtOx_5]_4$). NMR measurements showed no signals for the porphyrin units in the aromatic region, presumably due to the ferromagnetic character of the copper ions (Figure S8). This effect was also observed in the case of non-symmetrically substituted porphyrins and could be reduced by the addition of a ligand to minimize the magnetic exchange interactions between Cu-Cu ions (29). In our case, both UV-Vis and NMR indicated the incorporation of Cu ions into the cavity of the porphyrin core for $[TPP\text{-}PEtOx_5]_4$. The formation of this Cu complex also occurred under different reaction conditions for the CuAAC step (80°C for 5–10 min, room temperature for <12 h).

For the synthesis of a metal-free $[TPP\text{-}PEtOx_5]_4$, $[Cu\text{-}TPP\text{-}PEtOx_5]_4$ was dissolved in neat sulfuric acid and stirred for 12 h at room temperature (28). Acid-catalyzed hydrolysis of PEtOx (37–39) under these conditions was not observed in NMR spectra. Afterwards, no significant change in the elution behavior was observed in SEC (Figure 2C; Table 1). Nevertheless, comparable UV-Vis spectra as for earlier described $[TPP\text{-}TB]_4$ were observed, hinting towards the successful removal of copper from the porphyrin cavity and the formation of $[TPP\text{-}PEtOx_5]_4$. More precisely, both the ratio and the position of the signals, in particular in the case of the bands at 519 and 554 nm, coincided with the measurements for $[TPP\text{-}TB]_4$ (Figure 2D; see Figure S10).

The incorporation of different metal ions into porphyrin cavities has been described in the literature (30, 40). Because of the similarity of porphyrin and hemoglobin as iron-centered porphyrin-based complexes, we were interested in whether iron(III) ions could be selectively introduced, leading to $[Fe\text{-}TPP\text{-}PEtOx_5]_4$. Direct exchange by heating $[Cu\text{-}TPP\text{-}PEtOx_5]_4$ in the presence of iron (III) chloride ($FeCl_3$) at 90°C for 24 h was not successful, presumably due to the strong complexation of the copper ion. Using $[TPP\text{-}PEtOx_5]_4$ for the inclusion of iron into the cavity was not successful either, as the remaining acid might lead to the direct removal of the iron again. Therefore, the inclusion of iron into $[TPP\text{-}PEtOx_5]_4$ was achieved by the synthesis of an iron-containing core ($[Fe\text{-}TPP\text{-}TB]_4$), which was prepared by direct addition of iron(III) chloride to $[TPP\text{-}TB]_4$. After 24 h at 80°C, $[Fe\text{-}TPP\text{-}TB]_4$ was obtained after purification in a yield of 54% (Figures S12 and S13). Because of the ferromagnetic character of iron(III), characterization via NMR was not possible and FTIR was

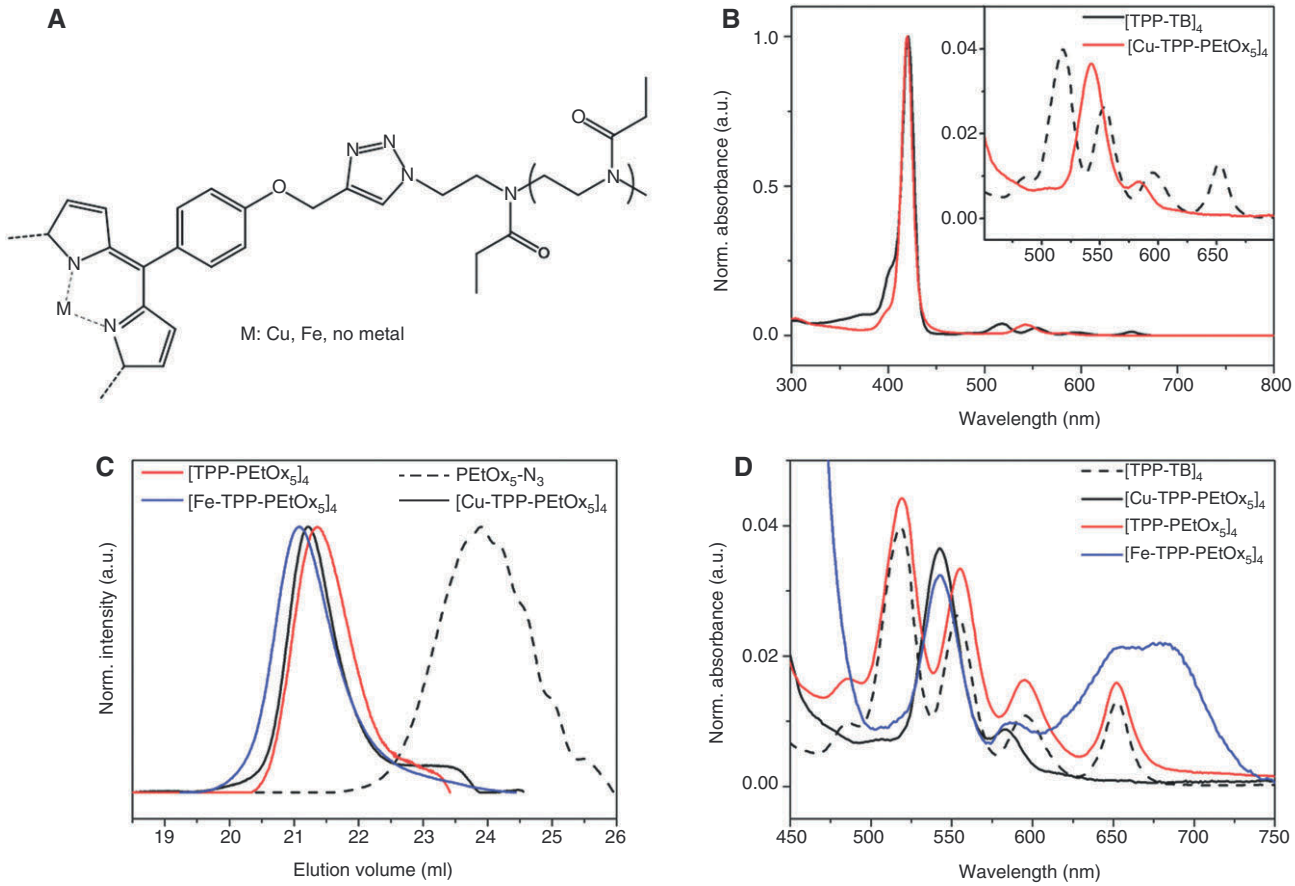

Figure 2: (A) Structure of $[Me\text{-}TPP\text{-}PEtOx_5]_4$; (B) comparison of UV-Vis spectra for $[TPP\text{-}TB]_4$ (black dashed line) and $[Cu\text{-}TPP\text{-}PEtOx_5]_4$; (C) comparison of SEC traces for $PEtOx_5\text{-}N_3$ (dashed line), $[Cu\text{-}TPP\text{-}PEtOx_5]_4$ (black line), $[Fe\text{-}TPP\text{-}PEtOx_5]_4$ (blue line), and $[TPP\text{-}PEtOx_5]_4$ (red line); (D) comparison of UV-Vis spectra for $[TPP\text{-}TB]_4$ (black dashed line), $[Cu\text{-}TPP\text{-}PEtOx_5]_4$ (straight black line), $[TPP\text{-}PEtOx_5]_4$ (red line), and $[Fe\text{-}TPP\text{-}PEtOx_5]_4$ (blue line).

applied instead. Compared to the FTIR of $[TPP\text{-}TB]_4$, that of $[Fe\text{-}TPP\text{-}TB]_4$ showed differences in the region associated with pyrrole moieties in the range of 1300 to 900 cm^{-1}, in particular at 995 cm^{-1} (Figure S12). Subsequently, $[Fe\text{-}TPP\text{-}TB]_4$ was used for CuAAC reactions with $PEtOx_5\text{-}N_3$ as described earlier. After precipitation, $[Fe\text{-}TPP\text{-}PEtOx_5]_4$ was characterized via SEC and FTIR, which showed an elution behavior comparable to those of $[Cu\text{-}TPP\text{-}PEtOx_5]_4$ and $[TPP\text{-}PEtOx_5]_4$ (Figure 2C; Table 1; Figure S16). Upon direct comparison of the FTIR spectra for $[Fe\text{-}TPP\text{-}PEtOx_5]_4$, $[Cu\text{-}TPP\text{-}PEtOx_5]_4$, and $[TPP\text{-}PEtOx_5]_4$, a signal, which can be attributed to pyrrole-metal complexes, being formed could be found at 995 cm^{-1}, whereas this individual signal disappeared in the case of $[TPP\text{-}PEtOx_5]_5$ (Figure S17).

Furthermore, the UV-Vis spectrum for $[Fe\text{-}TPP\text{-}PEtOx_5]_4$ in comparison to that for $[Cu\text{-}TPP\text{-}PEtOx_5]_4$ also showed a combined band at 542 nm, indicating metal complexation, and a new broad signal from 600 to 750 nm (Figure S14). The second broad signal was also indicated by the brownish color of the obtained material. As $[Fe\text{-}TPP\text{-}PEtOx_5]_4$ shows certain similarity to hemoglobin, selective complexation of oxygen by $[Fe\text{-}TPP\text{-}PEtOx_5]_4$ when stored under air can be assumed. This was already observed in SEC for $[Fe\text{-}TPP\text{-}PEtOx_5]_4$ after several days, where an additional distribution at higher molar masses could be found, which might indicate the presence of partially bridged or

Table 1: Selected characterization data of linear and star-shaped porphyrin-centered polymers synthesized in this study.

Polymer	M_n [a] (g mol^{-1})	$Đ$ [a]	M_p [b] (g mol^{-1})
$PEtOx_5\text{-}N_3$	710	1.37	
$[TPP\text{-}PEtOx_5]_4$	4600	1.12	2965
$[Cu\text{-}TPP\text{-}PEtOx_5]_4$	4900	1.10	3004
$[Fe\text{-}TPP\text{-}PEtOx_5]_4$	5100	1.14	2996
$[Cu\text{-}TPP\text{-}PEtOx_{11}]_4$	6100[c]	1.12	4700
$[Cu\text{-}TPP\text{-}PEtOx_{15}]_4$	8800[c]	1.07	6400

[a]SEC (DMAC/LiCl) PS calibration.
[b]MALDI-ToF MS.
[c]SEC ($CHCl_3$/TEA/iPrOH) PS calibration.

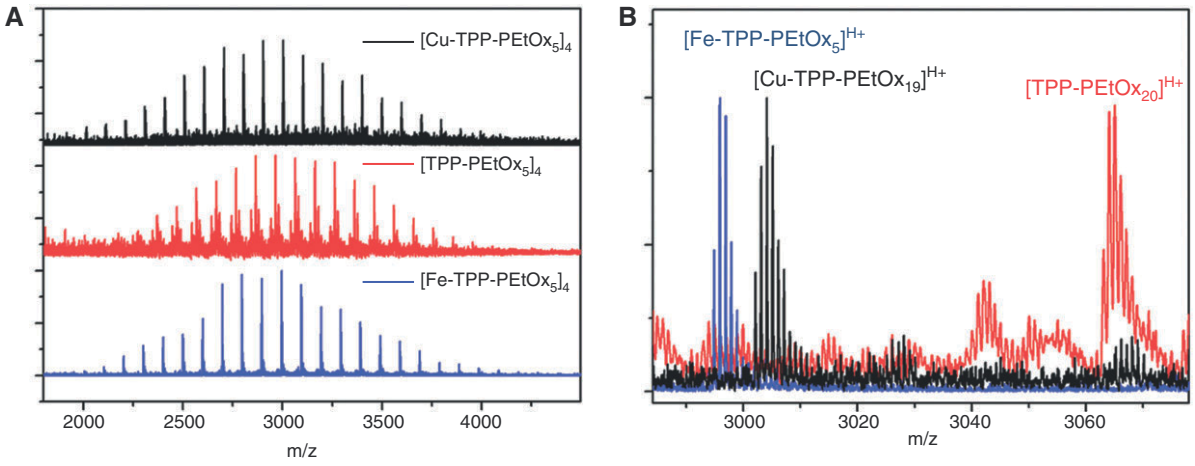

Figure 3: (A) Comparison of MALDI-ToF MS spectra for $[Cu\text{-}TPP\text{-}PEtOx_5]_4$ (black trace), $[TPP\text{-}PEtOx_5]_4$ (red trace), and $[Fe\text{-}TPP\text{-}PEtOx_5]_4$ (blue trace); (B) comparison of the major peak measured by MALDI-ToF MS spectra for $[Fe\text{-}TPP\text{-}PEtOx_{19}]$ (blue trace), $[Cu\text{-}TPP\text{-}PEtOx_{19}]$ (black trace), and $[TPP\text{-}PEtOx_{20}]$ (red curve).

oxidized $[Fe^{ox}\text{-}TPP\text{-}PEtOx_5]_4$ (Figure S18A). Oxidation or a low solubility of $[Fe\text{-}TPP\text{-}TB]_4$ might also explain the broad absorption bands in the UV-Vis spectra (Figure S13) at ≈375 and 490 nm. The solubility in the case of $[Fe\text{-}TPP\text{-}PEtOx_5]_4$ in THF increased in comparison to that of $[Fe\text{-}TPP\text{-}TB]_4$ by the attached polymer chains, and, presumably, both oxidation and aggregation decreased in THF.

We additionally subjected $[Fe\text{-}TPP\text{-}PEtOx_5]_4$, $[Cu\text{-}TPP\text{-}PEtOx_5]_4$, and $[TPP\text{-}PEtOx_5]_4$ to MALDI-ToF MS. The overall molar mass obtained for $[Fe\text{-}TPP\text{-}PEtOx_5]_4$, $[Cu\text{-}TPP\text{-}PEtOx_5]_4$, and $[TPP\text{-}PEtOx_5]_4$ could be determined at around 3000 g mol^{-1}, respectively, which is in good agreement with the desired composition (Figure 3A; Table 1). The calculated and measured isotopic patterns both showed differences corresponding to the according cavity-metal-intercalations (Figure 3B). In Figure 3B, the overlay shows a clear difference between the spectra for one peak corresponding to the same number of PEtOx arms, and the cationization agent of the individual star-macromolecules is illustrated, which shows a dependency on the specific composition. Depending on the incorporated metal for the porphyrin stars, shifts in the molar mass distributions were determined. The calculated isotopic patterns and the experimental data from MS for $[Fe\text{-}TPP\text{-}PEtOx_5]_4$, $[Cu\text{-}TPP\text{-}PEtOx_5]_4$, and $[TPP\text{-}PEtOx_5]_4$ fit, taking into account the architecture and ionization of the macromolecules (Figures S9, S11, and S15). Moreover, $[Fe^{ox}\text{-}TPP\text{-}PEtOx_5]_4$ showed at least two molar mass distributions at 3500 and 5000 g mol^{-1}, indicating bridging between two $[Fe\text{-}TPP\text{-}PEtOx_5]_4$ macromolecules.

The aforementioned outlined concept of the synthesis of star-shaped $[TPP\text{-}PEtOx_x]_4$ materials can also be applied for side chains with higher molar mass. Exemplarily, this has been shown using $PEtOx_{11}\text{-}N_3$ and $PEtOx_{15}\text{-}N_3$ as azide-functionalized building blocks. Comparable one-pot CuAAC reactions led to the formation of $[Cu\text{-}TPP\text{-}PEtOx_x]_4$ star-shaped polymers (Figure S19; Table 1).

3 Conclusion

Well-defined star-shaped polymers featuring a porphyrin core and PEtOx side chains of different lengths can be readily synthesized using CuAAC chemistry starting from alkyne-functionalized porphyrin and azide-functionalized poly(2-ethyl-2-oxazoline) ($PEtOx\text{-}N_3$). Mass spectrometry was used to investigate material characteristics as well as the intercalation of copper or iron into the porphyrin cavity of $[TPP\text{-}PEtOx_5]_4$ in addition to UV-Vis and FTIR. Such well-defined hybrid building blocks with defined amounts of metal cations are promising materials for future self-assembly studies. Another interesting feature is the herein observed susceptibility of $[Fe\text{-}TPP\text{-}PEtOx_5]_4$ to oxidation in the presence of oxygen.

4 Materials and methods

4.1 Methods

4.1.1 Nuclear magnetic resonance spectroscopy

Proton nuclear magnetic resonance (^{1}H NMR) spectra were recorded in $CDCl_3$ on a Bruker AC 300-MHz spectrometer at 298 K. Chemical shifts are given in parts per million (ppm, δ scale) relative to the residual signal of the deuterated solvent.

4.1.2 Size-exclusion chromatography

Size-exclusion chromatography was performed on a Agilent (Agilent Technology, Waldbronn, Germany) system equipped with an SCL-10A system controller, an G1329A pump, an G1362A refractive index detector, and both a PSS Gram30 and a PSS Gram1000 column series, whereby *N,N*-dimethylacetamide (DMAC) with 5 mmol of LiCl was used as an eluent at 1 ml min^{-1} of flow rate and the column oven was set to 40°C. The system was calibrated using polystyrene (PS; 100–1,000,000 g mol^{-1}) standards. Furthermore, a Shimadzu (Shimadzu, Duisburg, Germany) equipped with an SCL-10A system controller, an LC-10AD pump, and an RID-10A refractive index detector using a solvent mixture containing chloroform ($CHCl_3$), triethylamine (TEA), and *iso*-propanol (*i*-PrOH) (94:4:2) at a flow rate of 1 ml min^{-1} on a PSS SDV linear M 5-µm column at 40°was used for the investigation of the polymers.

4.1.3 Fourier-transform infrared spectroscopy

Dry powders of the copolymers were directly placed on the crystal of the ATR-FTIR (Affinity-1 FTIR, Shimadzu) or ATR-FT-IR (ALPHA's Platinum ATR, Bruker) for measurements in the range of 4000 to 600 cm^{-1}.

4.1.4 Microwave-assisted polymerizations

Microwave-assisted polymerizations were carried out utilizing an Initiator Sixty single-mode microwave synthesizer (Biotage, Uppsala, Sweden) equipped with a noninvasive IR sensor (accuracy: 2%). Microwave vials (conical, 0.5–2 ml) were heated at 110°C overnight and allowed to cool to room temperature under nitrogen atmosphere. All polymerizations were carried out using temperature control.

4.1.5 Matrix-assisted laser desorption ionization time-of-flight mass spectrometer

Matrix-assisted laser desorption/ionization time-of-flight mass spectrometry was performed on an Ultraflex III TOF/TOF (Bruker Daltonics, Bremen, Germany) equipped with a Nd:YAG laser and without any matrix and using NaCl as a doping agent in reflector and linear mode. The instrument was calibrated prior to each measurement following an external PMMA standard from PSS Polymer Standards Services GmbH (Mainz, Germany).

4.1.6 UV-Vis Spectroscopy

UV-Vis absorption spectra were recorded on a Specord 250 spectrometer (Analytik Jena, Jena, Germany) in Suprasil quartz glass cuvettes (104-QS, Hellma Analytics) with a thickness of 10 mm. The temperature at the measurements was controlled by a Jumo dTRON 08.1 instrument (Analytik Jena).

4.2 Materials

5,10,15,20-Tetrakis(4-hydroxyphenyl)-21H,23H-porphine (TPP), potassium carbonate, sodium azide, iron (III) chloride, and propargyl bromide (80 wt.% in toluene) were purchased from Sigma Aldrich. Propargyl bromide was distilled from $CaCl_2$ and stored under argon. 2-Ethyl-2-oxazoline was distilled from barium oxide under vacuum and stored under argon in a glove box.

4.2.1 Synthesis of alkyne modified tetrakisphenylporphyrin (TB-TPP)

5,10,15,20-Tetrakis(4-hydroxyphenyl)-21*H*,23*H*-porphyrin (TPP, 500 mg, 0.734 mmol) was dissolved in a solvent mixture of tetrahydrofuran and methanol (15 ml THF and 3 ml MeOH) together with 1.5 g of potassium carbonate (10.85 mmol). Propargyl bromide (3 ml, 26.9 mmol) was added to the solution under vigorous stirring and stirred for 24 h at 45°C. The solvent was removed under reduced pressure, dissolved in THF (concentrated), filtered, and dried under vacuum to obtain a purple solid. Yield: 95%, 590 mg.

^{1}H NMR (300 MHz, DMSO): 8.85 (s, pyrrole protons), 8.15 (d, phenyl), 7.43 (d, phenyl), 5.10 (s, -C*H*$_2$-C-CH), 3.77 (s, -CH$_2$-C-C*H*), -2.91 (s, -N*H*-) ppm.

FT-IR: 3290 (-CH), 1025 (C-O-C) cm^{-1}.

4.2.2 Synthesis of alkyne-modified iron(III) containing tetrakisphenylporphyrin ([Fe-TPP-TB]$_4$)

TB-TPP (92 mg, 0.11 mmol) was dissolved together with iron(III) chloride ($FeCl_3$, 52 mg, 0.19 mmol) in a THF/methanol mixture (10:4, v/v) and heated in an oil bath at 90°C overnight. The reaction mixture was diluted with dichloromethane and extracted with water, and the organic phase was dried over sodium sulfate, filtered, and then dried under vacuum. The product was obtained as a brownish solid. Yield: 54%, 54 mg.

ATR-FT-IR: 3300 (-CH), 1017 (C-O-C), 995 (pyrrole-metal) cm^{-1}.

4.2.3 Synthesis of azide-functionalized $PEtOx_5$-N_3

Methyl *p*-toluenesulfonate and EtOx were dissolved in ACN at a monomer-to-initiator ratio ([M]/[I]) of 5 and at a monomer concentration of 4 mol l^{-1}. The capped vials were placed in a microwave synthesizer at 140°C. The polymerization was terminated via the addition of dried sodium azide under inert conditions. The polymers were obtained after filtering the excess sodium azide and washing with dichloromethane; the organic phase was dried under vacuum. After precipitation in cold diethyl ether, the polymer was filtered and dried under vacuum.

SEC ($CHCl_3$/*i*-PrOH/Et_3N): M_n=900 g mol^{-1}; $Đ$=1.12 (PS calibration). SEC (DMAC/LiCl): M_n=710 g mol^{-1}; $Đ$=1.37 (PS calibration).

^{1}H NMR (300 MHz, $CDCl_3$, δ): 3.6–3.2 (br, -N-CH_2-CH_2-), 2.5–2.2 (br, CO-CH_2-CH_3), 1.2–0.9 (br, CO-CH_2-CH_3) ppm.

ATR-FT-IR: 2096 (azide), 1630 (carbonyl) cm^{-1}.

4.2.4 CuAAC reaction between $[TPP\text{-}TB]_4$ and azide-modified PEtOx ($PEtOx_5$-N_3) forming $[Cu\text{-}TPP\text{-}PEtOx_5]_4$

The core ($[TPP\text{-}TB]_4$) and $PEtOx_5$-N_3 (6 eq.) were dissolved in THF. The solution was purged with argon for 5 min, while CuBr (6 eq.) and PMDETA (6 eq.) were added under argon stream. The solution was heated up to 80°C in an oil bath for 10 min, diluted with chloroform, and passed over an aluminum oxide (AlOx N) column to remove the copper. The solvent was removed under reduced pressure and precipitated in cold diethyl ether. The purple precipitate was filtered and dried under vacuum, obtaining the porphyrin-centered polymer.

SEC (DMAC/LiCl): M_n=4900 g mol^{-1}; $Đ$=1.10 (PS calibration).

^{1}H NMR (300 MHz, $CDCl_3$, δ): 8.0–7.65 (tetrazine), 5.5-5.2 (tetrazine-CH_2-CH_2-), 4.8–4.6 (tetrazine-CH_2-O-), 4.0–3.8 (tetrazine-CH_2-CH_2-), 3.8–3.1 (backbone), 2.5–2.2 (br, CO-CH_2-CH_3), 1.2–0.9 (br, CO-CH_2-CH_3) ppm.

ATR-FT-IR: 1630 (carbonyl), 995 (pyrrole-metal) cm^{-1}.

4.2.5 Synthesis of metal-free $[TPP\text{-}PEtOx_5]_4$

For the synthesis of metal-free $[TPP\text{-}PEtOx_5]_4$, $[Cu\text{-}TPP\text{-}PEtOx_5]_4$ was dissolved in concentrated sulfuric acid and stirred at room temperature for 24 h. The product was obtained after dilution with water (caution during the addition of water to sulphuric acid) and then extracted with dichloromethane and water, dried under vacuum, and precipitated in diethyl ether.

SEC (DMAC/LiCl): M_n=4600 g mol^{-1}; $Đ$=1.12 (PS calibration).

^{1}H NMR (300 MHz, $CDCl_3$, δ): 8.0–7.65 (tetrazine), 5.7-5.4 (tetrazine-CH_2-CH_2-), 4.8–4.6 (tetrazine-CH_2-O-), 4.0–3.8 (tetrazine-CH_2-CH_2-), 3.8–3.1 (backbone), 2.5–2.2 (br, CO-CH_2-CH_3), 1.2–0.9 (br, CO-CH_2-CH_3) ppm.

ATR-FT-IR: 1630 (carbonyl) cm^{-1}.

4.2.6 CuAAC reaction between $[Fe\text{-}TPP\text{-}TB]_4$ and azide-modified PEtOx ($PEtOx_5$-N_3) forming $[Fe\text{-}TPP\text{-}PEtOx_5]_4$

The core ($[Fe\text{-}TPP\text{-}TB]_4$) and $PEtOx_5$-N_3 (6 eq.) were dissolved in THF. The solution was purged with argon for 5 min, while CuBr (6 eq.) and PMDETA (6 eq.) were added under argon stream. The solution was heated up to 80°C in an oil bath for 10 min, diluted with chloroform, and passed over an aluminum oxide (AlOx N) column to remove the copper. The solvent was removed under reduced pressure and precipitated in cold diethyl ether. The brownish precipitate was filtered and dried under vacuum, obtaining the porphyrin-centered polymer.

SEC (DMAC/LiCl): M_n=5100 g mol^{-1}; $Đ$=1.14 (PS calibration).

ATR-FT-IR: 1630 (carbonyl), 995 (pyrrole-metal) cm^{-1}.

Acknowledgments: F.H.S. thanks the VCI for an independent researcher fellowship, and T.R. the Carl-Zeiss foundation for a PhD scholarship. F.H.S. and U.S.S. also acknowledge the Thuringian Ministry for Education, Science and Culture (grant nos.: B514-09051 and B715-08011, NanoConSens; B515-10065, ChaPoNano) for financial support. T.R. would like to thank Katrin Knop for scientific discussions concerning TPP, as well as Benjamin Kintzel and Martin Obst for help during laboratory courses. We thank Bruker Daltonics for their help and support.

References

1. Pitsikalis M, Pispas S, Mays J, Hadjichristidis N. Nonlinear block copolymer architectures. Adv Polym Sci. 1998;135:1–137.
2. Hadjichristidis N, Iatrou H, Pitsikalis M, Mays J. Macromolecular architectures by living and controlled/living polymerizations. Prog Polym Sci. 2006;31(12):1068–32.
3. Blencowe A, Tan JF, Goh TK, Qiao GG. Core cross-linked star polymers via controlled radical polymerisation. Polymer 2009;50(1):5–32.

4. High LRH, Holder SJ, Penfold HV. Synthesis of star polymers of styrene and alkyl (meth)acrylates from a porphyrin initiator core via ATRP. Macromolecules 2007;40(20):7157–65.
5. Steinschulte AA, Schulte B, Drude N, Erberich M, Herbert C, Okuda J, Möller M, Plamper FA. A nondestructive, statistical method for determination of initiation efficiency: dipentaerythritol-aided synthesis of ternary ABC_3 miktoarm stars using a combined "arm-first" and "core-first" approach. Polym Chem. 2013;4:3885–3895.
6. Wu L, McHale R, Feng G, Wang X. RAFT synthesis and self-assembly of free-base porphyrin cored star polymers. Int J Polym Sci. 2011;2011:1–11.
7. Dai XH, Dong CM, Fa HB, Yan D, Wei Y. Supramolecular polyp-seudorotaxanes composed of star-shaped porphyrin-cored poly(ε-caprolactone) and α-cyclodextrin. Biomacromolecules 2006;7(12):3527–33.
8. Jia M, Ren T, Wang A, Yuan W, Ren J. Amphiphilic star-shaped poly(e-caprolactone-*block*-poly(L-Lysin) copolymers with porphyrin core: synthesis, self-assembly, and cell viability assay. J Appl Polym Sci. 2014;131:40097.
9. Jin RH. Water soluble star block poly(oxazoline) with porphyrin label: a unique emulsion and its shape direction. J Mater Chem. 2004;14:320–7.
10. Hoogenboom R, Fijten MWM, Kickelbick G, Schubert US. Synthesis and crystal structures of multifunctional tosylates as basis for star-shaped poly(2-ethyl-2-oxazoline)s. Beilstein J Org Chem. 2010;6:773–83.
11. Kolb HC, Finn MG, Sharpless KB. Click chemistry: diverse chemical function from a few good reactions. Angew Chem Int Ed. 2001;40(11):2004–21.
12. Binder WH, Sachsenhofer R. 'Click' chemistry in polymer and materials science. Macromol Rapid Commun. 2007;28(1):15–54.
13. Fournier D, Hoogenboom R, Schubert US. Clicking polymers: a straightforward approach to novel macromolecular architectures. Chem Soc Rev. 2007;36(8):1369–80.
14. Barner-Kowollik C, Du Prez FE, Espeel P, Hawker CJ, Junkers T, Schlaad H, Van Camp W. "Clicking" polymers or just efficient linking: what is the difference? Angew Chem Int Ed. 2011;50(1):60–2.
15. Xi W, Scott TF, Kloxin CJ, Bowman CN. Click chemistry in materials science. Adv Funct Mater. 2014;24(18):2572–90.
16. Espeel P, Du Prez FE. "Click"-inspired chemistry in macromolecular science: matching recent progress and user expectations. Macromolecules 2015;48(1):2–14.
17. Xu LQ, Yao F, Fu GD, Kang ET. Interpenetrating network hydrogels via simultaneous "click chemistry" and atom transfer radical polymerization. Biomacromolecules 2010;11(7):1810–7.
18. Koschella A, Hartlieb M, Heinze T. A "click-chemistry" approach to cellulose-based hydrogels. Carbohyd Polym. 2011;86(1):154–61.
19. Durmaz H, Dag A, Altintas O, Erdogan T, Hizal G, Tunca U. One-pot synthesis of ABC type triblock copolymers via in situ click [3 + 2] and Diels-Alder [4 + 2] reactions. Macromolecules 2007;40(2):191–8.
20. Zhu J, Zhu X, Kang ET, Neoh KG. Design and synthesis of star polymers with hetero-arms by the combination of controlled radical polymerizations and click chemistry. Polymer 2007;48(24):6992–9.
21. Rudolph T, Nunns A, Schwenke AM, Schacher FH. Synthesis and self-assembly of poly(ferrocenyldimethylsilane)-block-poly(2-alkyl-2-oxazoline) block copolymers. Polym Chem. 2015;6:1604–12.
22. Rudolph T, Crotty S, Lühe Mvd, Pretzel D, Schubert US, Schacher FH. Synthesis and solution properties of double hydrophilic poly(ethylene oxide)-block-poly(2-ethyl-2-oxazoline) (PEO-b-PEtOx) star block copolymers. Polymers 2013;5(3):1081–101.
23. Kempe K, Krieg A, Becer CR, Schubert US. "Clicking" on/with polymers: a rapidly expanding field for the straightforward preparation of novel macromolecular architectures. Chem Soc Rev. 2012;41(1):176–91.
24. Sternberg ED, Dolphin D, Brückner C. Porphyrin-based photosensitizers for use in photodynamic therapy. Tetrahedron 1998;54(17):4151–202.
25. Meunier B. Metalloporphyrins as versatile catalysts for oxidation reactions and oxidative DNA cleavage. Chem. Rev. 1992;92(6):1411–56.
26. Li Y, Auras F, Lobermann F, Doblinger M, Schuster J, Peter L, Trauner D, Bein T. A photoactive porphyrin-based periodic mesoporous organosilica thin film. J Am Chem Soc. 2013;135(49):18513–9.
27. Zhamkochyan GA, Akopyan ME, Akopyan LM, Kurtikyan TS. Synthesis of new unsaturated mesotetraarylporphyrins. Chem Heterocycl Compounds 1987;23(2):186–91.
28. Speckbacher M, Yu L, Lindsey JS. Formation of porphyrins in the presence of acid-labile metalloporphyrins: a new route to mixed-metal multiporphyrin arrays. Inorg Chem. 2003;42(14):4322–37.
29. Garate-Morales JL, Reyes-Ortega Y, Alvarez-Toledano C, Gurierrez-Perez R, Ramirez-Rosales D, Zamorano-Ulloa R, Basurto-Uribe E, Hernandez-Diaz J, Contreras R. Spectroscopic studies of novel porphyrin-copper(II) and zinc(II) complexes that share the pinch-porphyrin family structure of iron(III) complex models of peroxidases. Trans Metal Chem. 2002;27(8):906–17.
30. Kumar A, Maji S, Dubey P, Abhilash GJ, Pandey S, Sarkar S. One-pot general synthesis of metalloporphyrins. Tetrahedron Lett. 2007;48(41):7287–90.
31. Rowan SJ, Cantrill SJ, Cousins GRL, Sanders JKM, Stoddart JF. Dynamic covalent chemistry. Angew Chem Int Ed. 2002;41: 898–952.
32. Roberts DA, Schmidt TW, Crossley MJ, Perrier S. Tunable self-assembly of triazole-linked porphyrin-polymer conjugates. Chem Eur J. 2013;19(38):12759–70.
33. Jin RH. Self-assembly of porphyrin-centered amphiphilic star block copolymer into polymeric vesicular aggregates. Macromol Rapid Commun. 2003;204(3):403–9.
34. Jin RH. Controlled location of porphyrin in aqueous micelles self-assembled from porphyrin centered amphiphilic star poly(oxazolines). Adv Mater. 2002;14:889–92.
35. Rudolph T, Kumar Allampally N, Fernández G, Schacher FH. Controlling aqueous self-assembly mechanisms by hydrophobic interactions. Chem Eur J. 2014;20(43):13871–5.
36. Dinçer H, Mert H, Şen BN, Dağ A, Bayraktar S. Synthesis and characterization of novel tetra terminal alkynyl-substituted phthalocyanines and their star polymers via click reaction. Dyes Pigm. 2013;98(2):246–54.
37. Lambermont-Thijs HML, van der Woerdt FS, Baumgaertel A, Bonami L, Du Prez FE, Schubert US, Hoogenboom R. Linear poly(ethylene imine)s by acidic Hydrolysis of poly(2-oxazoline)s: kinetic screening, thermal properties, and temperature-induced solubility transitions. Macromolecules 2009;43(2):927–33.

38. Tauhardt L, Kempe K, Knop K, Altuntaş E, Jäger M, Schubert S, Fischer D, Schubert US. Linear polyethyleneimine: optimized synthesis and characterization – On the way to "Pharmagrade" batches. Macromol Chem Phys. 2011;212:1918–24.
39. de la Rosa VR, Bauwens E, Monnery BD, De Geest BG, Hoogenboom R. Fast and accurate partial hydrolysis of poly(2-ethyl-2-oxazoline) into tailored linear polyethylenimine copolymers. Polym Chem. 2014;5(17):4957–64.
40. Lemon CM, Brothers PJ, Boitrel B. Porphyrin complexes of the period 6 main group and late transition metals. Dalton Trans. 2011;40(25):6591–609.

Supplemental Material: The online version of this article (DOI: 10.1515/epoly-2015-0041) offers supplementary material, available to authorized users.

Graphical abstract

Tobias Rudolph, Sarah Crotty, Ulrich S. Schubert, Felix H. Schacher

Star-shaped poly(2-ethyl-2-oxazoline) featuring a porphyrin core: synthesis and metal complexation

DOI 10.1515/epoly-2015-0041
e-Polymers 2015; xx(x): xxx–xxx

Full length article: We demonstrate the synthesis of star-shaped porphyrin-centered poly(2-ethyl-2-oxazoline) via cationic ring-opening polymerization and CuAAC cycloaddition chemistry. Furthermore, the porphyrin cavity was used for the complexation of metal ions.

Keywords: metal-containing polymers; poly(2-ethyl-2-oxazoline); porphyrins; star-shaped polymers.

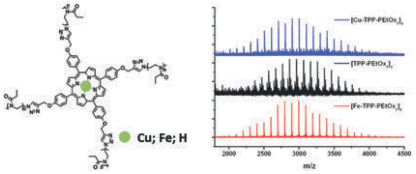

Supporting information

Star-Shaped Poly(2-ethyl-2-oxazoline) Featuring a Porphyrin Core: Synthesis and Metal Complexation

Tobias Rudolph,[1,2] Sarah Crotty,[1,2] Ulrich S. Schubert,[1,2] Felix H. Schacher[1,2,*]

[1] Institute of Organic Chemistry and Macromolecular Chemistry (IOMC), Friedrich Schiller University Jena, Humboldtstr. 10, 07743 Jena, Germany

E-mail: felix.schacher@uni-jena.de

[2] Jena Center for Soft Matter (JCSM), Friedrich Schiller University Jena, Philosophenweg 7, 07743 Jena, Germany

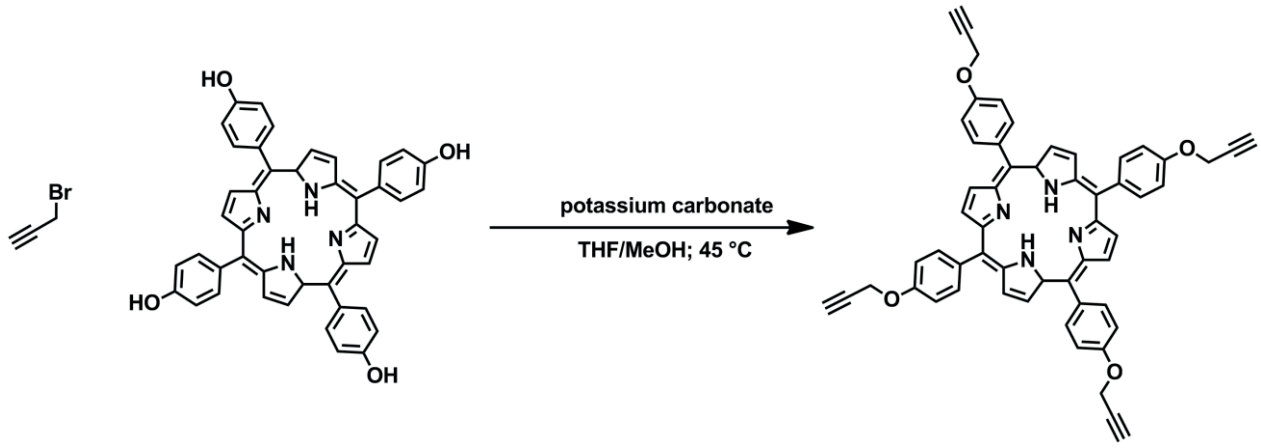

Scheme S1: 5,10,15,20-Tetrakis(4-hydroxyphenyl)-21H,23H-porphin $[TPP\text{-}OH]_4$ modification *via* etherification with propargyl bromide, forming alkyne-modified $[TPP\text{-}TB]_4$.

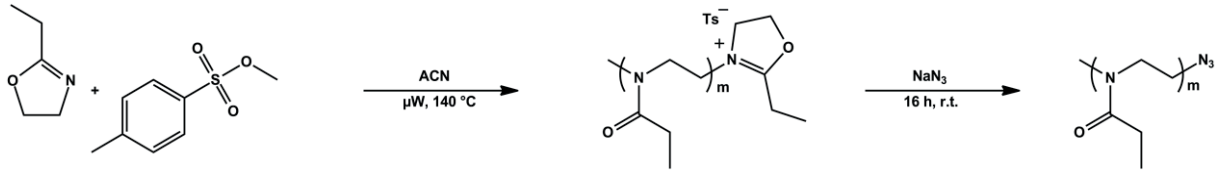

Scheme S2: Microwave-assisted cationic ring-opening polymerization (CROP) of 2-ethyl-2-oxazoline (EtOx) initiated *via* methyl *p*-toluenesulfonate and terminated using sodium azide.

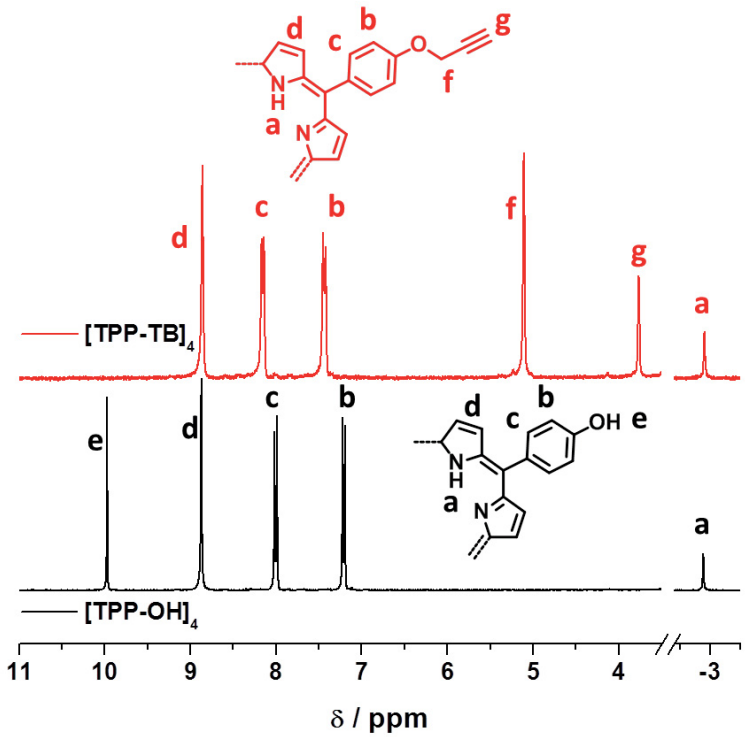

Figure S1: Comparison of ^{1}H-NMR spectra for $[TPP\text{-}OH]_4$ (black curve) and alkyne-modified $[TPP\text{-}TB]_4$ (red curve, DMSO- d_6; 300 MHz).

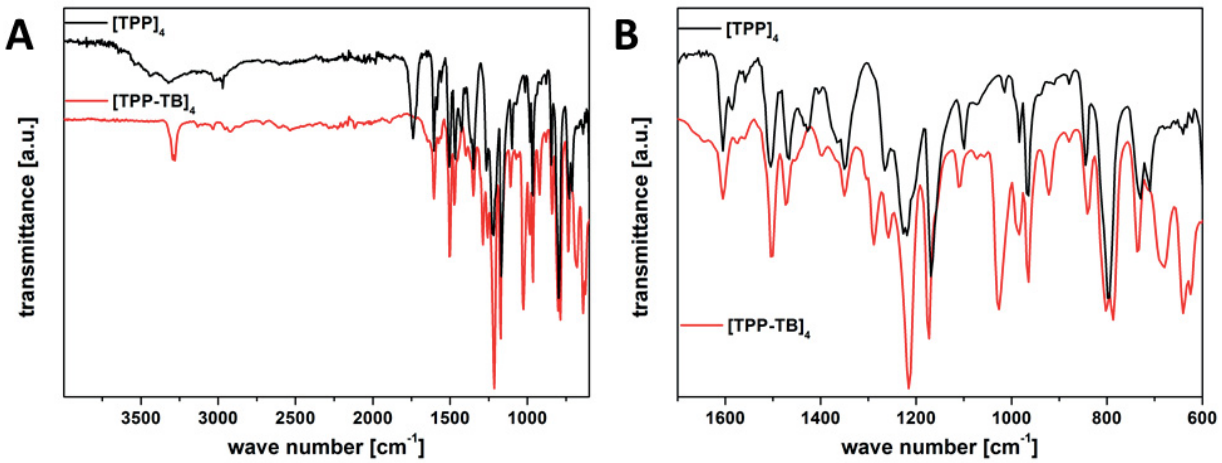

Figure S2: Comparison of FT-IR spectra for $[TPP\text{-}OH]_4$ (black curve) and alkyne-modified $[TPP\text{-}TB]_4$ (red curve).

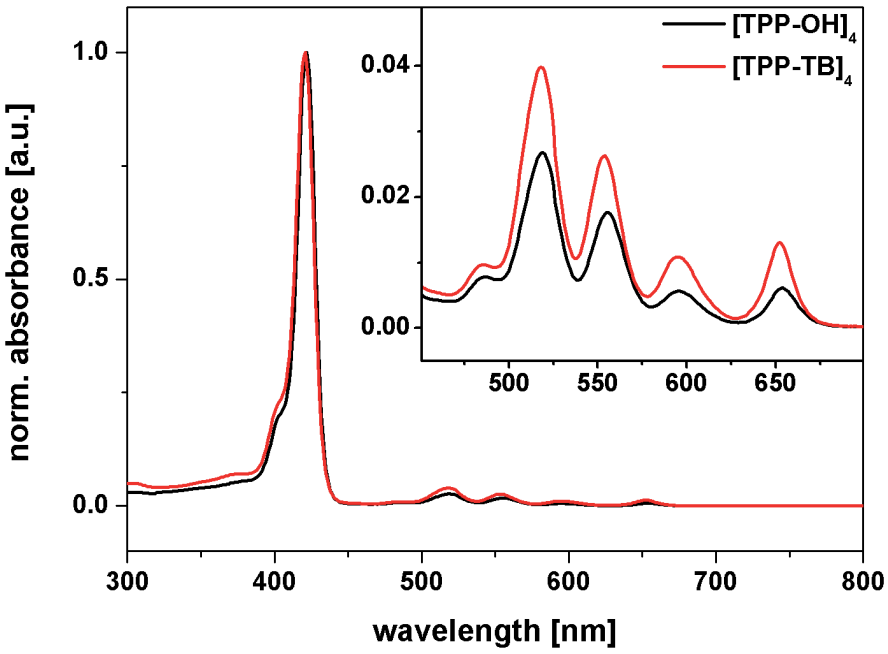

Figure S3: Comparison of UV-Vis spectra for $[TPP\text{-}OH]_4$ (black curve) and $[TPP\text{-}TB]_4$ (red trace) in THF with an inset showing the region between 450-700 nm in more detail.

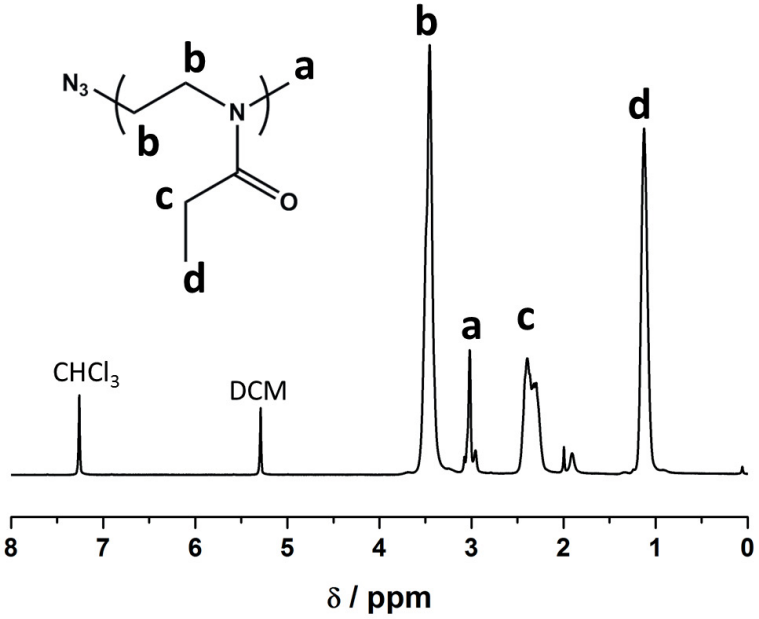

Figure S4: ^{1}H-NMR spectrum for $PEtOx_5\text{-}N_3$ ($CDCl_3$; 300 MHz).

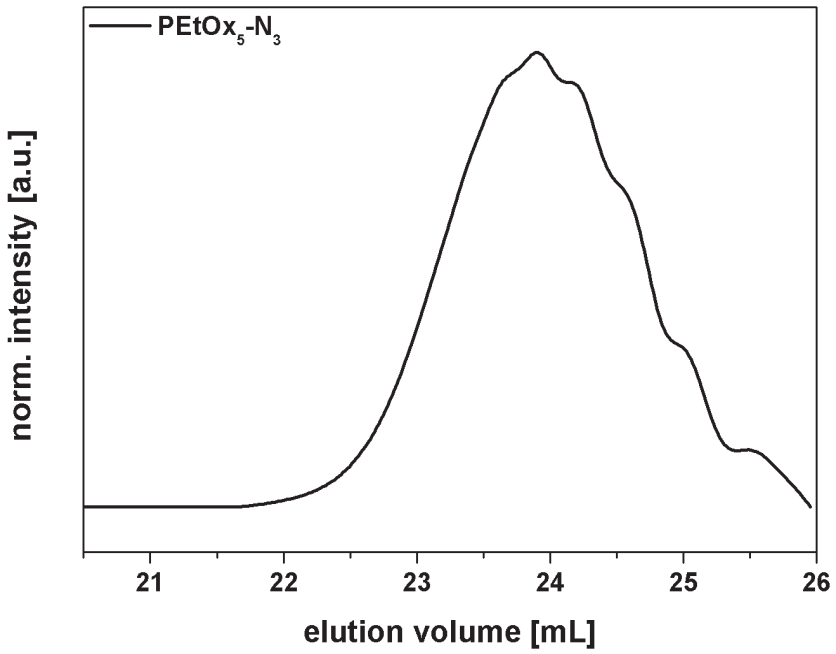

Figure S5: SEC elution trace for PEtOx-N_3 with DMAC/LiCl as eluent.

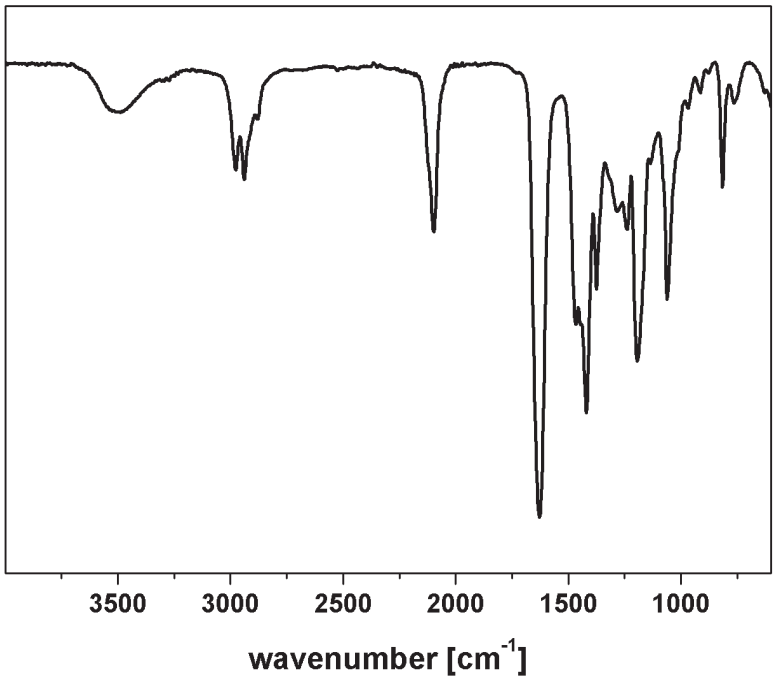

Figure S6: FT-IR spectrum for PEtOx$_5$-N_3 with the characteristic peak for the azide functionality at 2096 cm^{-1}.

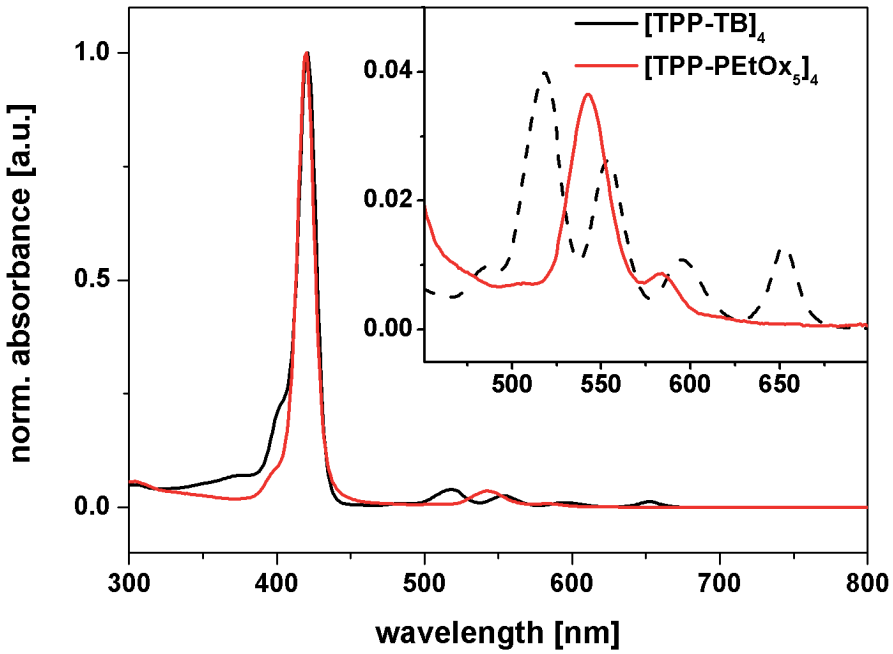

Figure S7: Comparison of UV-Vis spectra for $[TPP\text{-}TB]_4$ (black curve), and $[TPP\text{-}PEtOx_5]_4$ (red trace) in THF with an inset for the region between 450-700 nm.

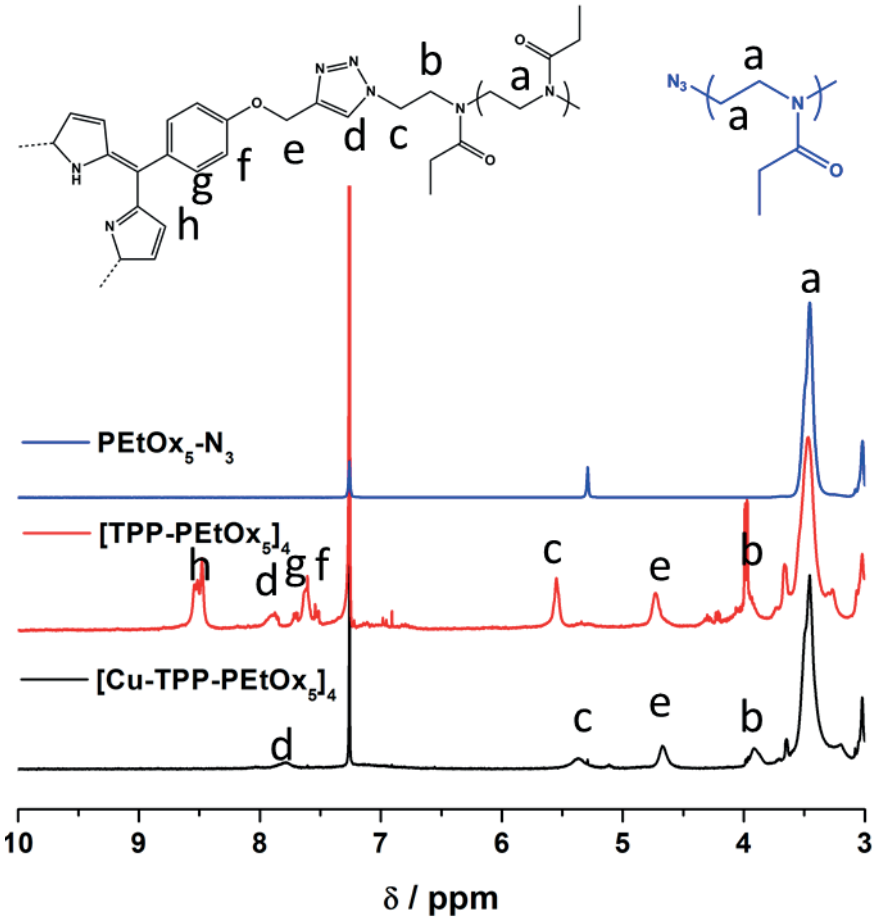

Figure S8: Comparison of ^{1}H-NMR spectra for $PEtOx_5$-N_3 (blue trace), $[TPP\text{-}PEtOx_5]_4$ (red trace), and $[Cu\text{-}TPP\text{-}PEtOx_5]_4$ (black trace) ($CDCl_3$; 300 MHz).

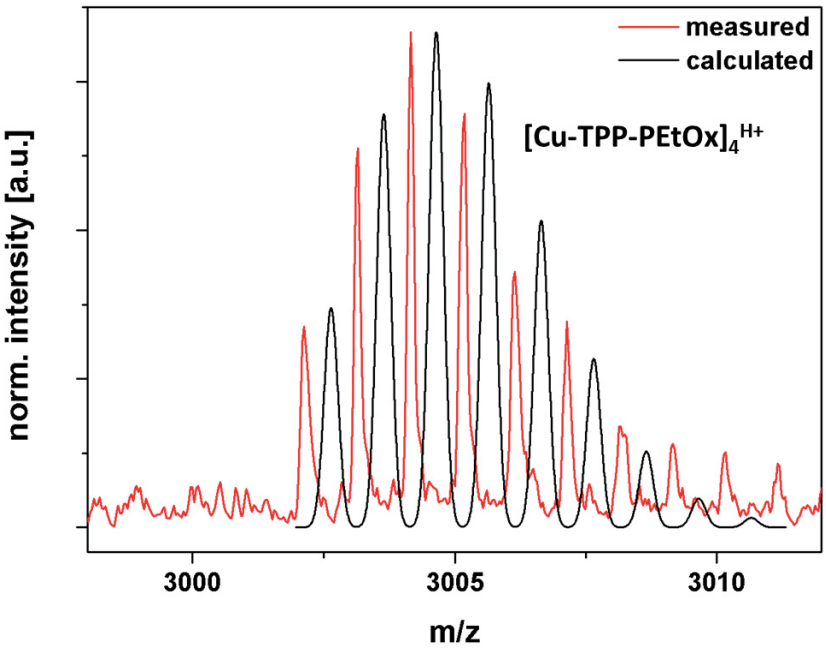

Figure S9: MALDI-ToF MS overlay of the measured (red curve) and calculated (black curve) spectra for $[Cu\text{-}TPP\text{-}PEtOx_5]_4$.

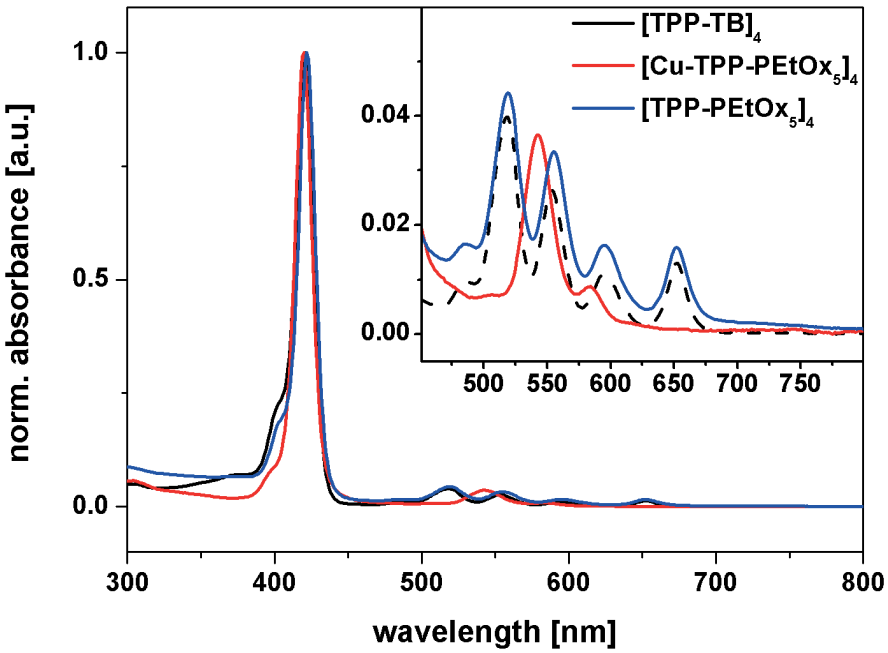

Figure S10: Comparison of UV-Vis spectra for $[TPP\text{-}TB]_4$ (black curve), $[Cu\text{-}TPP\text{-}PEtOx_5]_4$ (red trace) and $[TPP\text{-}PEtOx_5]_4$ (blue trace) in THF with an inset for the region between 450-800 nm.

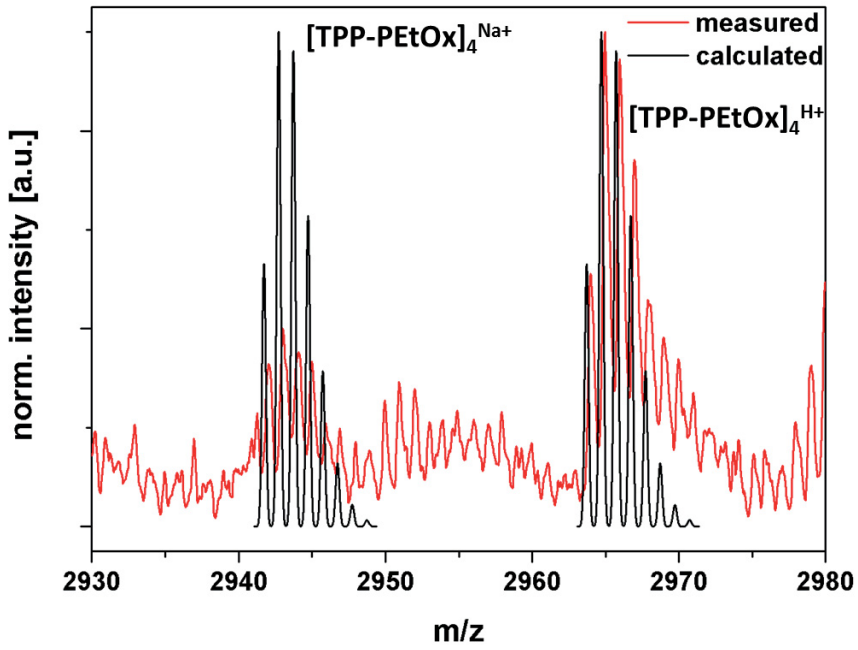

Figure S11: MALDI-ToF MS overlay of the measured (red curve) and calculated (black curve) spectra for $[TPP\text{-}PEtOx_5]_4$.

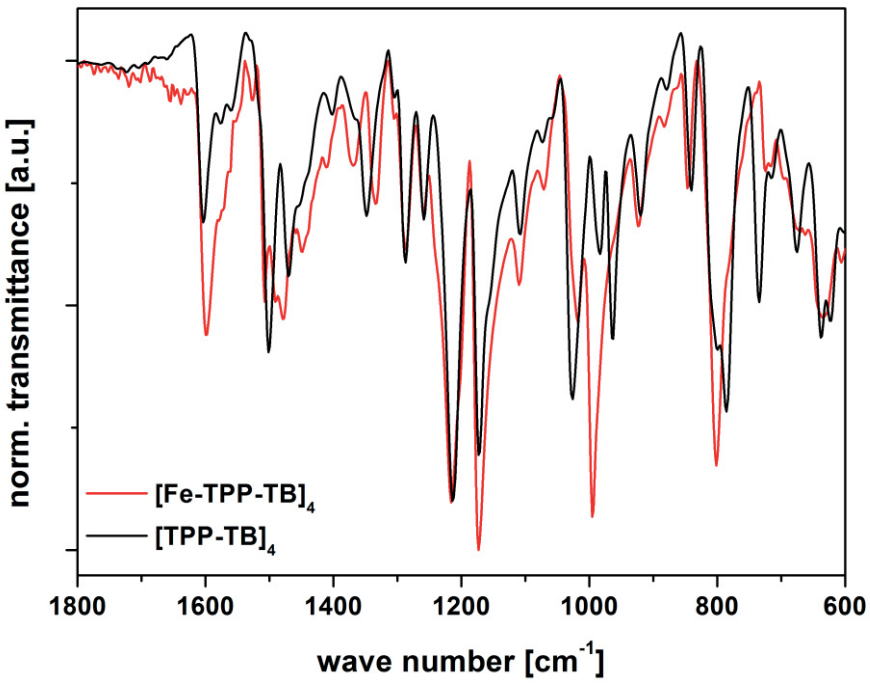

Figure S12: Comparison of FT-IR spectra for $[TPP\text{-}TB]_4$ (black trace) and $[Fe\text{-}TPP\text{-}TB]_4$ (red trace).

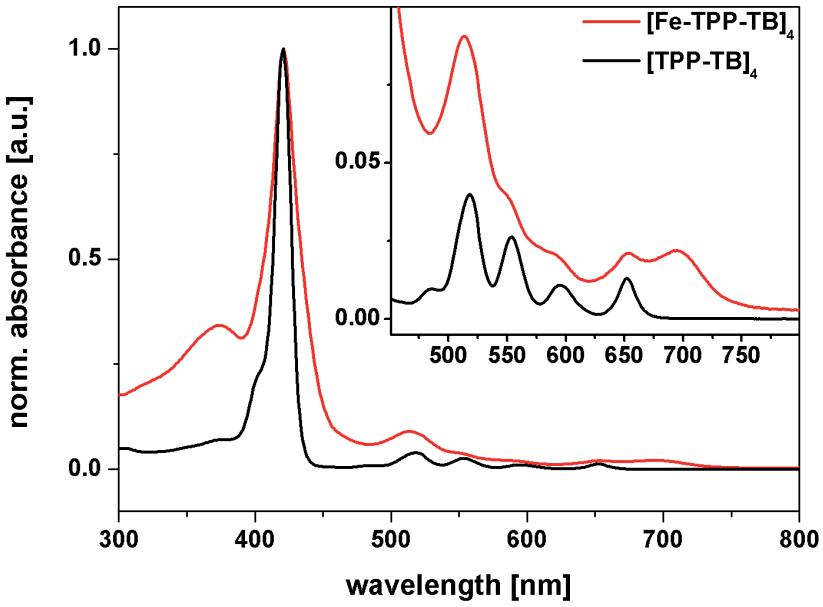

Figure S13: Comparison of UV-Vis spectra for $[TPP\text{-}TB]_4$ (black curve), and $[Fe\text{-}TPP\text{-}TB]_4$ (red trace) in THF with an inset of the region between 450-800 nm.

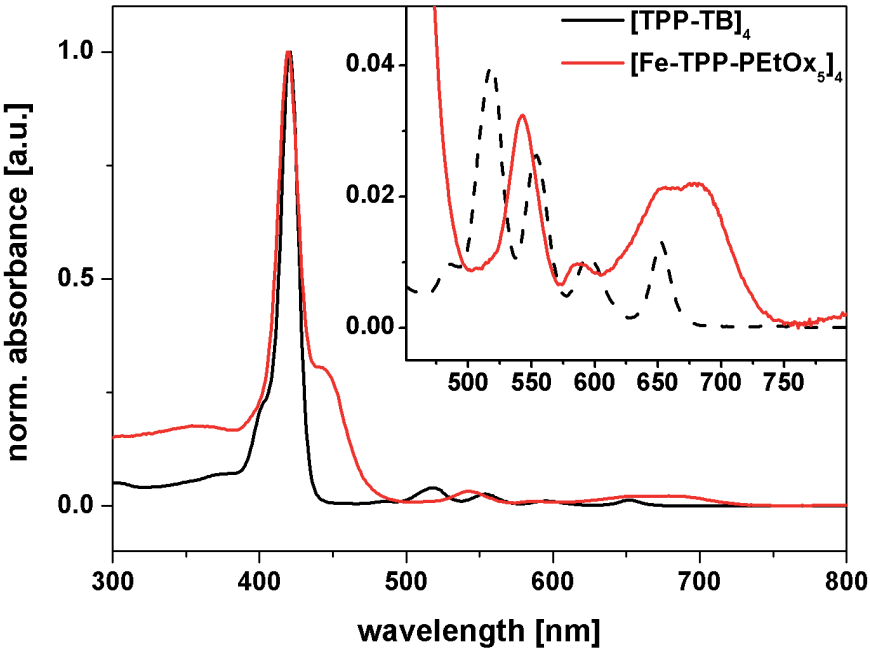

Figure S14: Comparison of UV-Vis spectra for $[TPP\text{-}TB]_4$ (black curve), and $[Fe\text{-}TPP\text{-}PEtOx_5]_4$ (red trace) in THF with an inset of the region between 450-800 nm.

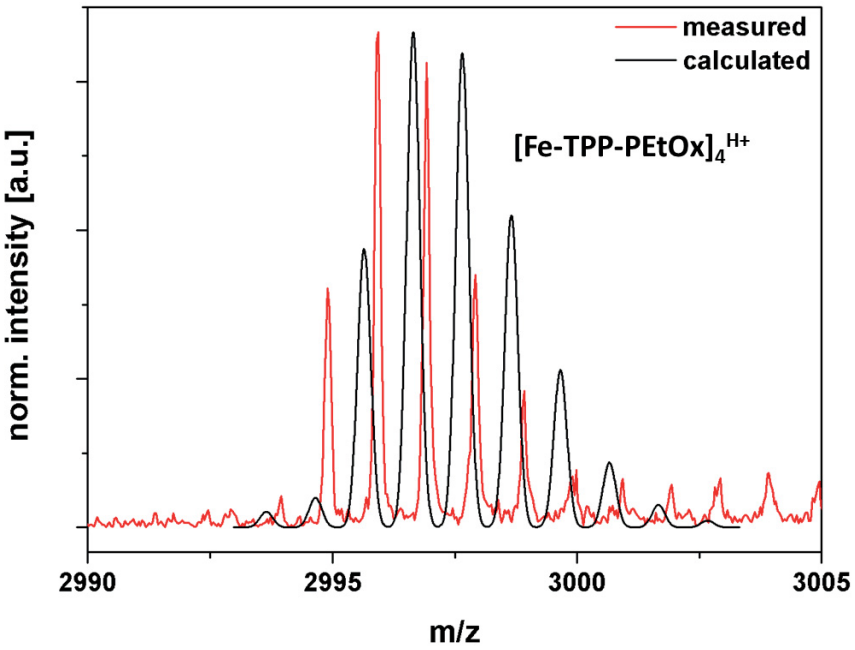

Figure S15: MALDI-ToF MS overlay of the measured (red curve) and calculated (black curve) spectra for $[Fe\text{-}TPP\text{-}PEtOx_5]_4$.

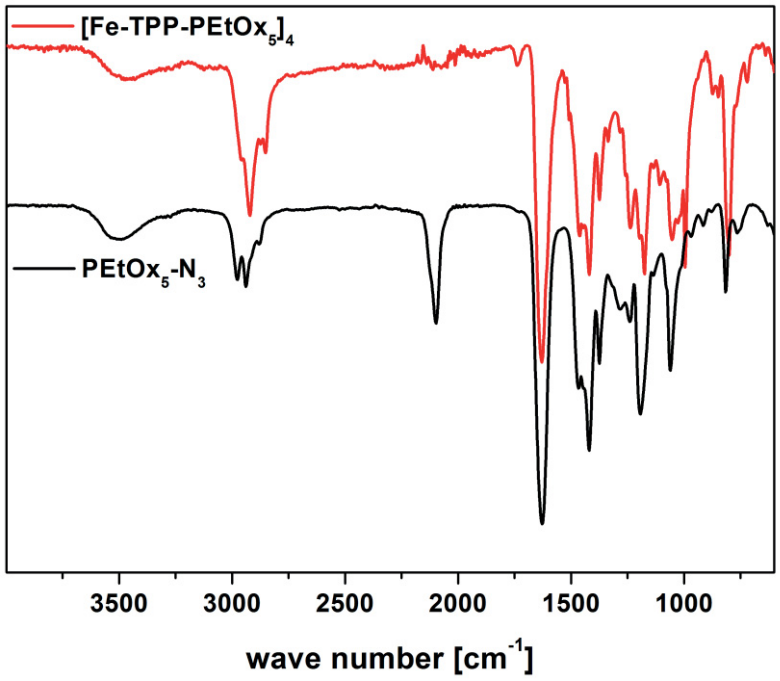

Figure S16: Comparison of FT-IR spectra for $PEtOx_5\text{-}N_3$ (black trace) and $[Fe\text{-}TPP\text{-}PEtOx_5]_4$ (red trace).

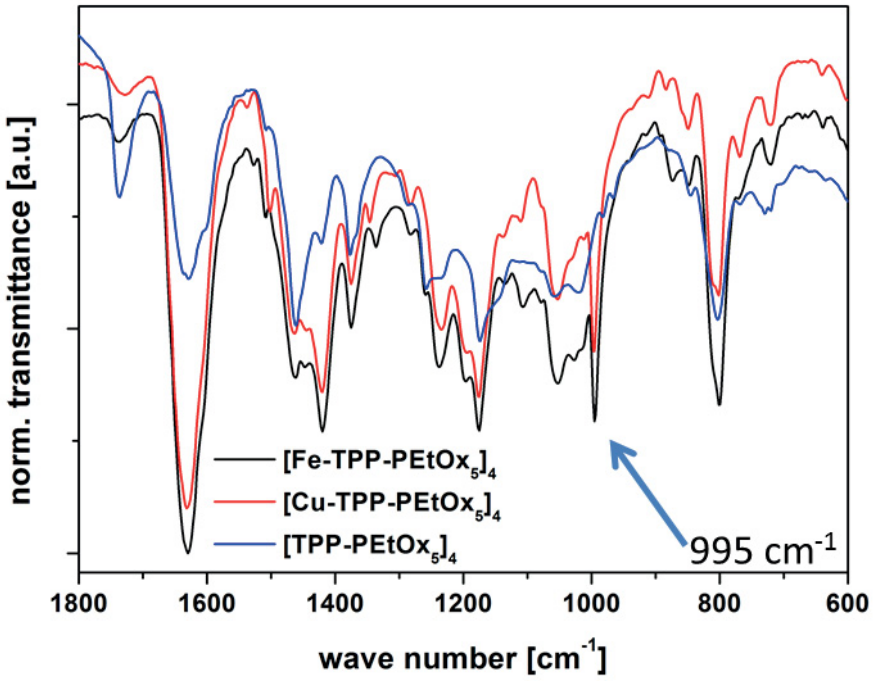

Figure S17: Comparison of FT-IR spectra for $[Cu\text{-}TPP\text{-}PEtOx_5]_4$ (red curve), $[TPP\text{-}PEtOx_5]_4$ (blue curve), and $[Fe\text{-}TPP\text{-}PEtOx_5]_4$ (black curve).

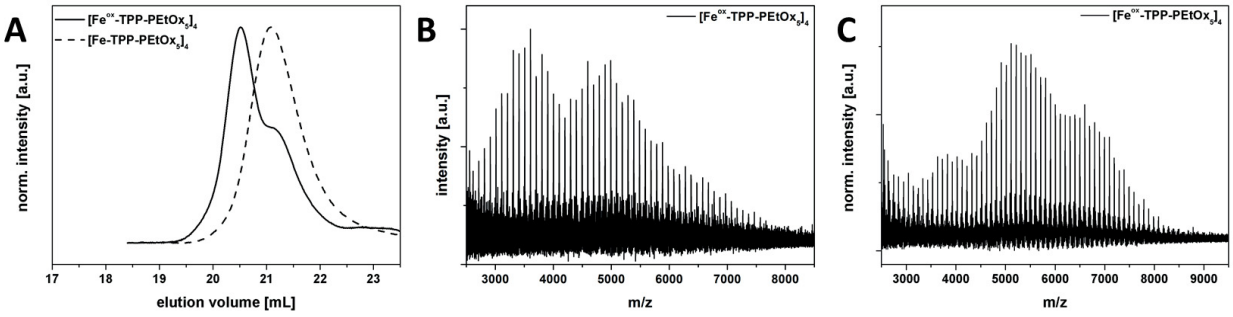

Figure S18: A) Comparison of SEC traces for $[Fe\text{-}TPP\text{-}PEtOx_5]_4$ (dashed curve) and a partially oxidized sample of $[Fe^{ox}\text{-}TPP\text{-}PEtOx_5]_4$ (straight curve); B-C) MALDI-ToF MS spectra for $[Fe^{ox}\text{-}TPP\text{-}PEtOx_5]_4$.

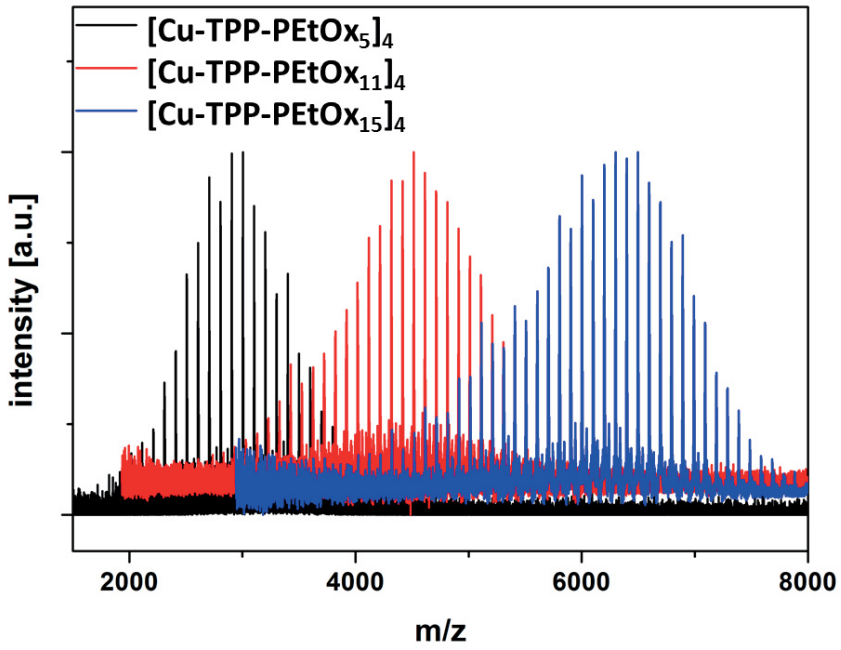

Figure S19: Overlay of MALDI-ToF MS spectra for $[Cu\text{-}TPP\text{-}PEtOx_5]_4$ (black trace), $[Cu\text{-}TPP\text{-}PEtOx_{11}]_4$ (red trace), and $[Cu\text{-}TPP\text{-}PEtOx_{15}]_4$ (blue trace).